THE DESIGN, SYNTHESIS, AND EVALUATION OF (I) ARYLPIPERAZINES AND (II) PYRAZOLOPYRIMIDINONES AS POTENTIAL ANTI-DIABETIC AGENTS.

A thesis submitted to Maynooth University in fulfilment of the requirements for the degree of

Doctor of Philosophy

by

Mark Kelada

Department of Chemistry,

Maynooth University,

Maynooth, Co. Kildare, Ireland

October 2018

Research Supervisor: Dr. John Stephens

Head of Department: Dr. Jennifer McManus

Table of Contents

<u>Declaration</u>

I declare that the work presented in this thesis was carried out in accordance with the regulations of Maynooth University. The work is original, except where indicated by reference, and has not been submitted before, in whole or in part, to this or any other university for any other degree.

Signed:_____Date: _____

Dedication

To my granny, inspiration and angel in heaven

Marie George Vlandis

(1937 – 2017)

Thank you for teaching me true love, kindness and joy.

Acknowledgments

"And whatever you do, whether in word or deed, do it all in the name of the Lord Jesus, giving thanks to God the Father through him." *Colossians 3:17*

I would like to first and foremost, thank my Lord and Saviour Jesus Christ who has brought me this far in my life and continues to support me in my journey. I am grateful for my Church, the Coptic Orthodox Church, for teaching me the true faith and showing me the unending love of our Lord.

I would also like to thank my parents, Sherif & Elvia, for their unlimited support and encouragement throughout my PhD and the past 25 years of my life. You have taught me so much about sacrifice, love and patience. I am sorry for all the difficult times I have put you through during my project and no matter what I do, I can never repay you for all your love. To my brother; Mina, thank you for being the best older brother. Thank you for supporting and motivating me. I hope I have made you all proud.

To my supervisor, Dr John Stephens, thank you so much for all your time, encouragement and support throughout the project. It has been wonderful getting to know you on a personal and professional level. Thank you for being a mentor and supervisor, but also thank you for being a friend. Also grateful for the Stephens group, John Walsh, Ross, Adam, Amanda, and Clara. Thank you all for your support and encouragement.

To my extended family; Gedo Roshdy and Teta Dalal, Gedo Wagih and Teta Marie, Teta Afaf, Uncle Atef, Aunt Rita, Shady, Katy, Uncle Paul, Aunt Daisy, Alex, Carol, Uncle Samir, Aunt Hanan, Michael, Mariam. Special thank you to Gedo Roshdy for inspiring me to enter into a career of chemistry. Thank you all so much for always being there for me and always encouraging me, especially when I needed it the most. Thank you for all your prayers and continued best wishes. I am so lucky to have such an amazing family and I hope we continue to grow in love and in Christ.

I would like to thank my best friend, father, and teacher; Bishop Antony. After receiving cancer more than 10 years ago, you still continue to serve every single day and never fail to inspire and teach me every time I see you. Thank you for your encouragement

and support since day one. Thank you for always smiling when the whole world seems sad. I wish one day I can do 1% of what you do.

To Father Rouies Anba Bishoy, somebody I can truly rely on and call a friend. Thank you for everything you do for us. We are so honoured and grateful for your presence among us. You are not just a teacher and a father to me, but also a friend that I can speak to about anything. Thank you for your continued prayers and unending love. I hope one day you can be cured of your diabetes and remember your son.

To my best friend and Dutch brother, Marco Boutrus, thank you for all the motivation, love and support you've given me. Life is so much better, crazier and more fun with people like you in my life. Sorry for all the hard times I've put you through and thank you for always listening to my endless rants. To my Irish best friend, Bishoy Abdou, brothers since we first met 17 years ago. Thank you for always having my back and understanding me. Your recent engagement in Paris to Solange was awesome. Asking me to be your witness was the icing on the cake for me. To my best friend, Bishoy Mesak, another person I consider a brother. Thank you for your all your help and support since day one. You're an amazing listener and a great friend. I am lucky and grateful to have you in my life and can't wait for many more years of crazy adventures.

To the amazing Sunday School class, St. Abanoub's Class, thank you all for your prayers and well wishes. The hug that I received from you all last Sunday meant a lot to me and serving you for the past few years has been awesome. I came to teach you all, but I ended up learning so much from you. Also, a huge thank you to the community of my Church, St Maximus & St Domadios Church, for all your prayers and well wishes. A true family and real love is always felt when seeing everybody there. Special thank you to Dr Adel for his daily prayers, and love and support to me over the many years.

Thank you to all my brothers and sisters of the Coptic Irish Youth, especially from Doxa. Special thank you to Michael Georgy, Pierre Metias, Marina (Zaki, Morcos, and Feekry), Sherry, Maria Farag, Rafik, and Abanoub Some. It's been great serving with all of you and going on many adventures. I can't wait for many more memories to be made. To the amazing newly formed Red Team; Michael, Edouard, Mena, and William. Thank you boys for your love and support. I can't wait to see what else we will do in this crazy and awesome friendship we have started. I am grateful for having you all in my life.

I would like to give a special thank you to His Holiness, Pope Tawadros II. Thank you for organising WYW 2018 and inviting me. It was a real pleasure getting to know you on a personal level and to go "back to the roots". However, I am most grateful for your strong encouragement to me about the PhD, the personal note you wrote to me, and especially the call two days before thesis submission. I pray that God continues to support you in leading our Church. To my second family, the youth of WYW 2018, thank you all so much. Meeting you all and going on the crazy adventures in August 2018 was exactly the motivation I needed to finish this project. You are all amazing and full of love, joy and kindness. I can't wait to continue meeting all of you throughout the world over the next few years.

Thank you to everyone in the Chemistry Department of Maynooth University. Special thank you to Harlei and Jessica for always being there for me and listening to my many rants. Thank you to Muhib, Sam, Xiang, Nan, Andrew, Luke, Chris, Barry, Justine, Grace, Mark G, Lucy, Anthony, and all the previous and current postgrads. Thank you to all the staff in the department for your continued help and care. Special thank you to Ria, Noel, Barbara, and all the technical staff, and the cleaning staff. Also thank you to Siobhan and Conor in Biology for all their help. Special thank you to Joanne for her kindess and amazing support. I will truly miss all of you.

I would like to thank everybody in the Admissions office in Maynooth University; John, Alice, Margaret, Fionnula, Barbara, Judith, Emer, Aoibheen, Kay, and Sheila, for their continuous encouragement. It's been an absolute pleasure working with you all and I hope we can meet again in the future. Also, thank you to everybody in the Conferring office and Exams office for all their support.

Finally, my PhD journey hasn't been easy. There haven't been many ups and downs. Difficult times where I thought I can't complete it, and harsh times when I thought circumstances were unfair. There have also been amazing times of great research, interesting findings, and innovative knowledge. But throughout all of it, the good and the bad, I have had endless support from all my family and friends mentioned above. I truly couldn't have completed it without them all and I am forever grateful.

Abstract

Diabetes is a worldwide condition that affects millions of people of all ages and backgrounds. It strikes the rich and the poor, old and young, healthy and sick. Diabetes is one of the largest global health emergencies of the 21st century, where some regions of the world have a much higher occurrence than others. Diabetes occurs when there are increased levels of glucose in the blood due to the lack of insulin, or the inability of the body's cells to respond to insulin. Type 2 diabetes accounts for approximately 90% of all cases of diabetes worldwide and continues to rise across all world regions.

The goal of our research was to investigate two families of heterocyclic compounds that have potential as anti-diabetic agents. We postulated that an anti-diabetic effect might be achieved through the inhibition of complex I of the electron transport chain, which would make oxidative phosphorylation less efficient, and therefore require increased glucose uptake from the blood in order to maintain ATP levels. This would consequently lower blood glucose levels and the inhibitor would thus have a hypoglycaemic effect.

Building on findings of previous members of our own research group and collaborators, we developed two families of compounds and evaluated them for their anti-diabetic biological activity. The first family investigated was the arylpiperazine family, which consisted of analogues of the hit compound RTC1. Here, structural variations were performed at five sites on RTC1. The second family explored was the pyrazolopyrimidinone bicycle family, which consisted of analogues of the hit compound RTC53. In this case, structural variations were carried out at two principle sites on RTC53. Hydrophobic, steric, and electronic effects were all explored for both families through the systematic structural modifications.

One of the aims of the project, in addition to access a large number of compounds, was to develop improved methods for the synthesis of both families. For the arylpiperazine family, a simpler and higher yielding procedure for their synthesis was achieved. This method no longer required anhydrous conditions or elaborate work-up procedures. For the pyrazolopyrimidinone bicycle family, method development focused on establishing a "one-pot" microwave-assisted synthesis of the pyrazolopyrimidinone bicycle. This

avoided the need to isolate and purify intermediates, and reduced total reaction times down to just over 2 hours.

Full characterisation of all compounds synthesised was carried out using techniques such as ^{1}H and ^{13}C NMR spectroscopy, including 2D-NMR experiments, X-ray crystal analysis, infrared spectroscopy, and high-resolution mass spectrometry.

A structure activity relationship study was performed by testing compounds from both families in (i) a whole cell, functional, glucose uptake assay and (ii) a complex I inhibition assay. The glucose uptake assay measured the amount of tritiated (^{3}H) deoxy-2-glucose taken up by C2C12 mouse muscle cells and quantified the fold change using a protein assay to determine the number of cells present. The complex I assay determined a compound's ability to inhibit NADH dehydrogenase, complex I of the electron transport chain, by measuring the change in ubiquinone absorbance. Using both these assays, we were able to establish active compounds, which had the potential of developing into anti-diabetic agents, and obtained a better understanding of the influence of structure on this anti-diabetic biological effect.

Chapter 1: Introduction

1.1 Diabetes

Diabetes Mellitus, more simply called diabetes, is a chronic condition that occurs when there are increased levels of glucose in the blood. Diabetes is a global worldwide issue. It kills and disables, strikes people at their most productive age, impoverishes families, and reduces the life expectancy of older people. Diabetes is a shared threat that does not respect borders or social class. No country is immune from diabetes and the epidemic is anticipated to continue. The burden of diabetes drains national healthcare budgets, reduces productivity, decreases economic growth, causes catastrophic expenditure for vulnerable households, and overwhelms healthcare systems.[1,2]

Diabetes is classed as a metabolism disorder. Metabolism refers to the way the body breaks down digested food into carbohydrates, fats, and proteins, which then makes its way into our bloodstream.[3] Glucose is a form of carbohydrate used by cells for energy and growth. However, cells cannot use glucose without insulin being present. Insulin is a hormone that is produced in the pancreas. It is an essential hormone as it plays a key role in the transport of glucose from the bloodstream into the body's cells where the glucose is converted into energy. The lack of insulin, or the inability of the cells to respond to insulin, leads to high levels of blood glucose, known as hyperglycaemia, causing diabetes.[1]

There are three main types of diabetes: type 1 diabetes, type 2 diabetes, and gestational diabetes. There are also some less common types of diabetes which include monogenic diabetes and secondary diabetes.[1] While type 1 and type 2 diabetes are caused by contributions of multiple genes and environmental factors, monogenic diabetes is the result of a single genetic mutation in an autosomal dominant gene. Neonatal diabetes mellitus and maturity-onset diabetes of the young (MODY) are examples of monogenic diabetes. Around 1-5% of all diabetes cases are due to monogenic diabetes.[4] Secondary diabetes arises as a complication of other diseases such as hormone disturbances, drugs, or diseases of the pancreas.[1]

Recent research has shown that diabetes has been increasing in patients with cystic fibrosis, occurring in 20 % of adolescents and up to 50 % of adults. Cystic fibrosis-related diabetes (CFRD) is a unique clinical entity but shares features of type 1 and type 2

diabetes. The complexity of management of CFRD is increased by other factors such as elevated energy expenditure, glucagon deficiency, and liver dysfunction.[5]

The most common symptoms of diabetes include fatigue, weight gain, cuts and bruises that do not heal, frequent urination, increased thirst and hunger, male sexual dysfunction, numbness and tingling in hands and feet. The risk of developing type 2 diabetes is elevated among those who are overweight, physically inactive, and have an unhealthy diet.[6]

Diabetic patients are typically advised to follow a healthy eating plan, perform adequate exercise and lose weight, take insulin regularly, and test their blood glucose levels regularly. Type 2 diabetics are also sometimes recommended to take oral medication to control their blood glucose levels.[6]

When diabetes is badly controlled, many complications can occur. These complications can affect the eye (glaucoma, cataracts, and diabetic retinopathy), leg/foot (ulcers), nerves (diabetic neuropathy), skin, heart, stomach (gastroparesis), and kidney (nephropathy). Complications from diabetes may also result in hypertension, hearing loss, gum disease, infections and stroke.[7,2,8] Acute complications can include diabetic ketoacidosis, hyperosmolar hyperglycaemic state, or death.[9]

In Ireland, recent research among children has shown that the risk of type 2 diabetes increases among obese children and adolescents. The extent of obesity has also been found to correlate with insulin resistance and occurrence of non-alcoholic steatohepatitis. Cardio-metabolic risk factors found in conjunction with obesity include impaired fasting glucose tolerance, impaired fasting blood glucose, as well as hypertension, low high-density lipoproteins, and high triglycerides.[10]

Prediabetes is a condition that normally develops into type 2 diabetes. It is diagnosed when blood glucose levels are higher than normal, but not high enough to merit a diabetes diagnosis. The cells in the body are gradually becoming resistant to insulin. Studies have indicated that even at the prediabetes stage, some damage to the circulatory system and the heart may have already occurred.[11]

1.1.1 Types of diabetes

As previously mentioned, there are several types of diabetes. However, there are three main types of diabetes: type 1 diabetes, type 2 diabetes, and gestational diabetes.

Type 1 diabetes tends to be diagnosed in childhood or early adult life, and always requires treatment with insulin injections. It is caused by the body's own immune system destroying the β-cells of the pancreas, whose function is to make insulin. As a result, the body produces none to very little insulin with a relative or absolute deficiency of insulin. The causes of this destructive process are not fully comprehended, but a combination of genetic susceptibility and environmental triggers have been suggested, such as viral infection, toxins or some dietary factors. People with type 1 diabetes need daily insulin injections in order to maintain a glucose level in the proper range.[1,12]

Type 2 diabetes usually develops slowly in adulthood and is commonly caused by excessive body weight and insufficient exercise. It begins with insulin resistance, where cells fail to respond to insulin properly, and may develop into a lack of insulin as the disease advances. It is progressive and can sometimes be treated with diet and exercise, but more frequently type 2 diabetes may require anti-diabetic medicine and/or insulin injections.[6,13]

Gestational diabetes is the third main form of diabetes, and occurs when women have very high levels of glucose in their blood during their pregnancy. In such a case, their bodies are unable to produce enough insulin to transport sufficient levels of glucose into their cells, resulting in progressively increasing levels of blood glucose. This is a result of the action of insulin being diminished (insulin resistance) due to hormone production by the placenta. Risk factors for gestational diabetes include older age, overweight or obesity, or a family history of diabetes. The majority of gestational diabetes patients can control their diabetes with exercise and diet.[14]

1.1.2 Diabetes prevalence globally

Diabetes is one of the largest global health emergencies of the 21st century. It is among the top ten causes of death globally and together with the other three major non-communicable diseases (NCDs) (cardiovascular disease, cancer, and respiratory disease) accounts for over 80% of all premature NCD deaths. A major contributor to the challenge of diabetes is that 80% of people with diabetes are undiagnosed.[15]

The occurrence of diabetes is increasing worldwide, but there is huge variation by country with some regions of the world having much higher occurrence than others (Figure 1). The reasons for this are unclear but an interplay between genetic and environmental factors is suspected.[1]
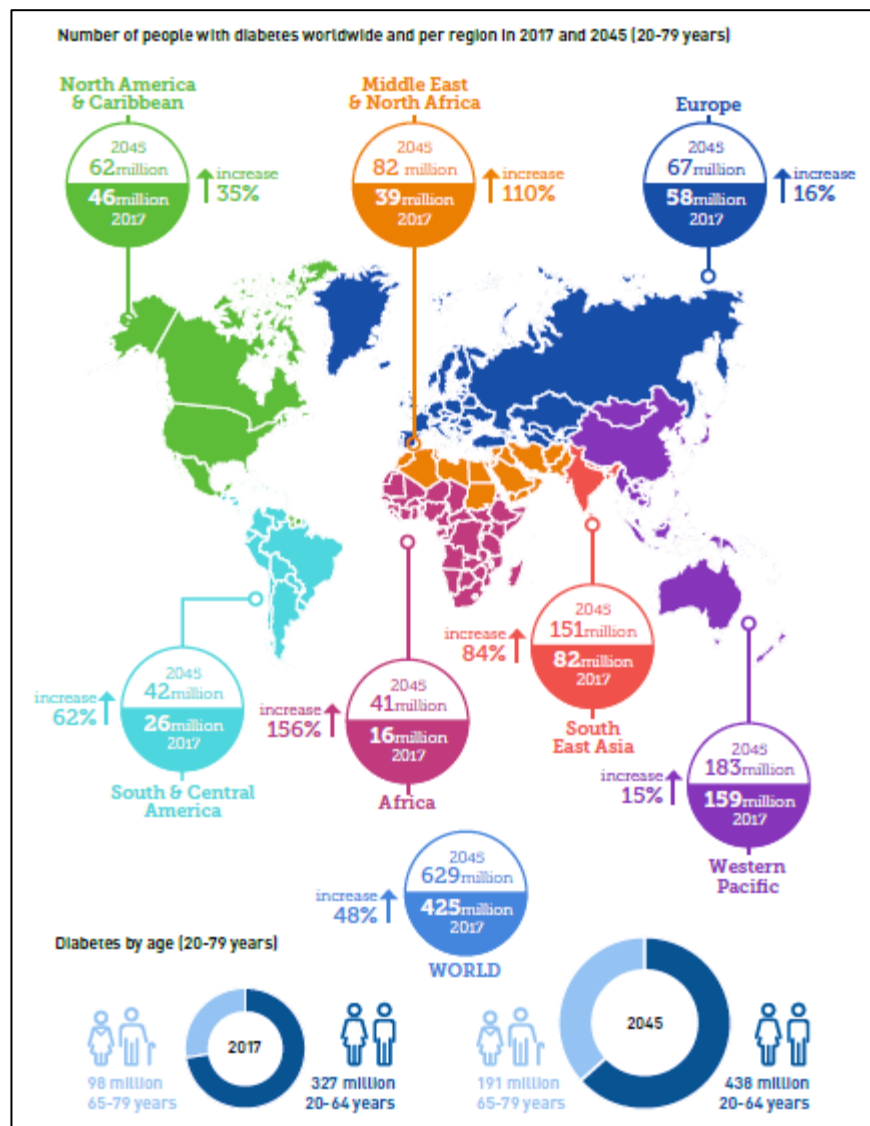
Figure 1: Number of people with diabetes worldwide and per region in 2017 and 2045 (20-79 years) (International Diabetes Federation – 8th Edition 2017).[1]

About 425 million people worldwide, or 8.8% of adults aged 20-79 years old, are estimated to have diabetes. From those, an estimated 79% live in low and middle income countries. If these trends continue, by 2045, 629 million people aged 20-79 years old are expected to have diabetes. The largest increases will take place in regions where economies are moving from low income to middle income levels.[1]

In high income countries, an estimated 10% of all diabetes cases are type 1 diabetes. In total, over one million of children and adolescents below 20 years of age are estimated to have type 1 diabetes globally. The United States, India, and Brazil have the largest incidence and prevalence of children with type 1 diabetes under 15 years old.[1]

Type 2 diabetes accounts for approximately 90% of all cases of diabetes worldwide and continues to rise across all world regions. This rise is likely fuelled by an aging population, economic development and increasing urbanisation, leading to more sedentary lifestyles and greater consumption of unhealthy foods linked with obesity.[16,17]

The International Diabetes Federation (IDF) 2017 (8th edition) showed that in 2017, China had the most number of people with diabetes aged 20-79 years old with 114.4 million people. Whereas by 2045, it is expected that India will have the most number of people for that age group with 134.3 million people. Other countries among the top ten in the world for the prevalence of diabetes included the United States of America, Indonesia, Brazil, and Egypt. This report also showed that the prevalence of diabetes for women aged 20-79 years old is estimated to be 203.9 million, which is slightly lower than among men, with 221.0 million. However, it has been estimated that approximately 212.4 million people (50%) of that age group are undiagnosed.[1]

It is estimated by the IDF that for 21.3 million (16.2%) live births in 2017, the mother had some form of hyperglycaemia in pregnancy. An estimated 86.4% of those cases were due to gestational diabetes, 6.2% due to diabetes detected prior to pregnancy, and 7.4% due to other types of diabetes first detected in pregnancy.[1]

The IDF also stated how diabetes shows high prevalence in people older than 65 years old. In 2017, it was estimated that 122.8 million people (18.8%) aged 65-99 years old were living with diabetes. If the trends continue, this number is expected to become 253.4 million people by the year 2045. The number of deaths due to diabetes from age

65 years and above currently stands at 3.2 million, which counts for more than 60% of all deaths attributable to diabetes among adults in total.[1]

As mentioned before, diabetes kills. According to the IDF, diabetes accounts for 10.7% of global all-cause mortality among people in the age of 20-79 years old. In 2017 alone, approximately 4 million people of this age group are estimated to have died from diabetes. This is higher than the combined number of deaths from infectious diseases, such as HIV, tuberculosis, and malaria. The continent which resulted in most deaths from diabetes before the age of 60 was Africa with 77% proportion of the deaths according to diabetes.[1]

According to the IDF, in 2017, Ireland had an estimate of 141,500 people aged 20-79 years old suffering from diabetes (prevalence of 4.3% of the population). Among those, an estimated 50,600 people (34%) are undiagnosed. People with type 1 diabetes account for approximately 15,000 people (11%) of the total diabetes population. It is estimated that there are over 15,600 people over 80 years of age living with type 2 diabetes. Ireland was ranked ninth in the top ten countries for the incidence rates of type 1 diabetes under 20 years of age in 2017, with 24,300 people.[1]

1.1.3 Cost of diabetes

The economic burden of diabetes on the Irish health care system is becoming a major challenge for the government and the Health Service Executive (HSE). The CODEIRE study published in 2006 was an international accredited study and examined the cost of treating type 2 diabetes in Ireland during Nov-Dec 1999.[18] This study suggested that 10% of the national health budget was being consumed treating diabetes alone. Of the overall cost, 50% was spent on hospitalization for complications and wages; 42% on drug costs; and 8% on ambulatory care and attending non-diabetes specialists for diabetes-related complications.[18] Globally, according to the IDF, diabetes results in $727 billion US dollars being spent annually by people with diabetes on healthcare alone, which corresponds to one of every eight dollars spent on healthcare.[1]

1.1.4 Treatments for diabetes

The first-line therapy for diabetes is diet and exercise plus hypoglycaemic drugs, as recommended by the American Diabetes Association (ADA) and European Association for the Study of Diabetes (EASD).[19] Regular monitoring of blood glucose levels for diabetic patients is essential, especially those who are overweight and obese. In order to save lives and prevent devastating complications resulting from diabetes, the IDF has suggested early detection, diagnosis and cost-effective treatment of diabetes.[1,19]

When inadequate glycaemic control prevails, pharmaceutical intervention in the form of an anti-diabetic oral agent is needed. There are currently seven distinct classes of hypoglycaemic agents with different mechanisms of action, adverse effect profiles, and toxicities. They are sulfonylureas, biguanides, meglitinides, thiazolidinediones, α-glucosidase inhibitors, incretin mimetics, and dipeptidyl peptidase IV (DPP-IV) inhibitors.[19,20,21]

1.1.4.1 Sulfonylureas

Sulfonylureas consist of first generation sulfonylureas (acetohexamide, chlorpropamide, tolbutamide and tolazamide), which are no longer in use due to undesirable cardiovascular effects, and second generation sulfonylureas (glipizide, gliclazide (Figure 2), glibenclamide, glimepiride) which are widely used worldwide. Sulfonylureas are used to enhance insulin secretion and improve insulin activity. They stimulate insulin release from the pancreatic β-cells, displaying a more pronounced action in the presence of glucose. They do so by inhibiting an adenosine triphosphate-dependent potassium channel that results in cell membrane depolarization.[22] This leads to calcium influx and release of stored insulin from secretory granules within the cell. The net outcome is increased responsiveness of β-cells to both glucose and non-glucose secretagogues, resulting in more insulin being released at all blood glucose concentrations.[19,21]
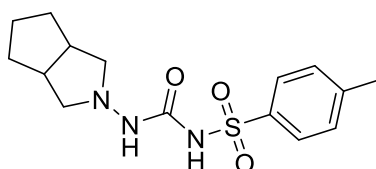
Figure 2: Structure of gliclazide.

The second generation sulfonylureas have a potency that allows them to be given in much lower doses than the first generation sulfonylureas. Due to the mechanism of action of sulfonylureas, studies have suggested concern with respect to patients with acute myocardial infarction (heart attack).[19] Sulfonylureas can be used as monotherapy, or in combination with insulin or other oral hypoglycaemic drugs. Sulfonylurea compounds have several adverse side-effects such as hypoglycaemia and hyponatraemia, or less severe side-effects such as headaches, dizziness, and gastrointestinal issues. Sulfonylureas are not suggested as first choice for obese patients as they have been associated with weight gain.[19,20,22,23] Sulfonylureas are also not recommended for patients with renal failure or high cardiovascular risk.[24]

1.1.4.2 Biguanides

Biguanides are a class of anti-hyperglycaemic agents that have been used in the control and treatment of type 2 diabetes for many years. They work by reducing hepatic glucose output and enhancing insulin sensitivity in hepatic and peripheral tissues. Originally three biguanides were used: metformin, phenformin and buformin. However metformin is the only drug of this class still administered to patients today as it does not cause lactic acidosis, unlike phenformin and buformin.[19]

1.1.4.2.1 Metformin

Metformin (Figure 3) is indicated either as a monotherapy or in combination with a sulfonylurea. Sulfonylureas and metformin cause a similar decrease in fasting blood glucose levels in diabetic patients. However, unlike sulfonylureas, metformin does not cause weight gain and does not directly stimulate insulin secretion. Its major effects are to increase insulin-mediated glucose utilization in peripheral tissues (such as muscle and liver), improve insulin action, and to decrease hepatic glucose output. It also reduces substrate availability for gluconeogenesis as it has an anti-lipolytic effect that lowers serum free fatty acid concentrations.[25] Furthermore, it decreases insulin resistance, which is often a problem in patients with type 2 diabetes, by increasing insulin sensitivity. Importantly, it is an anti-hyperglycaemic agent and not a hypoglycaemic agent, as are the sulfonylureas, as it decreases the blood glucose level of diabetic patients but not that of non-diabetic patients.[19,20]
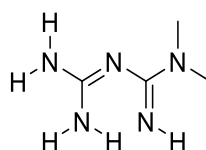
Figure 3: Structure of metformin.

Metformin undergoes almost no hepatic metabolism and is 90-100% excreted by the kidneys. Metformin has therefore proved effective and safe. It has been used in Europe for over thirty years, and in the United States for over twenty years. Metformin is commonly prescribed to type 2 diabetic patients, unless contraindicated.[19,20]

Although the exact mechanism by which metformin exerts its anti-diabetic effect in the body is not fully known, it has been found to activate adenosine monophosphate-activated protein kinase (AMPK). AMPK is a heterotrimeric protein complex that is involved in cellular energy homeostasis where it regulates energy levels by monitoring the amounts of adenosine triphosphate (ATP) and adenosine monophosphate (AMP). AMPK also regulates lipid and glucose metabolism. Activation of AMPK by small molecules such as metformin has shown to reduce hepatic gluconeogenesis and to stimulate the uptake of glucose by skeletal muscles. A commonly proposed mechanism for the metformin induced activation of AMPK is the inhibition of mitochondrial respiration by acting at complex I of the electron transport chain.[26,27]

Recently, metformin was found to lower the increase in enzyme activity exhibited by the pancreatic mitochondrial complex I, in both type 1 and type 2 diabetes, in response to nicotinamide adenine dinucleotide (NAD^+) versus NADH (reduced form) redox imbalance, as well as NADH overload of complex I.[28] Recent research has also shown that metformin does not produce the mitochondrial damage observed with more hydrophobic guanide-containing drugs. Instead, it was found to inhibit the mitochondria by a distinctive mechanism resulting in oxidation of the NADH/NAD^+ couple. It inhibits the energy transduction by selectively suppressing efficient coupling of the redox and proton transfer domains of complex I. In addition, unlike other biguanides, metformin does not exhibit any toxic properties nor induce lactic acidosis, but it does suppress weight gain.[29]

Metformin is available as tablet and liquid formulations. Metformin tablet formulations are either immediate release or extended release. The most common side-effects of metformin are gastrointestinal, including diarrhoea, nausea, and mild anorexia. These effects are usually mild and brief. They can be managed by dose reduction or discontinuation of the drug.[19] The use of metformin in the elderly has been associated with adverse events such as hyporexia, gastrointestinal intolerance, dysgeusia, and vitamin B12 deficiency.[24] Metformin extended release causes fewer gastrointestinal side-effects than metformin IR.[30]

Metformin cannot be administered to patients who have certain conditions such as acute heart failure, tissue hypoxia, respiratory failure, hepatic impairment, or a risk of

functional renal failure. The usefulness of metformin has been found to be highly limited in patients with anorexia and low weight. Five percent of patients who use metformin have been found to discontinue using it due to poor gastrointestinal tolerance. This rate has been reported to be higher in elderly patients.[24]

Metformin is commonly prescribed for women with gestational diabetes as it is associated with lower gestational weight gain, displays a reduced risk of hypoglycaemia, and shows no compromise of the motor and linguistic development. Despite all these benefits however, up to half of the women with gestational diabetes require insulin supplementation, as adequate glycaemic control is not achieved with metformin alone.[31]

1.1.4.3 Meglitinides

The meglitinides (repaglinide (Figure 4) and nateglinide) are short-acting glucose-lowering drugs for treatment of patients with type 2 diabetes, where they can be used alone or in combination with metformin. They were designed to achieve more physiologic insulin release and less risk for hypoglycaemia. Their mechanism of action closely resembles that of sulfonylureas. They also act by regulating ATP-dependent potassium channels in pancreatic β-cells, which leads to depolarization of cell membrane, opening of calcium channels, and consequently releasing insulin. However, they are structurally different than sulfonylureas and they stimulate the release of insulin from the pancreatic β-cells through a different binding site than the "sulfonylurea receptor". Meglitinides also have a shorter onset and duration of action compared with sulfonylureas, due to their weaker binding affinity and faster dissociation.[19,21]
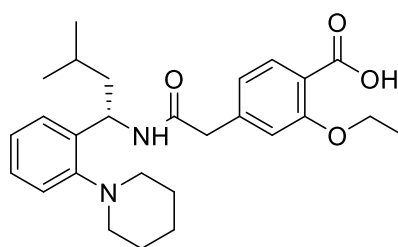
Figure 4: Structure of repaglinide.

Nateglinide is hepatically metabolized, with renal excretion of active metabolites. Repaglinide is the drug of choice in patients with impaired renal function as it is principally metabolized by the liver. Hypoglycaemia is the most common side effect associated with meglitinides.[19,21,24]

1.1.4.4 Thiazolidinediones

Thiazolidinediones (pioglitazone (Figure 5)) are another class of drugs for type 2 diabetes which act by increasing peripheral insulin sensitivity. Thiazolidinediones provide longer-lasting glycaemic control than sulfonylureas and metformin.[24] They improve glycaemia by reducing insulin resistance and preserving pancreatic β-cell function with a different mechanism of action than biguanides. They act mainly by improving peripheral uptake and utilization of glucose in muscle and fat, to decrease liver glucose production.[19,21]
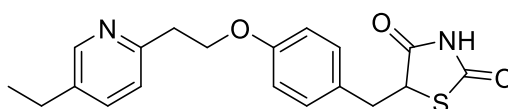
Figure 5: Structure of pioglitazone.

Pioglitazone does not produce hypoglycaemia and acts favourably on the lipid profile. The drug has also been shown to histologically improve non-alcoholic steatohepatitis in patients with prediabetes. However, pioglitazone has various adverse effects that limit its use in the elderly, such as weight gain, dilutional anaemia, salt and fluid retention, increased risk of fractures, and increased risk of heart failure.[24]

Thiazolidinediones are among the most expensive oral agents and therefore are not generally indicated over metformin for initial therapy of type 2 diabetes. Thiazolidinediones have been reported to have anti-inflammatory, anti-thrombotic, and anti-atherogenic properties. However, thiazolidinediones have also been found to cause severe side-effects. They were reported to increase the risk of heart attack in many patients. They cause weight gain due in part by fluid retention, but also from the proliferation of new adipocytes. They also have an effect on bone metabolism through the activation of peroxisome proliferator-activated receptor (PPAR), so a relationship between their assumption and an increased risk of fractures has been suggested.[19,21]

1.1.4.5 α-Glucosidase inhibitors

α-Glucosidase inhibitors (acarbose and miglitol (Figure 6)) act on the α-glucosidase enzyme which is found in brush border cells of the small intestine and cleaves more complex carbohydrates into simpler sugars. α-Glucosidase inhibitors prevent the breakdown and absorption of carbohydrates. The largest impact of α-glucosidase inhibitors is on postprandial hyperglycaemia and on fasting plasma glucose (FPG) levels.[19,21]
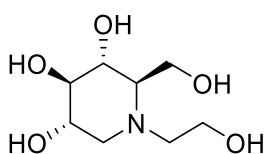
Figure 6: Structure of miglitol.

The main side-effects of α-glucosidase inhibitors are abdominal discomfort, flatulence, bloating, and diarrhoea. Although hypoglycaemia is not typically associated with monotherapy with α-glucosidase inhibitors, it can occur in combination with other drugs.[19] Although α-glucosidase inhibitors can be potentially useful for some elderly diabetic patients, their use can be limited by their low efficacy and high rate of adverse gastrointestinal effects both in monotherapy and especially in combination with metformin.[24]

1.1.4.6 Incretin mimetics

Incretins are enteroendocrine hormones released into bloodstream from L and K cells dispersed throughout the gastrointestinal tract. Examples of incretins are Glucagon Like Peptide-1 (GLP-1) and Glucose Dependent Insulinotropic Polypeptide (GIP). GLP-1 is secreted in response to nutrients and its levels are decreased in type 2 diabetes. It acts by stimulating glucose-dependent insulin release from the pancreatic islets and therefore prevents hypoglycaemia, which is the major advantage over sulfonylureas. It also slows gastric emptying, inhibits inappropriate post-meal glucagon release, and reduces food intake.[19,21,32]

Therapy with GLP-1 and its analogues is associated with weight loss, owing in part to the effects of GLP-1 on slowed gastric emptying and its well-recognized side-effects of nausea and vomiting.[19] GLP-1 analogue therapy has also been shown recently to decrease proinflammatory macrophages and reduce inflammation in type 2 diabetes.[33] GLP-1 can also regulate invariant natural killer T (iNKT) cells, which are a rare subset of innate T cells involved in the regulation of macrophage and adipose tissue biology.[32,34]

GLP-1 exhibits a short half-life of 1-2 minutes due to N-terminal degradation by the enzyme DPP-IV. Research has focused on analogues of GLP-1 (incretin mimetics) that are resistant to DPP-IV degradation, and on agents that increase GLP-1 via inhibition of DPP-IV. Experimental studies have suggested that GLP-1 stimulate proliferation of developed β-cells and inhibits β-cell apoptosis, suggesting a potential role of incretin-mimetics *in vivo* in limiting β-cells dysfunction, which typically occurs in people with type 2 diabetes.[19,21]

1.1.4.6.1 Exenatide

Exenatide is a 39-amino acid peptide incretin mimetic that exhibits glucose regulatory activities like those observed with human GLP-1 but with increased resistance to deactivation by DPP-IV. Exenatide binds to the GLP-1 receptor, stimulates glucose-dependent insulin secretion, reduces gastric emptying, suppresses glucagon secretion, and lowers food intake. More interestingly, exenatide appears to have beneficial effects on β-cell function as it normalizes the loss of first-phase insulin secretion as well as

hypersecretion of glucagon from α-cells, thereby lowering hepatic glucose production in the postprandial state.[19,21]

Commonly reported adverse effects of exenatide are nausea, diarrhoea, weight loss and vomiting. Hypoglycaemic events are mainly observed when combinations are used, such as with sulfonylureas and thiazolidinediones, but not when with metformin.[19]

1.1.4.7 Dipeptidyl peptidase-IV inhibitors

Dipeptidyl peptidase IV (DPP-IV) is a 110 kDa plasma membrane-spanning cell surface glycoprotein ectopeptidase. It is ubiquitously expressed in tissues such as liver, kidney, lung, lymphocytes, and endothelial cells. As previously discussed, DPP-IV rapidly degrades and inactivates GLP-1, GIP, and other peptides *in vivo* via cleavage of the N-terminal amino acids. Inhibition of DPP-IV therefore leads to an increase in circulating endogenous GLP-1 and GIP levels. DPP-IV inhibitors are therefore not incretin mimetics, but incretin enhancers. DPP-IV inhibitors can be administered orally, unlike other GLP-1 based therapies.[19,21]
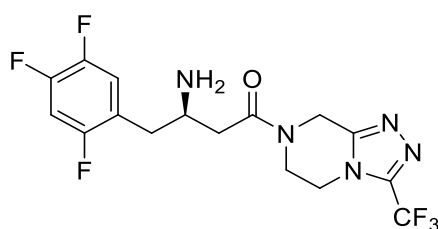
Figure 7: Structure of sitagliptin.

DPP-IV inhibitors (sitagliptin (Figure 7), vildagliptin and saxagliptin) can be used as a second agent if a single agent, such as a sulfonylurea, metformin or a thiazolidinedione, does not provide enough of a response. They can also be used as a third agent when dual therapy with metformin and a sulfonylurea does not provide adequate glycaemic control. These oral drugs are well tolerated, safe, and effective in the short and long term, in elderly and young diabetic patients. They have no effect on gastric emptying, do not induce reduced central intake, and do not cause gastrointestinal intolerance or weight loss.[24]

DPP-IV inhibitors mimic the therapeutic effects of incretin mimetics including inhibition of glucagon secretion, stimulation of insulin secretion, and inhibition of apoptosis. These drugs are weight neutral and have a low potential for hypoglycaemia when used as monotherapy. One safety concern involves the potential of DPP-IV inhibitors to interfere with immune functions causing infections and headaches. Other adverse effects occurring with sitagliptin include osteoarthritis, back pain, and extremities pain.[19]

1.2 ATP Production

Glucose in the blood acts as the main source of energy for our bodies. A major part of the use of the energy from glucose oxidation is the conversion of adenosine diphosphate (ADP) to adenosine triphosphate (ATP), which can be further used as the energy currency of the cell. ATP is produced in a process known as cellular respiration (Figure 8), which is a cumulative process that consists of glycolysis, Krebs' cycle, and oxidative phosphorylation.[35]
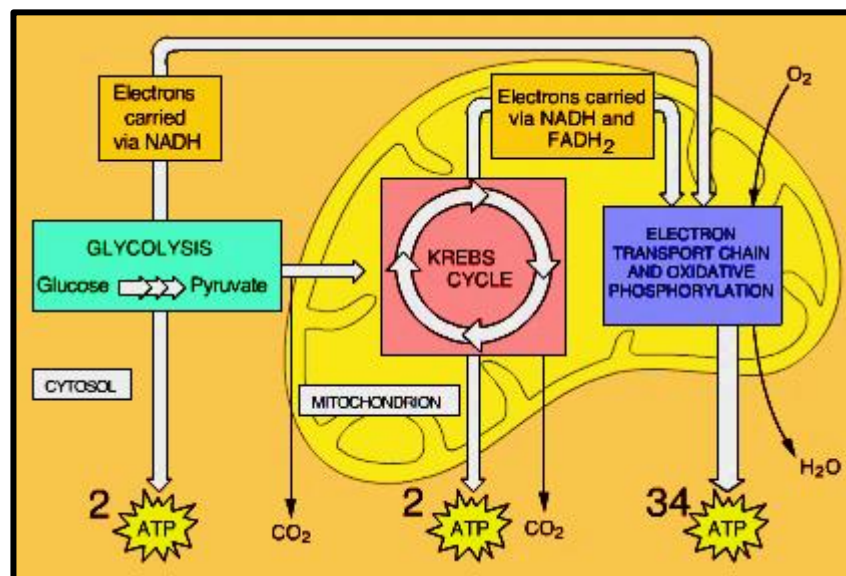
Figure 8: Overview of Cellular Respiration (Campbell's Biology, 5th Edition).

In eukaryotic cells, glycolysis takes place in the cytosol, whereas the Krebs' cycle and oxidative phosphorylation occur within the mitochondrion. In prokaryotic cells, these reactions take place in the cytoplasm. Glycolysis and the Krebs' cycle catabolically break down glucose and other organic substances. Redox reactions are key processes of both glycolysis and the Krebs' cycle.[35]

Glycolysis is the process where glucose is converted into smaller molecules through many chemical transformations. It occurs in two phases, known as the energy investment phase and the energy pay-off phase. It produces two molecules of ATP, two molecules of pyruvate and two electron-carrying molecules of NADH.[35]

The Krebs' cycle (also known as the citric acid cycle) oxidizes a pyruvate derivative to acetyl Coenzyme A and carbon dioxide. Through a series of intermediate steps, NAD^+

22

and flavin adenine dinucleotide (FAD), are produced along with two ATP molecules. NAD^+ and FAD molecules are capable of storing hydride electrons and are reduced in the process. The reduced forms, NADH and $FADH_2$, carry the hydride electrons to the next stage; oxidative phosphorylation (Figure 9).[35]
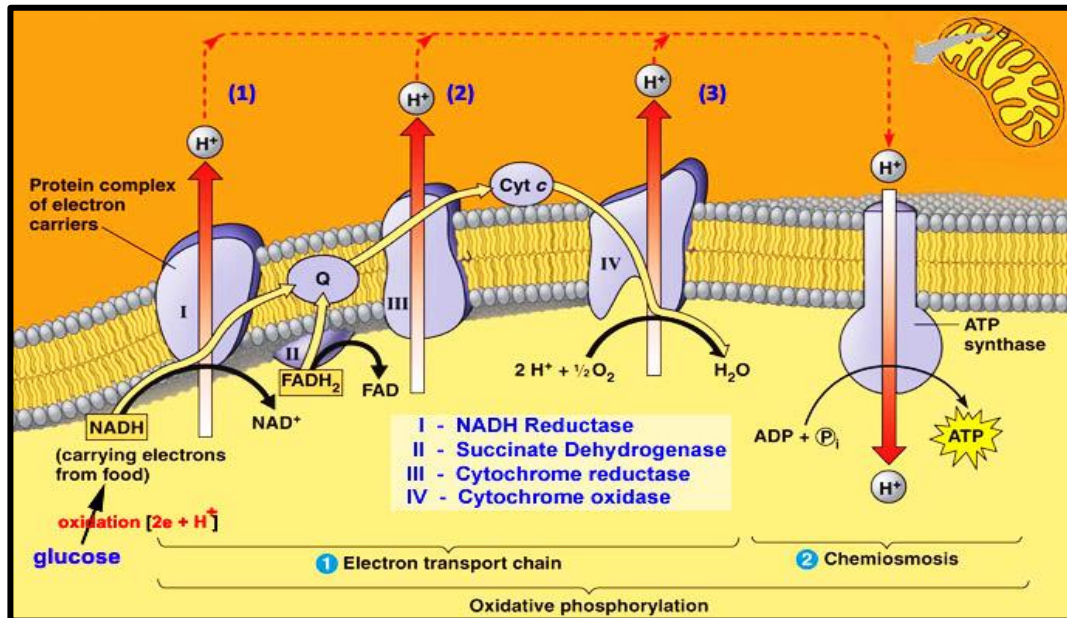
Figure 9: Oxidative Phosphorylation (Campbell Biology 7th Edition).

During the oxidative phosphorylation step, NADH and $FADH_2$ unload their electrons in the electron transport chain (ETC) and return to their original forms, NAD^+ and FAD. The electrons then move across the ETC to release energy. The major function of the ETC is to establish a proton gradient. The ETC ends when oxygen accepts the electrons and bonds with protons, forming water. The protons produced in the proton gradient return to the matrix via an enzyme called ATP synthase, which synthesises ATP in a process known as chemiosmosis. ATP synthase is an integral protein consisting of several different subunits. This protein is directly responsible for the production of ATP via chemiosmotic phosphorylation. It uses the proton gradient created by several of the other carriers in the ETC to drive a mechanical rotor, whose energy is then used to phosphorylate ADP to ATP. This couples the redox reactions of the ETC to ATP synthesis. Prokaryotic cells may yield a maximum of 38 ATP molecules, while eukaryotic cells may have a net yield of 36 ATP molecules.[35,36]

1.2.1 The Electron Transport Chain (ETC)

The ETC consists of a series of proteins, which exist in multi-protein complexes numbered I-IV. Tightly bound to these proteins are prosthetic groups, which are non-protein components essential for the catalytic functions of certain enzymes. In eukaryotes, the ETC components are found in the inner mitochondrial membrane. In prokaryotes, the ETC components are found in the plasma membrane.[35]

The ETC is an energy converter that uses the exergonic flow of electrons from NADH and FADH$_2$ to pump protons across the membrane. Electron carriers alternate between reduced and oxidized states as they accept and donate electrons. Each component of the chain reduces when it accepts electrons from its uphill neighbour and oxidizes when it passes electrons to its downhill neighbour. There are four complexes in the ETC, which are complex I (NADH reductase), complex II (succinate dehydrogenase), complex III (cytochrome reductase) and complex IV (cytochrome oxidase).[35,36]

Complex I, also known as NADH-ubiquinone oxidoreductase, or simply as NADH reductase, is an important protein that receives electrons in the form of hydride ions from NADH and passes them on to ubiquinone (Q). Complex II, also known as succinate dehydrogenase, is a peripheral protein that receives electrons from succinate (an intermediate metabolite of the Krebs' cycle) to yield fumarate and FADH$_2$. Electrons are received from succinate by FAD, which then becomes FADH$_2$. The electrons then pass onto ubiquinone.[36]

Ubiquinone is a small hydrophobic molecule which resides within the membrane and is the only member of the electron transport chain that is not a protein. It receives electrons from complex I and complex II, becomes the reduced form, ubiquinol, and passes its electron off to complex III. Complex III, also known as cytochrome reductase, is a vital protein that receives electrons from ubiquinol and passes them on to complex IV. Complex IV, also known as cytochrome c oxidase, is an essential protein that receives electrons from complex III and transfers them to oxygen, producing water within the mitochondria matrix. Cytochrome c is found within the intermembrane space but only transfers electrons from complex III to complex IV.[36,37]

The driving force of the ETC is the fact that each electron carrier has a higher standard reduction potential than the one that it accepts electrons from. Standard reduction potential is a measure of the ability to accept or donate electrons. Oxygen has the highest standard reduction potential which means that it is most likely to accept electrons from other carriers. That is precisely why it is found at the end of the ETC.[37]

1.2.1.1 Complex I of the ETC

Complex I of the ETC, also known as NADH reductase, is an essential protein that receives electrons in the form of hydride ions from NADH and passes them on to flavoprotein, then to an iron-sulphur (FeS) protein, and then onto ubiquinone (Q) (Figure 10). Flavoprotein has a prosthetic group attached called flavin mononucleotide (FMN).[38]
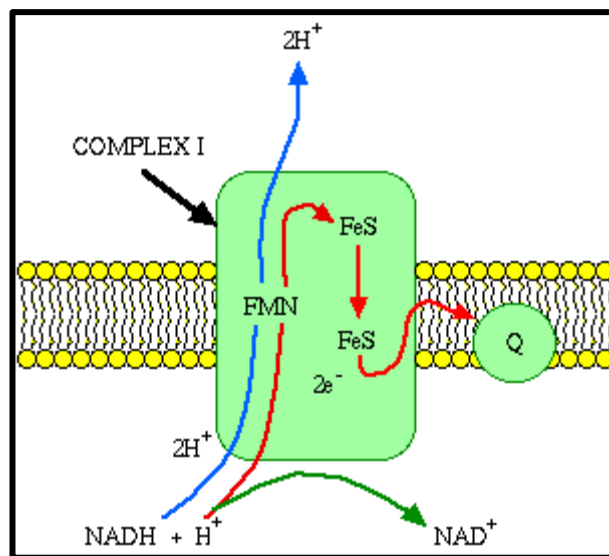
Figure 10: Simplified structure of complex I of the ETC.[38]

Electrons enter the ETC via complex I or complex II, as mentioned before. Electrons pass from complex I to ubiquinone (Q), which is embedded by itself in the membrane. From ubiquinone, electrons are then passed to complex III, which is associated with another proton translocation event. The path of electrons is therefore from complex I to ubiquinone to complex III.

Complex II is a separate starting point and is not a part of the NADH pathway. From succinate, the sequence is complex II (by-passing complex I) to ubiquinone to complex III to cytochrome c to complex IV. Thus there is a common electron transport pathway beyond the entry point, i.e. beyond either complex I or complex II.[38]

Complex I is one of the largest known membrane proteins. This mitochondrial enzyme consists of about 44 different subunits, divided into 30 accessory subunits and 14 core subunits. The 30 accessory subunits are thought to form a protective shell around the core, although some may have a specialized functional role. The simpler prokaryotic version of complex I normally comprises of just the 14 core subunits, highly conserved

from bacteria to humans, suggesting that the mechanism also conserves. Both enzymes contain equivalent redox components and have a similar L-shaped structure, formed by the hydrophilic and membrane domains.[39]

The structure of an entire, intact complex I was published for the first time by Sazanov et al. in 2013 (Figure 11).[40] They reported that the structure of the 536-kDa complex, from Thermus thermophiles, comprises 14 different subunits, with a total of 64 transmembrane helices and nine iron–sulphur clusters.[40]
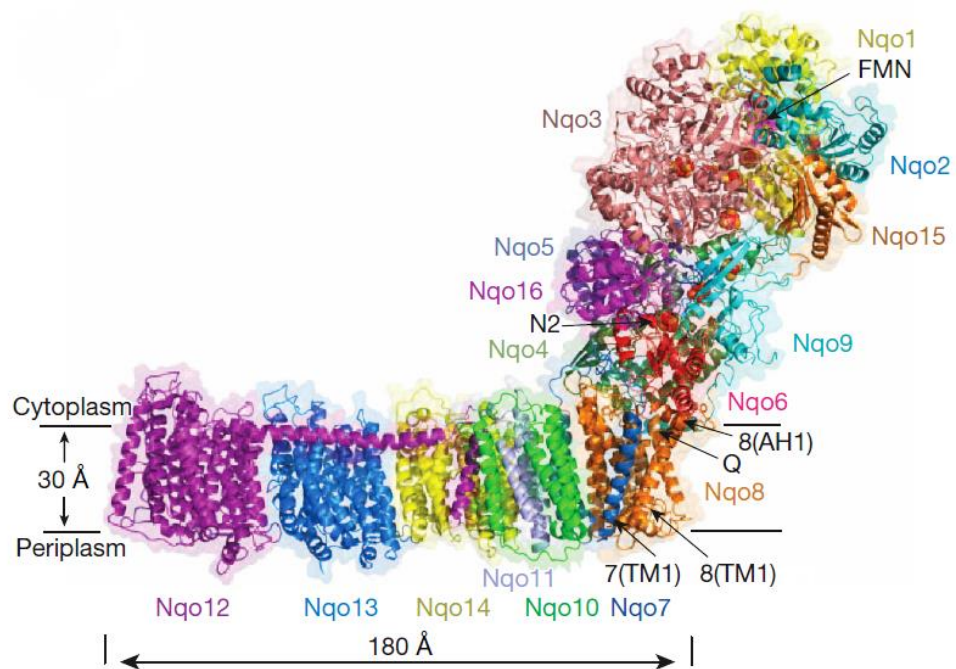
Figure 11: Structure of the entire complex I from T. thermophilus. FMN and Fe–S clusters shown as magenta and red–orange spheres, respectively, with cluster N2 labelled.[40]

They found that the core fold of subunit Nqo8 (ND1 in humans) was unexpectedly similar to a half-channel of the antiporter-like subunits. Small subunits nearby form a linked second half-channel, which completes the fourth proton-translocation pathway. They also reported that the ubiquinone-binding site was unusually "long, narrow and enclosed" and that the quinone head group binds at the deep end of this chamber, near iron–sulphur cluster N2.[40] The iron–sulphur cluster participates in the oxidative half reaction by accepting an electron from FAD, which is in a reduced state because it participates in the reductive half reaction with the substrate.[41] The chamber links to the

fourth channel by a "funnel" of charged residues. The link continues over the entire membrane domain as a flexible central axis of charged and polar residues, and probably has "a leading role in the propagation of conformational changes, aided by coupling elements". This structure suggested that a unique, out-of-the-membrane quinone-reaction chamber enables the redox energy to drive concerted long-range conformational changes in the four antiporter-like domains, resulting in translocation of four protons per cycle.[40]

The primary electron acceptor, FMN, is within electron transfer distance of cluster N3, leading to the main redox pathway, and of the distal cluster N1a, which is a possible antioxidant. The terminal cluster N2 coordinates, uniquely, by two consecutive cysteines. The novel subunit Nqo15 has a similar fold to the mitochondrial iron chaperone frataxin, and it may be involved in iron-sulphur cluster regeneration in the complex.[39]

In literature, research focused on complex I and its inhibition has mainly focused on two binding sites: the NADH binding site and the ubiquinone binding site. Some of the inhibitors currently targeting complex I such as rotenone, piericidin and pyridaben are considered to bind at the ubiquinone binding site.[42,43] It has been found that hydrophobic inhibitors like rotenone or piericidin most likely disrupt the electron transfer between the terminal FeS cluster N2 and ubiquinone. Some of the common complex I inhibitors, e.g. rotenone and metformin, have some unwanted side-effects, such as hepatotoxicity.[42]

Previous work by the Stephens group established the inhibition of complex I as a possible method of targeting diabetes, leading to AMP-activated protein kinase activation and subsequent increased glucose uptake by the cells, as measured in the mouse C2C12 muscle cell line. They also discovered that inhibiting complex I does not shut down the ETC, nor affects the ADP: ATP ratio. Instead, the cell maintains its levels of ATP production, perhaps via increased levels of succinate which is the alternative route for the electron entry. In order to generate sufficient levels of succinate, the cell increases its uptake of glucose (via Glut4) and hence lowers blood glucose levels.[44] Recent research involving restoring the NADH/NAD$^+$ redox balance and attenuating oxidative stress has proven that complex I could be a promising therapeutic target for

diabetes.[28] Building on this work, the aim of this project was to synthesise compounds which could increase glucose uptake by inhibiting complex I and therefore act as potential anti-diabetic agents.

1.3   Discovery of hit compounds

Previous work in this project involved computational techniques and biological assays in order to determine the hit compounds with potential as anti-diabetic agents.[45]

The initial biological mechanism targeted was the inhibition of a protein-protein interaction between retinol binding protein 4 (RBP4) and transthyretin (TTR).

The retinol transporter, RBP4, has been shown to have the potential to be used as a target for the control and treatment of type 2 diabetes. RBP4 has been reported to have a possible involvement in preventing cellular responses to insulin, generating insulin resistance and the development of type 2 diabetes.[46,47]

RBP4 is a member of the lipocalin family of proteins which are extracellular proteins that bind small, typically hydrophobic molecules, such as retinoids and steroids. RBP4 is composed of an N-terminal coil, eight anti-parallel β-strands, which form a β-barrel, and a short α-helix near the C-terminus. There are four highly variable loops that connect the β-strands A and B, C and D, E and F, and G and H (Figure 12).[46]
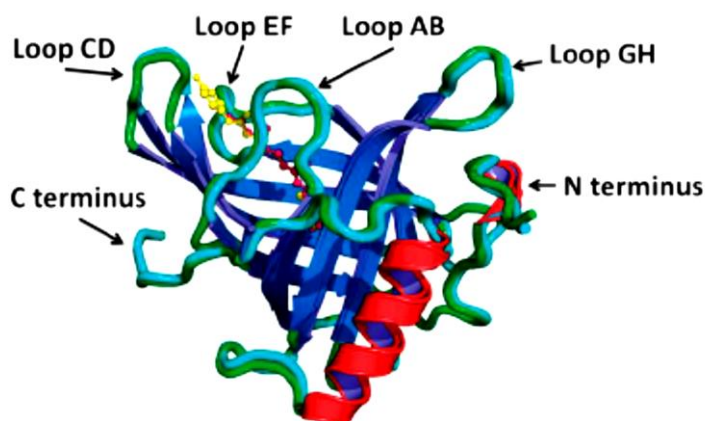
Figure 12: Structure of *holo*-RBP4 with ROH bound.[47]

The 21 kDa monomeric RBP4 is synthesised primarily in the liver but also in adipose tissue. Its main function is to transport retinol (ROH) (Figure 13) to extrahepatic tissues.[46,47]
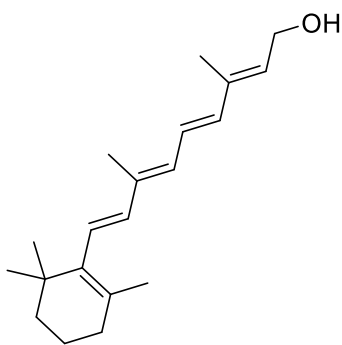
Figure 13: Structure of ROH.

During transportation, the vitamin molecule, ROH, is accommodated within the β-barrel of RBP4. The protein cavity is lined with hydrophobic residues that make specific interactions with ROH, thus stabilising the vitamin within the β-barrel.[47]

Holo-RBP4 is RBP4 with ROH bound inside the β-barrel. *Holo*-RBP4 is released from the liver complexed to a second homotetrameric protein, transthyretin (TTR). TTR is a thyroid binding hormone, synthesised in hepatic tissues, whose purpose is to distribute thyroids. It is a 55 kDa protein that binds to *holo*-RBP4 and stabilises the RBP4-ROH complex. The absence of ROH from the RBP4 β-barrel results in a weaker interaction between RBP4 and TTR. As *holo*-RBP4 is small enough to be removed from circulation by renal filtration, the formation of the 76 kDa RBP4-TTR complex prevents this renal filtration due to its increased size.[47]

The presence of ROH is very important in the formation of the RBP4-TTR complex and demonstrates that replacing ROH with an alternative ligand may disrupt the formation of the RBP4-TTR complex, which will result in the renal filtration of RBP4. Thus, the serum levels of RBP4 will be reduced and may improve the diabetic condition.[47]

Computational techniques were used to identify ligands that could bind to RBP4 and involved the use of the eHiTS (electronic High Throughput Screening) software package (SimBioSys Inc.). The eHiTS software docked flexible ligands within the RBP4 receptor and rapidly and systematically counted mappings of interacting atoms between the RBP4 receptor and the ligand database using an exhaustive search algorithm. The binding pocket was first determined from the X-ray crystal structure of RBP4. The binding mode for each conformation was determined and a binding score was assigned based on binding affinity for RBP4.[45]

From a database of 57,576 compounds, three compounds were uncovered, two of which are RTB70 and RTB69 (Figure 14). These compounds passed Lipinski's guidelines (< 5 hydrogen bond donors; < 10 hydrogen bond acceptors; molecular weight < 500; logP < 5), which indicated that the compound had potential to be used as a bioavailable and orally administered drug. The compounds were purchased from Maybridge (www.Maybridge.com) and tested in the surface plasmon resonance (SPR) assay to elucidate if they were capable of disrupting the RBP4-TTR complex formation.[45]
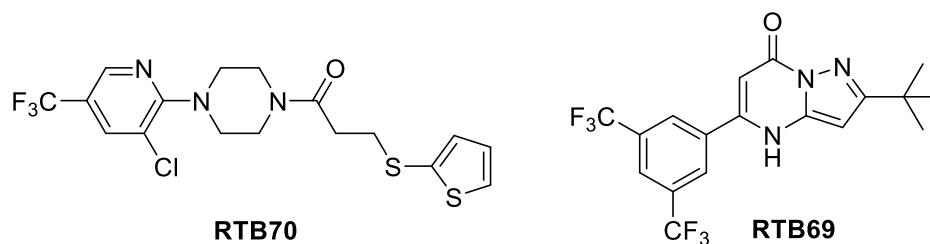
Figure 14: Structure of RTB70 and RTB69.

The SPR assay is an optical method used for measuring molecular interactions by immobilizing a binding molecule (e.g. *holo*, His-RBP4) onto the surface of a sensor chip. Next, a certain concentration of test compound is injected over the chip surface in a solution of SPR running buffer. This is followed by an injection of another binding molecule (e.g. untagged TTR). Binding of molecules (i.e. formation of a complex) causes a change in mass on the sensor chip resulting in changes in the refractive index of the SPR running buffer. Changes to the refractive index indicate if binding has occurred and appears as an increase in resonance units. This assay showed that RTB70 and RTB69 are capable of docking within the β-barrel of RBP4 and disrupting/preventing the formation of the RBP4-TTR complex.[45]

1.3.1 Glucose tolerance test (GTT) and an insulin tolerance test (ITT)

As discussed previously in section **1.3**, the ability to disrupt the RBP4-TTR complex, thus lowering serum RPB4, is linked to improvements in insulin resistance. The use of the retinoid like compound Fen has shown this to be true as its use prevents high-fat diet (HFD) induced obesity, and the development of insulin resistance in mice, through the lowering of serum RBP4 levels.[45,48]

Following this logic, the next investigation was focused on the ability of RTB70 and RTB69 to control and reduce insulin resistance in mice. A study examining the effects of these compounds on a group of mice exposed to a HFD was thus performed by our collaborators in the Biology department in Maynooth University, and the results were published.[45,49]

This study focused on two tests, a glucose tolerance test (GTT) and an insulin tolerance test (ITT). GTT examined how quickly glucose is cleared from the blood after a bolus of glucose is administered, whereas ITT examined insulin sensitivity. With regards to mice treated with RTB70, GTT showed improved glucose handling and the ability to clear glucose more rapidly was observed, as well as improved insulin sensitivity from ITT. With regards to mice treated with RTB69, GTT also showed improved glucose handling and the ability to clear glucose more rapidly, but not as effective in the ITT as RTB70.[45,49]

As well as showing improved insulin and glucose profiles, the mice treated with RTB70 also exhibited a reduced weight gain over the eight-week period when compared to a control. Although RTB69 was not as effective at reducing weight gain as RTB70, a reduction in weight gain was still observed.[49]

1.3.2 Discovery of RTC1 and RTC53

The results from the SPR assay and animal studies stimulated an effort to optimise RTB70 so as to improve its anti-diabetic properties. A small number of compounds were synthesised by removing functional groups from RTB70 and tested using SPR, fluorometric binding assay, and glucose uptake (GU) assay. From the compounds synthesised, RTC1 (compound **1**, Figure 15) was shown to be the most active.
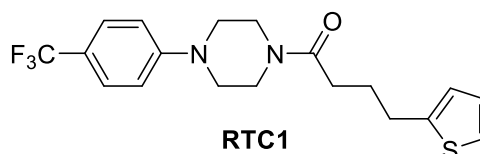
Figure 15: Structure of RTC1, compound **1**.

Results of the SPR assay showed that RTC1 was a highly effective disruptor of the RBP4-TTR complex with results indicating that it was more potent than RTB70. The fluorometric binding assay quantitatively measures a compounds ability to dock within *apo*-RBP (i.e. RBP4 without ROH bound inside the β-barrel), by measuring the level of tryptophan fluorescence quenching that occurs. RTC1 was found to show an increase in fluorescence due to conformational changes at or around the tryptophan residue. This may also indicate some level of interaction between RTC1 and RBP4.[48]

The glucose uptake assay measures the amount of tritiated (^{3}H) deoxy-2-glucose taken up by muscle cells. Tritiated deoxy-2-glucose is used as its biochemical properties allow for it to be easily traced and measured within a cell.[50] The glucose uptake assay is independent of RBP4. Therefore, one would not have expected the hit compounds to be active in this assay. However, RTC1 was very active, more so than RTB70. This suggested that a different mechanism of action was occurring that results in glucose uptake.

RTC53 (Figure 16), a member of the pyrazolopyrimidinone bicycle family and a derivative of RTB69, was also found to be highly active in the glucose uptake assay.[45]
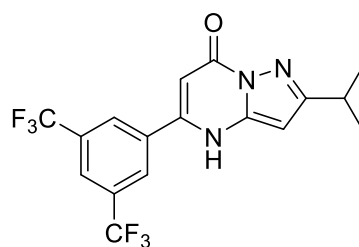
Figure 16: Structure of RTC53.

1.3.3 Alternative mechanism of action: effect of RTC1 on complex I

A concerted effort was undertaken, with our collaborators, to determine the mechanism of action. Recent work published with our collaborators in Maynooth University has shown the effect of RTC1 on inhibiting complex I (NADH:ubiquinone oxidoreductase), which can counteract many of the cellular abnormalities associated with type 2 diabetes. During this research, they compared RTC1 with the current leading therapy for type 2 diabetes, metformin. The result of their research showed that RTC1 demonstrated a superior effect at much lower concentrations in amending *in vitro* representations of the type 2 diabetes phenotype. They established that RTC1 stimulates the inhibition of complex I, which leads to the activation of AMPK, and an increase in glucose uptake at much lower concentrations than the common anti-diabetic therapy.[51]

It was predicted that the superior influence of RTC1 may lie with the structural differences of the compound, which could favour binding of RTC1 to distinctive regions of the enzyme complex, and could occupy a similar binding pocket to that discussed in section **1.2.1.1**. They concluded that although metformin is substantially more hydrophilic and reliant on organic cation transporters to enter the cell, RTC1 has lipophilic properties (logP value of 4.79), which might also allow easier target engagement. They also concluded that the cell was able to maintain its energy status as the ATP levels remained within normal levels.[51]

Overall, they demonstrated from this study that RTC1 can prevent weight gain, restore normal glucose uptake, and augment insulin sensitivity in a murine diet-induced model of type 2 diabetes. They concluded that RTC1 can act as an insulin sensitizer as well as an insulin substitute, through its potent influence on complex I and AMPK activation.[51]

1.4 Aims of this Project

Building on from all the previous work mentioned, this project was focused on expanding both families of compounds in order to create a large library of compounds that could potentially develop into novel small anti-diabetic agents. The first family is an arylpiperazine family with variations on five different sites of RTC1 (compound **1**, Figure 17). These sites are the aryl group (site A), the piperazine ring (site B), the carbonyl group (site C), the alkyl chain (site D), and the thiophene ring (site E).
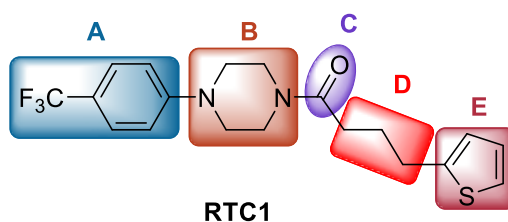
Figure 17: Structure of RTC1 with variations at five sites, A-E.

The second family is a pyrazolopyrimidinone bicycle family where analogues of RTC53 were synthesised with variations at the R and R^1 groups (Figure 18).
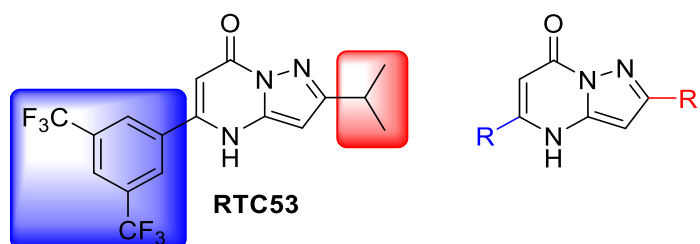
Figure 18: Structure of RTC53 and general structure of pyrazolopyrimidinone bicycle with variations at R and R^1 groups.

A structure activity relationship (SAR) study of both families was conducted in order to explore the effect the key functional groups had on biological activity. Full characterisation of all the compounds synthesised was carried out using techniques such as melting point, nuclear magnetic resonance (NMR) spectroscopy, including ^1H, ^{13}C NMR and 2D-NMR experiments, infrared (IR) spectroscopy, high-resolution mass spectrometry (HR-MS), and X-ray crystal analysis when appropriate. Variations were made with electron donating and electron withdrawing groups and adding/removing certain elements of the parent active structure to determine source of activity.

Another aim of the project was to develop an improved method for synthesising both families. This was carried out in the arylpiperazine family by developing a less laborious method of synthesis that does not require any anhydrous conditions and employs a simplified work-up. In the pyrazolopyrimidinone bicycle family, method development focused around microwave synthesis of the pyrazole starting materials and the pyrazolopyrimidinone bicycle final compounds. This involved the development of a "one-pot" synthesis for these compounds.

Active compounds from both families were identified using the glucose uptake assay and complex I assay. The complex I assay can determine a compound's ability to inhibit NADH dehydrogenase in complex I of the electron transport chain by measuring the change in ubiquinone absorbance. Using both these assays, we were able to establish active compounds, which had the potential of developing into anti-diabetic agents.

Chapter 2: Arylpiperazine Family

2.1 Introduction

Arylpiperazine compounds consist of a piperazine moiety bonded to an aryl group. They are commonly used in the development of novel drugs. To access the necessary arylpiperazine derivative, various synthetic approaches can be utilised such as nucleophilic aromatic substitutions (S_NAr) reactions, metal catalysed reactions, and cyclocondensation reactions.[52,53] Asymmetric synthesis of arylpiperazines has been widely reported and includes resolution of racemic materials, separation of diastereomers, and diastereoselective reduction at the benzylic position.[32]

Arylpiperazines have been used for many years in various applications. For example, (i) *m*-chlorophenylpiperazine was patented by American Cyanamid in the 1960s as an appetite suppressant, (ii) 2-chloro-6-(piperazin-1-yl)pyrazine, the pyrazine isoster of *m*-chlorophenylpiperazine, was patented by Merck & Co. for its anorectic effect in the 1970s, and (iii) 1-(4-fluoro-3-(trifluoromethyl)phenyl)piperazine has also been patented as an anorectic agent in the early 1970s (Figure 19).[52]
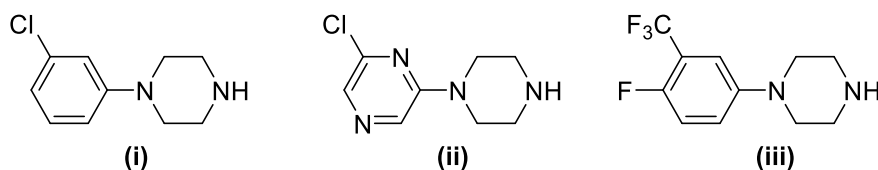
Figure 19: Structure of arylpiperazines found in literature.[52]

More recently, arylpiperazines are used in antidepressant drugs which act as monoamine neurotransmitter reuptake inhibitors and exhibit antidepressant activity. Some of these drugs include trazodone, which is a serotonin reuptake inhibitor and is comparatively safer than conventional antidepressants, and buspirone, which can cause metabolic acidosis in diabetic patients (Figure 20).[54]
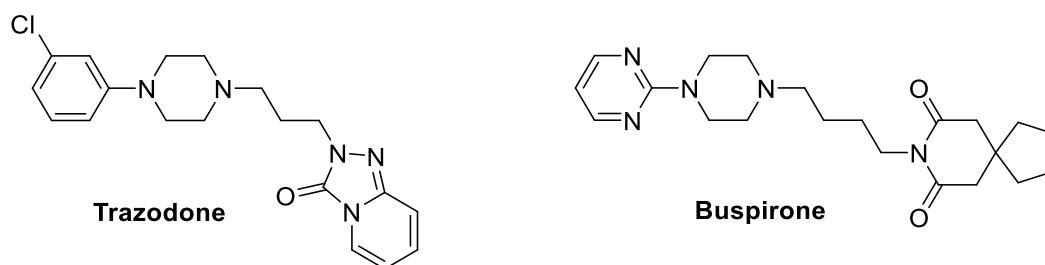
Figure 20: Structure of trazodone and buspirone.[54]

Studies have shown that compounds with arylpiperazine moieties have anti-proliferative properties. Naftopidil (Figure 21), an arylpiperazine ether derivative, has been shown to induce apoptosis in malignant mesothelioma cell lines, as well as exert an anticancer effect and inhibit prostate cancer cell growth by arresting the G1 cell cycle phase.[54,55]
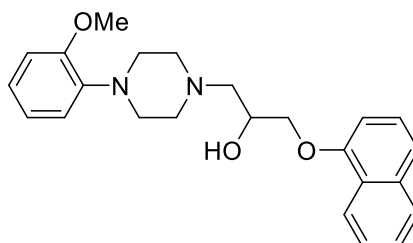
Figure 21: Structure of naftopidil.[54]

More recently, other arylpiperazine derivatives have been reported to act as novel anti-cancer agents as they have been shown to exhibit *in vitro* strong cytotoxic activity against prostate cancer cell lines. These compounds were derivatives of naftopidil and their synthesis consisted of a four-step reaction (Scheme 1). This consisted of (i) a reduction reaction of the carboxylic acid starting material into an alcohol, (ii) a nucleophilic substitution reaction, (iii) activation of the primary alcohol via a tosylation reaction, and (iv) reaction with arylpiperazines.[54,55]
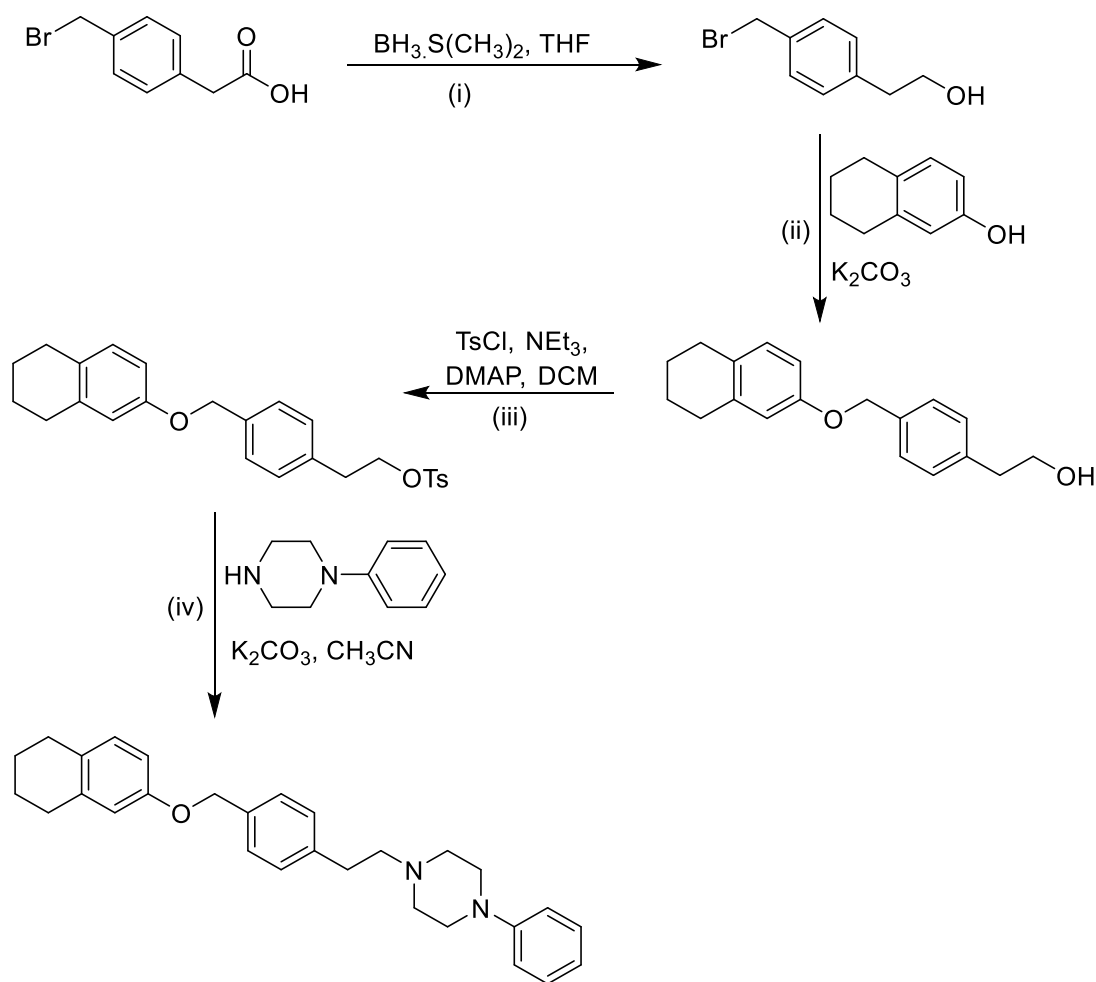
Scheme 1: Synthesis of naftopidil derivatives.[54]

An efficient protocol for the synthesis of various substituted arylpiperazines was recently reported using sulfolane as solvent (Scheme 2).[54] Sulfolane is an aprotic, dipolar, high boiling and recoverable solvent, and can be used as a substitute for common organic solvents. The developed protocol was clean, high yielding and products were obtained in high purities. The final products were precipitated as hydrochloride salts and could be obtained by filtration, thus making the new protocol also fast and convenient.[54]
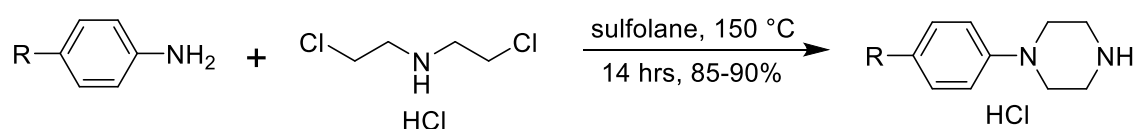
Scheme 2: The synthesis of arylpiperazines using sulfolane as solvent.[54]

The synthesis of an amide bond is one of the most important reactions in biochemistry, as it is the bond that links amino acids together in peptides and proteins. It is a common

feature in small and complex molecules, whether naturally-occurring or synthetically made.[56] Carboxamides are compounds which contain an amide functional group and have been reported to appear in more than 25% of known drugs, such as Penicilline G (Figure 22).[57] This is due to carboxamides being neutral and stable as well as having both hydrogen-bond accepting and donating properties.
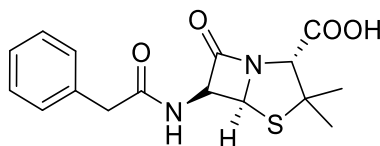
Figure 22: Structure of Penicilline G.

The amide bond is commonly synthesised using coupling reagents to activate the carboxylic acid *in situ*. Coupling reagents are used to generate more reactive intermediates such as acid chlorides, anhydrides, carbonic anhydrides or activated esters.[56] The *N*-acylpiperazine moiety consists of a piperazine bonded to a carbonyl group through an amide bond. This moiety is also found in many drugs with various medicinal uses such as antibacterial, antiulcer, anticancer and as nootropic agents.[58]

The arylpiperazine family that I worked with consisted of novel analogues of the lead compound of 4-(thiophen-2-yl)-1-(4-(4-(trifluoromethyl)phenyl)piperazin-1-yl)butan-1-one (RTC1) (compound **1**) (Figure 23). My family of arylpiperazine compounds were added to a family of arylpiperazines that had been generated by a previous group member.[45] This combination resulted in a larger library of arylpiperazines, which underwent biological evaluation and allowed for a more comprehensive investigation of the SAR. RTC1 was systematically modified at five different sites, A-E (Figure 23). This allowed us to investigate the importance of the aryl substituent and the nature of the aryl group (site A), the piperazine ring (site B), the carbonyl group (site C), the length and nature of the alkyl chain (site D), as well as the terminal group (site E), on anti-diabetic activity.
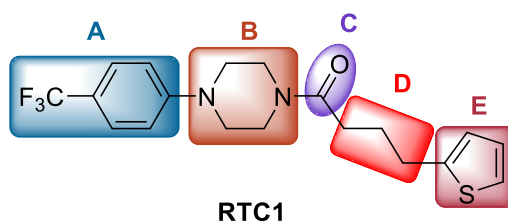
Figure 23: Structure of RTC1 with variations at five sites, A-E.

2.2 Synthesis of 4-(thiophen-2-yl)-1-(4-(4-(trifluoromethyl)phenyl)piperazin-1-yl)butan-1-one (RTC1) 1

The previously reported procedure for the generation of the amide bond in 4-(thiophen-2-yl)-1-(4-(4-(trifluoromethyl)phenyl)piperazin-1-yl)butan-1-one (RTC1) **1** and its analogues, consisted of coupling the starting aryl piperazine, 1-(4-(trifluoromethyl)phenyl)piperazine (MK17) **2**, with the corresponding carboxylic acid, 4-(2-thienyl)butyric acid, under rigorous air-free conditions.[44,45] The reaction was carried out using coupling reagent (e.g. hydroxybenzotriazole (HOBt) and N,N,N',N'-tetramethyl-O-(benzotriazol-1-yl)uronium tetrafluoroborate (TBTU) combination, or benzotriazol-1-yloxy)tris(dimethylamino)phosphonium hexafluorophosphate (BOP)), anhydrous dimethylformamide (DMF), anhydrous triethylamine (NEt$_3$), in an oven-dried Schlenk tube, and overnight stirring at rt under a N$_2$ atmosphere (Scheme 3).[44,45]
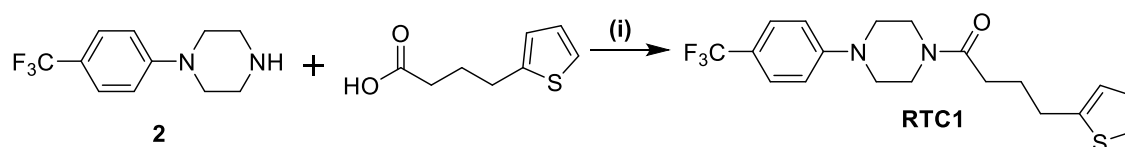
Scheme 3: Synthesis of RTC1, (i) HOBt, TBTU, anhydrous DMF, anhydrous NEt$_3$, N$_2$, rt, overnight, 80% yield.[44,45]

A somewhat elaborate work-up procedure was then followed, including evaporation under reduced pressure, acidification, extraction, base wash, brine wash, drying, and finally column chromatography.

2.2.1 Method development for the synthesis of arylpiperazines

The original procedure for the preparation of RTC1 was somewhat cumbersome and as a result a study was undertaken to identify improved reaction conditions. We first explored the need for anhydrous reaction conditions. To achieve this, we did not dry reactants, reagents, or solvents (i.e. non-anhydrous). We also avoided Schlenk conditions and carried out the reaction in a normal air atmosphere and round-bottom flask. Furthermore, we postulated that the work-up procedure could be simplified and upon reaction completion, move straight from evaporation under reduced pressure to column chromatography. This greatly reduced the amount of sample manipulation and removed the acidification, washing, extraction, and drying steps.

A comparison of the two methods was performed using the synthesis of methyl 9-oxo-9-(4-(4-(trifluoromethyl)phenyl)piperazin-1-yl)nonanoate (MK16) **3** (Scheme 4).
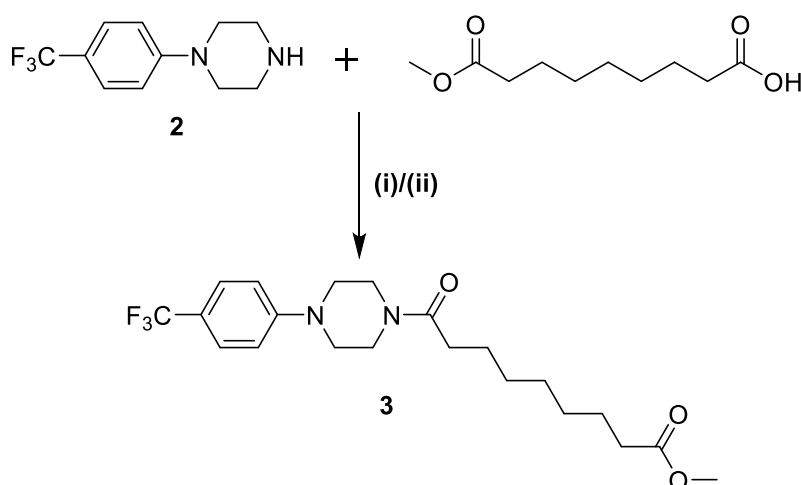
Scheme 4: Synthesis of compound **3** using: (i) the old method of BOP, anhydrous NEt₃, anhydrous dichloromethane (DCM), nitrogen (N₂) atmosphere, rt, overnight, 43% yield; versus (ii) the new method of BOP, NEt₃, DCM, rt, air atmosphere, overnight, 55% yield.

The old method consisted of coupling methyl hydrogen azelate with compound **2** using BOP, anhydrous NEt₃ and anhydrous dichloromethane (DCM) in an oven-dried two-neck flask under a nitrogen (N₂) atmosphere with overnight stirring. Purification of the reaction mixture consisted of acidification using 0.1 M aqueous hydrochloric acid (HCl), extraction using DCM, wash with aqueous sodium hydrogen carbonate (NaHCO₃), wash

with brine, and drying using magnesium sulfate (MgSO$_4$). The residue was purified using column chromatography to give compound **3** as an off-white solid in a 43% yield.

The new method involved coupling methyl hydrogen azelate with compound **2** using BOP, non-anhydrous NEt$_3$, and non-anhydrous DCM in a round-bottom flask and stirred at room temperature overnight. Purification of the crude product consisted of evaporation under reduced pressure followed by column chromatography to give compound **3** as an off-white solid in a 55% yield.

Most of the compounds were synthesised using this improved method and HOBt/TBTU coupling reagents, with non-anhydrous DMF as the solvent. However, because DMF is a reproductive toxin (category 1B) with a high boiling point (153 °C), an alternative solvent was sought. DCM was used instead as it has a much lower boiling point (39.6 °C) and is less toxic than DMF. This resulted in the synthesis of arylpiperazine derivatives with similar, and in some cases higher yields, than when using DMF as before.

For example, the original synthesis of 1-(4-cyclohexylpiperazin-1-yl)-4-(thiophen-2-yl)butan-1-one (MK43) **4** (Figure 24) using anhydrous conditions and anhydrous DMF resulted in a 70% yield.[45] Using the new method and DCM, the yield increased to 82%. A more significant difference was observed with the synthesis of 4-(1*H*-Pyrazol-4-yl)-1-(4-(4-(trifluoromethyl)phenyl)piperazin-1-yl)butan-1-one (MK69) **5** (Figure 24), which consisted of a 10% yield with the original synthesis method[45] and a 93% yield with the new synthesis method.
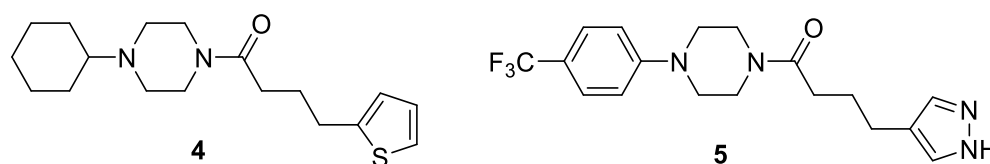
Figure 24: Structure of compound **4** and compound **5.**

The new method was therefore adopted and employed in the synthesis of most of the compounds reported in this thesis, with the exception of compounds **3** and **24**.

2.2.2 Mechanism for the synthesis of RTC1 (compound 1) and RTC1 analogues

The coupling of the carboxylic acid starting material with compound **2** is suggested to take place using the following general mechanism (Scheme 5):
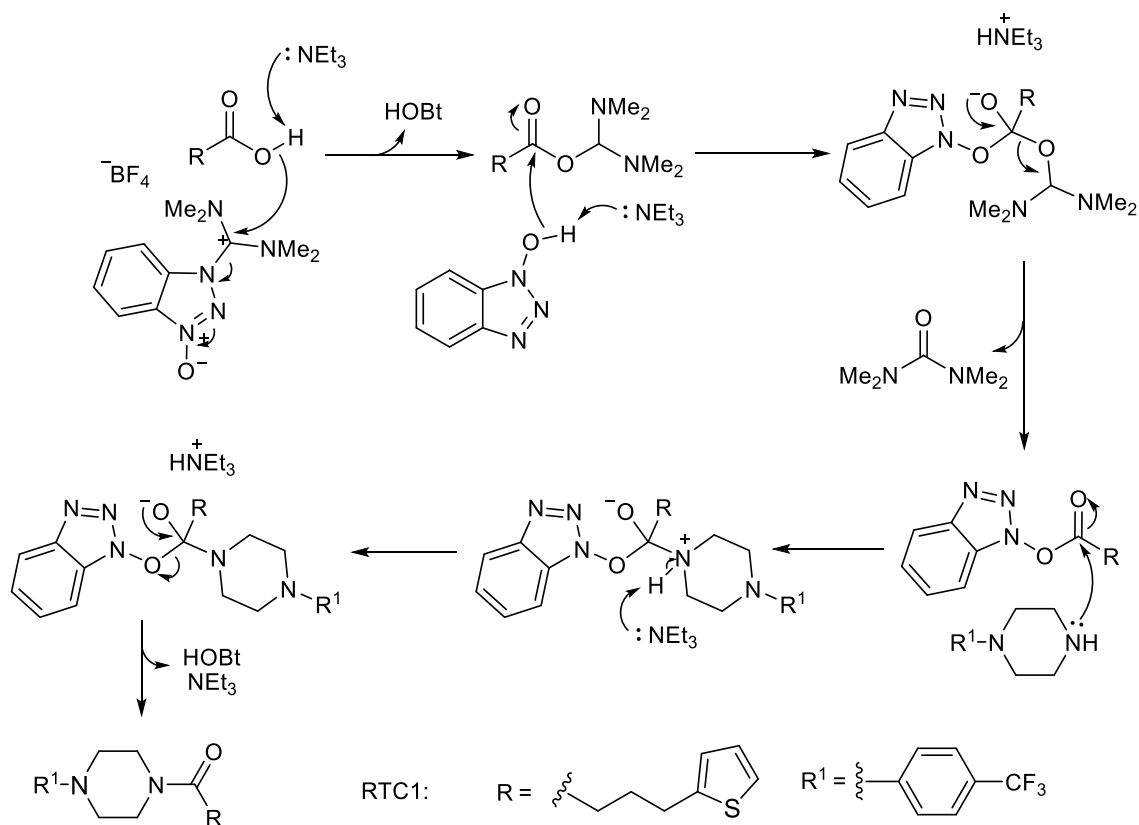
Scheme 5: Mechanism for the synthesis of RTC1.

The mechanism begins with a general base catalysis where NEt$_3$ deprotonates the carboxylic acid while the carboxylic acid attacks the electrophilic carbon of TBTU. This step creates an activated ester with a more electrophilic carbonyl group. This in turn can get attacked by HOBt which gets deprotonated at the same time via general base catalysis, generating a tetrahedral intermediate, with a better leaving group. The carbonyl group is then reformed and the 1,1,3,3-tetramethylurea group is eliminated. Finally, the carbonyl group of the resulting ester gets attacked by the arylpiperazine nucleophile to give a tetrahedral intermediate, which subsequently gets deprotonated and eliminates $^-$OBT leaving group to generate the final product.

2.2.3 Characterisation of RTC1, compound 1

All compounds synthesised in the arylpiperazine family were characterised using ^{1}H NMR, ^{13}C NMR, HR-MS and IR spectroscopy. Some of the compounds containing a trifluoromethyl group were also characterised using ^{19}F NMR spectroscopy. Proton and carbon signals were assigned with the aid of DEPT and 2D-NMR experiments such as ^{1}H $-$ ^{1}H COSY, ^{1}H $-$ ^{13}C HSQC, and ^{1}H $-$ ^{13}C HMBC. The numbering scheme shown below (Figure 25) will be used in the following discussion on the structural characterisation of RTC1.
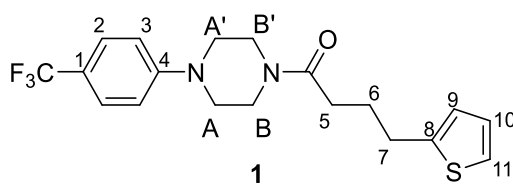
Figure 25: Structure of RTC1 with labelled protons and carbons for characterisation.

2.2.3.1 The ^{1}H NMR spectrum of RTC1

The ^{1}H NMR spectrum of RTC1 is shown below (Figure 26). The spectrum consists of ten signals in two main regions; four signals in the more deshielded aromatic region and six signals in the more shielded aliphatic region.
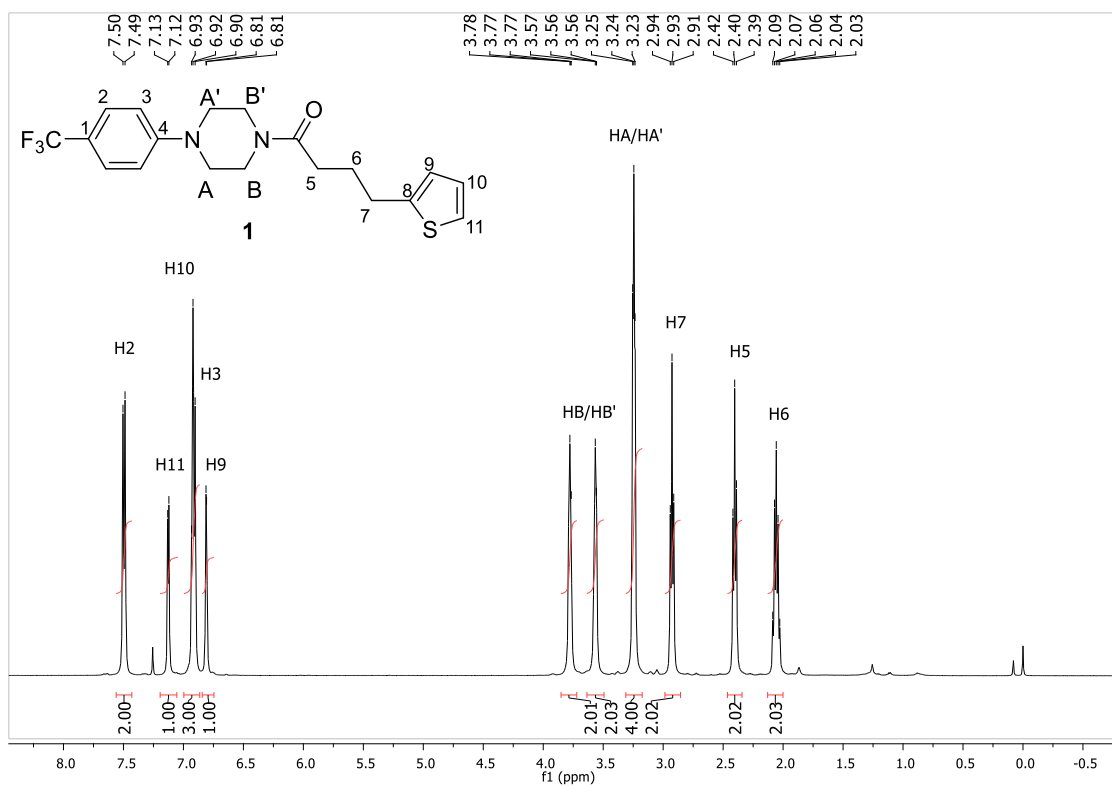
Figure 26: The ^{1}H NMR spectrum of RTC1.

2.2.3.1.1 Aromatic region of the ^{1}H NMR spectrum of RTC1

The four signals in the aromatic region (Figure 27) of the ^{1}H NMR spectrum of RTC1 integrate to 7H and account for the four protons of the aromatic ring and the three protons of the thiophene ring.
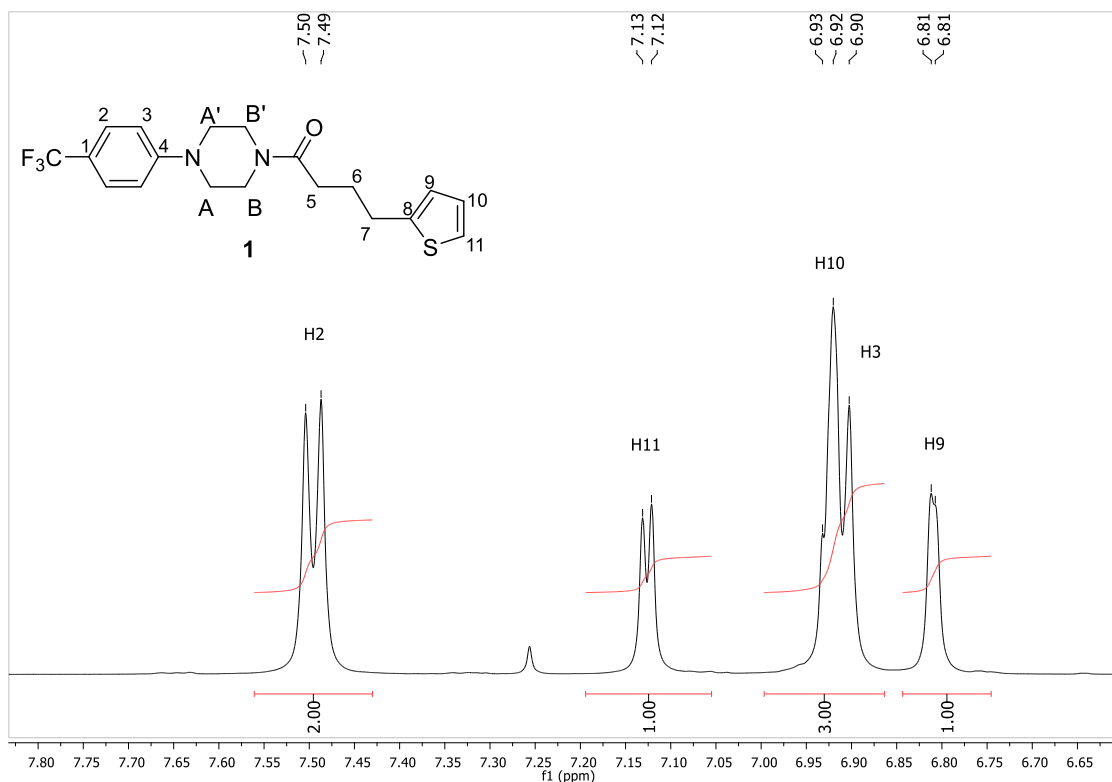
Figure 27: Aromatic region of the ^{1}H NMR spectrum of RTC1.

The most downfield signal is a doublet at 7.50 ppm and can be assigned as the two H2 protons of the aromatic ring. They are *ortho* to the electron withdrawing trifluoromethyl group (CF₃) and therefore appear as the most deshielded signals. A plane of symmetry exists through the aromatic ring and hence the signal at 7.50 ppm integrates for both protons *ortho* to the trifluoromethyl group. The coupling constant (*J* value) is a measure of the coupling interaction between a pair of protons. This signal appears as a doublet with a *J* value of 8.5 Hz as it couples with the neighbouring protons on the aromatic ring, H3. The signal for the two other protons in the aromatic ring (H3) should also appear as a doublet as they are only coupled with protons H2. However, they overlap with one of the protons of the thiophene ring (H10) and therefore appear as a multiplet in the region of 6.94 – 6.89 ppm integrating for three protons.

Without the overlap, the signal for H10 of the thiophene ring was expected to appear as a double of doublets (dd) as it is coupled to two non-equivalent protons, H9 and H11. Both H9 and H11 signals must therefore appear as doublets as they are both coupled to H10. The signal for H11 is more deshielded as it is adjacent to the electron withdrawing sulphur group and therefore appears more downfield. Its multiplicity is that of a doublet and occurs at 7.13 ppm with a J value of 4.9 Hz. The signal for H9 is more upfield as it is further away from the sulphur group and appears as a doublet at 6.81 ppm with a J value of 2.2 Hz.

The assignment of the aromatic region of the ^{1}H NMR spectrum is further supported by a 2D-NMR experiment known as ^{1}H–^{1}H Homonuclear Correlation Spectroscopy (^{1}H-^{1}H COSY) (Figure 28), which is used to identify protons coupled to each other. COSY spectra show two types of signals; diagonal signals and cross signals. Diagonal signals have the same frequency coordinate on each axis and appear along the diagonal of the plot, while cross signals have different values for each frequency coordinate and appear off the diagonal. Diagonal signals correspond to the signals in a 1D-NMR experiment, while the cross signals indicate couplings between pairs of nuclei. Using a ^{1}H–^{1}H COSY spectrum it is possible to map the coupling network in the molecule.
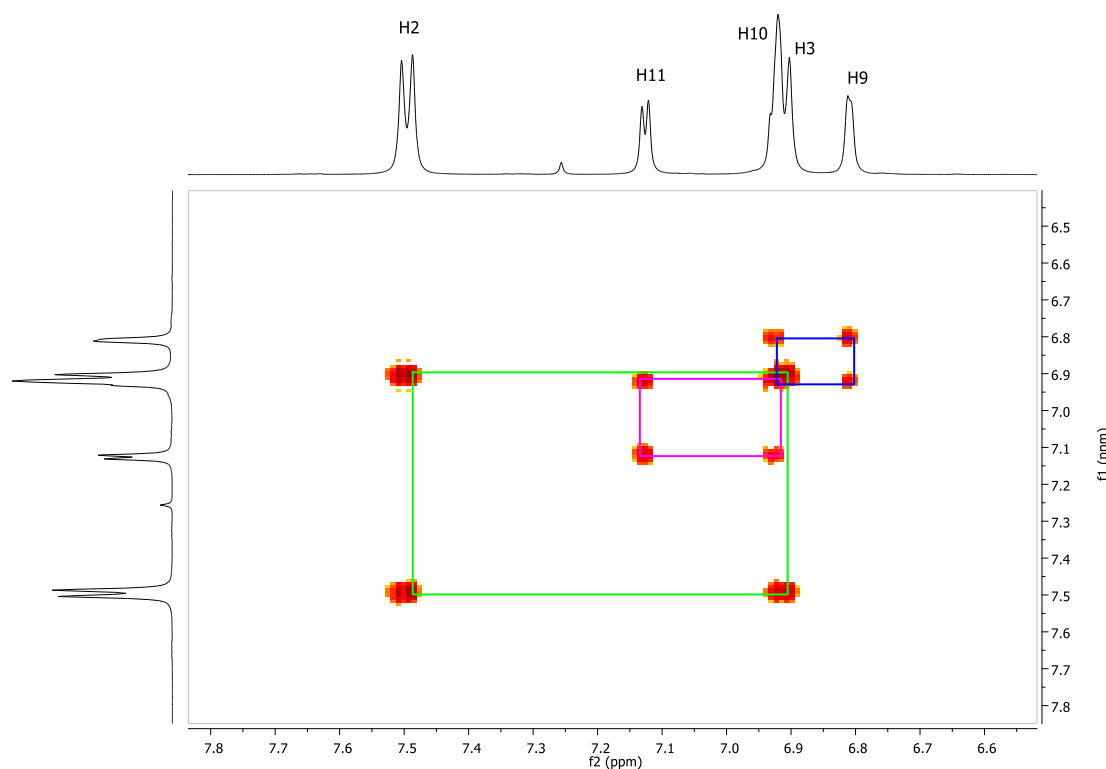
Figure 28: The aromatic region of the ^{1}H-^{1}H COSY spectrum of RTC1.

In the aromatic region of the ^{1}H – ^{1}H COSY spectrum of RTC1, the aromatic ring protons H2 and H3 are confirmed to be coupled to each other (green square). Proton H10 of the thiophene ring can also be seen to be coupled to both H11 (purple square) and H9 (blue square).

2.2.3.1.2 Aliphatic region of the ^{1}H NMR spectrum of RTC1

The aliphatic region of the ^{1}H NMR spectrum (Figure 29) of RTC1 consists of six different signals integrating for the eight protons of the piperazine ring and the six protons of the alkyl chain (H5 – H7). The three most deshielded multiplet signals in this region, resonating at 3.85 – 3.72 ppm, 3.64 – 3.49 ppm and 3.31 – 3.17 ppm, are due to the eight protons of the piperazine ring. The signals at 3.85 – 3.72 ppm and 3.64 – 3.49 ppm can be assigned as the HB/HB' protons of the piperazine ring, whereas the signal at 3.31 – 3.17 ppm can be assigned as the HA/HA' protons of the piperazine ring (this assignment was confirmed using the ^{1}H-^{13}C Heteronuclear Multiple Bond Correlation (^{1}H-^{13}C HMBC) spectrum, section **2.2.3.2.1**). The signals for the HB/HB' protons appear as two separate signals due to the anisotropy effect with respect to the carbonyl oxygen. These signals appear downfield as they are deshielded by the electronegative nitrogen adjacent to them. The remaining three signals in the aliphatic region can be assigned to the six protons from the alkyl chain with each signal integrating to two.
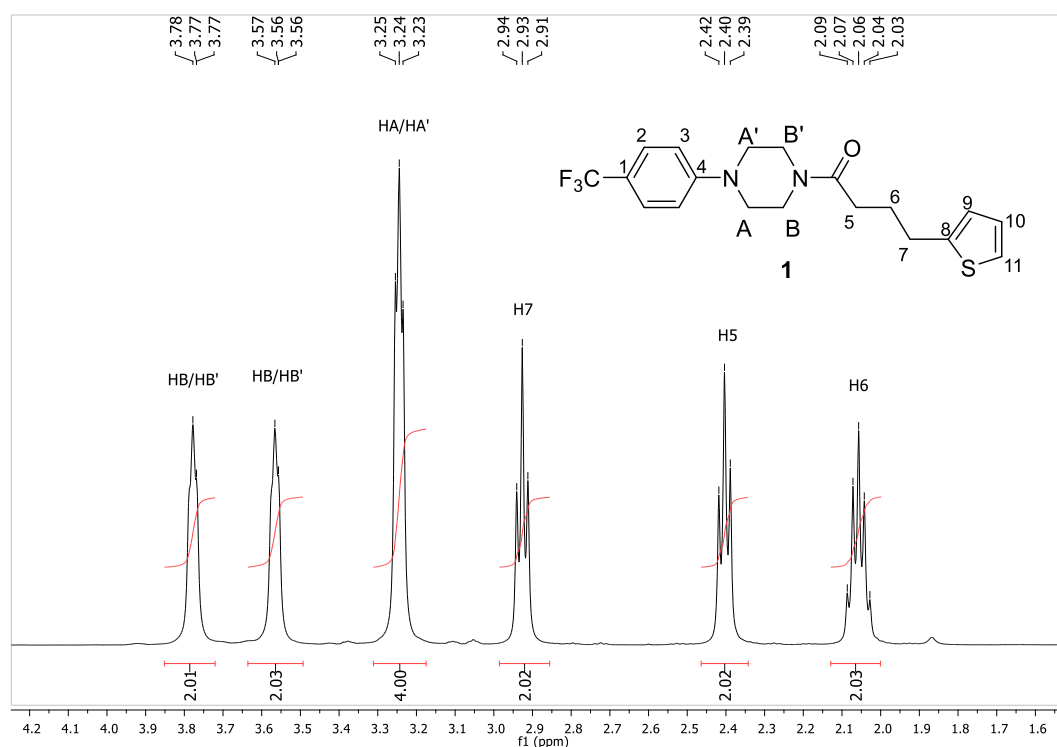
Figure 29: Aliphatic region of the ^{1}H NMR spectrum of RTC1.

51

The triplet signal resonating at 2.93 ppm can be assigned to the protons (H7) adjacent to the thiophene ring. This assignment was confirmed using the ^{1}H-^{13}C HMBC spectrum, section **2.2.3.2.1**. The signal appears as a triplet as it is coupled to two equivalent protons (i.e. H6) with a *J* value of 7.2 Hz. This signal is the most deshielded signal of the alkyl chain as it is adjacent to an electron withdrawing thiophene ring. Similarly, the signal at 2.40 ppm also appears as a triplet with a *J* value of 7.4 Hz and can be assigned to the two protons at H5. The H5 protons are deshielded due to the adjacent carbonyl group and are coupled to two equivalent protons at H6 (hence appear as a triplet). This assignment was also confirmed using the ^{1}H-^{13}C HMBC spectrum, section **2.2.3.2.1**. The two protons in the middle of the alkyl chain (H6) are therefore coupled to both H5 and H7 and appear as a quintet in the region of 2.13 – 2.00 ppm.

The coupling network of the signals can be clearly seen in the aliphatic region of the ^{1}H–^{1}H COSY spectrum of RTC1 (Figure 30).
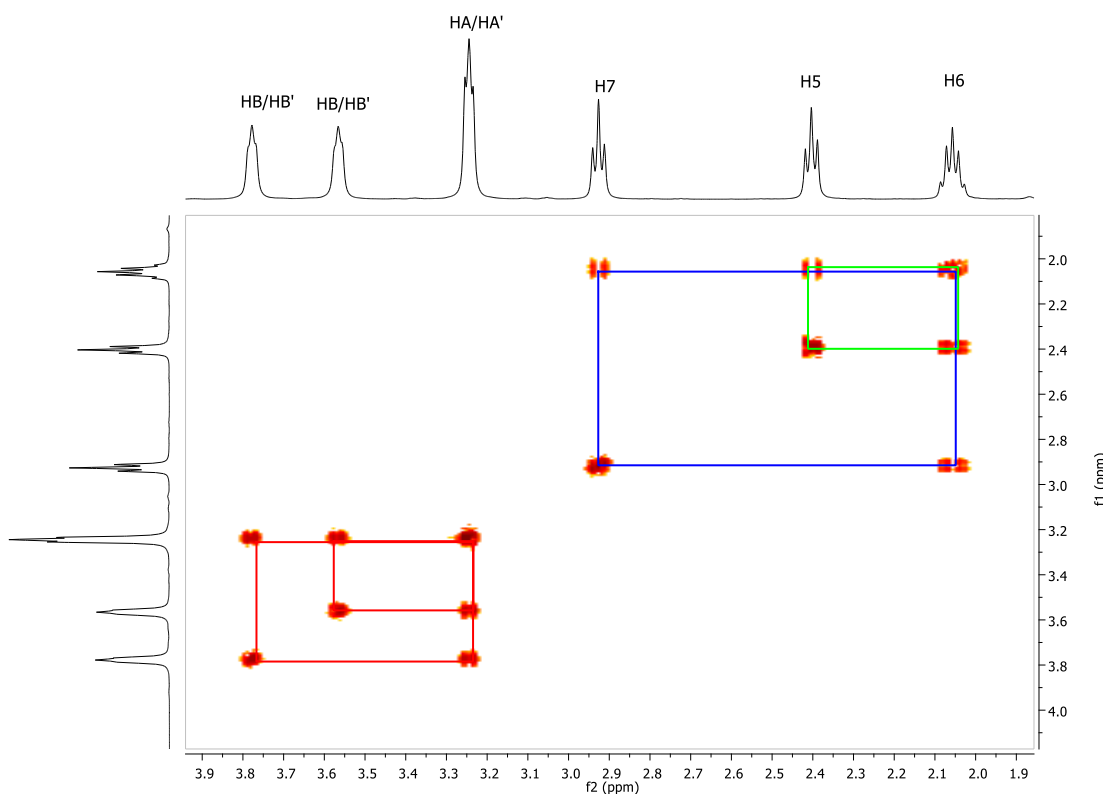
Figure 30: Aliphatic region of the ^{1}H–^{1}H COSY spectrum of RTC1.

The piperazine protons (HA/HA' and HB/HB') are coupled to each other as expected (red square). The protons in the middle of the alkyl chain, H6, can be seen to couple to both

the protons adjacent to the thiophene ring, H7, (blue square) and the protons adjacent to the carbonyl group, H5 (green square).

2.2.3.2 The ^{13}C NMR spectrum of RTC1

The ^{13}C NMR spectrum of RTC1 is shown below (Figure 31). For ease of explanation, this spectrum can be divided into three regions; A, B, and C.
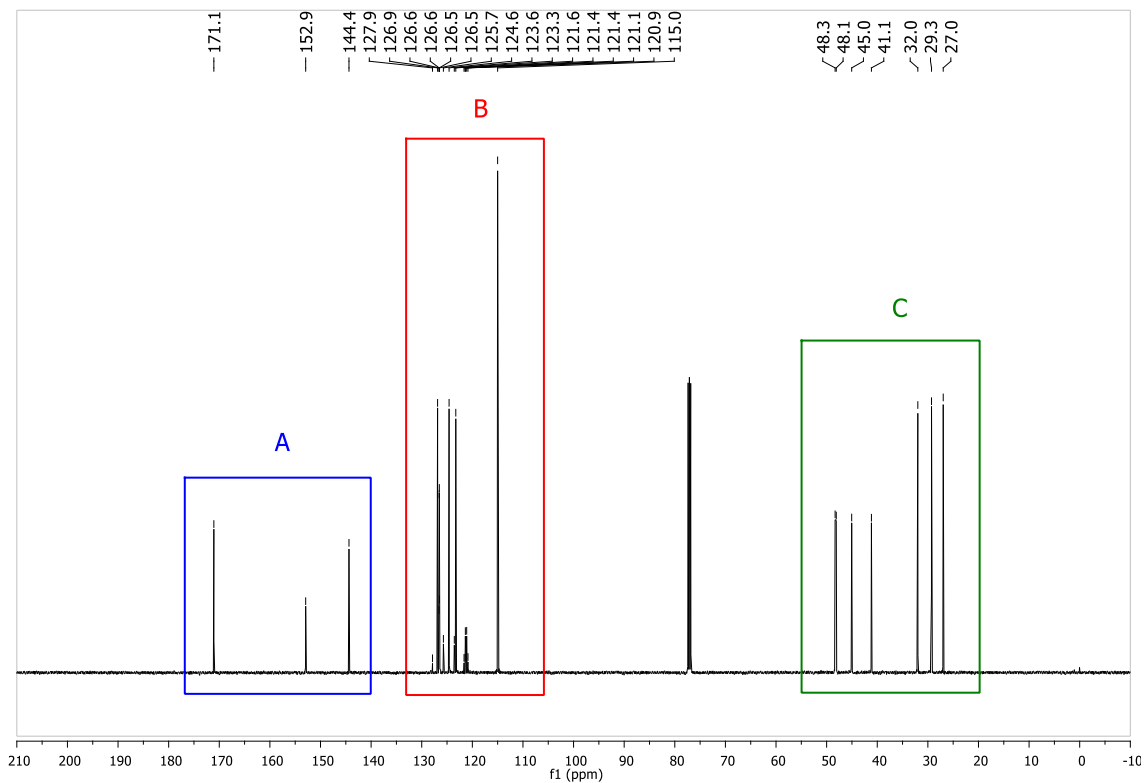
Figure 31: The ^{13}C NMR spectrum of RTC1 with three regions A, B, and C.

2.2.3.2.1 Region A of the ^{13}C NMR spectrum of RTC1

Region A of the ^{13}C NMR spectrum of RTC1 consists of three signals for three quaternary carbons; the carbonyl carbon (*C*=O), the *ipso* carbon of the aromatic ring (C4), and the *ipso* carbon of the thiophene ring (C8) (Figure 32).
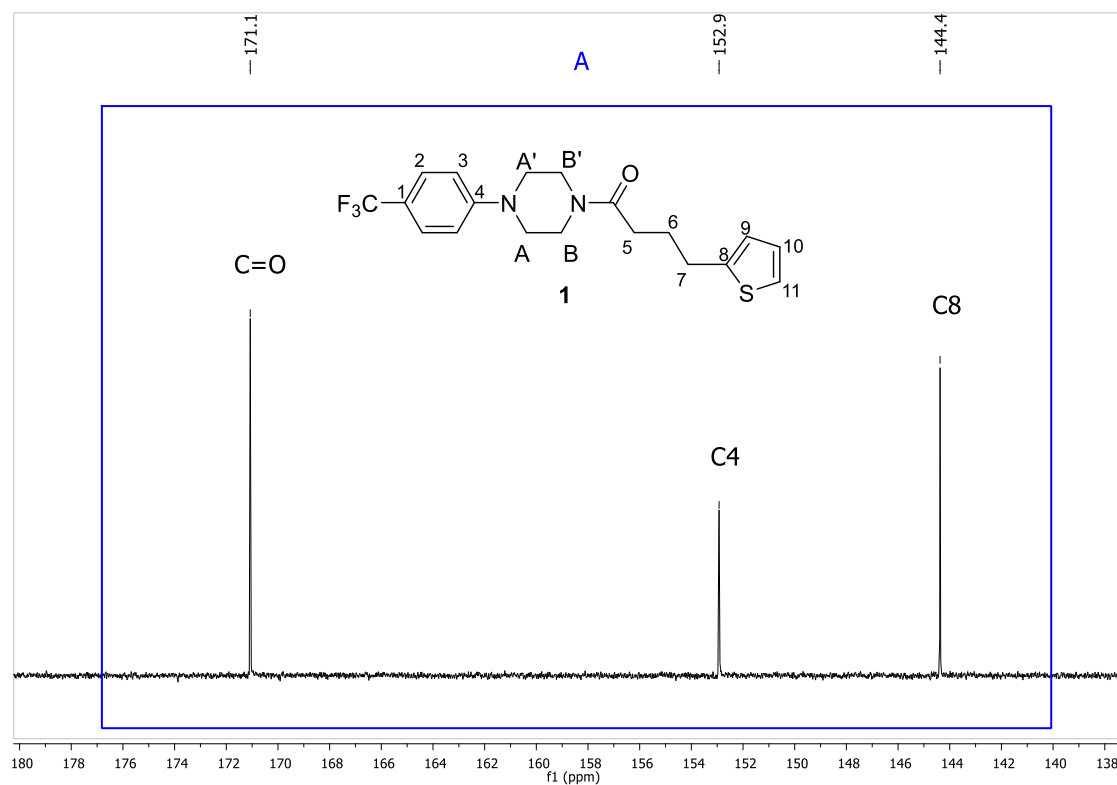
Figure 32: Region A of the ^{13}C NMR spectrum of RTC1.

These signals were identified using the 2D-NMR ^{1}H-^{13}C HMBC spectrum (Figure 33), which correlates chemical shifts of ^{1}H and ^{13}C nuclei separated from each other by two or more chemical bonds. HMBC spectra are particularly useful in identifying the connectivity of a molecule. The most deshielded quaternary carbon signal is due to the carbonyl carbon (*C*=O) and resonates at 171.1 ppm. This chemical shift is characteristic of a carbonyl carbon found in an amide. The ^{1}H-^{13}C HMBC spectrum (Figure 33) shows this carbon signal coupling to the two B/B' piperazine proton signals but is not coupled to the other A/A' piperazine proton signals, as they are too many bonds away. It is also coupled to the H5 and H6 proton signals from the alkyl chain (red lines), which are within two bonds (H5) or three bonds (H6) of the carbonyl carbon. Noticeably, it is not coupled to H7 of the alkyl chain as they are four bonds away.
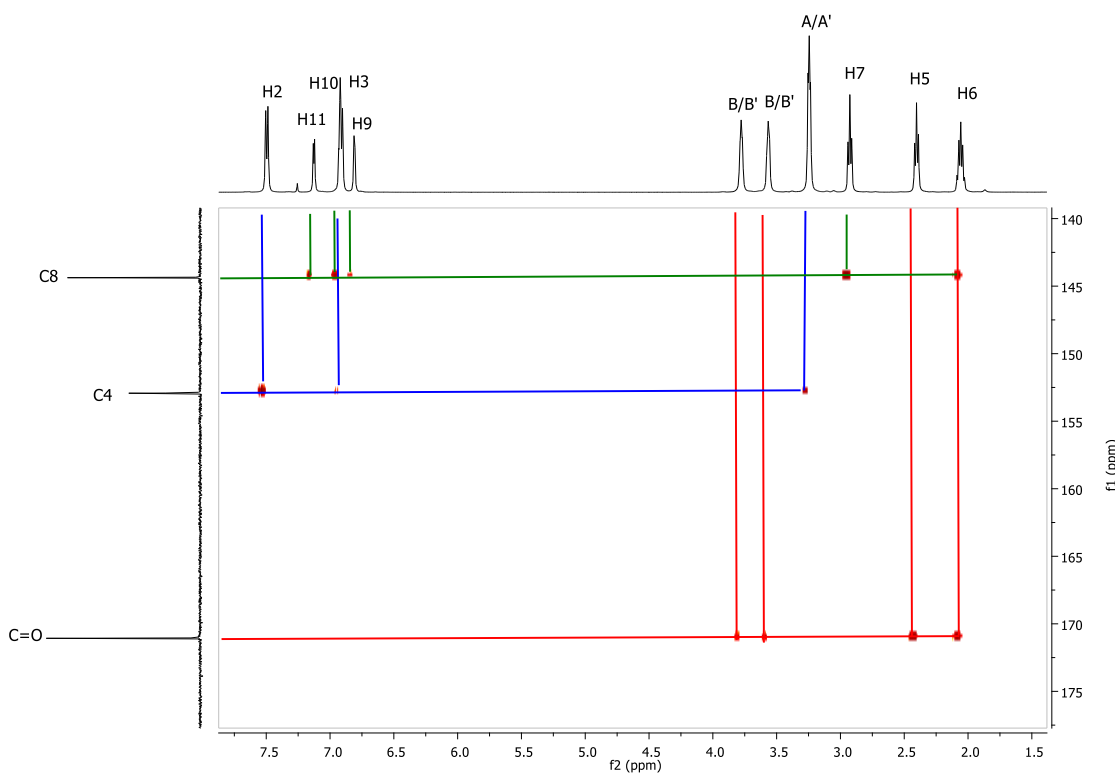
Figure 33: The ^{1}H-^{13}C HMBC spectrum of RTC1 showing the assignment of the three quaternary carbon signals.

The second signal in region A of the ^{13}C NMR spectrum at 152.9 ppm is assigned to the *ipso* quaternary carbon of the aromatic ring (C4). In the ^{1}H-^{13}C HMBC spectrum (Figure 33), this carbon is coupled to the aromatic protons (H2 and H3), as well as the piperazine A/A' protons adjacent to it (blue lines). It is not coupled to the other piperazine B/B' protons as they are too many bonds away.

The third signal in region A of the ^{13}C NMR spectrum at 144.4 ppm is assigned to the *ipso* quaternary carbon of the thiophene ring (C8). This signal can be seen in the ^{1}H-^{13}C HMBC spectrum (Figure 33) to be coupled to the three protons from the thiophene ring (H9, H10, H11), as well as protons from the alkyl chain (H6 and H7) which are 2-3 bonds away (green lines). It is not coupled to H5 protons of the alkyl chain as they are four bonds away.

2.2.3.2.2 Region B of the ^{13}C NMR spectrum of RTC1

Region B of the ^{13}C NMR spectrum (Figure 34) of RTC1 consists of multiple signals that can be assigned to seven carbons. The tertiary carbons of the thiophene ring appear as singlet signals at 126.9 ppm (C10), 124.6 ppm (C9) and 123.3 ppm (C11). The two tertiary carbons of the aromatic ring (C3), which are *meta* to the trifluoromethyl group, are equivalent and appear as a single singlet at 115.0 ppm.
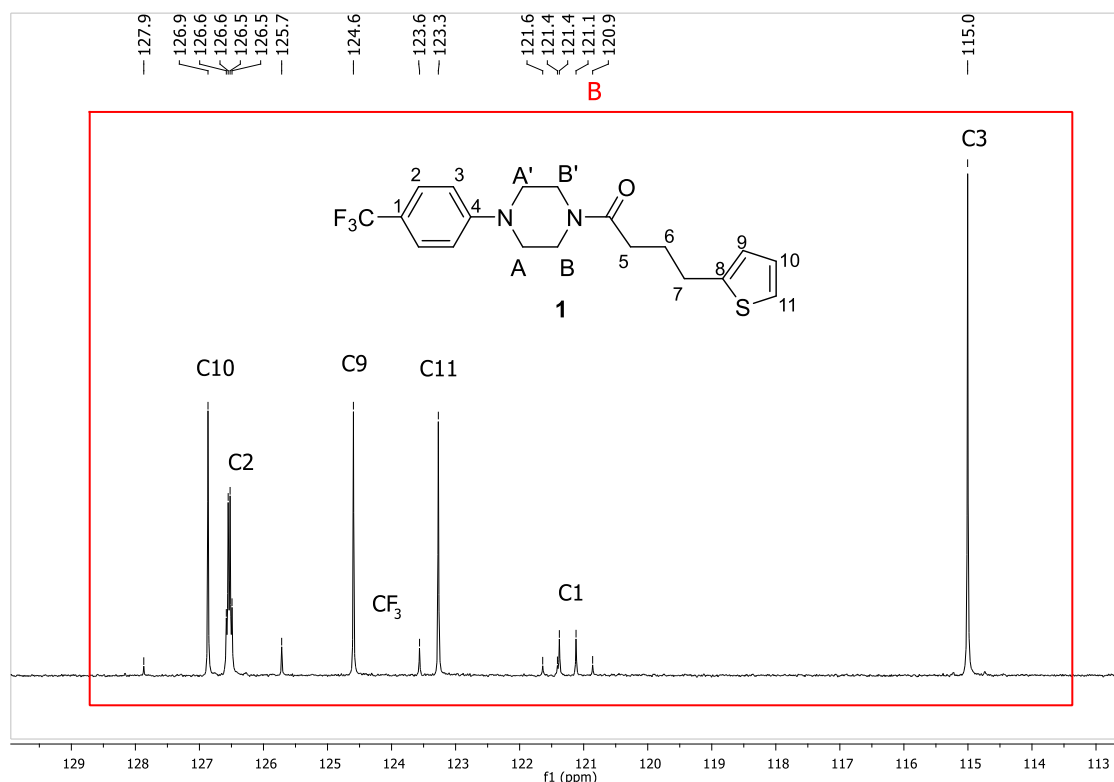
Figure 34: Region B of the ^{13}C NMR spectrum of RTC1.

The three other signals present in region B of the ^{13}C NMR spectrum of RTC1 appear as quartets due to the coupling between the ^{13}C nucleus and the NMR-active ^{19}F nucleus, which is the third most receptive NMR nucleus and has a nuclear spin of a half.[59] The carbon spectra generated are not fluorine-19 decoupled so coupling between ^{13}C-^{19}F was observed. The signal of the tertiary carbon *ortho* to the trifluoromethyl group (C2) appears as a quartet at 126.6 ppm with a *J* value of 3.7 Hz. The signal of the trifluoromethyl carbon appears as a quartet at 125.6 ppm with a *J* value of 271.3 Hz. The signal of the quaternary carbon bonded to the trifluoromethyl group (C1) appears as a quartet at 121.2 ppm with a *J* value of 32.8 Hz.

The assignment of the quaternary carbons in region B of the ^{13}C NMR spectrum employed a Distortionless Enhancement of Polarization Transfer (DEPT) experiment. This experiment uses a 135-degree decoupler pulse (DEPT-135) to produce a carbon spectrum with positive signals for methyl (CH$_3$) and methine (CH) carbons, and negative signals for methylene (CH$_2$) carbons. As the quaternary carbons are not bonded to any protons, they can be identified due to their absence from the DEPT-135 spectrum of RTC1 (Figure 35). The tertiary carbons of the aromatic ring (C2 & C3) and thiophene ring (C9, C10 and C11) all appear as positive signals in the DEPT-135 spectrum as they are each bonded to one proton.
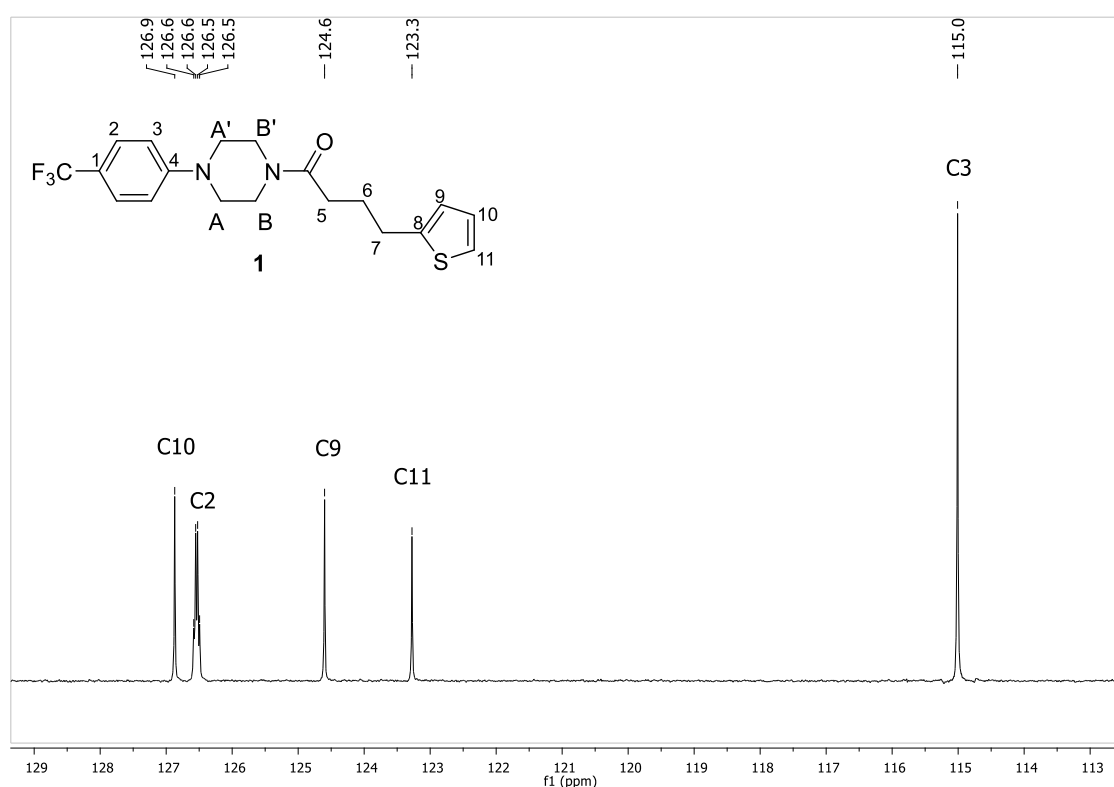
Figure 35: DEPT-135 spectrum of region B of the ^{13}C NMR spectrum of RTC1.

The assignment of the tertiary carbon signals in region B was also confirmed using a ^{1}H-^{13}C Heteronuclear Single Quantum Correlation (^{1}H-^{13}C HSQC) experiment (Figure 36) which is a 2D-NMR technique that correlates chemical shifts of directly bound nuclei (i.e. ^{1}H with ^{13}C). Using the information already obtained from the ^{1}H NMR spectrum (section **2.2.3.1**), the tertiary carbons from region B of the ^{13}C NMR spectrum were assigned by correlating their ^{13}C signal with the corresponding ^{1}H signal in the HSQC spectrum. For

example, the carbon signal at 123.3 ppm was identified as C11 as it correlates with the H11 proton signal at 7.13 ppm (red lines) (Figure 36).
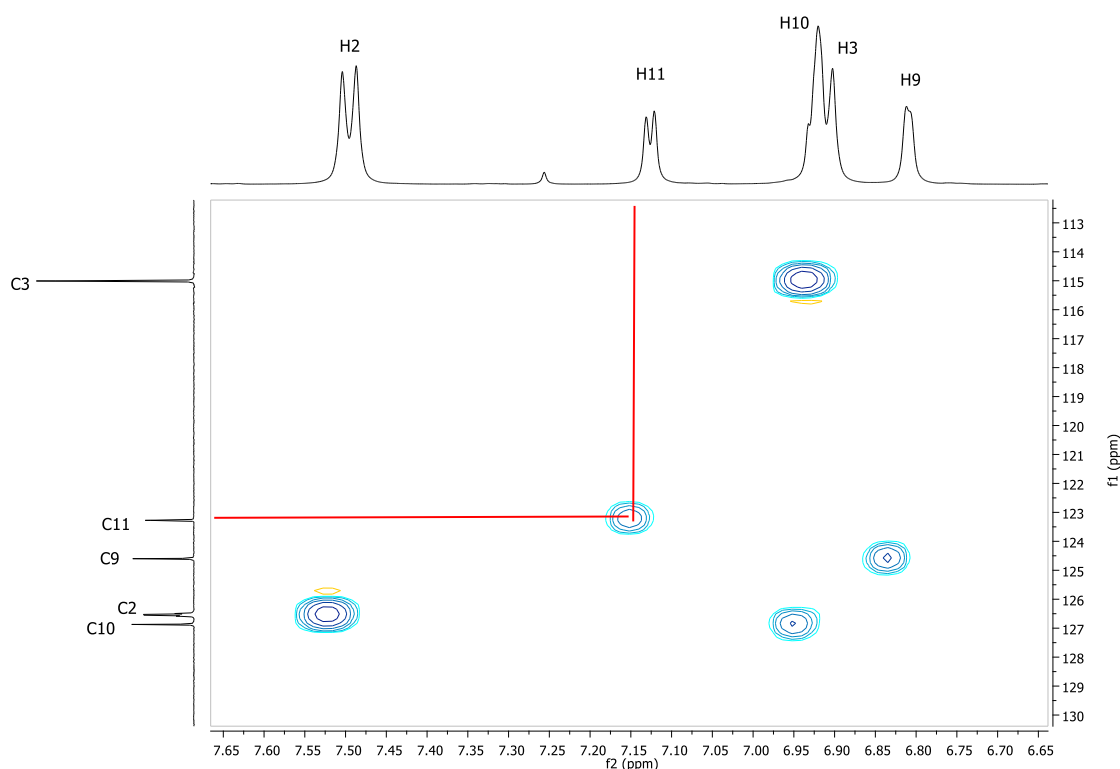
Figure 36: Region B of the ^{1}H-^{13}C HSQC spectrum of RTC1.

The assignments made using the DEPT and ^{1}H-^{13}C HSQC experiments were also confirmed using the ^{1}H-^{13}C HMBC experiment (Figure 37) which shows long range ^{1}H-^{13}C coupling. The quaternary *ipso* carbon (C1) was shown to couple with the aromatic protons (H2 & H3) (red lines) while the quaternary carbon from the trifluoromethyl group coupled to just H2 (blue lines). The tertiary carbons were all coupled to the neighbouring protons which were 2-3 bonds away from them. For example, C10 of the thiophene ring was observed to couple to H9 and H11, and weakly to H7 of the alkyl chain (green lines). H7 of the alkyl chain was observed to be strongly coupled to C9 as it was closest to it, and weakly coupled to C10 and C11, which were further away from it.
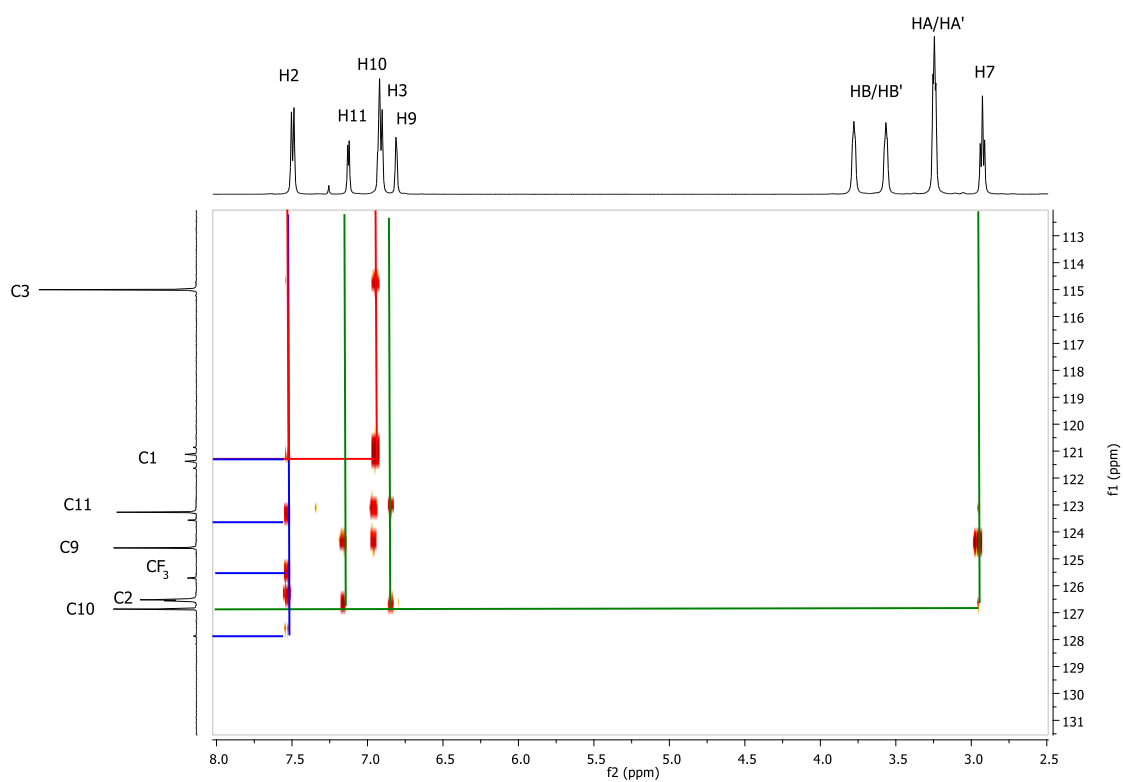
Figure 37: Region B of the ^{1}H-^{13}C HMBC spectrum of RTC1.

2.2.3.2.3 Region C of the ^{13}C NMR spectrum of RTC1

Region C of the ^{13}C NMR spectrum of RTC1 consists of seven signals that can be assigned to the secondary carbons of the piperazine ring and the alkyl chain (Figure 38).
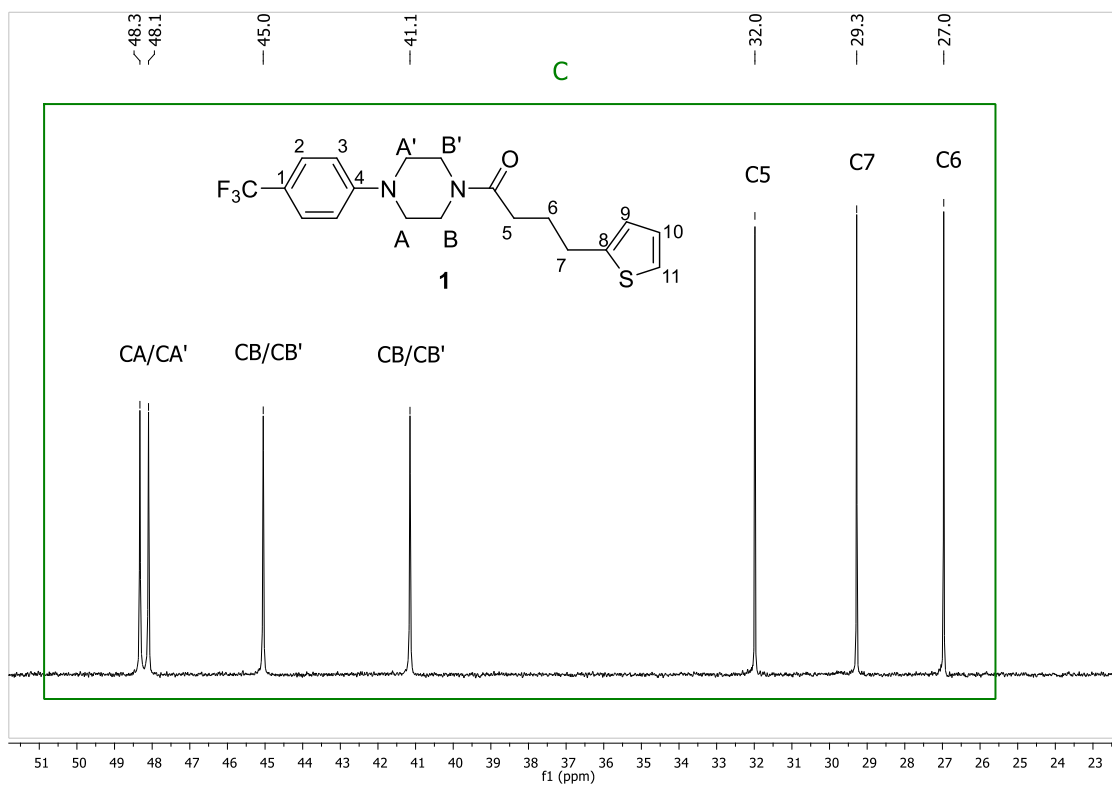
Figure 38: Region C of the ^{13}C NMR spectrum of RTC1.

These seven signals all appear negative in the DEPT-135 spectrum (Figure 39) as the carbons they represent are bonded to two hydrogens.
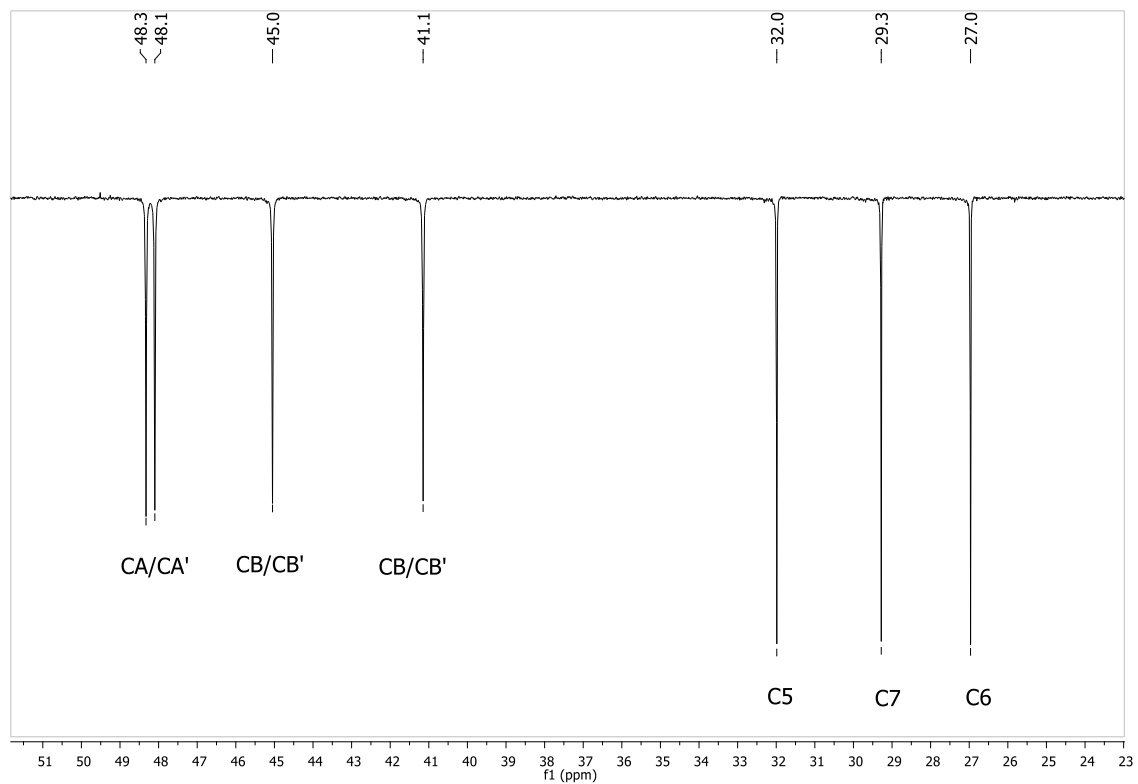
Figure 39: Region C of the DEPT-135 spectrum of RTC1.

These signals were assigned using the 2D-NMR ^{1}H–^{13}C HSQC spectrum (Figure 40). Here, the four signals resonating most downfield (48.3, 48.1, 45.0, and 41.1 ppm) are the secondary carbons of the piperazine (CA/CA' and CB/CB') and show a coupling to the piperazine protons (HA/HA' and HB/HB'). The signal at 32.0 ppm can be assigned to C5, the signal at 29.3 ppm to C7, and the signal at 27.0 ppm to C6. Again, in the HSQC, clear coupling can be seen with their corresponding proton signals.
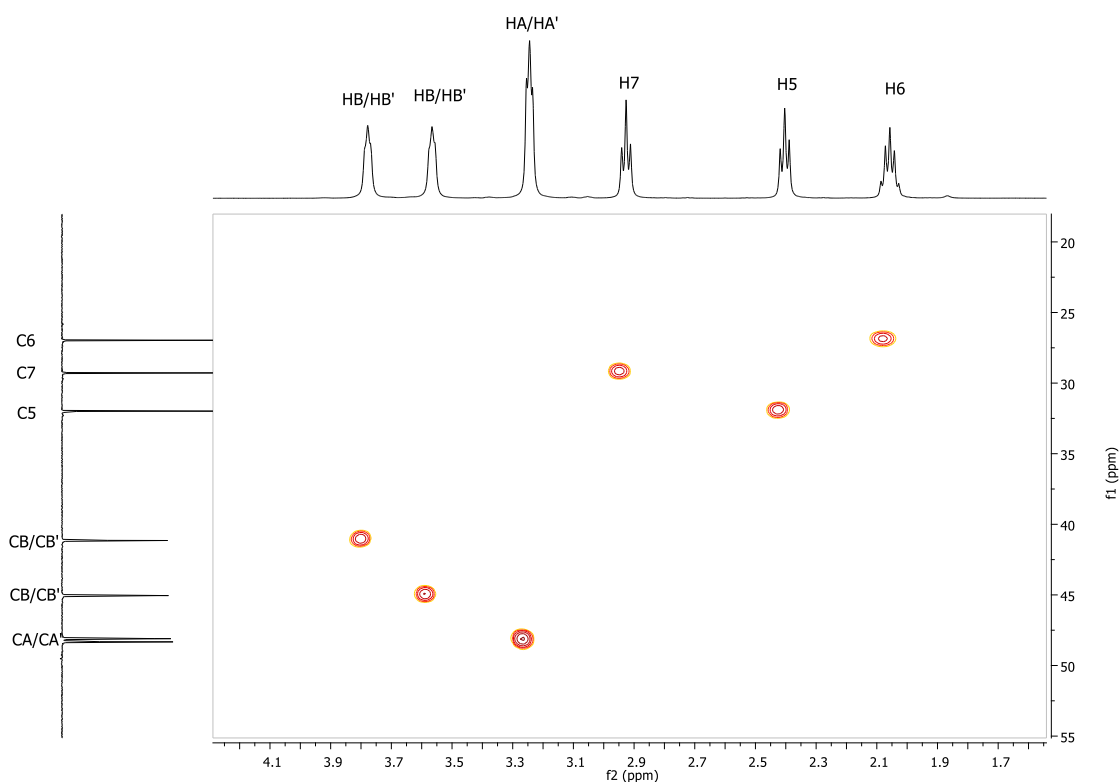
Figure 40: Region C of ^{1}H-^{13}C HSQC spectrum of RTC1.

The assignments made using the DEPT and ^{1}H-^{13}C HSQC experiments were confirmed using the ^{1}H-^{13}C HMBC experiment (Figure 41) which show long range ^{1}H-^{13}C coupling. Each carbon signal was shown to be coupled with the neighbouring protons within 2-3 bonds. For example, C6 of the alkyl chain was observed to be coupled to H5 and H7 (red lines). Similarly, C5 was coupled to H6 and H7. The carbon of the alkyl chain closest to the thiophene ring, C7, did not only couple to H5 and H6 of the alkyl chain, but also coupled to H9 of the thiophene ring, as it was three bonds away (blue lines). The other protons of the thiophene ring, H10 and H11, were more than three bonds away and therefore no coupling was observed. The piperazine carbons showed coupling to the piperazine protons as expected.
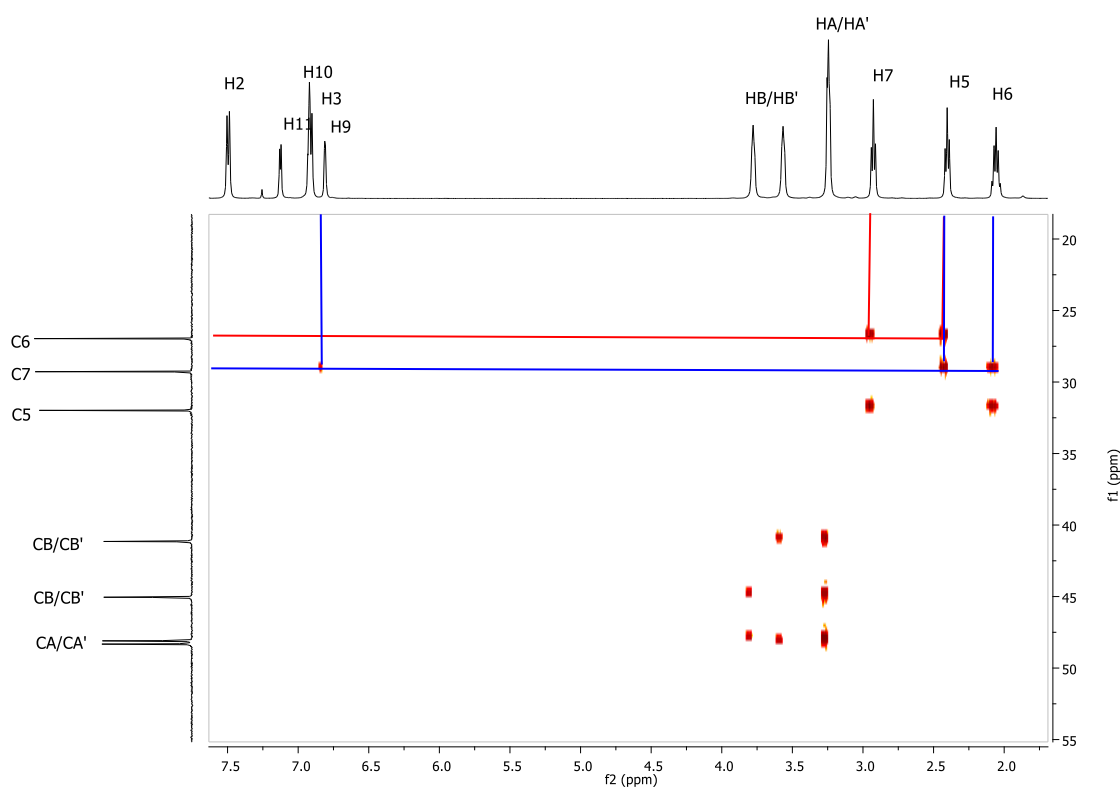
Figure 41: Region C of the ^{1}H-^{13}C HMBC spectrum of RTC1.

2.2.3.3 The ^{19}F NMR spectrum of RTC1

As mentioned previously, fluorine has an NMR-active ^{19}F isotope with a nuclear spin of a half (I = ½). It is the third most receptive NMR nucleus with many applications in medicinal chemistry and chemical biology.[60] The ^{19}F spectrum is ^{1}H and ^{13}C decoupled in order to just show the signals arising from the fluorine atoms in the compounds. For the ^{19}F spectrum of RTC1 (Figure 42), a singlet signal was observed at -61.4 ppm for the three equivalent fluorines of the trifluoromethyl group.
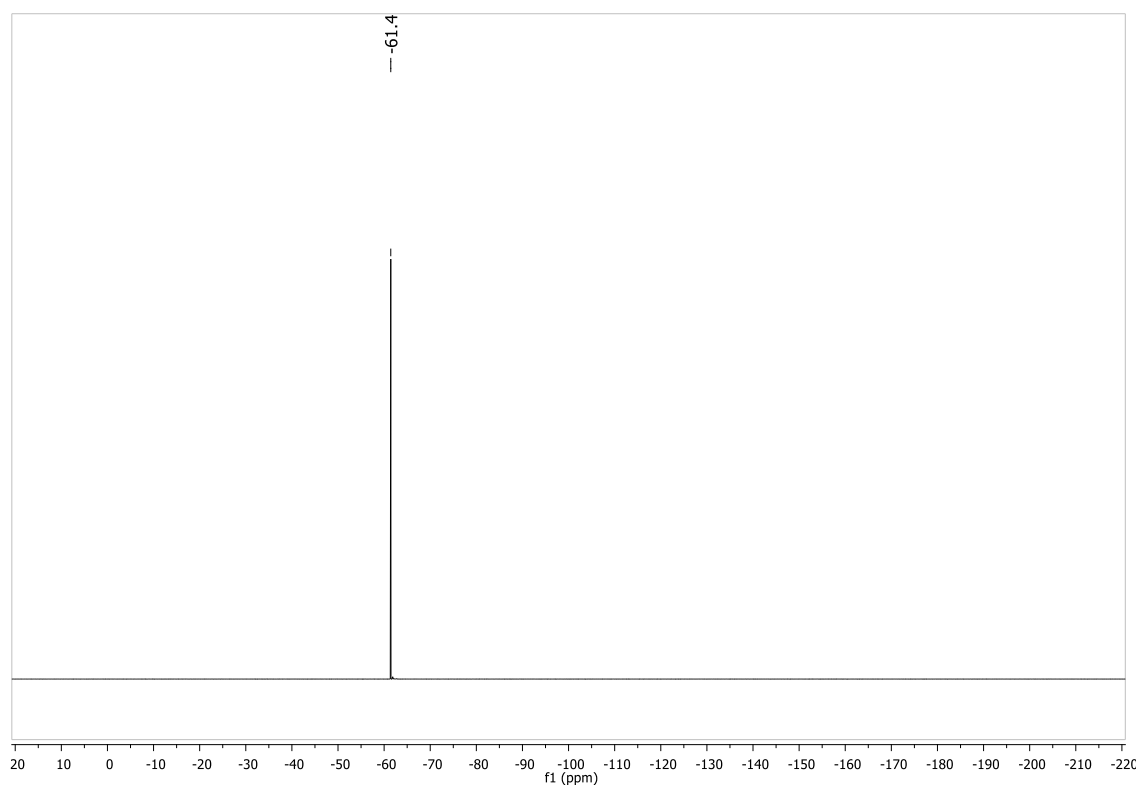
Figure 42: The ^{19}F NMR spectrum of RTC1.

A 2D-NMR experiment known as ¹H-¹⁹F Heteronuclear Overhauser Effect Spectroscopy (HOESY) can be used to assess the spatial proximity between two heteronuclei such as ¹H and ¹⁹F. The ¹H-¹⁹F HOESY spectrum of RTC1 (Figure 43) shows that the fluorine of the trifluoromethyl group is in close spatial proximity to the protons of the aromatic ring (H2 and H3) as well as the piperazine protons (HA/HA').
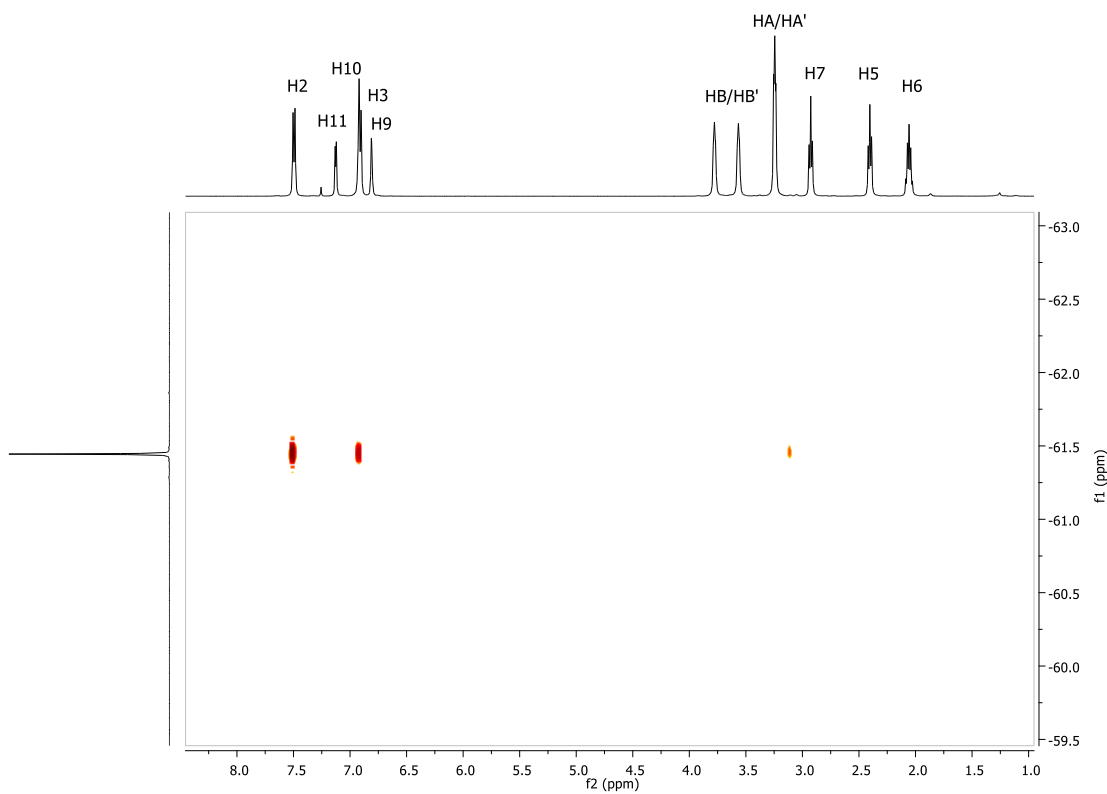
Figure 43: The ¹H-¹⁹F HOESY spectrum of RTC1.

2.2.3.4 Mass spectrum of RTC1

Mass spectrometry (MS) is a powerful analytical technique used to quantify known materials, to identify unknown compounds within a sample, and to help elucidate the structure of molecules. A typical process of mass spectrometry involves the conversion of the sample into gaseous ions, with or without fragmentation, which are then characterized by their mass to charge ratios (m/z) and relative abundances. Mass spectrometry was used in the characterisation of our compounds to further confirm the presence or absence of the target compounds. The mass (m/z) obtained for each compound was within 5 ppm of the calculated mass for that compound.

The mass spectrum (Figure 44) of RTC1 showed that the high-resolution mass obtained for $C_{19}H_{22}F_3N_2OS$, the protonated version of the product (i.e. $[M + H]^+$), is 383.1398 m/z, which is -0.26 ppm from the calculated mass of 383.1399 m/z. It also found the mass for $C_{19}H_{21}F_3N_2OSNa$, the product plus a sodium cation (i.e. $[M + Na]^+$), was found to be 405.1228 m/z, which is 2.2 ppm different from the calculated mass of 405.1219 m/z .
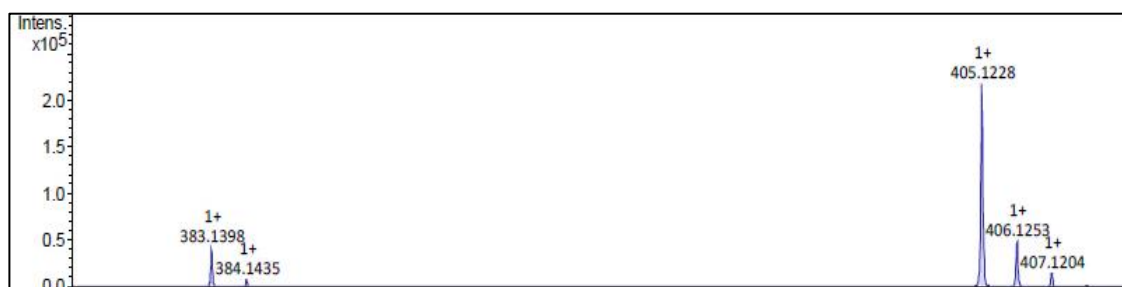
Figure 44: Mass spectrum of RTC1.

2.2.3.5 Infrared spectrum of RTC1

Infrared (IR) spectroscopy is an optical technique that detects molecular bond vibrations and rotations upon absorption of infrared light.[61] IR spectroscopy can be used for chemical structure analysis, chemical fingerprinting, and chemical imaging as different chemical functional groups absorb IR light at different frequencies. An IR spectrum displays transmittance on the vertical axis versus wavelength on the horizontal axis, and can be obtained using a fourier-transform infrared (FTIR) spectrometer. Liquid samples can be tested using sodium chloride plates, whereas solid samples are typically grinded with potassium bromide (KBr) to form KBr disks.

More recently, test compounds can be analysed by the more efficient attenuated total reflection (ATR) method, which enables samples to be examined directly in the solid or liquid state without further preparation.[62] ATR-FTIR operates by measuring the changes that occur in an internally reflected IR beam when it encounters the test sample. The way this takes place is that an IR beam is directed onto an optically dense crystal with a high refractive index at a certain angle. This internal reflectance creates an evanescent wave that extends beyond the surface of the crystal onto the sample held in contact with the crystal.[63] In regions of the IR spectrum where the sample absorbs energy, the evanescent wave will be attenuated. The attenuated beam then returns to the crystal, exits the opposite end of the crystal, and is directed onto the detector in the IR spectrometer. The detector records the attenuated IR beam as an interferogram signal, which can be used to generate an IR spectrum.[63]

The IR spectrum of RTC1 (Figure 45) showed an absorption band of 2925 cm^{-1} characteristic of the aliphatic C-H bonds, 1652 cm^{-1} characteristic of the carbonyl group C=O stretch, 1612 cm^{-1} characteristic of the C=C bond stretch, and 1329 cm^{-1} for the C-F bond stretch. These characteristic functional groups further confirmed the successful formation of RTC1.
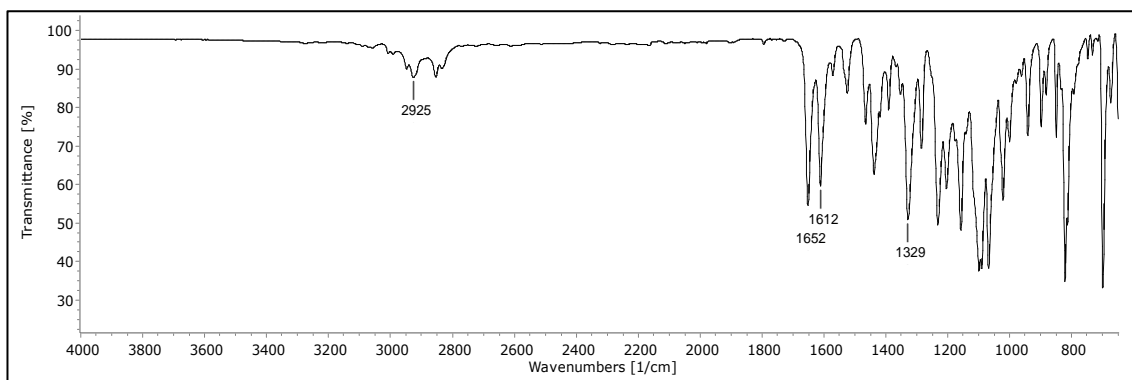
Figure 45: IR spectrum of RTC1.

2.3 Synthesis of compounds with structural variations at site A: the aryl group

As mentioned previously, structure modifications were carried out on RTC1 (Figure 46) at five different sites in order to explore the relationship between structure and biological activity. The first site examined was site A, where variations were made on the aryl group. For RTC1, site A consisted of an aromatic ring with a *para* substituted trifluoromethyl group.
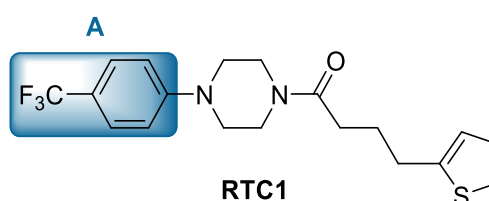
Figure 46: Structure of RTC1 showing site A – the aryl group.

Fluorine is the most electronegative element and has its 2s and 2d electrons close to the nucleus.[64,65] It has been found that a strong bond between carbon and fluorine leads to high thermal and chemical stabilities of fluorinated compounds.[64] These compounds also have a low dielectric constant due to the low polarizability of the C–F bond along with its hydrophobic character.[65] The trifluoromethyl (CF_3) group is significantly electron withdrawing and is often described as being intermediate between the electronegativities of fluorine and chlorine.[66] The CF_3 group has been used in many medicinal agents due to its unique chemical and physiological stability[67], and has been widely reported to result in pharmacological and chemotherapeutic effects.[68] Agents containing the trifluoromethyl group include anaesthetic, antidepressant, antiviral, and diuretic agents.[64] It has also been found in the selective PPAR-δ agonist pyridyloxybenzene-acylsulfonamides, which is a potential novel agent for the treatment of type 2 diabetes.[69]

Compounds containing variations at site A were synthesised using the new method discussed in section **2.2.1**. This involved the coupling of the corresponding arylpiperazine with 4-(2-thienyl)butyric acid using HOBt/TBTU coupling reagents and NEt_3. The reaction mixture in DMF or DCM was stirred at room temperature overnight and purified using column chromatography (Scheme 6).
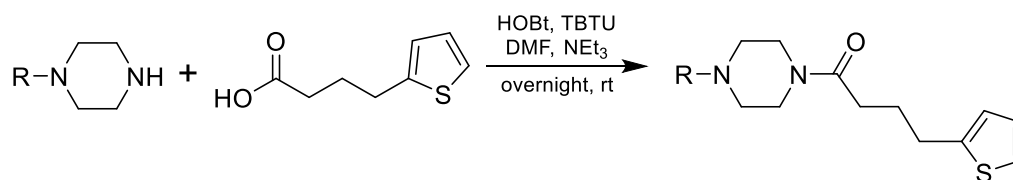
Scheme 6: General reaction of compounds made with variations at site A.

The acid derivative, 4-(2-thienyl)butyric acid, was commercially available and all the corresponding arylpiperazine starting materials were commercially available, with the exception of 1-(2-chloro-4-(trifluoromethyl)phenyl)piperazine (MK21) **6**. The synthesis of this starting material consisted of dissolving 3-chloro-4-fluorobenzotrifluoride and piperazine in *N*-methyl-2-pyrrolidone (NMP) and heating the reaction at 200 °C for 30 minutes in a microwave (MW) reactor (Scheme 7). The reaction mixture was purified using column chromatography to give the product as an orange oil in a 63% yield.
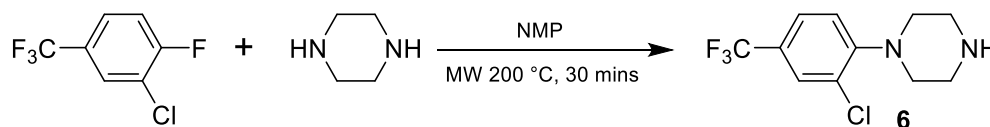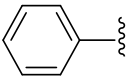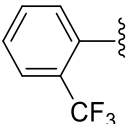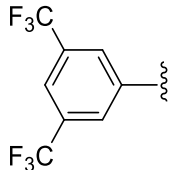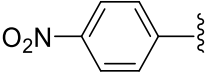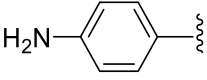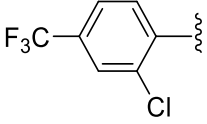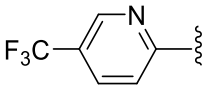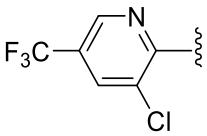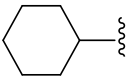
Scheme 7: Synthesis of compound **6**, 63% yield.

Structure variations of the aryl group (site A) of RTC1 consisted of removing the CF$_3$ group, i.e. an unsubstituted phenyl ring (compound **7**), moving the CF$_3$ group to the *ortho* position (compound **8**), and adding a second CF$_3$ group, i.e. the bistrifluoromethyl substitution pattern (compound **9**). Compounds were also made that replaced the *para* trifluoromethyl group with another electron withdrawing group, a nitro group (compound **10**), and an electron donating group, an amine group (compound **11**). We also wanted to explore the addition of a second halogen substituent and this resulted in the chlorine substituted compound **12**. Additionally, we examined if replacing the aromatic ring with a heterocyclic ring would affect the biological activity. To do this, we synthesised the pyridine-containing compounds **13** and **14** (Table 1).

Triflouromethyl groups are hydrophobic in nature. Hence, we were interested to know if replacing the *para* CF$_3$ aromatic ring with other hydrophobic groups, e.g. cyclohexyl (compound **4**) or methyl (compound **15**), would have a negative effect on biological activity (Table 1).

Table 1: Compounds synthesised with variations at site A.

Compound	R	Yield
7 (MK38)		78%
8 (MK41)		82%
9 (MK44)		86%
10 (MK39)	O_2N-	84%
11 (MK70)	H_2N-	35%
12 (MK20)	F_3C-, Cl	83%
13 (MK42)	F_3C-	91%
14 (MK45)	F_3C-, Cl	87%
4 (MK43)		82%
15 (MK36)	Me	70%

All yields for the final step were in the range of 70 – 90%, except for 1-(4-(4-aminophenyl)piperazin-1-yl)-4-(thiophen-2-yl)butan-1-one (MK70) **11**. The synthesis of this compound consisted of a reduction reaction of 1-(4-(4-nitrophenyl)piperazin-1-yl)-4-(thiophen-2-yl)butan-1-one (MK39) **10** (Scheme 8).
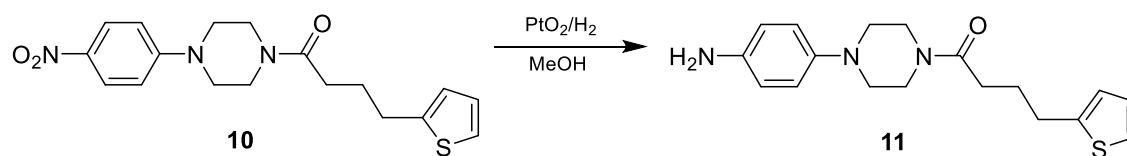
Scheme 8: Synthesis of compound **11** by the reduction of compound **10** using H_2 gas and PtO_2 (Adam's catalyst), 35% yield.

This reduction reaction was carried out using platinum oxide (PtO_2), also known as Adam's catalyst, in methanol (MeOH) with overnight stirring under an atmosphere of H_2 gas. The reaction mixture was passed through a bed of Celite to remove the platinum oxide and the filtrate was concentrated under reduced pressure, before purification using column chromatography. The lower yield of this compound was not totally unexpected as primary amines are often difficult to purify.

2.3.1 Structural characterisation of compounds made with variations at site A

Structural characterisation of compounds **4**, **7**-**15** was carried out in the same manner as for RTC1, whose structural characterisation was explained in detail in section **2.2.3**, and employed ^{1}H, ^{13}C, ^{19}F, and 2D-NMR spectroscopy, IR spectroscopy, and mass spectrometry.

2.3.1.1 Structural characterisation of 1-(4-phenylpiperazin-1-yl)-4-(thiophen-2-yl)butan-1-one (compound 7)
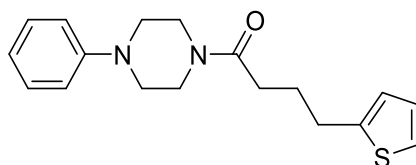
Figure 47: Structure of compound **7**.

Compound **7** (Figure 47) only differs from RTC1 at the aromatic ring. Hence, the spectroscopic data for compound **7** is very similar to RTC1 and only significantly differs for the aromatic signals. The aromatic region of the ^{1}H NMR spectrum for this compound contains four signals. The thiophene ring generates a doublet signal at 7.11 ppm and a multiplet signal in the range of 6.77 – 6.83 ppm, both integrating for 1H as expected. The multiplet signal in the range of 7.23 – 7.30 ppm, integrating for 2H, is assigned to the aromatic ring. The remaining multiplet signal in the range of 6.85 – 6.95 ppm is assigned to the three remaining hydrogens of the aromatic ring, and the remaining hydrogen of the thiophene ring. This signal integrates for 4H as expected.

The ^{13}C NMR spectrum also contains some differences compared to that for RTC1. We no longer see splitting due to F atoms and an additional CH signal can be observed at 116.6 ppm. The three ^{13}C CH signals for the aromatic ring in compound **7** occur at 129.2 ppm, 126.8 ppm, and 116.6 ppm. In addition, the signal at 1328 cm^{-1} for the C-F bond stretch in the IR spectrum of RTC1 is absent from the IR spectrum of this compound. The MS data also confirmed the generation of compound **7**.

2.3.1.2 Structural characterisation of 4-(thiophen-2-yl)-1-(4-(2-(trifluoromethyl)phenyl)piperazin-1-yl)butan-1-one (compound 8)
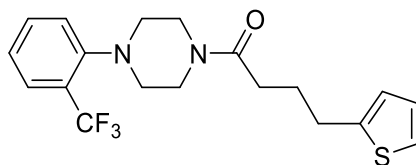
Figure 48: Structure of compound **8**.

The ^{1}H NMR spectrum of compound **8** (Figure 48) contains all the expected signals, many of which are again similar to those found for RTC1. The ^{1}H NMR signals of note occur in the aromatic region and were typical of an *ortho* substituted aromatic ring. The key ^{1}H NMR signals of the aromatic ring occur as a doublet at 7.64 ppm, integrating for 1H, a multiplet in the range of 7.48 – 7.56 ppm, also integrating for 1H, and a multiplet in the range of 7.21 – 7.33 ppm, integrating for 2H.

The ^{13}C NMR spectrum also displayed the expected signals along with ^{13}C-^{19}F splitting due to the presence of F atoms. The aromatic carbon *ipso* to the piperazine now appears as a doublet at 151.7 ppm due to ^{13}C-^{19}F splitting instead of the singlet signal in RTC1. Quartet signals appear at 123.9, 127.4, and 127.2 ppm for the trifluoromethyl group carbon (*C*F$_3$), the carbon bonded to the trifluoromethyl group (*C*-CF$_3$), and the CH carbon *ortho* to the trifluoromethyl group (*C*-C-CF$_3$), respectively. Singlet signals appear at 132.8, 124.0, and 123.1 ppm for the remaining carbons in the *para*, *meta*, and *ortho* position (relative to the piperazine) of the aromatic ring, which are four or more bonds away from the F atoms and therefore appear as singlet signals. The IR and MS data also confirmed the generation of compound **8**.

2.3.1.3 Structural characterisation of 1-(4-(3,5-bis(trifluoromethyl)phenyl)piperazin-1-yl)-4-(thiophen-2-yl)butan-1-one (compound 9)

Figure 49: Structure of compound **9**.

The ^{1}H NMR spectrum of compound **9** (Figure 49) differs from the ^{1}H NMR spectrum of RTC1 at the aromatic ring signals due to the bistrifluoromethyl substitution pattern. The ^{1}H NMR spectrum for this compound contains two singlet signals for the aromatic ring protons at 7.33 ppm and 7.24 ppm, representing the proton at the *para* position and the two protons at the *ortho* position of the aromatic ring (relative to the piperazine). The carbons bonded to these protons have corresponding signals in the ^{13}C spectrum at 112.7 ppm and 115.1 ppm, respectively, both appearing as multiplets due to ^{13}C-^{19}F coupling with the two trifluoromethyl groups. For the same reason, the signal for the trifluoromethyl carbon (CF$_3$) and the signal for the carbons bonded to the trifluoromethyl groups (C-CF$_3$) appear as quartets at 123.5 ppm and 132.5 ppm, respectively. The IR and MS data also confirmed the generation of compound **9**.

2.3.1.4 Structural characterisation of 1-(4-(4-nitrophenyl)piperazin-1-yl)-4-(thiophen-2-yl)butan-1-one (compound 10)

Figure 50: Structure of compound **10**.

Compound **10** (Figure 50) showed differences from RTC1 in the ^{1}H and ^{13}C NMR spectra as well as the IR spectrum due to the presence of the *para* nitro group in the aromatic ring. An important ^{1}H NMR signal is a doublet at 8.14 ppm, which is part of a double of doublets, and is assigned to the two aromatic protons *ortho* to the nitro group. This signal is more downfield than that for the corresponding CH signals in RTC1 due to the

deshielding effect caused by the electron withdrawing nitro group (Scheme 9). The aromatic ring signals appear as a double of doublets as the two pairs of protons on the aromatic ring are in different chemical environments. The other doublet signal of the aromatic ring is overlapping with a thiophene CH signal and hence appears as a multiplet in the range of 6.78 – 6.86 ppm, integrating for 3H as expected.
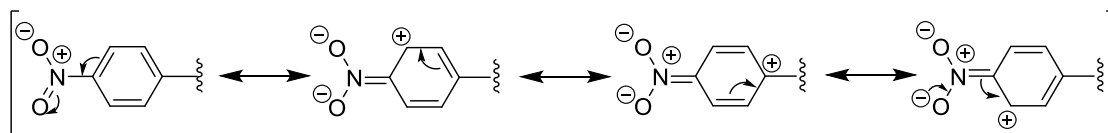
Scheme 9: Resonance structures for an aromatic ring with a *para* substituted nitro group.

The IR spectrum of compound **10** showed that the absorbance band for the C-F stretch from RTC1 was absent and an absorbance band at 1321 cm^{-1} for an NO_2 group was present. The MS data also confirmed the generation of compound **10**.

2.3.1.5 Structural characterisation of 1-(4-(4-aminophenyl)piperazin-1-yl)-4-(thiophen-2-yl)butan-1-one (compound 11)
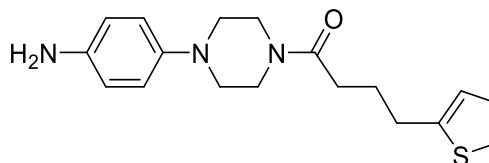
Figure 51: Structure of compound **11**.

While the ^{1}H NMR spectrum of compound **10** shows that the aromatic protons *meta* to the piperazine appear more downfield than in RTC1, due to the electron withdrawing nitro group, the ^{1}H NMR spectrum of compound **11** (Figure 51) shows the opposite effect. This is due to the presence of an electron donating *para* substituted amino group causing a shielding effect. The aromatic protons *meta* to the piperazine now appear as a multiplet more upfield in the ^{1}H NMR spectrum in the range of 6.77 – 6.82 ppm. As with compound **10**, the aromatic protons are expected to appear as a double of doublets due to the two pairs of protons being in different chemical environments. This can be explained by considering the resonance structures shown in Scheme 10, where electrons are delocalised into the aromatic ring from the amino group. For compound

11, the expected double of doublets appears as a somewhat poorly resolved double of multiplets.
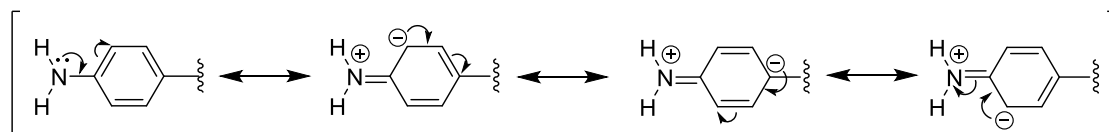
Scheme 10: Resonance structures for an aromatic ring with a *para* substituted amino group.

The IR spectrum shows an absorbance band at 3337 cm^{-1}, which is characteristic of a N-H bond stretch, and did not contain the C-F bond stretch that was found in the IR spectrum of RTC1. The MS data also confirmed the generation of compound **11**.

2.3.1.6 Structural characterisation of 1-(4-(2-chloro-4-(trifluoromethyl)phenyl)piperazin-1-yl)-4-(thiophen-2-yl)butan-1-one (compound 12)
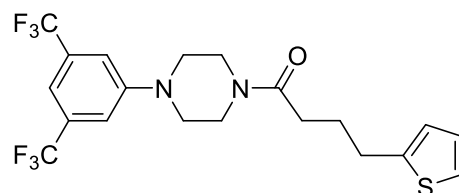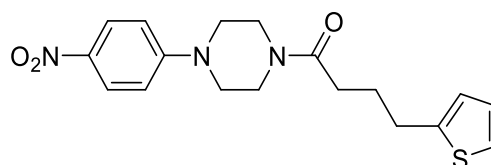

Figure 52: Structure of compound **12**.

Compound **12** (Figure 52) showed differences from RTC1 in the ^{1}H and ^{13}C NMR spectra as well as the IR spectrum, due to the presence of the *ortho* chloro substituent on the aromatic ring. In the ^{1}H NMR spectrum, the aromatic protons appear as three signals due to the absence of a plane of symmetry, as expected. The most deshielded signal at 7.64 ppm was assigned to the proton between the electron withdrawing CF$_3$ and chlorine substituents, which was further deshielded due to the electron withdrawing properties of the neighbouring chlorine substituent.

This signal appears as a doublet (*J* = 1.7 Hz) due to long range coupling with the proton in the *meta* position (relative to the piperazine), which is four bonds away from it. This coupling is common in aromatic rings and is known as *meta* coupling or "W-coupling" (Figure 53). The signal at 7.48 ppm was assigned to the other *meta* proton (relative to

the piperazine) which appears as a double of doublets (J = 8.4, 1.7 Hz) due to coupling to two non-equivalent protons (Figure 53). The third signal is a doublet at 7.05 ppm, which results from the *ortho* proton (relative to the piperazine) and has a coupling constant of J = 8.4 Hz.
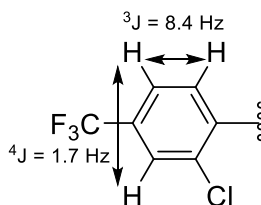
Figure 53: Long-range *meta* ("W") coupling between the *meta* protons (J = 1.7 Hz) and short-range coupling between the *ortho* and *meta* protons (J = 8.4 Hz) of the aromatic ring.

The ^{13}C NMR spectrum of compound **12** also confirms its synthesis as it contains two extra signals when compared to the ^{13}C spectrum of RTC1. The first signal is a quaternary ^{13}C signal at 128.8 ppm for the CH carbon bonded to the chlorine. The second signal is a quartet at 128.0 ppm for the carbon between the CF$_3$ and Cl groups. In the IR spectrum, an absorbance band at 694 cm^{-1}, which can be assigned to the C-Cl bond. The MS data also confirmed the generation of compound **12**.

2.3.1.7 Structural characterisation of 4-(thiophen-3-yl)-1-(4-(5-(trifluoromethyl)pyridin-2-yl)piperazin-1-yl)butan-1-one (compound 13)
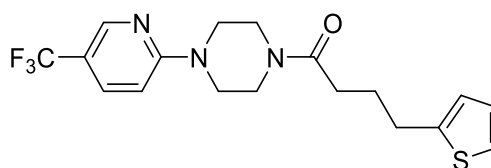
Figure 54: Structure of compound **13**.

The ^{1}H NMR spectrum of compound **13** (Figure 54) shows three pyridine signals in the aromatic region. The proton adjacent to the nitrogen of the pyridine ring appears most deshielded at 8.41 ppm due to the electron withdrawing effect of the nitrogen, as expected, with a multiplicity of a singlet. The other proton adjacent to the trifluoromethyl group, in the *meta* position relative to the piperazine, appears as a

double of doublets at 7.66 ppm. The multiplicity is due to coupling with the other *meta* proton (long-range "W" coupling as before) and also with its neighbouring proton (*ortho* to the piperazine). The third pyridine proton in the *ortho* position appears most upfield at 6.64 ppm and is a doublet due to coupling with the neighbouring proton. The key ^{13}C NMR signals appear as a quartet at 145.8 ppm for the CH carbon bonded to the nitrogen, a quartet at 134.7 ppm for the other *meta* carbon relative to the piperazine coupling with CF$_3$, and a singlet at 105.7 ppm for the CH carbon in the *ortho* position, relative to the piperazine. The IR and MS data also confirmed the generation of compound **13**.

2.3.1.8 Structural characterisation of 1-(4-(3-chloro-5-(trifluoromethyl)pyridin-2-yl)piperazin-1-yl)-4-(thiophen-2-yl)butan-1-one (compound 14)
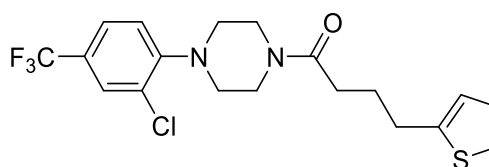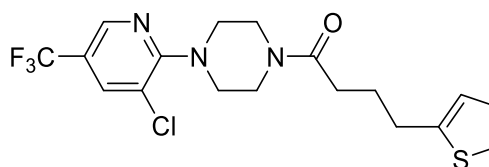

Figure 55: Structure of compound **14**.

Similar to compound **13**, compound **14** (Figure 55) also contained a pyridine. However, compound **14** also had an *ortho* substituted chlorine, which resulted in only two pyridine signals in the ^{1}H NMR spectrum. These signals appear more deshielded than the corresponding signals in RTC1 as expected. This is due to the electron withdrawing effects of the nitrogen and chlorine. As with compound **13**, the first proton appears as a singlet at 8.40 ppm, which represents the proton adjacent to the nitrogen. The second proton also appears as a singlet at 7.79 ppm, which represents the proton between the CF$_3$ and chlorine. The carbons bonded to these protons appear as quartets in the ^{13}C NMR spectrum at 143.0 ppm (*J* = 4.2 Hz) and 136.1 ppm (*J* = 3.3 Hz), respectively. In the IR spectrum, an absorbance band at 847 cm^{-1} can be observed for the C-Cl bond stretch. The MS data also confirmed the generation of compound **14**.

2.3.1.9 Structural characterisation of 1-(4-cyclohexylpiperazin-1-yl)-4-(thiophen-2-yl)butan-1-one (compound 4)
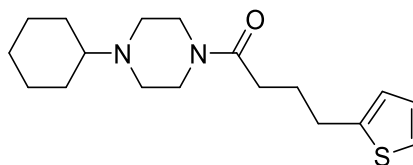
Figure 56: Structure of compound **4**.

The ^{1}H and ^{13}C NMR spectra of compound **4** (Figure 56) are significantly different from the spectra of RTC1 due to the replacement of the aromatic ring with a cyclohexyl group. The ^{1}H NMR spectrum for compound **4** shows five additional multiplet signals in the aliphatic region. The proton signal for CH attached to the piperazine appears in the range of 2.25 – 2.32 ppm, integrating for 1H, and is most deshielded due to its close proximity to an electronegative nitrogen. The protons in the 2- and 3-positions appear in the range of 1.73 – 1.93 ppm and 1.14 – 1.31 ppm respectively, each signal integrating for 4H. The protons in the 4-position appear as two multiplet signals in the range of 1.56 – 1.69 ppm and 1.04 – 1.14 ppm, each integrating for 1H.

The ^{13}C NMR spectrum contains four signals for the cyclohexyl carbons. The most downfield signal at 63.6 ppm is for the CH carbon bonded to the piperazine ring, which is the most deshielded cyclohexyl carbon as it is directly bonded to the electronegative nitrogen. The signals for the carbons in the 2, 3 and 4-position appear at 28.8 ppm, 25.8 ppm, and 26.2 ppm, respectively. The IR and MS data also confirmed the generation of compound **4**.

2.3.1.10 Structural characterisation of 1-(4-methylpiperazin-1-yl)-4-(thiophen-2-yl)butan-1-one (compound 15)
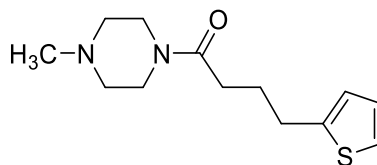
Figure 57: Structure of compound **15**

The final compound in the group with variations at site A is compound **15** (Figure 57), and also shows some differences in the ^{1}H and ^{13}C NMR spectra when compared to those of RTC1. Similar to compound **4**, the ^{1}H and ^{13}C NMR spectra of course do not contain any signals for the aromatic ring as found with RTC1. Instead, an extra singlet signal for the methyl group protons appears at 2.29 ppm, integrating for 3H, while the corresponding carbon appears at 46.0 ppm in the ^{13}C NMR spectrum. The IR and MS data also confirmed the generation of compound **15**.

2.4 Synthesis of compounds with structural variations at site B: the piperazine ring

The second site of variation examined was the piperazine ring (site B) (Figure 58). It is important to have variations at this site to establish whether a nitrogen-containing heterocyclic ring, such as a piperazine ring or indeed a piperidine ring, is needed for activity, or if instead a simple amide linkage can maintain biological activity. The piperidine ring will also indicate the importance of having the second nitrogen of the piperazine ring on biological activity.
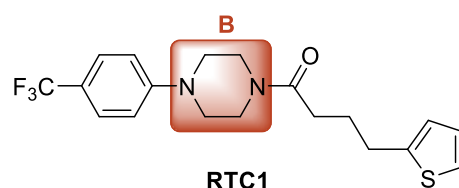
Figure 58: Structure of RTC1 showing site B – the piperazine ring.

The piperazine ring contains two nitrogen atoms in a 1,4-relationship within a 6-membered heterocyclic ring. It has many medicinal applications such as antiviral[70], antiobesity[52], antidepressant[71], antibacterial[72], and antiulcer[72] (Figure 59). It has many uses as an antithelmintic agent where it works to paralyze parasites that may invade the host body and cause disease[73], and act as a gamma-amino-butyric acid receptor agonist in nematodes.[74] It has also been associated with network formation and photoluminescence in copper(I) halide complexes.[75] Medicines containing piperazine are used to treat diseases such as ascariasis or enterobiasis.[73]
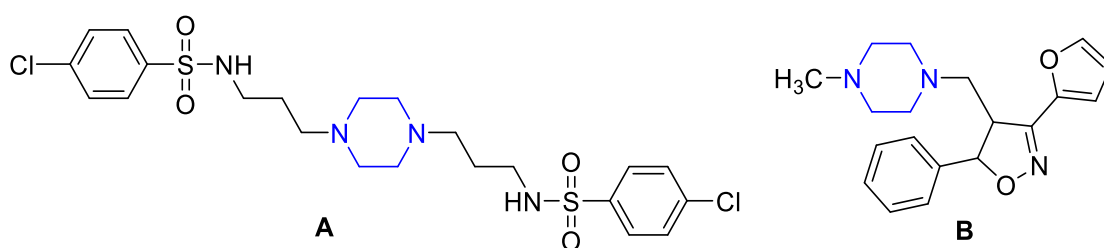
Figure 59: Structure of piperazine-based analogues that act as an antiviral (A)[70] or antidepressant (B)[71] agents.

Two derivatives of RTC1 were synthesised with variations at the piperazine ring (site B). For compound **16**, the piperazine ring was replaced by a piperidine ring and for compound **17**, the piperazine ring was replaced by an NH (amine linkage).

2.4.1 Synthesis and structural characterisation of 4-(thiophen-2-yl)-1-(4-(4-(trifluoromethyl)phenyl)piperidin-1-yl)butan-1-one (compound 16)

Compound **16** was synthesised using the new method discussed in section **2.2.1**. Again, coupling of 4-(4-(trifluoromethyl)phenyl)piperidine with 4-(2-thienyl)butyric acid, using HOBt/TBTU coupling reagents and NEt$_3$, was utilised (Scheme 11). The reaction mixture, in DMF, was stirred at room temperature for 24 hours and purified using column chromatography (3:2, ethyl acetate (EtOAc):*n*-hexane) to give an off-white solid in a 67% yield.
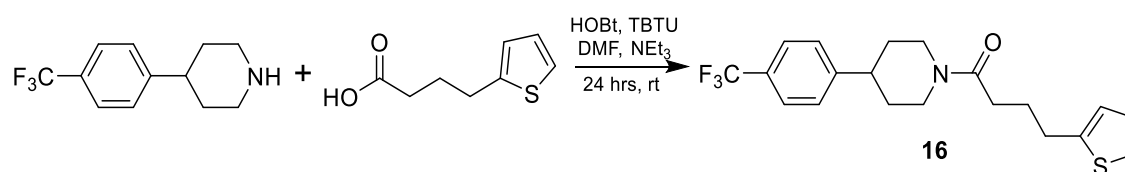
Scheme 11: Synthesis of compound **16**, 67% yield.

This compound has different ^{1}H and ^{13}C NMR spectra in comparison with RTC1 due to the replacement of the piperazine ring with a piperidine ring, most noticeably in the area where the piperazine signals occurred. Seven signals appear in the ^{1}H NMR spectrum due to the piperidine ring. The protons bonded to the carbons adjacent to the electronegative nitrogen appear as four separate signals; two doublet signals at 4.82 and 3.92 ppm, and two triplet signals at 3.10 ppm and 2.63 ppm. These four signals were shown to couple with the quaternary carbonyl carbon at 170.9 ppm in the ^{1}H-^{13}C HMBC spectrum (Figure 60).

The four protons further from the nitrogen appear as two multiplet signals in the range of 1.84 – 1.93 ppm and 1.52 – 1.68 ppm. The proton furthest to the nitrogen appears as a multiplet in the range of 2.74 – 2.85 ppm, integrating for 1H. These three signals coupled to the quaternary carbon of the aromatic ring at 149.2 ppm in the ^{1}H-^{13}C HMBC spectrum (Figure 60). The carbons bonded to these protons appear in the ^{13}C NMR spectrum at 46.0 ppm and 42.2 ppm for the carbons bonded to the nitrogen, at 33.7 ppm and 32.6 ppm for the carbons further from the nitrogen, and 42.7 ppm for the *ipso* carbon. The IR and MS data also confirmed the generation of compound **16**.
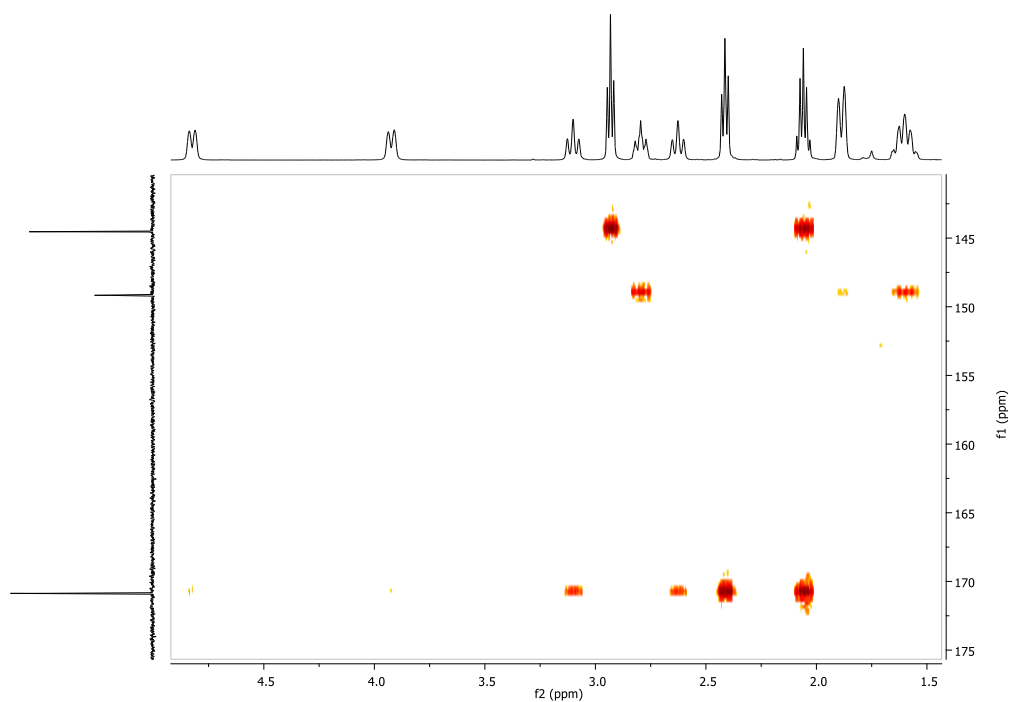
Figure 60: The ^{1}H-^{13}C HMBC spectrum of compound **16**

2.4.2 Synthesis and structural characterisation of 4-(thiophen-2-yl)-*N*-(4-(trifluoromethyl)phenyl)butanamide (compound 17)

Compound **17** was also synthesised using the new method discussed in section **2.2.1**. Once more, coupling 4-(trifluoromethyl)aniline with 4-(2-thienyl)butyric acid was carried out using HOBt/TBTU coupling reagents and NEt$_3$ (Scheme 12). The reaction mixture, in DMF, was stirred at room temperature for 20 hours and purified using column chromatography (3:2, EtOAc:*n*-hexane) to give a white solid in a 90% yield.
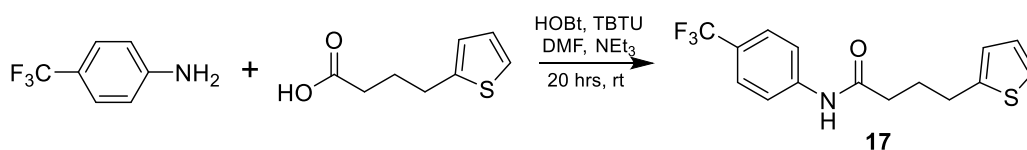
Scheme 12: Synthesis of compound **17**, 90% yield.

The replacement of the piperazine ring in RTC1 with a NH results in significantly different ^{1}H and ^{13}C NMR spectra. For compound **17** there are no piperazine signals present. Instead, a broad singlet at 7.29 ppm is observed in the ^{1}H NMR spectrum, which is assigned as the proton of the amide. Furthermore, the IR spectrum shows an absorbance band at 3304 cm^{-1}, which also confirms the presence of the amide linkage. The MS data also confirmed the generation of compound **17**.

2.5 Synthesis of compounds with structural variations at site C: the carbonyl group

The third site of variation examined on RTC1 was the carbonyl group (site C) (Figure 61). We deemed it important to establish the affect this group was having on biological activity.
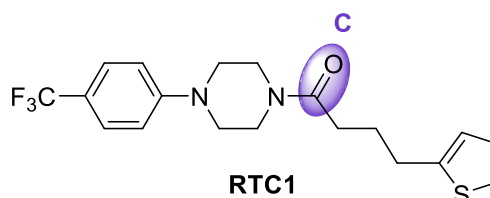
Figure 61: Structure of RTC1 showing site C – the carbonyl group.

A carbonyl group consists of a carbon atom double bonded to an oxygen atom. It is found in several functional groups such as aldehydes, ketones, anhydrides, and carboxylic acids. As oxygen is more electronegative than carbon, compounds containing a carbonyl group are polar, which results in an increase in the melting and boiling points as well as influencing their solubility. The polarity of the carbonyl bond allows it to partake in a variety of chemical reactions as nucleophilic reagents react at the carbonyl carbon atom (e.g. addition-elimination reactions), whereas electrophilic reagents, such as Lewis acid, interact with the carbonyl oxygen. It is found in many medicines due to its ability to participate in many non-covalent interactions with protein targets such as hydrogen-bonding, as it is a well-known hydrogen-bond acceptor.[76,77]

2.5.1 Synthesis and structural characterisation of 1-(4-(thiophen-2-yl)butyl)-4-(4-(trifluoromethyl)phenyl)piperazine (compound 18)

A single derivative was generated with the carbonyl group (site C) removed, 1-(4-(thiophen-2-yl)butyl)-4-(4-(trifluoromethyl)phenyl)piperazine (MK34) (compound **18**). The synthesis of this compound consisted of a three-step process involving (i) a reduction reaction, (ii) a mesylation reaction, and (iii) a nucleophilic substitution reaction (Scheme 13).
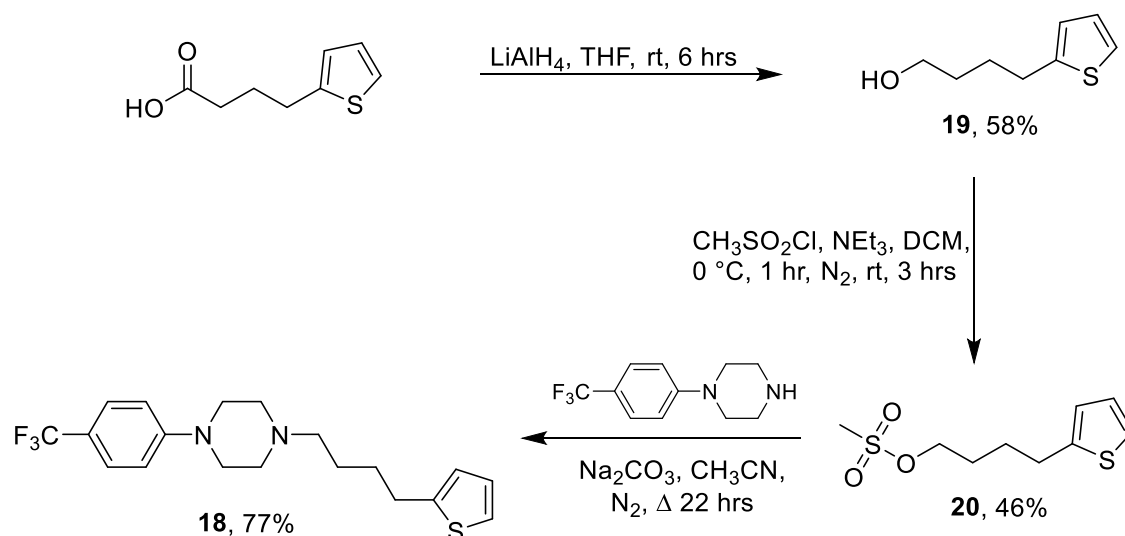
Scheme 13: Synthetic route to compound **18** using reduction, mesylation and nucleophilic substitution reactions.

The first reaction consists of the synthesis of 4-(thiophen-2-yl)butan-1-ol (MK32) **19** via the reduction of 4-(2-thienyl)butyric acid using lithium aluminium hydride (LiAlH₄) in anhydrous tetrahydrofuran (THF). After quenching the reaction mixture using deionised water (H₂O), and a work-up using HCl and EtOAc, the product was dried over MgSO₄ and under reduced pressure. The product was obtained as a pure orange oil in a 58% yield.

The second reaction, the mesylation reaction of compound **19**, used methanesulfonyl chloride and NEt₃ in anhydrous DCM. Work-up of this reaction also consisted of several washes using HCl and EtOAc, purification using column chromatography, and drying under reduced pressure, to obtain the product (compound **20**) as a colourless oil in a 46% yield.

The mesylation reaction converts the hydroxy group of the alcohol into a good leaving group, the methanesulfonyl group. The mesylation mechanism (Scheme 14) begins with the elimination of HCl from sulfonyl chloride to give the sulfene intermediate, followed by the nucleophilic attack of compound **19** to give 4-(thiophen-2-yl)butyl methanesulfonate (MK33) **20**.
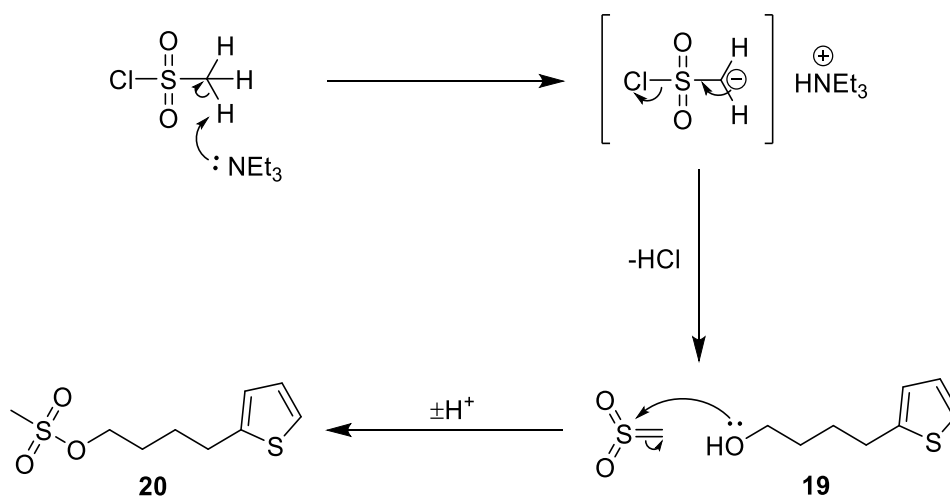
Scheme 14: Proposed mechanism for the synthesis of compound **20**.

The final reaction is a nucleophilic substitution reaction of compound **20** using the arylpiperazine as the nucleophile, and sodium carbonate (Na_2CO_3) as base. The reaction mixture in acetonitrile was refluxed for 22 hours with vigorous agitation and under a nitrogen atmosphere. After purification using column chromatography, the product, compound **18**, was obtained as a white solid in a 77% yield.

Compound **18** showed the expected differences in the ^1H and ^{13}C NMR spectra, and IR spectra from those of RTC1. The ^{13}C NMR spectrum no longer has a signal at 171.1 ppm due to the absence of the carbonyl carbon. Also, an extra proton signal at 2.87 ppm in the ^1H NMR spectrum and corresponding 29.8 ppm in the ^{13}C NMR spectrum is observed. These signals can be assigned to the CH_2 group that has replaced the carbonyl group. Furthermore, the IR spectrum does not contain a carbonyl absorbance band at 1652 cm^{-1}, as found in the IR spectrum of RTC1. The MS data also confirmed the generation of compound **18**.

2.6 Synthesis of compounds with structural variations at site D: the alkyl chain

The fourth site of variation examined was the alkyl chain (site D) (Figure 62) which links the carbonyl group to the thiophene ring.
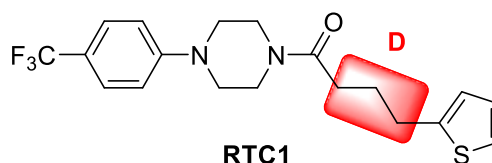
Figure 62: Structure of RTC1 showing site D – the alkyl chain.

The length and nature of the alkyl chain could have a significant effect on biological activity. Hence, investigating the optimum length for this alkyl chain was considered important, as was varying the nature of the linking chain.

Five compounds (compounds **21-25**) were made as part of this study (Table 2). Compounds **21**, **22**, **24**, and **25** were synthesised using the optimised method as discussed in section **2.2.1**. Again, coupling of compound **2** with the corresponding carboxylic acid derivative was performed using HOBt/TBTU as coupling reagents (Scheme 15). Purification was carried out using column chromatography.
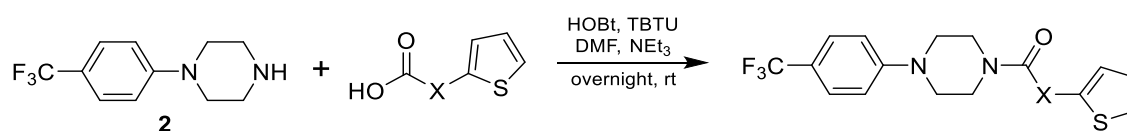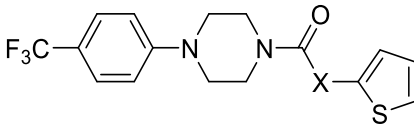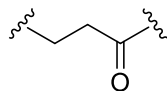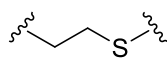
Scheme 15: General reaction for the synthesis of compounds **21**, **22**, **24**, and **25**.

Compound **23** was synthesised using the old method consisting of anhydrous conditions, HOBT/TBTU, oven-dried Schlenk tube and under nitrogen atmosphere at the beginning of this project and not repeated under the improved conditions.

Structure variations of RTC1 on the alkyl chain (site D) consisted of compounds without an alkyl chain (compound **21**), a shorter alkyl chain (compound **22**), and a longer alkyl chain (compound **23**). Further variations on the alkyl chain consisted of substituting the CH_2 group adjacent to the thiophene ring with a carbonyl group (compound **24**), or a

sulphur atom (compound **25**). Yields of 60-84% were obtained for compounds **21-25** (Table 2).

Table 2: Compounds made with variations at site D of RTC1 at the alkyl chain.

Compound	X	Yield
21 (MK37)	-	69%
22 (MK47)	CH_2	82%
23 (MK18)	C_4H_8	73%
24 (MK40)		84%
25 (MK22)		60%

2.6.1 Structural characterisation of thiophen-2-yl (4-(4-(trifluoromethyl)phenyl)piperazin-1-yl) methanone (compound 21)
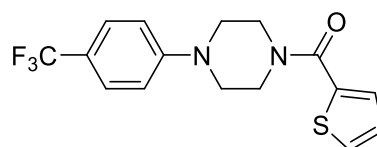
Figure 63: Structure of compound **21**.

As expected, the ^{1}H and ^{13}C NMR spectra of compound **21** (Figure 63) do not contain any alkyl chain signals. Instead, both spectra just contain the typical signals for the *para* CF$_3$ substituted aromatic ring and the thiophene ring, as well as the signals for the piperazine motif. The IR and MS data also confirmed the generation of compound **21**.

2.6.2 Structural characterisation of 2-(thiophen-2-yl)-1-(4-(4-(trifluoromethyl)phenyl)piperazin-1-yl)ethanone (compound 22)

Figure 64: Structure of compound **22**.

90

The three signals for the alkyl chain of RTC1 are also absent in the ^{1}H NMR spectrum of compound **22** (Figure 64). Instead, just one singlet signal at 3.96 ppm appears for the single CH_2 group, integrating for 2H. The carbon signal for this CH_2 group appears at 35.2 ppm in the ^{13}C NMR spectrum. The expected ^{1}H and ^{13}C NMR signals for the *para* CF_3 substituted aromatic ring, the thiophene ring, and the piperazine ring are all present. The IR and MS data also confirmed the generation of compound **22**.

2.6.3 Structural characterisation of 5-(thiophen-2-yl)-1-(4-(4-(trifluoromethyl)phenyl)piperazin-1-yl)pentan-1-one (compound 23)

Figure 65: Structure of compound **23**.

Compound **23** (Figure 65) contains an alkyl chain with four repeating CH_2 units. The ^{1}H NMR spectrum contains three signals for the alkyl chain, with one of the signals, a multiplet in the range of 1.68 – 1.81 ppm, integrating for four protons and the remaining two signals integrating for two protons each. The extra CH_2 group also shows an extra carbon signal in the ^{13}C NMR spectrum at 31.4 ppm, which further confirms the synthesis of this compound. The IR and MS data also confirmed the generation of compound **23**.

2.6.4 Structural characterisation of 1-(thiophen-2-yl)-1-(4-(4-(trifluoromethyl)phenyl)piperazin-1-yl)butan-1,4-dione (compound 24)
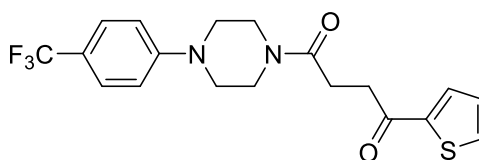
Figure 66: Structure of compound **24**.

Compound **24** (Figure 66) contains one less signal in the ^{1}H NMR spectrum, when compared to that of RTC1, due to the replacement of one of the CH_2 groups with an electron withdrawing carbonyl group. This second carbonyl group causes the signals for the two CH_2 groups to be deshielded and appear as an unresolved multiplet in the range

of 3.25 – 3.27 ppm and a triplet at 2.82 ppm. Both signals integrate for 2H. The ^{13}C NMR spectrum for compound **24** also confirms its synthesis as it has one less CH$_2$ signal in the aliphatic region, when compared to the ^{13}C NMR spectrum of RTC1, and instead has an extra quaternary carbonyl carbon signal at 191.9 ppm. Furthermore, the IR spectrum shows a second carbonyl group absorbance band at 1647 cm^{-1}. The MS data also confirmed the generation of compound **24**.

2.6.5 Structural characterisation of 3-(thiophen-2-ylthio)-1-(4-(4-(trifluoromethyl)phenyl)piperazin-1-yl)propan-1-one (compound 25)
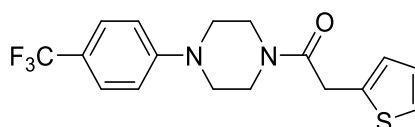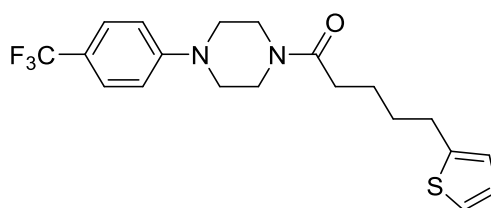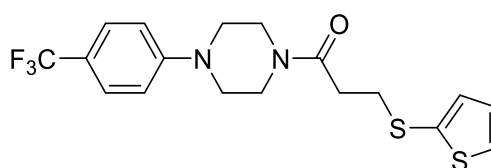

Figure 67: Structure of compound **25**.

Similar to compound **24**, compound **25** (Figure 67) also has a one less signal in the ^{1}H NMR spectrum, when compared to that of RTC1. This is due to the replacement of one of the CH$_2$ groups with an electronegative sulphur atom. This also causes the signals of the two CH$_2$ groups to be deshielded, occurring at 2.68 ppm and 3.12 ppm. Both signals appear as triplets and integrate for 2H. The ^{13}C NMR spectrum also showed one CH$_2$ signal less when compared to the spectrum for RTC1. The IR and MS data also confirmed the generation of compound **25**.

2.7 Synthesis of compounds with structural variations at site E: the thiophene ring

The final site of variation examined on RTC1 was the thiophene ring (site E) (Figure 68).
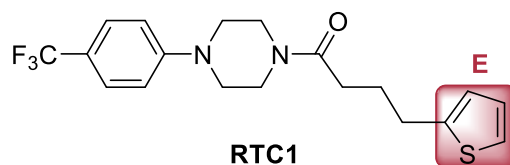
Figure 68: Structure of RTC1 showing variations at site E – the thiophene ring.

The thiophene ring is a planar five-membered heterocyclic ring, which is present in many agrochemicals, pharmaceuticals and dyes, with applications in many areas such as material science, coordination chemistry, and organic synthesis.[78,79] Many molecules incorporating the thiophene ring have shown important pharmacological activities.[79] It can partake in many reactions such as oxidation, halogenation, acylation, alkylation and polymerisation, and has many useful applications as an electron acceptor, a hydrogen-poor heterocycle, or an organic conductors.[80,81] It can react with oxidising agents, nucleophilic reagents, bases and radical agents.[81]

Structure variations of RTC1 at the thiophene ring (site E) consisted of just one derivative where the thiophene ring was replaced with a different heterocycle, namely the nitrogen containing pyrazole ring (compound **5**) (Figure 69).
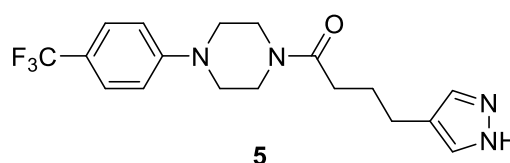
Figure 69: Structure of compound **5**.

2.7.1 Synthesis and structural characterisation of 4-(1*H*-pyrazol-4-yl)-1-(4-(4-(trifluoromethyl)phenyl)piperazin-1-yl)butan-1-one (compound 5)

The synthesis of compound **5** consisted of using the new method as discussed in section **2.2.1**. Again, coupling of the arylpiperazine with 4-(1*H*-pyrazol-4-yl-)butanoic acid was

carried out using HOBt/TBTU as coupling reagents (Scheme 16). Purification using column chromatography generated the desired product as a brown solid in a 93% yield.
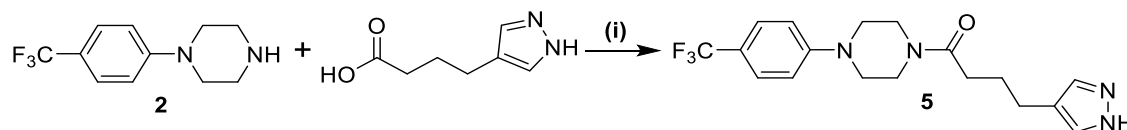
Scheme 16: Synthesis of compound **5**, (i) HOBt, TBTU, DCM, NEt$_3$, 24 hrs, rt, 93% yield.

Compound **5** contains two different signals in the ^{1}H NMR spectrum in comparison with RTC1 due to the replacement of the thiophene ring with a pyrazole ring. These signals are a singlet at 7.43 ppm representing the two C-H protons, and a broad singlet at 5.57 ppm representing the N-H proton of the pyrazole ring. The C-H carbons of the pyrazole ring also show a signal at 132.9 ppm in the ^{13}C NMR spectrum. Furthermore, the IR spectrum shows an absorbance band for the N-H at 3055 cm^{-1}, with the MS data also confirming the generation of compound **5**.

2.8   Synthesis of compounds with structural variations at multiple sites

After making individual changes to the five different sites of RTC1 (Figure 70), additional compounds were synthesised that consisted of variations at multiple sites. These compounds were synthesised from the corresponding arylpiperazine and carboxylic acid using coupling chemistry.
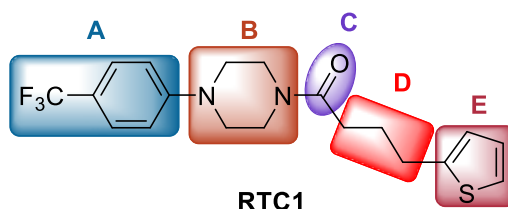
Figure 70: Structure of RTC1 with variation sites, A-E.

2.8.1   Synthesis of compounds with structural variations at site A and site B – compounds 26 and 27

Two compounds were synthesised with variations at the aryl group (site A) and piperazine ring (site B) (Figure 71). Compound **26** was synthesised where the entire arylpiperazine motif of RTC1 was replaced by a dimethylamino group. For compound **27**, the trifluoromethyl group of RTC1 was replaced with a hydrogen, and the piperazine ring replaced with a piperidine ring.
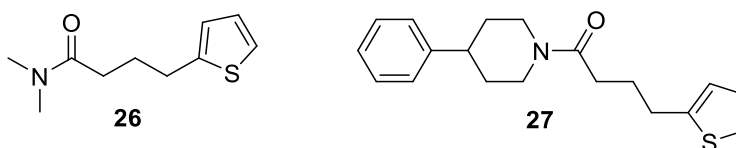
Figure 71: Structure of compound **26** and compound **27**.

2.8.1.1 Synthesis   and   structural   characterisation   of   *N,N*-dimethyl-4-(thiophen-2-yl)butanamide (compound 26)

Compound **26** was synthesised using the new method discussed in section **2.2.1** which involved coupling of dimethylamine with 4-(2-thienyl)butyric acid, using HOBt/TBTU coupling reagents and NEt$_3$ (Scheme 17). The reaction mixture, in DMF, was stirred at

95

room temperature for 16 hours and purified using column chromatography (3:2, EtOAc:*n*-hexane) to give a grey oil in a 43% yield.
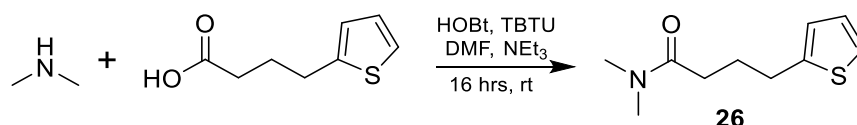
Scheme 17: Synthesis of compound **26**, 43% yield.

Compound **26** differed from the ^{1}H and ^{13}C NMR spectra of RTC1 in that it did not contain any signals for the aryl or piperazine groups. Instead a multiplet signal, due to bond rotation, appears in the ^{1}H NMR spectrum in the range of 2.74 – 3.11 ppm for the two methyl groups of the dimethylamine group. The carbon signals for these methyl groups appear at 35.5 ppm and 37.3 ppm in the ^{13}C NMR spectrum. The IR and MS data also confirmed the generation of compound **26**.

2.8.1.2 Synthesis and structural characterisation of 1-(4-phenylpiperidin-1-yl)-4-(thiophen-2-yl)butan-1-one (compound 27)

Compound **27** was also synthesised using the new method discussed in section **2.2.1**. Again, HOBt/TBTU coupling reagents were used to couple 4-phenylpiperidine with 4-(2-thienyl)butyric acid, and NEt$_3$ (Scheme 18). The reaction mixture, in DCM this time, was stirred at room temperature for 18 hours and purified using column chromatography (3:2, EtOAc:*n*-hexane) to give a clear oil in a 98% yield.

Scheme 18: Synthesis of compound **27**, 98% yield.

Differences in the ^{1}H and ^{13}C NMR spectra of compound **27** compared to the spectra of RTC1 are due to the absence of the trifluoromethyl group, and the replacement of the piperazine ring with a piperidine ring. The aromatic region of the ^{1}H NMR spectrum of this compound contains two signals for the phenyl ring. The first signal is for the *ortho* proton at 7.32 ppm which appears as a p*seudo* triplet instead of a double of doublet as expected due to short-range splitting with the proton in the *meta* position and long-

range splitting with the proton in the *para* position. The second signal appears as a multiplet at 7.16 – 7.25 ppm integrating for 3H for the protons in the *ortho* and *para* positions. The carbons bonded to these protons appear in the ^{13}C NMR spectrum as singlet signals at 126.5 ppm (*ortho* carbons), 126.8 ppm (*meta* carbons), and 128.6 ppm (*para* carbons).

The piperidine ring results in multiple signals in the ^{1}H and ^{13}C NMR spectra. The piperidine CH proton appears at 2.73 ppm in the ^{1}H NMR spectrum as a triplet of triplet signal as expected due to splitting with two sets of two adjacent protons. The carbon bonded to this proton appears at 42.8 ppm in the ^{13}C NMR spectrum. The protons adjacent to the nitrogen results in 4 different signals; two triplet of doublet signals at 2.63 ppm and 3.09 ppm, and two doublet signals at 3.91 ppm and 4.82 ppm. The carbons bonded to these protons appear in the ^{13}C spectrum at 42.4 ppm and 46.2 ppm. The protons further from the nitrogen appear in the ^{1}H NMR spectrum as multiplet signals in the range of 1.54 – 1.67 ppm and 1.84 – 1.93 ppm, each integrating for 2H. The carbons bonded to these protons appear at 32.9 ppm and 34.0 ppm in the ^{13}C NMR spectrum. The IR and MS data also confirmed the generation of compound **27**.

2.8.1.3 Synthesis of compound with structural variations at site B and site D – 1-(thiophen-2-yl)-4-(4-(4-(trifluoromethyl)phenyl)piperidin-1-yl)butane-1,4-dione (compound 28)

Compound **28** consisted of replacing the piperazine ring (site B) with a piperidine ring, and a methylene group on the alkyl chain (site D) with a carbonyl group. It was synthesised using the new method discussed in section **2.2.1** by coupling 4-(4-trifluoromethyl)phenyl)piperidine with 4-oxo-4-(2-thienyl)butanoic acid, using HOBt/TBTU coupling reagents, and NEt$_3$ (Scheme 19). The reaction mixture, also in DCM, was stirred at room temperature for 19 hours and purified using column chromatography (4:1, EtOAc:*n*-hexane) to give a white solid in a 87% yield.
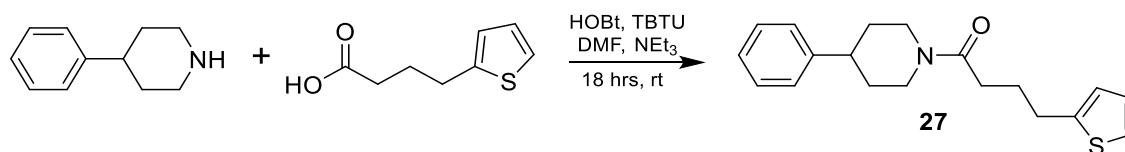

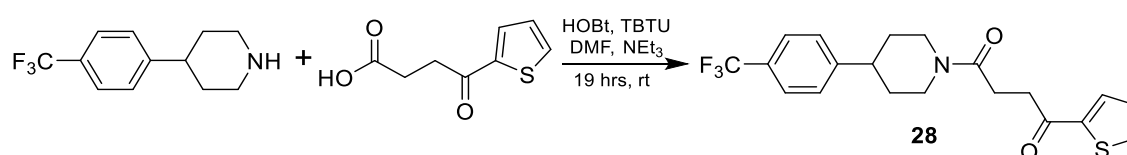**Scheme 19:** Synthesis of compound **28**, 87% yield.

The ^{1}H and ^{13}C NMR spectra of compound **28** showed all the expected signals. The piperidine ring generated very similar signals in the ^{1}H and ^{13}C NMR spectra to those of compound **27**. As anticipated, the extra carbonyl group results in one less signal in the aliphatic region of the ^{1}H NMR spectrum in comparison to RTC1. Furthermore, the two signals of the alkyl chain of compound **28** appear as multiplet signals at 2.77 – 2.90 ppm and 3.14 – 3.23 ppm, more deshielded than the corresponding signals in RTC1. The alkyl carbonyl group also produces an extra quaternary carbon signal at 192.2 ppm in the ^{13}C NMR spectrum. The IR and MS data also confirmed the generation of compound **28**.

2.8.1.4 Synthesis of compounds with structural variations at site D and site E – compounds 3, 29 and 30

The next set of compounds synthesised consisted of variations of RTC1 at both the alkyl chain (site D) and thiophene ring (site E). The first compound (compound **3**) was previously discussed in the method development section **2.2.1**. For compound **3**, the alkyl chain is elongated with the thiophene heterocycle being replaced with a methyl ester group. The second compound (compound **29**) also consisted of elongating the alkyl chain but this time the thiophene is replaced with a phenyl ring. The third compound (compound **30**) consisted of replacing both the alkyl chain and the thiophene ring with a methyl group (Figure 72).
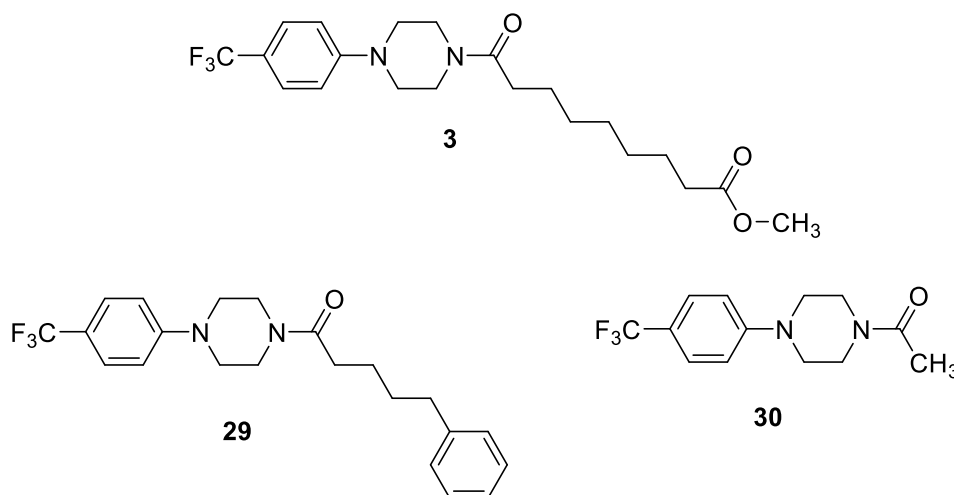
Figure 72: Structure of compounds **3**, **29** and **30**.

2.8.1.4.1 Synthesis and structural characterisation of methyl 9-oxo-9-(4-(4-(trifluoromethyl)phenyl)piperazin-1-yl)nonanoate (compound 3)

The synthesis of compound **3** was previously discussed in the method development section **2.2.1** which consisted of coupling methyl hydrogen azelate with 1-(4-(trifluoromethyl)phenyl)piperazine (compound **2**) using BOP and NEt$_3$ in a round-bottom flask and stirred, in DCM, at room temperature overnight. Purification consisted of evaporation under reduced pressure followed by column chromatography to give the product as an off-white solid, in a 55% yield (Scheme 20).
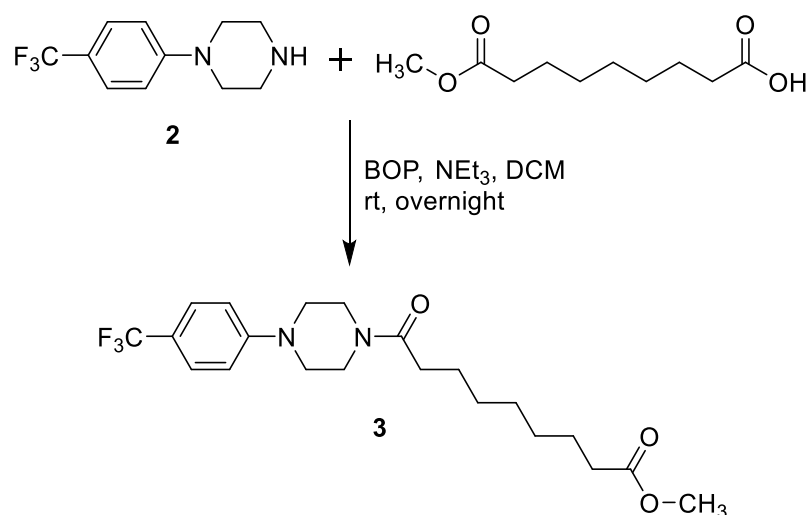
Scheme 20: Synthesis of compound **3**, 55% yield.

The ^{1}H NMR spectrum of compound **3** contains three signals for the seven CH$_2$ groups. The α-protons from the two CH$_2$ groups adjacent to the two carbonyl groups appear most deshielded at 2.32 ppm and as a doublet of triplet signal, integrating for 4H. The next signal appears as a multiplet in the range of 1.58 – 1.69 ppm and can be assigned to the β-protons of the two CH$_2$ groups further from the carbonyl groups.

The third signal appears as a broad singlet at 1.34 ppm integrating for the 6H of the γ-protons of the remaining three CH$_2$ groups in the middle of the alkyl chain. The CH$_3$ signal of the ester group appears as a multiplet in the range of 3.52 – 3.72 ppm. The ^{13}C NMR spectrum for compound **3**, in comparison with the spectrum of RTC1, also shows the expected additional signals for the elongated alkyl chain, as well as an extra carbonyl carbon signal at 174.3 ppm. The ester CH$_3$ signal appears at 51.5 ppm. The MS and IR data for compound **3** also confirms its synthesis, with the IR spectrum showing an absorbance band at 1736 cm^{-1}, characteristic of an ester carbonyl group.

2.8.1.4.2 Synthesis and structural characterisation of 5-phenyl-1-(4-(4-(trifluoromethyl)phenyl)piperazin-1-yl)pentan-1-one (compound 29)

The synthesis of compound **29** involved using the new method as discussed in section **2.2.1** which consisted of coupling of the arylpiperazine with 5-phenylpentanoic acid using HOBt/TBTU as coupling reagents, and NEt$_3$, and carrying the reaction in DMF

(Scheme 21). Purification using column chromatography (4:1, EtOAc:*n*-hexane) generated the desired product as an orange oil in a 65% yield.
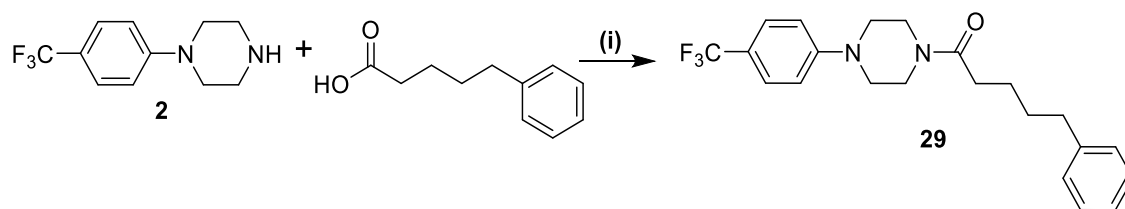

Scheme 21: Synthesis of compound **29**, (i) HOBt, TBTU, DMF, NEt$_3$, 21 hrs, rt, 65% yield.

The ^{1}H and ^{13}C NMR spectra for compound **29** differ from those of RTC1 as expected. The ^{1}H NMR spectrum contains a multiplet signal in the range of 1.65 – 1.75 ppm, which integrates for 4H instead of 2H as in RTC1, due to the extra CH$_2$ group of compound **29**. An extra carbon signal at 31.1 ppm can be found in the ^{13}C NMR spectrum of compound **29**, again due to the extra CH$_2$ group. The phenyl ring results in multiplet signals in the ^{1}H NMR spectrum in the range of 7.23 – 7.26 ppm and 7.13 – 7.19 ppm for the protons in the *ortho* position and *meta* position respectively. The carbons in the *ortho*, *meta*, and *para* position of the aromatic ring appear at 128.5 ppm, 128.4 ppm, and 125.8 ppm respectively, while the *ipso* carbon appears at 142.2 ppm. The IR and MS data also confirmed the generation of compound **29**.

2.8.1.4.3 Structural characterisation of 1-(4-(4-(trifluoromethyl)phenyl)piperazin-1-yl)ethan-1-one (compound 30)

Compound **30** was also synthesised using the new method as discussed in section **2.2.1** by using HOBt/TBTU coupling reagents to couple the arylpiperazine with 1-(4-(trifluoromethyl)phenyl)piperazine, using NEt$_3$, and carrying the reaction in DMF (Scheme 22). Purification using column chromatography (4:1, EtOAc:*n*-hexane) generated the desired product as an off-white solid in a 73% yield.
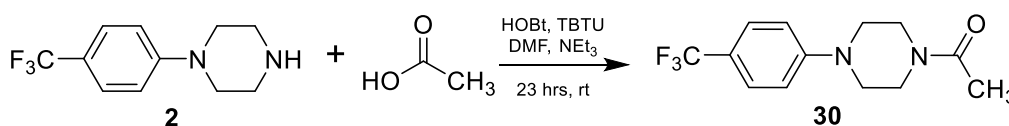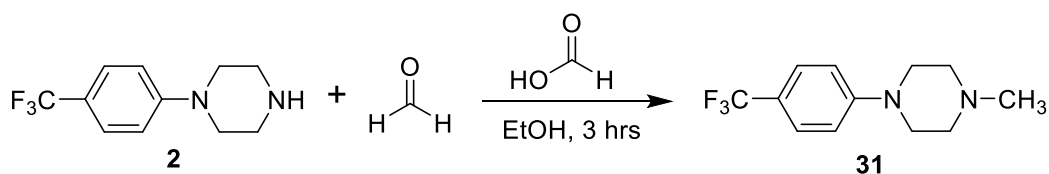

Scheme 22: Synthesis of compound **30**, 73% yield.

The ^1H and ^{13}C NMR spectra of compound **30** does not contain any signals for the alkyl chain or thiophene ring of RTC1 as they have been replaced by a methyl group. Instead, a singlet signal at 2.14 ppm in the ^1H NMR spectrum, integrating for 3H, and a signal at 21.3 ppm in the ^{13}C NMR spectrum, confirms the presence of the methyl group. The IR and MS data also confirmed the generation of compound **30**.

2.8.1.5 Synthesis and structural variation of compound 31 with structural variation at sites C, D and E – 1-methyl-4-(4-(trifluoromethyl)phenyl)piperazine (compound 31)

The final compound, 1-methyl-4-(4-(trifluoromethyl)phenyl)piperazine (MK35) (compound **31**) consisted of completely removing the thiophene-linker motif, including the carbonyl carbon, of RTC1 and replacing it with a simple methyl group. The synthesis of compound **31** utilised the Eschweiler-Clarke reaction,[82] a reductive amination, and consisted of dissolving compound **2** in ethanol (EtOH) and reacting it with formic acid and formaldehyde, under refluxing conditions for three hours (Scheme 23). After successful work-up and purification using column chromatography, the product appeared as a white solid in a 70% yield.

Scheme 23: Synthesis of compound **31**, 70% yield.

The proposed mechanism for this reaction (Scheme 24) begins with the protonation of formaldehyde by formic acid to form a more electrophilic carbonyl carbon, which in turn undergoes nucleophilic attack by the arylpiperazine **2**. After protonation and deprotonation, water is removed as the leaving group to form the electrophilic iminium intermediate. The formate then acts as a hydride donor with the iminium ion being reduced to an amine. Deprotonation of the amine reforms formic acid and compound **31** as the final product.
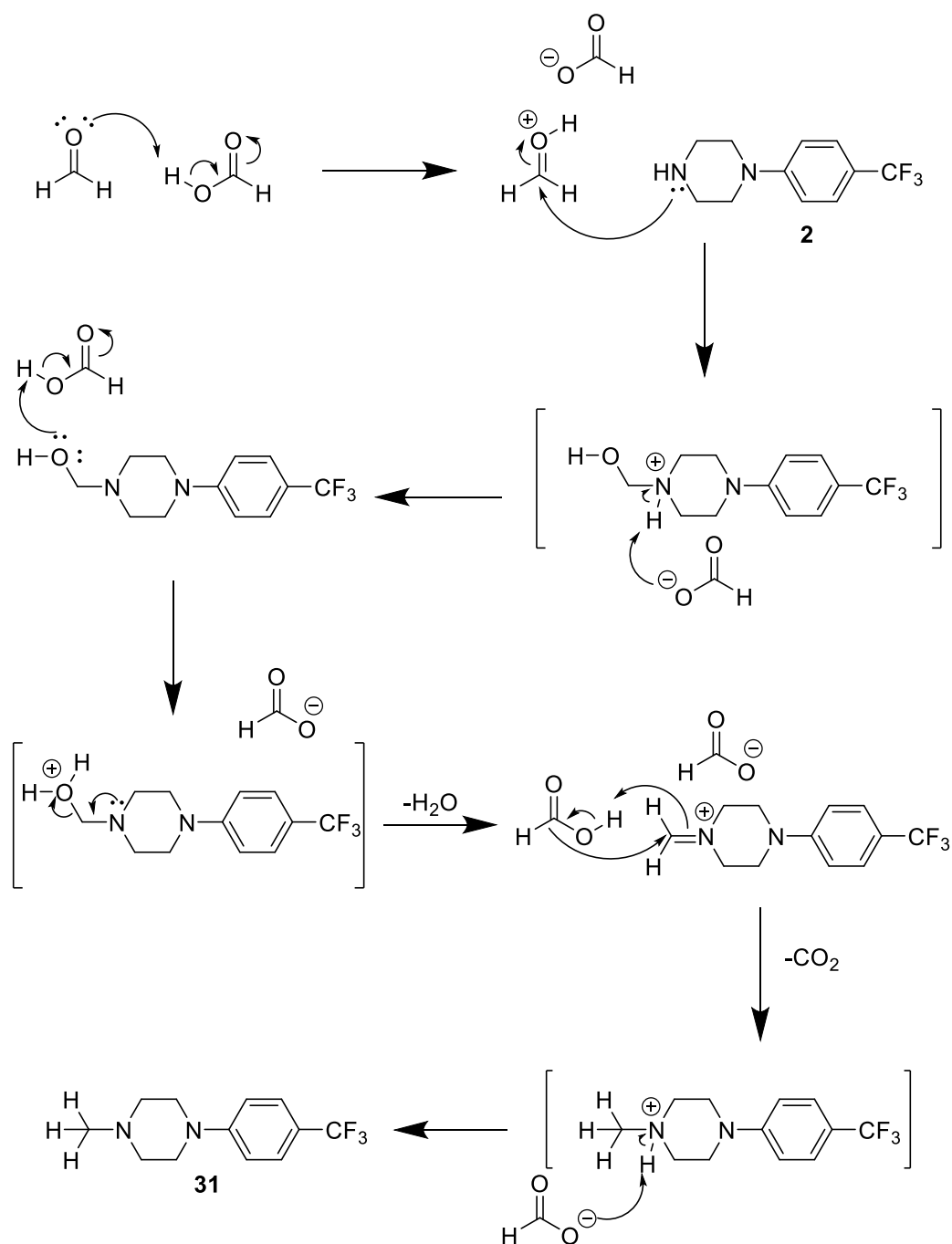
Scheme 24: Proposed mechanism for the synthesis of compound **31.**

As with compound **30**, the ^{1}H and ^{13}C NMR spectra of compound **31** does not contain any signals for the alkyl chain or thiophene ring of RTC1. Also, the quaternary carbonyl carbon signal is absent in the ^{13}C NMR spectrum. The methyl group signals appear as a singlet signal at 2.35 ppm in the ^{1}H NMR spectrum, integrating for 3H, and at 54.8 ppm in the ^{13}C NMR spectrum. The IR and MS data also confirmed the generation of compound **30**.

2.9 Conclusion

The arylpiperazine moiety is found in many medicinal agents and has multiple pharmacological applications. To access the arylpiperazine derivative, various synthetic approaches can be utilised such as nucleophilic aromatic substitutions (S_NAr) reactions, metal catalysed reactions, and cyclocondensation reactions.[52,53] Arylpiperazines have been used for many years in various applications such as an appetite suppressant, an anorectic agent, an antidepressant drug, and an anti-cancer agent.[54,55]

The arylpiperazine family generated in this project consisted of analogues of RTC1 with variations at five sites, Figure 73. The purpose of generating this family was to explore the relationship between chemical structure and biological function (anti-diabetic effect) for this compound class. The five sites of variation are the aryl group (A), piperazine ring (B), carbonyl group (C), alkyl chain (D), and thiophene ring (E). Additional compounds were also synthesised that contained variations at multiple sites.
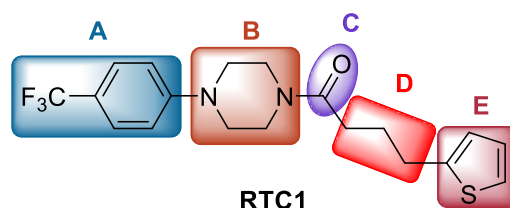

Figure 73: Structure of RTC1 with five sites of variation, A-E.

Synthetic method development for this family involved using non-anhydrous conditions and removing the post-reaction work-up to provide a more facile and quicker method of synthesising the target compounds. This optimised method resulted in a reduction of time required to synthesise and purify target compounds as well as giving a higher yield. This method was therefore utilised for the synthesis of most compounds in this family.

Each member of the arylpiperazine family was fully characterised using ^{1}H and ^{13}C NMR spectroscopy, including 2D-NMR spectroscopy, as well as IR spectroscopy, and accurate HR-MS. Some of the compounds containing a trifluoromethyl group were also characterised using ^{19}F NMR spectroscopy. Compounds synthesised in this group were added to arylpiperazines generated by previous group members to create a large family of arylpiperazines.

Compounds from this larger family were then made available for biologically evaluation in order to explore the relationship between their structure and biological activity. This SAR type study was performed using a glucose uptake assay and a complex I assay in order to determine their anti-diabetic activity.

Chapter 3: Pyrazolopyrimidinone Bicycle Family

3.1 Introduction

Members of the pyrazolopyrimidinone bicycle family are composed of a fused nitrogen-containing heterocyclic bicycle system with substituents at R and R^1 group, Figure 74.
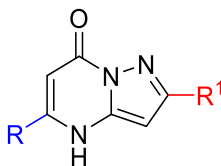

Figure 74: General structure for the pyrazolopyrimidinone bicycle family.

This family is of interest due to its role as a basic core scaffold in many bioactive and pharmaceutically relevant compounds. Derivatives of the pyrazolopyrimidinone bicycle core structure have found use in the battle against several illnesses including cancer[83] (GSK), obesity[84] (Pfizer), and cystic fibrosis[85] (Vertex) (Figure 75).
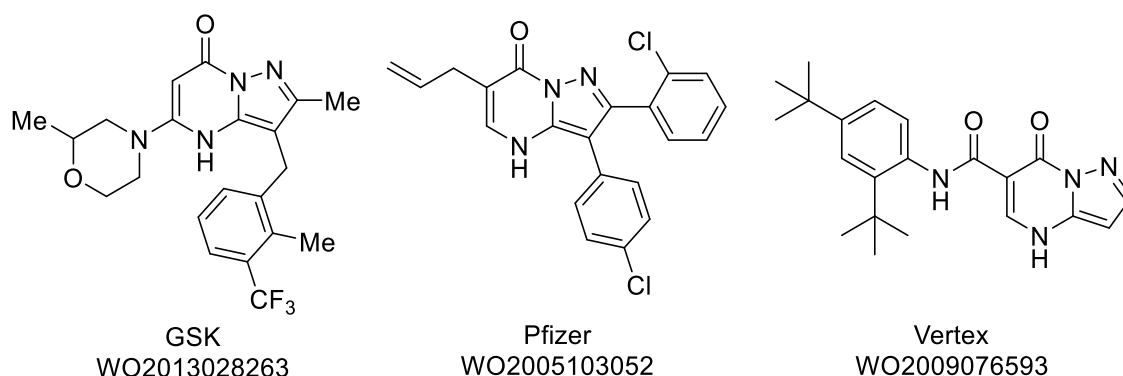

GSK	Pfizer	Vertex
WO2013028263	WO2005103052	WO2009076593

Figure 75: Structure of bioactive pyrazolopyrimidinones as agents for cancer[83], obesity[84] and cystic fibrosis[85].

They have also been found as KCNQ channel openers. KNCQ are a member of potassium channel proteins that belong to the 6-transmemberance gene family of ion channels[86] (Figure 76). Some derivatives have also been discovered to have anti-trypanosomal or anti-schistosomal activities, while others show potential activity against respiratory diseases.[87]
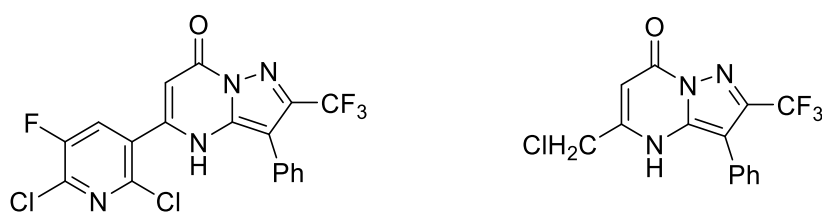

Figure 76: Structures of bioactive pyrazolopyrimidinones as KCNQ channel openers.[86]

Due to the continuous discoveries of interesting biological properties of this ring system, research has been stimulated for new and efficient procedures of synthesising compounds containing this core scaffold. Solvent-free conditions for the synthesis of these compounds have been employed, particularly with cyclocondensation reactions, due to the drive towards clean technology in organic synthesis. This resulted in higher yields in most cases, while using benign synthetic procedures. Most methods found in literature for the synthesis of pyrazolopyrimidinones (or pyrazolo[1,5-a]pyrimidones) involve the reaction between 5-amino-1*H*-pyrazoles with 1,3-bis-electrophilic reagents, such as β-dicarbonyl, α,β-unsaturated carbonyl, alkoxy methylene-β-dicarbonyl, or β-enaminone compounds.[87]

The method by which we synthesise the pyrazolopyrimidinone bicycle compounds in this project is via a condensation reaction of the aminopyrazoles with the corresponding β-ketoesters. This method was recently reported by Azeredo et al. where they carried out this reaction under traditional reflux to produce the desired pyrazolo[1,5-a]pyrimidinones in 71-93% yield after 5-16 hours reflux (Scheme 25).[88] They then submitted these pyrazolopyrimidinones to a chlorodehydroxylation reaction with phosphorus oxychloride to produce the desired 7-chloro-pyrazolo[1,5-a]pyrimidines. These compounds underwent an aromatic nucleophilic substitution with the corresponding anilines to produce the target 7-arylaminopyrazolo[1,5-a]pyrimidines.[88]
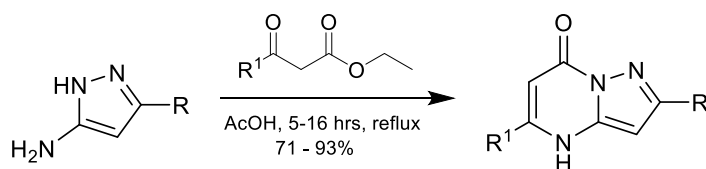
Scheme 25: Synthesis of pyrazolo[1,5-*a*]pyrimidinones.[88]

Recent research published by Portilla et al. have reported the regioselective synthesis of fused pyrazolo[1,5-a]pyrimidines and pyrazolo[1,5-a]pyrimidones by reaction of 5-amino-1*H*-pyrazoles and β-dicarbonyl compounds containing five-membered rings.[87] One of the reactions discussed in this research consisted of the synthesis of cyclopenta[*d*]pyrazolo[1,5-*a*]pyrimidones via a solvent-free cyclocondensation procedure using 3-substituted-5-amino-1*H*-pyrazoles and 2-ethoxycarbonylcyclopentanone (Scheme 26). This reaction was performed using fusion and microwave irradiation methods in 2-3 minutes to yield 82-92% yield. This was a

higher yield in comparison with the traditional reflux method in EtOH for 15-20 hours with 19-27% yields.[87]
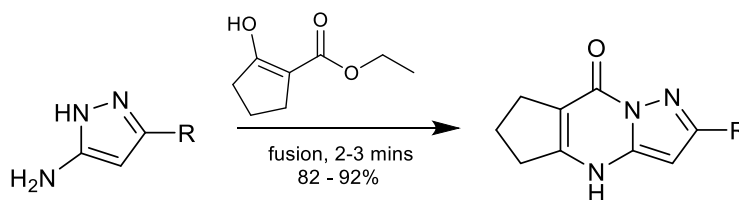
Scheme 26: Synthesis of cyclopenta[*d*]pyrazolo[1,5-a]pyrimidones.[87]

The pyrazolopyrimidinone bicycle RTC53 is one of our lead anti-diabetic compounds and showed good activity in the glucose uptake assay, Figure 77 and section **1.3.3**.[45] In order to better understand the potential of pyrazolopyrimidinones as anti-diabetic agents, it was necessary to synthesise and biologically evaluate a large family of pyrazolopyrimidinones.
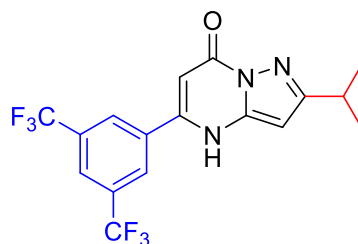

Figure 77: Structure of RTC53.

Proposed structural variations of RTC53 were categorised as follows: (i) variations of the R group on the bicycle core (Figure 78) i.e. vary the 3,5-bistrifluoromethyl aryl substituent on RTC53; (ii) the R^1 group on the bicycle core (Figure 78) i.e. vary the isopropyl substituent on RTC53; (iii) variations on both R and R^1 groups.
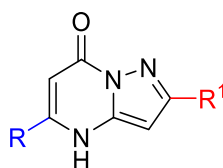

Figure 78: General structure for the pyrazolopyrimidinone bicycle family.

By maintaining the bicycle core while varying the R and R^1 groups, we hoped to gain a better understanding of how structure relates to biological activity (glucose uptake) for the pyrazolopyrimidinones.

3.2 Retrosynthesis of the pyrazolopyrimidinone bicycle

A retrosynthetic analysis of the pyrazolopyrimidinone bicycle is shown below (Scheme 27), where we proposed that the synthesis could be achieved via a condensation reaction between the appropriate β-ketoester and corresponding aminopyrazole. Some of the β-ketoesters and aminopyrazoles were commercially available. When the β-ketoester was not available, we considered forming it through the use of a coupling reaction of the corresponding carboxylic acid derivative with Meldrum's acid. The carboxylic acid itself was not always commercially available however, and in such cases, we proposed its synthesis using Grignard formation from the starting bromide and subsequent quenching with carbon dioxide. When the aminopyrazole was not commercially available, we proposed its synthesis from the corresponding β-ketonitrile derivative and hydrazine.
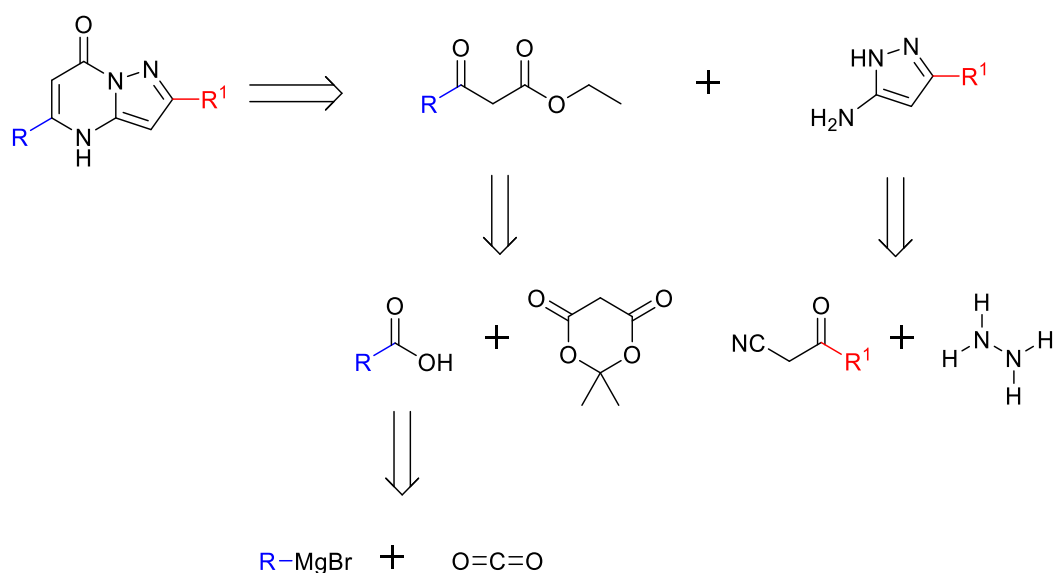

Scheme 27: Retrosynthesis of the pyrazolopyrimidinone bicycle.

3.3 Synthetic method development for the pyrazolopyrimidinone bicycle family

Due to the welcomed commercial availability of β-ketoesters, the key steps in the proposed synthetic route to the pyrazolopyrimidinones were considered to be the generation of the aminopyrazole and its subsequent reaction with the appropriate β-ketoester. As such, synthetic method development for the pyrazolopyrimidinone bicycle family focused on generating efficient and effective reactions for both these steps. We also postulated that a "one-pot" method, incorporating both of these reactions in a single pot, for the synthesis of the pyrazolopyrimidinones may be possible. Such a "one-pot" approach would remove the need to isolate and purify the intermediate aminopyrazole. In order to establish reaction conditions for this "one-pot" approach, we first turned our attention to developing general reaction conditions for the microwave-assisted generation of the intermediate aminopyrazoles. Once these reaction conditions were established, we sought to use them as a starting point for developing the "one-pot" approach. The novel "one-pot" method was ultimately published in a peer-reviewed journal.[89]

3.3.1 Solvent screen for the synthesis of aminopyrazoles

Typical methods for preparing aminopyrazoles require conventional heating of the appropriate β-ketonitrile in the presence of hydrazine monohydrate for 17 – 24 hours (Scheme 28).[86,90]
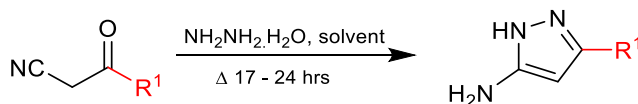

Scheme 28: Synthesis of aminopyrazoles using conventional heating.

The proposed mechanism for the synthesis of the aminopyrazole from the β-ketonitrile is shown below (Scheme 29). The synthesis begins with nucleophilic attack by hydrazine on the carbonyl carbon of the β-ketonitrile. This generates a tetrahedral intermediate. This intermediate cyclises via nucleophilic attack of the second nitrogen of the hydrazine on the electrophilic carbon of the nitrile group. After several proton transfers, and the elimination of water, the aminopyrazole is generated.
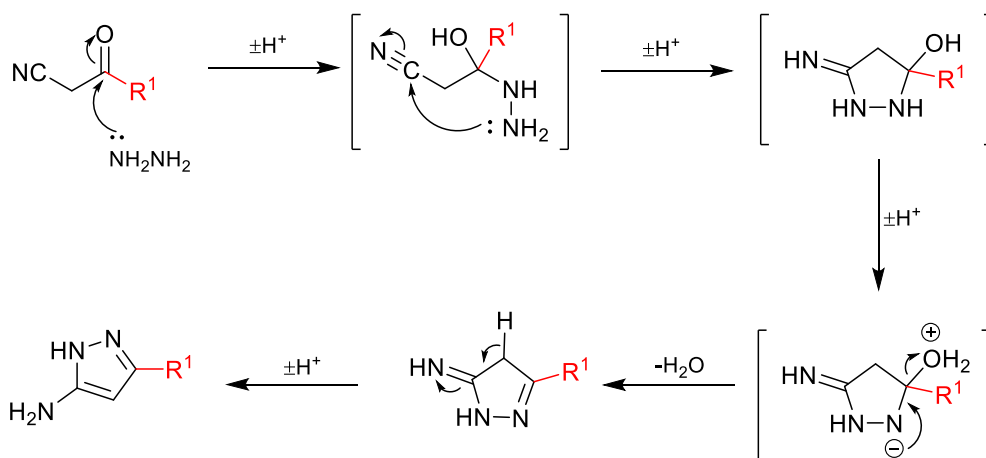
Scheme 29: Proposed mechanism of the synthesis of aminopyrazoles from β-ketonitrile.

Method optimisation was carried out on the reaction of 3-oxo-3-phenylpropanenitrile with hydrazine monohydrate to form 3-phenyl-1*H*-pyrazol-5-amine (MK12) **32** (Scheme 30).[89] Under conventional reflux conditions, this reaction in MeOH takes 17 hours to go to completion with a 60% isolated yield. Under microwave conditions at 150 °C for only five minutes, this reaction, also in MeOH, gave higher yields of 99%.
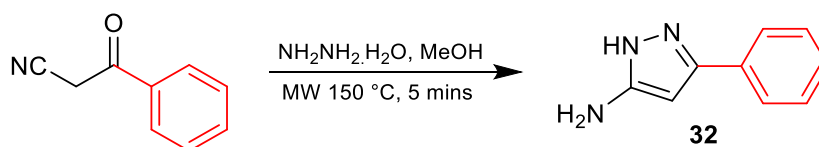
Scheme 30: Synthesis of compound **32** using optimised microwave conditions, 99% yield.

Microwave-assisted synthesis is increasingly becoming a popular method in modern chemical synthesis and drug discovery as it has revolutionized chemical synthesis. [91,92] It can be used in organic, inorganic, polymer and peptide synthesis, as well as nanotechnology.[93,94] It has also been extended to medicinal, analytical, environmental, and green chemistry as well as biochemistry and materials science.[93,95] It allows fast heating of reaction mixtures to high pressures and temperatures far above the boiling point of the used solvent.[95] Microwave-assisted synthesis reduces reaction times from several hours down to only a few minutes by employing closed vessel conditions.[91,94] This rate acceleration is based on the Arrhenius Law, which states that the reaction rate is doubled when increasing the reaction temperature by 10 °C.[92]

Microwave-assisted synthesis has proven to be an interesting alternative for heating chemical reactions and offers considerable advantages over conventional heating methods.[92] These include enhanced reaction rates, greater selectivity, simple purification procedures, and higher product purity as decomposition is minimized.[91] By controlling the specific parameters such as temperature, pressure, and time, as well as choice of solvents, researchers can now achieve similar and often better results using microwave-assisted synthesis with experiments previously performed using conventional heating methods.[93,94]

Microwave chemistry is based on the efficient heating of materials, particularly solvents, by dielectric heating effects. Dielectric heating works by two major mechanisms: dipolar polarization, and ionic conduction.[91]

When the molecular structure of a substance is partly negatively charged and partly positively charged, it contains a dipole. The presence of a dipole is important for a substance to be able to generate heat when irradiated with microwaves. Since the

microwave field is oscillating, the dipoles in the field align to the oscillating field. This alignment causes rotation, which results in friction and ultimately in heat energy.[91,92]

During ionic conduction, dissolved charged particles oscillate back and forth under the influence of microwave irradiation, which causes collisions of the charged particles with neighbouring molecules creating heat energy.[91,92]

A material or solvent must possess certain dielectric properties in order to be efficiently heated in the microwave field. The heating characteristics of a particular substance under microwave irradiation conditions are dependent on its ability to convert electromagnetic energy into heat.[94] Solvents such as MeOH, EtOH and formic acid are therefore useful for rapid heating in the microwave field. Although solvents such as chloroform, acetone, and toluene have low heating efficiencies, they can still be used for microwave-assisted synthesis.[95]

Previous group members established the optimum temperature and time needed for the synthesis of aminopyrazoles to be 150 °C and five minutes respectively.[89] To do this, they initially began with 120 °C and 40 minutes, as previously reported by Bagley et al.[94], where they generated the product in 84% yield. Increasing the temperature to 130 °C and decreasing the time to 30 minutes resulted in a 96% yield of the product. Maintaining temperature at 130 °C but reducing the time to only five minutes decreased the yield to 53%. The penultimate attempt consisted of increasing the temperature to 140 °C for 20 minutes, which produced 98% yield of the product. The final and most successful variation consisted of 150 °C for five minutes, which generated the product in 99% yield (Table 3).[89]

Table 3: Temperature and time variations for the synthesis of 3-phenyl-1*H*-pyrazol-5-amine.[89]

| T (°C)	Time (min)	Yield (%)
120	40	84
130	30	96
130	5	53
140	20	98
150	5	99

The final parameter needed to be investigated for the synthesis of these aminopyrazoles was the optimum solvent. This was performed by myself by carrying out the reaction in different solvent, while keeping the reaction time constant at five minutes and the temperature constant at 150 °C. High yields were obtained for all solvents under microwave conditions, all with only five minutes reaction time. Results for the solvent screen can be found below (Table 4). Based on these results, MeOH was subsequently selected as the solvent of choice, due to the higher yield generated and the lower cost when compared with acetonitrile. When the same reaction was carried out under conventional heating, refluxing in MeOH, for the same five minutes, the yield drops to only 30%.[89]

Table 4: Solvent screen for the synthesis of 3-phenyl-1*H*-pyrazol-5-amine.[89]

Solvent	Yield
DCM	82%
Toluene	83%
Petroleum Ether	88%
EtOAc	92%
Acetonitrile	96%
9:1, Petroleum ether:MeOH	99%
MeOH	99%

3.4   Synthesis of aminopyrazoles

Some of the aminopyrazoles used to synthesise the pyrazolopyrimidinone bicycle compounds were commercially available. When this was not the case, they were synthesised from the corresponding β-ketonitrile by reacting it with hydrazine monohydrate and MeOH solvent in the microwave at 150 °C for five minutes (Scheme 31).
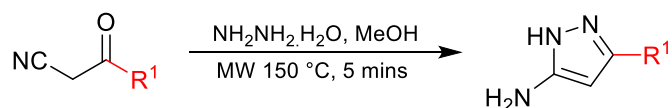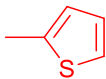
Scheme 31: Synthesis of aminopyrazole from the corresponding β-ketonitrile.

The aminopyrazoles synthesised in this project, and yields obtained, are shown in Table 5, where the R^1 substituent is an aromatic ring, a heterocyclic ring, or an alkyl group. Purification of these compounds consisted of evaporation under reduced pressure followed by column chromatography to give the product a solid in the yields reported below.

Table 5: Synthesised aminopyrazoles with isolated yields.

Compound	R^1	Yield
32 (MK12)		99%
33 (MK14)		72%
34 (MK50)		74%
35 (MK57)		67%
36 (MK52)		59%

37 (MK51)		81%
38 (MK54)	Et	54%
39 (MK53)	*t*-Butyl	77%

Structural characterisation of these compounds consisted of ^{1}H and ^{13}C NMR analysis, IR spectroscopy, and HR-MS. An example is shown below of the full structural characterisation of compound **32**. The same approach was carried out on all the remaining compounds.

3.4.1 Structural characterisation of 3-phenyl-1*H*-pyrazol-5-amine (compound 32)

The numbering scheme shown below (Figure 79) will be used in the following discussion on the structural characterisation of compound **32** which consisted of ^{1}H and ^{13}C NMR analysis, IR spectroscopy, and HR-MS.
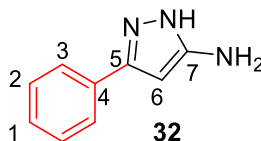
Figure 79: Structure of compound **32** with all protons and carbons assigned for characterisation.

3.4.1.1 The ^{1}H NMR spectrum of compound 32

The ^{1}H NMR spectrum of compound **32** (Figure 80) shows four signals as expected in the aromatic region. The most deshielded signal was assigned for the H3 protons of the aromatic ring as a multiplet in the range of 7.51 – 7.54 ppm. The H2 protons which are *meta* to the pyrazole ring also appear as a multiplet in the range of 7.36 – 7.38 ppm. The third signal from the aromatic ring appears as a multiplet in the range of 7.28 – 7.33 ppm for the proton in the *para* position. The proton of the pyrazole ring appeared at 5.90 ppm as a singlet signal.
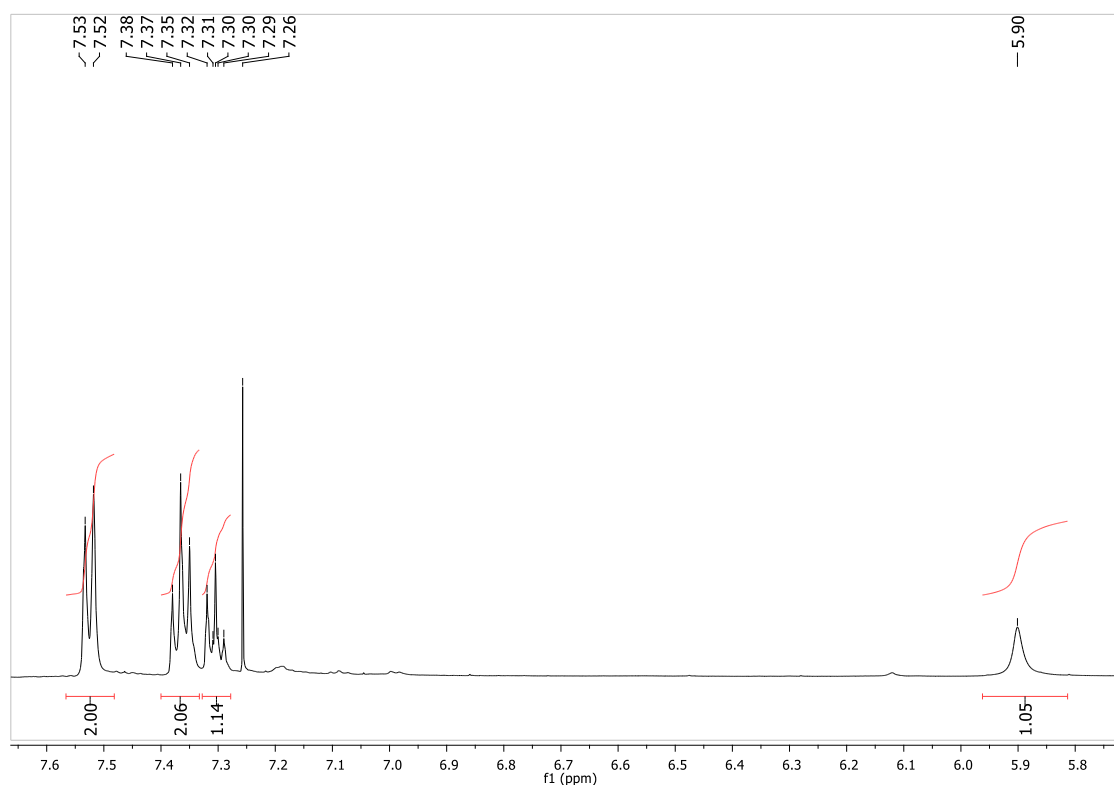
Figure 80: The ^{1}H NMR spectrum of compound **32**.

3.4.1.2 The ^{13}C NMR spectrum of compound 32

The ^{13}C NMR spectrum of compound **32** (Figure 81) contained seven signals, one for each carbon. The quaternary carbon of the pyrazole ring bonded to the amine group appears at 154.5 ppm, whereas the other quaternary carbon of the pyrazole ring bonded to the aromatic ring appears at 145.6 ppm. The quaternary carbon of the aromatic ring, *ipso* to the pyrazole ring, appears at 130.3 ppm. The CH proton signals of the aromatic ring appear at 128.9 ppm, 128.3 ppm, and 125.4 ppm, for C2, C1, and C3 respectively. The CH pyrazole carbon signal appears at 90.5 ppm.
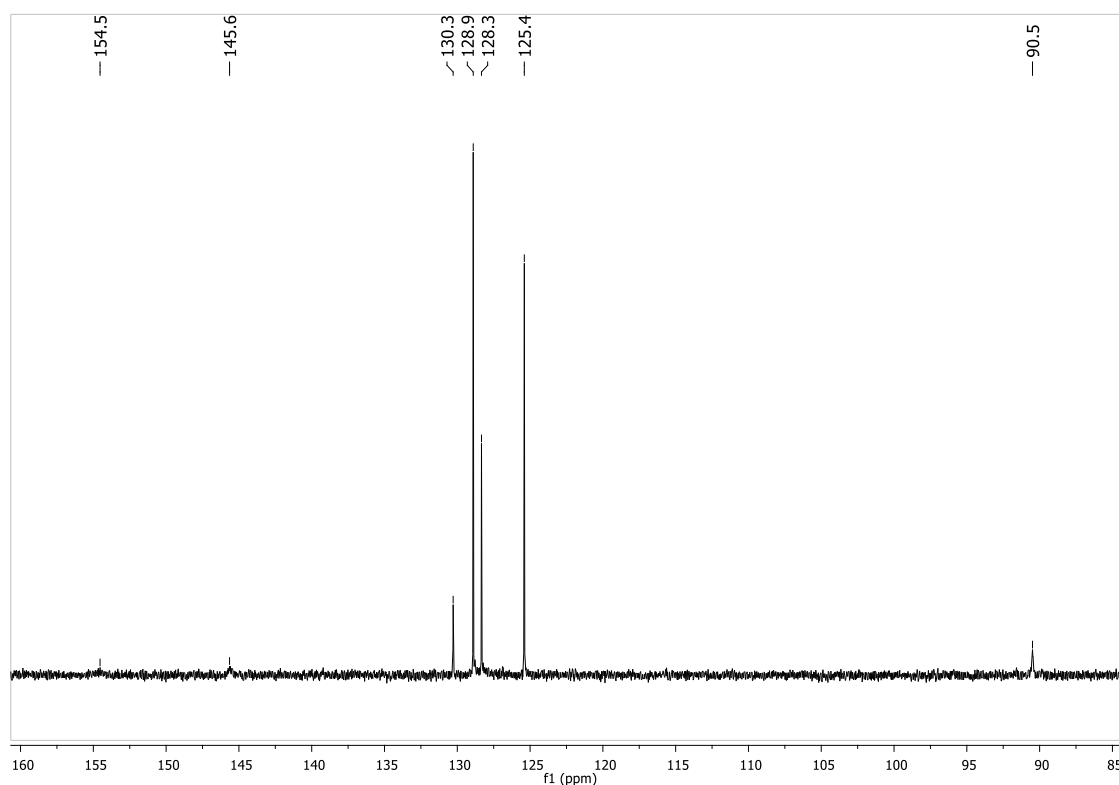
Figure 81: The ^{13}C NMR spectrum of compound **32**.

3.4.1.3 Mass spectrum of compound 32

Mass spectrometry was used in the characterisation of the aminopyrazoles to further confirm their successful synthesis. The high-resolution mass spectrum of compound **32** showed the mass obtained for $C_9H_{10}N_3$, the protonated version of the molecule (i.e. $[M+H]^+$), to be 160.0872 m/z which is -1.9 ppm different from the calculated mass of 160.0869 m/z.

3.4.1.4 IR spectrum of compound 32

IR spectroscopy identified key functional groups in the aminopyrazole which further confirmed its presence. Some of these functional groups are labelled in the IR spectrum of compound **32** below (Figure 82). They include an absorption band at 3296 cm^{-1} and 1564 cm^{-1} which are characteristic of an NH bond, and 1506 cm^{-1} and 1468 cm^{-1} for the C-C bond.
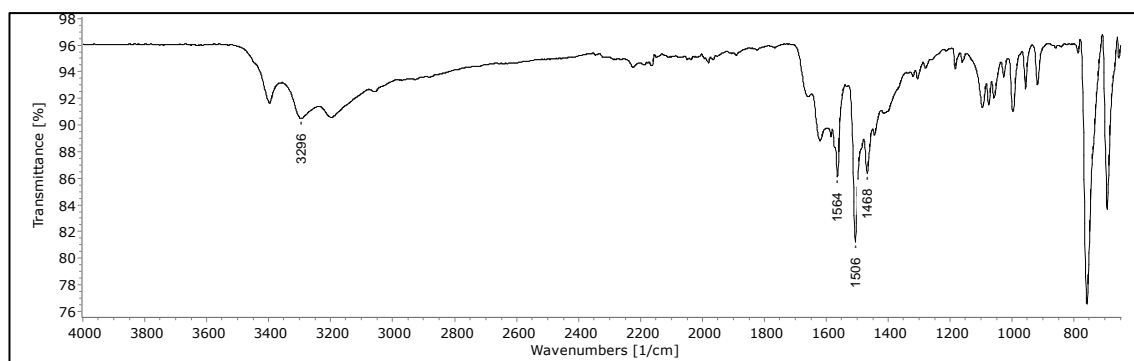
Figure 82: IR spectrum of compound **32**.

3.5 "One-pot" synthesis of the pyrazolopyrimidinone bicycle family

After developing a convenient and efficient method for the synthesis of aminopyrazoles, our attention focused on finding a "one-pot" synthesis of the pyrazolopyrimidinone bicycle using microwave-assisted synthesis as discussed earlier. Once established, such a method would eliminate the need to isolate and purify the intermediate aminopyrazole (Scheme 32). The synthesis begins with the appropriate β-ketonitrile reacting with hydrazine monohydrate, with MeOH as solvent, in the microwave at 150 °C for five minutes. Without isolating the resultant intermediate aminopyrazole, the synthesis is then continued, in the same reaction vessel, by adding the appropriate β-ketoester and acetic acid. The reaction mixture is then heated in the microwave at 150 °C for a further two hours.
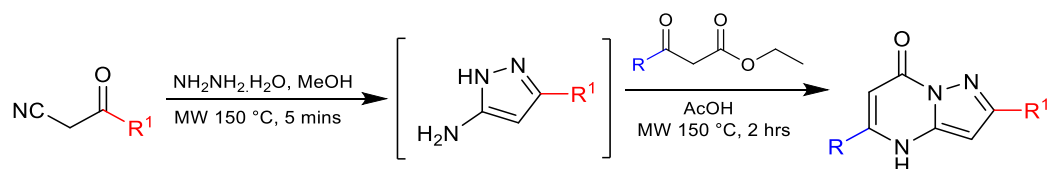
Scheme 32: "One-pot" synthesis of pyrazolopyrimidinones.

A comparative study was carried out using the synthesis of 2,5-diphenylpyrazolo[1,5-*a*]pyrimidin-7(4*H*)-one (MK15) (compound **40**). By conventional reflux heating (Scheme 33), the first reaction to synthesise 3-phenyl-1*H*-pyrazol-5-amine (MK12) (compound **32**) required 17 hours to go to completion, and the second reaction to synthesise compound **40** required 18 hours to go to completion. Therefore, in total, using conventional reflux heating, the synthesis of this product took over 35 hours to complete. This method also required isolation and purification of the intermediate aminopyrazole. This method of synthesis resulted in 15% overall yield for the two steps.
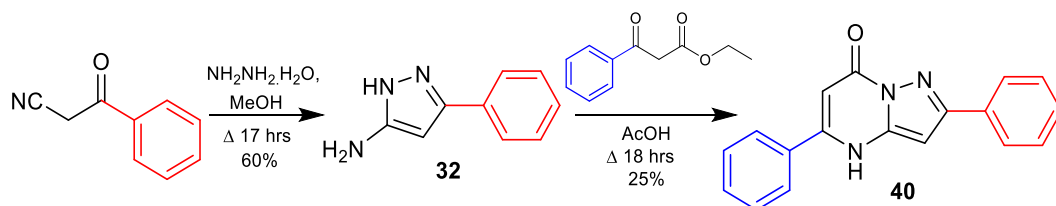
Scheme 33: Synthesis of compound **40** using conventional heating conditions.

Using microwave irradiation (Scheme 34), the first reaction to synthesise compound **32** as shown previously required only five minutes for completion, and the second reaction to synthesise compound **40** required a further two hours for completion. Therefore, in total, using microwave irradiation, the synthesis of this product took just over two hours to complete. In addition to the higher yield, this method also involved a "one-pot" approach which eliminated the need to isolate the intermediate aminopyrazole.[89] This method of synthesis resulted in 52% yield of the product over the two steps.
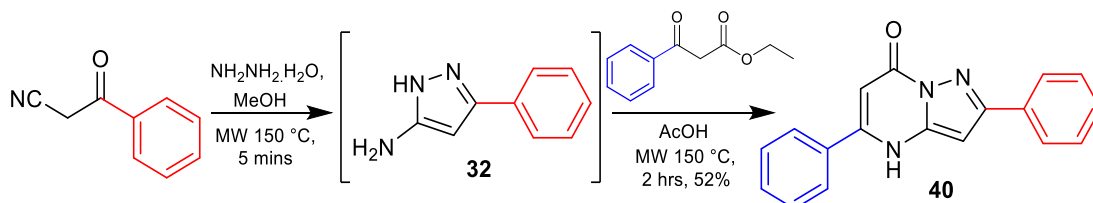
Scheme 34: Synthesis of compound **40** using microwave conditions using a "one-pot" approach.[89]

In direct comparison with the above microwave-assisted "one-pot" approach, we attempted a "one-pot" conventional heating reaction that employed the same times as the microwave heating conditions (i.e. five minutes for step one and two hours for step two). We did not isolate the intermediate aminopyrazole as per the microwave method. The final product was isolated in this case, but a complex mixture resulted. A further comparison was carried out using purified compound **32** and reacting it with the β-ketoester, ethyl 3-oxo-3-phenylpropanoate, in acetic acid and MeOH using conventional reflux heating but for only two hours. This resulted in the product isolation, but only in an 11% yield. Another comparison consisted of also reacting compound **32** with the β-ketoester, ethyl 3-oxo-3-phenylpropanoate, in acetic acid and MeOH, but using microwave heating for two hours, which resulted in 53% yield. The microwave-assisted "one-pot" approach was used for most of the pyrazolopyrimidinones reported in this thesis.

3.6 Mechanism of the formation of the pyrazolopyrimidinone bicycle

The formation of the pyrazolopyrimidinone bicycle from the appropriate β-ketoester and aminopyrazole can be explained through the following proposed mechanism (Scheme 35):
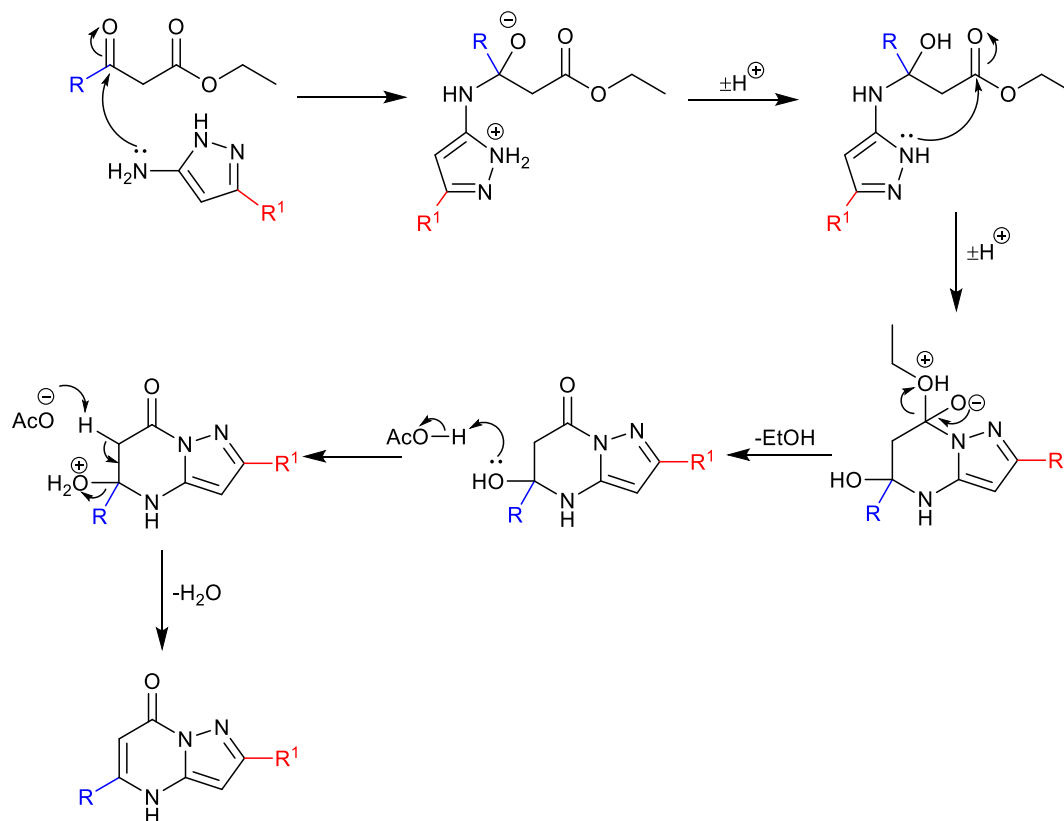
Scheme 35: Proposed mechanism for the final step of the synthesis of the pyrazolopyrimidinone bicycle.

The mechanism begins with a nucleophilic attack of the primary amine on the aminopyrazole to the first carbonyl group of the β-ketoester. Proton transfer step takes place to form an alcohol intermediate. The second cyclisation step occurs by another nucleophilic attack from the NH on the aminopyrazole to the second carbonyl group of the β-ketoester. Once the bicycle is formed, the carbonyl group is reformed by the elimination of EtOH. The hydroxyl group is protonated using acetic acid to form water, which is eliminated after the deprotonation of the α-hydrogen, resulting in the formation of the final pyrazolopyrimidinone bicycle product.

3.7 Structure variations on RTC53

As mentioned previously, structure variations were performed on the hit compound RTC53 (Figure 83) in an effort to better understand the relation between chemical structure and biological activity in the glucose uptake assay.
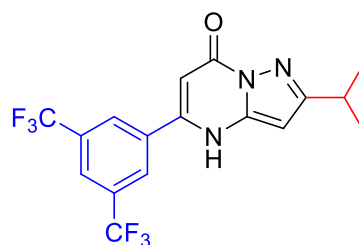
Figure 83: Structure of RTC53.

Variations in this family of compounds can be divided into three categories. Category 1 consists of variations on both sides of the pyrazolopyrimidinone bicycle (both R and R^1). Category 2 consists of variations of the R substituent on the left of the bicycle, i.e. the aromatic bis-CF_3 group, while keeping the isopropyl group. Category 3 consists of maintaining the aromatic bis-CF_3 group on the left and varying the R^1 group on the right, i.e. the isopropyl group (Figure 84).

Category 1   **Category 2**   **Category 3**
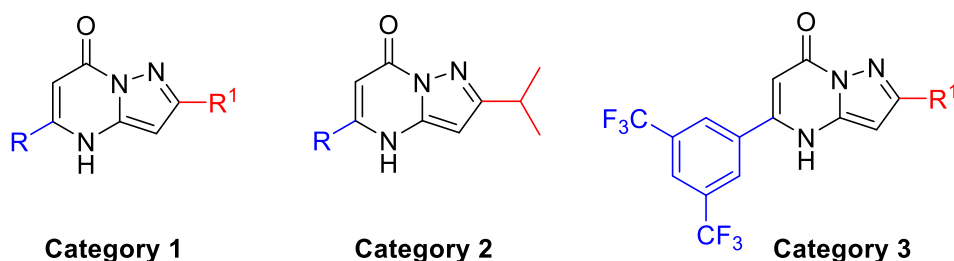
Figure 84: Structural variations of RTC53.

3.7.1 Category 1: Substituent variation on both sides of the pyrazolopyrimidinone core (R and R^1)

The first category of variations of RTC53 consisted of changing both the aromatic bis-CF$_3$ group on the left (R) and the isopropyl group on the right (R^1) of the pyrazolopyrimidinone bicycle (Figure 85).
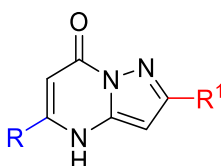
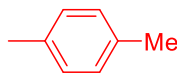

Figure 85: Category 1 variations on both sites, R and R^1.
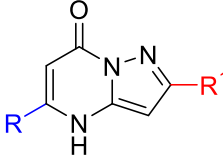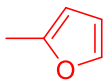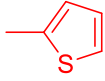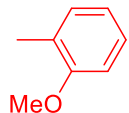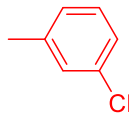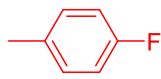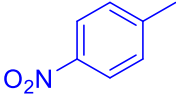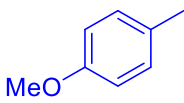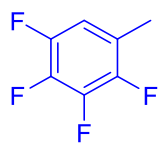
Compounds produced in this category of variations were synthesised using the "one-pot" microwave-assisted method as described in section **3.5**. Starting from the β-ketonitrile, reaction with hydrazine generated the intermediate aminopyrazole and subsequent addition of the corresponding β-ketoester resulted in the desired pyrazolopyrimidinone bicycle (Scheme 36). After removing volatiles under reduced pressure, products were purified using column chromatography or trituration using a suitable solvent such as MeOH or EtOAc.
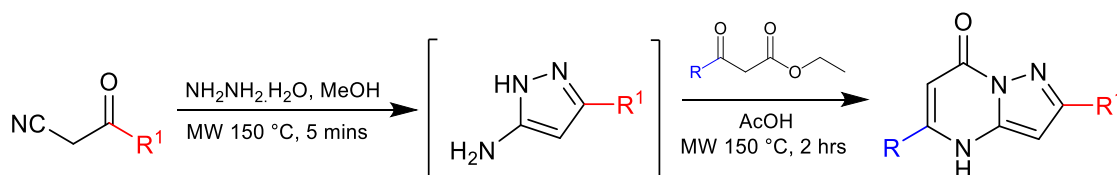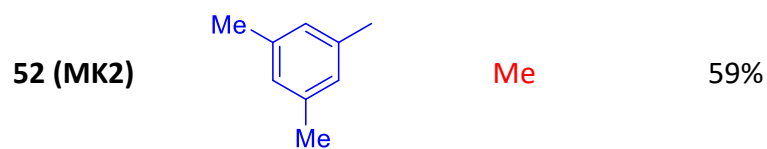

Scheme 36: Synthesis of pyrazolopyrimidinones of group 1 using the "one-pot" synthesis.

Twelve compounds were made in total with category 1 variations. The R group was maintained as an aromatic ring, be that a phenyl ring or a substituted aromatic ring. Substituent variations at the R^1 site included alkyl groups, substituted aromatic rings, heterocyclic rings, and a phenyl ring. Aromatic ring substitutions included those at the *ortho, meta* and *para* positions of the aromatic rings, and consisted of electron donating (e.g. methyl and methoxy) and electron withdrawing groups (e.g. nitro group) (Table 6).

Table 6: Pyrazolopyrimidinone bicycles synthesised category 1 variations (at R and R^1).

Compound	R	R^1	Yield
41 (MK56)	Ph		50%
42 (MK55)	Ph		40%
43 (MK62)	Ph	Me	33%
44 (MK59)	Ph		17%
45 (MK58)	Ph		32%
46 (MK7)	Ph		45%
47 (MK8)	Ph		67%
48 (MK9)	Ph		45%
40 (MK15)	Ph	Ph	29%
49 (MK61)		Ph	30%
50 (MK66)		Ph	16%
51 (MK63)		Ph	22%

52 (MK2)	Me Me Me	Me	59%

The successful synthesis of these compounds was confirmed by using ^{1}H and ^{13}C NMR spectroscopy, HR-MS, and IR spectroscopy. Section **3.7.1.1** details the approach taken for the structural characterisation of the pyrazolopyrimidinone family, using the furan substituted pyrazolopyrimidinone (compound **41**) as an example. Common absorption bands found in the IR spectra of all these compounds appear at 3251 cm^{-1}, which is characteristic of an N-H bond stretch, 3060 cm^{-1} for the aromatic C-H bonds, 1665 for the carbonyl C=O bond, and 1597 cm^{-1} for the aromatic C-C bonds. Each compound was analysed using HR-MS and the correct mass was found for all compounds with a difference of less than 5.0 ppm from the calculated mass.

3.7.1.1 Structural characterisation of 2-(furan-2-yl)-5-phenylpyrazolo[1,5-a]pyrimidin-7(4*H*)-one (compound 41)

The numbering scheme shown below (Figure 86) will be used in the following discussion on the structural characterisation of compound **41**. Structural characterisation of this compound involved ^{1}H and ^{13}C NMR spectroscopy, IR spectroscopy, and mass spectrometry. The ^{1}H and ^{13}C NMR signals were assigned with the aid of 2D-NMR experiments such as ^{1}H – ^{1}H COSY, ^{1}H – ^{13}C HSQC, and ^{1}H – ^{13}C HMBC. Furthermore, an X-ray crystal structure of this compound was obtained in order to further confirm its formation.
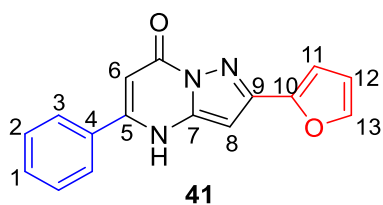
Figure 86: Structure of compound **41** with all protons and carbons numbered for characterisation.

3.7.1.1.1 The ^{1}H NMR spectrum of compound 41

The ^{1}H NMR spectrum of compound **41** (Figure 87) has eight signals.
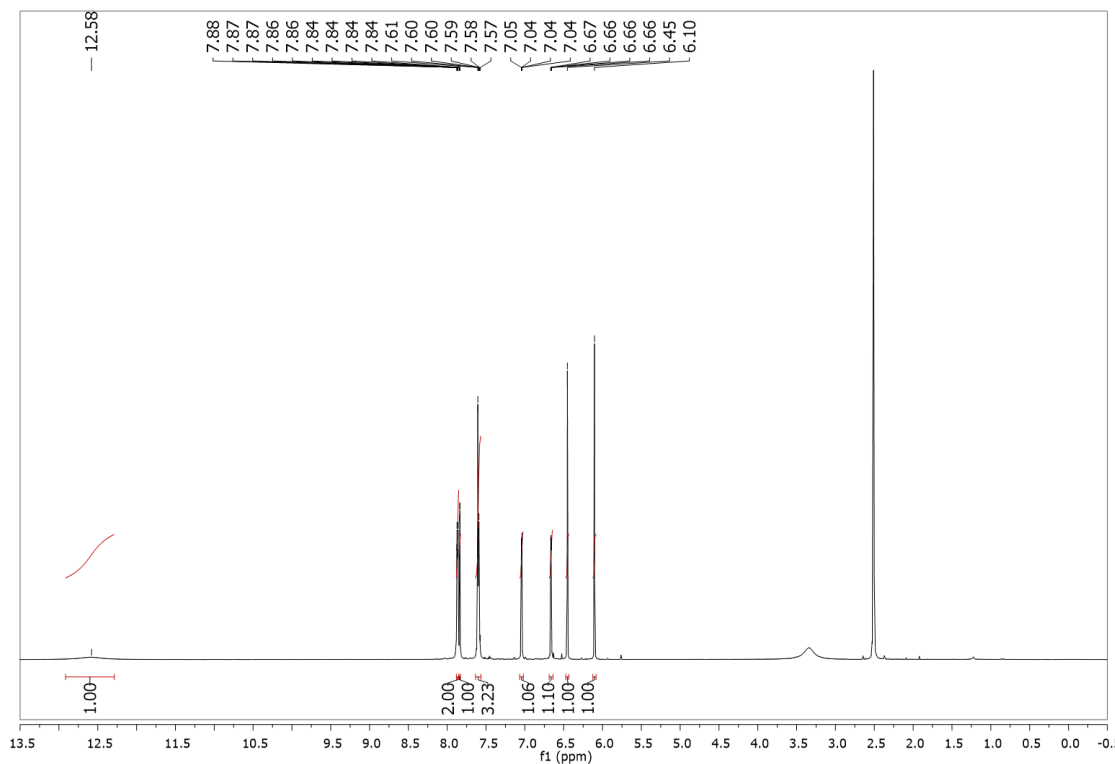
Figure 87: ^{1}H NMR spectrum of compound **41.**

The most downfield signal at 12.58 ppm is a broad singlet for the NH signal, integrating for 1H. This signal appears deshielded as the hydrogen atom is directly bonded to an electronegative nitrogen. The most upfield signals appear as singlets with a chemical shift of 6.45 ppm, representing the pyrazole proton (H8), and 6.10 ppm, representing the α-proton (H6), each integrating for 1H.

The next five signals appear in the aromatic region (Figure 88) and can be assigned to the protons of the phenyl and furan rings. The protons arising from the phenyl ring in the *ortho* position (H3) appear as a multiplet in the range of 7.85 – 7.90 ppm, integrating for 2H. The protons arising from the phenyl ring in the *meta* position (H2), and *para* position (H1), appear as a multiplet in the range of 7.56 – 7.64 ppm, integrating for 3H.
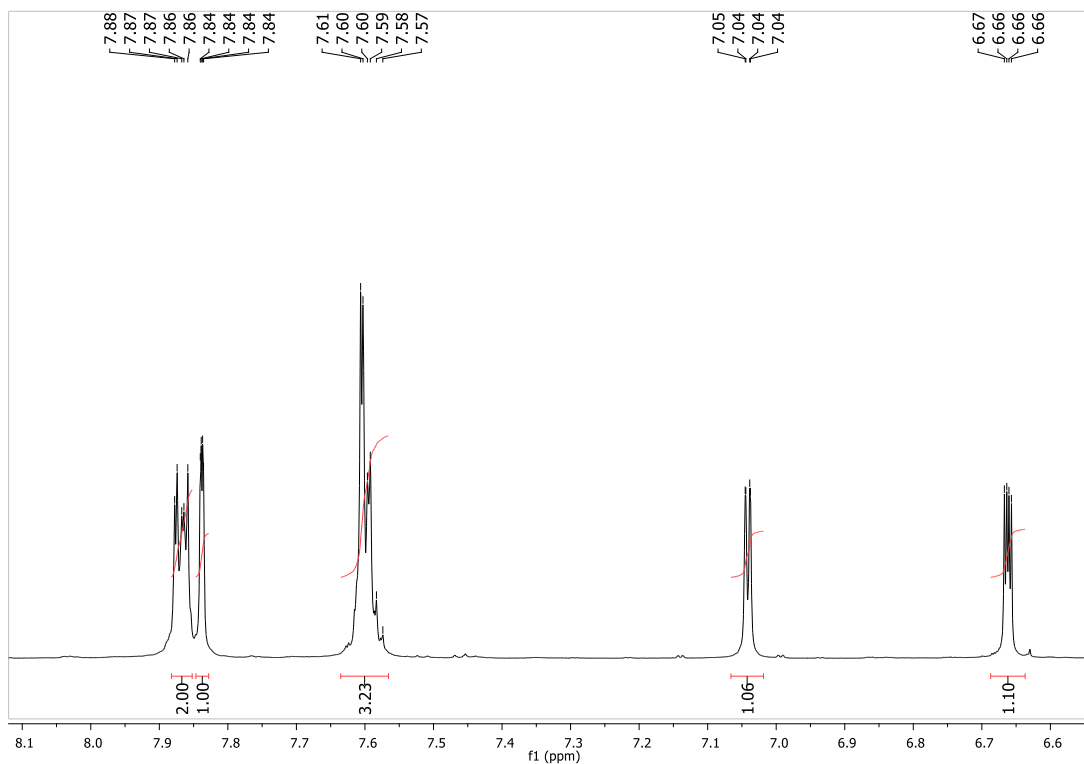
Figure 88: The aromatic region of the ^{1}H spectrum of compound **41.**

The signals arising from the furan ring appear at 6.66 ppm (H12), 7.04 ppm (H11), and 7.84 ppm (H13). Each proton was split by two non-equivalent protons and therefore all appear a double of doublets. The *J* value was calculated for these 3 signals and helped distinguish which protons they represent. The *J* value due to the coupling between H11 and H12 was calculated to be 3.3 Hz. The *J* value due to the coupling between H12 and H13 was found to be 1.7 Hz, and the longer-range coupling between H11 and H13 was 0.6 Hz.

3.7.1.1.1.1   The ^{1}H–^{1}H COSY 2D-NMR spectrum of compound 41

As previously discussed in section **2.2.3.1.1**, the ^{1}H–^{1}H COSY NMR is a 2D-NMR experiment which shows coupling between protons in the same coupling system. The ^{1}H – ^{1}H COSY spectrum (Figure 89) of compound **41** showed the coupling systems within the aromatic region. The phenyl ring contained coupling between H3, H1 and H2 (red square), and the furan ring contained coupling between H13 and H12 (green square) as well as between H11 and H12 (blue square). The coupling between H11 and H13 was too weak to be observed in the ^{1}H – ^{1}H COSY spectrum but was evident from the splitting of the peaks (i.e. double of doublets). The ^{1}H – ^{1}H COSY spectrum confirms the assignment of H12 as it is coupled to both H11 and H13. The signal for H13 can be distinguished from H11 as it is more deshielded, as is expected for a furan ring since it is adjacent to the electronegative oxygen of the furan ring, unlike H11.
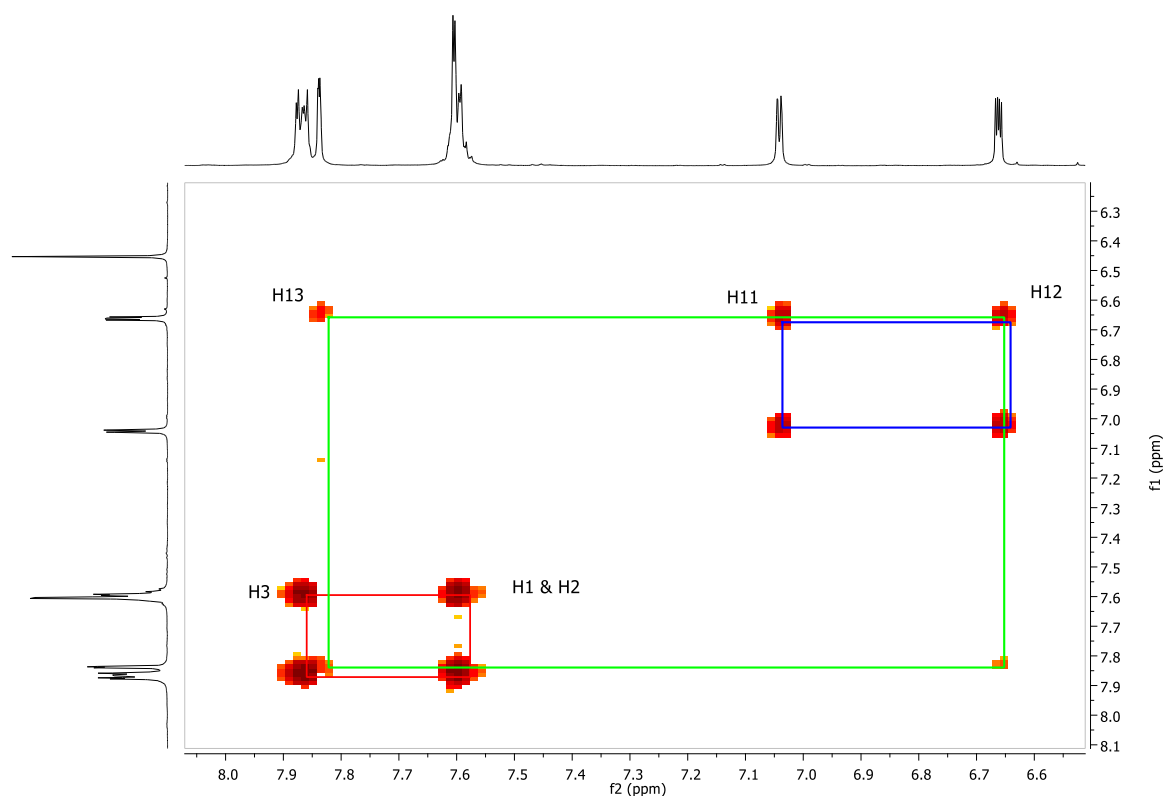
Figure 89: ^{1}H – ^{1}H COSY 2D spectrum of compound **41.**

3.7.1.1.2 The ^{13}C NMR spectrum of compound 41

Structural characterisation of compound **41** (Figure 90) also involved the use of a ^{13}C NMR experiment.
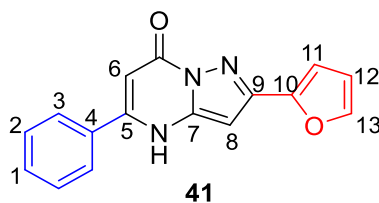

Figure 90: Structure of compound **41** with all protons and carbons numbered.

The ^{13}C NMR spectrum of compound **41** (Figure 91) generated 14 signals. These consist of six quaternary carbons and eight tertiary carbons. The assignment of these signals was confirmed by the 2D-NMR experiments ^{1}H – ^{13}C HSQC and ^{1}H – ^{13}C HMBC.
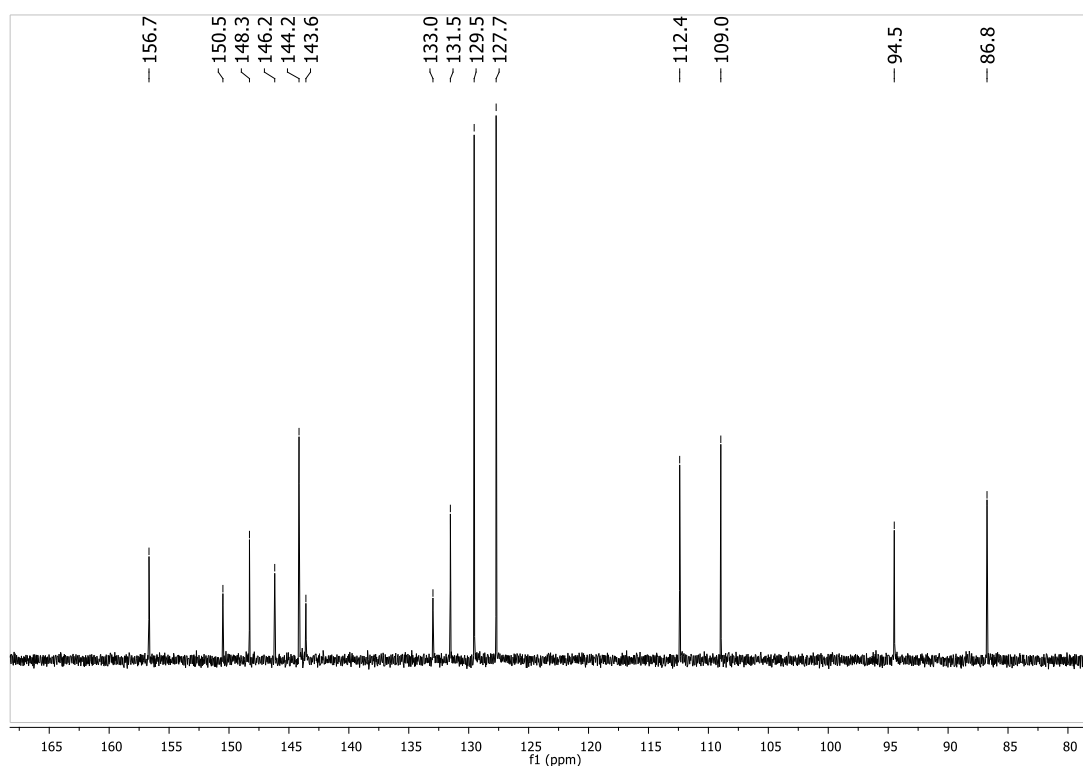
Figure 91: ^{13}C NMR spectrum of compound **41**.

Six quaternary carbons were identified; the carbonyl carbon at 156.7 ppm, the β-carbon (C5) at 150.5 ppm, the *ipso* carbon of the furan ring (C10) at 148.3 ppm, the carbon of the bicycle core bonded to the furan ring (C9) at 146.2 ppm, the bridgehead carbon of the bicycle core (C7) at 143.6 ppm, and the *ipso* carbon of the phenyl ring (C4) at 133.0 ppm.

The carbon adjacent to the electronegative oxygen of the furan ring (C13) appears downfield at 144.2 ppm. The other two carbon signals of the furan ring appear at 112.4 ppm (C12) and 109.0 ppm (C11). The carbon signals of the phenyl ring appear in close proximity to each other at 131.5 ppm (C1), 129.5 ppm (C2), and 127.7 ppm (C3). Finally, the most upfield signals consist of the signal for the α-carbon (C6) at 94.5 ppm, and for the pyrazole carbon of the bicycle core (C8) at 86.8 ppm.

3.7.1.1.2.1 The ^{1}H–^{13}C HSQC 2D-NMR spectrum of compound 41

As previously discussed in section **2.2.3.2.2**, the ^{1}H-^{13}C HSQC experiment is a 2D-NMR technique that correlates chemical shifts of directly bound nuclei (i.e. ^{1}H with ^{13}C). The ^{1}H–^{13}C HSQC spectrum (Figure 92) of compound **41** helped confirm the identity of the eight tertiary carbon signals already discussed. This was achieved by correlating each ^{13}C NMR signal with the corresponding ^{1}H signal in the ^{1}H-^{13}C HSQC spectrum. For example, the ^{1}H NMR signal at 6.45 ppm representing H8 correlated with the ^{13}C NMR signal at 86.8 ppm, therefore the signal at 86.8 ppm was assigned to C8.
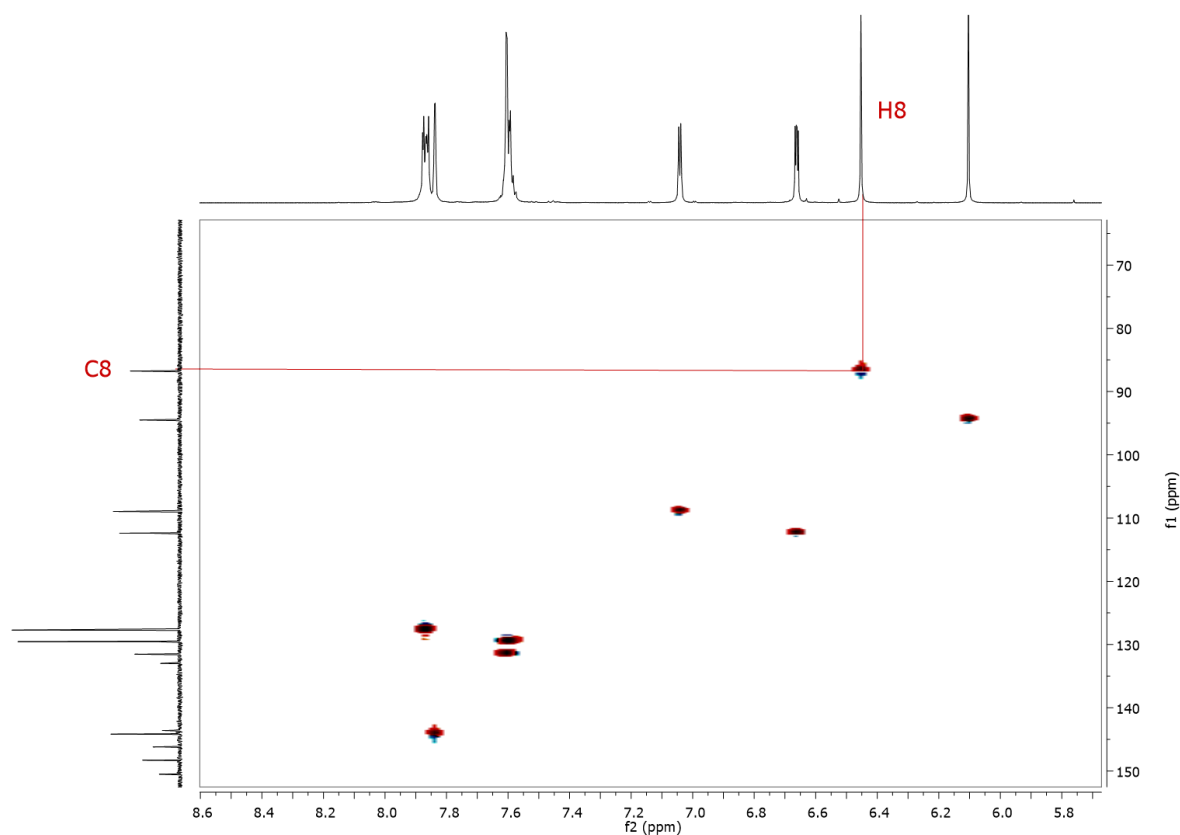
Figure 92: ^{1}H – ^{13}C HSQC 2D-NMR spectrum of compound **41**.

3.7.1.1.2.2 The ^{1}H–^{13}C HMBC 2D-NMR spectrum of compound 41

Another useful 2D-NMR experiment that was employed used was the ^{1}H–^{13}C HMBC, which, as previously mentioned in section **2.2.3.2.1**, correlates the ^{1}H NMR signals with the ^{13}C NMR signals generated by atoms that are two or three bonds away from each other. The ^{1}H – ^{13}C HMBC spectrum (Figure 93) of compound **41** further confirmed the assignment of the tertiary carbons but was essential for identification of the quaternary carbons.

With regards to the tertiary carbons, an example is the signal for C12 at 112.4 ppm, which correlates with H11 at 7.04 ppm, and H13 at 7.84 ppm (red lines), as expected based on the proposed structure. In the same way, C11 at 109.0 ppm correlates with H12 at 6.66 ppm, and H13 at 7.84 ppm (green lines). The same technique was used to confirm the identity of C13 and the tertiary carbons of the phenyl ring.
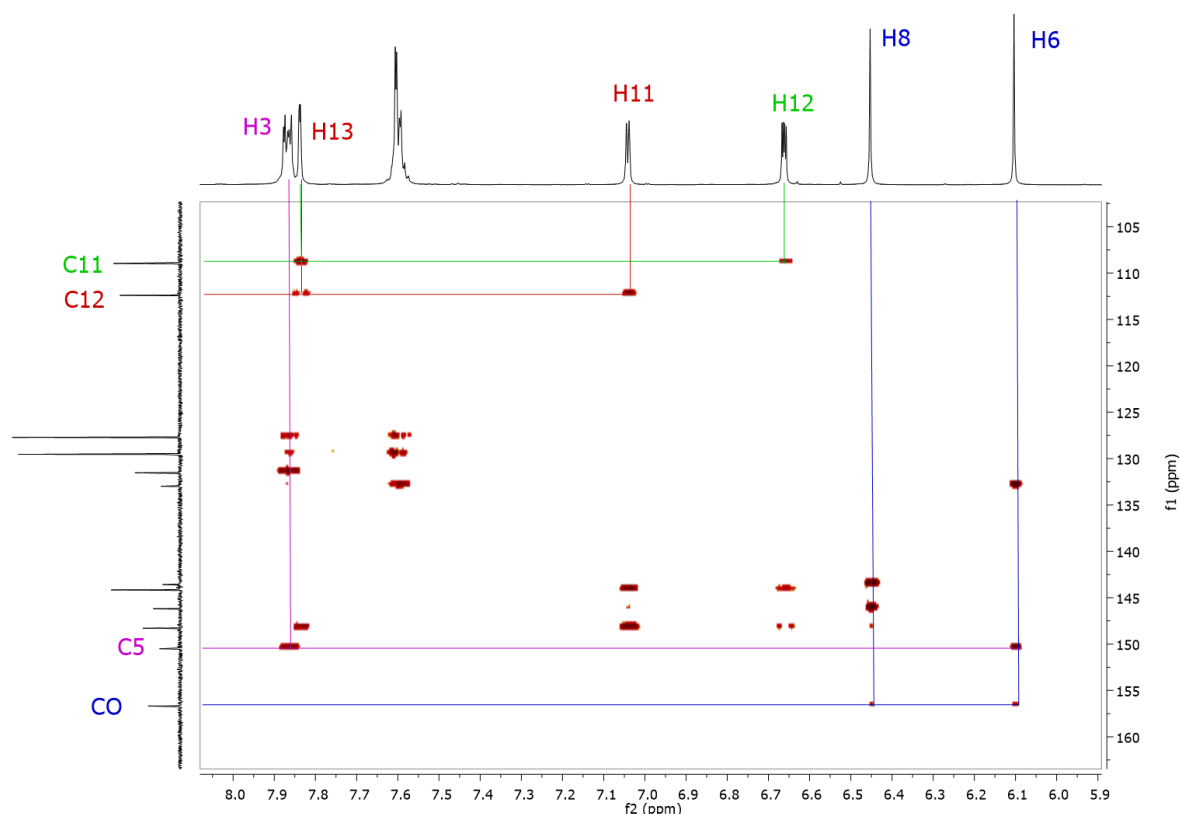
Figure 93: The ^{1}H – ^{13}C HMBC 2D-NMR spectrum of compound **41**.

The ^{1}H – ^{13}C HMBC spectrum was of critical importance for the assignment of the six quaternary carbons. The ^{13}C signal at 156.7 ppm was assigned as the carbonyl carbon signal as it correlates with the H8 proton of the pyrazole at 6.45 ppm, and the α-proton

(H6) adjacent to it at 6.10 ppm (blue lines). The ^{13}C signal at 150.5 ppm was assigned as the carbon β to the carbonyl (C5) as it correlates with the protons at the *ortho* position (H3) of the aromatic ring in the range of 7.89 – 7.90 ppm, and the α-proton (H6) at 6.10 ppm (magenta lines).

The ^{13}C signal at 148.3 ppm was assigned as the *ipso* carbon of the furan ring (C10) as it correlates with all three protons of the furan ring (H11, H12 and H13). The ^{13}C signal at 146.2 ppm was assigned as the carbon of the bicycle core bonded to the furan ring (C9) as it correlates with the H8 proton of the pyrazole ring adjacent to it, and weakly with H11, which is three bonds away from it. The ^{13}C signal at 143.6 ppm was assigned as the C7 carbon of the bicycle core as it only correlates with the H8 pyrazole proton adjacent to it. The final ^{13}C signal at 133.0 ppm was assigned as the *ipso* carbon of the phenyl ring (C4) as it correlates with the α-proton (H6), and with the aromatic protons (H1, H2 and H3).

3.7.1.1.3 Mass spectrum of compound 41

Mass spectrometry was used in the characterisation of these compounds to further confirm the presence or absence of the target compounds. The high-resolution mass spectrum (Figure 94) of compound **41** showed the mass obtained for $C_{16}H_{11}N_3O_2Na$, the ionised version of the molecule with a sodium cation (i.e. $[M + Na]^+$), was found to be 300.0757 m/z which is 4.70 ppm different from the calculated mass of 300.0743 m/z. It also found the mass of $(C_{16}H_{11}N_3O_2)_2Na$ (i.e. $[2M + Na]^+$) ion to be 577.1615 m/z which is 3.47 ppm different from the calculated mass of 577.1595 m/z.
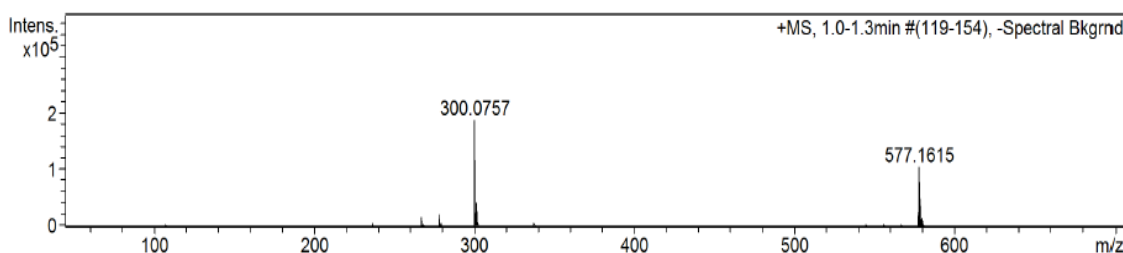
Figure 94: Mass spectrum of compound **41**.

3.7.1.1.4 Infrared spectrum of compound 41

IR spectroscopy identified key functional groups which further confirmed the presence of our target compound. The IR spectrum (Figure 95) of compound **41** shows an absorption frequency of 3122 cm^{-1} characteristic of the secondary amine (N-H), 3059 cm^{-1} for the aromatic C-H's, and 1670 cm^{-1} for the carbonyl group (C=O stretch).
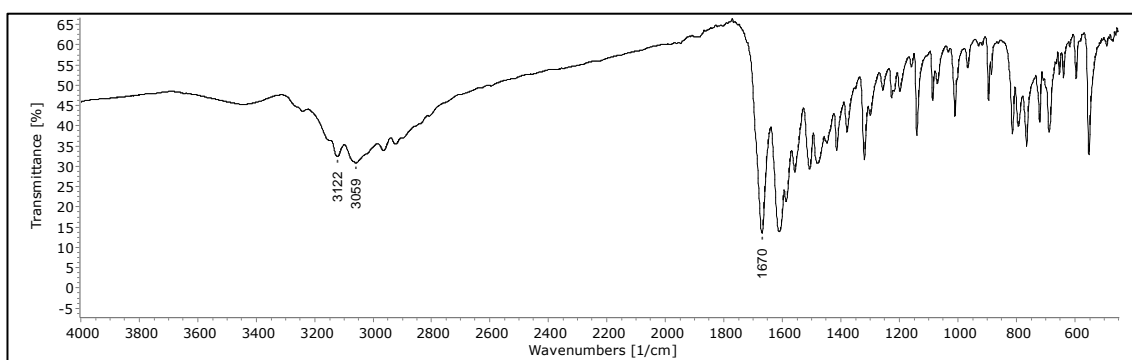
Figure 95: IR spectrum of compound **41**.

3.7.1.1.5 X-ray crystal structure of compound 41

The final characterisation carried out for compound **41** was an X-ray crystal structure analysis which confirmed the correct structure of our compound. Recrystallization of the sample was performed using the solvent system 4:1, EtOH:H_2O at room temperature. The X-ray crystal structure (Figure 96) obtained shows the phenyl ring on the left (C7 – C12), the pyrazolopyrimidinone bicycle core structure in the middle with the carbonyl oxygen (O1) and the three nitrogens (N1 – N3), and the furan ring on the right (C13 – C16) with the furan oxygen (O2).
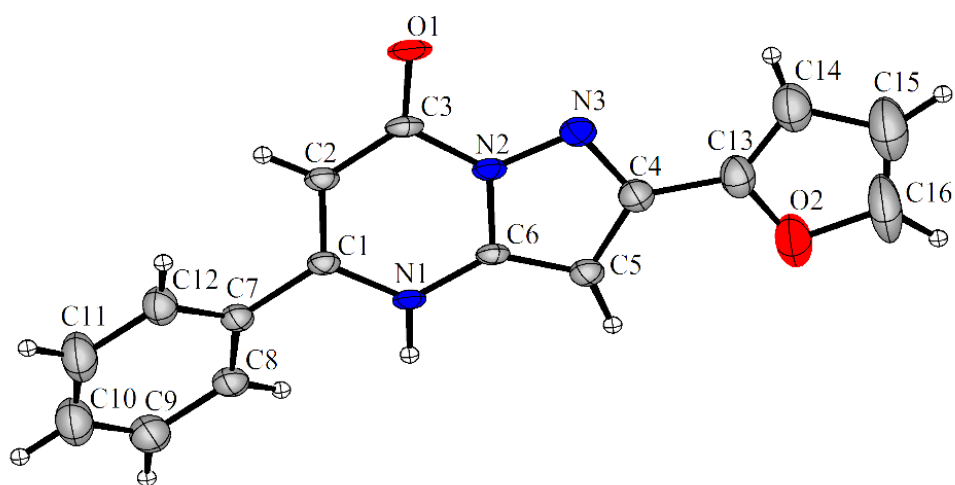
Figure 96: X-ray crystal structure of compound **41**.

3.7.1.2 Structural characterisation of 5-phenyl-2-(thiophen-2-yl)pyrazolo[1,5-a]pyrimidin-7(4*H*)-one (compound 42)

42
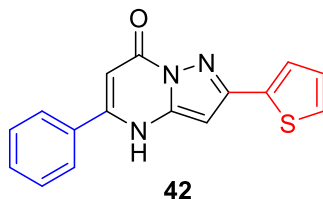
Figure 97: Structure of compound **42**.

The compound containing a thiophene ring at the R^1 site, compound **42** (Figure 97), generated three ^{1}H NMR signals and five ^{13}C NMR signals for the thiophene ring. The ^{1}H NMR signal for the proton adjacent to the electronegative sulphur is the most deshielded signal and appears as a doublet at 7.61 ppm, as it is coupled to the neighbouring proton. The carbon bonded to this proton appears at 125.7 ppm in the ^{13}C NMR spectrum.

The proton furthest from the sulphur appears as a doublet at 7.53 ppm in the ^{1}H NMR spectrum. It is also coupled to the neighbouring proton, with the carbon bonded to it appearing at 126.2 ppm in the in the ^{13}C NMR spectrum. The remaining thiophene proton is coupled to two non-equivalent protons and therefore appears as a double of doublets at 7.13 ppm, with the carbon bonded to it appearing at 128.1 ppm in the ^{13}C NMR spectrum. The quaternary *ipso* carbon of the thiophene ring appears at 148.3 ppm, and the quaternary carbon, of the bicycle core, directly bonded to the thiophene ring appears at 137.7 ppm. The phenyl substituted pyrazolopyrimidine core generated all the expected signals in both the ^{1}H and ^{13}C NMR spectra. The IR and MS data also confirmed the generation of compound **42**.

### 3.7.1.3 Structural characterisation of 2-methyl-5-phenylpyrazolo[1,5-a]pyrimidin-7(4H)-one (compound 43)
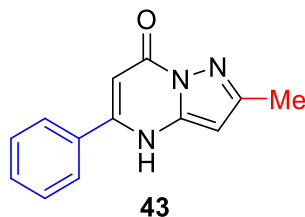
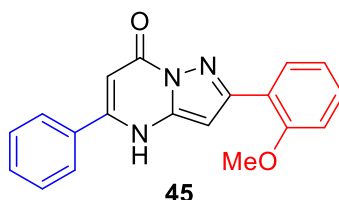**Figure 98:** Structure of compound **43**.

Compound **43** (Figure 98) contains a methyl group at the R^1 site and a phenyl ring at the R site and generated all the expected NMR signals. The presence of the methyl group results in a singlet in the ^1H NMR spectrum at 2.32 ppm. The same methyl group also generates a signal at 14.6 ppm in the ^{13}C NMR spectrum. The quaternary carbon bonded to the methyl group appears at 152.6 ppm in the ^{13}C NMR spectrum. The IR spectrum of this compound showed an absorbance band at 1327 cm^{-1}, which is characteristic of an alkyl C-H bond. The MS data also confirmed the generation of compound **43**.

3.7.1.4 Structural characterisation of 2-(tert-butyl)-5-phenylpyrazolo[1,5-a]pyrimidin-7(4H)-one (compound 44)
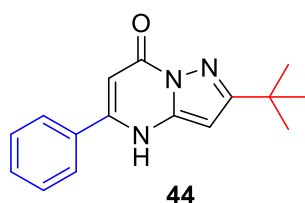
Figure 99: Structure of compound **44**.

The compound containing a t-butyl group at the R^1 site, compound **44** (Figure 99), like compound **43**, also contained a singlet signal in the alkyl region of the ^1H NMR spectrum. This time the signal occurs at 1.42 ppm and integrates for the nine protons of the t-butyl group. The carbon signal for the three equivalent methyl groups appears at 30.6 ppm in the ^{13}C NMR spectrum. The carbonyl carbon appears at 165.2 ppm, the quaternary carbon bonded to the t-butyl group appears at 142.8 ppm, whereas the quaternary carbon of the t-butyl group appears at 32.9 ppm. The phenyl substituted pyrazolopyrimidinone generated all the expected ^1H and ^{13}C NMR signals. Similar to

before, the IR spectrum showed an absorbance band at 1324 cm^{-1}, which is characteristic of an alkane C-H bond, and the MS data also confirmed the generation of compound **44**.

3.7.1.5 Structural characterisation of 2-(2-methoxyphenyl)-5-phenylpyrazolo[1,5-*a*]pyrimidin-7(4*H*)-one (compound 45)
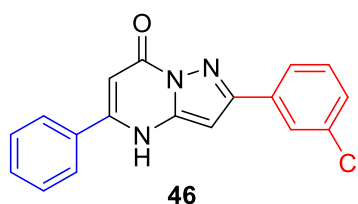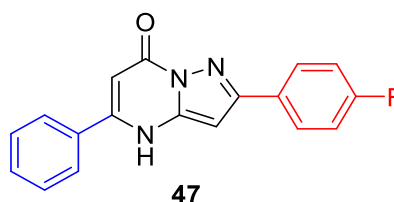

Figure 100: Structure of compound **45**.

Compound **45** (Figure 100), contains an *ortho* methoxy substituted aryl ring at the R^1 site. The NMR spectra for compound **45** contains four aromatic proton signals in the ^{1}H NMR spectrum and seven carbon signals in the ^{13}C NMR spectrum. The most deshielded signal in the ^{1}H NMR spectrum is a broad singlet at 7.99 ppm for the aromatic ring proton *ortho* to the pyrazolopyrimidinone bicycle core. The carbon attached to this proton appears at 128.9 ppm in the ^{13}C NMR spectrum. The proton *para* to the bicycle core appears as a *pseudo* triplet at 7.30 ppm instead of the expected double of doublets shape as it is coupled by two non-equivalent protons. The carbon bonded to this proton appears at 129.4 ppm in the ^{13}C NMR spectrum.

The proton adjacent to the methoxy group (*meta* to the bicycle core) appears as multiplet in the range of 7.02 – 7.05 ppm, while the other *meta* proton appears as a multiplet in the range of 6.95 – 6.98 ppm. These protons appear more shielded than expected due to the presence of the methoxy group (Scheme 37). The corresponding carbons bonded to these protons appear at 112.3 ppm and 120.8 ppm, respectively. The protons from the methyl group appear as a singlet at 3.89 ppm, which was more deshielded than typical methyl proton signals due to the electron withdrawing effect of oxygen.
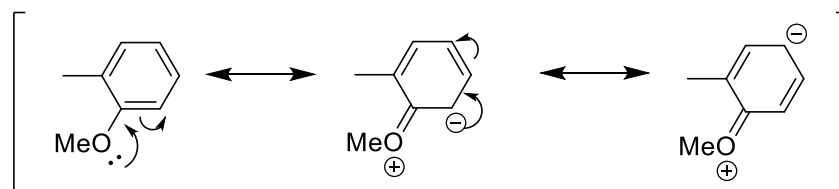
Scheme 37: Resonance contributors of the methoxy substituted aromatic ring.

The carbon of the methyl group appears at 56.0 ppm in the ^{13}C NMR spectrum. The quaternary carbon bonded to the methoxy group appears at 157.4 ppm, the quaternary carbon bonded to the aromatic ring from the bicycle core appears at 152.0 ppm, and the quaternary *ipso* carbon from the aromatic ring appears at 123.3 ppm. The IR spectrum showed an absorbance band at 1248 cm^{-1}, which is characteristic of the C-O bond stretch of the methoxy group. The MS data also confirmed the generation of compound **45**.

3.7.1.6 Structural characterisation of 2-(3-chlorophenyl)-5-phenylpyrazolo[1,5-*a*]pyrimidin-7(4*H*)-one (compound 46)


46

Figure 101: Structure of compound **46**.

The compound containing a *meta* substituted chlorine aryl ring at the R^1 site, compound **46** (Figure 101), generated four proton signals and six carbon signals for the aromatic ring. The most deshielded signal appearing as a singlet at 8.07 ppm in the ^{1}H NMR spectrum was due to the proton in the *ortho* position adjacent to the electron withdrawing chlorine. The carbon bonded to this proton appears at 129.6 ppm in the ^{13}C NMR spectrum. The other proton adjacent to the chlorine group in the *para* position appears as a doublet at 8.00 ppm in the ^{1}H NMR spectrum, due to coupling with one non-equivalent proton, and the corresponding carbon at 129.2 ppm.

The other two protons from the aromatic ring had overlapping signals and therefore appears as a multiplet in the range of 7.46 – 7.56 ppm, with corresponding carbons at 126.2 ppm and 125.3 ppm in the ^{13}C NMR spectrum. The quaternary carbon bonded to

the chlorine appears at 158.9 ppm, the quaternary carbon from the bicycle core bonded to the aromatic ring appears at 152.3 ppm, and the quaternary *ipso* carbon appears at 128.1 ppm. The IR spectrum showed an absorbance band at 772 cm^{-1}, which is characteristic of a C-Cl bond. The MS data also confirmed the generation of compound **46**.

3.7.1.7 Structural characterisation of 2-(4-fluorophenyl)-5-phenylpyrazolo[1,5-*a*]pyrimidin-7(4*H*)-one (compound 47)
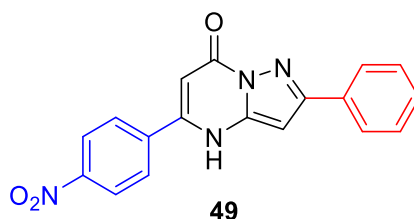

Figure 102: Structure of compound **47**.

Compound **47** (Figure 102) contains a *para* fluoro substituted aryl ring at the R^1 site and a phenyl ring at the R site. There are two multiplet signals in the ^{1}H NMR spectrum for the four protons of the aryl ring, as opposed to four signals. These signals occur in the range of 8.02 – 8.12 ppm for the protons *ortho* to the pyrazolopyrimidinone, and 7.31 – 7.37 ppm for the protons *meta* to the pyrazolopyrimidinone. Each signal integrates for two protons. These signals appear more deshielded due to the effect of the electron withdrawing fluoro substituent.

The multiplet shape of the peaks may have been due to coupling of the aromatic protons with the NMR-active ^{19}F atom. The carbons bonded to these protons both appear as doublets in the ^{13}C NMR spectrum due to bonding with fluorine at 128.8 ppm (J_{CF} = 8.4 Hz) and 116.2 ppm (J_{CF} = 21.5 Hz) respectively. The quaternary carbon bonded to the fluorine also appears as a doublet at 163.1 ppm (J_{CF} = 246.3 Hz) and the quaternary carbon of the bicycle core that is bonded to the fluoro aryl ring appears as a singlet at 152.9 ppm. The fluoro aryl quaternary carbon *ipso* to the pyrazolopyrimidinone appears as a doublet at 129.4 ppm (J_{CF} = 3.0 Hz). The IR and MS data also confirmed the generation of compound **43**.

3.7.1.8 Structural characterisation of 5-phenyl-2-(*p*-tolyl)pyrazolo[1,5-*a*]pyrimidin-7(4*H*)-one (compound 48)
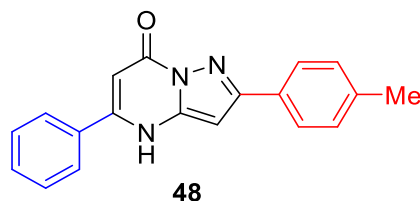
Figure 103: Structure of compound **48**.

The compound containing a *para* methyl aryl ring at the R^1 site, compound **48** (Figure 103), like for compound **47** has free rotation about the bond between the *para* methyl substituted aryl ring and the pyrazolopyrimidinone bicycle. As a result, one would expect the aryl ring to contain two sets of equivalent protons generating two signals in the ^{1}H NMR spectrum. For compound **48**, there are overlapping signals in the aromatic region of the ^{1}H NMR spectrum. The ^{1}H NMR spectrum contains a signal for the protons *ortho* to the pyrazolopyrimidinone as a multiplet in the range of 7.82 – 7.96 ppm, which overlapped with the *ortho* protons of the phenyl ring. The carbon bonded to this proton appears as a singlet at 129.5 ppm in the ^{13}C NMR spectrum.

The protons of the methyl substituted aromatic ring *meta* to the pyrazolopyrimidinone appear as a doublet (J = 7.8 Hz) in the ^{1}H NMR spectrum at 7.30 ppm as they coupled with the neighbouring *ortho* protons. The carbons bonded to these protons appear at 127.7 ppm in the ^{13}C NMR spectrum. The methyl group protons appear as a singlet at 2.37 ppm in the ^{1}H NMR spectrum, and the methyl carbon appears at 21.4 ppm in the ^{13}C NMR spectrum. The quaternary carbon of the bicycle core that is bonded to the methyl substituted aromatic ring appears at 153.8 ppm, the quaternary carbon bonded to the methyl group appears at 138.9 ppm, and the quaternary carbon *ipso* to the pyrazolopyrimidinone appears at 130.1 ppm. The IR and MS data also confirmed the generation of compound **48**.

### 3.7.1.9 Structural characterisation of 2,5-diphenylpyrazolo[1,5-*a*]pyrimidin-7(4*H*)-one (compound 40)
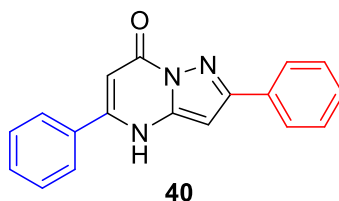
Figure 104: Structure of compound **40**.

Compound **40** (Figure 104) contains a phenyl ring at both the R and R[1] sites. The ^{1}H NMR spectrum showed two signals for the aromatic protons; a multiplet in the range of 7.94 – 8.02 ppm, with an integration of two, for the *ortho* protons, and a multiplet in the range of 7.55 – 7.63 ppm, with an integration of three, for the *meta* and *para* protons. The ^{13}C NMR spectrum showed the *ortho* carbon at 131.1 ppm, *meta* carbon at 128.7 ppm, and the *para* carbon at 128.9 ppm. The quaternary carbon of the bicycle core bonded to the phenyl group at R[1] appears at 143.2 ppm, and the quaternary carbon *ipso* to the pyrazolopyrimidinone appears at 132.3 ppm. The IR and MS data also confirmed the generation of compound **40**.

3.7.1.10 Structural characterisation of 5-(4-nitrophenyl)-2-phenylpyrazolo[1,5-*a*]pyrimidin-7(4*H*)-one (compound 49)

The next three compounds, compounds **49**-**51**, all contain a phenyl group at the R^1 site, with different aromatic rings at the R site.

Figure 105: Structure of compound **49**.

Compound **49** (Figure 105) contains a *para* nitro substituted aromatic ring at the R site and a phenyl ring at the R^1 site. There is free rotation about the bond between the *para* nitro substituted aryl ring and the pyrazolopyrimidinone core. This would be expected to result in two sets of equivalent protons. As such, in the ^{1}H NMR spectrum, there are two doublet signals, as opposed to four signals, for the four protons of the aryl ring. The *meta* protons (*meta* to the pyrazolopyrimidinone) appear more deshielded as a doublet at 8.40 ppm, with a *J* value of 8.8 Hz, due to the electron withdrawing effect of the nitro group (see Scheme 9, section **2.3.1.4**).

The *ortho* protons (*ortho* to the pyrazolopyrimidinone), are less shielded and appear as a doublet at 8.14 ppm, with a matching *J* value of 8.8 Hz. The carbons bonded to the *meta* protons appear at 128.7 ppm in the ^{13}C NMR spectrum, whereas the *ortho* carbons appear at 123.9 ppm. The quaternary carbon of the bicycle core bonded to the *para* nitro aryl ring appears at 148.9 ppm and the quaternary carbon bonded to the nitro group itself appears at 147.7 ppm. The quaternary carbon of the *para* nitro aryl ring *ipso* to the pyrazolopyrimidinone appears at 138.6 ppm. The IR and MS data also confirmed the generation of compound **49**.

3.7.1.11 Structural characterisation of 5-(4-methoxyphenyl)-2-phenylpyrazolo[1,5-*a*]pyrimidin-7(4*H*)-one (compound 50)
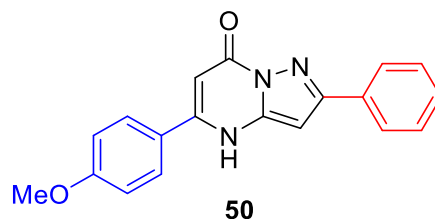
Figure 106: Structure of compound **50**.

Compound **50** (Figure 106) contained a *para* methoxy aryl ring at the R site and a phenyl ring at the R^1 site. As previously discussed for other *para* substituted aryl systems, it was expected that the *para* methoxy aryl ring would generate twos sets of ^{1}H NMR signals, as a double of doublets. This was indeed the case. The *meta* protons (*meta* to the pyrazolopyrimidinone) appear as a more deshielded doublet at 7.85 ppm due to the electron withdrawing effect of the oxygen, with a *J* value of 8.8 Hz. The *ortho* protons (*ortho* to the pyrazolopyrimidinone) appear as a doublet at 7.14 ppm, with a matching coupling constant of 8.8 Hz. The carbons bonded to the *meta* protons appear at 114.4 ppm in the ^{13}C NMR spectrum, whereas the *ortho* carbons appear at 128.7 ppm.

The protons of the methoxy group appear as a singlet at 3.86 ppm in the ^{1}H NMR spectrum, and the carbon of the methoxy group appears at 55.5 ppm in the ^{13}C NMR spectrum. The quaternary carbon bonded to the methoxy group appears at 161.5 ppm, the quaternary carbon of the bicycle core bonded to the *para* methoxy aryl ring appears at 130.7 ppm, and the quaternary carbon of the *para* methoxy aryl ring *ipso* to the pyrazolopyrimidinone bicycle appears at 124.4 ppm. The IR and MS data also confirmed the generation of compound **50**.

3.7.1.12 Structural characterisation of 2-phenyl-5-(2,3,4,5-tetrafluorophenyl)pyrazolo[1,5-*a*]pyrimidin-7(4*H*)-one (compound 51)
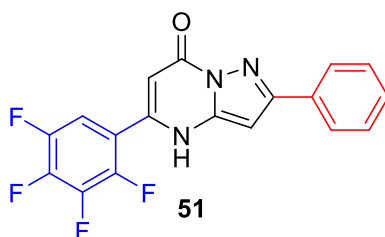
Figure 107: Structure of compound **51**.

Compound **51** (Figure 107) generated a more complex set of NMR spectra due to the presence of the four ^{19}F NMR active atoms. The single proton of the fluorinated aromatic ring at the R site generated a multiplet signal in the region of 7.87 – 7.94 ppm in the ^{1}H NMR spectrum due to ^{1}H-^{19}F coupling. The carbon bonded to this proton appears as a doublet in the ^{13}C NMR spectrum at 113.3 ppm with a coupling constant of 19.3 Hz. Interestingly, the α-proton on the pyrazolopyrimidinone core, no longer appear as a singlet at approximately 6.1 ppm. Instead, it appears as a doublet signal at 6.01 ppm with a coupling constant of 0.8 Hz due to long-range coupling with one of the fluorine atoms. In the ^{13}C NMR spectrum, the quaternary carbon of the pyrazolopyrimidinone core bonded to the fluorinated aromatic ring appears at 156.2 ppm and the quaternary carbon of the fluorinated aromatic ring *ipso* to the pyrazolopyrimidinone core appears at 143.5 ppm. The ^{19}F NMR spectrum shows four multiplet peaks at -140.2, -141.8, -154.9 and -156.9 ppm. The IR spectrum shows an absorbance band at 1089 cm^{-1}, which is characteristic of a C-F bond stretch. The MS data also confirmed the generation of compound **51**.

3.7.1.13 Synthesis and characterisation of 5-(3,5-dimethylphenyl)-2-methylpyrazolo[1,5-*a*]pyrimidin-7(4*H*)-one (compound 52)
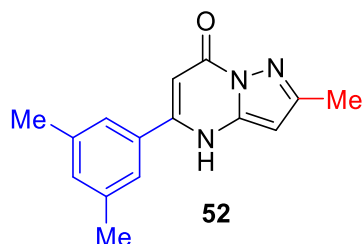
Figure 108: Structure of compound **52**.

Almost all the compounds in category 1 were synthesised using the "one-pot" microwave-assisted approach described previously. The only exception was compound **52** (Figure 108) which contains a 3,5-dimethyl substituted aryl ring at the R site, and a phenyl ring at the R^1 site. The synthesis of this compound was performed by the conventional reflux heating of ethyl 3-(3,5-dimethylphenyl)-3-oxopropanoate (MK1) (compound **53**) with 3-amino-5-methylpyrazole in acetic acid for 21 hours. After volatiles were removed under reduced pressure, the product was purified by column chromatography (100 % DCM) to generate the product as a beige solid with 59% yield (Scheme 38). The starting β-ketoester, compound **53**, was not commercially available and had to be synthesised. The synthesis of this compound and other β-ketoesters is discussed in detail in section **3.7.2**.
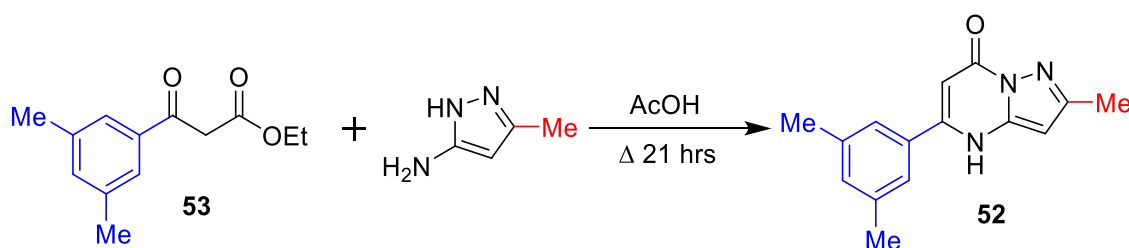
Scheme 38: Synthesis of compound **52**, 59% yield.

The ^{1}H NMR spectrum of compound **52** shows two signals for the aromatic ring, both appear**ing** as singlets, one at 7.42 ppm for the *ortho* protons and 7.26 ppm for the *para* proton. The carbons bonded to these protons appear in the ^{13}C NMR spectrum at 124.5 ppm and 132.3 ppm respectively. The CH proton of the pyrazole ring appears as a singlet at 6.13 ppm and the α-proton appears as a singlet at 6.05 ppm. The three methyl groups had overlapping signals and appear as overlapping singlets in the range of 2.34 – 2.53 ppm in the ^{1}H NMR spectrum, and their carbons appear at 19.9 ppm in the ^{13}C NMR spectrum. The IR and MS data also confirmed the generation of compound **52**.

3.7.2 Category 2: Substituent variations at the R site only (the bis-CF₃ aryl site)

The second category of RTC53 analogues consisted of only varying the R, bis-CF$_3$ aryl, group of RTC53 (Figure 109).
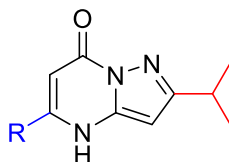
Figure 109: Category 2 - variations at the R site.
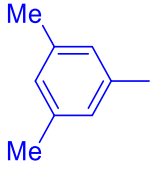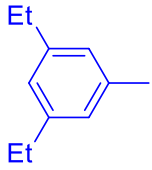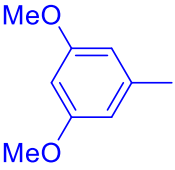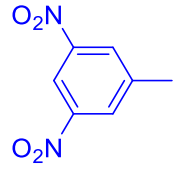
The synthesis of the pyrazolopyrimidinone bicycles in the category was carried out by reaction of the corresponding β-ketoester with the commercially available 3-isopropyl-1*H*-pyrazol-5-amine in acetic acid using microwave irradiation (Scheme 39). For some compounds, conventional heating at reflux was employed instead of microwave irradiation.
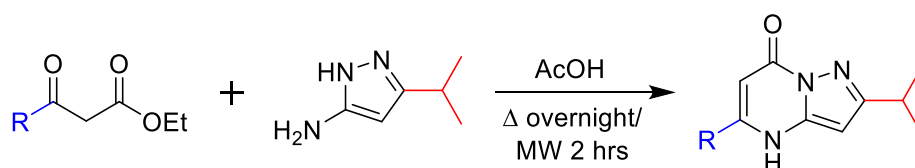
Scheme 39: Synthesis of category 2 pyrazolopyrimidinones.

The β-ketoesters starting materials used in the synthesis of the category 2 pyrazolopyrimidinone bicycles were not always commercially available and therefore had to be synthesised. This was achieved via a coupling type reaction of the corresponding benzoic acid starting materials with Meldrum's acid, using the coupling reagent *N,N'*-dicyclohexylcarbodiimide (DCC). The β-ketoesters synthesised in this group are summarised below (Table 7).

Table 7: β-ketoesters made for the synthesis of pyrazolopyrimidinone bicycles.

	Reaction scheme	
R–C(=O)OH + Meldrum's acid	1) DMAP, DCC, DCM 0 °C - rt, 2 hrs → 2) *p*-TSA.H$_2$O, EtOH N$_2$, 1 hr	R–C(=O)CH$_2$C(=O)OEt

Compound	R	Yield
53 (MK1)	3,5-dimethylphenyl (Me, Me)	67%
54 (MK4)	3,5-diethylphenyl (Et, Et)	74%
55 (MK10)	3,5-dimethoxyphenyl (MeO, MeO)	37%
56 (MK11)	3,5-dinitrophenyl (O$_2$N, O$_2$N)	11%

The proposed mechanism for the synthesis of these β-ketoesters (Scheme 40) begins with nucleophilic attack of the benzoic acid on to DCC to generate an ester with a more electrophilic carbonyl carbon. General base catalysis occurs where Meldrum's acid is deprotonated by the base 4-dimethylaminopyridine (DMAP), which removes the acidic α-proton, and the deprotonated Meldrum's acid acts as a nucleophile and attacks the electrophilic carbonyl carbon to generate the tetrahedral intermediate. Removal of *N,N'*-dicyclohexylurea (DCU) leaving group regenerates the carbonyl group. The second carbonyl group gets protonated using *para*-toluenesulfonic acid (*p*-TSA) to generate a more electrophilic carbonyl carbon which gets attacked by EtOH. A hydroxyl group is generated by protonation of the oxygen by *p*-TSA. The second carbonyl group is regenerated by deprotonation using *p*-TSA and the cleavage of the bond to the hydroxyl group. The final step of the synthesis involves decarboxylation which generates the product as two tautomers, keto and enol tautomers, with carbon dioxide and acetone as bi-products.

151
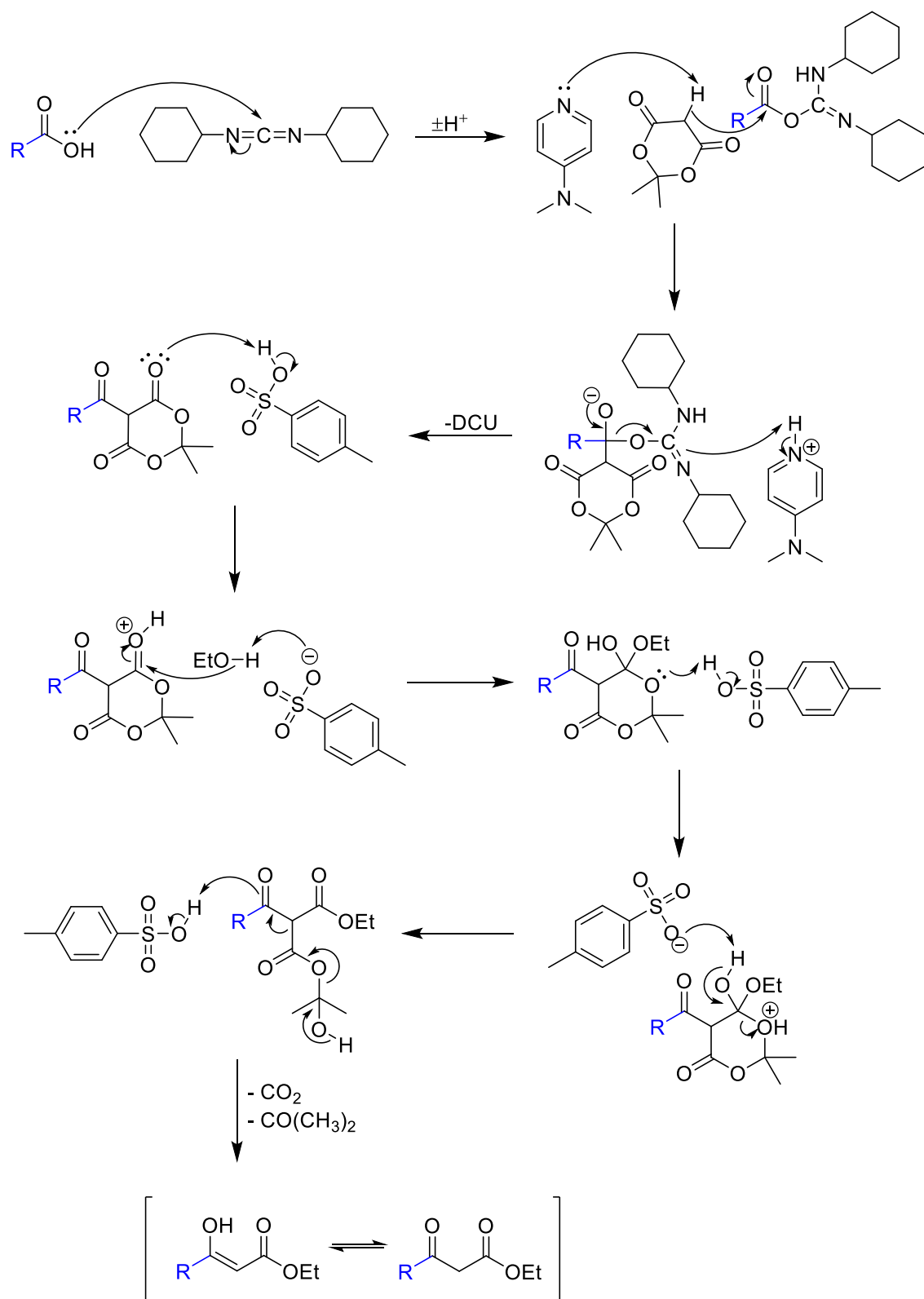
Scheme 40: Mechanism of the synthesis of β-ketoesters using Meldrum's acid and DCC.

The benzoic acid starting material used in the synthesis of the β-ketoesters was commercially available for all compounds except one of the target compounds.

Compound **54**, ethyl 3-(3,5-diethylphenyl)-3-oxopropanoate (MK4), contains a diethyl *meta* substituted aryl ring, whose incorporation required the use and synthesis of 3,5-diethylbenzoic acid (MK3) (compound **57**). We proposed the synthesis of benzoic acid **57** via the generation of the corresponding aryl Grignard and its subsequent reaction with carbon dioxide. The synthesis of 3,5-diethylbenzoic acid **57** was successfully completed via the formation of the aryl Grignard from 1-bromo-3,5-diethylbenzene using magnesium turnings and iodine in THF (Scheme 41). Subsequent reaction with carbon dioxide and acidic work-up gave the desired benzoic acid in a 93% yield.
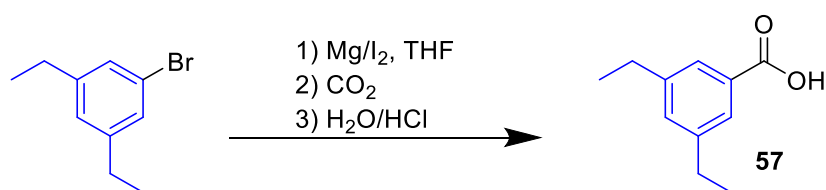
Scheme 41: Synthesis of benzoic acid **57**, 93% yield.

After successfully synthesising the required β-ketoesters, the four corresponding pyrazolopyrimidinone bicycles were made, see Table 8.

Table 8: Pyrazolopyrimidinone bicycles synthesised with category 2 variations (at R site).

Compound	R	Yield
58 (MK6)		42%
59 (MK5)		20%

60 (MK13)		18%
61 (MK49)		13%
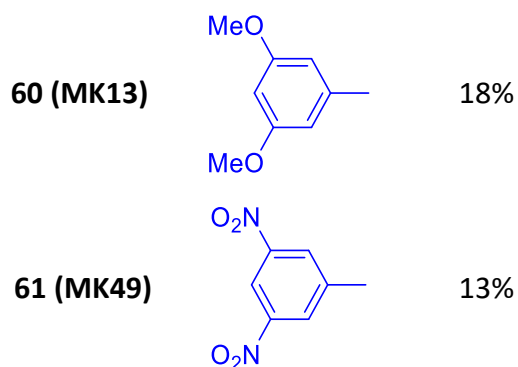
The synthesis of the first three pyrazolopyrimidinone bicycles (compounds **58, 59** and **60**) was performed towards the beginning of my PhD studies by reaction of the corresponding β-ketoester with the commercially available 3-isopropyl-1*H*-pyrazol-5-amine in acetic acid, with overnight conventional heating at reflux (Scheme 42).
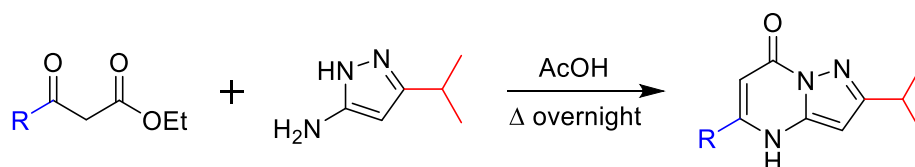
Scheme 42: Synthesis of compounds **58 – 60**.

The synthesis of 5-(3,5-dinitrophenyl)-2-isopropylpyrazolo[1,5-*a*]pyrimidin-7(4*H*)-one (MK49) (compound **61**), was carried out at a later stage and hence employed the "one-pot" microwave assisted approach described previously in section **3.5**. This synthesis consisted of reaction of the commercially available β-ketonitrile, 4-methyl-3-oxopentanenitrile with hydrazine monohydrate, in the microwave at 150 °C for five minutes to synthesise the intermediate aminopyrazole, 3-isopropyl-1*H*-pyrazol-5-amine. This was followed by addition of the previously synthesised β-ketoester, ethyl 3-(3,5-dinitrophenyl)-3-oxopropanoate (MK11) (compound **56**) and acetic acid and microwave heating at 150 °C for a further two hours (Scheme 43).
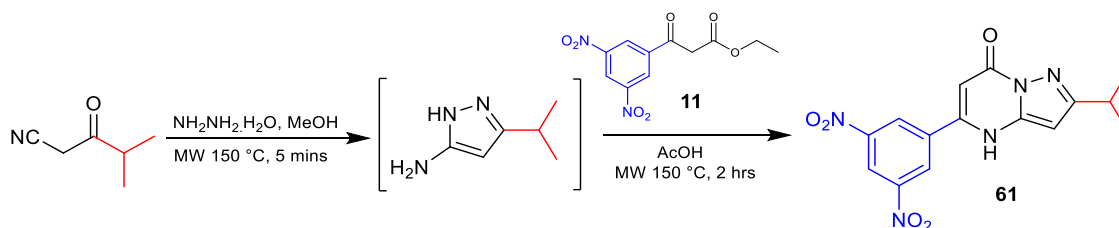
Scheme 43: Synthesis of compound **61**, 13% yield.

Structural characterisation of these four pyrazolopyrimidinone bicycles employed ^{1}H and ^{13}C NMR spectroscopy, HR-MS, and IR spectroscopy. DEPT and 2D-NMR experiments, such as ^{1}H-^{1}H COSY, ^{1}H-^{13}C HSQC and ^{1}H-^{13}C HMBC, were used to help assign the ^{1}H and ^{13}C NMR signals.

Common signals were present in the ^{1}H NMR and ^{13}C NMR spectra arising from the bicycle core structure and the isopropyl group of all four compounds. For compound **58**, a broad singlet signal at 9.51 ppm in the ^{1}H NMR spectrum is assigned to the NH, a multiplet signal at 6.00 ppm for the pyrazole proton and the α-proton of the bicycle core, a septet signal at 3.10 ppm for the single proton of the isopropyl group, and a doublet signal at 1.28 ppm for the two methyl groups of the isopropyl group. The single proton of the isopropyl group is coupled to six equivalent protons from the two methyl groups and therefore appears as a septet.

The ^{13}C NMR spectrum for the same compound contained quaternary signals for the bridgehead carbon adjacent to the amine at 139.1 ppm, and the carbon bonded to the aromatic ring at 132.8 ppm. Tertiary carbon signals appear at 94.6 ppm for the carbon α to the carbonyl group, 86.7 ppm for the pyrazole carbon, and 28.6 ppm for the isopropyl CH carbon. The carbon signals for the two methyl groups of the isopropyl group appear at 22.5 ppm.

All four compounds were analysed by high-resolution mass spectrometry where an accurate mass was obtained for each compound which was less than 5 ppm from the calculated expected mass.

An IR spectrum was obtained for all these compounds. With regards to the bicycle core and isopropyl group, the IR spectrum shows absorbance bands at 3199 cm^{-1} and 1595 cm^{-1} characteristic of the amine (N-H) bond, 3081 cm^{-1} for the aromatic C-H bond and 1651 cm^{-1} for the carbonyl (C=O) bond.

3.7.2.1 Structural characterisation of 5-(3,5-dimethylphenyl)-2-isopropylpyrazolo[1,5-*a*]pyrimidin-7(4*H*)-one (compound 58)
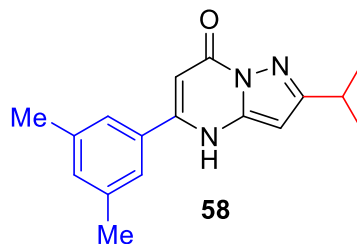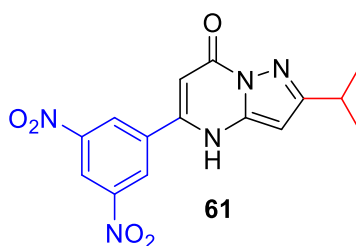

Figure 110: Structure of compound **58**.

The ^{1}H and ^{13}C NMR data was as expected for the compound containing an aromatic ring on the R site with two *meta* substituted methyl groups, compound **58** (Figure 110). The signals for the aromatic ring appear as singlets in the ^{1}H NMR spectrum at 7.25 ppm (two protons *ortho* to the pyrazolopyrimidinone) and 7.13 ppm (*para* proton), and at 124.5 ppm and 132.7 ppm in the ^{13}C NMR spectrum for the carbons bonded to these protons respectively. The quaternary carbons of the aromatic ring appear in the ^{13}C NMR spectrum at 157.7 ppm for the carbon *ipso* to the pyrazolopyrimidinone and at 141.6 ppm for the carbon bonded to the methyl groups. The signal for the methyl groups appears as a singlet in the ^{1}H NMR spectrum at 2.34 ppm integrating for the six equivalent protons, and at 21.3 ppm in the ^{13}C NMR spectrum. The IR and MS data also confirmed the successful synthesis of compound **58**.

3.7.2.2 Structural characterisation of 5-(3,5-diethylphenyl)-2-isopropylpyrazolo[1,5-*a*]pyrimidin-7(4*H*)-one (compound 59)
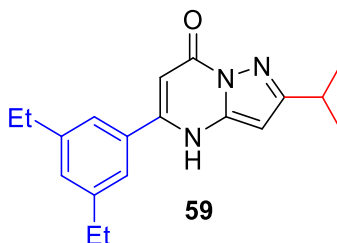
Figure 111: Structure of compound **59**.

The same approach was taken for the compound containing an aromatic ring on the R site with two *meta* substituted ethyl groups, compound **59** (Figure 111). The aromatic proton signals appear similarly to the previous compound at 7.37 ppm and 7.12 ppm,

and 123.8 ppm and 130.5 ppm, for the two *ortho* C-H's of the aromatic ring, and the *para* C-H respectively. The two ethyl groups appear as a quartet at 2.60 ppm, resonating for the two CH_2 groups of the ethyl groups and integrating for four protons, and at 1.16 ppm for the CH_3 groups of the ethyl groups, integrating for six protons (overlap was observed with the isopropyl methyl groups). In the ^{13}C NMR spectrum, the corresponding carbon signals for the CH_2 of the ethyl groups resonated at 28.7 ppm, and at 15.3 ppm for the ethyl CH_3 groups. The IR and MS data also confirmed the successful synthesis of compound **59**.

3.7.2.3 Structural characterisation of 5-(3,5-dimethoxyphenyl)-2-isopropylpyrazolo[1,5-*a*]pyrimidin-7(4*H*)-one (compound 60)
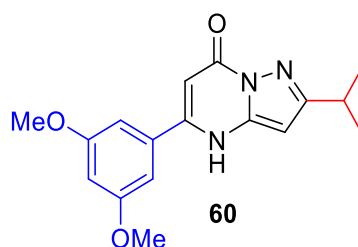
Figure 112: Structure of compound **60**.

For the compound containing an aromatic ring on the R site with two *meta* substituted methoxy groups, compound **60** (Figure 112), the aromatic proton signals in the ^1H NMR spectrum appear more upfield at 7.08 ppm (two protons *ortho* to the pyrazolopyrimidinone) and 6.60 ppm (*para* proton). This was expected as the methoxy groups are electron donating groups due to resonance (Scheme 44). The corresponding ^{13}C signals appear in the ^{13}C NMR spectrum at 105.4 ppm (two *ortho* C-H's) and 102.1 ppm (*para* C-H).
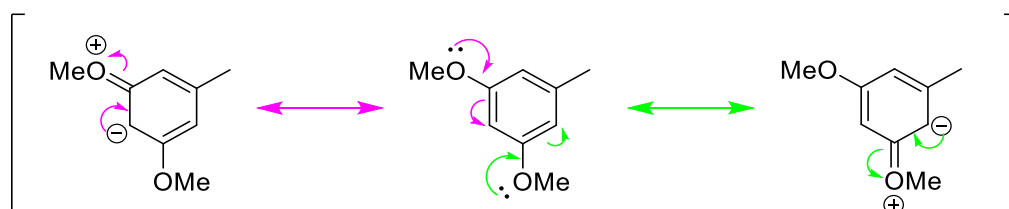
Scheme 44: Resonance structures due to delocalisation of electrons from methoxy group into the aromatic ring.

The methoxy protons resonate as a singlet signal integrating for six protons at 3.83 ppm in the ^{1}H NMR spectrum. The carbons of the methoxy groups resonate at 55.9 ppm in the ^{13}C NMR spectrum. Both signals are downfield due to the deshielding effect of the electronegative oxygen. Finally, the IR and MS data also confirmed the successful synthesis of compound **60**.

3.7.2.4 Structural characterisation of 5-(3,5-dinitrophenyl)-2-isopropylpyrazolo[1,5-*a*]pyrimidin-7(4*H*)-one (compound 61)

Figure 113: Structure of compound **61**.

For the compound containing an aromatic ring on the R site with two *meta* substituted nitro groups, compound **61** (Figure 113), the opposite effect was observed in the ^{1}H and ^{13}C NMR spectra to that which was observed to the dimethoxy substituted compound **60**. This was due to the electron withdrawing effect of the nitro groups which resulted in the aromatic proton and carbon signals being deshielded and appearing more downfield. The aromatic protons appear in the ^{1}H NMR spectrum at 9.07 ppm and 8.92 ppm for the *ortho* and *para* protons respectively. The corresponding carbon signals appear at 127.3 ppm and 119.8 ppm respectively, according to the ^{1}H-^{13}C HSQC spectrum. Furthermore, the presence of this compound was additionally confirmed by the MS data and IR spectrum, with absorbance bands of 1533 cm^{-1} and 1341 cm^{-1} which are typical absorbance for N-O bond stretches.

3.7.3 Category 3: Substituent variations at R^1 site only (the isopropyl group)

The third category of variations of RTC53 consisted of changing the isopropyl group at the R^1 site while maintaining the aromatic bis-CF$_3$ group (Figure 114).
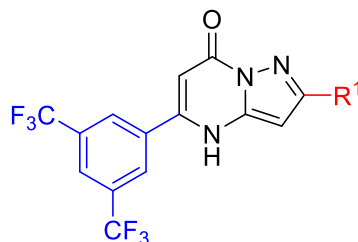
Figure 114: Category 3 variations at the R^1 site.
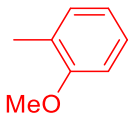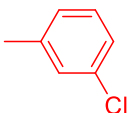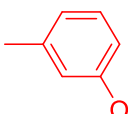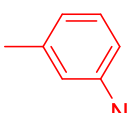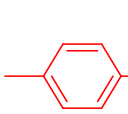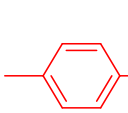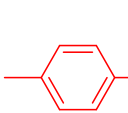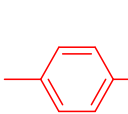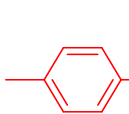
Compounds produced in category 3 were synthesised using the "one-pot" microwave assisted method as described previously in section **3.5**. This consisted of reacting a commercially available β-ketonitrile with hydrazine monohydrate in MeOH using microwave heating at 150 °C for five minutes. This was followed by addition of the commercially available β-ketoester, ethyl 3-(3,5-bis(trifluoromethyl)phenyl)-3-oxopropanoate, along with acetic acid with microwave heating for a further two hours to yield the pyrazolopyrimidinone bicycle (Scheme 45).
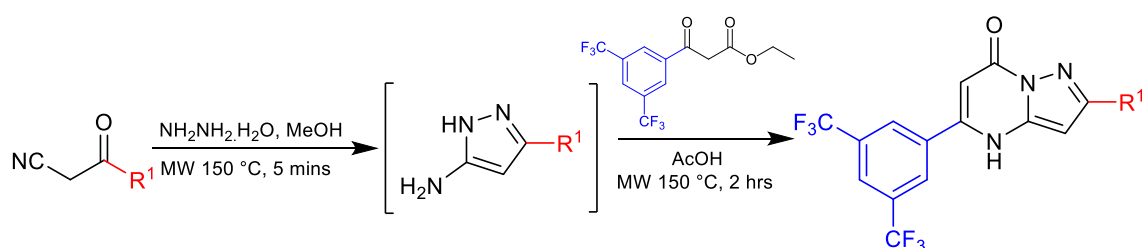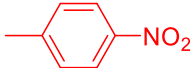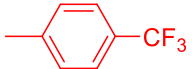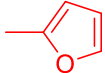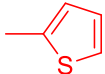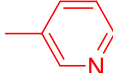
Scheme 45: General synthesis of category 3 pyrazolopyrimidinone bicycles using the "one-pot" microwave assisted method.

In total, 15 compounds were made with category 3 variations at R^1. Variations consisted of substituted aromatic rings or heterocyclic rings. The aromatic rings contained substitutions at the *ortho*, *meta* and *para* positions, with electron donating (e.g. methyl and methoxy) and electron withdrawing groups (e.g. nitro and halogens). Heterocyclic rings consisted of furan, thiophene, and pyridine (Table 9).

Table 9: Pyrazolopyrimidinone bicycles synthesised with category 3 variations.

Compound	R^1	Yield
62 (MK80)		3%
63 (MK79)		16%
64 (MK82)		8%
65 (MK81)		7%
66 (MK83)		7%
67 (MK71)		9%
68 (MK72)		6%
69 (MK75)		7%
70 (MK73)		10%
71 (MK74)		19%

72 (MK76)		—⟨⟩—NO$_2$	78%
73 (MK78)		—⟨⟩—CF$_3$	11%
74 (MK84)		O	8%
75 (MK85)		S	8%
76 (MK86)		N	3%

The isolated yields obtained for most of these compounds were poor due to a complex mixture being formed and the difficulty in isolation of the product. All these compounds were purified by column chromatography when other purification methods, such as filtration, recrystallisation, or trituration, were unsuccessful. The only exception was the compound containing the aromatic ring with the nitro group substituted at the *para* position, 5-(3,5-bis(trifluoromethyl)phenyl)-2-(4-nitrophenyl)pyrazolo[1,5-*a*]pyrimidin-7(4*H*)-one (MK76) (compound **72**), which was purified by trituration with cold MeOH.

The synthesis of these compounds was confirmed as before using ^{1}H and ^{13}C NMR spectroscopy, HR-MS, and IR spectroscopy. DEPT and 2D NMR techniques were used to support signal assignments. The mass spectrum of each compound was analysed, and the correct mass was found for all compounds with a difference of less than 5.0 ppm from the calculated mass.

Common signals in the NMR spectra for these compounds arose from the protons of the bis-CF$_3$ substituted aromatic ring and bicycle core, which were present in all the compounds. Taking compound **62** as an example, the aromatic ring with the bis *meta* substituted trifluoromethyl groups generated ^{1}H NMR signals at 8.73 ppm (*ortho* protons) and 8.15 ppm (*para* proton), and corresponding ^{13}C NMR signals at 127.2 ppm and 122.1 ppm. The ^{13}C NMR also displayed a signal at 152.9 ppm for the *ipso* quaternary carbon, a quartet at 130.9 ppm ($J = 33.4$ Hz) for the carbon of the trifluoromethyl group,

and a quartet at 124.0 ppm (J = 273.6 Hz) for the carbon bonded to the trifluoromethyl group. The IR spectrum also displayed absorbance bands at 1276 cm^{-1} and at 1126 cm^{-1}, which are characteristic of the C-F bond stretches.

The bicycle core of the same compound displayed ^{1}H NMR signals at 6.69 ppm for the pyrazole proton adjacent to the R^1 group, and at 6.33 ppm for the α-proton (α to the carbonyl group), with the corresponding ^{13}C NMR signals at 94.8 ppm and 89.6 ppm, respectively. The ^{13}C NMR spectra also displayed quaternary carbon signals arising from the bicycle core for the carbonyl group (159.1 ppm), the bridgehead carbon adjacent to the NH group (152.1 ppm), the carbon bonded to the R^1 group (149.6 ppm), and the β-carbon bonded to the bistrifluoromethyl substituted aryl ring (128.5 ppm).

3.7.3.1 Structural characterisation of 5-(3,5-bis(trifluoromethyl)phenyl)-2-(2-chlorophenyl)pyrazolo[1,5-*a*]pyrimidin-7(4*H*)-one (compound 62)
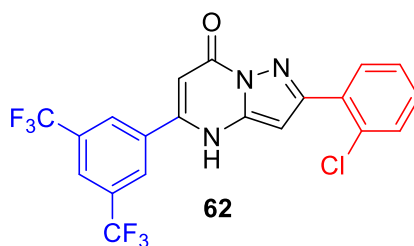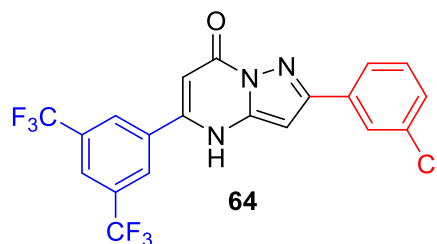

Figure 115: Structure of compound **62**.

Compound **62** (Figure 115) contains an *ortho* chloro substituted aromatic ring at R^1. The proton of the chloro substituted aromatic ring *ortho* to the pyrazolopyrimidinone core appears as a doublet at 8.03 ppm, with a coupling constant of 8.4 Hz, in the ^{1}H NMR spectrum and a corresponding signal in the ^{13}C NMR spectrum at 131.6 ppm. The proton adjacent to the C-Cl bond also appears as a doublet at 7.61 ppm, with a coupling constant of 7.2 Hz, in the ^{1}H NMR spectrum and a corresponding ^{13}C NMR signal at 130.6 ppm. This was expected due to the deshielding effect of the electron withdrawing chlorine atom.

The remaining protons of the chloro substituted aromatic ring generate overlapping signals and appear as a multiplet between 7.42 – 7.56 ppm and integrate for two. The corresponding ^{13}C signals occur at 129.6 ppm and 127.5 ppm. The IR and MS data also confirmed the generation of compound **62**.

162

3.7.3.2 Structural characterisation of 5-(3,5-bis(trifluoromethyl)phenyl)-2-(2-methoxyphenyl)pyrazolo[1,5-*a*]pyrimidin-7(4*H*)-one (compound 63)
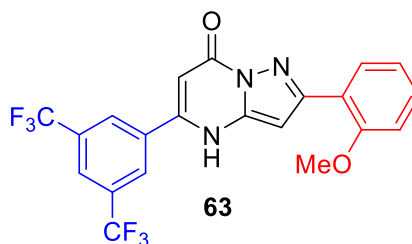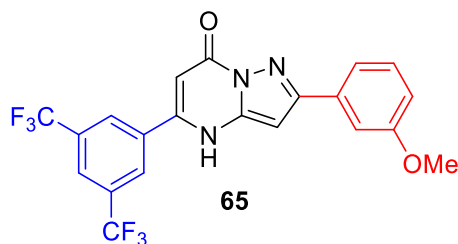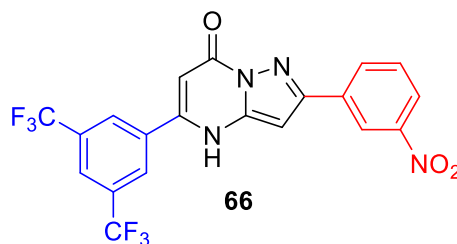

Figure 116: Structure of compound **63**.

Compound **63** (Figure 116) contains an aromatic ring with an *ortho* methoxy substituent at R^1 and generated the expected signals for the pyrazolopyrimidinone core and the bistrifluoromethyl aryl ring. The proton of the methoxy substituted aromatic ring *ortho* to the pyrazolopyrimidinone core resonates as a multiplet in the range of 8.04 – 8.15 ppm as it overlapped with the proton in the *para* position of the other aromatic ring.

The proton adjacent to the methoxy group appears as a doublet at 7.13 ppm with a coupling constant of 8.2 Hz as it was coupled with just one non-equivalent proton. The remaining two protons of the methoxy aryl ring might both have been expected to appear as a double of doublets, as they are each coupled to two non-equivalent protons. However, for each the double of doublets overlapped slightly and they appear as *pseudo* triplet at 7.02 ppm (*meta* proton) and 7.34 ppm (*para* proton). The *meta* proton is slightly more shielded than the *para* proton due to the effect of the methoxy group (see Scheme 37, section **3.7.1.5**).

The ^{13}C NMR spectrum displays signals for the methoxy aryl ring at 129.7 ppm (carbon *meta* to pyrazolopyrimidinone), 129.5 ppm (carbon adjacent to OMe), 120.8 ppm (*para* C-H), and 112.4 ppm (*ortho* C-H). Quaternary signals consist of the carbon bonded to the methoxy group at 157.5 ppm and the *ipso* carbon at 123.1 ppm. The signal for the methyl group of the methoxy group appears as a singlet at 3.91 ppm in the ^1H NMR spectrum and at 56.1 ppm in the ^{13}C NMR spectrum. The IR and MS data also confirmed the generation of compound **63**.

3.7.3.3 Structural characterisation of 5-(3,5-bis(trifluoromethyl)phenyl)-2-(3-chlorophenyl)pyrazolo[1,5-a]pyrimidin-7(4H)-one (compound 64)
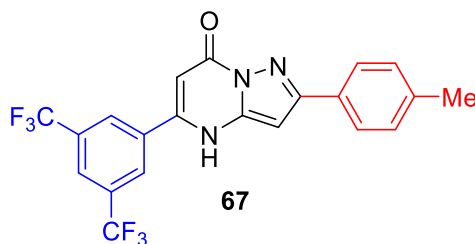

Figure 117: Structure of compound **64**.

The *meta* chloro aryl ring of compound **64** (Figure 117) generated four signals in both the ^{1}H and ^{13}C NMR spectra. The proton adjacent to the C-Cl bond, in the *ortho* position of the aromatic ring, appears as a singlet at 8.02 ppm in the ^{1}H NMR spectrum, with a corresponding ^{13}C signal at 125.8 ppm for the carbon bonded to it. This signal is deshielded due to the electron withdrawing effect of the chlorine atom as previously discussed. This signal was confirmed using ^{1}H-^{1}H COSY spectrum (see spectra of compound **64**) as it did not couple with the other three proton signals of the aromatic ring. The protons in the *para* position and *ortho* position of the aromatic ring both appear as doublets at 7.92 ppm and 7.39 ppm respectively, as they are both coupled by the *meta* proton between them. The carbons bonded to these protons appear at 124.9 ppm and 127.8 ppm respectively. Finally, the remaining *meta* proton appears as a *pseudo* triplet (resulting from slightly overlapped double of doublets) at 7.48 ppm, with a corresponding ^{13}C NMR signal at 130.8 ppm for the carbon bonded to it. The IR spectrum shows an absorbance at 768 cm^{-1} which is characteristic of a C-Cl bond. The MS data also confirmed the generation of compound **64**.

3.7.3.4 Structural characterisation of 5-(3,5-bis(trifluoromethyl)phenyl)-2-(3-methoxyphenyl)pyrazolo[1,5-*a*]pyrimidin-7(4*H*)-one (compound 65)

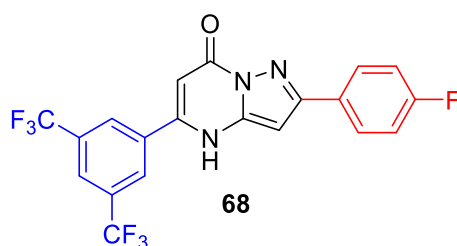**Figure 118:** Structure of compound **65**.

The compound containing a *meta* methoxy aromatic ring at the R^1 site, compound **65** (Figure 118), generated all the expected ^{1}H and ^{13}C NMR signals. The two protons adjacent to the methoxy group on each side had overlapping signals in the ^{1}H NMR spectrum and appear as a multiplet in the range of 7.49 – 7.61 ppm, and at 118.7 ppm and 111.5 ppm in the ^{13}C NMR spectrum. The proton in the *meta* position of the aromatic ring appears as a *pseudo* triplet at 7.36 ppm (*J* = 7.8 Hz), with a corresponding ^{13}C signal at 130.0 ppm.

The proton in the *ortho* position of the aromatic ring appears as a double of doublets at 6.92 ppm with a coupling constant of 8.6 Hz and 2.1 Hz due to coupling with its neighbouring proton (*meta* proton), as well as a proton four bonds away (*ortho* or *para* proton) through aromatic long-range coupling or "W-coupling". The carbon bonded to this proton appears at 114.2 ppm in the ^{13}C NMR spectrum. Finally, the methyl group protons of the methoxy group appear as a singlet at 3.84 ppm in the ^{1}H NMR spectrum with the corresponding carbon appearing at 55.6 ppm in the ^{13}C NMR spectrum. The IR and MS data also confirmed the generation of compound **65**.

3.7.3.5 Structural characterisation of 5-(3,5-bis(trifluoromethyl)phenyl)-2-(3-nitrophenyl)pyrazolo[1,5-*a*]pyrimidin-7(4*H*)-one (compound 66)
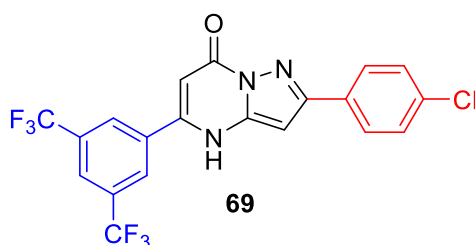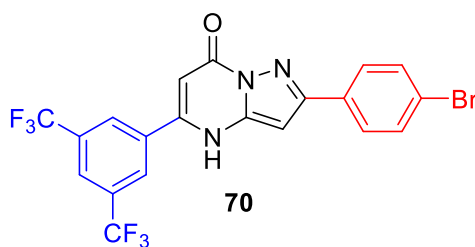

Figure 119: Structure of compound **66**.

Compound **66** (Figure 119) contains a *meta* nitro substituted aryl ring at the R^1 site. The ^{1}H NMR signals arising for the nitro substituted aromatic protons are quite deshielded as nitro is significantly electron withdrawing (see Scheme 9, section **2.3.1.4**). The signal for the proton in the *ortho* position between the nitro group and the pyrazolopyrimidinone is most deshielded and appears as a singlet at 8.42 ppm, with the corresponding ^{13}C NMR signal for the carbon bonded to it found at 120.4 ppm using ^{1}H-^{13}C HSQC.

The signal for the other proton adjacent to the nitro group (*para* to the pyrazolopyrimidinone) overlapped with the signal for the other *ortho* proton and appears as a multiplet in the range of 7.82 – 7.93 ppm, with corresponding ^{13}C NMR signals at 132.5 ppm and 122.3 ppm, respectively. The remaining proton, in between these protons, appears as a *pseudo* triplet at 7.38 ppm, with a corresponding ^{13}C NMR signal at 129.1 ppm. The IR spectrum for this compound showed an absorbance band at 1347 cm^{-1}, which is characteristic of a N-O bond stretch. The MS data also confirmed the generation of compound **66**.

3.7.3.6 Structural characterisation of 5-(3,5-bis(trifluoromethyl)phenyl)-2-(*p*-tolyl)pyrazolo[1,5-*a*]pyrimidin-7(4*H*)-one (compound 67)
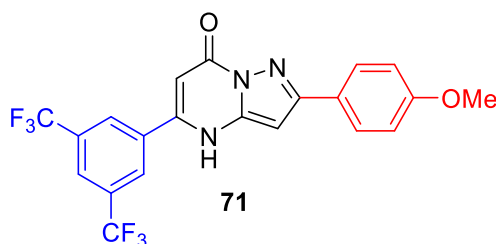

Figure 120: Structure of compound **67**.

Compound **67** (Figure 120) contains a *para* methyl substituted aryl ring at R^1. The *p*-tolyl group generated the expected pair of doublets in the aromatic region of ^{1}H NMR spectrum at 7.92 ppm and 7.32 ppm, for the protons *ortho* and *meta* to the pyrazolopyrimidinone respectively, with a matching coupling constant of 7.9 Hz for each. The carbons bonded to these protons appear in the ^{13}C NMR spectrum at 126.7 ppm and 129.8 ppm respectively, as identified using ^{1}H-^{13}C HSQC experiment. The protons from the *p*-tolyl methyl group appear as a singlet at 2.38 ppm in the ^{1}H NMR spectrum, and the corresponding carbon appears at 21.4 ppm in the ^{13}C NMR spectrum. The IR and MS data also confirmed the generation of compound **67**.

3.7.3.7 Structural characterisation of 5-(3,5-bis(trifluoromethyl)phenyl)-2-(4-fluorophenyl)pyrazolo[1,5-*a*]pyrimidin-7(4*H*)-one (compound 68)
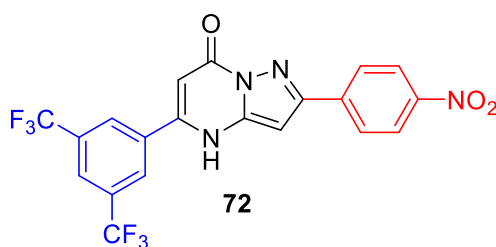

Figure 121: Structure of compound **68**.

The presence of the additional NMR active fluorine atom, of the *para* fluoro aryl ring, in compound **68** (Figure 121) resulted in a more complex set of NMR spectra. In ^{1}H NMR spectrum, the protons *ortho* to the pyrazolopyrimidinone appear as a double of doublets at 8.02 ppm (*J* = 8.5, 5.7 Hz). The splitting pattern is due to coupling with the neighbouring *meta* protons and the fluorine atom. The ^{13}C NMR spectrum shows the

carbon bonded to the *ortho* protons as a doublet at 128.6 ppm. The splitting was due to the ^{13}C-^{19}F coupling and had a coupling constant of 8.0 Hz.

The proton at the *meta* position of the aromatic ring appears as a *pseudo* triplet at 7.27 ppm (J = 8.8 Hz), again due to coupling with the neighbouring protons, as well as the fluorine. This signal was expected to appear as a double of doublets but overlap of the two middle peaks resulted in a *pseudo* triplet appearance. The fluorine atom itself was expected to have a similar deshielding effect on the protons *meta* to the pyrazolopyrimidinone as before.

The carbons bonded to the *meta* protons are equivalent and appear as a doublet in the ^{13}C NMR spectrum at 115.8 ppm due to ^{13}C-^{19}F coupling with a coupling constant of 21.6 Hz. The quaternary carbon bonded to the fluorine also appears as a doublet at 162.7 ppm (J_{CF} = 245.6 Hz) and the carbon *ipso* to the pyrazolopyrimidinone appears as a quartet at 131.1 ppm (J_{CF} = 33.0 Hz). The IR and MS data also confirmed the generation of compound **68**.

3.7.3.8 Structural characterisation of 5-(3,5-bis(trifluoromethyl)phenyl)-2-(4-chlorophenyl)pyrazolo[1,5-*a*]pyrimidin-7(4*H*)-one (compound 69)
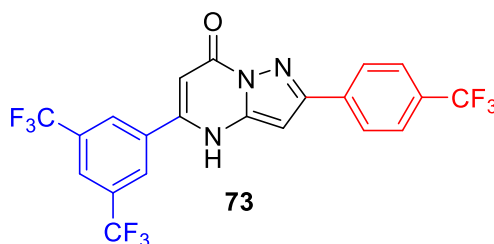

Figure 122: Structure of compound **69**.

Compound **69** (Figure 122) contains a *para* chloro substituted aromatic ring at R^1. This aryl ring generated the expected pair of doublets in the aromatic region of the ^1H NMR spectrum at 7.97 ppm and 7.48 ppm. These signals were assigned to the protons *ortho* and *meta* to the pyrazolopyrimidinone respectively. Both doublets have a matching coupling constant of 8.4 Hz. The deshielding effect of the chloro substituent is as expected and similar to that discussed previously**.** The carbons bonded to these protons appear as singlets in the ^{13}C NMR spectrum at 128.1 ppm and 128.9 ppm respectively.

This assignment was supported by the HSQC spectrum. The IR spectrum shows an absorbance band at 806 cm^{-1}, which is characteristic of the C-Cl bond stretch. The MS data also confirmed the generation of compound **69**.

3.7.3.9 Structural characterisation of 5-(3,5-bis(trifluoromethyl)phenyl)-2-(4-bromophenyl)pyrazolo[1,5-*a*]pyrimidin-7(4*H*)-one (compound 70)
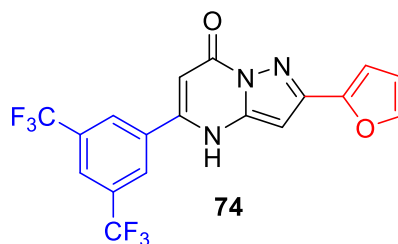

Figure 123: Structure of compound **70**.

The *para* bromo aryl substituted pyrazolopyrimidinone compound **70** (Figure 123) generated all the expected NMR signals. The *para* bromo aromatic ring itself produced two doublet aromatic signals in the ^{1}H NMR spectrum at 7.94 ppm and 7.62 ppm, for the protons ortho and *meta* to the pyrazolopyrimidinone respectively. The doublets have matching coupling constants of 8.3 Hz. The deshielding effect of the bromo substituent is as expected and again similar to that discussed for the *para* fluoro derivative, compound **68**. The carbons bonded to these protons appear as singlets in the ^{13}C NMR spectrum at 128.5 ppm and 131.8 ppm respectively, this was supported by ^{1}H-^{13}C HSQC data. The IR and MS data also confirmed the generation of compound **70**.

3.7.3.10 Structural characterisation of 5-(3,5-bis(trifluoromethyl)phenyl)-2-(4-methpxyphenyl)pyrazolo[1,5-*a*]pyrimidin-7(4*H*)-one (compound 71)
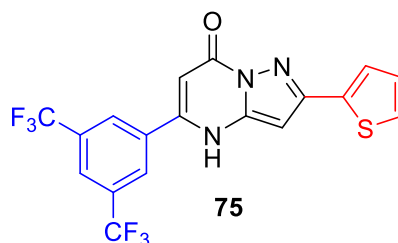

Figure 124: Structure of compound **71**.

169

Compound **71** (Figure 124) contains a *para* methoxy substituted aryl ring at R^1. The methoxy aromatic ring did not generate the expected pair of doublets in the aromatic region of the ^1H NMR spectrum. Instead a pair of multiplets are observed in the ^1H NMR spectrum for the protons *ortho* and *meta* to the pyrazolopyrimidinone bicycle, and four corresponding carbon signals are observed in the ^{13}C NMR spectrum. This led us to believe that the *ortho* and *meta* protons were not equivalent. The two protons in the *meta* position appear as a multiplet in the region of 7.82 – 7.90 ppm, with corresponding ^{13}C signals at 127.8 ppm and 127.9 ppm.

Similarly, the two protons in the *ortho* position appear as a multiplet in the region of 6.90 – 6.97 ppm with corresponding ^{13}C signals at 114.1 ppm and 114.2 ppm. The quaternary carbon *ipso* to the pyrazolopyrimidinone appears at 152.9 ppm. The signals for the methyl group appear as a multiplet in the range of 3.74 – 3.80 ppm in the ^1H NMR spectrum, and a corresponding signal in the ^{13}C NMR spectrum for the carbon of the methyl group at 55.5 ppm. The IR spectrum shows an absorbance band at 1174 cm^{-1} which is characteristic of the C-O bond stretch. The MS data also confirmed the generation of compound **71**.

3.7.3.11 Structural characterisation of 5-(3,5-bis(trifluoromethyl)phenyl)-2-(4-nitrophenyl)pyrazolo[1,5-*a*]pyrimidin-7(4*H*)-one (compound 72)
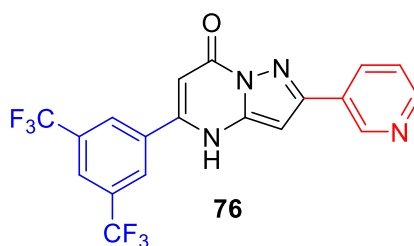

Figure 125: Structure of compound **72**.

Compound **72** (Figure 125) contains a *para* nitro substituted aryl ring at R^1. The electron withdrawing nature of a nitro group and its deshielding effect in NMR spectroscopy has already been discussed in for compound **66** (Scheme 9, section **2.3.1.4**). For compound **72**, the *para* nitro aromatic ring generated the expected NMR data. The two ^1H NMR aromatic signals for the nitro substituted aryl ring were overlapping with each other and with one of the protons from the bistrifluoromethyl aromatic ring and appear as a

multiplet in the range of 8.24 – 8.46 ppm, integrating for five hydrogens. The carbons bonded to the aromatic protons appear in the ^{13}C NMR spectrum at 127.8 and 124.5 ppm. The IR spectrum showed an absorbance band at 1364 cm^{-1}, which is characteristic of the N-O symmetric bond stretch. The MS data also confirmed the generation of compound **72**.

3.7.3.12 Structural characterisation of 5-(3,5-bis(trifluoromethyl)phenyl)-2-(4-trifluoromethyl)phenyl)pyrazolo[1,5-*a*]pyrimidin-7(4*H*)-one (compound 73)

Figure 126: Structure of compound **73**.

The compound containing the *para* trifluoromethyl aromatic ring at R^1 (compound **73**) (Figure 126) generated a somewhat complex set of NMR spectra due to the additional coupling with the NMR active fluorine atoms. The ^{1}H NMR spectrum shows the proton *meta* to the pyrazolopyrimidinone resonating as a multiplet in the range of 8.14 – 8.20 ppm and overlaps with a proton from the other aromatic ring. The *ortho* proton of the aromatic ring appears as a doublet at 7.77 ppm with a coupling constant of 8.1 Hz due to coupling with its neighbouring proton.

The carbon bonded to the *meta* proton appears as a poorly resolved quartet at 125.6 ppm in the ^{13}C NMR spectrum due to coupling with the fluorine (^{13}C-^{19}F coupling) of the trifluoromethyl group, with a coupling constant of 6.9 Hz. The carbon attached to the *ortho* proton was too distant from the fluorine to display any coupling and therefore appears as a singlet at 126.9 ppm. However, the carbon *ipso* to the pyrazolopyrimidinone core appears as a poorly resolved quartet at 151.8 ppm (J = 32.8 Hz), the carbon of the trifluoromethyl group appears as a quartet at 137.5 ppm (J = 313.3 Hz), and the carbon bonded to the trifluoromethyl group appears as a quartet at 124.9 ppm (J = 274.8 Hz). The IR and MS data also confirmed the generation of compound **73**.

3.7.3.13 Structural characterisation of 5-(3,5-bis(trifluoromethyl)phenyl)-2-(furan-2-yl)pyrazolo[1,5-*a*]pyrimidin-7(4*H*)-one (compound 74)

Figure 127: Structure of compound **74**.

Compound **74** (Figure 127) contains a furan heterocyclic ring at R^1. Clear signals for the furan ring could be observed in the ^{1}H NMR spectrum. The proton adjacent to the oxygen appears as a broad singlet at 7.48 ppm, which was the most deshielded proton due to the electron withdrawing effect of oxygen. The proton furthest away from the oxygen also appears as a broad singlet at 6.89 ppm, while the middle proton appears as a broad singlet at 6.47 ppm. Although these three signals had a broad singlet appearance, the ^{1}H-^{1}H COSY spectrum (see spectra for compound **74**) confirmed that they are coupled to each other but are poorly resolved. The ^{13}C NMR signals for the carbons bonded to these protons appear at 142.5 ppm, 107.6 ppm, and 110.1 ppm respectively. These assignments were confirmed using the ^{1}H-^{13}C HSQC spectrum. The IR and MS data also confirmed the generation of compound **74**.

3.7.3.14 Structural characterisation of 5-(3,5-bis(trifluoromethyl)phenyl)-2-(thiophen-2-yl)pyrazolo[1,5-*a*]pyrimidin-7(4*H*)-one (compound 75)

Figure 128: Structure of compound **75**.

Compound **75** (Figure 128) also contained a heterocyclic ring at R^1, this time a thiophene ring. The ^{1}H NMR spectrum consists of three signals for the thiophene ring; a poorly resolved broad singlet for the proton adjacent to the sulphur at 7.55 ppm which was

confirmed by ^{1}H-^{1}H COSY spectrum (see spectra of compound **75**), a doublet for the proton adjacent to the previous proton at 7.51 ppm, and a multiplet for the proton furthest away from the sulphur in the range of 7.10 – 7.16 ppm. The carbons bonded to these protons appear as singlets in the ^{13}C NMR spectrum at 125.0 ppm, 125.8 ppm and 128.0 ppm. The IR and MS data also confirmed the generation of compound **75**.

3.7.3.15 Structural characterisation of 5-(3,5-bis(trifluoromethyl)phenyl)-2-(pyridin-3-yl)pyrazolo[1,5-*a*]pyrimidin-7(4*H*)-one (compound 76)

Figure 129: Structure of compound **76**.

Compound **76** (Figure 129) had the nitrogen containing pyridine heterocycle at R^1. The proton in the *ortho* position of the pyridine ring, and adjacent to the nitrogen, appears as a singlet at 9.20 ppm, being most deshielded due to the electron withdrawing effect of the nitrogen. The carbon bonded to this proton appears at 147.6 ppm in the ^{13}C NMR spectrum. The other *ortho* proton appears as a double of doublets at 8.55 ppm as it coupled with its neighbouring proton and through long-range coupling to the proton in the *para* position, which itself appears as a multiplet in the range of 8.31 – 8.37 ppm. The carbons bonded to these protons appear at 149.2 ppm and 133.4 ppm respectively.

The proton in the *meta* position was between these two protons and therefore coupled with both. It also shows a small coupling with the first *ortho* proton (adjacent to the nitrogen), which resulted in a multiplet signal at 7.46 – 7.50 ppm. The carbon bonded to this proton appears at 124.1 ppm in the ^{13}C NMR spectrum. These assignments were supported by ^{1}H-^{1}H COSY and ^{1}H-^{13}C HSQC data. The IR and MS data also confirmed the generation of compound **76**.

3.8   Conclusion

The pyrazolopyrimidinone bicycle core is commonly found in many pharmaceutical and biomedical agents. Derivatives of this core structure can be found in medicines for the treatment of cancer, obesity, and cystic fibrosis. Other research groups have reported the synthesis of this pyrazolopyrimidinone bicycle core using conventional heating and microwave methods.

A family of pyrazolopyrimidinones were synthesised in order to establish how structural variations can influence biological activity, namely their ability to stimulate glucose uptake and inhibit complex I. The hit compound RTC53 was used as a starting point and a large number of RTC53 derivatives were synthesised using a selection of structural variations at R and R^1, Figure 130.
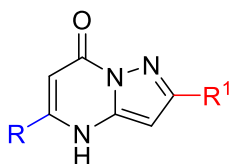
Figure 130: General structure for the pyrazolopyrimidinone bicycle family.

These structural variations can be grouped in three categories. Category 1: derivatives of RTC53 where variations were made at both the R and R^1 sites; Category 2: derivatives of RTC53 where variations were made at the R site only; Category 3: derivatives of RTC53 where variations were made at the R^1 site only. Variations included alkyl groups, phenyl ring, substituted aromatic rings, and heterocyclic rings. Aromatic ring substitutions included those at the *ortho, meta*, and *para* positions of the aromatic rings, and consisted of electron donating (e.g. methyl and methoxy) and electron withdrawing groups (e.g. nitro group). Heterocyclic rings consisted of furan, thiophene, and pyridine.

Synthetic method development for this family consisted of developing a microwave-assisted "one-pot" approach for the generation of the pyrazolopyrimidinone bicycles. The conventional reflux heating method for the synthesis of the intermediate aminopyrazole typically takes 17–24 hours and for the subsequent synthesis of pyrazolopyrimidinone takes a further 21–24 hours. This two step synthesis was reduced down to just over 2 hours using the "one-pot" microwave-assisted method. Furthermore, isolation and purification of the intermediate aminopyrazole could be

avoided as the second step of the synthesis could be conducted in the same reaction vessel ("one-pot"), by adding in the relevant β-ketoester to produce the required pyrazolopyrimidinone bicycle.

Purification of some pyrazolopyrimidinones proved to be difficult with yields averaging between 30-50% for the three categories. Category 3 compounds where the most challenging group of compounds to isolate and purify, and here our focus moved to accessing sufficient quantities of pure material for biological evaluation, regardless of yield. For all categories, purification typically consisted of column chromatography with a solvent mixture, or in a few cases, trituration with the appropriate solvent.

Structural characterisation of the pyrazolopyrimidinones employed ^{1}H and ^{13}C NMR spectroscopy, HR-MS, and IR spectroscopy. An X-ray crystal structure was also obtained for the furan-substituted pyrazolopyrimidinone. The ^{1}H NMR and ^{13}C NMR spectral assignments were confirmed using DEPT NMR experiments, as well as 2D-NMR experiments such as ^{1}H-^{1}H COSY, ^{1}H-^{13}C HSQC and ^{1}H-^{13}C HMBC. All compounds were analysed by high-resolution mass spectrometry to obtain a mass which was less than five ppm from the calculated mass of the compound. This also confirmed the presence of the desired compound. Finally, IR spectroscopy displayed absorption bands for the key functional groups present in each compound and further verified the successful synthesis of the target compound. The pure and fully characterised pyrazolopyrimidinones were then available for biological evaluation.

Chapter 4: Biological Evaluation

4.1   Introduction

As previously mentioned, biological evaluation of the two families of compounds, the arylpiperazine family and the pyrazolopyrimidinone bicycle family, involved a glucose uptake assay and a complex I assay.

The results presented in this chapter are for compounds synthesised by myself, and whose synthesis was discussed in the previous two chapters. In addition, some biological results are included for compounds that were synthesised by previous members of the Stephens group; Robert Devine and John Walsh. For clarity, compounds synthesised by Robert Devine will be assigned a subscript "a", and compounds synthesised by John Walsh will be assigned a subscript "b". All other compounds will have been synthesised by myself. The biological evaluation itself was carried out by myself, Robert Devine, John Walsh, Darren Martin (collaborator), and Siobhan Leonard (also a previous member of the Stephens group). Biological data generated by another group member will be assigned a subscript "c" (all the complex I inhibition data, including that using the compounds I synthesised, was generated by Siobhan Leonard). All other biological data will have been generated by myself.

The glucose uptake assay is a whole cell assay carried out on C2C12 mouse muscle cells. Cells were stimulated with the test compounds 16 hours before the glucose uptake assay was performed. The glucose uptake assay used was a radiolabelled assay that employed tritiated deoxy-2-glucose, see section **4.2**. After 16 hours of stimulation of the cells with the test compounds or controls, tritiated (^{3}H) deoxy-2-glucose was added. Tritium (^{3}H) is a radioactive isotope of hydrogen. This allowed us to quantitatively measure how much radio labelled deoxy-2-glucose has been taken up by the cells after stimulation of the test compounds, in comparison with the controls. Deoxy-2-glucose is used, as opposed to glucose itself, as it is a derivative of glucose that cannot be metabolized and so will remain in the cell after uptake.[50]

The glucose uptake assay is a whole cell assay, where the cell membrane and cell components are all in place. We used the glucose uptake assay as our first screening assay. This is because a whole cell assay more closely resembled what the compounds

will encounter in the body, as opposed to an enzyme inhibition assay (such as our second assay, complex I inhibition assay). Compounds that are active in enzyme inhibition assays have been known to be inactive in whole cell assays due to difficulties in passing through the cell membrane, and/or degradation by the cell components.[96]

The second assay performed, a complex I inhibition assay, was performed on compounds that were active in the glucose uptake assay (we also evaluated some compounds that were inactive in the glucose uptake assay). This assay utilised isolated rat liver mitochondria. A liver extraction, washing, chopping, homogenization, centrifugation process was followed, see section **4.4**, which resulted in a mitochondrial pellet with which the assay could be carried out. The pelleted mitochondria were then permeabilized and the reaction initiated with the addition of ubiquinone and the resulting decrease in absorbance of ubiquinone measured for 3 minutes. Varying concentrations of the test compounds were then added, and absorbance was measured for a further 3 minutes in each case. The effect of the compounds on complex I was determined by comparing activity before and after addition, relative to the vehicle control, dimethyl sulfoxide (DMSO).

4.2 Glucose Uptake Assay

The glucose uptake assay was carried out on C2C12 mouse muscle cells, an immortalized myoblast cell line, which is derived from a subclone of a mouse cell line.[97] Subcloning is the targeted transfer of a specific DNA sequence from the parent vector to the target one.[98] C2C12 is a muscle tissue cell line, which exhibits mononucleated myoblast morphology. This cell line acts as a good transfection model, but can rapidly differentiate into contractile multinucleated myotubes, producing muscle-specific proteins. Due to this ability for rapid differentiation, these cells are ideal for *in vitro* studies in biomedical research and cell biology, especially of mammalian myoblast cells.[97] C2C12 cells have been used to study the differentiation of myoblasts, osteoblasts, and myogenesis, to explore mechanistic biochemical pathways such as protein degradation[99], gene expression[100], and glucose transport[101], and to express various target proteins.

C2C12 cells used for the assay were stored in liquid nitrogen in DMSO in a process known as cryopreservation.[102] This process preserves the cells at low temperatures (-196 °C) to prevent any enzymatic or chemical activity from occurring. All media, equipment, and reagents must be sterile during cell culture to prevent microbial growth. Once removed from liquid nitrogen, cells were split multiple times in a sterilised biosafety cabinet before being used for experiments.

Splitting of the cells is an essential component of tissue culture as it allows for the cells to grow in a healthy and suitable environment. This process begins by rinsing the cells with phosphate-buffered saline to remove any dead cells, detaching cells from the bottom of the flask using trypsin, adding in fresh medium to transport the cells into a falcon tube, and spinning the cells down using a centrifuge. Cells can then be counted under a microscope using a haemocytometer, which is a glass plate accurately engraved with a grid of squares. New T75 flasks can be seeded with cells of the desired density. Once these cells become 80% confluent after 2-3 days, they can be split again into new flasks and the process continues until cells are no longer growing at the same rate as before.

Cells were cultured in 6-, 12-, or 24-well plates using high-glucose Dulbecco's Modified Eagle's Medium (DMEM) containing 10% (v/v) fetal bovine serum, 2 mM L-glutamine,

and 100 μg/ml penicillin-streptomycin, and stored in 5% CO_2 sterilised biosafety incubator with a constant temperature of 37 °C. When the myoblast cells reached 80 % confluence, differentiation into myotubes was induced by switching the growth medium to DMEM supplemented with 2% (v/v) horse serum for three days, after which the myotube cells were ready for use in the assay.

Cells were stimulated with the test compounds 16 hours before the glucose uptake assay in a 0.1% (v/v) horse serum DMEM medium. Compounds were prepared by dissolution in 100 μL DMSO to achieve a 50 mM concentration stock solution, which was diluted down to 1 mM working solution in Krebs' Ringer Buffer (KRB). KRB was prepared using 1 litre of distilled water containing sodium chloride (136 mM), Hepes (20 mM), potassium chloride (4.6 mM), magnesium sulfate (1 mM), calcium chloride (1 mM), sodium phosphate dibasic (4.05 mM), and sodium phosphate monobasic (0.95 mM). After the pH of KRB was adjusted to pH 7.4 using sodium hydroxide, it was sterilised filtered using a syringe and a 0.2 μM filter and stored at 4 °C.

Two controls were prepared in all experiments. DMSO acted as the standard control, to which all the cells were compared with, and insulin (or in some cases metformin) acted as the positive control to ensure cells are performing correctly. Insulin was stimulated for only 30 minutes to the cells at a concentration of 100 nM. This was done by pipetting 5 μL of a 10 μM working solution into 245 μL of 5 mM glucose solution inside the cells. The 10 μM working solution of insulin was prepared by pipetting 2.9 μL out of a 10 mg/mL stock solution of insulin inside 500 μL of 5 mM glucose solution. The 5 mM glucose solution was prepared by dissolving 0.04504 g of glucose in 50 mL KRB solution and sterilise filtering it. Metformin was stimulated in the same concentration as the test compounds for 16 hours.

After 16 hours of stimulation of the cells with the test compounds and controls, tritiated (^{3}H) deoxy-2-glucose was added to quantitatively measure how much glucose has been taken up by the cells after stimulation of the test compounds, in comparison with the controls. Tritium (^{3}H) is a radioactive isotope of hydrogen containing one proton and two neutrons with a half-life of over 12 years. It emits β-particles which cannot travel far through air and are incapable of passing through skin. Caution was taken while handling ^{3}H deoxy-2-glucose and disposing its waste by carrying out swabs before and

after every experiment, using designated equipment and reagents in the radiation suite, reducing the amount of time exposed to tritium to a minimum, and carrying out all the work inside the safety cabinet or fume-hood.

Following treatment of the cells with ^{3}H deoxy-2-glucose, cells were incubated for 10 minutes then washed three times in ice-cold KRB to stop any further uptake and solubilized in 0.1% (w/v) sodium dodecyl sulfate for 30-45 minutes. After this time, tritiated glucose uptake was evaluated via scintillation counting of the lysates diluted 1:4 in β-scintillation fluid using a scintillation counter. A protein assay accompanied the glucose uptake assay by quantitatively measuring the protein concentration of each sample via the bicinchoninic acid assay method to account for the different number of cells present in each sample.[103] A standard solution curve was made in this assay using distilled water and bovine serum albumin.

Protein concentration of each sample was correlated with the corresponding counts from the glucose uptake assay to express the result as counts per minute per mg protein. Each result was compared with the control (DMSO) to generate the fold change. All data was expressed as means ± standard error of the means (SEM) of a number of experiments (n) performed for that sample. Statistical analysis was performed using one-way analysis of variance (ANOVA) using GraphPad Prism 5.0 with a threshold of significance defined as a p-value <0.05 (95% confidence in result) or a one star significance (*), p-value < 0.01 or two stars significance (**), and p-value < 0.0001 or three stars significance (***). Only compounds which received stars significance in the glucose uptake assay were considered "active" compounds as their results meant that their ability to increase the uptake of glucose in cells was reliable and reproducible.

4.3   Glucose uptake results of the arylpiperazine family

As discussed in chapter 2, the arylpiperazine family consists of compounds synthesised by structural variation of RTC1 at five sites (Figure 131). Variations were carried out at the aryl group (site A), the piperazine ring (site B), the carbonyl group (site C), the alkyl chain (site D), and the thiophene ring (site E).
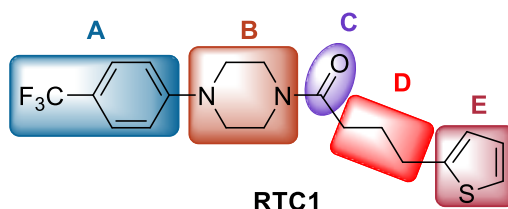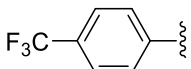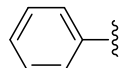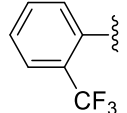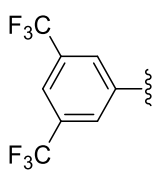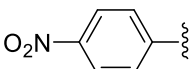
Figure 131: Structure of RTC1 with variations sites, A-E.
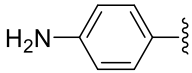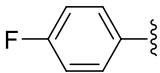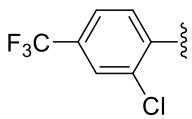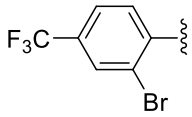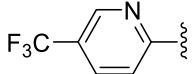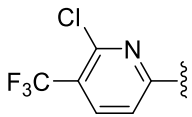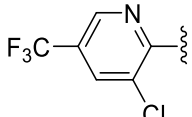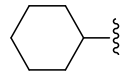
The results from the glucose uptake assay can be divided into the same sites/subfamilies, and hence allow the relationship between chemical structure and biological activity to be explored. As previously mentioned, and in order to describe the complete compound library, some compounds have been included that were synthesised by previous group members. All the biological data was generated by Siobhan Leonard, except for compounds **4** and **15**, which were tested by myself.

4.3.1 Glucose uptake results for structure variations at site A: the aryl group

Glucose uptake data for compounds with variations at site A of RTC1 can be found in Table 10. The first entry in Table 10 is for the parent compound, RTC1, which was active and gave a glucose uptake result of 2.57 fold change over the vehicle control with three stars significance. The fold change value illustrates how active RTC1 was in comparison with the vehicle control (fold change of 1). This calculation is performed by combining the number of ^3H deoxy-2-glucose counts (per minute) the cells contained after stimulation with RTC1, and the number of proteins (i.e. cells) these counts correspond to, in order to achieve the counts per minute per mg of protein. Three stars significance indicates that the results obtained from RTC1 have a p-value of less than 0.0001 and are therefore accurate and reliable, and RTC1 should be consistently active.

Table 10: Glucose uptake results for site A variations of RTC1.

Compound	R	Glucose Uptake Result	
		Fold change ± SEM	Active (Y) with stars significance, or inactive (N)
1 (RTC1/MK24)	F$_3$C—⟨phenyl⟩—	2.57 ± 0.08	Y (***)
7 (MK38)^c	⟨phenyl⟩—	0.96 ± 0.07	N
8 (MK41)^c	⟨phenyl-CF$_3$⟩—	0.85 ± 0.02	N
9 (MK44)^c	F$_3$C—⟨phenyl⟩—CF$_3$	1.42 ± 0.09	Y (*)
10 (MK39)^c	O$_2$N—⟨phenyl⟩—	1.06 ± 0.10	N

184

Compound	Structure	Fold change	Significant
11 (MK70)[c]	H_2N—⟨aryl⟩	1.32 ± 0.12	N
RTC11[a,c]	F—⟨aryl⟩	1.16 ± 0.09	N
12 (MK20)[c]	F_3C—⟨aryl⟩, Cl	1.58 ± 0.15	Y (***)
RTC62[a,c]	F_3C—⟨aryl⟩, Br	1.02 ± 0.04	N
13 (MK42)[c]	F_3C—⟨pyridyl, N⟩	1.00 ± 0.09	N
RTC44[a,c]	F_3C—⟨pyridyl, N⟩, Cl	1.22 ± 0.10	N
14 (MK45)[c]	F_3C—⟨pyridyl, N⟩, Cl	1.13 ± 0.02	Y (*)
4 (MK43)	⟨cyclohexyl⟩	1.29 ± 0.04	Y (***)
15 (MK36)	Me	0.84 ± 0.03	N

[a]Compounds synthesised by Dr Robert Devine.

[c]Compounds tested by Dr Siobhan Leonard.

From these results, it is observed that changes to the trifluoromethyl group or its position may result in loss of activity. This was the case when the trifluoromethyl group was removed (compound 7), substituted in the *ortho* position instead of the *para* position (compound 8), or replaced by a nitro (compound 10), amine (compound 11), or fluorine (RTC11) groups. The result for compound 10 is interesting as replacement of a hydrophobic electron withdrawing group (CF_3) with a considerable less hydrophobic electron withdrawing group (NO_2) resulted in loss of activity. Activity was found with the compound containing two trifluoromethyl groups, *meta* substituted, (compound 9) but with a lower fold change and only one star significance in comparison with RTC1. From these results, it could be concluded that one trifluoromethyl group at the *para* position of the aromatic ring may play an important role in the biological activity of the

compounds. Trifluoromethyl groups are well known for the hydrophobic and lipophilic nature, and can aid transport across cell membranes as well as contribute to binding in hydrophobic enzyme pockets.[68]

Some further changes to the aromatic ring also resulted in complete loss of activity, including those where an additional bromine *ortho* substituent was added (**RTC62**), where a *para* CF_3 pyridine ring replaced the *para* CF_3 aryl ring (compound **13**), or a *para* CF_3 pyridine ring with an additional chlorine *meta* substituent replaced the *para* CF_3 aryl ring (**RTC44**). However, some changes could be somewhat tolerated, albeit with a drop in activity. When a chlorine group was added at the *ortho* position of the aromatic ring (compound **12**), the glucose uptake fold change dropped but still showed activity with three stars significance. Similarly, an increase in glucose uptake over vehicle control was observed for compound **14**, where the *para* CF_3 pyridine ring had an additional chloro *ortho* substituent. Although, here the fold change was small but did have one star significance.

An increase in glucose uptake over the vehicle control, with three stars significance, was observed for compound **4** where the hydrophobic *para* CF3 aryl ring was replaced by a hydrophobic cyclohexyl ring. This activity was not shown when the hydrophobic *para* CF_3 aryl group was replaced with a simple methyl group (MK36) (compound **14**). These results may suggest that a somewhat large hydrophobic group at site A may be important for biological activity. The presence of such a group could impact on transport across cell membranes and on binding in enzyme hydrophobic pockets.

The results of each experiment were generated using a bar graph similar to the one shown below (Figure 132), which shows the activity of compounds **4** and **15**, in comparison with the vehicle control (DMSO) and the two positive controls; insulin and RTC1.
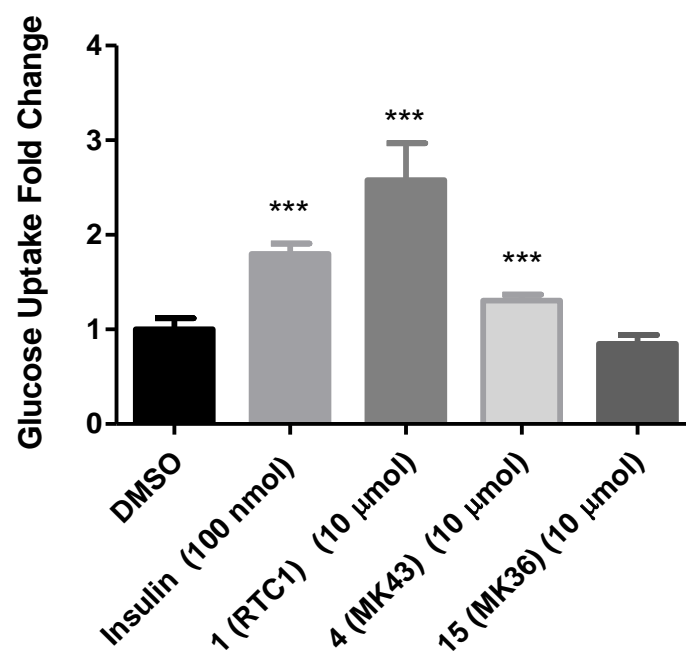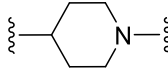
Figure 132: Glucose uptake results of RTC1, compound **4**, and compound **15** in comparison with DMSO as the vehicle control and insulin as the positive control.

4.3.2 Glucose uptake results for structure variations at site B: the piperazine ring

The next set of glucose uptake results are for site B variations, the piperazine ring of RTC1 (Table 11).

Table 11: Glucose uptake results for site B variations of RTC1.

Compound	X	Glucose Uptake Result	
		Fold change ± SEM	Active (Y) with stars significance or inactive (N)
16 (MK19)[c]		2.14 ± 0.30	Y (***)
17 (MK90)	NH	1.11 ± 0.08	N
RTC21[a,c]	(NH)$_2$	1.24 ± 0.05	Y (**)

[a]Compound synthesised by Dr Robert Devine.

[c]Compounds tested by Dr Siobhan Leonard.

It is observed from these results that good activity is maintained if the piperazine ring in RTC1 is replaced by a piperidine ring (compound **16**), which had three stars significance and a 2.14 fold change over the vehicle control. Replacement of the piperazine ring with a hydrazine motif (**RTC21**) resulted in an active compound, albeit with lower fold change (two stars significance). Activity was lost when the piperazine ring was replaced by a secondary amine (compound **17**). It can therefore be concluded that the piperazine ring appears to be important for biological activity and that changing to a piperidine ring is not optimal but does generate a compound with good activity. However, removal of the saturated six membered ring heterocycle altogether, as was the case with the hydrazine and amine motifs, results in a large drop in or complete loss of activity.

4.3.3 Glucose uptake results for structure variations at site C: the carbonyl group

The next glucose uptake result is for site C variations of RTC1, the carbonyl group (Figure 133). Here, a single compound was made without the carbonyl group, 1-(4-(thiophen-2-yl)butyl)-4-(4-(trifluoromethyl)phenyl)piperazine (MK34) (compound **18**). This compound was active in the glucose uptake assay with a fold change value of 1.36 ± 0.09 and three-star significance. This compound was tested by Dr Siobhan Leonard.
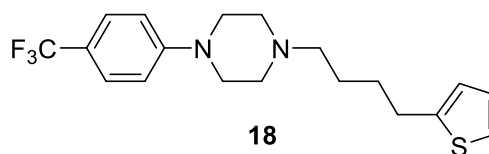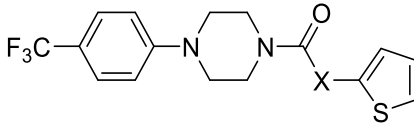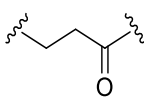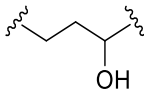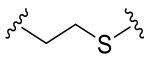
Figure 133: Structure of compound **18.**

Although activity was still maintained without the carbonyl group, the fold change of this compound was lower than RTC1. It can therefore be concluded that the carbonyl group improves biological activity and its presence is important, but perhaps not absolutely essential.

4.3.4 Glucose uptake results for structure variations at site D: the alkyl chain

The following set of glucose uptake results are for site D variations of RTC1, the alkyl chain (Table 12).

Table 12: Glucose uptake results for site D variations of RTC1.

Compound	X	Glucose Uptake Result	
		Fold change ± SEM	Active (Y) with stars significance or inactive (N)
21 (MK37)[c]	-	0.93 ± 0.07	N
22 (MK47)[c]	CH_2	1.33 ± 0.04	Y (***)
RTC532[a,c]	C_2H_4	1.09 ± 0.08	N
1 (RTC1)	C_3H_6	2.57 ± 0.08	Y (***)
23 (MK18)	C_4H_8	1.78 ± 0.13	Y (***)
RTC537[a,c]	C_5H_{10}	1.33 ± 0.05	Y (***)
24 (MK40)[c]		1.19 ± 0.03	Y (***)
RTC29[a,c]		1.41 ± 0.04	Y (***)
25 (MK22)[c]		2.14 ± 0.23	Y (***)

[a]Compounds synthesised by Dr Robert Devine.

[c]Compounds tested by Dr Siobhan Leonard.

The lead compound RTC1 has a three carbon alkyl chain linking the carbonyl carbon with the thiophene heterocycle. The results of the glucose uptake assay suggest that the alkyl chain in RTC1 is important for biological function, as activity was lost when the chain was completely removed (compound **21**). Activity was also reduced when the alkyl chain was shortened but not fully removed, as was the case for compound **22** (low activity) and **RTC532** (not active). Lengthening the alkyl chain (compound **23** and **RTC537**) also

resulted in a decrease in activity but not a complete loss in activity. One possible explanation is that a certain length of alkyl chain is required for the molecule to strongly bind to the active site. Too short or too long a chain may result in a poor fit and weak binding. Also, an entropy effect could also be considered for the longer chain compounds. Longer chain compounds will be more "floppy" in nature and be able to adopt a larger number of conformations when unbound. As such, upon binding there will a large increase in order, entropy cost, and hence the binding of such molecules may be less thermodynamically favourable when compare to shorter chained molecules.

A large drop in activity levels was observed when an additional carbonyl group (compound **24**) or when a hydroxyl group (**RTC29**) was placed at the γ-carbon. Carbonyl groups can act as H-bond acceptors via the lone pairs on the carbonyl oxygen.[77] Hydroxyl groups can act as both H-bond acceptors and H-bond donors.[104] Carbonyl groups and hydroxyl groups are also polar in nature. Hence, the addition of such groups may result in unfavourable H-bonding or electrostatic interactions between the molecule and the target protein. This could cause a weakening in binding and poorer biological function.
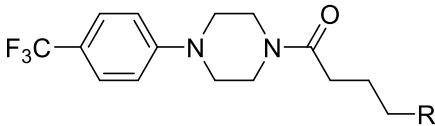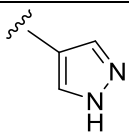
When the γ-CH_2 was replaced with a sulphur atom (compound **25**), a small drop in activity was observed, but with a 2.14 fold change compared with the vehicle control and with three-star significance. Sulphur has two lone pairs, but is considered to be a significantly weaker H-bond acceptor that oxygen,[105] and hence may not have large negative impact on binding strength.

All the active compounds in this subfamily had activity with three stars significance, but with a lower fold change than RTC1. It could therefore be concluded that the alkyl chain in RTC1, which connects the carbonyl group to the thiophene ring, is important for biological activity. An optimal alkyl chain length appears to be three carbons in length, and that the addition of motifs to the chain that could result in additional substrate-target interactions could reducing binding/activity.

4.3.5 Glucose uptake results for structure variations at site E: the thiophene ring

The next set of glucose uptake results are for site E variations of RTC1, the thiophene ring (Table 13).

Table 13: Glucose uptake results for site E variations of RTC1.

Compound	R	Glucose Uptake Result	
		Fold change ± SEM	Active (Y) with stars significance or inactive (N)
5 (MK69)[c]		1.35 ± 0.11	Y (**)
RTC194[a,c]	CH_3	1.28 ± 0.11	Y (**)

[a]Compound synthesised by Dr Robert Devine.
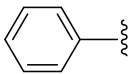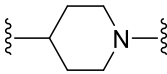
[c]Compounds tested by Dr Siobhan Leonard.

It can be observed from these glucose uptake results that replacing the thiophene ring in RTC1 with a different heterocycle, a pyrazole ring (compound **5**), or with an alkyl group, a methyl group (**RTC194**), caused a decrease in activity. However, both compounds did remain active, with two stars significance, and hence it could be suggested that a thiophene may be important but not be essential for activity, and that alternatives to a thiophene may result in reduced activity.

4.3.6 Glucose uptake results for structure variations at a combination of sites

The following sets of glucose uptake results are for compounds with a combination of variations of RTC1. Table 14 summaries the results for the first set, which contains compounds with variation at both site A, the aryl group, and site B, the piperazine.

Table 14: Glucose uptake results for compounds with a combination of variations at sites A and B.

Compound	R	X	Glucose Uptake Result	
			Fold change ± SEM	Active (Y) with stars significance or inactive (N)
27 (MK89)			1.25 ± 0.12	Y (*)
RTC1 acid[c]	-	OH	1.16 ± 0.04	Y (*)
RTC19[a,c]	-	OMe	1.09 ± 0.04	N

[a]Compound synthesised by Dr Robert Devine.

[c]Compounds tested by Dr Siobhan Leonard.

Removal of the CF_3 group from RTC1 at the same time as replacing the piperazine ring with a piperidine ring (compound **27**) resulted a large drop in activity. A reduction in activity may not be very surprising, if one considers the result for compound **7** where removal of the CF_3 group alone, Table 10, resulted in complete loss of activity. What perhaps is more surprising is that activity was observed at all for compound **27**, albeit at very low levels. Very low levels of activity were also observed when the starting material used in the synthesis of RTC1 (**RTC1 acid**) was evaluated in the glucose uptake assay. For both these compounds, the fold change was marginally above 1 (1.2-1.3, one star significance) and hence are not very promising candidates for development.

When the aryl group and piperazine ring were both replaced by a methoxy group, activity was lost. This is not surprising as this molecule is significantly different from the

hit compound RTC1. This set of tests further suggests that having a *para* substituted trifluoromethyl aryl ring and a piperazine ring are important for biological activity.

The next set of glucose uptake results are for a combination of site A (aryl group) and site D (alkyl chain) variations of RTC1 (Table 15).

Table 15: Glucose uptake results for compounds with for a combination of variations at sites A and D.

Compound	R	X	Glucose Uptake Result	
			Fold change ± SEM	Active (Y) with stars significance or inactive (N)
RTB70[a,c]			1.31 ± 0.02	Y (***)
RTC4[a,c]			1.26 ± 0.06	Y (*)
RTC3[a,c]			1.22 ± 0.06	N

[a]Compounds synthesised by Dr Robert Devine.

[c]Compounds tested by Dr Siobhan Leonard.

Although active, all three compounds evaluated in this subfamily showed large drops in biological activity. Such a decrease in activity may not be that surprising if one considers the results for compound **13** and **14** in Table 10, where the same pyridine rings replaced the *para* trifluoromethyl aryl ring of RTC1, and a large drop in activity was also observed. These compounds reaffirm previous suggestions that compounds with chlorine substituted in the *ortho* position of a pyridine ring can result in an active compound but with much low levels of activity in comparison with RTC1.

The next glucose uptake result is for 1-(thiophen-2-yl)-4-(4-(4-(trifluoromethyl)phenyl)piperidin-1-yl)butane-1,4-dione (MK88) (compound **28,** Figure 134). Here a combination of variations was employed at both site B (the piperazine ring) and site D (the alkyl chain).
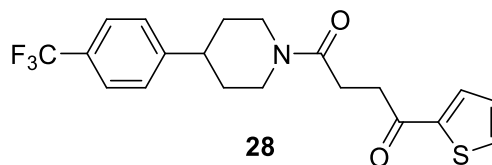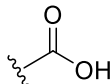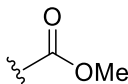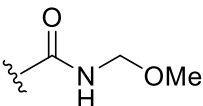
Figure 134: Structure of compound **28**.

As discussed earlier, compound **16**, Table 11, replacing the piperazine ring by a piperidine ring seemed to maintain high levels of activity. However, adding an extra carbonyl group in the alkyl chain was observed to lower activity in the glucose uptake assay. As such, combining both these changes would be expected to show a reduction in activity but perhaps still some lower level of activity. This indeed turned out to be the case as the glucose uptake assay for this compound showed a fold change of 1.31 ± 0.05 compared to the vehicle control, with three stars significance.

The next set of glucose uptake results are for compounds with a combination of variations at site D (the alkyl chain) and site E (the thiophene ring) (Table 16).

Table 16: Glucose uptake results for compounds with a combination of variations at sites D and E.

Compound	X	R	Glucose Uptake Result	
			Fold change ± SEM	Active (Y) with stars significance or inactive (N)
30 (MK29)	CH_3	-	1.43 ± 0.09	Y (***)
RTC535[a,c]	C_2H_4		1.11 ± 0.04	N
29 (MK30)	C_4H_8	Ph	1.95 ± 0.09	Y (***)

Compound		R	Fold change	Active
RTC533[a,c]	C$_6$H$_{12}$	CH$_3$	1.38 ± 0.05	Y (***)
RTC15[a,c]	C$_7$H$_{14}$		1.38 ± 0.06	Y (***)
3 (MK16)[c]	C$_7$H$_{14}$		1.08 ± 0.08	N
RTC18[a,c]	C$_7$H$_{14}$		2.35 ± 0.25	Y (***)
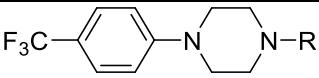
[a]Compounds synthesised by Dr Robert Devine.

[c]Compounds tested by Dr Siobhan Leonard.

All the compounds in this subfamily contain changes in length of the alkyl chain compared to RTC1. Such changes would be expected to reduce, but perhaps not eliminate, biological activity in the glucose uptake assay, based on results shown for related compounds in Table 12. Changes to the thiophene ring, site E, Table 13, could also be expected to reduce, but not eliminate, activity. The results in Table 16 above are reflective of this, with lower activity resulting for all compounds. Compounds **3** and **RTC35** both showed complete loss of activity. **RTC18**, on the other hand, is perhaps the surprise result from this subfamily as while the activity was lower than for RTC1, the drop was only marginal.

The next set of glucose uptake results are for a combination of variations at site C (the carbonyl group), site D (the alkyl chain), and site E (the thiophene ring) (Table 17).

Table 17: Glucose uptake results for a combination of variations at sites C, D, and E.

Compound	R	Glucose Uptake Result	
		Fold change ± SEM	Active (Y) with stars significance or inactive (N)
RTC1 amine[c]	H	1.16 ± 0.06	Y (*)
31 (MK35)	CH$_3$	0.92 ± 0.07	N

[c]Compound tested by Dr Siobhan Leonard.

It can be observed from these glucose uptake results that the starting material of RTC1 (**RTC1 amine**), which does not have a carbonyl group, alkyl chain, or thiophene ring show a very large drop in activity, as would be expected. It is perhaps surprising that any activity was observed, but it is worth noting that the activity level was very low at 1.2 fold change compared with the vehicle control. Furthermore, if a methyl group is used to replace the carbonyl group, alkyl chain, and thiophene ring then activity is no longer observed. Again, this would be as expected. These results suggest the presence of an arylpiperazine alone is not sufficient for substantial levels of activity.

For this compound family, RTC1 remained the most active compound in the glucose uptake assay. The presence of a *para* trifluoromethyl aryl piperazine motif appears essential for high levels of glucose uptake activity. An alkyl chain linker of three carbons also appears important. The terminal moiety appears to be variable to some extent, although a preference for the thiophene ring could be suggested.

4.4 NADH:ubiquinone oxidoreductase (complex I) assay, aryl piperazine family

Compounds that were active in the glucose uptake assay were brought forward for testing in a second assay, the NADH:ubiquinone oxidoreductase (complex I) assay. This would allow us to evaluate the compounds ability to inhibit complex I of the electron transport chain. As discussed previously, the inhibition of complex I of the electron transport chain has been discovered to be a potential target for treatment of type 2 diabetes.[44] Recent research published by our group examined how compounds of the arylpiperazine family were able to inhibit complex I and restore the glucose-handling abilities of mice fed with a high-fat diet.[44] The complex I assay used isolated rat liver mitochondria for the animal studies. Inhibition of complex I was shown to lead to activation of AMP-activated protein kinase (AMPK), which in turn increased glucose uptake by the cells.[44]

Inhibition of complex I was shown to lead to activation of AMP-activated protein kinase (AMPK).[44] AMPK is a heterotrimeric protein complex that is involved in cellular energy homeostasis where it regulates energy levels by monitoring the amounts of adenosine triphosphate (ATP) and adenosine monophosphate (AMP).[26] Activation of AMPK by small molecules such as arylpiperazines and metformin has shown to reduce hepatic gluconeogenesis, increase oxidation of fatty acids, increase glycolysis, and, most importantly, increase the uptake of glucose by skeletal muscles.[26,51]

Metformin is one of the most widely used treatments for type 2 diabetes today and it can be used as a monotherapy or as a combination therapy with other treatments.[30] Metformin achieves its anti-diabetic role by reducing the activity of complex I of the electron transport chain which in turn activates AMPK, inhibits liver gluconeogenesis, and antagonises glucagon action.[25,27,29] However, metformin is known for causing many undesirable side-effects such as diarrhoea, nausea and mild anorexia. Compounds from the arylpiperazine family were shown to have a greater anti-diabetic effect than metformin and at a lower dose when tested on mice, with no known side-effects.[44]

The complex I assay was carried out on isolated rat liver mitochondria which were isolated by the method described by Chappell and Hansford (1972).[106] Immediately after

extraction, liver samples were washed free of excess blood, trimmed of any fat and connective tissue, finely chopped, and placed in ice-cold isolation medium containing sucrose, tris-hydrochloric acid, and egtazic acid. The tissue was homogenized and centrifuged and the supernatant was filtered through a sieve before being centrifuged. The resulting mitochondrial pellet was resuspended in ice-cold isolation medium supplemented with defatted bovine serum albumin (BSA) and washed twice by centrifugation. The final mitochondrial pellet was resuspended in a small volume of isolation medium, and the aliquots were frozen at −20°C.

Immediately before the assay, the isolated mitochondria were diluted in a hypotonic buffer and permeabilized with three cycles of freeze thawing. The assay was carried at 30°C in a 1 mL cuvette. Permeabilized mitochondria were incubated with potassium phosphate dibasic, fatty acid-free BSA, potassium cyanide, and NADH. Baseline activity was measured at 340 nm for 1 minute. The reaction was initiated with the addition of ubiquinone (60 µmol L^{-1}) and the resulting decrease in absorbance was measured for three minutes. Varying concentrations of the test compounds were then added, and absorbance was measured for a further three minutes. The effect of the compounds on complex I was determined by comparing activity before and after addition, relative to the vehicle control, DMSO. Rotenone (1 µmol L^{-1}) was used as a positive control in this assay due to its known ability to inhibit complex I.[107,108]
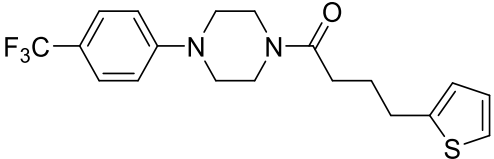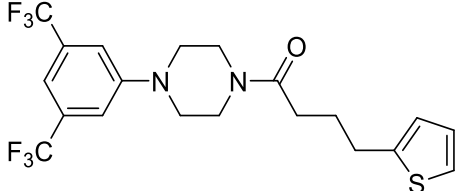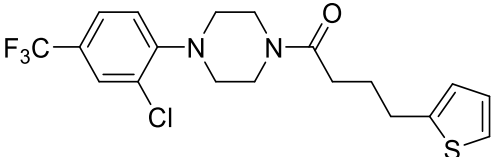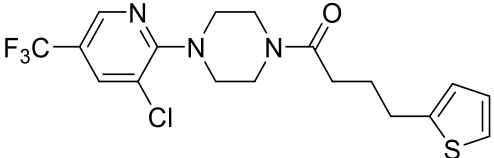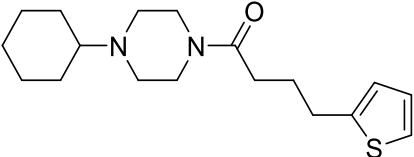
To determine the percentage activity of complex I, the slope of the line obtained with the addition of ubiquinone was divided by the slope of the line produced with the addition of the test compound. This value was then expressed as a percentage, relative to the value calculated for the vehicle control, DMSO, and the protein concentration of the mitochondrial sample. Compounds were tested at five different concentrations, in triplicate, to generate their half maximal inhibitory concentration (IC_{50}) values which is a quantitative measure that indicates the concentration of the compound which inhibits a biological process by 50%. It is commonly used in pharmacological research as a measure of antagonist drug potency and represents the concentration of a drug that is required for 50% inhibition *in vitro*.

As previously mentioned, all the compounds evaluated in the complex I assay were tested by Dr Siobhan Leonard.

4.4.1 Complex I assay results of the active arylpiperazine compounds

Complex I assay results for the aryl piperazine compounds that were active in the glucose uptake assay are shown in Table 18. The IC_{50} value of all the compounds was compared to the IC_{50} value of the parent molecule, RTC1. Rotenone has an IC_{50} value of 3.1375 µM.[43] The results of the complex I assay showed a range of IC_{50} values for the evaluated compounds in the arylpiperazine family.

Table 18: Complex I assay results of the active arylpiperazine compounds.

Compound	Structure	IC_{50} (µM)
1 (RTC1)		27
9 (MK44)		107
12 (MK20)		46
14 (MK45)		154
4 (MK43)		359

16 (MK19)		15
RTC21[a]		378
18 (MK34)		4
22 (MK47)		7
23 (MK18)		60
RTC537[a]		9
24 (MK40)		15
RTC29[a]		9

25 (MK22)

14

5 (MK69)

67

RTC194[a]

4

27 (MK89)

78

RTB70[a]

6

RTC4[a]

21

28 (MK88)

289

30 (MK29)

702

29 (MK30)		6
RTC533[a]		33
RTC15[a]		370
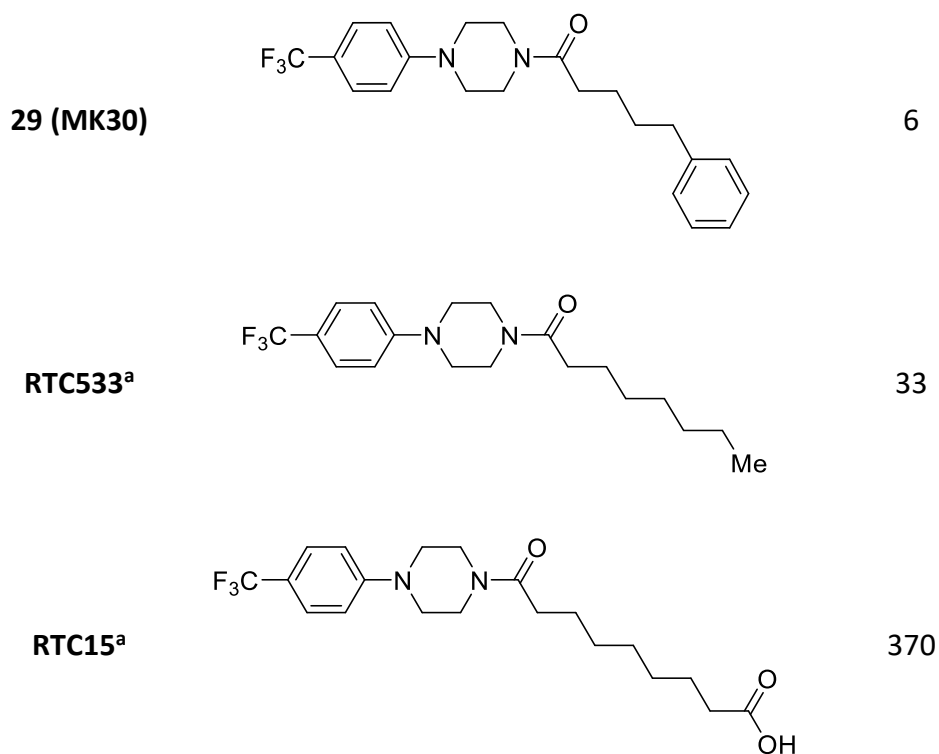
[a]Compounds synthesised by Dr Robert Devine.

All the compounds which were active in the glucose uptake assay were found to also be active in the complex I assay. The parent molecule, RTC1, had an IC$_{50}$ value of 27 μM, which is the concentration of that compound required to give 50% inhibition of complex I activity (Figure 135).
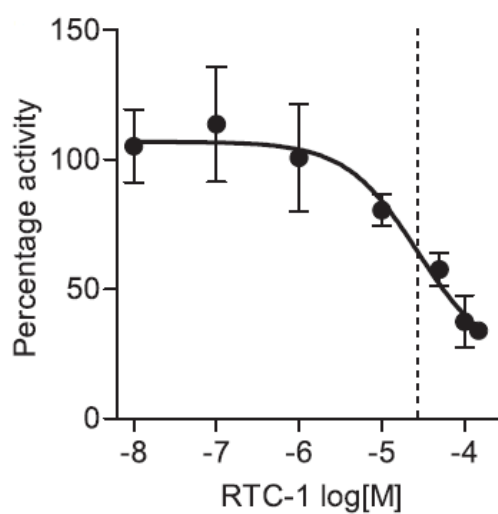
Figure 135: Plot of RTC1-induced inhibition of NADH oxidation in disrupted mitochondria showing the IC$_{50}$ to be 27 μM.
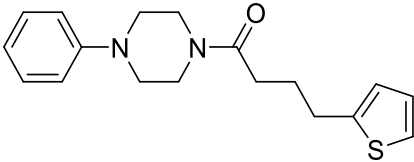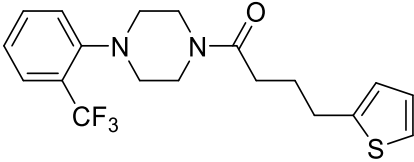
Some compounds had a much higher IC_{50} value, (e.g. compound **4**), where other compounds had a lower IC_{50} value (e.g. compound **22**). From the active compounds, the compound with the highest IC_{50} value of 702 µM was compound **30**, which contained a methyl group instead of the alkyl chain and a thiophene ring. This means it would take 28 times the concentration of RTC1 for this compound to have the same effect of inhibiting 50% of complex I activity. The lowest IC_{50} value of 4 µM was reported with compound **18**, the analogue of RTC1 without the carbonyl group. This value was very close to the IC_{50} value of the positive control, rotenone, which had an IC_{50} value of 3.14 µM.[43] Of all the compounds which were active in the glucose uptake assay with three stars significance, twelve of them had a similar or lower IC_{50} value to RTC1. These compounds are: **16**, **18**, **22**, **RTC537**, **24**, **RTC29**, **25**, **RTC194**, **RTB70**, **RTC4**, **29**, **RTC533**.
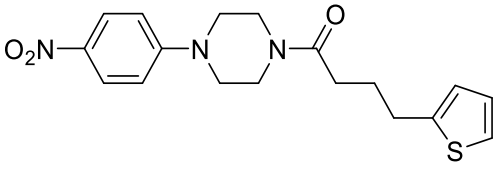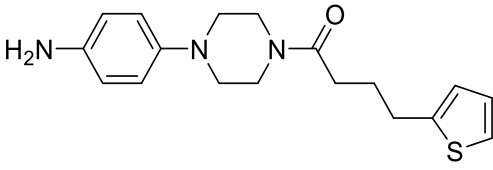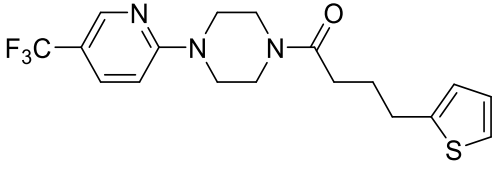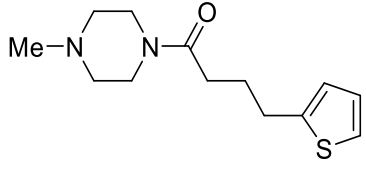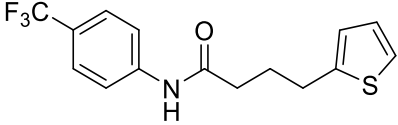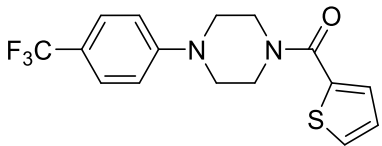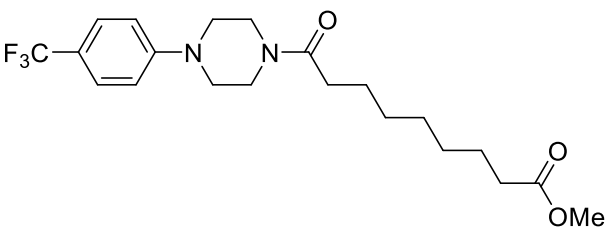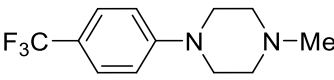
4.4.2 Complex I assay results of the inactive arylpiperazine compounds

A number of the aryl piperazine compounds that I had synthesised were not active in the glucose uptake assay. Even though this was the case, they were evaluated in the complex I assay as we had material to hand. To our surprise, all of the inactive compounds showed some activity in the complex I inhibition assay (Table 19). One possible explanation is that in the whole cell glucose uptake assay, the compounds could not pass the cell membrane, avoid efflux mechanisms, or survive the cells internal "machinery" (e.g. hydrolysis, enzyme catalysed degradation) and hence were inactive.[96,106]

In an inhibition assay, such as the complex I assay, these barriers and problems are removed, and this could allow the compounds to access the complex I active site and inhibit its activity. Hollenback et al. have reported a similar trend in their research where they tested substrate specificity in membrane and whole cell assays.[109] A research by Hernandez et al. also compared enzyme assays with a whole cells based assay. They concluded that whole cell based assays have the advantage of only selecting compounds that are able to penetrate cells and reach the intracellular targets.[110]

Table 19: Complex I assay results of the inactive arylpiperazine compounds.

Compound	Structure	IC_{50} (μM)
7 (MK38)		133
8 (MK41)		30

10 (MK39)		17
11 (MK70)		10
13 (MK42)		27
15 (MK36)		161
17 (MK90)		92
21 (MK37)		14
3 (MK16)		91
31 (MK35)		67

As previously mentioned, all the compounds showed activity in the complex I assay. However, only three compounds were reported to have an IC_{50} value lower than RTC1,

namely compounds **10**, **11**, and **21**. Compounds **8** and **31** had similar values to RTC1, and all other compounds had a higher IC$_{50}$ value.

4.5 Glucose uptake results of the pyrazolopyrimidinone bicycle family

As mentioned before, a family of pyrazolopyrimidinones, analogues of RTC53 (Figure 136) were synthesised in order to evaluate their activity in the glucose uptake assay and study the affect different structural variations had on activity levels.
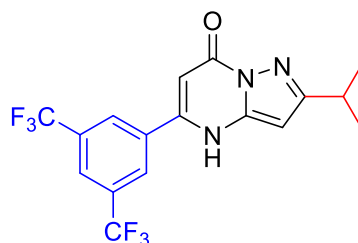
Figure 136: Structure of RTC53.

The 32 compounds already discussed in chapter 3 were tested by myself for biological activity in the glucose uptake assay. These compounds were added to the library of compounds synthesised and tested by previous group members. Structural variations in this family of compounds were divided into three categories as discussed previously (Figure 137). The first subfamily was categorised as variations on both R and R^1 sites. The second category consisted of variations on the R site only (aromatic bis-CF$_3$ group). The third category consisted of varying the R^1 site (isopropyl group). The results from the glucose uptake assay were divided up into the same three categories.
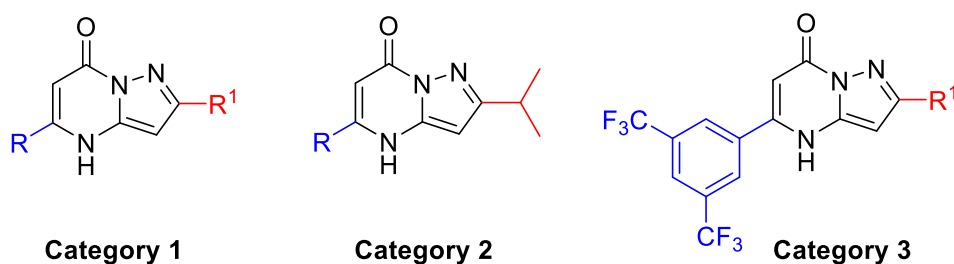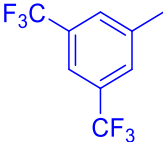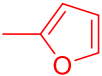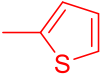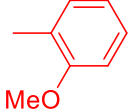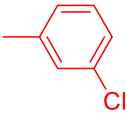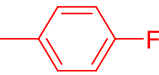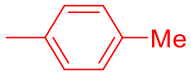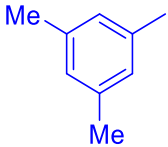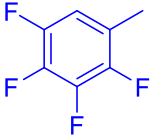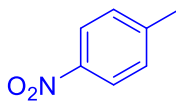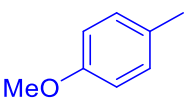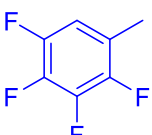
Figure 137: Structural variations of RTC53.

4.5.1 Glucose uptake results for pyrazolopyrimidinone category 1: variations at both R and R^1 sites

Category 1 consisted of variations at both the R and R^1 sites on the bicycle core. Variations at the R site consisted of a phenyl ring, substituted aromatic rings with electron donating and electron withdrawing groups, and alkyl groups. Variations to the R^1 site consisted of alkyl groups, heterocyclic rings, phenyl ring, or substituted aromatic rings with electron donating and electron withdrawing groups. The effect of these variations on glucose uptake in the cells is shown in Table 20).

Table 20: Glucose uptake results for pyrazolopyrimidinone category 1 variations.

Compound	R	R^1	Glucose Uptake Result	
			Fold change ± SEM	Active (Y) with stars significance or inactive (N)
RTC53[a,c]		iPr	1.99 ± 0.15	Y (***)
43 (MK62)	Ph	Me	0.80 ± 0.11	N
44 (MK59)	Ph	tBu	0.79 ± 0.14	N
41 (MK56)	Ph		1.10 ± 0.26	N
42 (MK55)	Ph		0.96 ± 0.16	N
40 (MK15)	Ph	Ph	0.90 ± 0.10	N
45 (MK58)	Ph		0.95 ± 0.29	N

Compound	R	R^1	Glucose uptake	Active
46 (MK7)	Ph	(3-Cl phenyl)	1.10 ± 0.26	N
47 (MK8)	Ph	(4-F phenyl)	0.61 ± 0.04	N
48 (MK9)	Ph	(4-Me phenyl)	0.85 ± 0.18	N
JW-06-006[b,c]	Me	Me	0.76 ± 0.04	N
52 (MK2)	(3,5-diMe phenyl)	Me	1.20 ± 0.18	N
JW-06-012[b,c]	(tetrafluoro phenyl)	Me	0.90 ± 0.08	N
RTC54[a,c]	Et	*t*Bu	1.08 ± 0.04	N
JW-04-053[b,c]	iPr	*t*Bu	0.96 ± 0.07	N
RTC55[a,c]	*t*Bu	*t*Bu	0.53 ± 0.05	N
JW-04-041[b,c]	Me	Ph	0.95 ± 0.05	N
49 (MK61)	(4-nitro phenyl, O₂N)	Ph	1.16 ± 0.06	N
50 (MK66)	(4-methoxy phenyl, MeO)	Ph	1.23 ± 0.07	Y (*)
51 (MK63)	(tetrafluoro phenyl)	Ph	1.27 ± 0.07	Y (*)

[a]Compounds synthesised by Dr Robert Devin.

[b]Compounds synthesised by Dr John Walsh.

[c]Compounds tested by Dr Siobhan Leonard.

The glucose uptake results from category 1 variations showed that very few compounds were active meaning that variations at both R and R^1 sites resulted a loss in activity

compared to RTC53. The first nine compounds after RTC53 in Table 20 had a phenyl ring at the R site, with variations at the R^1 site that included alkyl groups (e.g. methyl, compound **43,** and *tert*-butyl, compound **44**), heterocyclic rings (e.g. furan, compound **41,** and thiophene, compound **42**), a phenyl ring (compound **40**), and substituted aromatic rings (compounds **45**-**48**).

None of these derivatives of RTC53, containing a phenyl ring at the R site, showed activity in the glucose uptake assay. This correlates well with the loss of activity for found for pyrazolopyrimidinone category 2 variations (section **4.5.2**), where the R site consisted of a phenyl group and the R^1 site remained as an isopropyl group.

The next three compounds contained a methyl group at the R^1 site and a methyl (**JW-06-006**), aromatic ring bis substituted with *meta* methyl groups (compound **52**), or an aromatic ring, with multiple fluoro substituents, (**JW-06-012**) at the R site. These three compounds also showed a loss of activity in the glucose uptake assay. This correlates well with the loss of activity found with a subset of the pyrazolopyrimidinone category 3 variations, where a methyl group was placed at the R^1 site.

The next three compounds contained a *tert*-butyl group at the R^1 site and an ethyl group (**RTC54**), isopropyl group (**JW-04-053**) or a *tert*-butyl group (**RTC55**) at the R site. All these compounds showed loss of activity. Although the *tert*-butyl group in the R^1 site resulted in activity in category 3 variations, activity was lost when the aromatic bistrifluoromethyl group at the R site was substituted with an ethyl, isopropyl or another *tert*-butyl groups, as was the case in the pyrazolopyrimidinone category two variations.

The final four compounds contained a phenyl ring at the R^1 site, while the R site consisted of a methyl (**JW-04-041**), a *para* nitro aromatic ring (compound **49**), *para* methoxy aromatic ring (compound **50**), and a tetrafluoro substituted aromatic ring (compound **51**). These final two compounds, compounds **50** and **51**, were the only compounds in pyrazolopyrimidinone category 1 which showed activity (Figure 138).
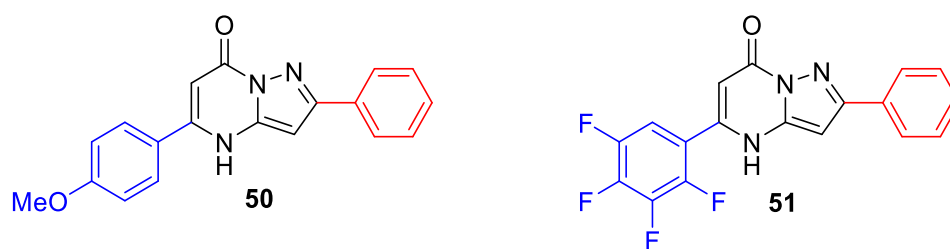
Figure 138: Structure of active compounds in category 1 variations at the R and R^1 site.

Both compounds had a smaller fold change than RTC53 and one star significance (Figure 139). This was also interesting as derivatives containing both groups in category 2 variations showed no activity in the glucose uptake assay when the R^1 contained an isopropyl group.
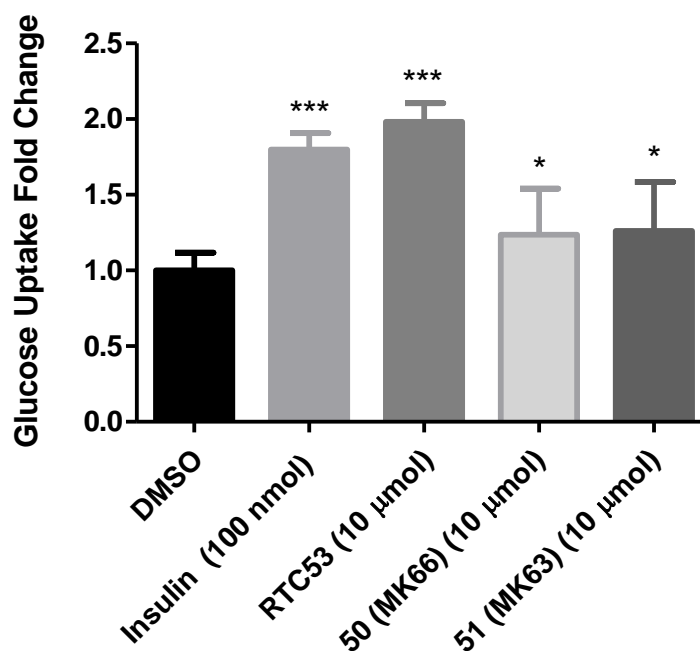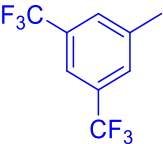
Figure 139: Glucose uptake results of RTC53, compound **50**, and compound **51** in comparison with DMSO as the control and insulin as the positive control.
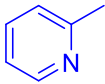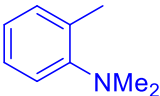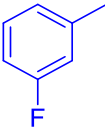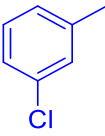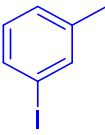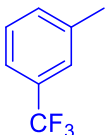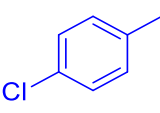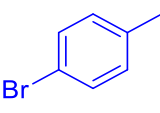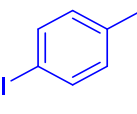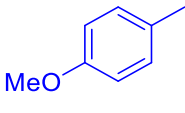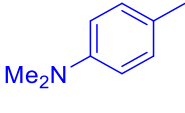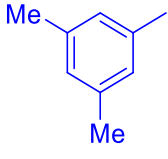
In summary, only two compounds were active in the glucose uptake assay of category 1 variations at the R and R^1 site. The glucose uptake results for pyrazolopyrimidinone category 1 variations can be better discussed in combination with results for category 2 and 3 variations.
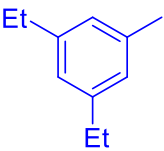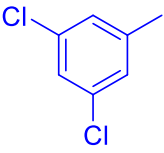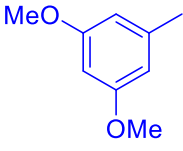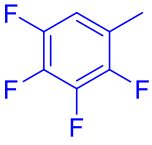
4.5.2 Glucose uptake results for pyrazolopyrimidinone category 2: variations at the R site (the bistrifluoromethyl substituted aryl site)

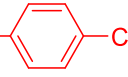The second category consisted of only variations at the R site (the bistrifluoromethyl substituted aryl site) of the bicycle core. In RTC53, this group consists of an aromatic ring with bistrifluoromethyl groups at both *meta* positions. Derivatives of RTC53 in category 2 all had the isopropyl group at R^1, with variations at the R site, which included a hydrogen, alkyl groups, a phenyl ring, heterocyclic rings, or substituted aromatic rings (with electron donating and electron withdrawing groups). The glucose uptake assay results for pyrazolopyrimidinone category 2 compounds are shown in Table 21.

Table 21: Glucose uptake results for pyrazolopyrimidinone category 2 variations.

Compound	R	Glucose Uptake Result	
		Fold change ± SEM	Active (Y) with stars significance or inactive (N)
RTC53[a,c]	F₃C–(3,5-bis-CF₃-phenyl)	1.99 ± 0.15	Y (***)
RTC80[a,c]	H	0.99 ± 0.07	N
RTC60[a,c]	Me	2.04 ± 0.43	Y (*)
RTC87[a,c]	Et	1.21 ± 0.09	N
RTC63[a,c]	nPr	0.99 ± 0.01	N
RTC58[a,c]	iPr	1.19 ± 0.17	N
RTC57[a,c]	iBu	0.83 ± 0.15	N
RTC61[a,c]	Ph	0.86 ± 0.13	N

JW-01-005[b,c]		1.10 ± 0.06	N
JW-06-011[b,c]		1.20 ± 0.08	N
MK26		1.14 ± 0.03	N
JW-01-023[b,c]		1.32 ± 0.19	N
JW-04-063[b,c]		1.03 ± 0.21	N
RTC84[a,c]		2.08 ± 0.20	Y (***)
JW-01-024[b,c]		1.12 ± 0.11	N
JW-01-018[b,c]		1.95 ± 0.22	Y (**)
JW-01-022[b,c]		2.01 ± 0.20	Y (***)
JW-01-037[b,c]		1.01 ± 0.05	N
JW-06-022[b,c]		1.11 ± 0.05	N
58 (MK6)		1.05 ± 0.32	N

59 (MK5)	Et / Et-substituted aryl ring	1.41 ± 0.53	N
JW-04-067[b,c]	Cl / Cl-substituted aryl ring	1.19 ± 0.19	N
60 (MK13)	MeO / OMe-substituted aryl ring	0.68 ± 0.07	N
61 (MK49)	O₂N / NO₂-substituted aryl ring	1.19 ± 0.40	N
JW-04-022[b,c]	F / F / F / F-substituted aryl ring	0.80 ± 0.08	N

[a]Compounds synthesised by Dr Robert Devin.

[b]Compounds synthesised by Dr John Walsh.

[c]Compounds tested by Dr Siobhan Leonard.

The glucose uptake results of category two variations at the R site showed that most changes at this site result in the loss of biological activity. The aromatic ring with the bistrifluoromethyl groups in the parent molecule RTC53 provides a steric bulk, which could be important for binding in the active site of the biological target. Furthermore, the trifluoromethyl groups contribute to the overall lipophilicity of a compound, which governs the compound's ability to pass through a lipid membrane and dock within a hydrophobic protein cavity. Adequate lipophilicity can help compounds to permeate through a lipid membrane.[111] The absence of the trifluoromethyl groups could result in a drop in lipophilicity and consequently a compound may find it difficult pass through the cell membrane and consequently may not reach the active site. The hydrophobic nature of the bistrifluoromethyl aryl ring may also play an important role in binding to a hydrophobic pocket in the active site.[69] Trifluoromethyl groups are also strongly

electron withdrawing in nature and this electronic effect may also have a role to play in binding at an active site.[66]

Replacing the substituted aromatic ring (R site) in RTC53 with a hydrogen (**RTC80**) resulted in a loss in activity, but activity was maintained with a methyl group at the R site (**RTC60**). This positive result may be due to the hydrophobicity of the methyl group. However, when other alkyl groups were attempted (**RTC87, RTC63, RTC58, and RTC57**), the same effect was not observed, and loss of activity was reported.

Loss of activity also occurred with a phenyl ring (**RTC61**) or a pyridine ring (**JW-01-005**) at the R site, suggesting that substituents on the ring could be important for activity. We postulated that these substituents might need to be hydrophobic and/or electron withdrawing in nature and hence systematically generated and evaluated a number of aryl rings with a variety of substituents. Substituents on the aromatic ring that were explored included derivatives with an *ortho* substituted electron donating dimethylamine group (**JW-06-011**), and *meta* substituted electron withdrawing halogens such as fluorine (**MK26**), chlorine (**JW-01-023**), and iodine (**JW-04-063**). None of these derivatives showed activity in the glucose uptake assay. When an aryl ring with a single *meta* substituted trifluoromethyl group was placed at the R site, activity was shown with three stars significance. This result initially supported our theory that a hydrophobic substituent was needed and may suggest that both electron withdrawing and hydrophobic properties may be required.

Compounds with *para* substituted halogens on the aromatic ring were also tested for activity. The compound containing the aromatic ring with *para* chlorine (**JW-01-024**) did not show any activity, whereas activity was reported for *para* bromine derivative (**JW-01-018**) and *para* iodine (**JW-01-022**) substitutions. Perhaps the size of the bromo and iodo groups, coupled with their electron withdrawing effect, may be important and the activity shown may be due to the steric properties that are not present with chlorine.

Other compounds that contained a *para* substituted aromatic ring at the R site consisted of the derivative with the *para* methoxy group (**JW-01-037**) and *para* dimethylamine group (**JW-06-022**). These electron donating groups did not show activity in the glucose uptake assay.

After monosubstituted aromatic rings were tested, bis substituted aromatic rings were evaluated at the R site, with substituents in the two *meta* positions of the aromatic ring. The derivatives containing aromatic rings with bis substituted alkyl groups, such as methyl (compound **58**) or ethyl (compound **59**), showed a loss of activity from RTC53. This was a little surprising as we thought that the hydrophobic nature of the methyl and ethyl substituents may be sufficient to maintain activity. However, methyl and ethyl groups are not electron withdrawing in nature and are instead slightly electron donating. Loss of activity was also found for derivatives containing bis *meta* chloro substituents (**JW-04-067**), bis *meta* methoxy substituents (compound **60**), and bis *meta* nitro substituents (compound **61**). Compound **61** was particularly interesting as the two nitro groups are very electron withdrawing but are not hydrophobic in nature. The loss of activity from these five compounds may be due to a loss of hydrophobicity in some cases, a loss of electron withdrawing ability in others, and perhaps a combination of both effects. The final compound containing a tetrafluoro aromatic ring also showed a loss of activity compared to RTC53.

In summary, five compounds from pyrazolopyrimidinone category 2 were active in the glucose uptake assay (Figure 140). The R site of these compounds contained a methyl group (**RTC60**), an aromatic ring with a *meta* substituted trifluoromethyl group (**RTC84**), an aromatic ring with bis *meta* trifluoromethyl substituents (**RTC53**), an aromatic ring with a *para* substituted bromine (**JW-01-018**), and an aromatic ring with a *para* substituted iodine (**JW-01-022**). The outlier of this group may be **RTC60**. The other four compounds contained substituted aryl rings with large, electron withdrawing groups. It could be suggested that a substituted aryl ring, bearing sterically bulky electron withdrawing groups may be important for activity. The hydrophobicity of that substituent may have a role to play as the use of the relatively large electron withdrawing nitro groups did not result in a biologically active compound.
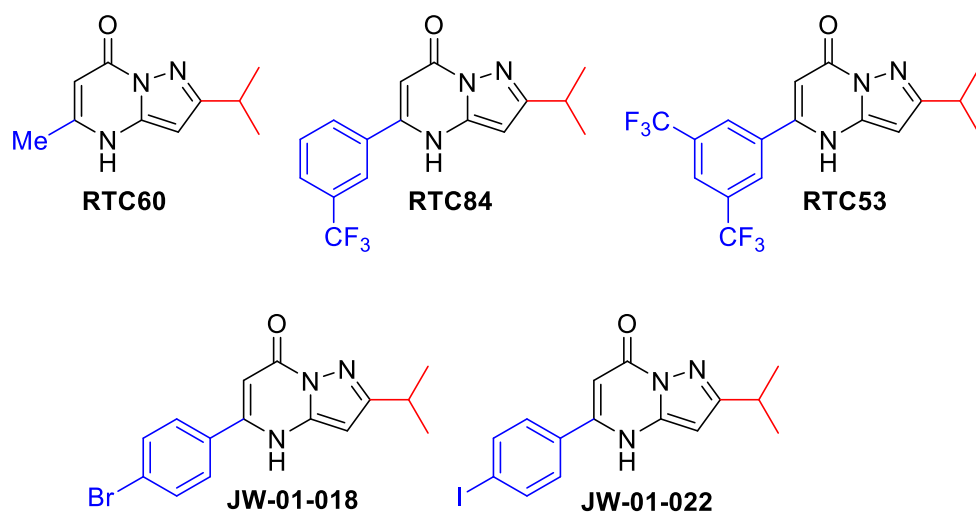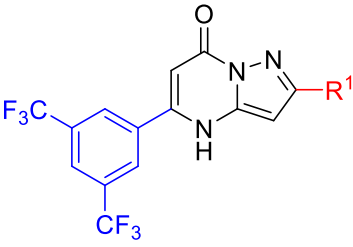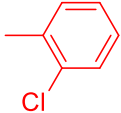
Figure 140: Structure of active compounds from pyrazolopyrimidinone category 2.
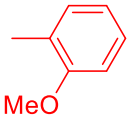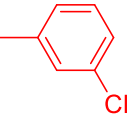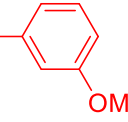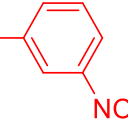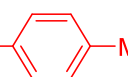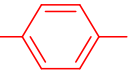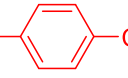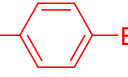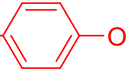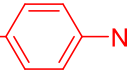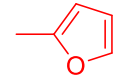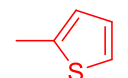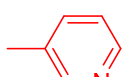
4.5.3 Glucose uptake results for pyrazolopyrimidinone category 3: variations at the R^1 site (the isopropyl group site)

The third category consisted of only variations at the R^1 site pyrazolopyrimidinone bicycle, which is an isopropyl group in the parent molecule, RTC53. Derivatives of RTC53 were made in where the aromatic bis-CF_3 group was maintained at the R site, with variations to the R^1 site that included alkyl groups, phenyl ring, heterocyclic rings, or substituted aromatic rings with electron donating and electron withdrawing groups. A summary of the glucose uptake results for the pyrazolopyrimidinone category 3 compounds can be found in Table 22.

Table 22: Glucose uptake results for pyrazolopyrimidinone category 3 variations.

Compound	R^1	Glucose Uptake Result	
		Fold change ± SEM	Active (Y) with stars significance or inactive (N)
RTC53[a,c]	iPr	1.99 ± 0.15	Y (***)
JW-04-054[b,c]	Me	0.94 ± 0.06	N
JW-06-001[b,c]	Et	1.29 ± 0.02	Y (**)
JW-01-033[b,c]	nBu	1.91 ± 0.10	Y (***)
JW-01-017[b,c]	iBu	2.34 ± 0.29	Y (**)
RTB69[a,c]	tBu	1.28 ± 0.05	Y (***)
RTC91[a,c]	Ph	1.67 ± 0.09	Y (**)
62 (MK80)		1.96 ± 0.87	Y (*)

Compound	Structure	Value	Active
63 (MK79)	2-MeO-phenyl	1.92 ± 0.58	Y (*)
64 (MK82)	3-Cl-phenyl	1.67 ± 0.81	Y (*)
65 (MK81)	3-OMe-phenyl	1.85 ± 1.00	Y (*)
66 (MK83)	3-NO_2-phenyl	0.77 ± 0.42	N
67 (MK71)	4-Me-phenyl	1.90 ± 1.19	Y (*)
68 (MK72)	4-F-phenyl	0.89 ± 0.29	N
69 (MK75)	4-Cl-phenyl	3.84 ± 2.23	Y (***)
70 (MK73)	4-Br-phenyl	0.79 ± 0.10	N
71 (MK74)	4-OMe-phenyl	1.33 ± 0.61	N
72 (MK76)	4-NO_2-phenyl	3.13 ± 1.35	Y (*)
73 (MK78)	4-CF_3-phenyl	1.36 ± 0.97	Y (*)
74 (MK84)	furan-2-yl	1.51 ± 1.09	Y (*)
75 (MK85)	thiophen-2-yl	0.86 ± 0.37	N
76 (MK86)	pyridin-3-yl	0.84 ± 0.33	N

[a]Compounds synthesised by Dr Robert Devin.

[b]Compounds synthesised by Dr John Walsh.

The isopropyl group at the R^1 site in RTC53 could increase the hydrophobicity of the compound and bind in a suitable hydrophobic pocket within the target active site. When this group was replaced by a methyl group (**JW-04-054**), it was seen that activity was lost, possibly due to the methyl group not binding strongly in a hydrophobic pocket due to its shorter chain length and reduced steric bulk in comparison to the isopropyl group. However, activity was reported with the derivative containing an ethyl group (**JW-06-001**) with a smaller fold change than RTC53 and with two stars significance. This may have been due to the smaller reduction in length and steric bulk for the ethyl group. The same effect can be seen with the derivative containing *n*-butyl group (**JW-01-033**), which has a similar fold change to RTC53 and with three stars significance. The other compounds with butyl groups, **JW-01-017** and **RTB69**, at R^1 also showed similar activity to RTC53. These results support the suggestion that a hydrophobic group with sufficient steric bulk may be required at R^1 for activity.

Replacing the isopropyl group at R^1, with a somewhat hydrophobic and sterically substantial phenyl ring did generate an active compound, albeit with a slightly slower fold change in activity. This result could suggest that an alkyl group is not absolutely required at R^1 and that a suitably hydrophobic and sterically bulky group can generate an active compound.

The next attempts consisted of compounds containing an aromatic ring with substituents at the *ortho*, *meta*, and *para* positions. The two derivatives containing an aromatic ring with *ortho* substituents, i.e. *ortho* chloro (compound **62**) and *ortho* methoxy (compound **63**), showed activity in the glucose uptake assay with a fold change similar to RTC53. The same effect was seen for aromatic rings with chloro and methoxy groups in the *meta* position, compound **64** and compound **65** respectively. For these two compounds a fold change similar to RTC53 was observed. Another derivative, compound **66**, contained a polar electron withdrawing nitro group in the *meta* position. However, this compound showed a loss of activity in the glucose uptake assay and could support the theory that polar groups at R^1 will lead to loss in activity and that a hydrophobic group at the R^1 site is preferred.

Seven derivatives were tested which contained an aromatic ring with *para* substituents. The first derivative consisted of an aromatic ring with a *para* methyl group (compound **67**), which is hydrophobic in nature and showed activity similar to RTC53. The same effect was not observed when the methyl group was replaced by a fluorine (compound **68**) as activity was lost. However, with the derivative containing an aromatic ring with a *para* chlorine (compound **69**), not only did it show activity, but it also had a much higher fold change than RTC53 (almost twice). This compound was found to be the most active compound of the pyrazolopyrimidinone bicycle family to date. This level of activity for compound **69** did not aligned well with our theory that a hydrophobic group is preferred at R^1.

The next two compounds consisted of an aromatic ring with a *para* bromine (compound **70**) and *para* methoxy (compound **71**) groups but neither showed activity. The next derivative contained an aromatic ring with a *para* nitro group (compound **72**) was not expected to be active due to the polar electron withdrawing nature of the nitro group and a similar result was expected as found with compound **66** where the nitro group was in the *meta* position. To our surprise, compound **72** was active and showed a fold change higher than that found for RTC53. The final compound containing an aromatic at R^1 was one with a *para* trifluoromethyl substituent (compound **73**). We had expected this compound to be active, and it was albeit with a lower fold change than RTC53.

The final three compounds tested in the pyrazolopyrimidinone category 3 variations consisted of derivatives of RTC53 with a heterocyclic ring instead of the isopropyl group at the R^1 site. The first compound consisted of a furan ring (compound **74**), which showed activity with a fold change lower than RTC53. The other two compounds contained a thiophene ring (compound **75**) and pyridine ring (compound **76**) at R^1, and neither compound showed activity in the glucose uptake assay.

In summary, fifteen compounds from the pyrazolopyrimidinone category 3 subfamily were active in the glucose uptake assay, while seven compounds were inactive. Derivatives containing an alkyl group at the R^1 site were all active, except the derivative which contained the smaller methyl group. Derivatives containing a phenyl ring or a substituted aromatic ring at the R^1 site were also all active, with initial results suggesting that a hydrophobic non-polar nature being preferred. However, this theory did not

always ring true as compounds with a *para* chloro and *para* nitro aryl ring at R^1 showed significant levels of activity in the glucose uptake assay, with fold changes greater than that found for RTC53. Finally, heterocyclic ring substitutions at R^1, did not appear to be that well tolerated with only the furan derivative showing activity, and both the thiophene and pyridine derivatives proving to be inactive.

4.6 Complex I assay results for the pyrazolopyrimidinone bicycle family

Only three compounds have been tested so far in the complex I assay to check whether they can inhibit complex I. These compounds were tested by Dr Siobhan Leonard. The parent molecule (**RTC53**) was tested along with the derivative containing a *tert*-butyl group instead of the isopropyl group (**RTB69**), and the derivative containing the isobutyl group (**JW-01-017**) (Figure 140). All three of these compounds were active in the glucose uptake assay.
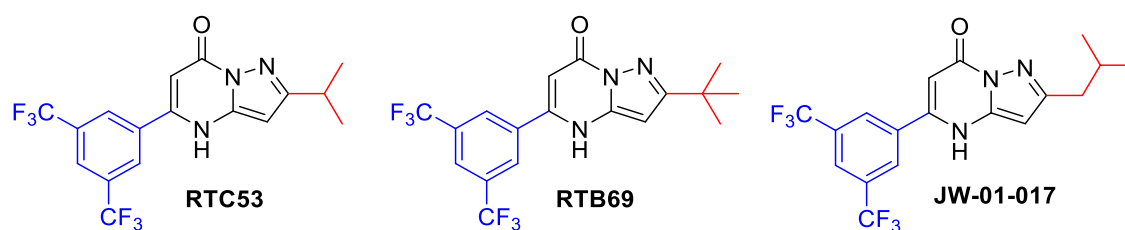
Figure 141: Structure of compounds tested in the complex I assay from the pyrazolopyrimidinone bicycle family.

These three compounds were shown to be inactive in the complex I assay which suggested that this family may increase the uptake of glucose from the cells through a different mechanism, other than the inhibition of complex I. It is suspected that pyrazolopyrimidinones may still result in AMPK activation through a different mechanism. Future work in this project can focus on determining the pathway by which these compounds increase glucose uptake and their mechanism of action.

4.7 Conclusion

A structure activity relationship study was performed through the biological evaluation of compounds from both the arylpiperazine and pyrazolopyrimidinone families using the glucose uptake assay and NADH : ubiquinone oxidoreductase (complex I) assay. The goal of this study, and indeed this project, was to explore the relationship between chemical structure and biological activity, and how changes in structure can generate more or less active compounds. The biological evaluation involved a whole cell functional assay to determine a given compounds ability to stimulate glucose uptake, as well as the enzyme inhibition assay to determine if compounds could inhibit complex I activity. Using both these assays, we were able to establish active compounds, which have the potential of developing into anti-diabetic agents.

The glucose uptake assay, i.e. the whole cell assay, measured the amount of tritiated (^{3}H) deoxy-2-glucose taken up by C2C12 mouse muscle cells and quantified the fold change using a protein assay to determine the number of cells present. The complex I assay, i.e. the enzyme inhibition assay, determined a compound's ability to inhibit NADH dehydrogenase, complex I of the electron transport chain, by measuring the change in ubiquinone absorbance.

The arylpiperazine family consisted of analogues of the hit compound RTC1, where structural variation occurred at five sites (A-E) (Figure 142).
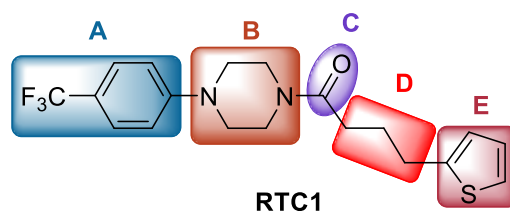
Figure 142: Structure of RTC1 with variations sites, A-E.

Site A consisted of variations of the aryl group of RTC1. Three of the four active compounds from site A variations contained a trifluoromethyl group. This suggests that this group is important for biological activity. Trifluoromethyl groups are large, electron withdrawing, and hydrophobic. It was interesting to note that removal of the CF$_3$ group resulted in a reduction in activity, as did moving it from the *para* to the *ortho* position. Replacement of the *para* CF$_3$ group with a *para* NO$_2$ group, which like the CF$_3$ group is

electron withdrawing but less hydrophobic, also resulted in loss of activity, which might point to an important hydrophobic role for the CF_3 group. This theory might gain some support from the compound where the entire para CF_3 aryl ring was replaced with the hydrophobic cyclohexyl ring. This cyclohexyl derivative was active in the glucose uptake assay, albeit with reduced activity. The trifluoromethyl group could play a key role by binding to a hydrophobic pocket of the target protein and may also have a very important role in aiding transport across cell membranes and cellular uptake.[68]

Variations at the piperazine ring (site B) of RTC1 showed some mixed results as replacement of the piperazine ring with either a piperidine ring or a hydrazine motif generated active compounds in the glucose uptake assay. Although, the hydrazine containing compound was significantly less active than the parent RTC1. Replacement of the piperazine with a simple amide bond motif resulted in complete loss of activity. It is therefore suggested that site B should be a saturated six membered heterocyclic ring, such as a piperazine or piperidine ring. Replacing the carbonyl group (site C) of RTC1 with a CH_2 also appeared undesirable, as while the resulting compound was active, its activity levels were lower than RTC1. It was concluded that the carbonyl group improves biological activity and its presence is important, but perhaps not absolutely essential.

Compounds synthesised with variations on the alkyl chain (site D) contained alkyl chains of different lengths and various substituents on the γ-CH_2. It was concluded that the alkyl chain in RTC1 is important for biological activity as removal of it resulted in a loss of activity. An optimal alkyl chain length appeared to be three carbons in length. The addition of motifs to the chain, such as a carbonyl or hydroxyl groups, could result in additional substrate-target interactions and this may be the reason behind their drop in activity.

Two compounds were synthesised with variations at site E of RTC1, the thiophene ring. One compound contained a pyrazole ring and the other a methyl group. Both compounds showed activity, but at lower levels than that of RTC1. It was concluded that a thiophene ring may be important, but not be essential, for activity, and that alternatives to a thiophene ring may result in reduced activity.

Combinations of structural variations on multiple sites were carried out on a few compounds. Although nine compounds maintained activity, they all resulted in a lower activity than RTC1. Overall, RTC1 still remained the most active compound in this family.

All the active and inactive compounds of this family were tested in the complex I assay to test their ability to inhibit complex I. All the active compounds from the glucose uptake assay were also found to be active in the complex I assay, with some variation in activity levels. To our surprise, some of the inactive compounds from the glucose uptake assay were found to have some activity in the complex I assay. This apparent contradiction may be as a result of the difference between a whole cell functional assay and an inhibition/binding assay. With a whole cell assay, the compound being tested must pass through the cell membrane barrier, get taken up by the cell, and survive the internal workings of the cell in order to reach the protein target and exert its biological effect. These barriers are not in place for inhibition/binding assays, where the compounds have direct access to the protein target. As such, some compounds that are not active in a whole cell assay, for reasons of cell permeability or enzymatic degradation, may show a positive result in an inhibition/binding assay where these challenges are not present. The two compounds which were active in the glucose uptake assay and had the lowest IC_{50} values were compounds **18** and **RTC194**.

The pyrazolopyrimidinone bicycle family consisted of analogues of RTC53 where variations were carried out on the bis-CF_3 aryl ring (R site) and the isopropyl group (R^1 site). Compounds were categorised as variations on both sites (category 1), variations on the R site (category 2), and variations on the R^1 site (category 3) (Figure 143).
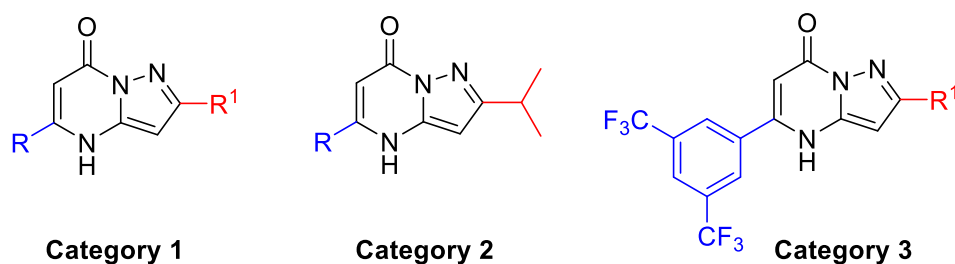
Figure 143: Structural variations of RTC53.

The glucose uptake results from category 1 variations showed that compounds which contained a phenyl ring at the R site and various substituents at the R^1 site did not show activity. Similarly, compounds containing a methyl group or a *t*-butyl group at the R^1 site, while varying the R site, also reported a loss in activity. Four compounds contained a phenyl ring at the R^1 site, with variations at the R site. Two of these compounds were inactive, where two were active. Therefore, the only two active compounds in this category were compounds **50** and **51** (Figure 144). Compound **50** contained a *para* methoxy aromatic ring on the R site, and a phenyl ring on the R^1 site. Compound **51** contained a tetrafluoro substituted aromatic ring on the R site, and also a phenyl ring on the R^1 site.
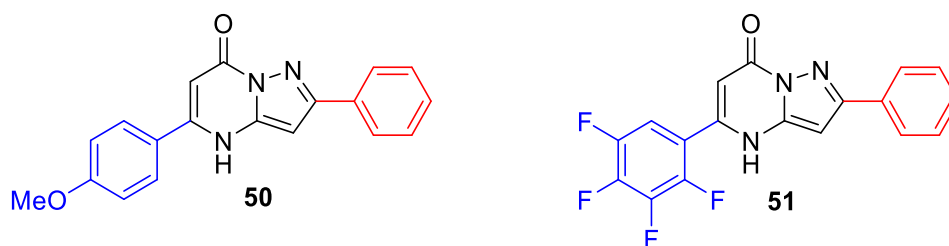
Figure 144: Structure of compounds **50** and **51**.

It was observed from the glucose uptake results of category 2 variations at the R site that most changes at this site resulted in the loss of biological activity. This could be due to the loss of steric bulk provided by the aromatic ring with the bistrifluoromethyl groups in the parent molecule RTC53, which could be important for binding in the active site of the biological target. As was previously mentioned with the arylpiperazine family, the absence of the trifluoromethyl groups could also result in a drop in hydrophobicity/lipophilicity and consequently a compound may lose some ability to bind in a hydrophobic pocket of the target active site and/or find it difficult to pass through the cell membrane. Trifluoromethyl groups are also strongly electron withdrawing in nature and this electronic effect may also have a role to play in binding at an active site.

All the compounds containing an alkyl group at the R site in category 2 variations, similar to category 1 variations, showed a loss of activity, except for the compound containing a methyl group (**RTC60**, Figure 145). This was surprising as compounds with a methyl group at the R site in category 1 variations, (compound **43** and **JW-06-006**, Figure 145)

did not show activity. The compound containing a phenyl ring at the R site in category 2 (**RTC61**) also showed a loss in activity, which correlated with compounds from category 1 that also contained a phenyl ring at the R site.
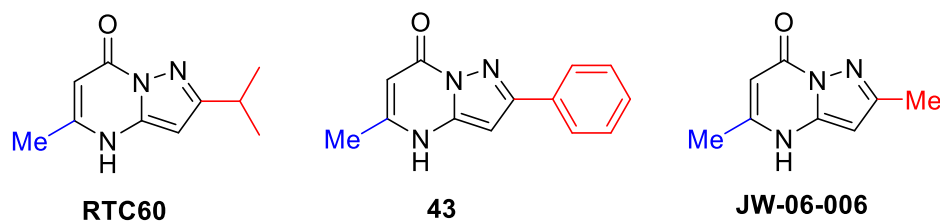
Figure 145: Structure of **RTC60,** compound **43**, and **JW-06-006**.

Out of the remaining compounds in category 2, those containing a substituted aryl or pyridine ring at the R site all showed a drop in activity with the exception of three compounds (**RTC84, JW-01-018, JW-01-022,** Figure 146). Compound **RTC84** contained an aryl ring with a single *meta* substituted trifluoromethyl group at the R site and showed strong activity. This result supported the theory that a hydrophobic substituent was needed and may suggest that both electron withdrawing and hydrophobic properties may be required. Compounds containing *para* substituted aromatic rings with bromo (**JW-01-018**) and iodo (**JW-01-022**) groups at the R site were also active (Figure 146). It could be suggested that the steric properties of these halogens, coupled with their electron withdrawing effect, were important for biological activity.
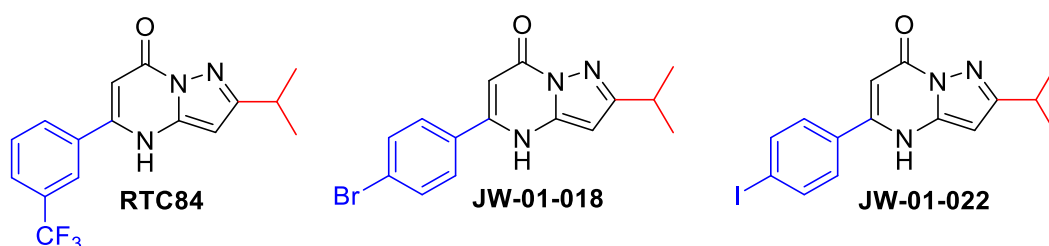
Figure 146: Structure of **RTC84**, **JW-01-018**, and **JW-01-022**.

More compounds were active in category 3 than category 2. This suggested that variations at the R^1 site are a lot more tolerable than those at the R site. In RTC53, the isopropyl group at the R^1 site could increase the hydrophobicity of the compound and bind in a suitable hydrophobic pocket within the target active sites. Activity was reported with compounds where this group was replaced by alkyl groups such as an ethyl, *n*-butyl, *t*-butyl, and isobutyl groups, but not with a methyl group. These results

support the suggestion that a hydrophobic group with sufficient steric bulk may be required at R^1 for activity.

Replacing the isopropyl group at R^1 with a somewhat hydrophobic and sterically substantial phenyl ring in category 3 variations did generate an active compound, albeit with a slightly lower fold change in activity than RTC53. This correlated with the two active compounds from category 1 variations which also had a phenyl ring at the R^1 site. This result could suggest that an alkyl group is not absolutely required at R^1 and that a suitably hydrophobic and sterically bulky group can generate an active compound. Compounds containing aromatic rings with methoxy or chloro groups, in the *ortho* or *meta* position, in the R^1 site in category 3 also showed activity in the glucose uptake assay.

The same result was not observed with an aromatic ring containing a polar electron withdrawing nitro group in the *meta* position as it resulted in a loss of activity. This result supported the theory that polar groups at R^1 could lead to loss in activity and that a hydrophobic group at the R^1 site is preferred. However, this theory was not supported with the derivatives containing an aromatic ring with a *para* chlorine or *para* nitro groups, which showed activity and had a higher fold change than RTC53. The compound containing a *para* chlorine substituted aromatic ring (compound **69**, Figure 147) was found to be the most active compound of the pyrazolopyrimidinone bicycle family to date. The derivatives containing an aromatic ring with a *para* methyl group and *para* trifluoromethyl group at R^1 also showed activity, as did the derivative containing a furan ring at the R^1 site. This was the only category 3 compound with a heterocycle at R^1 that showed activity, those with a thiophene or pyridine ring at R^1 were inactive.
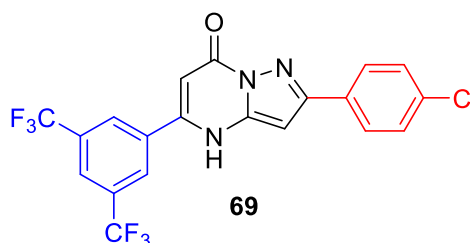
Figure 147: Structure of compound **69**.

Three compounds of the pyrazolopyrimidinone bicycle family (**RTC53, RTB69,** and **JW-01-017**), which were active in the glucose uptake assay, were tested in the complex I

assay and shown to be inactive. This suggests that this family may increase the uptake of glucose from the cells through a different mechanism other than the inhibition of complex I.

Experimental

5.1　General information

Reagents and reactants which were commercially available were purchased from Sigma Aldrich, Fluorochem or Alfa Aesar, and used without further purification.

NMR spectra were recorded using Bruker Ascend 500 spectrometer at 293 K operating at 500 MHz for the ^{1}H nucleus, 126 MHz for the ^{13}C nucleus, and 471 MHz for the ^{19}F nucleus. All chemical shifts were referenced relative to the relevant deuterated solvent residual peaks or TMS. Deuterated solvents used were CDCl$_3$, MeOD, CD$_3$CN and DMSO. Assignments of the NMR spectra were deduced using ^{1}H NMR, ^{13}C NMR, and ^{19}F NMR, along with 2D-NMR experiments; ^{1}H-^{1}H COSY, ^{1}H-^{13}C HMBC, ^{1}H-^{13}C HSQC, and ^{1}H-^{19}F HOESY. The following abbreviations were used to explain the observed multiplicities; s (singlet), d (doublet), t (triplet), q (quartet), m (multiplet), bs (broad singlet), pt (*pseudo* triplet). Chemical shifts were given in ppm downfield from the internal standard and coupling constants were given in Hz. ^{13}C NMR spectra were recorded with complete proton decoupling. ^{19}F NMR spectra were recorded with proton and carbon decoupling.

Microwave reactions were carried out using a CEM Discover Microwave Synthesizer with a vertically focused floor mounted infrared temperature sensor, external to the microwave tube. The 10 mL reaction vessels used were supplied from CEM and were made of borosilicate glass. Melting point analyses were carried out using a Stewart Scientific SMP11 melting point apparatus and are uncorrected.

High-resolution mass spectrometry (HRMS) was performed in Maynooth University (MU) and the University of Bath (UoB). HRMS in MU was conducted on an Agilent-LC 1200 Series coupled to a 6210 or 6530 Agilent Time-Of-Flight (TOF) mass spectrometer equipped with an electrospray source in both positive and negative (ESI+/−) modes.

In UoB, HPLC-ESI-TOF analysis was conducted using an electrospray time-of-flight (MicrOTOF) mass spectrometer (Bruker Daltonik GmbH, Bremen, Germany), which was coupled to an Agilent HPLC stack (Agilent, Santa Clara, CA, United States) consisting of Agilent G1312A binary pump with G1329A autosampler and G1316A column oven. Analyses were performed in ESI positive and negative mode. The capillary voltage was set to 4500 V, nebulizing gas at 2.2 bar, drying gas at 10.2 L/min at 220°C in each case. The TOF scan range was from 50 − 500 or 50 -1500 mass-to-charge ratio (*m/z*). In each

case 10 µL injections were made. Data processing was performed using the Compass Data Analysis software scripts (Bruker Daltonik GmbH, Bremen, Germany). Samples were dissolved first in 1000 µL of MeOH (LC-MS grade, VWR), and then to aid additional solubilisation 200 µL H_2O (LC-MS grade, VWR) was added. From this solution, 10µL was added to 990 µL of 70% MeOH to get to effective 8.33 µg/ml concentration (or 4.16 µg/ml for the 0.5 mg initial sample).

Infrared spectra were recorded on a Perkin Elmer Spectrum 100 FT-IR spectrophotometer using a smart endurance single bounce diamond, attenuated total reflection (ATR) cell or potassium bromide (KBr) disks. Spectra were recorded in the region of 4000–600 cm^{-1} and were obtained by the co-addition of 4 scans with a resolution of 4 cm^{-1}.

Scintillation counts were obtained using a Wallac MicroBeta scintillation counter (Perkin Elmer). Reactions were monitored with thin layer chromatography (TLC) on Merck Silica Gel F$_{254}$ plates. Developed sheets were visualised using a portable UVltec CV-006 lamp (λ = 254, 365 nm). Flash column chromatography was performed using Merck Silica gel 60.

5.2 Experimental procedures

5.2.1 General procedure for arylpiperazine synthesis using HOBt and TBTU coupling reagents

Carboxylic acid, HOBt, TBTU, NEt$_3$ and DMF were placed in a round-bottom flask and stirred at rt for 15 minutes. A second round-bottom flask was prepared containing amine and DMF. The resulting solution was transferred to the first round-bottom flask containing the carboxylic acid. The solution was stirred overnight. The DMF was removed under reduced pressure. The residue was purified using column chromatography.

5.2.2 Synthesis of 4-(thiophen-2-yl)-1-(4-(4-(trifluoromethyl)phenyl)piperazin-1-yl)butan-1-one RTC1 (MK24) (1)
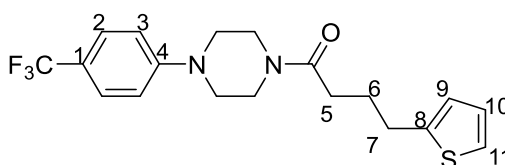
Prepared from 1-(4-(trifluoromethyl)phenyl)piperazine (compound **2**) (100 mg, 0.43 mmol) and 4-(2-thienyl)butyric acid (50 μL, 0.34 mmol), using HOBt (58 mg, 0.43 mmol), TBTU (140 mg, 0.43 mmol), NEt$_3$ (100 μL, 0.69 mmol) and DMF (3 mL) and following the general procedure described in section **5.2.1**. The reaction mixture was stirred at rt overnight. DMF was removed under reduced pressure and the residue was purified using column chromatography (3:2, EtOAc:*n*-hexane) to give a white solid, 112 mg (86%).

^{1}H NMR: (500 MHz, CDCl$_3$) δ 7.50 (d, *J* = 8.5 Hz, 2H, H2), 7.13 (d, *J* = 4.9 Hz, 1H, H11), 6.94 − 6.89 (m, 3H, H3, H10), 6.81 (d, *J* = 2.2 Hz, 1H, H9), 3.85 − 3.72 (m, 2H*), 3.64 − 3.49 (m, 2H*), 3.31 − 3.17 (m, 4H*), 2.93 (t, *J* = 7.2 Hz, 2H, H7), 2.40 (t, *J* = 7.4 Hz, 2H, H5), 2.13 − 2.00 (m, 2H, H6).*Piperazine. ^{1}H NMR matches literature data.[45] **^{13}C NMR:** (126 MHz, CDCl$_3$) δ 171.1 (C=O), 152.9 (C4), 144.4 (C8), 126.9 (C10), 126.6 (q, *J* = 3.7 Hz, C2), 125.6 (q, *J* = 271.3 Hz, CF$_3$), 124.6 (C9), 123.3 (C11), 121.2 (q, *J* = 32.8 Hz, C1), 115.0 (C3), 48.3 (C*), 48.1 (C*), 45.0 (C*), 41.1 (C*), 32.0 (C5), 29.3 (C7), 27.0 (C6). *Piperazine.

^{13}C NMR matches literature data.[45] **^{19}F NMR:** (471 MHz, CDCl$_3$) δ -61.4 (C*F*$_3$). **HR-MS:** calcd for C$_{19}$H$_{21}$F$_3$N$_2$OSNa m/z: [M + H]$^+$, 405.1219; found: 405.1228 [Diff(ppm) = 2.2]. **R$_f$:** 0.5 (3:2, EtOAc:*n*-hexane). **IR (ATR):** 2925 (C-H), 2853 (C-H), 1652 (C=O), 1611 (C=C), 1328 (C-F), 1068 (C-N) cm^{-1}.

5.2.3 Synthesis of 1-(4-(trifluoromethyl)phenyl)piperazine (MK17) (RD269) (2)
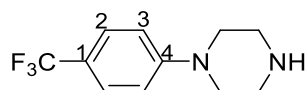
Prepared from 1-chloro-4-(trifluoromethyl)benzene (1.59 mL, 11.91 mmol) and piperazine (2.00 g, 23.82 mmol) dissolved in NMP (5 mL) and heated at 200 °C for 30 mins in a microwave reactor. The reaction mixture was purified using column chromatography (9:1, DCM:MeOH) to give a white solid, 417 mg (15%).

^{1}H NMR: (500 MHz, CDCl$_3$) δ 7.48 (d, *J* = 8.8 Hz, 2H, H2), 6.92 (d, *J* = 8.8 Hz, 2H, H3), 3.28 − 3.21 (m, 4H*), 3.07 − 3.00 (m, 4H*), 2.01 (bs, 1H, NH).*Piperazine. ^{1}H NMR data matches literature data.[112] **^{13}C NMR:** (126 MHz, CDCl$_3$) δ 153.7 (C4), 126.4 (q, *J* = 3.8 Hz, C2), 124.7 (q, *J* = 270.9 Hz, CF$_3$), 120.6 (q, *J* = 32.6 Hz, C1), 114.6 (C3), 49.1 (C*), 45.9 (C*).*Piperazine. ^{13}C NMR data matches literature data.[112] **HR-MS:** calcd for C$_{11}$H$_{14}$F$_3$N$_2$ m/z: [M + H]$^+$, 231.1104; found: 231.1106 [Diff (ppm) = 0.87]. **R$_f$:** 0.2 (9:1, DCM:MeOH). **IR (ATR)**: 3257 (Ar C-H), 2836 (alkane C-H), 1668 (N-H), 1613 (C-C), 1323 (C-N), 1101 (C-F), 1067 (C-N) cm^{-1}.

5.2.4 Synthesis of methyl 9-oxo-9-(4-(4-(trifluoromethyl)phenyl)piperazin-1-yl)nonanoate (MK16) (RTC56) (3)
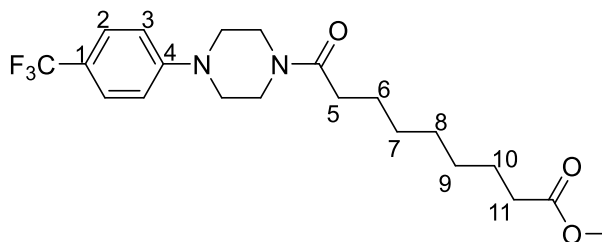
Anhydrous method:[45] Prepared from methyl hydrogen azelate (48 mg, 0.23 mmol), BOP (114 mg, 0.26 mmol), anhydrous NEt_3 (51.2 μL, 0.36 mmol) and anhydrous DCM (10 mL) in an oven-dried two-neck flask under a N_2 atmosphere, and stirred at rt for 15 mins. 1-(4-(trifluoromethyl)phenyl)piperazine (compound **2**) (60 mg, 0.26 mmol) was added and the reaction mixture stirred under a N_2 atmosphere. After 17 hrs, DCM was removed under reduced pressure and the resulting oil was acidified to pH = 3 using a 0.1 M aqueous HCl. The aqueous mixture was extracted with DCM (3 x 10 mL) and the organic layer washed with a saturated aqueous solution of $NaHCO_3$ (3 x 10 mL) and brine (3 x 10 mL). The organic layer was dried over $MgSO_4$. Volatiles were removed under reduced pressure and the residue was purified using column chromatography (3:2, EtOAc:Pet.Ether) to give an off white solid, 41 mg (43%).

Non-anhydrous method: Prepared from methyl hydrogen azelate (48 mg, 0.23 mmol), BOP (114 mg, 0.26 mmol), NEt_3 (51.2 μL, 0.36 mmol) and DCM (10 mL) in a round-bottom flask and stirred at rt for 15 mins. 1-(4-(trifluoromethyl)phenyl)piperazine (compound **2**) (60 mg, 0.26 mmol) was added and the reaction mixture stirred for 17 hrs. Volatiles were removed under reduced pressure and the residue was purified using column chromatography (3:2, EtOAc:Pet.Ether) to give an off white solid, 53 mg (55%).

¹H NMR: (500 MHz, $CDCl_3$) δ 7.49 (d, *J* = 8.6 Hz, 2H, H2), 6.92 (d, *J* = 8.7 Hz, 2H, H3), 3.85 − 3.71 (m, 2H*), 3.72 − 3.52 (m, 2H*, 3H, OCH_3), 3.39 − 3.14 (m, 4H*), 2.32 (dt, *J* = 29.1, 7.5 Hz, 4H, H5, H11), 1.69 − 1.58 (m, 4H, H6, H10), 1.36 − 1.32 (m, 6H, H7, H8, H9).*Piperazine. ¹H NMR matches literature data.[45] **¹³C NMR:** (126 MHz, $CDCl_3$) δ 174.3 (ester C=O), 171.7 (amide C=O), 149.2 (C4), 126.5 (q, *J* = 3.3 Hz, C2), 124.5 (q, *J* = 269.7 Hz, CF_3), 121.2 (q, *J* = 32.8 Hz, C1), 115.0 (C3), 51.5 (OCH_3), 48.5 (C*), 48.2 (C*), 45.2 (C*),

41.1 (C*), 34.1 (H11), 33.2 (H5), 29.3 (C8), 29.1 (C6), 29.0 (C7), 25.2 (C10), 24.9 (C6). *Piperazine. ^{13}C NMR matches literature data.[45] **HR-MS:** calcd for $C_{21}H_{30}F_3N_2O_3$ m/z: [M + H]$^+$, 415.2203; found: 415.2217 [Diff (ppm) = 3.37]. **R$_f$:** 0.65 (3:2, EtOAc:Pet. Ether). **IR (ATR):** 2934 (Ar C-H), 1736 (ester C=O), 1614 (amide C=O), 1157 (C-N), 1102 (C-O) cm^{-1}.

5.2.5 Synthesis of 1-(4-cyclohexylpiperazin-1-yl)-4-(thiophen-2-yl)butan-1-one (MK43) (RTC13) (4)
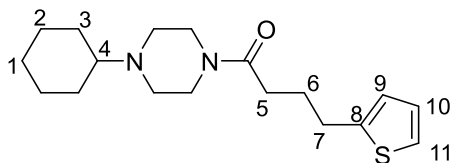
Prepared from 1-cyclohexylpiperazine (150 mg, 0.89 mmol) and 4-(2-thienyl)butyric acid (118 μL, 0.81 mmol) using HOBt (120 mg, 0.89 mmol), TBTU (285 mg, 0.89 mmol), NEt$_3$ (180 μL, 1.29 mmol) and DCM (6 mL) and following the general procedure described in section **5.2.1**. The reaction mixture was stirred at room temperature overnight for 17.5 hours. DCM was removed under reduced pressure and the residue was purified using column chromatography (9:1, DCM:MeOH) to give a red solid, 213 mg (82%).

^{1}H NMR: (500 MHz, CDCl$_3$) δ 7.11 (dd, J = 5.1, 1.0 Hz, 1H, H11), 6.91 (dd, J = 5.1, 3.4 Hz, 1H, H10), 6.79 (dd, J = 3.4, 1.0 Hz, 1H, H9), 3.70 – 3.55 (m, 2H*), 3.45 – 3.31 (m, 2H*), 2.90 (t, J = 7.3 Hz, 2H, H7), 2.67 – 2.40 (m, 4H*), 2.40 – 2.32 (m, 2H, H5), 2.32 – 2.25 (m, 1H, H4), 2.07 – 1.96 (m, 2H, H6), 1.90 – 1.73 (m, 4H, H3), 1.69 – 1.56 (m, 1H, H1), 1.31 – 1.14 (m, 4H, H2), 1.14 – 1.04 (m, 1H, H1). *Piperazine. ^{1}H NMR matches literature data.[45]

^{13}C NMR: (126 MHz, CDCl$_3$) δ 170.8 (*C*=O), 144.5 (C8), 126.8 (C11), 124.6 (C10), 123.1 (C12), 63.6 (C4), 49.3 (C*), 48.7 (C*), 45.9 (C*), 41.9 (C*), 32.0 (C5), 29.3 (C7), 28.8 (C3), 27.1 (C6), 26.2 (C1), 25.8 (C2). *Piperazine. ^{13}C NMR matches literature data.[45] **HR-MS:** calcd for $C_{18}H_{29}N_2OS$ m/z: [M + H]$^+$, 321.1995; found: 321.2005 [Diff(ppm) = 3.1]. **R$_f$:** 0.56 (9:1, DCM:MeOH). **IR (ATR):** 2928 (Ar C-H), 2851 (alkane C-H), 1632 (C=O), 1445 (C=C) cm^{-1}.

5.2.6 Synthesis of 4-(1*H*-Pyrazol-4-yl)-1-(4-(4-(trifluoromethyl)phenyl)piperazin-1-yl)butan-1-one (MK69) (RTC193) (5)
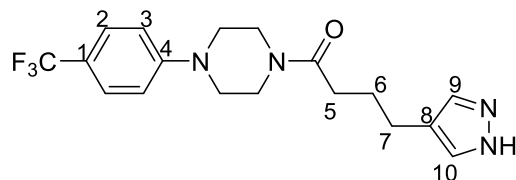
Prepared from 1-(4-(trifluoromethyl)phenyl)piperazine (compound **2**) (100 mg, 0.43 mmol) and 4-(1*H*-pyrazol-4-yl)butanoic acid (52 mg, 0.34 mmol), using HOBt (58 mg, 0.43 mmol), TBTU (140 mg, 0.43 mmol), NEt$_3$ (100 µL, 0.69 mmol) and DCM (3 mL) and following the general procedure described in section **5.2.1**. The reaction mixture was stirred at rt for 24 hours. DCM was removed under reduced pressure and the residue was purified using column chromatography (3:2, EtOAc:*n*-hexane) to give a brown solid, 116 mg (93%).

^{1}H NMR: (500 MHz, CDCl$_3$) δ 7.50 (d, *J* = 8.5 Hz, 2H, H2), 7.43 (s, 2H, H9 and H10), 6.91 (d, *J* = 8.6 Hz, 2H, H3), 5.57 (bs, 1H, NH), 3.85 – 3.72 (m, 2H*), 3.64 – 3.54 (m, 2H*), 3.26 (s, 4H*), 2.59 (t, *J* = 7.4 Hz, 2H, H7), 2.44 – 2.35 (m, 2H, H5), 2.00 – 1.90 (m, 2H, H6). *Piperazine. ^{1}H NMR matches literature data[45]. **^{13}C NMR:** (126 MHz, CDCl$_3$) δ 171.4 (C=O), 152.9 (C4), 132.9 (C9 and C10), 126.5 (q, *J* = 3.9 Hz, C2), 124.6 (q, *J* = 271.3 Hz, CF$_3$), 121.4 (q, *J* = 32.6 Hz, C1), 120.3 (C8), 115.0 (C3), 48.4 (C*), 48.1 (C*), 45.1 (C*), 41.2 (C*), 32.3 (C5), 26.2 (C6), 23.6 (C7). *Piperazine. ^{13}C NMR matches literature data[45]. **HR-MS:** calcd for C$_{18}$H$_{21}$F$_3$N$_4$ONa m/z: [M + Na]$^+$, 389.156; found: 389.1563 [Diff (ppm) = 0.9]. **R$_f$:** 0.1 (3:2, EtOAc:n-hexane). **IR (ATR)**: 3055 (N-H), 2947 (Ar C-H), 1649 (C=O), 1614 (N-H), 1226 (C-N) cm^{-1}.

5.2.7 Synthesis of 1-(2-chloro-4-(trifluoromethyl)phenyl)piperazine (MK21) (RD20) (6)
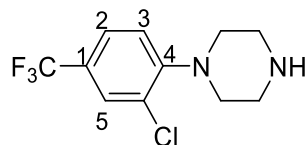
Prepared from 3-chloro-4-fluorobenzotrifluoride (100 µL, 0.75 mmol) and piperazine (129 mg, 1.5 mmol) dissolved in NMP (3 mL) and heated at 200 °C for 30 mins in a microwave reactor. The reaction mixture was purified using column chromatography (100% DCM to 8:2, DCM:MeOH) to give an orange oil, 124 mg (63%).

^{1}H NMR: (500 MHz, CDCl$_3$) δ 7.61 (d, J = 1.4 Hz, 1H, H5), 7.47 (dd, J = 8.4, 1.4 Hz, 1H, H2), 7.08 (d, J = 8.4 Hz, 1H, H3), 3.10 (s, 8H*), 2.78 (bs, 1H, NH).*Piperazine. ^{1}H NMR data matches literature data[113]. **^{13}C NMR:** (126 MHz, CDCl$_3$) δ 152.5 (C4), 128.6 (C-Cl), 127.9 (q, J = 3.8 Hz, C5), 125.3 (q, J = 33.3 Hz, C-CF$_3$), 124.7 (q, J = 3.9 Hz, C2) 123.6 (q, J = 272.2 Hz, CF$_3$), 120.2 (C3), 51.9 (C*), 51.4 (C*), 50.9 (C*), 45.9 (C*).*Piperazine. ^{13}C NMR matches literature data[45]. **HR-MS:** calcd for C$_{19}$H$_{20}$F$_3$N$_2$OSClNa m/z: [M + Na]$^+$, 439.0829; found: 439.085 [Diff (ppm) = 4.8]. **R$_f$:** 0.2 (9:1, DCM:MeOH).

5.2.8 Synthesis of 1-(4-phenylpiperazin-1-yl)-4-(thiophen-2-yl)butan-1-one (MK38) (RTC162) (7)
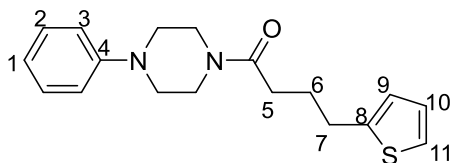
Prepared from 1-phenylpiperazine (100 µL, 0.64 mmol) and 4-(2-thienyl)butyric acid (84 µL, 0.58 mmol) using HOBt (86 mg, 0.64 mmol), TBTU (205 mg, 0.64 mmol), NEt$_3$ (129 µL, 0.93 mmol) and DMF (5 mL) and following the general procedure described in section **5.2.1**. The reaction mixture was stirred at rt for 16.5 hrs. DMF was removed under reduced pressure and the residue was purified using column chromatography (3:2, EtOAc:*n*-hexane) to give a dark red oil, 142 mg (78%).

^{1}H NMR: (500 MHz, CDCl$_3$) δ 7.30 – 7.23 (m, 2H, H3), 7.11 (d, *J* = 5.1 Hz, 1H, H11), 6.95 – 6.85 (m, 4H, H1, H2, H10), 6.83 – 6.77 (m, 1H, H9), 3.81 – 3.70 (m, 2H*), 3.59 – 3.48 (m, 2H*), 3.16 – 3.08 (m, 4H*), 2.92 (t, *J* = 7.3 Hz, 2H, H7), 2.43 (t, *J* = 7.3 Hz, 2H, H5), 2.05 (p, *J* = 7.3 Hz, 2H, H6).*Piperazine. ^{1}H NMR matches literature data[45]. **^{13}C NMR:** (126 MHz, CDCl$_3$) δ 171.0 (C=O), 151.0 (C4), 144.4 (C8), 129.2 (C3), 126.8 (C2), 124.5 (C9), 123.2 (C11), 120.5 (C10), 116.6 (C1), 49.7 (C*), 49.4 (C*), 45.4 (C*), 41.5 (C*), 32.0 (C5), 29.3 (C7), 27.0 (C6).*Piperazine. ^{13}C NMR matches literature data[45]. **HR-MS:** calcd for C$_{18}$H$_{23}$N$_2$OS m/z: [M + H]$^+$, 315.1526; found: 315.1531 [Diff (ppm) = 1.59]. **R$_f$:** 0.65 (3:2, EtOAc:*n*-hexane). **IR (ATR):** 2915 (C-H), 1639 (C=O), 1597 (C=C), 1227 (C-N) cm^{-1}.

5.2.9 Synthesis of 4-(thiophen-2-yl)-1-(4-(2-(trifluoromethyl)phenyl)piperazin-1-yl)butan-1-one (MK41) (RTC20) (8)
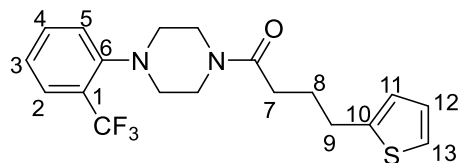
Prepared from 1-(2-(trifluoromethyl)phenyl)piperazine (83 µL, 0.43 mmol) and 4-(2-thienyl)butyric acid (57 µL, 0.39 mmol) using HOBt (58 mg, 0.43 mmol), TBTU (139 mg, 0.43 mmol), NEt$_3$ (60 µL, 0.62 mmol) and DMF (4 mL) and following the general procedure described in section **5.2.1**. The reaction mixture was stirred at rt for 22 hrs. DMF was removed under reduced pressure and the residue was purified using column chromatography (3:2, EtOAc:n-hexane) to give a colourless oil, 122 mg (82%).

^{1}H NMR (500 MHz, CDCl$_3$) δ 7.64 (d, J = 7.9 Hz, 1H, H2), 7.56 – 7.48 (m, 1H, H4), 7.33 – 7.21 (m, 2H, H3, H5), 7.12 (dd, J = 5.1, 1.1 Hz, 1H, H13), 6.92 (dd, J = 5.1, 3.4 Hz, 1H, H12), 6.82 (dd, J = 3.3, 0.9 Hz, 1H, H11), 3.76 (bs, 2H*), 3.59 – 3.48 (m, 2H*), 2.97 – 2.82 (m, 2H, H7, 4H*), 2.41 (t, J = 7.5 Hz, 2H, H9), 2.06 (p, J = 7.4 Hz, 2H, H8).*Piperazine. ^{1}H NMR matches literature data[45]. **^{13}C NMR:** (126 MHz, CDCl$_3$) δ 171.0 (C=O), 151.7 (d, J = 1.1 Hz, C6), 144.4 (C10), 132.8 (C3), 127.4 (q, J = 28.7 Hz, C1), 127.2 (q, J = 5.4 Hz, C2), 126.7 (C12), 125.3 (C13), 124.4 (C11), 124.0 (C4), 123.9 (q, J = 273.7 Hz, CF$_3$), 123.1 (C5) 53.7 (C*), 53.0 (C*), 46.0 (C*), 42.0 (C*), 32.1 (C9), 29.3 (C7), 27.0 (C8).*Piperazine. ^{13}C NMR matches literature data[45]. **HR-MS:** calcd for C$_{19}$H$_{22}$F$_3$N$_2$OS m/z: [M + H]$^+$, 383.1399; found: 383.1406 [Diff (ppm) = 1.8]. **R$_f$:** 0.74 (3:2, EtOAc:n-hexane). **IR (ATR):** 2916 (C-H), 1642 (C=O), 1312 (C-F), 1107 (C-N) cm^{-1}.

5.2.10 Synthesis of 1-(4-(3,5-bis(trifluoromethyl)phenyl)piperazin-1-yl)-4-(thiophen-2-yl)butan-1-one (MK44) (RTC26) (9)
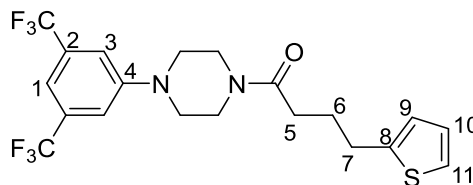
Prepared from 1-(3,5-bis(trifluoromethyl)phenyl)piperazine (194 mg, 0.65 mmol) and 4-(2-thienyl)butyric acid (85 µL, 0.58 mmol) using HOBt (87 mg, 0.65 mmol), TBTU (207 mg, 0.65 mmol), NEt$_3$ (129 µL, 0.92 mmol) and DMF (5 mL) and following the general procedure described in section **5.2.1**. The reaction mixture was stirred at rt for 14.5 hrs. DMF was removed under reduced pressure and the residue was purified using column chromatography (3:2, EtOAc:n-hexane) to give a clear oil, 223 mg (86%).

¹H NMR: (500 MHz, CDCl$_3$) δ 7.33 (s, 1H, H1), 7.24 (s, 2H, H3), 7.12 (dd, J = 5.0 Hz, H11), 6.96 – 6.89 (m, 1H, H10), 6.81 (s, 1H, H9), 3.86 – 3.76 (m, 2H*), 3.65 – 3.55 (m, 2H*), 3.34 – 3.21 (m, 4H*), 2.93 (t, J = 7.2 Hz, 2H, H7), 2.41 (t, J = 7.2 Hz, 2H, H5), 2.11 – 2.02 (m, 2H, H6).*Piperazine. ¹H NMR matches literature data[45]. **¹³C NMR:** (126 MHz, CDCl$_3$) δ 171.1 (C=O), 151.3 (C4), 144.3 (C8), 132.5 (q, J = 32.8 Hz, C2), 126.8 (C10), 124.6 (C9), 123.5 (q, J = 273.3 Hz, CF$_3$), 123.2 (C11), 115.1 (m, C3), 112.7 (m, C1), 48.4 (C*), 48.3 (C*), 44.9 (C*), 41.0 (C*), 31.9 (C7), 29.2 (C5), 26.9 (C6).*Piperazine. ¹³C NMR matches literature data[45]. **¹⁹F NMR:** (471 MHz, CDCl$_3$) δ -60.5 (CF_3). **HR-MS:** calcd for C$_{20}$H$_{20}$F$_6$N$_2$OSNa m/z: [M + Na]$^+$, 473.1093; found: 473.1107 [Diff (ppm) = 2.96]. **R$_f$:** 0.78 (3:2, EtOAc:n-hexane). **IR (ATR):** 2835 (C-H), 1655 (C=O), 1273 (C-N), 1120 (C-O) cm^{-1}.

5.2.11 Synthesis of 1-(4-(4-nitrophenyl)piperazin-1-yl)-4-(thiophen-2-yl)butan-1-one (MK39) (RTC22) (10)
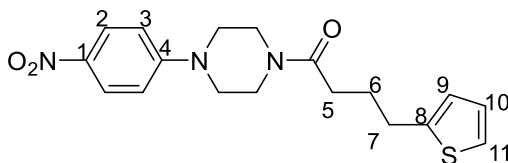
Prepared from 1-(4-nitrophenyl)piperazine (150 mg, 0.72 mmol) and 4-(2-thienyl)butyric acid (95 µL, 0.66 mmol) using HOBt (97 mg, 0.72 mmol), TBTU (232 mg, 0.72 mmol), NEt$_3$ (146 µL, 1.05 mmol) and DMF (6 mL) and following the general procedure described in section **5.2.1**. The reaction mixture was stirred at rt for 22.5 hrs. DMF was removed under reduced pressure and the residue was purified using column chromatography (7:3, EtOAc:DCM) to give an orange solid, 199 mg (84%).

^{1}H NMR: (500 MHz, CDCl$_3$) δ 8.14 (dd, *J* = 9.1, 1.4 Hz, 2H, H2), 7.13 (dd, *J* = 5.1, 1.1 Hz, 1H, H11), 6.95 − 6.90 (m, 1H, H10), 6.86 − 6.78 (m, 3H, H3, H9), 3.84 − 3.76 (m, 2H*), 3.65 − 3.56 (m, 2H*), 3.47 − 3.39 (m, 4H*), 2.93 (t, *J* = 7.2 Hz, 2H, H7), 2.40 (t, *J* = 7.2 Hz, 2H, H5), 2.10 − 2.03 (m, 2H, H6). *Piperazine. ^{1}H NMR matches literature data[45]. **^{13}C NMR:** (126 MHz, CDCl$_3$) δ 171.2 (C=O), 154.4 (C4), 144.3 (C8), 139.1 (C1), 126.9 (C9), 126.0 (C2), 124.6 (C10), 123.3 (C11), 112.9 (C3), 47.0 (C*), 46.9 (C*), 44.7 (C*), 40.8 (C*), 31.9 (C5), 29.2 (C7), 26.8 (C6).*Piperazine. ^{13}C NMR matches literature data[45]. **HR-MS:** calcd for C$_{18}$H$_{21}$N$_3$O$_3$SNa m/z: [M + Na]$^+$, 382.1196; found: 382.1212 [Diff (ppm) = 4.2]. **R$_f$:** 0.7 (7:3, EtOAc:DCM). **IR (ATR):** 2857 (C-H), 1648 (C=O), 1599 (C=C), 1321 (N-O), 1163 (C-N) cm^{-1}.

5.2.12 Synthesis of 1-(4-(4-aminophenyl)piperazin-1-yl)-4-(thiophen-2-yl)butan-1-one (MK70) (RTC23) (11)
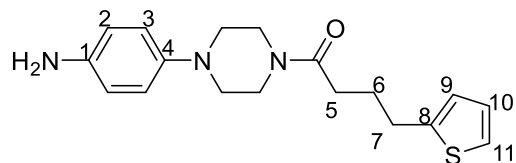
Prepared from 1-(4-(4-nitrophenyl)piperazin-1-yl)-4-(thiophen-2-yl)butan-1-one (compound **10**) (143 mg, 0.39 mmol) dissolved in MeOH (10 mL) in a round bottom flask with PtO_2 (10 mg, 0.04 mmol). The resulting mixture was degassed and purged with H_2 (x3), stirred vigorously at rt for 16.5 hrs under an atmosphere of H_2 gas and monitored by TLC (7:1, EtOAc:DCM). The reaction mixture was passed through a bed of Celite and the filtrate was concentrated under reduced pressure. The residue was purified using column chromatography (7:1, EtOAc:DCM) to give a brown solid, 23 mg (35%).

^{1}H NMR: (500 MHz, $CDCl_3$) δ 7.12 (dd, J = 5.1, 1.2 Hz, 1H, H11), 6.92 (dd, J = 5.1, 3.4 Hz, 1H, H10), 6.82 – 6.77 (m, 3H, H2, H9), 6.67 – 6.63 (m, 2H, H3), 3.77 – 3.74 (m, 2H*), 3.56 – 3.52 (m, 2H*), 2.99 – 2.90 (m, 6H, 4H*, 2H, H5), 2.42 – 2.38 (m, 2H, H7), 2.08 – 5.2.1 (m, 2H, H6). *Piperazine. ^{1}H NMR matches literature data[45]. **^{13}C NMR:** (126 MHz, $CDCl_3$) δ 171.0 (C=O), 144.5 (C4), 144.0 (C1), 140.9 (C8), 126.8 (C10), 124.5 (C9), 123.2 (C11), 119.3 (C2), 116.2 (C3), 51.6 (C*), 51.2 (C*), 45.7 (C*), 41.7 (C*), 32.1 (C7), 29.3 (C5), 27.1 (C6).*Piperazine. ^{13}C NMR matches literature data[45]. **HR-MS:** calcd for $C_{18}H_{24}F_3N_3OS$ m/z: [M + H]$^+$, 330.1635; found: 330.1649 [Diff (ppm) = 4.3]. **R_f:** 0.4 (7:1, EtOAc:DCM). **IR (ATR):** 3337 (N-H), 2815 (C-H), 1638 (C=O), 1510 (C=C), 1223 (C-N) cm^{-1}.

5.2.13 Synthesis of 1-(4-(2-chloro-4-(trifluoromethyl)phenyl)piperazin-1-yl)-4-(thiophen-2-yl)butan-1-one (MK20) (RTC8) (12)
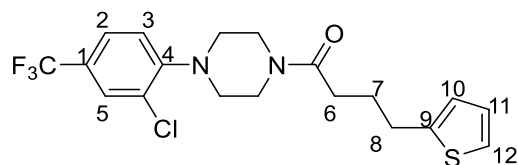
Prepared from 1-(2-chloro-4-(trifluoromethyl)phenyl)piperazine (compound **6**) (90 mg, 0.34 mmol) and 4-(2-thienyl)butyric acid (46 µL, 0.32 mmol) using HOBt (47 mg, 0.34 mmol), TBTU (111 mg, 0.34 mmol), NEt$_3$ (47 µL, 0.51 mmol) and DMF (3 mL) and following the general procedure described in section **5.2.1**. The reaction mixture was stirred at rt overnight. DMF was removed under reduced pressure and the residue was purified using column chromatography (3:2, EtOAc:Pet. Ether) to give a grey oil, 111 mg (83%).

^{1}H NMR: (500 MHz, CDCl$_3$) δ 7.64 (d, J = 1.7 Hz, 1H, H5), 7.48 (dd, J = 8.4, 1.7 Hz, 1H, H2), 7.13 (dd, J = 5.1, 1.0 Hz, 1H, H12), 7.05 (d, J = 8.4 Hz, 1H, H3), 6.95 – 6.91 (m, 1H, H9), 6.84 – 6.79 (m, 1H, H10), 3.86 – 3.76 (m, 2H*), 3.64 – 3.56 (m, 2H*), 3.09 – 3.02 (m, 4H*), 2.93 (t, J = 7.3 Hz, 2H, H8), 2.42 (t, J = 7.5 Hz, 2H, H6), 2.06 (p, J = 7.4 Hz, 2H, H7). *Piperazine. ^{1}H NMR matches literature data[45]. **^{13}C NMR:** (126 MHz, CDCl$_3$) δ 171.2 (C=O), 151.6 (C4), 144.4 (C9), 128.8 (C-Cl), 128.0 (q, J = 3.8 Hz, C5), 126.8 (C11), 126.0 (q, J = 33.4 Hz, C1), 124.9 (q, J = 3.7 Hz, C2), 124.6 (C10), 123.5 (q, J = 272.2 Hz, CF_3), 123.3 (C12), 120.4 (C3), 51.2 (C*), 50.7 (C*), 45.6 (C*), 41.6 (C*), 32.1 (C6), 29.3 (C8), 27.0 (C7). *Piperazine. ^{13}C NMR matches literature data[45]. **HR-MS:** calcd for C$_{19}$H$_{20}$F$_3$N$_2$OSClNa m/z: [M + Na]$^+$, 439.0829; found: 439.085 [Diff (ppm) = 4.8]. **R$_f$:** 0.7 (3:2, EtOAc:Pet. Ether). **IR (ATR):** 2823 (C-H), 1624 (C=O), 1325 (C-F), 1111 (C-N), 694 (C-Cl) cm^{-1}.

5.2.14 Synthesis of 4-(thiophen-3-yl)-1-(4-(5-(trifluoromethyl)pyridin-2-yl)piperazin-1-yl)butan-1-one (MK42) (RTC5) (13)
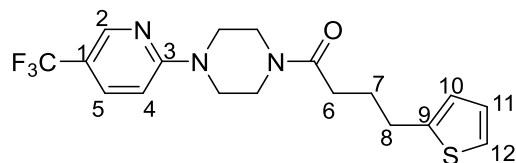
Prepared from 1-(5-(trifluoromethyl)pyridin-2-yl)piperazine (99 mg, 0.43 mmol) and 4-(2-thienyl)butyric acid (50 µL, 0.34 mmol) using HOBt (58 mg, 0.43 mmol), TBTU (140 mg, 0.43 mmol), NEt$_3$ (100 µL, 0.69 mmol) and DMF (3 mL) and following the general procedure described in section **5.2.1**. The reaction mixture was stirred at room temperature overnight. DMF was removed under reduced pressure and the residue was purified using column chromatography (3:2 EtOAc:*n*-hexane) to give a white solid, 119 mg (91%).

^{1}H NMR: (500 MHz, CDCl$_3$) δ 8.41 (s, 1H, H2), 7.66 (dd, *J* = 9.0 Hz, *J* = 2.2 Hz, 1H, H5), 7.14 – 7.10 (m, 1H, H12), 6.94 – 6.91 (m, 1H, H11), 6.82 – 6.80 (m, 1H, H10), 6.64 (d, *J* = 9.0 Hz, 1H, H4), 3.79 – 3.68 (m, 4H*), 3.66 – 3.56 (m, 2H*), 3.56 – 3.49 (m, 2H*), 2.93 (t, *J* = 7.4 Hz, 2H, H8), 2.41 (t, *J* = 7.4, 2H, H6), 2.06 (p, *J* = 7.4 Hz, 2H, H7).*Piperazine. ^{1}H NMR matches literature data[45]. **^{13}C NMR:** (126 MHz, CDCl$_3$) 171.3 (*C*=O), 160.1 (C3), 145.8 (q, *J* = 4.3 Hz, C2), 144.3 (C9), 134.7 (q, *J* = 3.2 Hz, C5), 126.8 (C11), 124.6 (C10), 124.5 (q, *J* = 270.9 Hz, CF$_3$), 123.2 (C12), 115.9 (q, *J* = 33.1 Hz, C1), 105.7 (C4), 45.0 (C*), 44.7 (C*), 44.4 (C*), 41.0 (C*), 32.0 (C6), 29.3 (C8), 26.9 (C7).*Piperazine. ^{13}C NMR matches literature data[45]. **HR-MS:** calcd for C$_{18}$H$_{21}$F$_3$N$_3$OS m/z: [M + H]$^+$, 384.1352; found: 384.1355 [Diff(ppm) = 0.8]. **R$_f$:** 0.5 (3:2, EtOAc:*n*-hexane). **IR (ATR):** 2912 (C-H), 1645 (C=O), 1609 (C=C), 1415 (C=C), 1318 (C-F), 1106 (C-N) cm^{-1}.

5.2.15 Synthesis of 1-(4-(3-chloro-5-(trifluoromethyl)pyridin-2-yl)piperazin-1-yl)-4-(thiophen-2-yl)butan-1-one (MK45) (RTC6) (14)
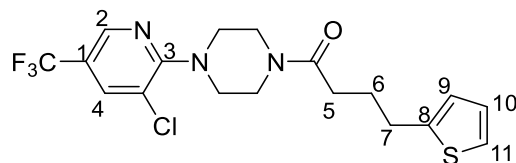
Prepared from 1-(3-chloro-5-(trifluoromethyl)pyridin-2-yl)piperazine (114 mg, 0.43 mmol) and 4-(2-thienyl)butyric acid (50 µL, 0.34 mmol) using HOBt (58 mg, 0.43 mmol), TBTU (140 mg, 0.43 mmol), NEt$_3$ (100 µL, 0.69 mmol) and DMF (3 mL) and following the general procedure described in section **5.2.1**. The reaction mixture was stirred at room temperature overnight. DMF was removed under reduced pressure and the residue was purified using column chromatography (3:2, EtOAc:*n*-hexane) to give a grey solid, 123 mg (87 %).

^{1}H NMR: (500 MHz, CDCl$_3$) δ 8.40 (s, 1H, H2), 7.79 (s, 1H, H4), 7.14 − 7.10 (m, 1H, H11), 6.95 − 6.89 (m, 1H, H10), 6.83 − 6.78 (m, 1H, H9), 3.81 − 3.74 (m, 2H*), 3.60 − 3.53 (m, 2H*), 3.51 − 3.44 (m, 4H*), 2.93 (t, *J* = 7.2 Hz, 2H, H7), 2.41 (t, *J* = 7.4 Hz, 2H, H5), 2.06 (p, *J* = 7.3 Hz, 2H, H6).*Piperazine. ^{1}H NMR matches literature data[45]. **^{13}C NMR:** (126 MHz, CDCl$_3$) 171.2 (C=O), 159.6 (C3), 144.4 (C8), 143.0 (q, *J* = 4.2 Hz, C2), 136.1 (q, *J* = 3.3 Hz, C4), 126.8 (C10), 124.5 (C9), 123.23 (q, *J* = 272.3 Hz, CF$_3$), 123.21 (C11), 121.1 (C-Cl), 120.6 (q, *J* = 33.5 Hz, C1), 48.6 (C*), 45.2 (C*), 41.3 (C*), 32.0 (C5), 29.3 (C7), 27.0 (C6).*Piperazine. ^{13}C NMR matches literature data[45]. **^{19}F NMR:** (471 MHz, CDCl$_3$) δ -61.3 (C*F*$_3$). **HR-MS:** calcd for C$_{18}$H$_{20}$F$_3$N$_3$OSCl m/z: [M + H]$^+$, 418.0971; found 418.0963 [Diff(ppm) = 0.24]. **R$_f$:** 0.78 (3:2, EtOAc:*n*-hexane). **IR (ATR):** 3036 (N-H), 2852 (C-H), 1646 (C=O), 1600 (C=C), 1438 (C=C), 1317 (C-F), 1117 (C-N), 847 (C-Cl) cm^{-1}.

5.2.16 Synthesis of 1-(4-methylpiperazin-1-yl)-4-(thiophen-2-yl)butan-1-one (MK36) (RTC32) (15)
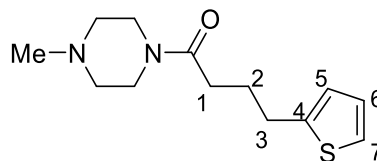
Prepared from 1-methylpiperazine (71 µL, 0.65 mmol) and 4-(2-thienyl)butyric acid (85 µL, 0.59 mmol) using HOBt (87 mg, 0.65 mmol), TBTU (207 mg, 0.65 mmol), NEt$_3$ (90 µL, 0.94 mmol) and DCM (4 mL) and following the general procedure described in section **5.2.1**. The reaction mixture was stirred at room temperature overnight for 18 hours. DCM was removed under reduced pressure and the residue was purified using column chromatography (3:2, EtOAc:n-hexane) to give a yellow oil, 104 mg (70 %).

^{1}H NMR: (500 MHz, CDCl$_3$) δ 7.11 (dd, J = 5.1, 1.2 Hz, 1H, H7), 6.91 (dd, J = 5.1, 3.4 Hz, 1H, H6), 6.80 (ddd, J = 3.4, 2.1, 1.2 Hz, 1H, H5), 3.65 − 3.61 (m, 2H*), 3.43 − 3.39 (m, 2H*), 2.90 (t, J = 7.3 Hz, 2H, H3), 2.38 − 2.33 (m, 4H*, 2H, H1), 2.29 (s, 3H, CH$_3$), 2.02 (p, J = 7.4 Hz, 2H, H2). *Piperazine. ^{1}H NMR matches literature data[45]. **^{13}C NMR:** (126 MHz, CDCl$_3$) δ 170.9 (C=O), 144.5 (C4), 126.8 (C6), 124.5 (C5), 123.1 (C7), 55.2 (C*), 54.7 (C*), 46.0 (CH$_3$), 45.4 (C*), 41.5 (C*), 32.0 (C1), 29.31 (C3), 27.0 (C2). *Piperazine. ^{13}C NMR matches literature data[45]. **HR-MS:** calcd for C$_{13}$H$_{21}$N$_2$OS m/z: [M + H]$^+$, 253.1369; found 253.1367 [Diff(ppm) = -0.8]. **R$_f$:** 0.56 (100% DCM). **IR (ATR):** 2936 (Ar C-H), 2792 (alkane C-H), 1635 (C=O), 1435 (C=C), 1289 (C-N) cm^{-1}.

5.2.17 Synthesis of 4-(thiophen-2-yl)-1-(4-(4-(trifluoromethyl)phenyl)piperidin-1-yl)butan-1-one (MK19) (RTC196) (16)
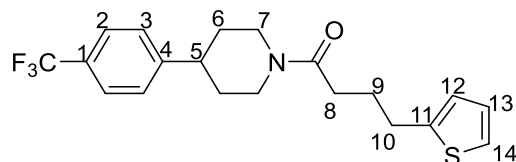
Prepared from 4-(4-(trifluoromethyl)phenyl)piperidine.HCl (100 mg, 0.38 mmol) and 4-(2-thienyl)butyric acid (50 µL, 0.34 mmol) using HOBt (51 mg, 0.38 mmol), TBTU (122 mg, 0.38 mmol), NEt$_3$ (55 µL, 0.54 mmol) and DMF (2 mL) and following the general procedure described in section **5.2.1**. The reaction mixture was stirred for 24 hrs at rt. DMF was removed under reduced pressure and the residue was purified using column chromatography (3:2, EtOAc:n-hexane) to give an off-white solid, 87 mg (67%).

^{1}H NMR: (500 MHz, CDCl$_3$) δ 7.56 (d, *J* = 8.0 Hz, 2H, H2), 7.30 (d, *J* = 8.0 Hz, 2H, H3), 7.12 (d, *J* = 5.1 Hz, 1H, H14), 6.97 − 6.87 (m, 1H, H13), 6.83 − 6.79 (m, 1H, H12), 4.82 (d, *J* = 13.2 Hz, 1H, H7), 3.92 (d, *J* = 13.5 Hz, 1H, H7), 3.10 (t, *J* = 12.9 Hz, 1H, H7), 2.93 (t, *J* = 7.3 Hz, 2H, H10), 2.85 − 2.74 (m, 1H, H5), 2.63 (t, *J* = 12.7 Hz, 1H, H7), 2.41 (t, *J* = 7.4 Hz, 2H, H8), 2.06 (p, *J* = 7.4 Hz, 2H, H9), 1.93 − 1.84 (m, 2H, H6), 1.68 − 1.52 (m, 2H, H6). ^{1}H NMR matches literature data[45]. **^{13}C NMR:** (126 MHz, CDCl$_3$) δ 170.9 (C=O), 149.2 (C4), 144.5 (C11), 128.9 (q, *J* = 32.5 Hz, C1), 127.1 (C3), 126.8 (C13), 125.6 (q, *J* = 3.8 Hz, C2), 124.5 (C12), 124.2 (q, *J* = 272.3 Hz, CF$_3$), 123.1 (C14), 46.0 (C7), 42.7 (C5), 42.2 (C7), 33.7 (C6), 32.6 (C6), 32.2 (C8), 29.4 (C10), 27.1 (C9). ^{13}C NMR matches literature data[45]. **HR-MS:** calcd for C$_{20}$H$_{22}$F$_3$NOSNa m/z: [M + Na]$^+$, 404.1266; found 404.1279 [Diff (ppm) = 3.2]. **R$_f$:** 0.7 (3:2, EtOAc:*n*-hexane). **IR (ATR):** 2850 (C-H), 1644 (C=O), 1323 (C-F), 1112 (C-N) cm^{-1}.

5.2.18 Synthesis of 4-(thiophen-2-yl)-N-(4-(trifluoromethyl)phenyl)butanamide (MK90) (17)
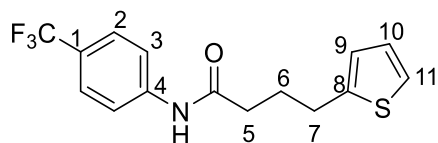
Prepared from 4-(trifluoromethyl)aniline (69 mg, 0.43 mmol) and 4-(thiophen-2-yl)butanoic acid (50 µL, 0.34 mmol) using HOBt (58 mg, 0.43 mmol), TBTU (140 mg, 0.43 mmol), NEt$_3$ (100 µL, 0.51 mmol) and DCM (6 mL) and following the general procedure described in section **5.2.1**. The reaction mixture was stirred at rt for 20 hrs. DCM was removed under reduced pressure and the residue was purified using column chromatography (3:2, EtOAc:n-hexane) to give a white solid, 96 mg (90%).

^{1}H NMR: (500 MHz, CDCl$_3$) δ 7.62 (d, J = 8.6 Hz, 2H, H2), 7.56 (d, J = 8.6 Hz, 2H, H3), 7.29 (bs, 1H, NH), 7.14 (ddd, J = 5.1, 1.2, 0.5 Hz, 1H, H9), 6.93 (dd, J = 5.1, 3.4 Hz, 1H, H10), 6.81 (dd, J = 2.2, 1.1 Hz, 1H, H11), 2.94 (t, J = 7.2 Hz, 2H, H7), 2.42 (t, J = 7.4 Hz, 2H, H5), 2.12 (p, J = 7.2 Hz, 2H, H6). **^{13}C NMR:** (126 MHz, CDCl$_3$) δ 171.0 (C=O), 143.8 (C8), 140.8 (C4), 126.9 (C10), 126.3 (q, J = 3.8 Hz, C2), 126.1 (q, J = 33.0 Hz, C1), 124.8 (C11), 124.1 (q, J = 272.1 Hz, CF$_3$), 123.4 (C9), 119.3 (C3), 36.4 (C5), 29.0 (C7), 27.0 (C6). **HR-MS:** calcd for C$_{19}$H$_{23}$NOSNa m/z: [M + H]$^+$, 336.1393; found 336.1393 [Diff (ppm) = 0.0]. **R$_f$:** 0.6 (3:2, EtOAc:*n*-hexane). **IR (ATR):** 3304 (N-H), 2926 (Ar C-H), 1670 (C=O), 1514 (Ar C=C), 1319 (C-F), 1125 (C-N) cm^{-1}.

5.2.19 Synthesis of 1-(4-(thiophen-2-yl)butyl)-4-(4-(trifluoromethyl)phenyl)piperazine (MK34) (RTC46) (18)
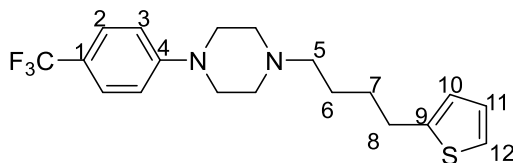
Prepared from a suspension of 4-(thiophen-2-yl)butyl methanesulfonate (compound **20**) (29 mg, 0.12 mmol) and Na_2CO_3 (26 mg, 0.24 mmol) in acetonitrile (5 mL), with 1-(4-(trifluoromethyl)phenyl)piperazine (compound **2**) (110 mg, 0.48 mmol). The mixture was heated at reflux for 22 hrs under vigorous agitation and a N_2 atmosphere. The solvent was removed under reduced pressure and the residue was purified using column chromatography (3:2, EtOAc:*n*-hexane) to give a white solid, 34 mg (77%).

1H NMR: (500 MHz, CDCl3) δ 7.48 (d, *J* = 8.7 Hz, 2H, H2), 7.12 – 7.10 (m, 1H, H12), 6.94 – 6.90 (m, 3H, H3, H11), 6.81 – 6.78 (m, 1H, H10), 3.32 – 3.24 (m, 4H*), 2.87 (t, *J* = 7.5 Hz, 2H, H5), 2.62 – 2.54 (m, 4H*), 2.42 (t, *J* = 7.5 Hz, 2H, H8), 1.74 (dt, *J* = 15.2, 7.5 Hz, 2H, H6), 1.66 – 1.57 (m, 2H, H7).*Piperazine. 1H NMR matches literature data[45]. **13C NMR:** (126 MHz, CDCl3) δ 153.3 (C4), 145.3 (C9), 126.7 (C11), 126.3 (q, *J* = 3.3 Hz, C2), 124.7 (q, *J* = 269.4 Hz, CF3), 124.1 (C10), 122.9 (C12), 120.4 (q, *J* = 32.4 Hz, C1), 114.4 (C3), 58.3 (C8), 53.0 (C*), 48.0 (C*), 29.8 (C5), 29.7 (C6), 26.3 (C7).*Piperazine. 13C NMR matches literature data[45]. **HR-MS:** calcd $C_{19}H_{24}F_3N_2S$ m/z: [M + H]+, 369.1067; found 369.1608 [Diff(ppm) = 0.3]. **Rf:** 0.8 (3:2, EtOAc:*n*-hexane). **IR (ATR):** 2839 (C-H), 1613 (C=C), 1325 (C-F), 1099 (C-N) cm-1.

5.2.20 Synthesis of 4-(thiophen-2-yl)butan-1-ol (MK32) (RD28) (19)
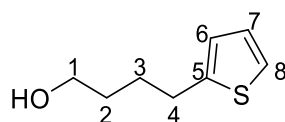
Prepared from a solution of 4-(2-thienyl)butyric acid (500 µL, 3.43 mmol) in anhydrous THF (2.5 mL) added to a suspension of $LiAlH_4$ (130 mg, 3.43 mmol) in anhydrous THF (2.5 mL) in an oven-dried two-necked round-bottom flask, over ice and with a positive flow of argon. The suspension was allowed to reach rt slowly and was stirred for 6 hrs at rt. The reaction mixture was quenched with H_2O (2 mL) added slowly dropwise. The solution was neutralised with 10% aqueous HCl (2 mL) and the aqueous layer extracted with EtOAc (4 x 10 mL). The combined organic layers were dried over $MgSO_4$ and the residue dried under reduced pressure to give an orange oil, 309 mg (58%).

^{1}H NMR: (500 MHz, CDCl$_3$) δ 7.11 – 7.05 (m, 1H, H8), 6.92 – 6.87 (m, 1H, H7), 6.79 – 6.74 (m, 1H, H6), 3.60 (t, J = 6.6 Hz, 2H, H1), 2.83 (t, J = 7.6 Hz, 2H, H4), 2.35 (bs, 1H, OH), 1.77 – 1.68 (m, 2H, H2), 1.64 – 1.55 (m, 2H, H3). ^{1}H NMR matches literature data[45]. **^{13}C NMR:** (126 MHz, CDCl$_3$) δ 145.3 (C5), 126.8 (C7), 124.2 (C6), 123.0 (C8), 62.4 (C1), 32.1 (C4), 29.7 (C2), 28.0 (C3). ^{13}C NMR matches literature data[45]. **HR-MS:** calcd for $C_8H_{12}OSNa$ m/z: [M + Na]$^+$, 179.0501; found: 179.0509 [Diff (ppm) = 4.47]. **R$_f$:** 0.2 (100% DCM). **IR (ATR)**: 3329 (O-H), 2934 (C-H) cm^{-1}.

5.2.21 Synthesis of 4-(thiophen-2-yl)butyl methanesulfonate (MK33) (RD31) (20)
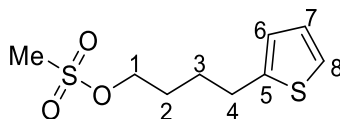
Prepared from a solution of 4-(thiophen-2-yl)butan-1-ol (compound **19**) (124 μL, 0.86 mmol), methanesulfonyl chloride (71 μL, 0.91 mmol), NEt$_3$ (142 μL, 1.01 mmol) in anhydrous DCM (3 mL) and kept at 0 °C. The reaction mixture was maintained at 0 °C for 1 hr followed by allowing it to reach rt slowly. It was maintained at rt under vigorous stirring and a N$_2$ atmosphere for 3 hrs. Volatiles were removed under reduced pressure and the product was purified by column chromatography (3:2, EtOAc:Pet. Ether). Residual NEt$_3$ remained which required additional work-up. The product was neutralised with 10% aqueous HCl (2 mL) and the aqueous layer extracted with EtOAc (4 x 10 mL). The combined organic layers were dried over MgSO$_4$ and the residue dried under reduced pressure to give a colourless oil, 92 mg (46%).

^{1}H NMR: (500 MHz, CDCl$_3$) δ 7.18 – 7.07 (m, 1H, H8), 6.95 – 6.88 (m, 1H, H7), 6.81 – 6.76 (m, 1H, H6), 4.27 – 4.20 (m, 2H*, H1), 2.98 (s, 3H, CH$_3$), 2.92 – 2.83 (m, 2H, H4), 1.87 – 1.75 (m, 4H, H2, H3). ^{1}H NMR matches literature data[45]. **^{13}C NMR:** (126 MHz, CDCl$_3$) δ 144.3 (C5), 126.8 (C7), 124.5 (C6), 123.2 (C8), 69.6 (C1), 37.4 (CH$_3$), 29.2 (C4), 28.4 (C2), 27.6 (C3). ^{13}C NMR matches literature data[45]. **HR-MS:** calcd for C$_9$H$_{14}$O$_3$S$_2$Na m/z: [M + Na]$^+$, 257.0277; found: 257.0271 [Diff (ppm) = -2.0]. **R$_f$:** 0.7 (3:2, EtOAc:Pet.Ether). **IR (ATR)**: 2938 (C-H), 1348 (S=O), 1169 (S=O), 930 (C-H) cm^{-1}.

5.2.22 Synthesis of thiophen-2-yl (4-(4-(trifluoromethyl)phenyl)piperazin-1-yl) methanone (MK37) (RTC93) (21)
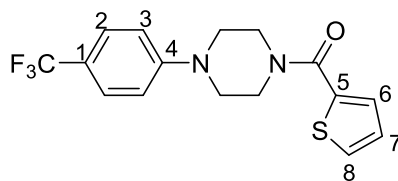
Prepared from 1-(4-(trifluoromethyl)phenyl)piperazine (compound **2**) (76 mg, 0.33 mmol) and thiophene-2-carboxylic acid (38 mg, 0.30 mmol) using HOBt (45 mg, 0.33 mmol), TBTU (107 mg, 0.33 mmol), NEt$_3$ (75 μL, 0.48 mmol) and DMF (4 mL) and following the general procedure described in section **5.2.1**. The reaction mixture was stirred at rt for 21 hours. DMF was removed under reduced pressure and the residue was purified using column chromatography (1:1, EtOAc:Pet. Ether) to give a green solid, 70 mg (69%).

^{1}H NMR: (500 MHz, CDCl$_3$) δ 7.55 – 7.45 (m, 3H, H2, H6), 7.35 (d, *J* = 3.2 Hz, 1H, H8), 7.13 – 7.02 (m, 1H, H7), 6.93 (d, *J* = 8.6 Hz, 2H, H3), 3.98 – 3.86 (m, 4H*), 3.42 – 3.27 (m, 4H*). *Piperazine. ^{1}H NMR matches literature data[45]. **^{13}C NMR:** (126 MHz, CDCl$_3$) δ 163.7 (C=O), 152.8 (C4), 136.6 (C5), 129.1 (C8), 129.0 (C6), 126.8 (C7), 126.5 (q, *J* = 3.8 Hz, C2), 124.5 (q, *J* = 271.3 Hz, CF$_3$), 121.3 (q, *J* = 32.8 Hz, C1), 114.9 (C3), 48.2 (C*). *Piperazine. ^{13}C NMR matches literature data[45]. **HR-MS:** calcd for C$_{16}$H$_{15}$F$_3$N$_2$OSNa m/z: [M + Na]$^+$, 363.0749; found: 363.0762 [Diff (ppm) = 3.58]. **R$_f$:** 0.6 (1:1, EtOAc:Pet.Ether). **IR (ATR):** 2838 (C-H), 1606 (C=O), 1334 (C-F), 1096 (C-N) cm^{-1}.

5.2.23 Synthesis of 2-(thiophen-2-yl)-1-(4-(4-(trifluoromethyl)phenyl)piperazin-1-yl)ethanone (MK47) (RTC536) (22)
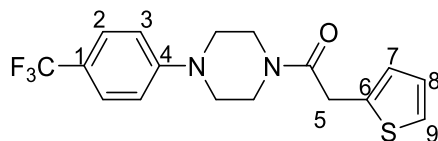
Prepared from 1-(4-(trifluoromethyl)phenyl)piperazine (compound **2**) (100 mg, 0.43 mmol) and 2-(thiophen-2-yl)acetic acid (48 mg, 0.34 mmol) using HOBt (58 mg, 0.43 mmol), TBTU (138 mg, 0.43 mmol), NEt$_3$ (87 μL, 0.63 mmol), DMF (4 mL) and following the general procedure described in section **5.2.1**. The reaction mixture was stirred at rt overnight. Purified using column chromatography (3:2, EtOAc:*n*-hexane) to give an orange solid, 98 mg (82%).

1H NMR: (500 MHz, CDCl$_3$) δ 7.49 (d, *J* = 8.7 Hz, 2H, H2), 7.21 (dd, *J* = 5.1 Hz, *J* = 1.2 Hz, 1H, H9), 6.97 – 6.88 (m, 4H, H3, H7, H8), 3.96 (s, 2H, H5), 3.84 – 3.78 (m, 2H*), 3.72 – 3.64 (m, 2H*), 3.29 – 3.23 (m, 2H*), 3.21 – 3.12 (m, 2H*). *Piperazine. ^{1}H NMR matches literature data[45]. **13C NMR:** (126 MHz, CDCl$_3$) δ 168.5 (C=O), 152.8 (C4), 136.2 (C6), 127.0 (C7), 126.5 (q, *J* = 3.3 Hz, C2), 126.1 (C8), 124.9 (C9), 124.6 (q, *J* = 271.3 Hz, CF$_3$), 121.4 (q, *J* = 32.8 Hz, C1), 115.0 (C3), 48.2 (C*), 47.9 (C*), 45.8 (C*), 41.5 (C*), 35.2 (C5). *Piperazine. ^{13}C NMR matches literature data[45]. **HR-MS:** calcd for C$_{17}$H$_{17}$F$_3$N$_2$O$_2$SNa m/z: [M + Na]$^+$, 377.0906; found: 377.0915 [Diff (ppm) = 2.4]. **R$_f$:** 0.9 (3:2, EtOAc:*n*-hexane). **IR (ATR):** 2826 (C-H), 1614 (C=O), 1409 (C=C), 1336 (C-F), 1229 (C-N) cm^{-1}.

5.2.24 Synthesis of 5-(thiophen-2-yl)-1-(4-(4-(trifluoromethyl)phenyl)piperazin-1-yl)pentan-1-one (MK18) (RTC195) (23)
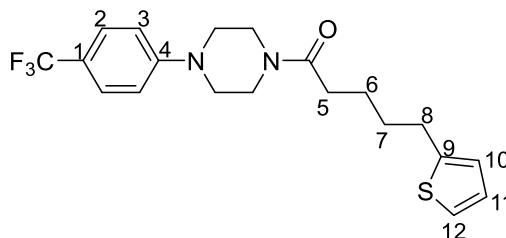
Prepared from 5-(thiophen-2-yl)pentanoic acid (72 mg, 0.39 mmol) using HOBt (58 mg, 0.43 mmol), TBTU (138 mg, 0.43 mmol), anhydrous NEt$_3$ (86 μL, 0.62 mmol) and anhydrous DMF (4 mL) in an oven-dried Schlenk tube under a N$_2$ atmosphere. The resulting solution was stirred at rt for 15 mins. A second Schlenk tube was prepared containing 1-(4-(trifluoromethyl)phenyl)piperazine (compound **2**) (100 mg, 0.43 mmol) and DMF (4 mL) under a N$_2$ atmosphere. The resulting solution was transferred, via a cannula, to the first Schlenk tube containing the carboxylic acid. The reaction mixture was stirred overnight at rt under a N$_2$ atmosphere. DMF was removed under reduced pressure. The resulting oil was acidified (pH = 3) using a 0.1 M aqueous HCl solution and purified using column chromatography (3:2 EtOAc:n-hexane) to give an orange solid, 113 mg (73 %).

^{1}H NMR: (500 MHz, CDCl$_3$) δ 7.50 (d, *J* = 8.8 Hz, 2H, H2), 7.09 (dd, *J* = 5.1, 1.2 Hz, 1H, H12), 6.94 – 6.86 (m, 3H, H3, H11), 6.81 – 6.74 (m, 1H, H10), 3.82 – 3.70 (m, 2H*), 3.66 – 3.53 (m, 2H*), 3.27 – 3.20 (m, 4H*), 2.87 (t, *J* = 6.7 Hz, 2H, H8), 2.39 (t, *J* = 7.0 Hz, 2H, H5), 1.81 – 1.68 (m, 4H, H6, H7). *Piperazine. ^{1}H NMR matches literature data[45]. **^{13}C NMR:** (126 MHz, CDCl$_3$) δ 171.4 (C=O), 152.9 (C4), 145.0 (C9), 126.7 (C11), 126.5 (q, *J* = 3.8 Hz, C2), 124.6 (q, *J* = 271.3 Hz, CF$_3$), 124.2 (C10), 123.0 (C12), 121.3 (q, *J* = 32.9 Hz, C1), 115.0 (C3), 48.4 (C*), 48.1 (C*), 45.1 (C*), 41.1 (C*), 33.0 (C5), 31.4 (C7), 29.7 (C8), 24.6 (C6). *Piperazine. ^{13}C NMR matches literature data[45]. **^{19}F NMR:** (471 MHz, CDCl$_3$) δ -61.8 (C*F*$_3$). **HR-MS:** calcd for C$_{20}$H$_{24}$F$_3$N$_2$OS m/z: [M + H]$^+$, 397.1556; found: 397.1572 [Diff (ppm) = 4.00]. **R$_f$:** 0.66 (3:2, EtOAc:n-hexane). **IR (KBr)**: 2862 (C-H), 1634 (C=O), 1612 (C=C), 1438 (C=C), 1326 (C-F), 1107 (C-N) cm^{-1}.

5.2.25 Synthesis of 1-(thiophen-2-yl)-1-(4-(4-(trifluoromethyl)phenyl)piperazin-1-yl)butan-1,4-dione (MK40) (RTC2) (24)
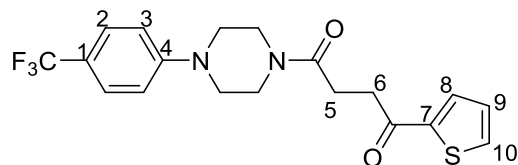
Prepared from 1-(4-(trifluoromethyl)phenyl)piperazine (compound **2**) (100 mg, 0.43 mmol) and 4-oxo-4-(thiophen-2-yl)butanoic acid (63 mg, 0.34 mmol), using HOBt (58 mg, 0.43 mmol), TBTU (140 mg, 0.43 mmol), NEt$_3$ (100 µL, 0.69 mmol) and DMF (3 mL) and following the general procedure described in section **5.2.1**. The reaction mixture was stirred at rt for 17 hrs. DMF was removed under reduced pressure and the residue was purified using column chromatography (3:2 EtOAc:*n*-hexane) to give an off-white solid, 114 mg (84%).

^{1}H NMR: (500 MHz, CDCl$_3$) δ 7.81 (d, *J* = 3.6 Hz, 1H, H8), 7.63 (d, *J* = 4.9 Hz, 1H, H10), 7.50 (d, *J* = 8.6 Hz, 2H, H2), 7.13 (t, *J* = 4.3 Hz, 1H, H9), 6.92 (d, *J* = 8.6 Hz, 2H, H3), 3.83 – 3.70 (m, 4H*), 3.34 – 3.32 (m, 4H*), 3.27 – 3.25 (m, 2H, H6), 2.82 (t, *J* = 6.5 Hz, 2H, H5).*Piperazine. ^{1}H NMR matches literature data[45]. **^{13}C NMR:** (126 MHz, CDCl$_3$) 191.9 (C=O), 170.1 (N-*C*=O), 152.9 (C4), 143.9 (C7), 133.6 (C10), 132.1 (C8), 128.2 (C9), 126.5 (q, *J* = 3.8 Hz, C2), 124.6 (q, *J* = 271.3 Hz, CF$_3$), 121.2 (q, *J* = 32.6 Hz, C1), 115.0 (C3), 48.2 (C*), 48.0 (C*), 45.0 (C*), 41.4 (C*), 34.2 (C5), 27.0 (C6). *Piperazine. ^{13}C NMR matches literature data[45]. **HR-MS:** calcd for C$_{19}$H$_{20}$F$_3$N$_2$O$_2$S m/z: [M + H]$^+$, 397.1192; found: 397.1179 [Diff(ppm) = -3.3]. **R$_f$:** 0.5 (3:2, EtOAc:*n*-hexane). **IR (ATR):** 2948 (C-H), 1647 (C=O), 1612 (N-*C*=*O*), 1325 (C-F), 1223 (C-N) cm^{-1}.

5.2.26 Synthesis of 3-(thiophen-2-ylthio)-1-(4-(4-(trifluoromethyl)phenyl)piperazin-1-yl)propan-1-one (MK22) (RTC7) (25)
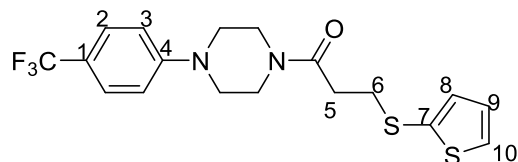
Prepared from 1-(4-(trifluoromethyl)phenyl)piperazine (compound **2**) (50 mg, 0.22 mmol) and 3-(thiophen-2-ylthio)propanoic acid (37 mg, 0.19 mmol) using HOBt (30 mg, 0.22 mmol), TBTU (70 mg, 0.22 mmol), NEt_3 (44 μL, 0.32 mmol) and DMF (2 mL) and following the general procedure described in section **5.2.1**. The reaction mixture was stirred at rt overnight. DMF was removed under reduced pressure and the residue was purified using column chromatography (3:2, EtOAc:Pet. Ether) to give a colourless oil, 45 mg (60%).

^{1}H NMR: (500 MHz, $CDCl_3$) δ 7.50 (d, J = 8.7 Hz, 2H, H2), 7.36 (dd, J = 5.4, 1.2 Hz, 1H, H10), 7.15 (dd, J = 3.6, 1.2 Hz, 1H, H8), 6.99 (dd, J = 5.4, 3.6 Hz, 1H, H9), 6.91 (d, J = 8.7 Hz, 2H, H3), 3.81 – 3.74 (m, 2H*), 3.61 – 3.54 (m, 2H*), 3.30 – 3.23 (m, 4H*), 3.12 (t, J = 7.3 Hz, 2H, H6), 2.68 (t, J = 7.3 Hz, 2H, H5). *Piperazine. ^{1}H NMR matches literature data[45]. **^{13}C NMR:** (126 MHz, $CDCl_3$) δ 169.4 (C=O), 152.9 (C4), 134.0 (C8), 134.0 (C7), 129.6 (C10), 127.7 (C9), 126.5 (q, J = 3.8 Hz, C2), 124.6 (q, J = 271.3 Hz, CF_3), 121.4 (q, J = 32.8 Hz, C1), 115.0 (C3), 48.3 (C*), 48.1 (C*), 45.0 (C*), 41.3 (C*), 34.1 (C5), 33.2 (C6). *Piperazine. ^{13}C NMR matches literature data[45]. **^{19}F NMR:** (471 MHz, $CDCl_3$) δ -61.4 (CF_3). **HR-MS:** calcd for $C_{18}H_{19}F_3N_2OS_2Na$ m/z: $[M + Na]^+$, 423.0783; found: 423.0797 [Diff (ppm) = 3.3]. **R_f:** 0.75 (3:2, EtOAc:Pet. Ether). **IR (ATR):** 2837 (C-H), 1640 (C=O), 1614 (C=C), 1331 (C-F), 1103 (C-N) cm^{-1}.

5.2.27 Synthesis of *N,N*-dimethyl-4-(thiophen-2-yl)butanamide (MK46) (26)
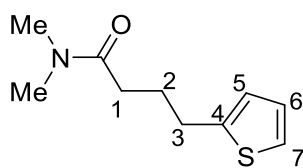
Prepared from dimethylamine (29 μL, 0.43 mmol) and 4-(2-thienyl)butyric acid (50 μL, 0.34 mmol) using HOBt (58 mg, 0.43 mmol), TBTU (139 mg, 0.43 mmol), NEt$_3$ (100 μL, 0.69 mmol) and DMF (3 mL) and following the general procedure described in section **5.2.1**. The reaction mixture was stirred at rt for 16 hrs. DMF was removed under reduced pressure and the residue was purified using column chromatography (3:2, EtOAc:*n*-hexane) to give a grey oil, 29 mg (43%).

^{1}H NMR: (500 MHz, CDCl$_3$) δ 7.16 – 7.03 (m, 1H, H7), 6.95 – 6.88 (m, 1H, H6), 6.83 – 6.76 (m, 1H, H5), 3.11 – 2.74 (m, 4H, H1, 2 x CH$_3$), 2.39 (dt, *J* = 25.2, 7.4 Hz, 2H, H3), 2.10 – 1.96 (m, 2H, H2). **^{13}C NMR:** (126 MHz, CDCl$_3$) δ 178.8 (C=O), 173.0 (C=O*), 144.6 (C4*), 143.9 (C4), 126.8 (C6), 126.8 (C6*), 124.6 (C7), 124.5 (C7*), 123.3 (C5), 123.1 (C5*), 37.3 (CH$_3$), 35.5 (CH$_3$), 33.0 (C3), 32.2 (C3*), 29.3 (C1*), 29.0 (C1), 26.9 (C2*), 26.6 (C2).*other tautomer. **HR-MS:** calcd for C$_{10}$H$_{16}$NOS m/z: [M + H]$^+$, 198.0947; found: 198.0944 [Diff (ppm) = -1.5]. **R$_f$:** 0.7 (3:2, EtOAc:*n*-hexane).

5.2.28 Synthesis of 1-(4-phenylpiperidin-1-yl)-4-(thiophen-2-yl)butan-1-one (MK89) (27)
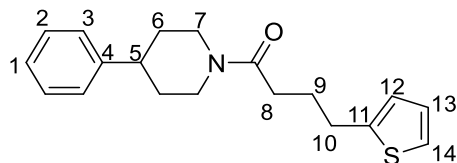
Prepared from 4-phenylpiperidine (69 mg, 0.43 mmol) and 4-(thiophen-2-yl)butanoic acid (50 μL, 0.34 mmol) using HOBt (58 mg, 0.43 mmol), TBTU (140 mg, 0.43 mmol), NEt$_3$ (100 μL, 0.51 mmol) and DCM (6 mL) and following the general procedure described in section **5.2.1**. The reaction mixture was stirred at rt for 18 hrs. DCM was removed under reduced pressure and the residue was purified using column chromatography (3:2, EtOAc:n-hexane) to give a clear oil, 105 mg (98%).

^{1}H NMR: (500 MHz, CDCl$_3$) δ 7.32 (*pseudo* t, J = 7.6 Hz, 2H, H3), 7.25 − 7.16 (m, 3H, H1, H2), 7.13 (dd, J = 5.1, 1.2 Hz, 1H, H14), 6.93 (dd, J = 5.1, 3.4 Hz, 1H, H13), 6.89 − 6.78 (m, 1H, H12), 4.82 (d, J = 13.2 Hz, 1H, H7), 3.91 (d, J = 13.5 Hz, 1H, H7), 3.09 (td, J = 13.2, 2.1 Hz, 1H, H7), 2.94 (t, J = 7.4 Hz, 2H, H10), 2.73 (tt, J = 12.2, 3.6 Hz, 1H, H5), 2.63 (td, J = 13.0, 2.1 Hz, 1H, H7), 2.46 − 2.38 (m, 2H, H8), 2.07 (p, J = 7.4 Hz, 2H, H9), 1.93 − 1.84 (m, 2H, H6), 1.67 − 1.54 (m, 2H, H6). **^{13}C NMR:** (126 MHz, CDCl$_3$) δ 170.8 (C=O), 145.3 (C4), 144.6 (C11), 128.6 (C3), 126.8 (C13), 126.8 (C2), 126.5 (C1), 124.5 (C12), 123.2 (C14), 46.2 (C7), 42.8 (C5), 42.4 (C7), 34.0 (C6), 32.9 (C6), 32.3 (C8), 29.4 (C10), 27.2 (C9). **HR-MS:** calcd for C$_{19}$H$_{23}$NOSNa m/z: [M + H]$^+$, 336.1393; found 336.1393 [Diff (ppm) = 0.0]. **R$_f$:** 0.6 (3:2, EtOAc:*n*-hexane). **IR (ATR):** 3026 (alkene C-H), 2933 (Ar C-H), 2850 (alkyl C-H), 1636 (alkene C=C), 1435 (Ar C=C) cm^{-1}.

5.2.29 Synthesis of 1-(thiophen-2-yl)-4-(4-(4-(trifluoromethyl)phenyl)piperidin-1-yl)butane-1,4-dione (MK88) (28)
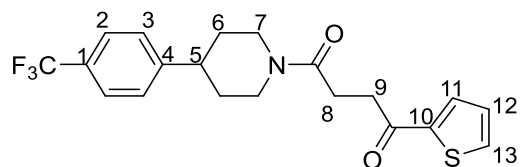
Prepared from 4-(4-trifluoromethyl)phenyl)piperidine (99 mg, 0.43 mmol) and 4-oxo-4-(2-thienyl)butanoic acid (63 mg, 0.34 mmol) using HOBt (58 mg, 0.43 mmol), TBTU (140 mg, 0.43 mmol), NEt$_3$ (100 µL, 0.51 mmol) and DCM (6 mL) and following the general procedure described in section **5.2.1**. The reaction mixture was stirred at rt for 19 hrs. DCM was removed under reduced pressure and the residue was purified using column chromatography (4:1, EtOAc:n-hexane) to give a white solid, 117 mg (87%).

^{1}H NMR: (500 MHz, CDCl$_3$) δ 7.82 (d, *J* = 3.2 Hz, 1H, H11), 7.63 (d, *J* = 4.9 Hz, 1H, H13), 7.57 (d, *J* = 8.1 Hz, 2H, H2), 7.32 (d, *J* = 8.1 Hz, 2H, H3), 7.17 – 7.08 (m, 1H, H12), 4.79 (d, *J* = 11.6 Hz, H7), 4.13 (d, *J* = 14.3 Hz, H7), 3.37 – 3.28 (m, 2H, H9), 3.23 – 3.14 (m, 1H, H7), 2.90 – 2.77 (m, 3H, H5, H8), 2.71 – 2.60 (m, 1H, H7), 1.91 (dd, *J* = 31.5, 13.1 Hz, 2H, H6), 1.75 – 1.57 (m, 2H, H6). **^{13}C NMR:** (126 MHz, CDCl$_3$) δ 192.2 (C=O), 169.9 (N-*C*=O), 149.2 (C4), 144.1 (C10), 133.6 (C13), 132.2 (C11), 128.9 (q, *J* = 32.4 Hz, C1), 128.2 (C12), 127.2 (C3), 125.6 (q, *J* = 3.8 Hz, C2), 124.3 (q, *J* = 272.4 Hz, CF$_3$), 46.0 (C7), 42.8 (C5), 42.5 (C7), 34.4 (C9), 33.6 (C6), 32.7 (C6), 27.3 (C8). **HR-MS:** calcd for C$_{20}$H$_{21}$F$_3$NO$_2$S m/z: [M + H]$^+$, 396.124; found 396.1251 [Diff (ppm) = 2.8]. **R$_f$:** 0.3 (4:1, EtOAc:*n*-hexane). **IR (ATR):** 2935 (Ar C-H), 1657 (C=O), 1633 (alkene C=C), 1330 (C-F), 1110 (C-N) cm^{-1}.

5.2.30 Synthesis of 5-phenyl-1-(4-(4-(trifluoromethyl)phenyl)piperazin-1-yl)pentan-1-one (MK30) (RTC16) (29)
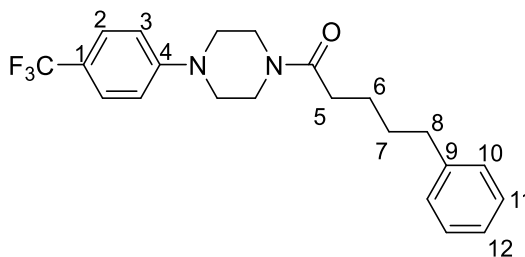
Prepared from 1-(4-(trifluoromethyl)phenyl)piperazine (compound **2**) (150 mg, 0.65 mmol) and 5-phenylpentanoic acid (105 mg, 0.59 mmol) using HOBt (87 mg, 0.65 mmol), TBTU (208 mg, 0.65 mmol), NEt$_3$ (131 µL, 0.94 mmol) and DMF (5mL) and following the general procedure described in section **5.2.1**. The reaction mixture was stirred at rt for 21 hours. DMF was removed under reduced pressure and the residue was purified using column chromatography (4:1, EtOAc:*n*-hexane) to give an orange oil, 150 mg (65%).

^{1}H NMR: (500 MHz, CDCl$_3$) δ 7.48 (d, *J* = 8.7 Hz, 2H, H2), 7.26 – 7.23 (m, 2H, H10), 7.19 – 7.13 (m, 3H, H11, H12), 6.88 (d, *J* = 8.7 Hz, 2H, H3), 3.81 – 3.68 (m, 2H*), 3.62 – 3.49 (m, 2H*), 3.24 – 3.17 (m, 4H*), 2.68 – 2.61 (m, 2H, H8), 2.40 – 2.32 (m, 2H, H5), 1.75 – 1.65 (m, 4H, H6, H7). *Piperazine. ^{1}H NMR matches literature data[45]. **^{13}C NMR:** (126 MHz, CDCl$_3$) δ 171.5 (C=O), 153.0 (C4), 142.2 (C9), 128.5 (C10), 128.4 (C11), 126.5 (q, *J* = 3.8 Hz, C2), 125.8 (C12), 124.7 (q, *J* = 271.3 Hz, CF$_3$), 121.2 (q, *J* = 32.8 Hz, C1), 115.0 (C3), 48.3 (C*), 48.1 (C*), 45.1 (C*), 41.1 (C*), 35.7 (C8), 33.1 (C5), 31.1 (C6), 24.9 (C7).*Piperazine. ^{13}C NMR matches literature data[45]. **HR-MS:** calcd for C$_{22}$H$_{26}$F$_3$N$_2$O m/z: [M + H]$^+$, 391.1992; found: 391.1996 [Diff (ppm) = 1.00]. **R$_f$:** 0.7 (4:1, EtOAc:*n*-hexane). **IR (ATR):** 2857 (C-H), 1636 (C=O), 1610 (C=C), 1436 (C=C), 1331 (C-F), 1068 (C-N) cm^{-1}.

5.2.31 Synthesis of 1-(4-(4-(trifluoromethyl)phenyl)piperazin-1-yl)ethanone (MK29) (RTC12) (30)
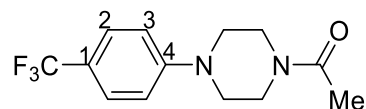
Prepared from 1-(4-(trifluoromethyl)phenyl)piperazine (compound **2**) (150 mg, 0.65 mmol) and acetic acid (33 µL, 0.59 mmol) using HOBt (87 mg, 0.65 mmol), TBTU (208 mg, 0.65 mmol), NEt$_3$ (131 µL, 0.94 mmol) and DMF (3 mL) and following the general procedure described in section **5.2.1**. The reaction mixture was stirred at rt for 23 hours. DMF was removed under reduced pressure and the residue was purified using column chromatography (4:1, EtOAc:*n*-hexane) to give an off-white solid, 117 mg (73%).

^{1}H NMR: (500 MHz, CDCl$_3$) δ 7.50 (d, *J* = 8.6 Hz, 2H, H2), 6.92 (d, *J* = 8.7 Hz, 2H, H3), 3.84 − 3.71 (m, 2H*), 3.70 − 3.57 (m, 2H*), 3.35 − 3.19 (m, 4H*), 2.14 (s, 3H, CH$_3$). *Piperazine. ^{1}H NMR matches literature data[45]. **^{13}C NMR:** (126 MHz, CDCl$_3$) δ 169.1 (*C*=O), 152.9 (C4), 126.5 (q, *J* = 3.3 Hz, C2), 124.6 (q, *J* = 277.2 Hz, CF$_3$), 121.2 (q, *J* = 32.8 Hz, C1), 115.0 (C3), 48.3 (C*), 48.0 (C*), 45.8 (C*), 41.0 (C*), 21.3 (*C*H$_3$).*Piperazine. ^{13}C NMR matches literature data[45]. **HR-MS:** calcd for C$_{13}$H$_{15}$F$_3$N$_2$ONa m/z: [M + Na]$^+$, 295.1029; found: 295.1037 [Diff (ppm) = 2.9]. **R$_f$:** 0.5 (4:1, EtOAc:*n*-hexane). **IR (ATR):** 3222 (C-H), 1614 (C=O), 1428 (C=C), 1324 (C-F), 1105 (C-N) cm^{-1}.

5.2.32 Synthesis of 1-methyl-4-(4-(trifluoromethyl)phenyl)piperazine (MK35) (RTC31) (35)
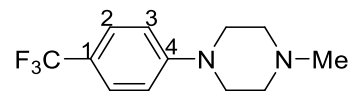
Prepared from 1-(4-(trifluoromethyl)phenyl)piperazine (compound **2**) (70 mg, 0.30 mmol) dissolved in absolute EtOH (3 mL) before formic acid (200 μL, 5.23 mmol) and formaldehyde (147 μL, 1.54 mmol) were consecutively added. The solution was heated at reflux for 3 hrs after which the EtOH was removed under reduced pressure and the residue dissolved in minimal H_2O (2 mL). The aqueous solution was neutralised to pH ~ 13 using saturated aqueous $NaHCO_3$ (4 mL) and extracted with DCM (4 x 10 mL). The organic layers were dried over $MgSO_4$ and concentrated *in vacuo*. The residue was purified using column chromatography (1:1, EtOAc: Pet. Ether) to give a white solid, 51 mg (70%).

^{1}H NMR: (500 MHz, CDCl$_3$) δ 7.47 (d, *J* = 8.7 Hz, 2H, H2), 6.92 (d, *J* = 8.7 Hz, 2H, H3), 3.33 − 3.26 (m, 4H*), 2.59 − 2.52 (m, 4H*), 2.35 (s, 3H, C*H$_3$*).*Piperazine. ^{1}H NMR matches literature data[45]. **^{13}C NMR:** (126 MHz, CDCl$_3$) δ 153.3 (C4), 126.4 (q, *J* = 3.8 Hz, C2), 124.8 (q, *J* = 271.1 Hz, CF$_3$), 120.5 (q, *J* = 32.7 Hz, C1), 114.5 (C3), 54.8 (C*H$_3$*), 48.0 (C*), 46.1 (C*). *Piperazine. ^{13}C NMR matches literature data[45]. **HR-MS:** calcd for $C_{12}H_{16}F_3N_2$ m/z: [M + H]$^+$, 245.1260; found: 245.1257 [Diff (ppm) = -1.22]. **R$_f$:** 0.1 (1:1, EtOAc:Pet. Ether). **IR (ATR):** 2851 (C-H), 1614 (C=C), 1104 (C-N) cm^{-1}.

5.2.33 General procedure of microwave synthesis of aminopyrazoles

A microwave tube (10 mL) was charged with ketonitrile (2.0 mmol), MeOH (1 mL), and hydrazine monohydrate (2.6 mmol) and subjected to microwave irradiation (100 W, 150 °C) for 5 minutes. Volatiles were subsequently removed under reduced pressure. The mixture was purified by either trituration with cold MeOH or cyclohexane, or by using column chromatography to give the final product.

5.2.34 General procedure of one-pot synthesis of pyrazolopyrimidinones

A microwave tube (10 mL) was charged with ketonitrile (0.9 mmol), MeOH (1 mL), and hydrazine monohydrate (1.2 mmol) and subjected to microwave irradiation (100 W, 150 °C) for 5 minutes. Subsequently, to this solution was added ketoester (0.9 mmol) and acetic acid (0.5 mmol), and the mixture was subjected to microwave irradiation (100 W, 150 °C) for 2 hours. Volatiles were removed under reduced pressure. The mixture was purified by either trituration with cold MeOH or ethyl acetate, or by using column chromatography to give the final product.

5.2.35 Synthesis of 3-phenyl-1*H*-pyrazol-5-amine (MK12, MK60, MK64, MK67) (32)
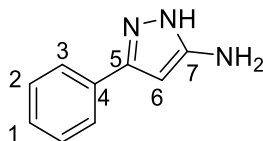
MK12: Prepared from benzoyl acetonitrile (290 mg, 2.0 mmol), hydrazine monohydrate (130 mg, 2.6 mmol) and solvent (1 mL) and following the general procedure described in section **5.2.33** to perform a solvent screen. Purified by column chromatography (1:1, EtOAc: Pet.Ether). Reaction with MeOH as solvent gave a white solid, 316 mg (99%).

MK60: Prepared from benzoyl acetonitrile (290 mg, 2.0 mmol), hydrazine monohydrate (130 mg, 2.6 mmol) and MeOH (2 mL) in a round-bottom flask and heated at reflux for 17 hours. Volatiles were removed under reduced pressure and the product was purified by column chromatography (7:3, EtOAc, Pet.Ether) to give a white solid, 191 mg (60%).

MK64: Prepared from benzoyl acetonitrile (290 mg, 2.0 mmol), hydrazine monohydrate (130 mg, 2.6 mmol) and MeOH (2 mL) and following the general procedure described in section **5.2.33**, except for temperature set at 130 °C. Volatiles were removed under reduced pressure and the product was purified by column chromatography (1:1, EtOAc, Pet.Ether) to give a brown solid, 169 mg (53 %).

MK67: Prepared from benzoyl acetonitrile (290 mg, 2.0 mmol), hydrazine monohydrate (130 mg, 2.6 mmol) and MeOH (2 mL) in a round-bottom flask and heated at reflux for 5 mins. Volatiles were removed under reduced pressure and the product was purified by column chromatography (1:1, EtOAc, Pet.Ether) to give a green solid, 94 mg (30%).

^{1}H NMR: (500 MHz, CDCl$_3$) δ 7.53 (d, *J* = 7.3 Hz, 2H, H3), 7.37 (t, *J* = 7.4 Hz, 2H, H2), 7.30 (t, *J* = 7.3 Hz, 1H, H1), 5.90 (s, 1H, CH), 3.80 (bs, 1H, NH). ^{1}H NMR data matches literature data[94]. **^{13}C NMR:** (126 MHz, CDCl$_3$) δ 154.5 (C7), 145.6 (C5), 130.3 (C4), 128.9 (C2), 128.3 (C1), 125.4 (C3), 90.5 (C6). ^{13}C NMR data matches literature data[94]. **HR-MS:** calcd for C$_9$H$_{10}$N$_3$ m/z: [M + H]$^+$, 160.0869; found: 160.0872 [Diff (ppm) = -1.9]. MS data matches literature data[94]. **R$_f$:** 0.42 (7:3, EtOAc:Pet.Ether). **IR (ATR)**: 3296 (N-H), 1564 (N-H), 1506 (C-C), 1467 (C-C), 759 (N-H) cm^{-1}.

5.2.36 Synthesis of 3-(3-chlorophenyl)-1*H*-pyrazol-5-amine (MK14) (33)
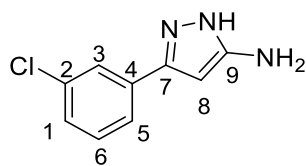
Prepared from 3-(3-chlorophenyl)-3-oxopropanenitrile (162 mg, 0.9 mmol), hydrazine monohydrate (59 mg, 1.2 mmol) and MeOH (1 mL) and following the general procedure described in section **5.2.33**. Volatiles were removed under reduced pressure and the product was purified by column chromatography (1:1, EtOAc:Pet. Ether) to give a red solid, 364 mg (94%).

¹H NMR: (500 MHz, CDCl₃) δ 7.53 (m, 1H, H3), 7.42 (dt, *J* = 7.2, 1.8 Hz, 1H, H5), 7.35 – 7.27 (m, 2H, H1 & H6), 5.91 (s, 1H, CH). ¹H NMR data matches literature data[114]. **¹³C NMR:** (126 MHz, CDCl₃) δ 154.0 (C9), 144.8 (C7), 134.9 (C4), 132.2 (C2), 130.2 (C6), 128.3 (C1), 125.5 (C3), 123.4 (C5), 90.8 (C8). **HR-MS:** calcd for $C_9H_9ClN_3$ m/z: [M + H]⁺, 194.0480; found: 194.0480 [Diff (ppm) = 0.06]. MS data matches literature data[114]. **R_f:** 0.11 (1:1, EtOAc:Pet.Ether). **IR (KBr)**: 3325 (N-H), 2928 (C-H), 2850 (C-H), 1621 (N-H), 1567 (N-H), 893 (C-Cl) cm⁻¹.

5.2.37 Synthesis of 3-(3-methoxyphenyl)-1*H*-pyrazol-5-amine (MK50) (34)
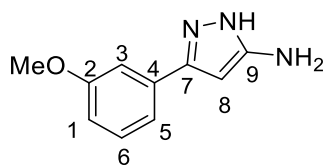
Prepared from 3-(3-methoxyphenyl)-3-oxopropanenitrile (350 mg, 2.0 mmol), hydrazine monohydrate (130 mg, 2.6 mmol) and MeOH (2 mL) and following the general procedure described in section **5.2.33**. Volatiles were removed under reduced pressure and the product was purified by column chromatography (3:2, EtOAc:Pet. Ether) to give a red solid, 278 mg (74%).

^{1}H NMR: (500 MHz, CDCl$_3$) δ 7.18 (*pseudo* t, J = 8.2 Hz, 1H, H1), 7.12 – 7.07 (m, 2H, H3 & H5), 6.80 – 6.76 (m, 1H, H6), 5.79 (s, 1H. CH), 3.68 (s, 3H, OCH$_3$). ^{1}H NMR data matches literature data[114]. **^{13}C NMR:** (126 MHz, CDCl$_3$) δ 159.8 (C2), 153.8 (C9), 146.1 (C7), 131.9 (C4), 129.9 (C1), 118.0 (C3), 113.9 (C6), 110.9 (C5), 90.1 (C8), 55.2 (CH$_3$). **HR-MS:** calcd for C$_{10}$H$_{12}$N$_3$O m/z: [M + H]$^+$, 190.0979; found: 190.0975 [Diff (ppm) = 1.97]. **R$_f$:** 0.18 (3:2, EtOAc:Pet.Ether). **IR (ATR)**: 3401 (N-H), 3203 (Ar C-H), 3001 (alkene C-H), 2942 (alkane C-H), 1612 (N-H), 1598 (N-H), 1506 (C-C), 1245 (C-N), 1039 (C-O), 758 (N-H) cm^{-1}.

5.2.38 Synthesis of 3-(3-nitrophenyl)-1*H*-pyrazol-5-amine (MK57) (35)
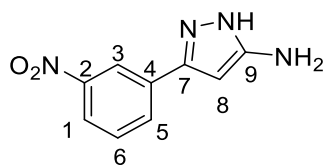
Prepared from 3-(3-nitrophenyl)-3-oxopropanenitrile (190 mg, 1.0 mmol), hydrazine monohydrate (65 mg, 1.3 mmol) and MeOH (1 mL) and following the general procedure described in section **5.2.33**. Volatiles were removed under reduced pressure and the product was purified by column chromatography (3:2, EtOAc:Pet. Ether) to give a yellow solid, 137 mg (67%).

^{1}H NMR: (500 MHz, CDCl$_3$) δ 8.47 (*pseudo* t, *J* = 1.8 Hz, 1H, H1), 8.10 (ddd, *J* = 8.2, 2.3, 1.0 Hz, 1H, H6), 7.98 (ddd, *J* = 7.9, 1.6, 1.0 Hz, 1H, H5), 7.57 (*pseudo* t, *J* = 7.9 Hz, 1H, H3), 5.98 (s, 1H, CH). ^{1}H NMR data matches literature data. **^{13}C NMR:** (126 MHz, CDCl$_3$) δ 152.3 (C9), 148.6 (C2), 146.3 (C7), 133.8 (C4), 130.8 (C5), 129.6 (C3), 121.8 (C6), 119.4 (C1), 88.3 (C8). **HR-MS:** calcd for C$_9$H$_9$N$_4$O$_2$ m/z: [M + H]$^+$, 205.0720; found: 205.0729 [Diff (ppm) = -4.4]. **R$_f$:** 0.1 (3:2, EtOAc:Pet.Ether). **IR (ATR)**: 3149 (N-H), 1607 (N-H), 1524 (N-O), 1504 (C-C), 1346 (N-O), 737 (C-H) cm^{-1}.

5.2.39 Synthesis of 3-(4-bromophenyl)-1*H*-pyrazol-5-amine (MK52) (36)
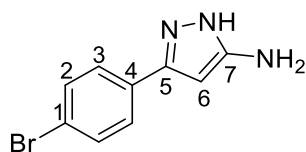
Prepared from (4-bromobenzoyl)acetonitrile (448 mg, 2.0 mmol), hydrazine monohydrate (130 mg, 2.6 mmol) and MeOH (2 mL) and following the general procedure described in section **5.2.33**. Volatiles were removed under reduced pressure and the product was purified by column chromatography (3:2, EtOAc:Pet. Ether) to give a yellow solid, 280 mg (59%).

¹H NMR: (500 MHz, DMSO) δ 7.61 (d, *J* = 8.5 Hz, 2H, H3), 7.55 (d, *J* = 8.5 Hz, 2H, H2), 5.76 (s, 1H, CH), 4.88 (bs, 2H, NH$_2$). **¹³C NMR:** (126 MHz, DMSO) δ 166.0 (C7), 151.2 (C5), 140.1 (C4), 132.7 (C1), 131.9 (C2), 127.2 (C3), 120.5 (C6). **HR-MS:** calcd for C$_9$H$_9$BrN$_3$ m/z: [M + H]$^+$, 237.9974; found: 237.9973 [Diff (ppm) = -0.37]. **R$_f$:** 0.1 (3:2, EtOAc:Pet.Ether). **IR (ATR)**: 3395 (N-H), 3172 (Ar C-H), 1592 (N-H), 1508 (C-C), 1408 (C-C) cm^{-1}.

5.2.40 Synthesis of 3-(thiophenyl-2-yl)-1*H*-pyrazol-5-amine (MK51) (37)
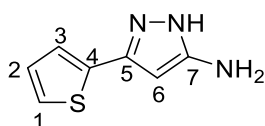
Prepared from 3-oxo-3-(thiophen-2-yl)propanenitrile (302 mg, 2.0 mmol), hydrazine monohydrate (130 mg, 2.6 mmol) and MeOH (2 mL) and following the general procedure described in section **5.2.33**. Volatiles were removed under reduced pressure and the product was purified by column chromatography (4:1, EtOAc:Pet. Ether) to give a yellow solid, 267 mg (81%).

^{1}H NMR: (500 MHz, CDCl$_3$) δ 7.22 (dd, *J* = 5.1, 1.1 Hz, 1H, H1), 7.19 (dd, *J* = 3.6, 1.1 Hz, 1H, H3), 6.99 (dd, *J* = 5.1, 3.6 Hz, 1H, H2), 5.78 (s, 1H, CH). **^{13}C NMR:** (126 MHz, CDCl$_3$) δ 152.8 (C7), 141.6 (C5), 133.6 (C4), 127.7 (C2), 124.9 (C1), 124.1 (C3), 90.1 (C6). **HR-MS:** calcd for C$_7$H$_8$N$_3$S m/z: [M + H]$^+$, 166.0433; found: 166.043 [Diff (ppm) = -2.3]. **R$_f$:** 0.1 (4:1, EtOAc:Pet.Ether). **IR (ATR**): 3366 (N-H), 3122 (Ar C-H), 2852 (alkene C-H), 1597 (N-H), 1515 (C-C), 1473 (C-C), 701 (N-H) cm^{-1}.

5.2.41 Synthesis of 3-ethyl-1*H*-pyrazol-5-amine (MK54) (38)
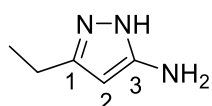
Prepared from 3-oxopentanenitrile (194 mg, 2.0 mmol), hydrazine monohydrate (130 mg, 2.6 mmol) and MeOH (2 mL) and following the general procedure described in section **5.2.33**. Volatiles were removed under reduced pressure and the product was purified by column chromatography (3:2, EtOAc:Pet. Ether) to give a red solid, 109 mg (49%).

1H NMR: (500 MHz, CDCl$_3$) δ 5.45 (s, 1H, CH), 2.57 (q, *J* = 7.5 Hz, 2H, CH$_2$), 1.23 (t, *J* = 7.5 Hz, 3H, CH$_3$). **13C NMR:** (126 MHz, CDCl$_3$) δ 154.7 (C3), 147.3 (C1), 91.2 (C2), 19.4 (*C*H$_2$), 13.1 (*C*H$_3$). **HR-MS:** calcd for C$_5$H$_{10}$N$_3$ m/z: [M + H]$^+$, 112.0869; found: 112.0874 [Diff (ppm) = 4.19]. **R$_f$:** 0.13 (3:2, EtOAc:Pet.Ether). **IR (ATR)**: 3181 (N-H), 2972 (alkane C-H), 1577 (Ar C-C) cm^{-1}.

5.2.42 Synthesis of 3-(*tert*-butyl)-1*H*-pyrazol-5-amine (MK53) (39)
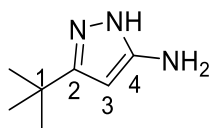
Prepared from pivaloylacetonitrile (250 mg, 2.0 mmol), hydrazine monohydrate (130 mg, 2.6 mmol) and MeOH (2 mL) and following the general procedure described in section **5.2.33**. Volatiles were removed under reduced pressure and the product was purified by column chromatography (3:2, EtOAc:Pet. Ether) to give a red solid, 216 mg (77%).

^{1}H NMR: (500 MHz, CDCl$_3$) δ 5.42 (s, 1H, CH), 1.26 (s, 9H, 3 x CH$_3$). **^{13}C NMR:** (126 MHz, CDCl$_3$) δ 155.2 (C4), 154.1 (C2), 89.3 (C3), 31.0 (C1), 30.0 (CH$_3$). **HR-MS:** calcd for C$_7$H$_{14}$N$_3$ m/z: [M + H]$^+$, 140.1182; found: 140.1185 [Diff (ppm) = 1.65]. **R$_f$:** 0.12 (3:2, EtOAc:Pet.Ether). **IR (ATR)**: 3360 (N-H), 3323 (N-H), 3115 (Ar C-H), 2962 (alkane C-H), 1592 (N-H), 1486 (C-C), 728 (C-H), 711 (N-H) cm^{-1}.

5.2.43 Synthesis of 2,5-diphenylpyrazolo[1,5-*a*]pyrimidin-7(4*H*)-one (MK15, MK65, MK68, MK91, MK92) (40)
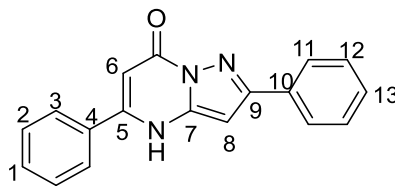
MK15: Prepared from benzoylacetonitrile (131 mg, 0.9 mmol) and ethyl benzoylacetate (173 mg, 0.9 mmol) and following the general procedure described in section **5.2.34**. The reaction mixture was purified by recrystallization using EtOH to give a white solid, 75 mg (29%).

MK65: Prepared by heating 3-phenyl-1*H*-pyrazol-5-amine (compound **12**) (143 mg, 0.9 mmol), ethyl benzoylacetate (173 mg, 0.9 mmol), AcOH (27 mg, 0.5 mmol), in MeOH (2 mL) in a round-bottom flask at reflux for 18 hours. Volatiles were subsequently removed under reduced pressure. The resulting residue was subjected to column chromatography (1:1, EtOAc:Pet. Ether) to give crude product that was further purified by trituration with EtOAc. The remaining residue, which contained the product, was dissolved in DCM (15 mL) and washed with aqueous NaHCO$_3$ (conc, 15 mL). The resulting organic layer was separated, and the solvent removed under reduced pressure to give the white solid, 64 mg (25%).

MK68: Prepared by heating 3-phenyl-1*H*-pyrazol-5-amine (compound **12**) (143 mg, 0.9 mmol), ethyl benzoylacetate (173 mg, 0.9 mmol), AcOH (27 mg, 0.5 mmol), in MeOH (2 mL) in a round-bottom flask at reflux for 2 hours. Volatiles were subsequently removed under reduced pressure. The resulting residue was subjected to column chromatography (1:1, EtOAc:Pet. Ether) to give crude product that was further purified by trituration with EtOAc. The remaining residue, which contained the product, was dissolved in DCM (15 mL) and washed with aqueous NaHCO$_3$ (conc, 15 mL). The resulting organic layer was separated, and the solvent removed under reduced pressure to give the white solid, 27 mg (11%).

MK91: Prepared from benzoyl acetonitrile (131 mg, 0.9 mmol), hydrazine monohydrate (59 mg, 1.2 mmol) and MeOH (4 mL) in a round-bottom flask and heated at reflux for 5

minutes. To this solution, ethyl benzoylacetate (173 mg, 0.9 mmol) and AcOH (27 mg, 0.5 mmol) were added and heated at reflux for 2 hours. Volatiles were subsequently removed under reduced pressure. The resulting residue was subjected to column chromatography (1:1, EtOAc:Pet. Ether) to give a complex mixture with mostly starting material.

MK92: Prepared from 3-phenyl-1*H*-pyrazol-5-amine (compound **12**) (143 mg, 0.9 mmol), ethyl benzoylacetate (173 mg, 0.9 mmol), AcOH (27 mg, 0.5 mmol), in MeOH (2 mL) in a MW reactor tube (10 mL) and subjected to MW irradiation for 2 hours. Volatiles were subsequently removed under reduced pressure. The resulting residue was subjected to column chromatography (1:1, EtOAc:Pet. Ether) to give a white solid, 137 mg (53%).

^{1}H NMR: (126 MHz, DMSO) δ 12.61 (bs, 1H, NH), 8.02 – 7.94 (m, 2H, H11), 7.91 – 7.82 (m, 2H, H3), 7.63 – 7.55 (m, 3H, H1 & H2), 7.48 – 7.40 (m, 3H, H12 & H13), 6.67 (s, 1H, CH), 6.10 (s, 1H, CHCO). **^{13}C NMR:** (126 MHz, DMSO) δ 156.2 (CO), 153.3 (C7), 149.8 (C5), 143.2 (C9), 132.4 (C4), 132.3 (C10), 131.1 (C1), 129.0 (C2), 128.9 (C13), 128.7 (C12), 127.2 (C3), 126.2 (C11), 94.0 (C6), 86.6 (C8). **HR-MS:** calcd for $C_{18}H_{14}N_3O$ m/z: $[M + H]^+$, 288.1131; found: 288.1118 [Diff (ppm) = -4.5] **IR (KBr)**: 3126 (N-H), 3033 (C-H), 1669 (C=O), 1610 (Ar C-H), 768 (C-H) cm^{-1}.

5.2.44 Synthesis of 2-(furan-2-yl)-5-phenylpyrazolo[1,5-*a*]pyrimidin-7(4*H*)-one (MK56) (41)
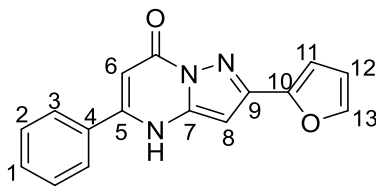
Prepared from 2-furoylacetonitrile (136 mg, 0.9 mmol) and ethyl benzoylacetate (173 mg, 0.9 mmol) and following the general procedure described in section **5.2.34**. Volatiles were removed under reduced pressure and the product was purified by column chromatography (9:1, DCM: MeOH) to give a brown solid, 200 mg (50%). Product was recrystallized using 4:1 EtOH:H$_2$O and a X-ray crystal structure was obtained.

^{1}H NMR: (500 MHz, DMSO) δ 12.58 (bs, 1H, NH), 7.90 – 7.85 (m, 2H, H3), 7.84 (dd, *J* = 1.7, 0.6 Hz, 1H, H13), 7.64 – 7.56 (m, 3H, H1 & H2), 7.04 (dd, *J* = 3.3, 0.6 Hz, 1H, H11), 6.66 (dd, *J* = 3.4, 1.7 Hz, 1H, H12), 6.45 (s, 1H, CH), 6.10 (s, 1H, CHCO). **^{13}C NMR:** (126 MHz, DMSO) δ 156.7 (CO), 150.5 (C5), 148.3 (C10), 146.2 (C9), 144.2 (C13), 143.6 (C7), 133.0 (C4), 131.5 (C1), 129.5 (C2), 127.7 (C3), 112.4 (C12), 109.0 (C11), 94.5 (C6), 86.8 (C8). **HR-MS:** calcd for C$_{16}$H$_{11}$N$_3$O$_2$Na m/z: [M + Na]$^+$, 300.0743; found: 300.0757 [Diff (ppm) = 4.70]. **R$_f$:** 0.5 (9:1, DCM: MeOH). **IR (KBr)**: 3122 (N-H), 3059 (Ar C-H), 1669 (C=O), 764 (C-H) cm^{-1}.

5.2.45 Synthesis of 5-phenyl-2-(thiophen-2-yl)pyrazolo[1,5-*a*]pyrimidin-7(4*H*)-one (MK55) (42)
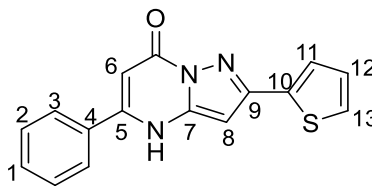
Prepared from 3-oxo-3-(thiophen-2-yl)propanenitrile (136 mg, 0.9 mmol) and ethyl benzoylacetate (173 mg, 0.9 mmol) and following the general procedure described in section **5.2.34**. Volatiles were removed under reduced pressure and the product was purified by column chromatography (3:2, EtOAc:Pet. Ether) to give a yellow solid, 105 mg (40%).

1H NMR: (500 MHz, DMSO) δ 7.98 (d, *J* = 6.8 Hz, 2H, H3), 7.61 (d, *J* = 3.5 Hz, 1H, H13), 7.53 (d, *J* = 5.0 Hz, 1H, H11), 7.51 – 7.38 (m, 3H, H1 & H2), 7.13 (dd, *J* = 5.0, 3.5 Hz, 1H, H12), 6.46 (s, 1H, CH), 6.09 (s, 1H, CHCO). **13C NMR:** (126 MHz, DMSO) δ 158.4 (CO), 155.6 (C5), 150.8 (C7), 148.3 (C10), 138.4 (C4), 137.7 (C9), 129.6 (C1), 128.9 (C2), 128.1 (C12), 127.2 (C3), 126.2 (C11), 125.7 (C13), 90.7 (C6), 89.4 (C8). **HR-MS:** calcd for $C_{16}H_{12}N_3OS$ m/z: [M + H]$^+$, 294.0696; found: 294.0696 [Diff (ppm) = 0.3]. **R$_f$:** 0.43 (3:2, EtOAc:Pet.Ether). **IR (KBr)**: 3402 (N-H), 1667 (C=O), 1661 (Ar C-H), 768 (C-H) cm^{-1}.

5.2.46 Synthesis of 2-methyl-5-phenylpyrazolo[1,5-*a*]pyrimidin-7(4*H*)-one (MK62) (43)
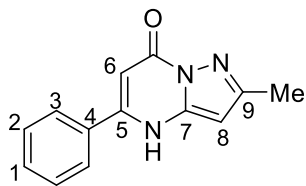
Prepared from 3-oxobutanenitrile (75 mg, 0.9 mmol) and ethyl benzoylacetate (173 mg, 0.9 mmol) and following the general procedure described in section **5.2.34**. Volatiles were removed under reduced pressure and the product was purified by trituration with EtOAc to give an off-white solid, 66 mg (33%).

^{1}H NMR: (500 MHz, DMSO) δ 12.34 (bs, 1H, NH), 7.86 – 7.81 (m, 2H, H3), 7.62 – 7.55 (m, 3H, H1 & H2), 6.05 (s, 1H, CH), 6.00 (s, 1H, CHCO), 2.32 (s, 3H, CH$_3$). ^{1}H NMR matches literature data.[115] **^{13}C NMR:** (126 MHz, DMSO) δ 156.6 (CO), 152.6 (C9), 149.7 (C5), 142.9 (C7), 132.9 (C4), 131.5 (C1), 129.5 (C2), 127.6 (C3), 94.1 (C6), 89.7 (C8), 14.6 (*C*H$_3$). **HR-MS:** calcd for C$_{13}$H$_{12}$N$_3$O m/z: [M + H]$^+$, 226.0975; found: 226.0979 [Diff (ppm) = -1.8]. **IR (KBr)**: 3441 (N-H), 3088 (Ar C-H), 1674 (C=O), 1327 (alkane C-H), 771 (C-H) cm^{-1}.

5.2.47 Synthesis of 2-(*tert*-butyl)-5-phenylpyrazolo[1,5-*a*]pyrimidin-7(4*H*)-one (MK59) (RTC81) (44)
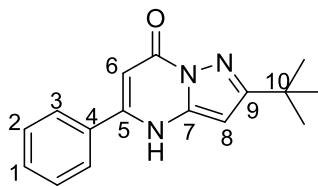
Prepared from pivaloylacetonitrile (113 mg, 0.9 mmol) and ethyl benzoylacetate (173 mg, 0.9 mmol) and following the general procedure described in section **5.2.34**. Volatiles were removed under reduced pressure and the product was purified by column chromatography (3:2, EtOAc:Pet.Ether) to give a white solid, 41 mg (17%).

^{1}H NMR: (500 MHz, DMSO) δ 12.45 (bs, 1H, NH), 7.95 – 7.89 (m, 2H, H3), 7.72 – 7.64 (m, 3H, H1 & H2), 6.18 (s, 1H, CH), 6.09 (s, 1H, CHCO), 1.42 (s, 9H, 3 x CH$_3$). **^{13}C NMR:** (126 MHz, DMSO) δ 165.2 (C=O), 156.9 (C7), 149.9 (C5), 142.8 (C9), 133.0 (C4), 131.4 (C1), 129.5 (C2), 127.7 (C3), 94.1 (C6), 86.5 (C8), 32.9 (C10), 30.6 (CH$_3$). **HR-MS:** calcd for C$_{16}$H$_{18}$N$_3$O m/z: [M + H]$^+$, 268.1444; found: 268.1442 [Diff (ppm) = -0.9]. **R$_f$:** 0.2 (3:2, EtOAc:Pet.Ether). **IR (KBr)**: 2966 (Ar C-H), 1659 (C=O), 1611 (C=C), 1324 (alkane C-H), 770 (C-H) cm^{-1}.

5.2.48 Synthesis of 2-(2-methoxyphenyl)-5-phenylpyrazolo[1,5-*a*]pyrimidin-7(4*H*)-one (MK58) (45)
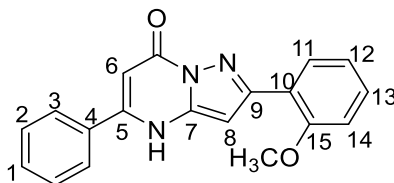
Prepared from 2-methoxybenzoylacetonitrile (158 mg, 0.9 mmol) and ethyl benzoylacetate (173 mg, 0.9 mmol) and following the general procedure described in section **5.2.34**. Volatiles were removed under reduced pressure and the product was purified by column chromatography (4:1, EtOAc:Pet.Ether) to give a white solid, 92 mg (32%).

^{1}H NMR: (500 MHz, MeOD) δ 7.99 (bs, 1H, H11), 7.85 (m, 2H, H3), 7.48 (m, 3H, H1 & H2), 7.30 (*pseudo* t, 1H, H13), 7.05 – 7.02 (m, 1H, H14), 6.98 – 6.95 (m, 1H, H12), 6.73 (s, 1H, CH), 6.12 (s, 1H, CHCO), 3.89 (s, 3H, CH$_3$). **^{13}C NMR:** (126 MHz, DMSO) δ 159.1 (CO), 157.4 (C10), 156.4 (C5), 152.0 (C9), 149.4 (C7), 140.1 (C4), 129.4 (C13), 129.3 (C1), 128.9 (C11), 128.7 (C2), 127.0 (C3), 123.3 (C15), 120.8 (C12), 112.3 (C14), 94.5 (C8), 89.0 (C6), 56.0 (CH$_3$). **HR-MS:** calcd for $C_{19}H_{16}N_3O_2$ m/z: [M + H]$^+$, 318.1237; found: 318.1241 [Diff (ppm) = 1.3]. **R$_f$:** 0.43 (3:2, EtOAc:Pet.Ether). **IR (KBr)**: 3444 (N-H), 1657 (C=O), 1602 (N-H), 1419 (C-C), 1248 (C-O), 760 (C-H) cm^{-1}.

5.2.49 Synthesis of 2-(3-chlorophenyl)-5-phenylpyrazolo[1,5-*a*]pyrimidin-7(4*H*)-one (MK7) (46)
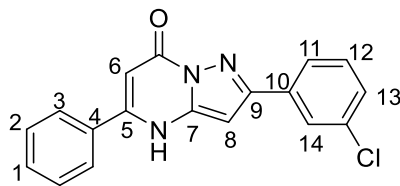
Prepared from 3-(3-chlorophenyl)-3-oxopropanenitrile (162 mg, 0.9 mmol) and ethyl benzoylacetate (173 mg, 0.9 mmol) and following the general procedure described in section **5.2.34**. The reaction mixture was purified by trituration using cold MeOH to remove impurities and give a green solid, 131 mg (45%).

¹H NMR: (500 MHz, DMSO) δ 12.69 (bs, 1H, NH), 8.07 (s, 1H, H14), 8.00 (d, *J* = 7.5 Hz, 1H, H13), 7.91 – 7.84 (m, 2H, H3), 7.67 – 7.56 (m, 3H, H1 & H2), 7.56 – 7.46 (m, 2H, H11 & H12), 6.76 (s, 1H, H8), 6.12 (s, 1H, H6). **¹³C NMR:** (126 MHz, DMSO) δ 158.9 (C-Cl), 156.8 (CO), 152.3 (C9), 150.7 (C5), 135.0 (C7), 134.1 (C4), 131.6 (C1), 131.2 (C2), 129.6 (C14), 129.2 (C13), 128.1 (C10), 127.8 (C3), 126.2 (C12), 125.3 (C11), 94.5 (C8), 87.7 (C6). **HR-MS:** calcd for $C_{18}H_{13}N_3O$ m/z: $[M + H]^+$, 322.0742, found 322.0744 [Diff (ppm) = 0.72]. **IR (KBr):** 3062 (N-H), 1662 (C=O), 1607 (N-H), 1321 (Ar C-N), 772 (C-Cl) cm^{-1}.

5.2.50 Synthesis of 2-(4-fluorophenyl)-5-phenylpyrazolo[1,5-*a*]pyrimidin-7(4*H*)-one (MK8) (47)
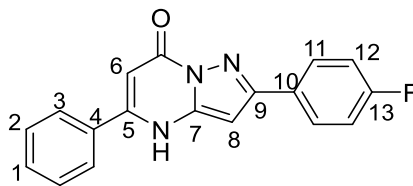
Prepared from 3-(4-fluorophenyl)-3-oxopropanenitrile (147 mg, 0.9 mmol) and ethyl benzoylacetate (173 mg, 0.9 mmol) and following the general procedure described in section **5.2.34**. The reaction mixture was purified by trituration using cold MeOH to remove impurities and give an orange solid, 183.7 mg (67%).

^{1}H NMR: (500 MHz, DMSO) δ 12.61 (bs, 1H, NH), 8.12 – 8.02 (m, 2H, H11), 7.91 – 7.84 (m, 2H, H3), 7.66 – 7.56 (m, 3H, H1 & H2), 7.37 – 7.31 (m, 2H, H12), 6.67 (s, 1H, H8), 6.10 (s, 1H, H6). **^{13}C NMR:** (126 MHz, DMSO) δ 163.1 (d, J_{CF} = 246.3 Hz, C13), 156.7 (CO), 152.9 (C9), 150.3 (C5), 143.7 (C7), 132.8 (C4), 131.6 (C1), 129.6 (C2), 129.4 (d, J_{CF} = 3.0 Hz, C10), 128.8 (d, J_{CF} = 8.4 Hz, C11), 127.8 (C3), 116.2 (d, J_{CF} = 21.5 Hz, C12), 94.6 (C8), 87.1 (C6). **HR-MS:** calcd for $C_{18}H_{13}FN_3O$ m/z: $[M + H]^+$, 306. 1037, found 306.1043 [Diff (ppm) = 1.92]. Matches literature MS data.[116] **IR (KBr):** 3060 (N-H), 1667 (C=O), 1609 (N-H), 1528 (Ar C-C), 767 (N-H) cm^{-1}.

## 5.2.51 Synthesis of 5-phenyl-2-(*p*-tolyl)pyrazolo[1,5-*a*]pyrimidin-7(4*H*)-one (MK9) (48)
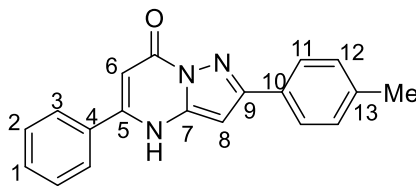
Prepared from 4-methylbenzoylacetonitrile (143.3 mg, 0.9 mmol) and ethyl benzoylacetate (173 mg, 0.9 mmol) and following the general procedure described in section **5.2.34**. The reaction mixture was purified by trituration using cold MeOH to remove impurities and give a white solid, 122.3 mg (45%).

¹H NMR: (500 MHz, DMSO) δ 12.57 (bs, 1H, NH), 7.96 – 7.82 (m, 4H, H11 & H3), 7.65 – 7.56 (m, 3H, H1 & H2), 7.30 (d, *J* = 7.8 Hz, 2H, H12), 6.62 (s, 1H, H8), 6.09 (s, 1H, H6), 2.37 (s, 3H, CH$_3$). **¹³C NMR:** (126 MHz, DMSO) δ 156.7 (CO), 153.8 (C9), 150.2 (C5), 143.6 (C7), 138.9 (C13), 132.8 (C4), 131.5 (C1), 130.1 (C10), 129.8 (C2), 129.5 (C11), 127.7 (C12), 126.6 (C3), 94.5 (C8), 86.9 (C6), 21.4 (CH$_3$). **HR-MS:** calcd for C$_{19}$H$_{16}$FN$_3$O m/z: [M + H]$^+$, 302.1288, found 302.1291 [Diff (ppm) = 1.1]. **IR (KBr):** 3019 (C-H), 1667 (C=O), 1609 (N-H), 1448 (C-H), 767 (N-H), 689 (C-H) cm^{-1}.

5.2.52 Synthesis of 5-(4-nitrophenyl)-2-phenylpyrazolo[1,5-*a*]pyrimidin-7(4*H*)-one (MK61) (49)
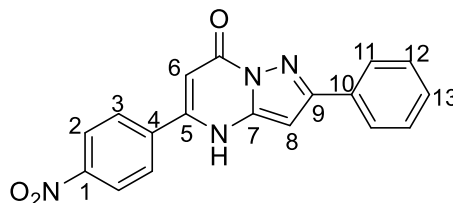
Prepared from benzoylacetonitrile (131 mg, 0.9 mmol) and ethyl 4-nitrobenzoylacetate (213 mg, 0.9 mmol) and following the general procedure described in section **5.2.34**. Volatiles were removed under reduced pressure and the product was purified by trituration with cold MeOH to give a yellow solid, 67 mg (22%).

¹H NMR: (500 MHz, DMSO) δ 8.40 (d, *J* = 8.8 Hz, 2H, H2), 8.14 (d, *J* = 8.8 Hz, 2H, H3), 8.01 (d, *J* = 6.9 Hz, 2H, H11), 7.57 – 7.36 (m, 3H, H12 & H13), 6.67 (s, 1H, CH), 6.19 (s, 1H, CHCO). **¹³C NMR:** (126 MHz, DMSO) δ 155.9 (CO), 153.6 (C7), 148.9 (C5), 147.7 (C1), 143.3 (C9), 138.6 (C4), 132.4 (C10), 128.9 (C13), 128.8 (C12), 128.7 (C3), 126.3 (C11), 123.9 (C2), 95.6 (C6), 86.9 (C8). **HR-MS:** calcd for $C_{18}H_{12}N_4O_3Na$ m/z: [M + Na]⁺, 355.0802; found: 355.0818 [Diff (ppm) = 4.6]. **IR (KBr)**: 3122 (N-H), 3032 (Ar C-H), 1667 (C=O), 1615 (C=C), 774 (C-H) cm⁻¹.

5.2.53 Synthesis of 5-(4-methoxyphenyl)-2-phenylpyrazolo[1,5-*a*]pyrimidin-7(4*H*)-one (MK66) (50)
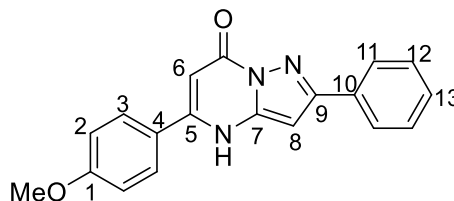
Prepared from benzoylacetonitrile (131 mg, 0.9 mmol) and ethyl 4-methoxybenzoylacetate (200 mg, 0.9 mmol) and following the general procedure described in section **5.2.34**. Volatiles were removed under reduced pressure and the product was purified by column chromatography (1:1, EtOAc:Pet. Ether) to give a white solid, 47 mg (16%).

¹H NMR: (500 MHz, DMSO) δ 8.00 (m, 2H, H11), 7.85 (d, *J* = 8.8 Hz, 2H, H2), 7.47 (m, 3H, H12 & H13), 7.14 (d, *J* = 8.8 Hz, 2H, H3), 6.63 (s, 1H, CH), 6.05 (s, 1H, CHCO), 3.86 (s, 3H, OCH₃). **¹³C NMR:** (126 MHz, DMSO) δ 161.5 (C1), 156.3 (CO), 153.0 (C9), 149.6 (C7), 132.5 (C10), 130.7 (C5), 128.9 (C13), 128.8 (C12), 128.7 (C3), 126.1 (C11), 124.4 (C4), 114.4 (C2), 92.8 (C6), 86.5 (C8), 55.5 (O-*C*H₃). **HR-MS:** calcd for C₁₉H₁₅N₃O₂Na m/z: [M + Na]⁺, 340.1056; found: 340.1071 [Diff (ppm) = 4.4]. **R_f:** 0.59 (1:1, EtOAc:Pet.Ether). **IR (KBr):** 3128 (N-H), 3061 (Ar C-H), 1662 (C=O), 1598 (N-H), 1575 (C=C), 1428 (alkane C-H), 770 (C-H) cm⁻¹.

5.2.54 Synthesis of 2-phenyl-5-(2,3,4,5-tetrafluorophenyl)pyrazolo[1,5-a]pyrimidin-7(4*H*)-one (MK63) (51)
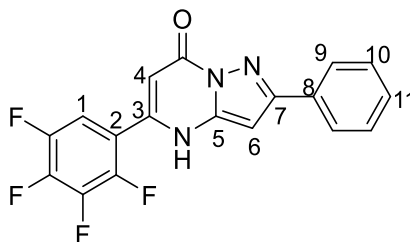
Prepared from benzoylacetonitrile (131 mg, 0.9 mmol) and ethyl (2,3,4,5-tetrafluorobenzoyl)acetate (323 mg, 0.9 mmol) and following the general procedure described in section **5.2.34**. Volatiles were removed under reduced pressure and the product was purified by trituration with cold MeOH to give a yellow solid, 71 mg (22%).

^{1}H NMR: (500 MHz, DMSO) δ 8.05 − 8.01 (m, 2H, H9), 7.94 − 7.87 (m, 1H, H1), 7.53 − 7.48 (m, 2H, H10), 7.46 − 7.42 (m, 1H, H11), 6.74 (s, 1H, CH), 6.01 (d, J_{HF} = 0.8 Hz, 1H, CHCO). **^{13}C NMR:** (126 MHz, DMSO) δ 156.2 (C3), 154.1 (C5), 143.5 (C2), 142.8 (C7), 132.7 (C8), 129.6 (C11), 129.2 (C10), 126.8 (C9), 113.3 (d, J_{CF} = 19.3 Hz, C1), 97.9 (C4), 87.4 (C6). **^{19}F NMR:** (471 MHz, MeOD) δ -140.2, -141.8, -154.8, -156.9. **HR-MS:** calcd for $C_{18}H_{10}F_4N_3O$ m/z: [M + H]$^+$, 360.0755; found: 360.0745 [Diff (ppm) = 2.8]. **IR (KBr)**: 3124 (N-H), 3066 (Ar C-H), 1664 (C=O), 1608 (C=C), 1089 (C-F), 769 (C-H) cm^{-1}.

5.2.55 Synthesis of 5-(3,5-dimethylphenyl)-2-methylpyrazolo[1,5-a]pyrimidin-7(4H)-one (MK2) (52)
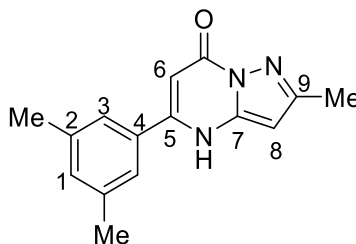
Ethyl 3-(3,5-dimethylphenyl)-3-oxopropanoate (compound **1**) (0.56 mL, 3.0 mmol) was added to a solution of 3-*a*mino-5-methylpyrazole (132 mg, 1.0 mmol) dissolved in AcOH (5 mL) and refluxed overnight for 21 hours. Volatiles were removed under reduced pressure. The product was purified by column chromatography (100 % DCM) to give a beige solid, 204 mg, (59%).

¹H NMR: (500 MHz, MeOD) δ 7.42 (s, 2H, H3), 7.26 (s, 1H, H1), 6.13 (s, 1H, H8), 6.05 (s, 1H, H6), 2.53 – 2.34 (m, 9H, CH$_3$ x 3). **¹³C NMR:** (126 MHz, MeOD) δ 138.9 (C2), 132.3 (C1), 124.5 (C3), 19.9 (CH$_3$). **HR-MS:** calcd for C$_{13}$H$_{16}$N$_3$O m/z: [M + H]$^+$, 254.1293; found: 253.1207 [Diff (ppm) = 3.3]. **R$_f$:** 0.11 (100% DCM). **IR (KBr):** 3251 (N-H), 2917 (C-H), 1665 (C=O), 1618 (N-H), 1597 (Ar C-C) cm^{-1}. **m.p.:** 220-227 ˚C.

5.2.56 Synthesis of ethyl 3-(3,5-dimethylphenyl)-3-oxopropanoate (MK1) (53)
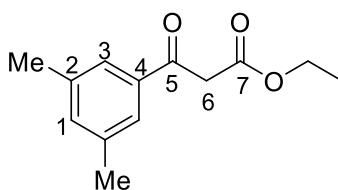
A solution of 3,5-dimethylbenzoic acid (255 mg, 2.0 mmol), Meldrum's acid (299 mg, 2.0 mmol), and DMAP (425 mg, 3.0 mmol), in anhydrous DCM (2.5 mL), was cooled to 0 °C. The reaction mixture was treated with a solution of DCC (386 mg, 2.0 mmol) in DCM (1.9 mL) and was allowed to stir at rt for 5.5 hrs. The white precipitate was removed by gravity filtration and the filtrate was concentrated at reduced pressure. The residue was dissolved in absolute EtOH (10 mL) and treated with a solution of p-TSA.H_2O (799 mg, 4.0 mmol) in absolute EtOH (2.5 mL).

The solution was heated at reflux under N_2 for 1 hr. The EtOH was removed under reduced pressure and EtOAc was added until the residue dissolved. The solution was washed sequentially with H_2O (2 x 10 mL), saturated aqueous $NaHCO_3$ (2 x 5 mL), 1 M aqueous HCl (2 x 5 mL), and brine (2 x 5 mL). The organic layer was dried over $MgSO_4$ and evaporated at reduced pressure. The residue was purified by column chromatography (5:95, EtOAc:Pet.Ether) to give a yellow oil, 251 mg (67%).

^{1}H NMR: (500 MHz, CDCl$_3$) (Keto form) δ 7.55 (s, 2H, H3), 7.22 (s, 1H, H1), 4.22 (q, J = 7.1 Hz, 2H, OCH_2CH$_3$), 3.96 (s, 2H, CH_2), 2.37 (s, 6H, Ar-CH_3 x 2), 1.26 (t, J = 7.1 Hz, 3H, OCH$_2$$CH_3$). ^{1}H NMR data matches literature data [117]. **^{13}C NMR:** (126 MHz, CDCl$_3$) (Keto form) δ 192.9 (C5), 167.7 (C7), 138.4 (C4), 135.4 (C2), 126.3 (C1), 123.9 (C3), 61.4 (C6), 46.0 (CH$_2$), 21.2 (Ar-CH$_3$), 14.1 (CH$_3$, C1). ^{13}C NMR data matches literature data[117] **HR-MS:** calcd for C$_{13}$H$_{16}$O$_3$ m/z: [M + H]$^+$, 221.1178; found: 221.1172 [Diff (ppm) = 1.15]. **R$_f$:** 0.27 (5:95, EtOAc:Pet.Ether). **IR (ATR**): 2963 (C-H), 1738 (C=O ester), 1682 (C=O ketone), 1595 (Ar C-C), 1031 (C-O), 801 (Ar C-H) cm^{-1}.

5.2.57 Synthesis of ethyl 3-(3,5-diethylphenyl)-3-oxopropanoate (MK4) (54)

A solution of 3,5-diethylbenzoic acid (compound **57**) (356 mg, 2.0 mmol), Meldrum's acid (340 mg, 2.0 moles), and DMAP (480 mg, 3.0 mmol), in anhydrous DCM (10 mL), was cooled to 0 °C. The reaction mixture was treated with a solution of DCC (442 mg, 2.0 mmol) in DCM (5 mL) and was allowed to stir overnight at rt. The white precipitate was removed by gravity filtration and the filtrate was concentrated at reduced pressure. The residue was dissolved in absolute EtOH (15 mL) and treated with a solution of p-TSA.H_2O (914 mg, 5.0 mmol) in absolute EtOH (5 mL).

The solution was heated at refluxed under N_2 for 2 hrs. The EtOH was removed under reduced pressure and EtOAc was added until the residue dissolved. The solution was washed sequentially with H_2O (2 x 25 mL), saturated aqueous $NaHCO_3$ (2 x 10 mL), 1 M aqueous HCl (2 x 15 mL), brine (2 x 20 mL). The organic layer was dried over MgSO4 and evaporated at reduced pressure. The residue was purified by column chromatography (elution gradient 5:95 DCM:Pet.Ether to DCM:Pet.Ether 4:6) to give a yellow oil, 359 mg (74%).

1H NMR: (500 MHz, CDCl3) (Keto form) δ 7.61 (s, 2H, H3), 7.28 (s, 1H, H1), 4.25 (q, J = 7.1 Hz, 2H, O*CH2*CH3), 3.99 (s, 2H, *CH2*), 2.69 (m, 4H, Ar-*CH2*CH3 x 2), 1.27 (m, 9H, OCH2*CH3* & Ar-CH2*CH3* x 2). **13C NMR:** (126 MHz, CDCl3) (Keto form) δ 192.9 (C5), 167.7 (C7), 144.9 (C2), 136.3 (C4), 133.1 (C1), 125.4 (C3), 60.8 (O*CH2*CH3), 46.1 (C6), 28.7 (Ar-*CH2*CH3), 15.5 (Ar-CH2*CH3*), 14.1 (OCH2*CH3*). **HR-MS:** calcd for $C_{15}H_{20}O_3$ m/z: [M + H]+, 248.1412; found: 248.142 [Diff (ppm) = 3.16]. **Rf:** 0.29 (3:7, DCM:Pet.Ether). **IR (ATR)**: 3322 (OH), 2928 (Ar C-H), 2850 (alkane C-H), 1683 (C=O ketone), 1570 (Ar C-C), 1241 (C-O), 891 (Ar C-H) cm-1.

5.2.58 Synthesis of ethyl 3-(3,5-dimethoxyphenyl)-3-oxopropanoate (MK10) (55)

A solution of 3,5-dimethoxybenzoic acid (1.439 g, 7.9 mmol), Meldrum's acid (1.368 g, 9.5 moles), and DMAP (1.93 g, 15.8 mmol), in anhydrous DCM (10 mL), was cooled to 0 °C. The reaction mixture was treated with a solution of DCC (1.79 g, 8.7 mmol) in DCM (5 mL) and was allowed to stir overnight at rt. The white precipitate was removed by gravity filtration and the filtrate was concentrated at reduced pressure. The residue was dissolved in absolute EtOH (10 mL) and treated with a solution of p-TSA.H_2O (3.68 g, 19 mmol) in absolute EtOH (5 mL).

The solution was heated at refluxed under N_2 for 2 hrs. The EtOH was removed under reduced pressure and EtOAc was added until the residue dissolved. The solution was washed sequentially with H_2O (2 x 15 mL), saturated aqueous $NaHCO_3$ (2 x 10 mL), 1 M aqueous HCl (2 x 10 mL), brine (2 x 10 mL). The organic layer was dried over $MgSO_4$ and evaporated at reduced pressure. The residue was purified by column chromatography (1:1, EtOAc:Pet.Ether) to give a yellow oil, 748 mg (37%).

^{1}H NMR: (500 MHz, CDCl$_3$) (Keto form) δ 7.05 (m, 2H, H3), 6.65 (m, 1H, H1), 4.22 (m, 2H, O*CH$_2$*CH$_3$), 3.94 (s, 2H, *CH$_2$*), 3.81 (s, 6H, O*CH$_3$* x 2), 1.25 (t, *J* = 7.2 Hz, 3H, OCH$_2$*CH$_3$*). ^{1}H NMR data matches literature data[118]. **^{13}C NMR:** (126 MHz, CDCl$_3$) (Keto form) δ 192.1 (C5), 167.4 (C7), 160.9 (C2), 137.8 (C4), 106.1 (C3), 105.9 (C1), 61.3 (CH$_2$), 55.4 (OCH$_3$ x 2), 46.0 (C6), 14.0 (CH$_3$, C1). ^{13}C NMR data matches literature data[118]. **HR-MS:** calcd for C$_{13}$H$_{16}$O$_5$Na m/z: [M + Na]$^+$, 275.0890; found: 275.0888 [Diff (ppm) = - 0.7]. **R$_f$:** 0.73 (1:1, EtOAc:Pet.Ether). **IR (KBr):** 2917 (C-H), 1737 (C=O), 1591 (Ar C-C), 1152 (C-O) cm^{-1}. IR data matches literature data[118].

5.2.59 Synthesis of ethyl 3-(3,5-dinitrophenyl)-3-oxopropanoate (MK11) (56)

A solution of 3,5-dinitrobenzoic acid (1.51 g, 7.1 mmol), Meldrum's acid (1.227 g, 8.5 moles), and DMAP (1.735 g, 14.2 mmol), in anhydrous DCM (10 mL), was cooled to 0 °C. The reaction mixture was treated with a solution of DCC (1.61 g, 7.8 mmol) in DCM (5 mL) and was allowed to stir overnight at rt. The white precipitate was removed by gravity filtration and the filtrate was concentrated at reduced pressure. The residue was dissolved in absolute EtOH (10 mL) and treated with a solution of p-TSA.H_2O (3.31 g, 17.4 mmol) in absolute EtOH (5 mL).

The solution was heated at refluxed under N_2 for 2 hrs. The EtOH was removed under reduced pressure and EtOAc was added until the residue dissolved. The solution was washed sequentially with H_2O (2 x 15 mL), saturated aqueous $NaHCO_3$ (2 x 10 mL), 1 M aqueous HCl (2 x 10 mL), brine (2 x 10 mL). The organic layer was dried over $MgSO_4$ and evaporated at reduced pressure. The residue was purified by column chromatography (1:1, EtOAc:Pet.Ether) to give a yellow solid, 211 mg (11%).

^{1}H NMR: (500 MHz, $CDCl_3$) (Keto form) δ 9.22 (m, 1H, H1), 8.90 (m, 2H, H3), 4.32 (q, J = 7.0 Hz, 2H, OCH_2CH$_3$), 4.12 (s, 2H, CH_2), 1.36 (t, J = 7.0 Hz, 3H, OCH$_2$$CH_3$). **^{13}C NMR:** (126 MHz, $CDCl_3$) (Keto form) δ 193.3 (C5), 172.3 (C2), 165.5 (C7), 148.8 (C4), 127.9 (C1), 125.8 (C3), 61.3 (CH_2), 45.9 (C6), 14.0 (CH_3). **HR-MS:** calcd for $C_{11}H_{10}O_7N_2Na$ m/z: [M + Na]$^+$, 305.0380; found: 305.0388 [Diff (ppm) = 2.6]. **R_f:** 0.8 (1:1, EtOAc:Pet.Ether). **IR (KBr):** 3098 (C-H), 1625 (C=O), 1535 (N-O), 1341 (N-O) cm^{-1}.

5.2.60 Synthesis of 3,5-diethylbenzoic acid (MK3) (57)
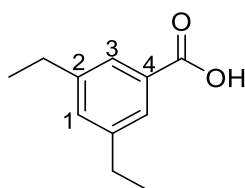
Magnesium turnings (170 mg, 7.0 mmol) were added under a N_2 atmosphere to an oven-dried 2-necked round bottom flask via the septum, followed by a crystal of iodine and anhydrous THF (10 mL). 1-Bromo-3,5-diethylbenzene (0.82 mL, 5.0 mmol) was added to another 2-necked round bottom flask followed by anhydrous THF (5 mL). This solution was added dropwise to the flask containing magnesium and iodine via a cannula. THF (2 mL) was added to the flask to rinse any remaining 1-Bromo-3,5-diethylbenzene solution, and transferred again via the cannula. The reaction was heated at reflux for 1 hr.

Carbon dioxide was added by sublimation of crushed crystals of dry ice. The resulting gaseous carbon dioxide was bubbled into the reaction solution using a cannula. The reaction was added to hot water to remove the remaining THF. A few drops of 6 M HCl were added to the solution until pH paper indicated sufficient acidity. Crystallization was achieved by cooling the solution on ice. The product was purified by filtration to give a white solid, 781 mg (93%).

^{1}H NMR: (500 MHz, CDCl$_3$) δ 7.77 (s, 2H, H3), 7.27 (s, 1H, H1), 2.69 (q, J = 7.6 Hz, 4H, CH$_2$ x 2), 1.27 (t, J = 7.6 Hz, 6H, CH$_3$ x 2). ^{1}H NMR data matches literature data[119]. **^{13}C NMR:** (126 MHz, CDCl$_3$) δ 170.7 (CO), 144.7 (C2), 133.2 (C1), 129.0 (C4), 127.0 (C3), 28.7 (CH$_2$), 15.5 (CH$_3$). ^{13}C NMR data matches literature data[119]. **HR-MS:** calcd for C$_{11}$H$_{15}$O$_2$ m/z: [M + H]$^+$, 179.1072; found: 178.0986 [Diff (ppm) = 4.45]. **IR (KBr):** 2968 (O-H), 1688 (C=O), 1601 (Ar C-C), 1460 (C-H), 1241 (C-O), 936 (O-H) cm^{-1}. IR data matches literature data[119]. **m.p.:** 120 – 122 °C.

5.2.61 Synthesis of 5-(3,5-dimethylphenyl)-2-isopropylpyrazolo[1,5-a]pyrimidin-7(4H)-one (MK6) (58)
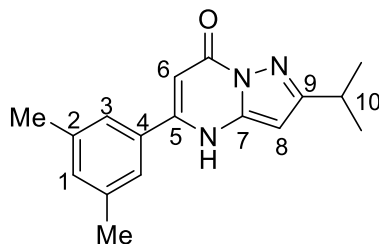
Ethyl 3-(3,5-dimethylphenyl)-3-oxopropanoate (compound **53**) (28 mL, 1.4 mmol) was added to a solution of 3-isopropyl-1H-pyrazol-5-amine (176 mg, 1.4 mmol) dissolved in AcOH (5 mL) and refluxed for 5.5 hrs. Volatiles were removed under reduced pressure. The product was purified by trituration using EtOAc (10 mL) to remove impurities and give a white solid, 165.4 mg (42%).

^{1}H NMR: (500 MHz, CDCl$_3$) δ 9.51 (bs, 1H, NH), 7.25 (s, 2H, H3), 7.13 (s, 1H, H1), 6.00 (m, 2H, H6 & H8), 3.10 (septet, 1H, H10), 2.34 (s, 6H, Ar-CH$_3$ x 2), 1.28 (d, J = 7.0 Hz, 6H, CH$_3$ x 2). **^{13}C NMR:** (126 MHz, CDCl$_3$) δ 157.7 (C4), 141.6 (C2), 139.1 (C7), 132.8 (C5), 132.7 (C1), 124.5 (C3), 94.6 (C6), 86.7 (C8), 28.6 (iPr-CH, C10), 22.5 (iPr-CH$_3$), 21.3 (Ar-CH$_3$). **HR-MS:** calcd for C$_{17}$H$_{20}$N$_3$O m/z: [M + H]$^+$, 281.1528 ; found: 281.1528 [Diff (ppm) = 0.06]. **IR (KBr):** 3199 (N-H), 3081 (C-H), 1651 (C=O), 1595 (N-H), 1291 (Ar C-N) cm^{-1}.

5.2.62 Synthesis of 5-(3,5-diethylphenyl)-2-isopropylpyrazolo[1,5-a]pyrimidin-7(4*H*)-one (MK5) (59)
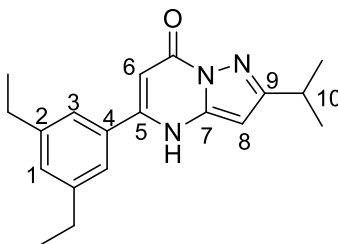
Ethyl 3-(3,5-diethylphenyl)-3-oxopropanoate (compound **54**) (50 mg, 0.2 mmol) was added to a solution of 3-isopropyl-1*H*-pyrazol-5-amine (25 mg, 0.2 mmol) dissolved in AcOH (5 mL) and refluxed overnight. Volatiles were removed under reduced pressure. The product was purified by trituration using EtOAc (5 mL) followed column chromatography (elution gradient 7:3 EtOAc:DCM to EtOAc: DCM 9:1) to give a light brown solid, 12.2 mg (20%).

¹H NMR: (500 MHz, CDCl₃) δ 11.00 (bs, 1H, NH), 7.37 (s, 2H, H3), 7.12 (s, 1H, H1), 6.03 (m, 2H, H6 & H8), 2.98 (bs, 1H, H10), 2.60 (q, *J* = 7.5 Hz, 4H, *CH₂*CH₃ x 2), 1.16 (m, 12H, CH₃ x 4). **¹³C NMR:** (126 MHz, CDCl₃) δ 145.4 (C2), 132.8 (C5), 130.5 (C1), 123.8 (C3), 94.3 (C6), 87.0 (C8), 28.7 (*CH₂*CH₃), 28.5 (*i*Pr-CH, H10), 22.4 (*i*Pr-CH₃), 15.3 (CH₂*CH₃*). **R_f:** 0.44 (7:3 EtOAc:DCM). **IR (KBr):** 2963 (N-H), 2924 (C-H), 1661 (C=O), 1619 (N-H), 1564 (Ar C-C) cm⁻¹.

5.2.63 Synthesis of 5-(3,5-dimethoxyphenyl)-2-isopropylpyrazolo[1,5-a]pyrimidin-7(4*H*)-one (MK13) (60)
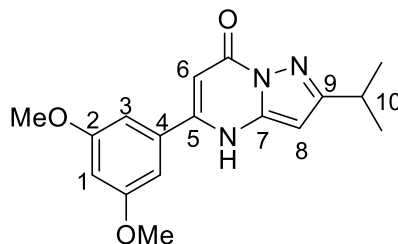
Ethyl 3-(3,5-dimethoxyphenyl)-3-oxopropanoate (compound **55**) (200 mg, 0.79 mmol) was added to a solution of 3-isopropyl-1*H*-pyrazol-5-amine (100 mg, 0.79 mmol) dissolved in AcOH (5 mL) and refluxed for 20 hrs. Volatiles were removed under reduced pressure. The product was purified by column chromatography (100% EtOAc) to give a yellow-brown solid, 45 mg (18%).

¹H NMR: (500 MHz, DMSO) δ 10.19 (s, 1H, NH), 7.08 (s, 2H, H3), 6.60 (s, 1H, H1), 6.07 (s, 1H, H6), 6.03 (s, 1H, H8), 3.83 (s, 6H, O-C*H₃* x 2), 3.13 – 3.06 (m, 1H, H10), 1.24 (d, *J* = 6.8 Hz, 6H, C*H₃* x 2). **¹³C NMR:** (126 MHz, DMSO) δ 162.4 (C9), 161.0 (C2), 153.7 (C4), 147.5 (C7), 138.8 (C5), 105.4 (C3), 102.1 (C1), 91.0 (C6), 88.5 (C8), 55.9 (O-C*H₃* x 2), 28.2 (C10), 23.2 (C*H₃* x 2). **HR-MS:** calcd for $C_{17}H_{20}N_3O_3$ m/z: [M + H]⁺, 314.1499; found: 314.1511 [Diff (ppm) = 3.8]. **R_f:** 0.59 (100% EtOAc). **IR (KBr)**: 2962 (C-H), 1660 (C=O), 1595 (N-H), 1542 (C-C), 1152 (C-O) cm⁻¹.

5.2.64 Synthesis of 5-(3,5-dinitrophenyl)-2-isopropylpyrazolo[1,5-a]pyrimidin-7(4*H*)-one (MK49) (61)
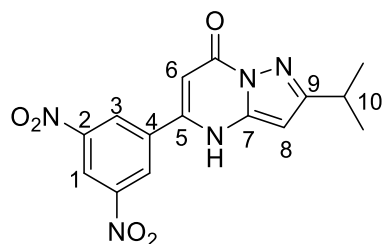
Prepared from 4-methyl-3-oxopentanenitrile (50 mg, 0.45 mmol) and ethyl 3-(3,5-dinitrophenyl)-3-oxopropanoate (compound **56**) (127 mg, 0.45 mmol) and following the general procedure described in section **5.2.34**. Volatiles were removed under reduced pressure and the reaction mixture was purified by column chromatography (1:1, EtOAc:Pet.Ether) to give a red solid, 20 mg (13%).

^{1}H NMR: (500 MHz, DMSO) δ 12.56 (s, 1H, NH), 9.07 (s, 2H, H3), 8.92 (s, 1H, H1), 6.09 (s, 1H, H8), 6.01 (s, 1H, H6), 2.79 (s, 1H, H10), 1.26 (d, *J* = 6.9 Hz, 6H, 2 x C*H₃*). ^{13}**C NMR:** (126 MHz, DMSO) δ 127.3 (C3), 119.8 (C1), 96.9 (C6), 22.7 (2 x C*H₃*), 18.9 (C10). **R$_f$:** 0.43 (1:1, EtOAc:Pet.Ether). **IR (KBr)**: 3106 (C-H), 1618 (C=O), 1533 (N-O), 1341 (N-O), 727 (C-H) cm^{-1}.

5.2.65 Synthesis of 5-(3,5-bis(trifluoromethyl)phenyl)-2-(2-chlorophenyl)pyrazolo[1,5-*a*]pyrimidin-7(4*H*)-one (MK80) (62)
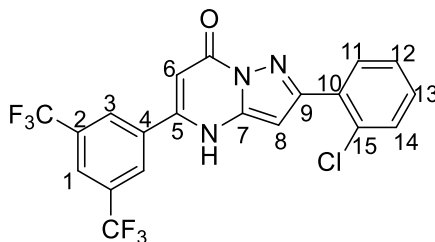
Prepared from 3-(2-chlorophenyl)-3-oxopropanenitrile (162 mg, 0.9 mmol) and ethyl 3-(3,5-bis(trifluoromethyl)phenyl)-3-oxopropanoate (295 mg, 0.9 mmol) and following the general procedure described in section **5.2.34**. Volatiles were removed under reduced pressure and the product was purified by column chromatography (3:2, EtOAc:DCM) to give a green solid, 12 mg (3%).

¹H NMR: (500 MHz, DMSO) δ 8.73 (s, 2H, H3), 8.15 (s, 1H, H1), 8.03 (d, *J* = 8.4 Hz, 1H, H14), 7.61 (d, *J* = 7.2 Hz, 1H, H11), 7.56 – 7.42 (m, 2H, H12, H13), 6.69 (s, 1H, CH), 6.33 (s, 1H, CHCO). **¹³C NMR:** (126 MHz, DMSO) δ 152.9 (C4), 144.8 (C15), 131.6 (C14), 130.6 (C11), 129.6 (C12), 128.5 (C5), 127.5 (C13), 127.2 (C3), 122.1 (C1), 94.8 (C8), 89.4 (C6). **HR-MS:** calcd for $C_{20}H_{10}ClN_3OF_6Na$ m/z: [M + Na]⁺, 480.0309; found: 480.0314 [Diff (ppm) = 1.04]. **R$_f$:** 0.3 (3:2, EtOAc:DCM). **IR (ATR):** 2923 (aromatic C-H), 1609 (C=C), 1540 (C=C), 1276 (C-F), 1126 (C-F) cm⁻¹.

5.2.66 Synthesis of 5-(3,5-bis(trifluoromethyl)phenyl)-2-(2-methoxyphenyl)pyrazolo[1,5-*a*]pyrimidin-7(4*H*)-one (MK79) (63)
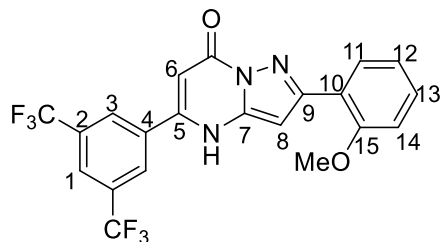
Prepared from 3-(2-methoxyphenyl)-3-oxopropanenitrile (158 mg, 0.9 mmol) and ethyl 3-(3,5-bis(trifluoromethyl)phenyl)-3-oxopropanoate (295 mg, 0.9 mmol) and following the general procedure described in section **5.2.34**. Volatiles were removed under reduced pressure and the product was purified by column chromatography (3:2, EtOAc:n-hexane) to give a yellow solid, 66 mg (16%).

^{1}H NMR: (500 MHz, DMSO) δ 8.67 (s, 2H, H3), 8.15 – 8.04 (m, 2H, H1, H14), 7.34 (*pseudo* t, J = 7.8 Hz, 1H, H12), 7.13 (d, J = 8.2 Hz, 1H, H11), 7.02 (t, J = 7.4 Hz, 1H, H13), 6.72 (s, 1H, CH), 6.31 (s, 1H, CHCO), 3.91 (s, 3H, CH$_3$). **^{13}C NMR:** (126 MHz, DMSO) δ 159.1 (C=O), 157.5 (C15), 152.9 (C4), 152.1 (C7), 149.6 (C9), 130.9 (q, J = 32.7 Hz, CF$_3$), 129.7 (C12), 129.5 (C14), 127.2 (C3), 124.0 (q, J = 273.2 Hz, C2), 123.1 (C10), 122.1 (C1), 120.8 (C13), 112.4 (C11), 95.4 (C8), 89.1 (C6), 56.1 (CH$_3$). **HR-MS:** calcd for C$_{21}$H$_{13}$N$_3$O$_2$F$_6$Na m/z: [M + Na]$^+$, 476.0804; found: 476.0817 [Diff (ppm) = 2.8]. **R$_f$:** 0.13 (3:2, EtOAc:n-hexane). **IR (ATR):** 3167 (aromatic C-H), 1602 (C=C), 1582 (C=C), 1275 (C-F), 1124 (C-F) cm^{-1}.

5.2.67 Synthesis of 5-(3,5-bis(trifluoromethyl)phenyl)-2-(3-chlorophenyl)pyrazolo[1,5-*a*]pyrimidin-7(4*H*)-one (MK82) (64)
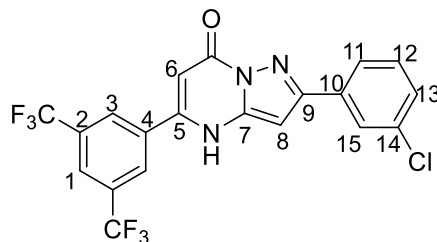
Prepared from 3-(3-chlorophenyl)-3-oxopropanenitrile (162 mg, 0.9 mmol) and ethyl 3-(3,5-bis(trifluoromethyl)phenyl)-3-oxopropanoate (295 mg, 0.9 mmol) and following the general procedure described in section **5.2.34**. Volatiles were removed under reduced pressure and the product was purified by column chromatography (3:2, EtOAc:DCM) to give a green solid, 34 mg (8%).

^{1}H NMR: (500 MHz, DMSO) δ 8.65 (s, 2H, H3), 8.09 (s, 1H, H1), 8.02 (s, 1H, H15), 7.92 (d, *J* = 7.9 Hz, 1H, H13), 7.48 (*pseudo* t, *J* = 7.8 Hz, 1H, H12), 7.39 (d, *J* = 7.0 Hz, 1H, H11), 6.67 (s, 1H, CH), 6.23 (s, 1H, CHCO). **^{13}C NMR:** (126 MHz, DMSO) δ 152.9 (C4), 130.8 (C12), 127.8 (C11), 127.2 (C3), 125.8 (C15), 125.1 (C2), 124.9 (C13), 121.9 (C1), 90.8 (C8), 89.6 (C6). **HR-MS:** calcd for $C_{20}H_{10}ClN_3OF_6Na$ m/z: [M + Na]$^+$, 480.0309; found: 480.0317 [Diff (ppm) = 1.7]. **R$_f$:** 0.25 (3:2, EtOAc:DCM). **IR (ATR):** 2924 (aromatic C-H), 1603 (C=C), 1541 (C=C), 1274 (C-F), 1125 (C-F), 768 (C-Cl) cm^{-1}.

5.2.68 Synthesis of 5-(3,5-bis(trifluoromethyl)phenyl)-2-(3-methoxyphenyl)pyrazolo[1,5-*a*]pyrimidin-7(4*H*)-one (MK81) (65)
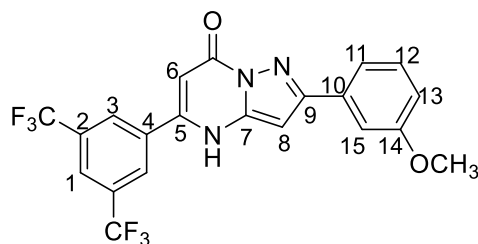
Prepared from 3-(3-methoxyphenyl)-3-oxopropanenitrile (158 mg, 0.9 mmol) and ethyl 3-(3,5-bis(trifluoromethyl)phenyl)-3-oxopropanoate (295 mg, 0.9 mmol) and following the general procedure described in section **5.2.34**. Volatiles were removed under reduced pressure and the product was purified by column chromatography (3:2, EtOAc:DCM) to give a green solid, 28 mg (7%).

^{1}H NMR: (500 MHz, DMSO) δ 8.65 (s, 2H, H3), 8.12 (s, 1H, H1), 7.61 – 7.49 (m, 2H, H13, H15), 7.36 (*pseudo* t, *J* = 7.8 Hz, 1H, H12), 6.92 (dd, *J* = 8.6, 2.1 Hz, 1H, H11), 6.67 – 6.59 (m, 1H, CH), 6.29 – 6.21 (m, 1H, CHCO), 3.84 (s, 3H, CH$_3$). **^{13}C NMR:** (126 MHz, DMSO) δ 159.9 (C14), 152.6 (C7), 152.4 (C4), 135.6 (C10), 130.0 (C12), 128.5 (C5), 127.3 (C3), 122.4 (C1), 118.7 (C15), 114.2 (C11), 111.5 (C13), 90.9 (C8), 89.8 (C6), 55.6 (CH$_3$). **HR-MS:** calcd for C$_{21}$H$_{13}$N$_3$O$_2$F$_6$Na m/z: [M + Na]$^+$, 476.0804; found: 476.0795 [Diff (ppm) = -1.89]. **R$_f$:** 0.27 (3:2, EtOAc:DCM). **IR (ATR):** 2939 (aromatic C-H), 1603 (C=C), 1540 (C=C), 1476 (alkane C-H), 1273 (C-F), 1125 (C-F) cm^{-1}.

5.2.69 Synthesis of 5-(3,5-bis(trifluoromethyl)phenyl)-2-(3-nitrophenyl)pyrazolo[1,5-*a*]pyrimidin-7(4*H*)-one (MK83) (66)
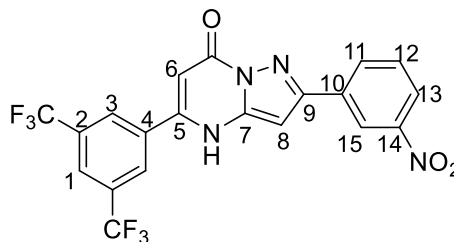
Prepared from 3-(3-nitrophenyl)-3-oxopropanenitrile (171 mg, 0.9 mmol) and ethyl 3-(3,5-bis(trifluoromethyl)phenyl)-3-oxopropanoate (295 mg, 0.9 mmol) and following the general procedure described in section **5.2.34**. Volatiles were removed under reduced pressure and the product was purified by column chromatography (100% EtOAc) to give a yellow solid, 28 mg (7%).

^{1}H NMR: (500 MHz, MeOD) δ 8.42 (s, 1H, H15), 8.37 (s, 2H, H3), 7.96 (s, 1H, H1), 7.93 – 7.82 (m, 2H, H11, H13), 7.38 (*pseudo* t, *J* = 7.9 Hz, 1H, H12), 6.27 (s, 1H, CH), 6.20 (s, 1H, CHCO). **^{13}C NMR:** (126 MHz, MeOD) δ 155.9 (C=O), 141.9 (C4), 132.5 (C13), 131.5 (C14), 129.1 (C12), 127.3 (C3), 127.2 (C2), 124.4 (CF$_3$), 122.3 (C11), 122.1 (C1), 120.4 (C15), 91.4 (C8), 90.5 (C6). **HR-MS:** calcd for C$_{20}$H$_{10}$N$_4$O$_3$F$_6$Na m/z: [M + Na]$^+$, 491.0549; found: 491.0562 [Diff (ppm) = 2.5]. **R$_f$:** 0.16 (100% EtOAc). **IR (ATR):** 3353 (N-H), 2923 (aromatic C-H), 1607 (C=C), 1533 (C=C), 1347 (N-O), 1277 (C-F), 1123 (C-F) cm^{-1}.

5.2.70 Synthesis of 5-(3,5-bis(trifluoromethyl)phenyl)-2-(p-tolyl)pyrazolo[1,5-a]pyrimidin-7(4H)-one (MK71) (67)
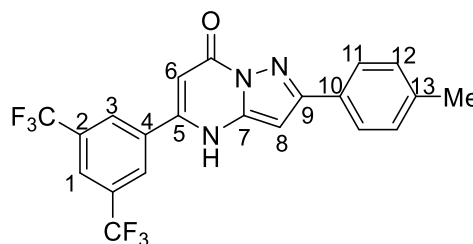
Prepared from 4-methylbenzoylacetonitrile (72 mg, 0.45 mmol) and ethyl 3-(3,5-bis(trifluoromethyl)phenyl)-3-oxopropanoate (148 mg, 0.45 mmol) and following the general procedure described in section **5.2.34**. Volatiles were removed under reduced pressure and the product was purified by column chromatography (3:2, EtOAc:DCM) to give a white solid, 17 mg (9%).

^{1}H NMR: (500 MHz, DMSO) δ 12.83 (s, 1H, NH), 8.56 (s, 2H, H3), 8.35 (s, 1H, H1), 7.92 (d, J = 7.9 Hz, 2H, H11), 7.32 (d, J = 7.9 Hz, 2H, H12), 6.68 (s, 1H, CH), 6.39 (s, 1H, CHCO), 2.38 (s, 3H, CH_3). **^{13}C NMR:** (126 MHz, DMSO) δ 153.9 (C10), 147.4 (C4), 143.9 (C9), 138.9 (C13), 135.7 (C5), 129.8 (C12), 128.9 (C3), 126.7 (C11), 124.6 (C1), 122.4 (C2), 95.8 (C6), 87.2 (C8), 21.4 (CH$_3$). **HR-MS:** calcd for C$_{21}$H$_{12}$N$_3$OF$_6$ m/z: [M - H]$^+$, 436.0890; found: 436.0902 [Diff (ppm) = 2.7]. **R$_f$:** 0.14 (3:2, EtOAc:DCM). **IR (ATR):** 3481 (N-H), 2923 (aromatic C-H), 1656 (C=O), 1605 (C=C), 1274 (C-F), 1122 (C-F) cm^{-1}.

5.2.71 Synthesis of 5-(3,5-bis(trifluoromethyl)phenyl)-2-(4-fluorophenyl)pyrazolo[1,5-*a*]pyrimidin-7(4*H*)-one (MK72) (68)
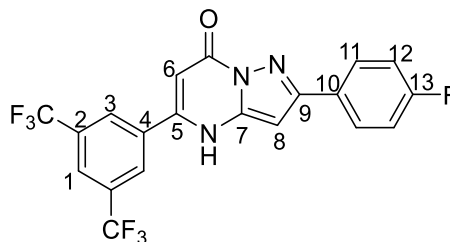
Prepared from 4-fluorobenzoylacetonitrile (75 mg, 0.45 mmol) and ethyl 3-(3,5-bis(trifluoromethyl)phenyl)-3-oxopropanoate (148 mg, 0.45 mmol) and following the general procedure described in section **5.2.34**. Volatiles were removed under reduced pressure and the product was purified by column chromatography (3:2, EtOAc:Pet. Ether) to give a yellow solid, 12 mg (6%).

^{1}H NMR: (500 MHz, DMSO) δ 8.62 (s, 2H, H3), 8.36 (bs, 1H, NH), 8.19 (s, 1H, H1), 8.02 (dd, *J* = 8.5, 5.7 Hz, 2H, H11), 7.27 (*pseudo* t, *J* = 8.8 Hz, 2H, H12), 6.65 (s, 1H, CH), 6.33 (s, 1H, CHCO). **^{13}C NMR:** (126 MHz, DMSO) δ 162.7 (d, J_{CF} = 245.6 Hz, C13), 152.2 (C9), 150.7 (C4), 149.7 (C7), 134.0 (C5), 131.1 (q, J_{CF} = 33.0 Hz, C10), 128.6 (d, J_{CF} = 8.0 Hz, C11), 127.9 (C3), 123.8 (q, *J* = 273.6 Hz, C2), 122.7 (C1), 115.80 (d, J_{CF} = 21.6 Hz, C12), 92.1 (C6), 89.4 (C8). **HR-MS:** calcd for $C_{20}H_{10}F_7N_3ONa$ m/z: [M - H]$^+$, 464.0604; found: 464.0604 [Diff (ppm) = -0.1]. **R$_f$:** 0.1 (3:2, EtOAc:DCM). **IR (ATR):** 1672 (C=O), 1607 (C=C), 1276 (C-F), 1125 (C-F) cm^{-1}.

5.2.72 Synthesis of 5-(3,5-bis(trifluoromethyl)phenyl)-2-(4-chlorophenyl)pyrazolo[1,5-*a*]pyrimidin-7(4*H*)-one (MK75) (69)
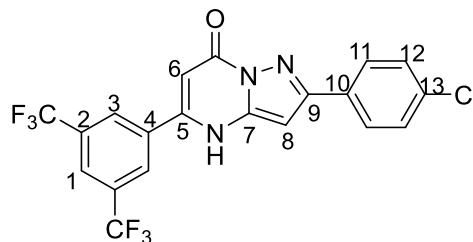
Prepared from 4-chlorobenzoylacetonitrile (162 mg, 0.9 mmol) and ethyl 3-(3,5-bis(trifluoromethyl)phenyl)-3-oxopropanoate (295 mg, 0.9 mmol) and following the general procedure described in section **5.2.34**. Volatiles were removed under reduced pressure and the product was purified by column chromatography (3:2, EtOAc:DCM) to give a yellow solid, 30 mg (7%).

¹H NMR: (500 MHz, DMSO) δ 8.65 (s, 2H, H3), 8.12 (s, 1H, H1), 7.97 (d, *J* = 8.4 Hz, 2H, H12), 7.48 (d, *J* = 8.4 Hz, 2H, H11), 6.63 (s, 1H, CH), 6.28 (s, 1H, CHCO). **¹³C NMR:** (126 MHz, DMSO) δ 128.9 (C11), 128.1 (C12), 127.4 (C3), 122.9 (C1), 90.4 (C8), 90.1 (C6). **HR-MS:** calcd for $C_{20}H_{10}ClN_3OF_6Na$ m/z: [M + Na]⁺, 480.0309; found: 480.0312 [Diff (ppm) = 0.62]. **R$_f$:** 0.14 (3:2, EtOAc:DCM). **IR (ATR):** 3091 (aromatic C-H), 1603 (C=C), 1541 (C=C), 1274 (C-F), 1125 (C-F), 806 (C-Cl) cm⁻¹.

5.2.73 Synthesis of 5-(3,5-bis(trifluoromethyl)phenyl)-2-(4-bromophenyl)pyrazolo[1,5-*a*]pyrimidin-7(4*H*)-one (MK73) (70)
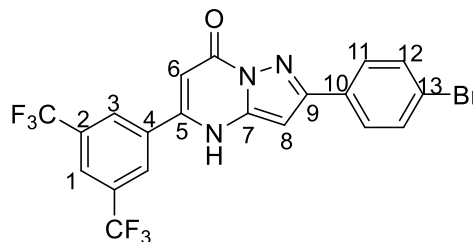
Prepared from 4-bromobenzoylacetonitrile (202 mg, 0.9 mmol) and ethyl 3-(3,5-bis(trifluoromethyl)phenyl)-3-oxopropanoate (295 mg, 0.9 mmol) and following the general procedure described in section **5.2.34**. Volatiles were removed under reduced pressure and the product was purified by column chromatography (3:2, EtOAc:n-hexane) to give a green-yellow solid, 47 mg (10%).

^{1}H NMR: (500 MHz, DMSO) δ 8.66 (s, 2H, H3), 8.09 (s, 1H, H1), 7.94 (d, *J* = 8.3 Hz, 2H, H12), 7.62 (d, *J* = 8.3 Hz, 2H, H11), 6.65 (s, 1H, CH), 6.28 (s, 1H, CHCO). **^{13}C NMR:** (126 MHz, DMSO) δ 153.4 (C7), 152.7 (C4), 151.3 (C9), 143.1 (C5), 134.1 (d, *J*$_{CBr}$ = 5.9 Hz, C13), 131.8 (C11), 128.5 (C12), 127.2 (C3), 124.0 (q, *J*$_{CF}$ = 273.2 Hz, C2), 122.1 (C1), 121.4 (C10), 90.9 (C8), 89.6 (C6). **HR-MS:** calcd for $C_{20}H_{10}BrN_3OF_6Na$ m/z: [M + Na]$^+$, 523.9804; found: 523.98526 [Diff (ppm) = 4.2]. **R$_f$:** 0.12 (3:2, EtOAc:n-hexane). **IR (ATR):** 1604 (C=C), 1541 (C=C), 1275 (C-F), 1128 (C-F) cm^{-1}.

5.2.74 Synthesis of 5-(3,5-bis(trifluoromethyl)phenyl)-2-(4-methpxyphenyl)pyrazolo[1,5-*a*]pyrimidin-7(4*H*)-one (MK74) (71)
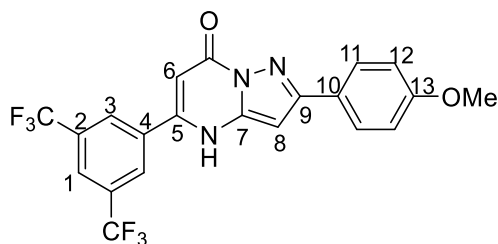
Prepared from 4-methoxybenzoylacetonitrile (158 mg, 0.9 mmol) and ethyl 3-(3,5-bis(trifluoromethyl)phenyl)-3-oxopropanoate (295 mg, 0.9 mmol) and following the general procedure described in section **5.2.34**. Volatiles were removed under reduced pressure and the product was purified by column chromatography (3:2, EtOAc:n-hexane) to give a yellow-brown solid, 77 mg (19%).

^{1}H NMR: (500 MHz, DMSO) δ 8.66 (s, 2H, H3), 8.10 (s, 1H, H1), 7.86 (dd, *J* = 8.6, 4.6 Hz, 2H, H12), 6.94 (dd, *J* = 11.8, 8.7 Hz, 2H, H11), 6.53 (s, 1H, CH), 6.32 (d, *J* = 16.1 Hz, 1H, CHCO), 3.76 (d, *J* = 8.4 Hz, 3H, CH$_3$). **^{13}C NMR:** (126 MHz, DMSO) δ 159.6 (C13), 159.2 (C7), 153.4 (C4), 152.8 (d, *J* = 20.7 Hz, C10), 142.8 (C5), 127.9 (d, *J* = 8.2 Hz, C12), 127.2 (C3), 127.0 (C9), 124.0 (q, *J$_{CF}$* = 273.6 Hz, C2), 122.2 (C1), 114.2 (d, *J* = 7.2 Hz, C11), 90.5 (C8), 89.3 (C6), 55.5 (d, *J* = 4.1 Hz, CH$_3$). **HR-MS:** calcd for C$_{21}$H$_{13}$N$_3$O$_2$F$_6$Na m/z: [M + Na]$^+$, 476.0804; found: 476.0813 [Diff (ppm) = 1.9]. **R$_f$:** 0.1 (3:2, EtOAc:n-hexane). **IR (ATR):** 1612 (C=C), 1524 (C=C), 1274 (C-F), 1174 (C-O), 1128 (C-F) cm^{-1}.

5.2.75 Synthesis of 5-(3,5-bis(trifluoromethyl)phenyl)-2-(4-nitrophenyl)pyrazolo[1,5-*a*]pyrimidin-7(4*H*)-one (MK76) (72)
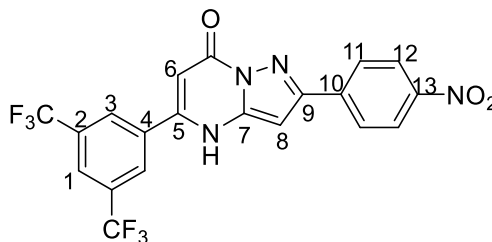
Prepared from 5-(4-nitrophenyl)-2*H*-pyrazol-3-amine (184 mg, 0.9 mmol) and ethyl 3-(3,5-bis(trifluoromethyl)phenyl)-3-oxopropanoate (295 mg, 0.9 mmol) in a microwave tube (10 mL) with AcOH (27 mg, 0.5 mmol) in MeOH (2 mL) and subjected to microwave irradiation (100 W, 150 °C) for 2 hours. Volatiles were removed under reduced pressure and the product was purified by trituration with cold MeOH to give a yellow solid, 330 mg (78%).

^{1}H NMR: (500 MHz, DMSO) δ 12.99 (s, 1H, NH), 8.56 (s, 2H, H3), 8.46 – 8.24 (m, 5H, H1, H11, H12), 6.91 (s, 1H, CH), 6.46 (s, 1H, CHCO). **^{13}C NMR:** (126 MHz, DMSO) δ 156.4 (C=O), 151.9 (C9), 148.0 (C13), 147.6 (C4), 143.8 (C7), 139.1 (C10), 135.3 (C5), 131.4 (q, *J* = 33.4 Hz, C2), 129.1 (C3), 127.8 (C11), 125.0 (C1), 124.5 (C12), 123.5 (q, *J* = 273.6 Hz, CF$_3$), 96.6 (C6), 88.5 (C8). **HR-MS:** calcd for $C_{20}H_{10}N_4O_3F_6Na$ m/z: [M + Na]$^+$, 491.0549; found: 491.0544 [Diff (ppm) = -1.2]. **IR (ATR):** 2927 (aromatic C-H), 1667 (C=O), 1612 (C=C), 1516 (N-O), 1438 (C=C), 1364 (N-O), 1129 (C-F).

5.2.76 Synthesis of 5-(3,5-bis(trifluoromethyl)phenyl)-2-(4-trifluoromethyl)phenyl)pyrazolo[1,5-*a*]pyrimidin-7(4*H*)-one (MK78) (73)
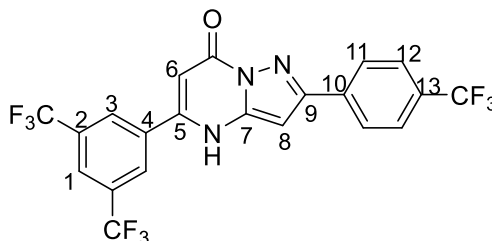
Prepared from 4-trifluoromethylbenzoylacetonitrile (192 mg, 0.9 mmol) and ethyl 3-(3,5-bis(trifluoromethyl)phenyl)-3-oxopropanoate (295 mg, 0.9 mmol) and following the general procedure described in section **5.2.34**. Volatiles were removed under reduced pressure and the product was purified by column chromatography (3:2, EtOAc:n-hexane) to give a green solid, 49 mg (11%).

^{1}H NMR: (500 MHz, DMSO) δ 8.71 (s, 2H, H3), 8.20 – 8.14 (m, 3H, H1, H12), 7.77 (d, *J* = 8.1 Hz, 2H, H11), 6.74 (s, 1H, CH), 6.36 (s, 1H, CHCO). **^{13}C NMR:** (126 MHz, DMSO) δ 159.0 (C=O), 153.3 (C4), 153.1 (C7), 151.8 (d, *J* = 32.8 Hz, C10), 150.9 (C9), 142.9 (C5), 137.5 (q, *J* = 313.3 Hz, CF$_3$), 130.9 (q, *J* = 32.8 Hz, CF$_3$), 127.3 (m, C3), 126.9 (C11), 125.6 (d, *J* = 6.9 Hz, C12), 125.1 (C2), 124.9 (q, *J* = 274.8 Hz, C13), 122.9 (C-CF$_3$), 122.2 (C1), 91.6 (C8), 89.8 (C6). **HR-MS:** calcd for C$_{21}$H$_{10}$N$_3$OF$_9$Na m/z: [M + Na]$^+$, 514.0572; found: 514.0576 [Diff (ppm) = 0.8]. **R$_f$:** 0.12 (3:2, EtOAc:n-hexane). **IR (ATR):** 1604 (C=C), 1527 (C=C), 1322 (C-F), 1274 (C-F), 1109 (C-F) cm^{-1}.

5.2.77 Synthesis of 5-(3,5-bis(trifluoromethyl)phenyl)-2-(furan-2-yl)pyrazolo[1,5-*a*]pyrimidin-7(4*H*)-one (MK84) (74)
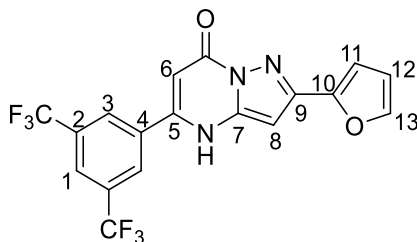
Prepared from 3-(furan-2-yl)-3-oxopropanenitrile (122 mg, 0.9 mmol) and ethyl 3-(3,5-bis(trifluoromethyl)phenyl)-3-oxopropanoate (295 mg, 0.9 mmol) and following the general procedure described in section **5.2.34**. Volatiles were removed under reduced pressure and the product was purified by column chromatography (3:2, EtOAc:DCM) to give a red-brown solid, 28 mg (8%).

¹H NMR: (500 MHz, MeOD) δ 8.49 (s, 2H, H3), 8.10 (s, 1H, H1), 7.48 (s, 1H, H13), 6.89 (s, 1H, H11), 6.50 (s, 1H, CH), 6.47 (s, 1H, H12), 6.33 (s, 1H, CHCO). **¹³C NMR:** (126 MHz, MeOD) δ 154.0 (C4), 146.3 (C9), 142.5 (C13), 132.5 (C7), 129.8 (C10), 127.3 (C3), 124.5 (CF₃), 122.5 (C1), 110.1 (C12), 107.6 (C11), 91.3 (C6), 89.0 (C8). **HR-MS:** calcd for $C_{18}H_{10}N_3O_2F_6$ m/z: [M + H]⁺, 414.0672; found: 414.0654 [Diff (ppm) = -4.35]. **R_f:** 0.22 (3:2, EtOAc:DCM). **IR (ATR):** 3111 (aromatic C-H), 1613 (C=C), 1542 (C=C), 1277 (C-F), 1169 (C-O), 1126 (C-F) cm⁻¹.

5.2.78 Synthesis of 5-(3,5-bis(trifluoromethyl)phenyl)-2-(thiophen-2-yl)pyrazolo[1,5-*a*]pyrimidin-7(4*H*)-one (MK85) (75)
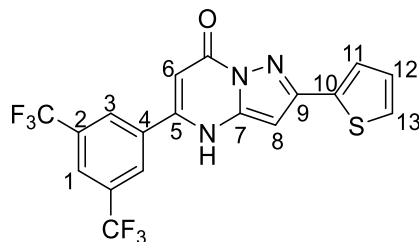
Prepared from 3-oxo-3-(thiophen-2-yl)propanenitrile (136 mg, 0.9 mmol) and ethyl 3-(3,5-bis(trifluoromethyl)phenyl)-3-oxopropanoate (295 mg, 0.9 mmol) and following the general procedure described in section **5.2.34**. Volatiles were removed under reduced pressure and the product was purified by column chromatography (3:2, EtOAc:DCM to 100% EtOAc) to give a yellow solid, 29 mg (8%).

¹H NMR: (500 MHz, DMSO) δ 8.64 (s, 2H, H3), 8.08 (s, 1H, H1), 7.89 (bs, 1H, NH), 7.55 (s, 1H, H13), 7.51 (d, *J* = 4.8 Hz, 1H, H12), 7.16 – 7.10 (m, 1H, H11), 6.47 (s, 1H, CH), 6.22 (s, 1H, CHCO). **¹³C NMR:** (126 MHz, DMSO) δ 153.2 (C7), 152.9 (C4), 148.0 (C9), 143.1 (C5), 138.5 (C10), 130.9 (q, *J* = 32.6 Hz, CF$_3$), 128.0 (C11), 127.2 (C3), 125.8 (C12), 125.0 (C13), 124.0 (q, *J* = 273.2 Hz, C2), 122.0 (C1), 90.3 (C8), 89.7 (C6). **HR-MS:** calcd for C$_{18}$H$_9$N$_3$OF$_6$SNa m/z: [M + Na]⁺, 452.0263; found: 452.0272 [Diff (ppm) = 1.99]. **R$_f$:** 0.36 (3:2, EtOAc:DCM). **IR (ATR):** 2924 (aromatic C-H), 1604 (C=C), 1533 (C=C), 1275 (C-F), 1125 (C-F) cm⁻¹.

5.2.79 Synthesis of 5-(3,5-bis(trifluoromethyl)phenyl)-2-(pyridin-3-yl)pyrazolo[1,5-*a*]pyrimidin-7(4*H*)-one (MK86) (76)
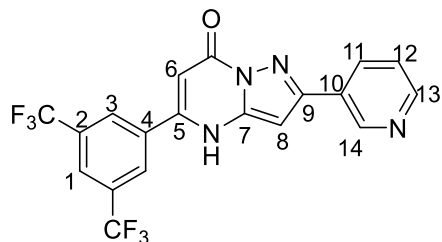
Prepared from 3-oxo-3-(pyridin-3-yl)propanenitrile (132 mg, 0.9 mmol) and ethyl 3-(3,5-bis(trifluoromethyl)phenyl)-3-oxopropanoate (295 mg, 0.9 mmol) and following the general procedure described in section **5.2.34**. Volatiles were removed under reduced pressure and the product was purified by column chromatography (9:1, DCM:MeOH) to give an off-white solid, 12 mg (3%).

¹H NMR: (500 MHz, DMSO) δ 9.20 (s, 1H, H14), 8.67 (s, 2H, H3), 8.55 (dd, *J* = 4.7, 1.6 Hz, 1H, H11), 8.37 – 8.31 (m, 1H, H13), 8.10 (s, 1H, H1), 7.63 – 7.59 (m, 1H, NH), 7.48 (ddd, *J* = 7.9, 4.8, 0.7 Hz, 1H, H12), 7.34 – 7.29 (m, 1H, NH), 6.74 (s, 1H, CH), 6.27 (s, 1H, CHCO).

¹³C NMR: (126 MHz, DMSO) δ 153.3 (C7), 152.9 (C4), 150.5 (C10), 149.7 (C9), 149.2 (C11), 147.6 (C14), 133.4 (C13), 127.1 (C3), 125.0 (C2), 124.1 (C12), 122.1 (C1), 90.8 (C8), 89.5 (C6). **HR-MS:** calcd for $C_{19}H_{11}N_4OF_6$ m/z: [M + H]⁺, 447.0651; found: 447.0652 [Diff (ppm) = 1.65]. **R$_f$:** 0.38 (9:1, DCM:MeOH). **IR (ATR):** 3094 (Ar C-H), 1607 (N-H), 1541 (C=N), 1364 (C-N), 1277 (C-F), 1126 (C-F).

Spectra

6.01 Spectra for 4-(thiophen-2-yl)-1-(4-(4-(trifluoromethyl)phenyl)piperazin-1-yl)butan-1-one RTC1 (MK24) (1)
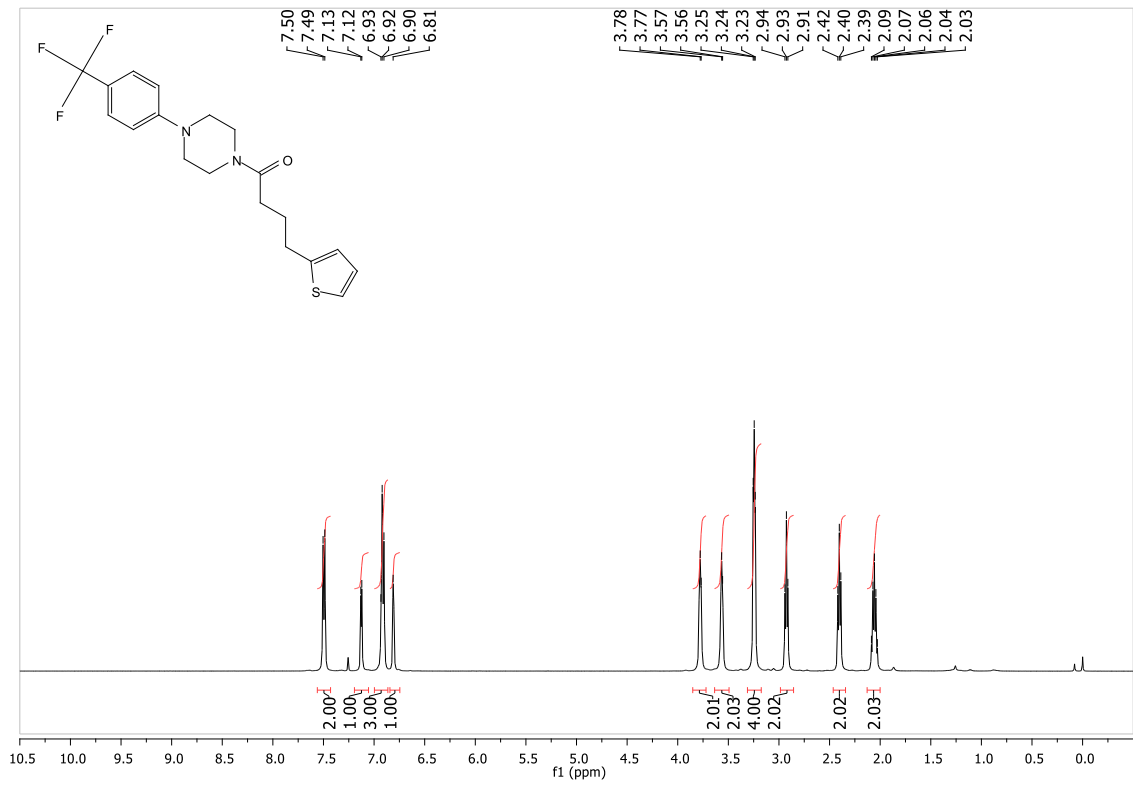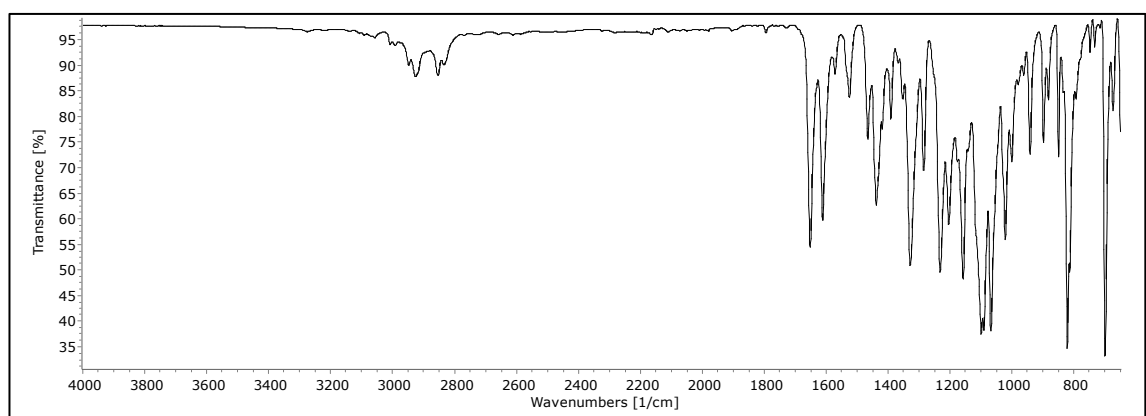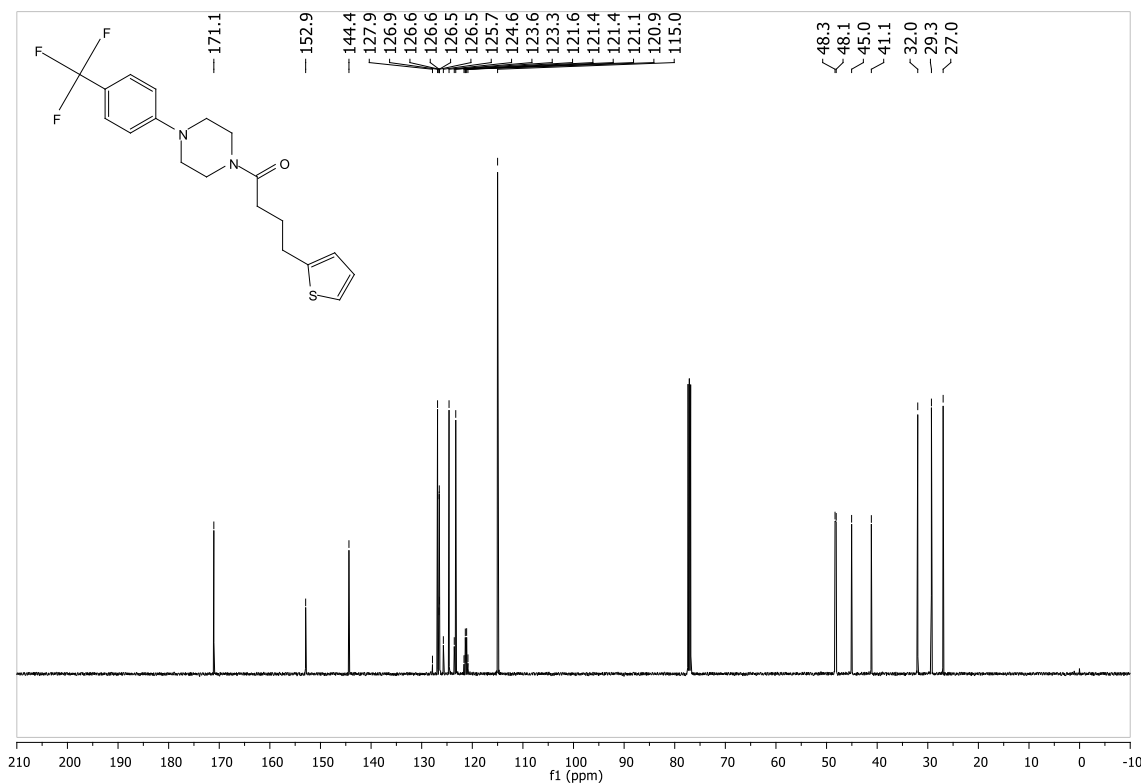
6.02 Spectra for 1-(4-(trifluoromethyl)phenyl)piperazine (MK17) (RD269) (2)
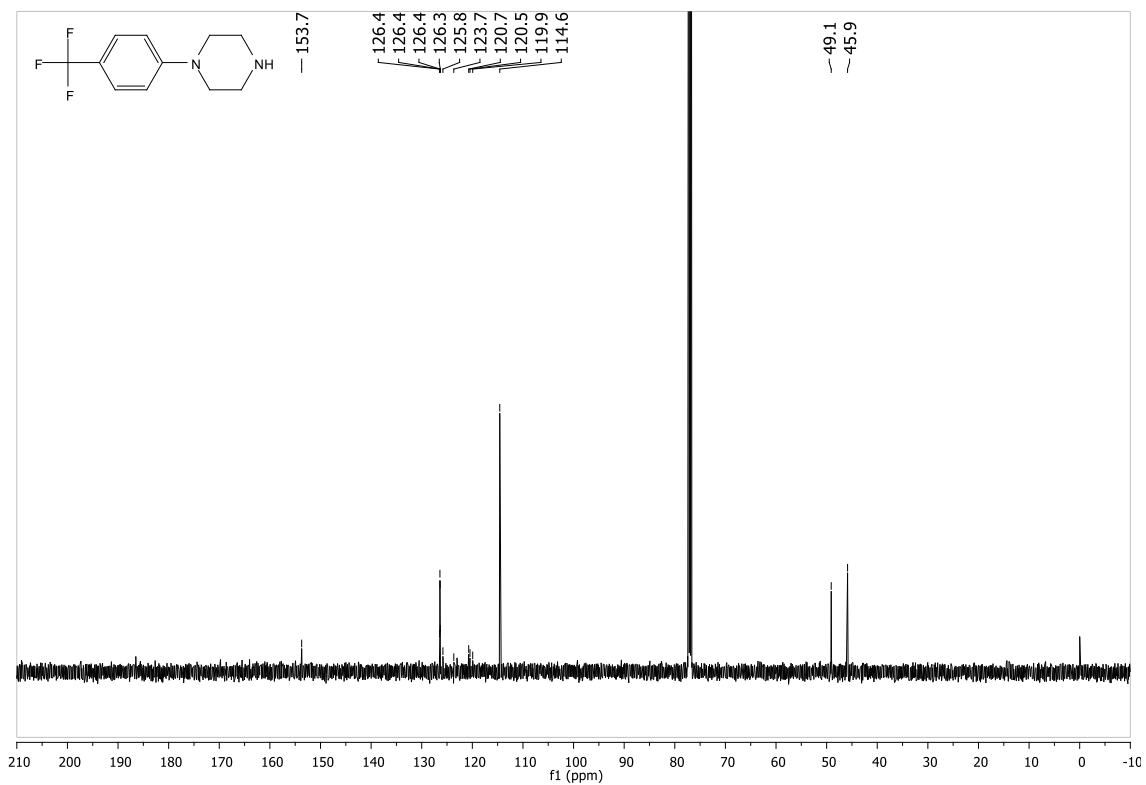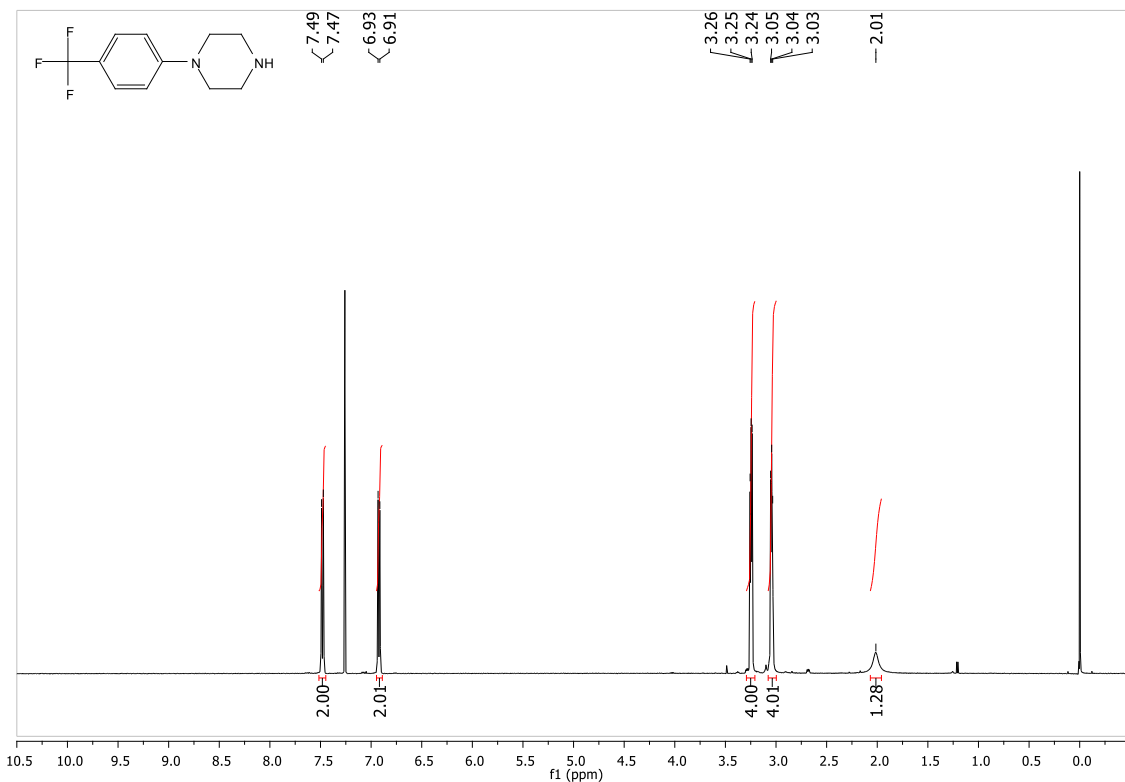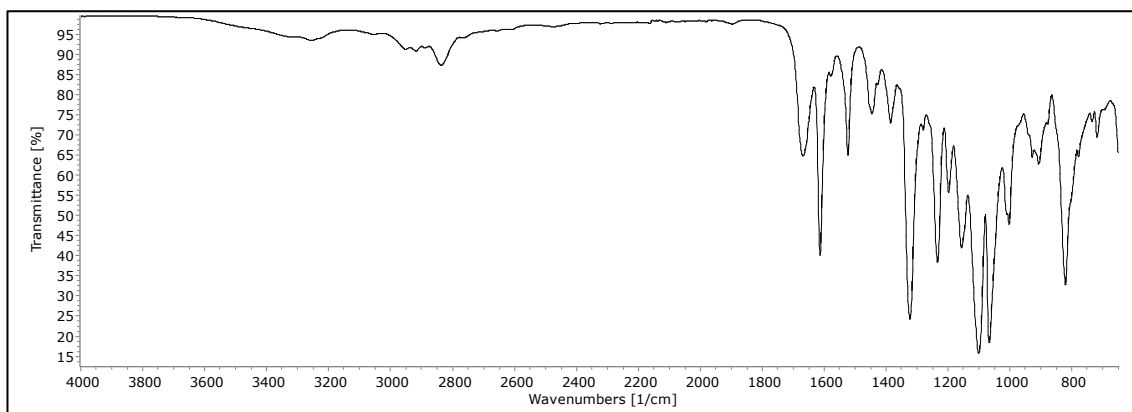
6.03   Spectra for methyl 9-oxo-9-(4-(4-(trifluoromethyl)phenyl)piperazin-1-yl)nonanoate (MK16) (RTC56) (3)
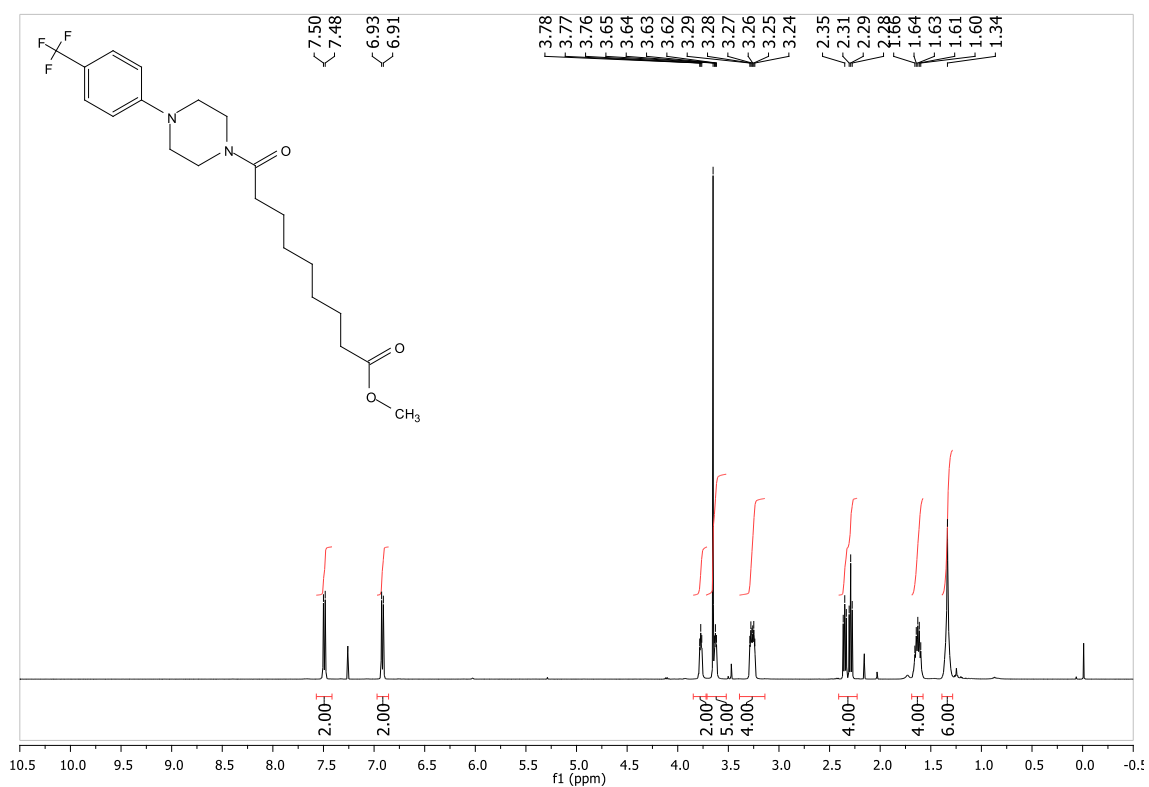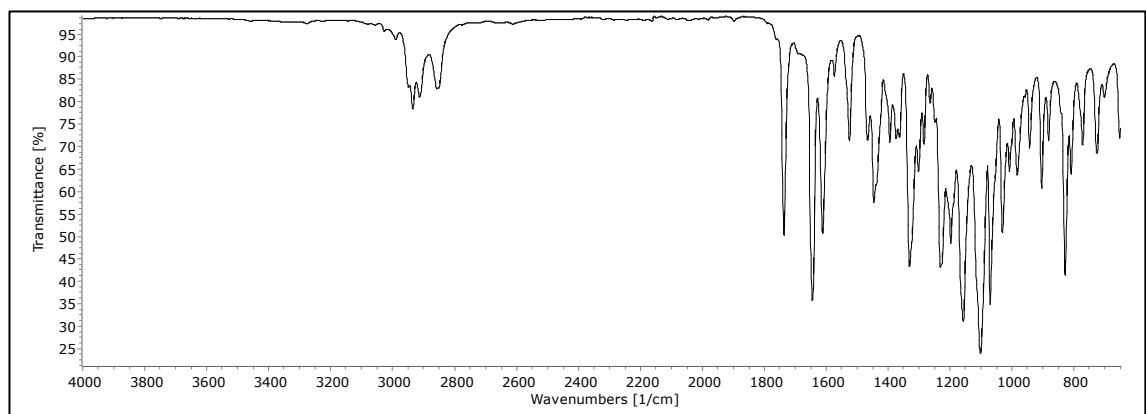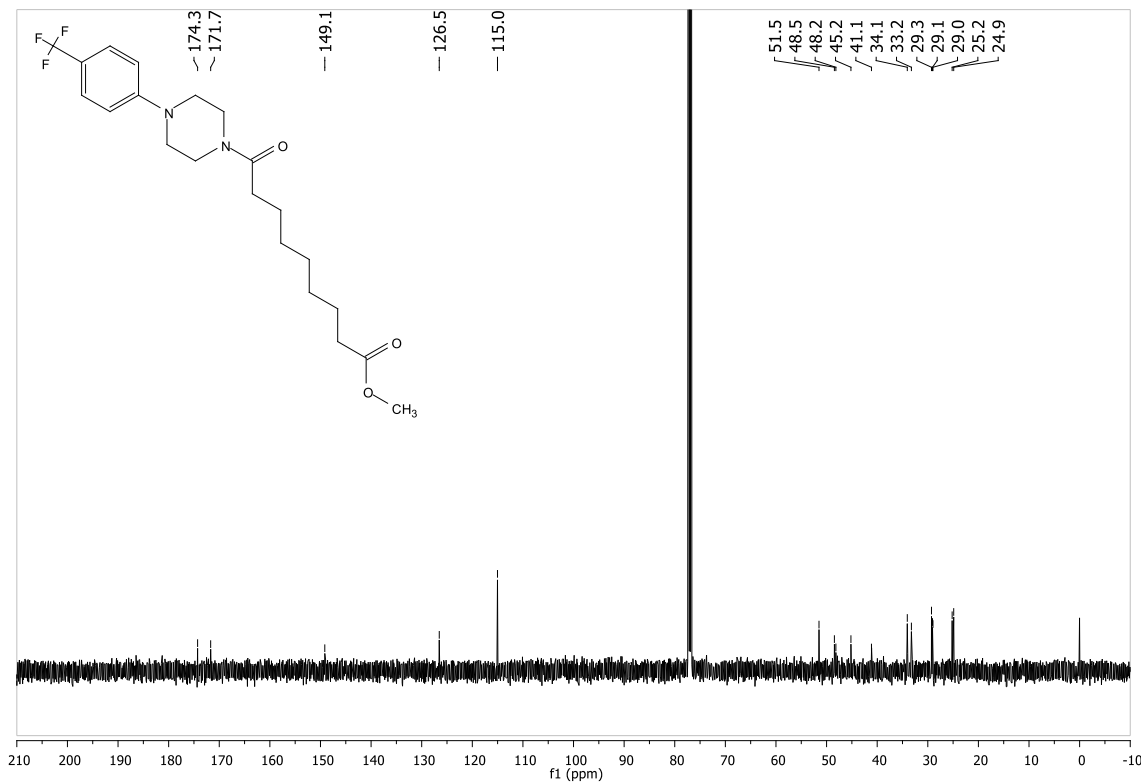
6.04 Spectra for 1-(4-cyclohexylpiperazin-1-yl)-4-(thiophen-2-yl)butan-1-one (MK43) (RTC13) (4)
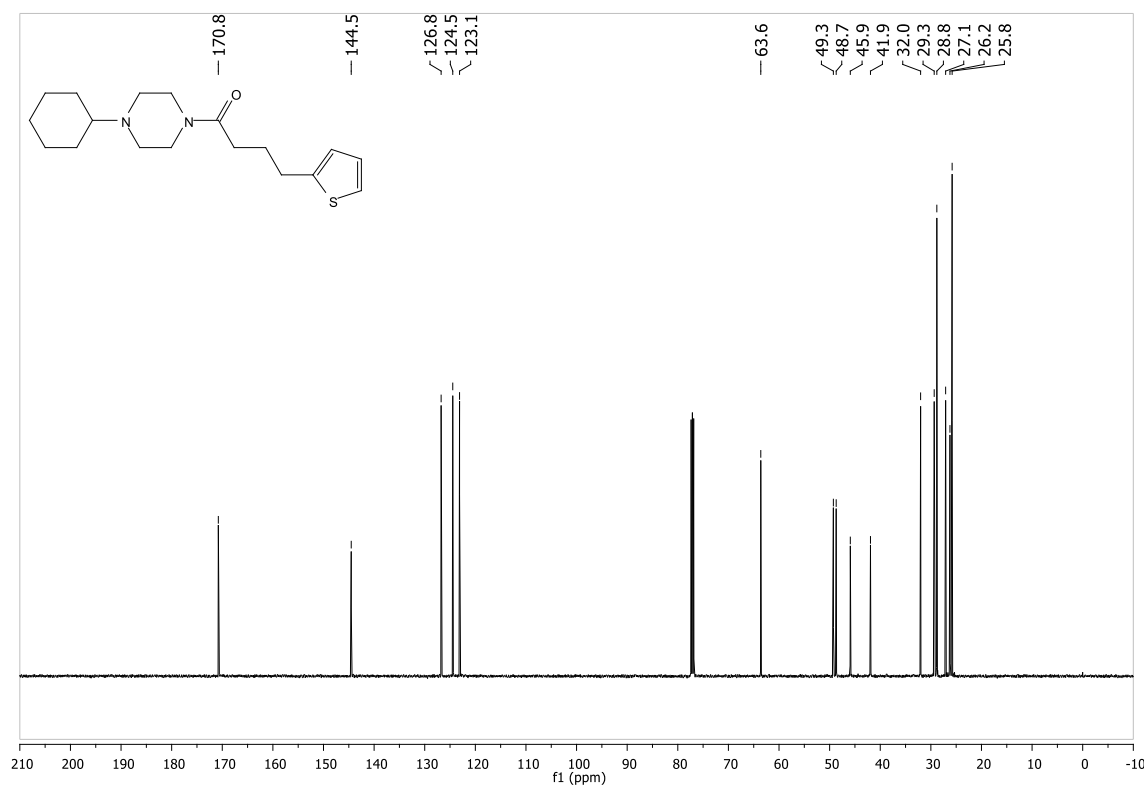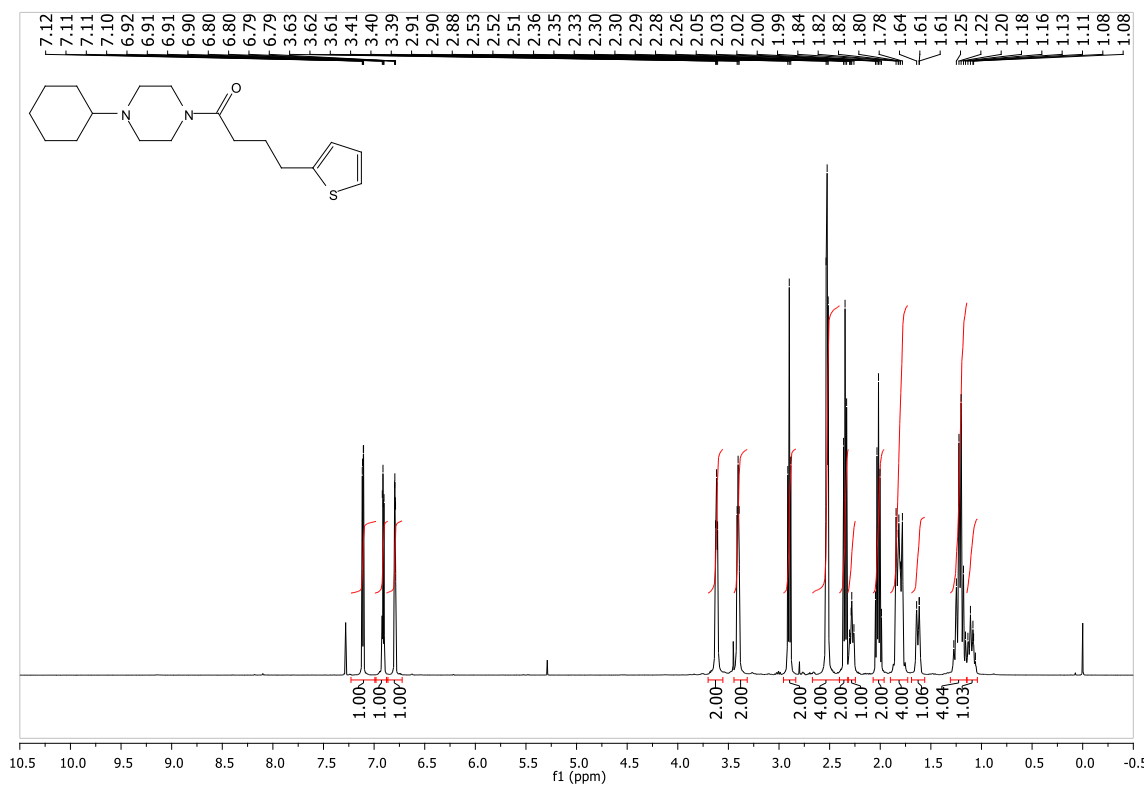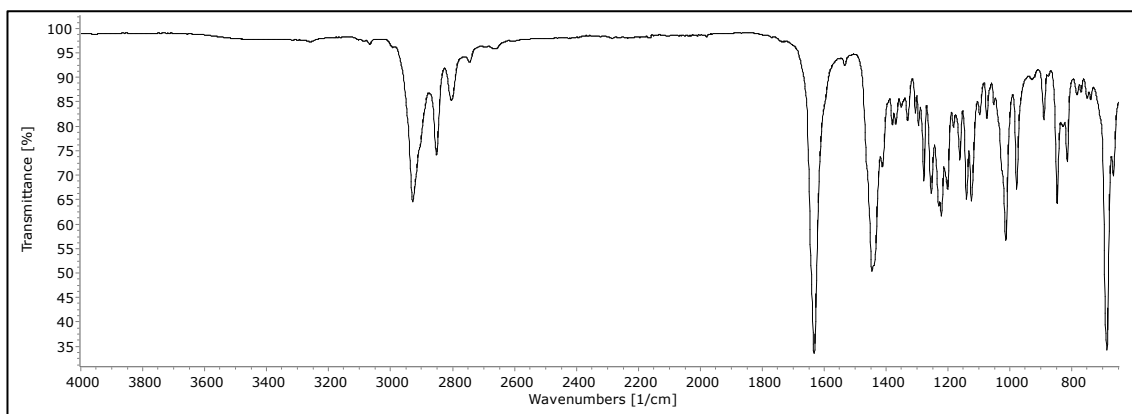
6.05 Spectra for 4-(1*H*-Pyrazol-4-yl)-1-(4-(4-(trifluoromethyl)phenyl)piperazin-1-yl)butan-1-one (MK69) (RTC193) (5)
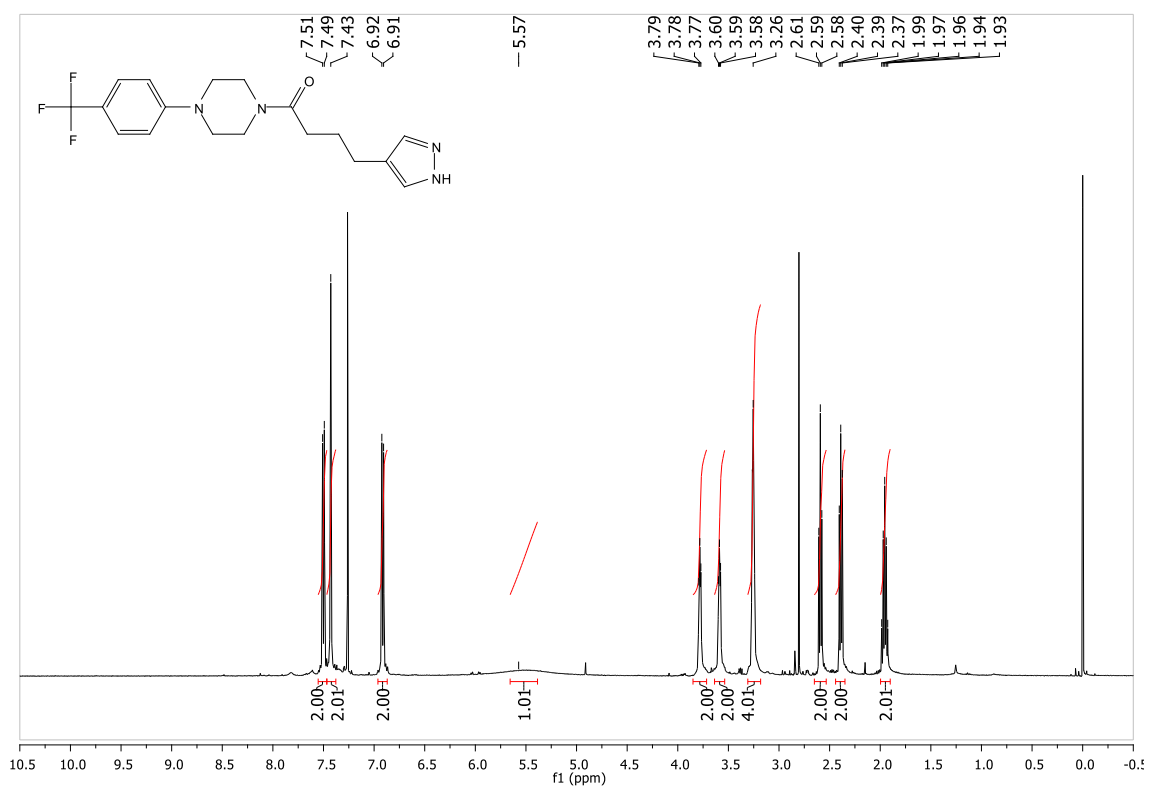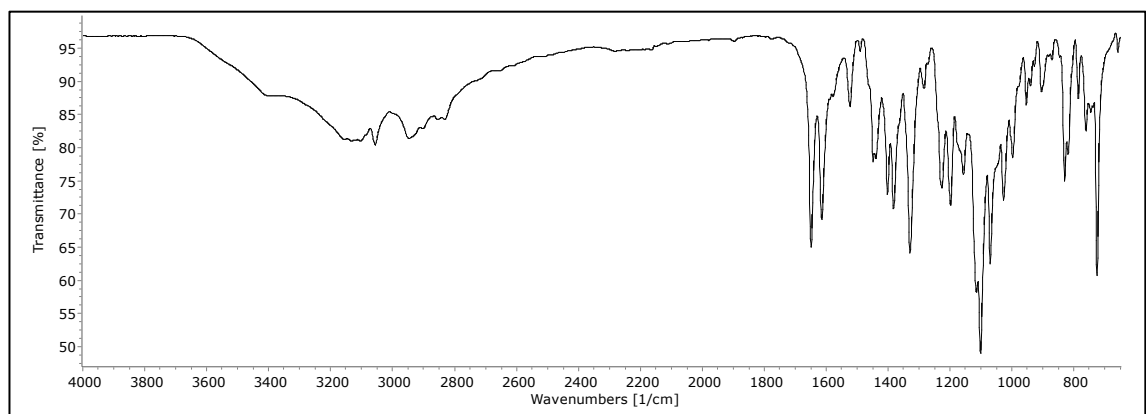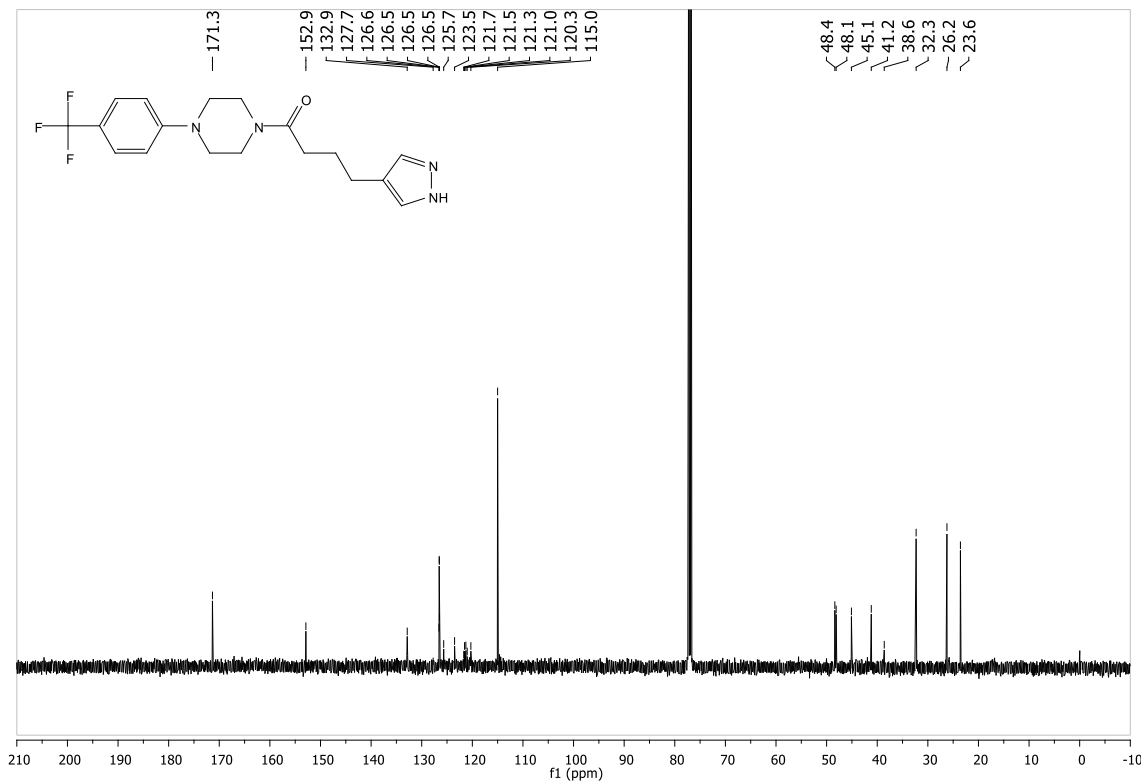
6.06 Spectra for 1-(2-chloro-4-(trifluoromethyl)phenyl)piperazine (MK21) (RD20) (6)
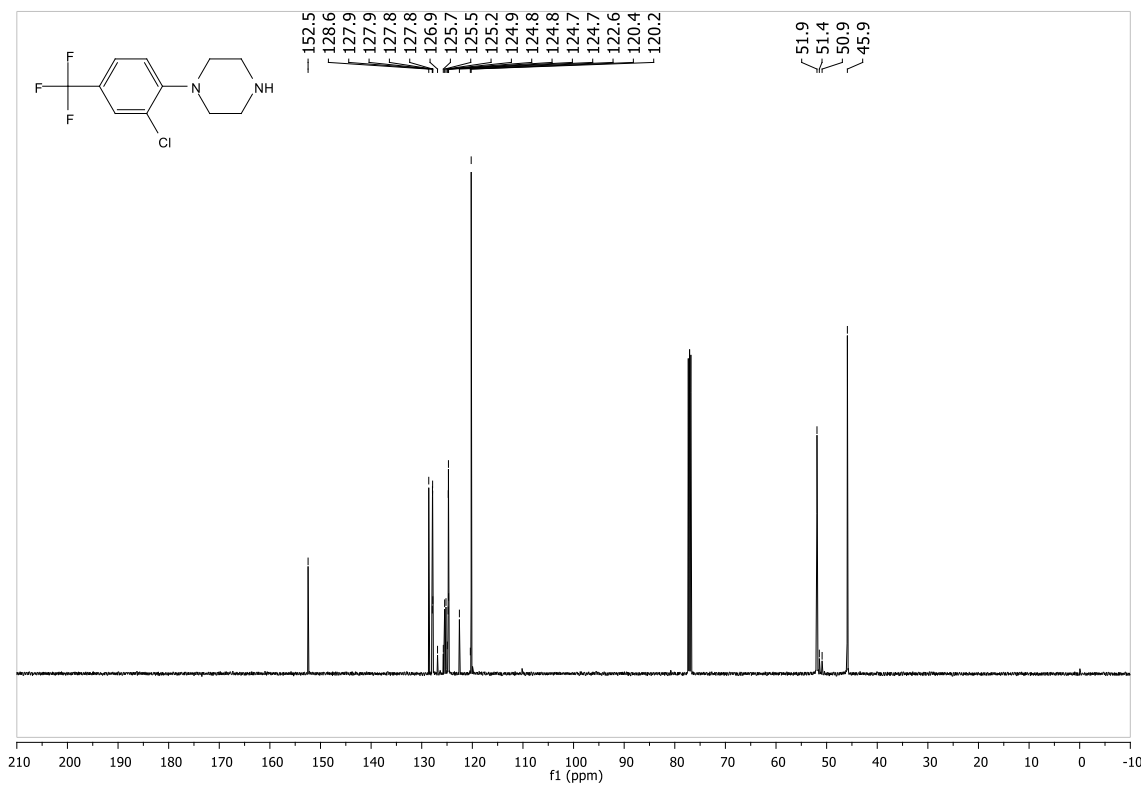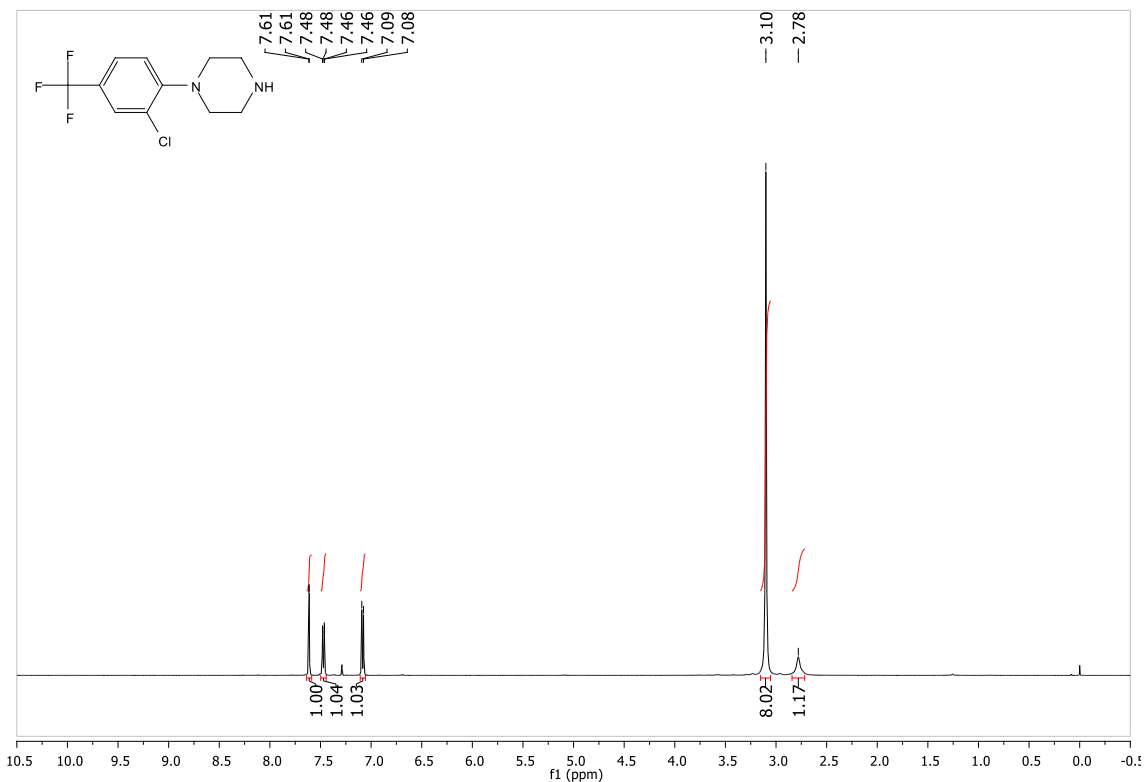
6.07 Spectra for 1-(4-phenylpiperazin-1-yl)-4-(thiophen-2-yl)butan-1-one (MK38) (RTC162) (7)
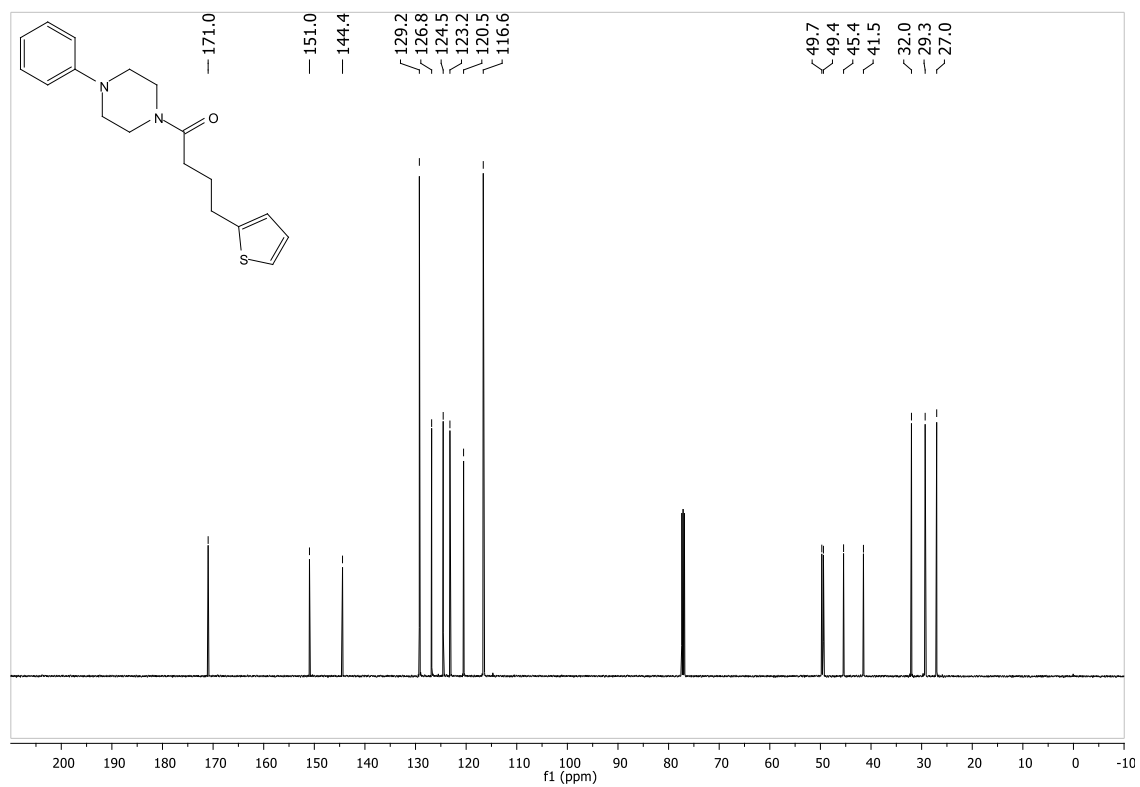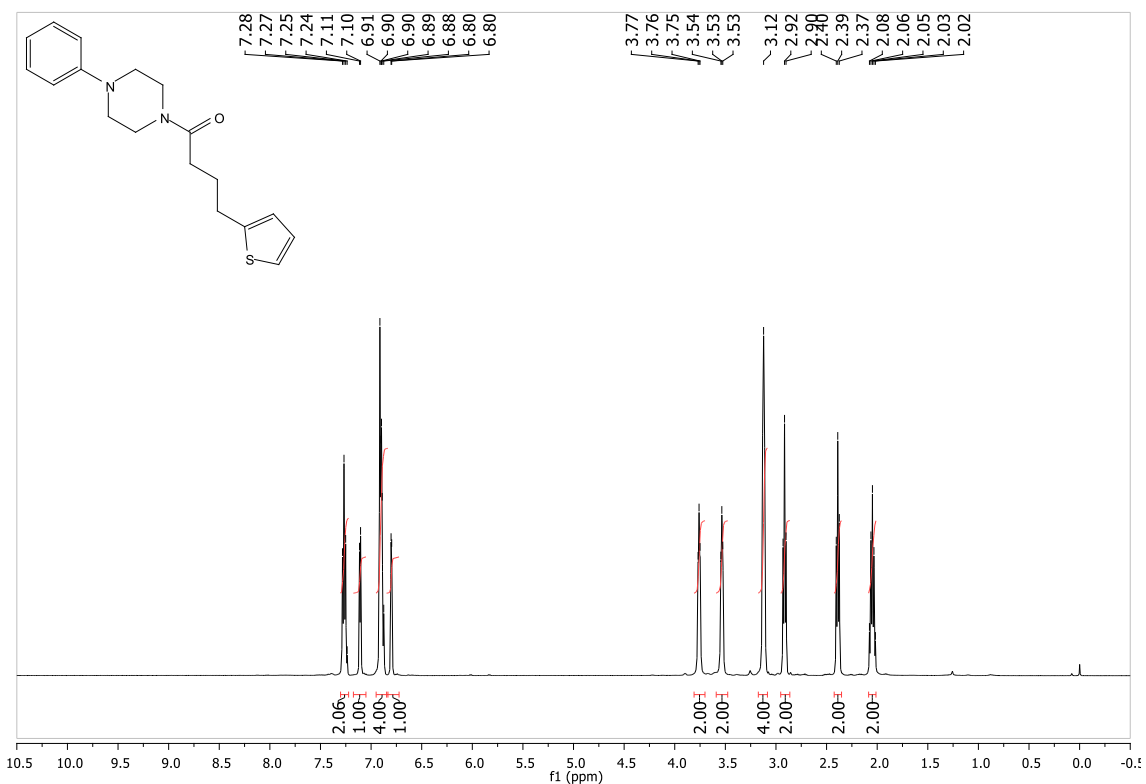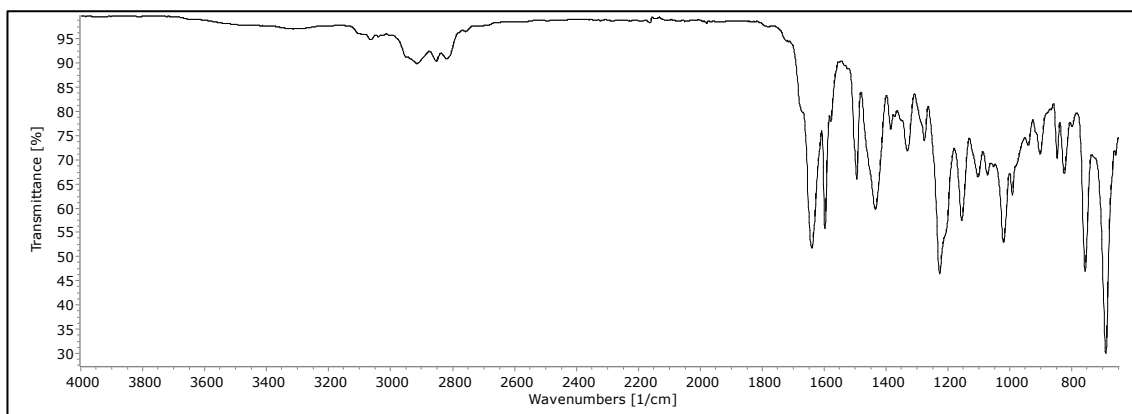
6.08 Spectra for 4-(thiophen-2-yl)-1-(4-(2-(trifluoromethyl)phenyl)piperazin-1-yl)butan-1-one (MK41) (RTC20) (8)

13C NMR peaks: 171.0

151.7, 151.7, 144.4, 132.8, 127.8, 127.6, 127.3, 127.2, 127.2, 127.2, 127.1, 126.7, 125.3, 125.0, 124.5, 124.0, 123.1, 122.8, 120.6

53.7, 53.1, 46.0, 42.0

32.1, 29.3, 27.0
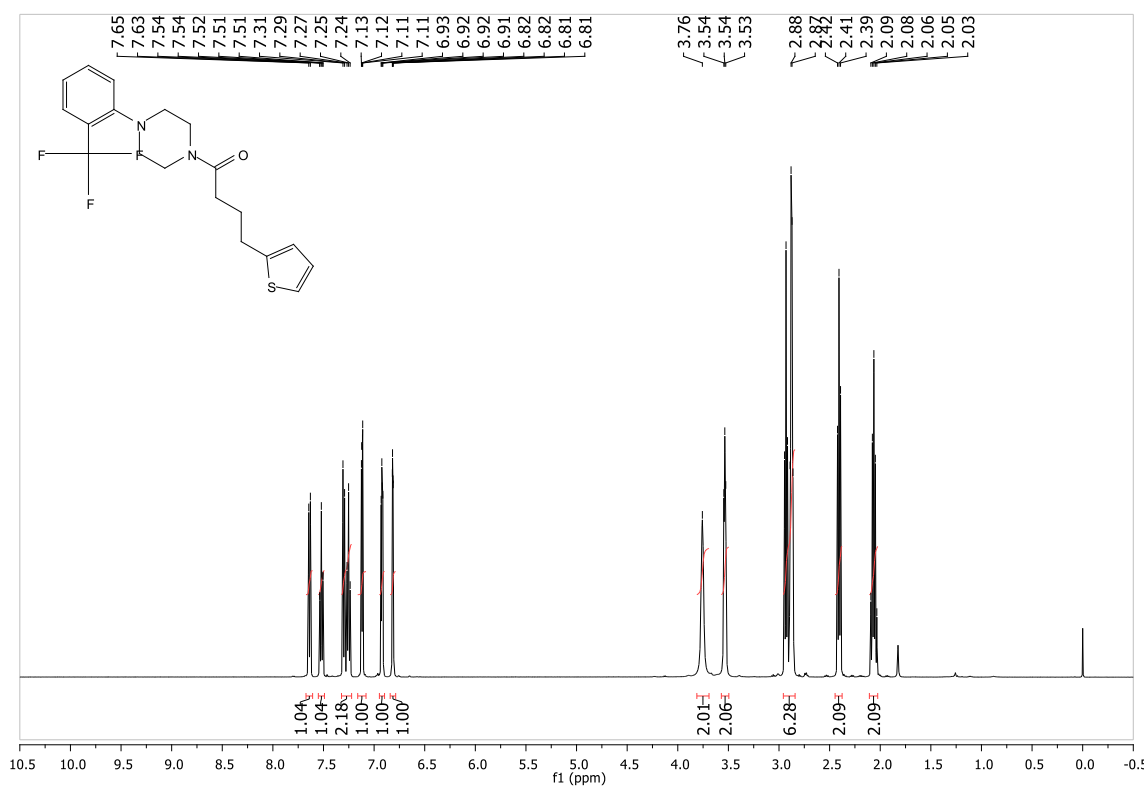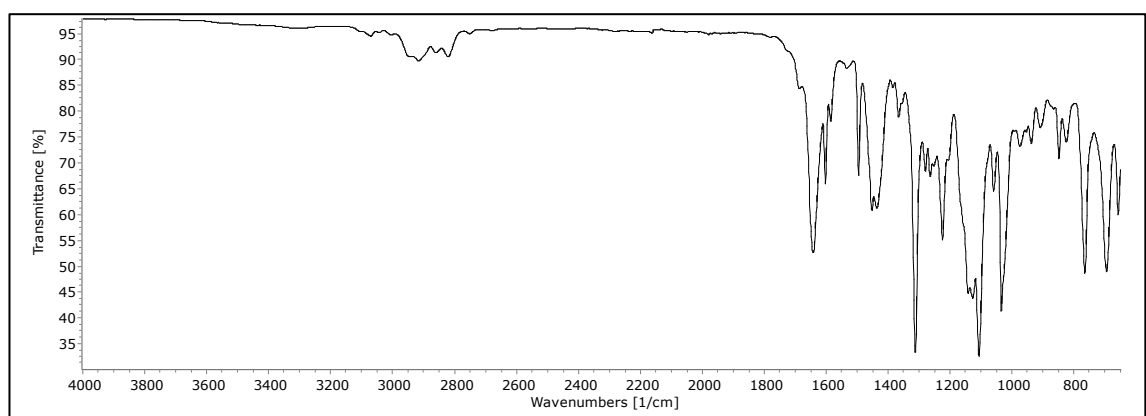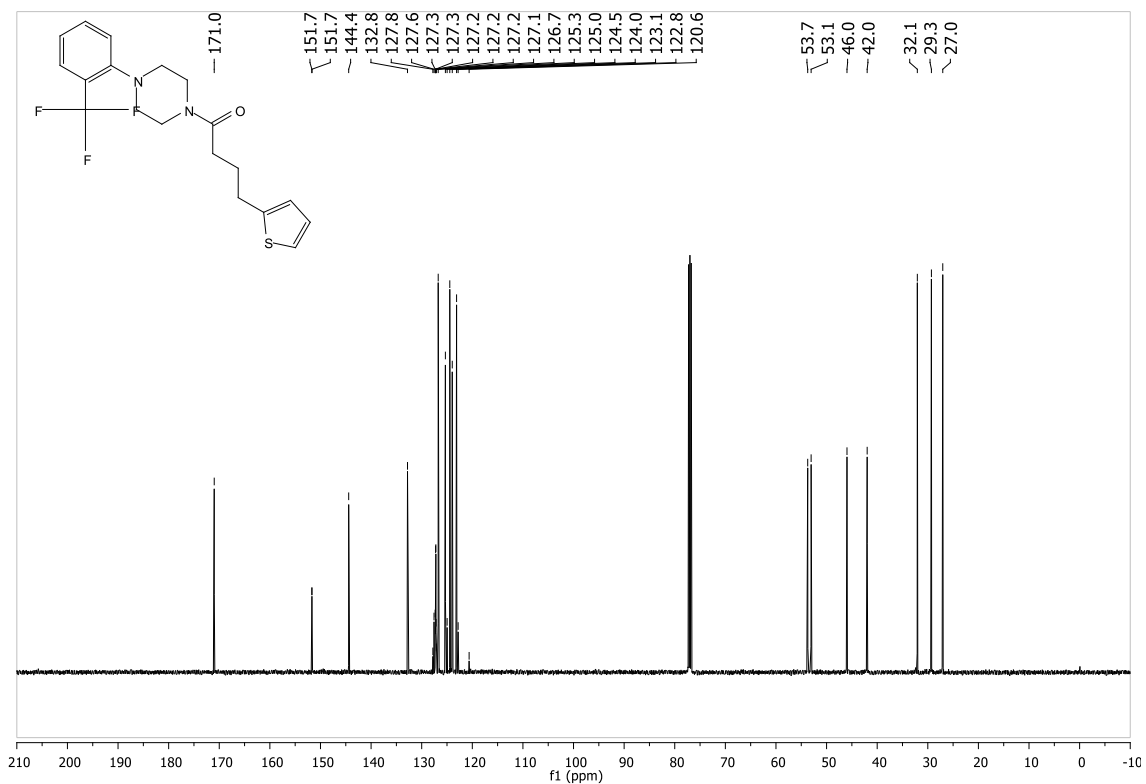
6.09   Spectra for 1-(4-(3,5-bis(trifluoromethyl)phenyl)piperazin-1-yl)-4-(thiophen-2-yl)butan-1-one (MK44) (RTC26) (9)
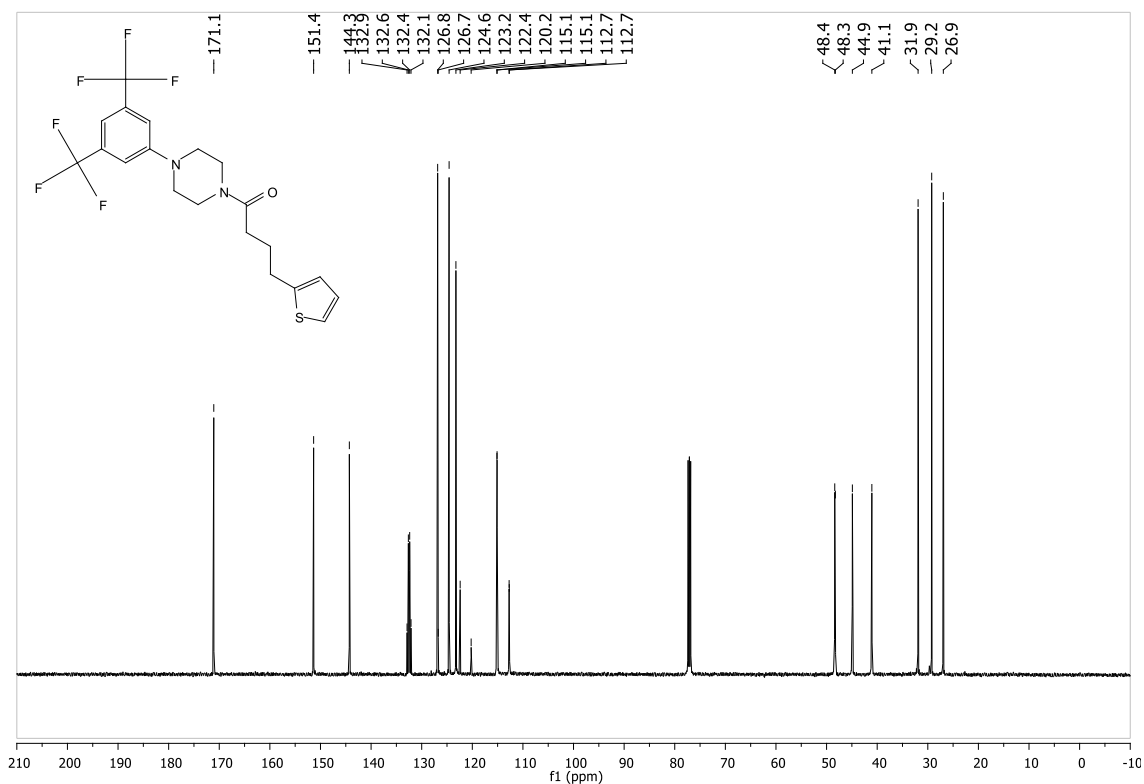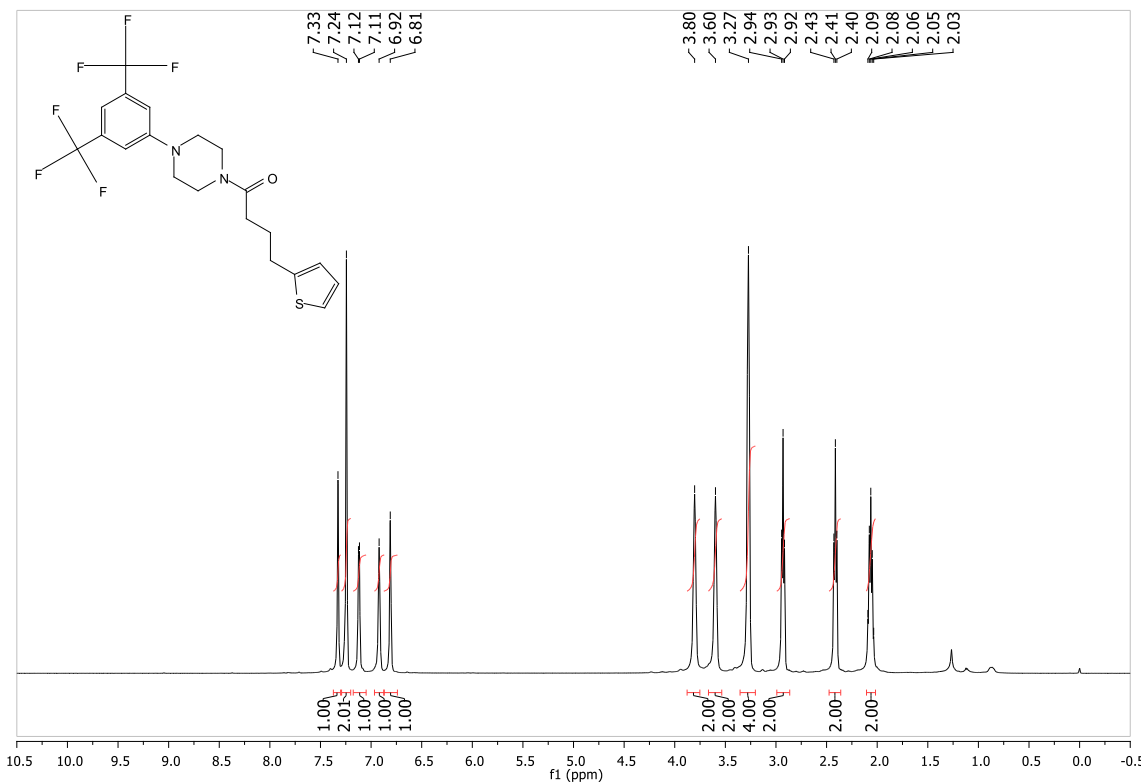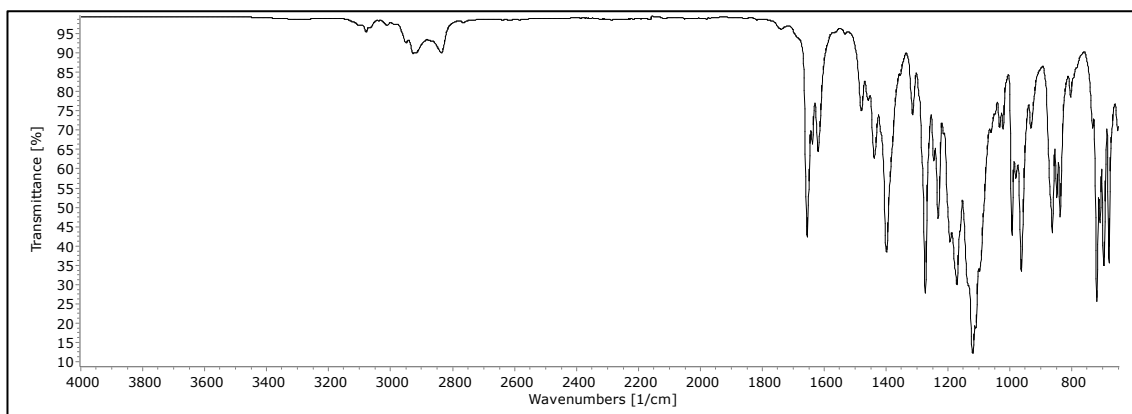
6.10   Spectra for 1-(4-(4-nitrophenyl)piperazin-1-yl)-4-(thiophen-2-yl)butan-1-one (MK39) (RTC22) (10)
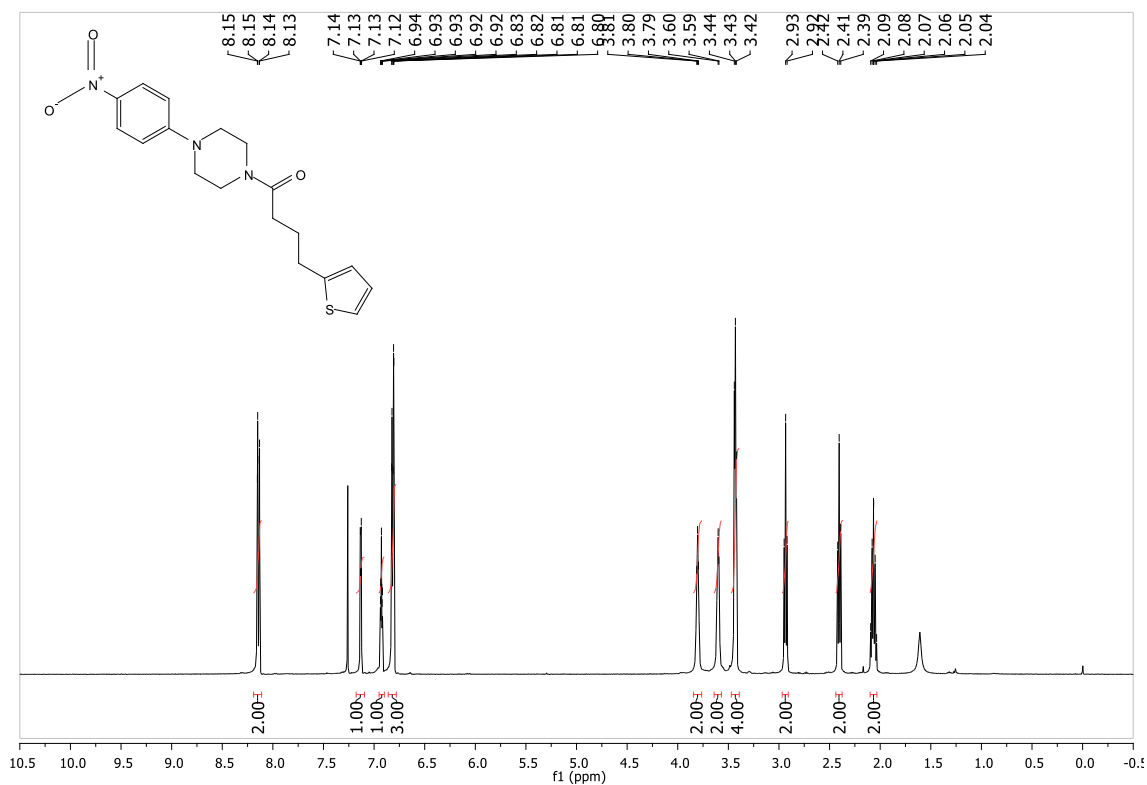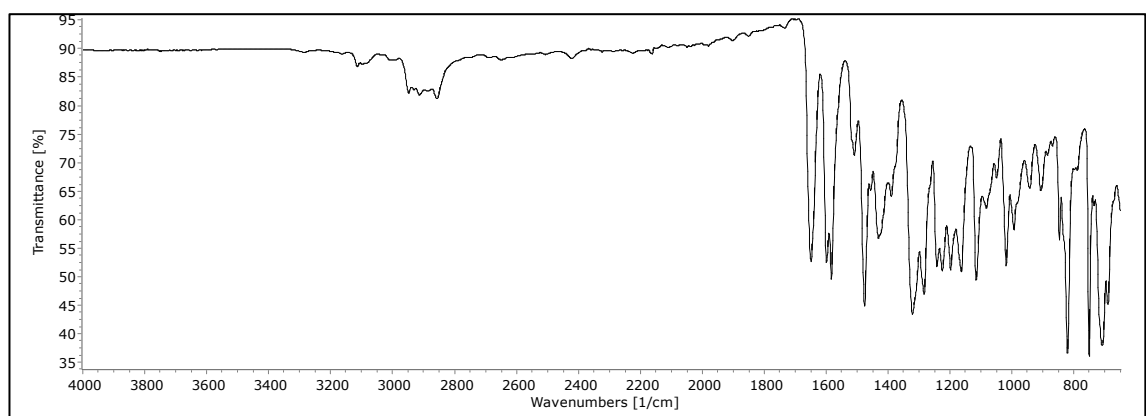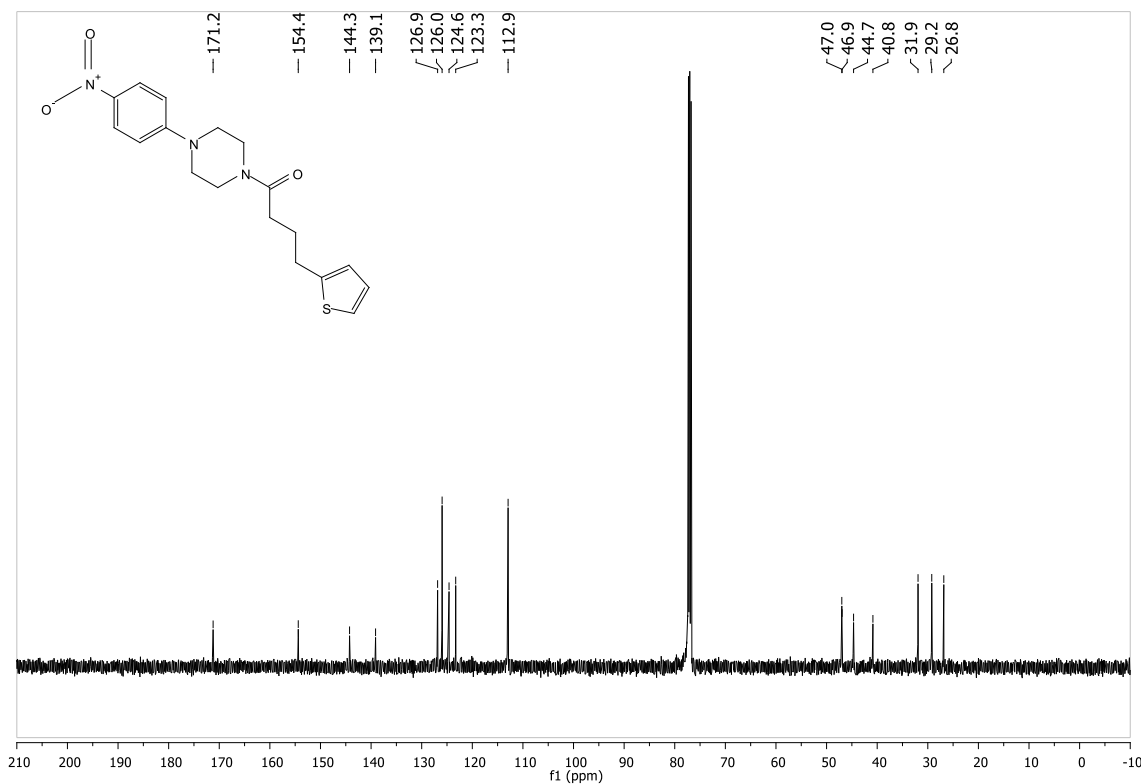
6.11 Spectra for 1-(4-(4-*a*minophenyl)piperazin-1-yl)-4-(thiophen-2-yl)butan-1-one (MK70) (RTC23) (11)
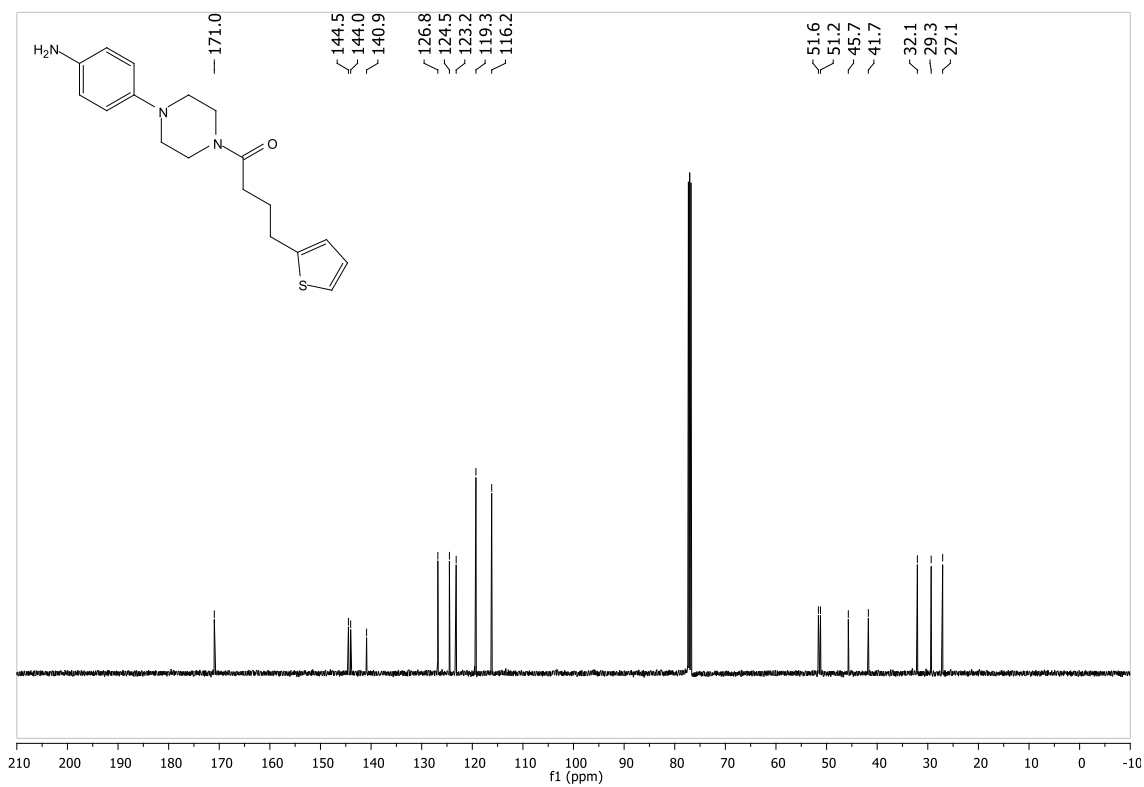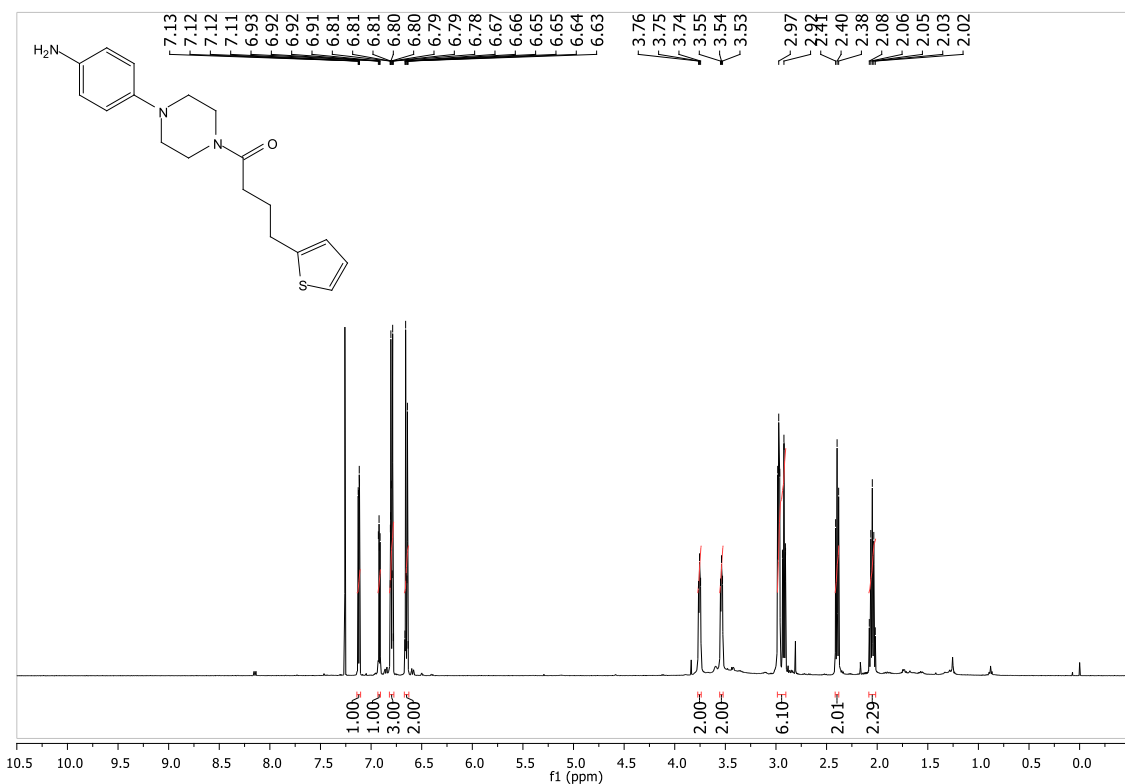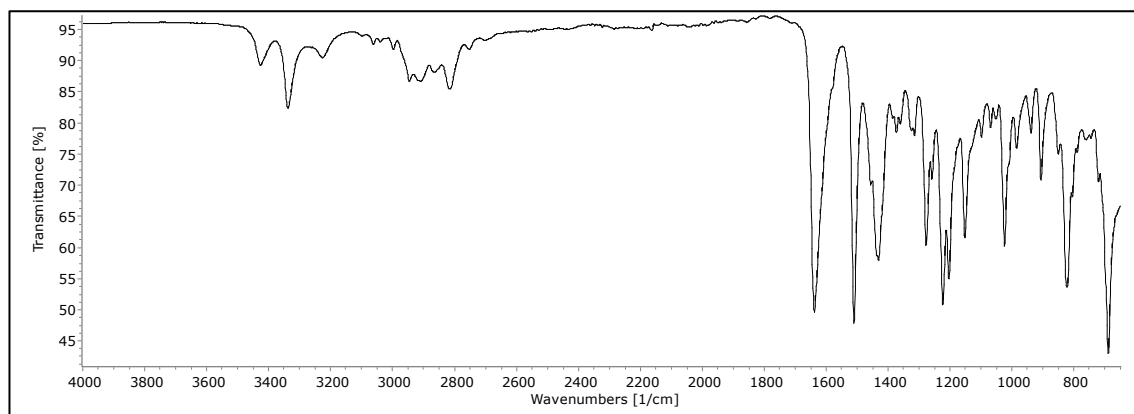
6.12   Spectra for 1-(4-(2-chloro-4-(trifluoromethyl)phenyl)piperazin-1-yl)-4-(thiophen-2-yl)butan-1-one (MK20) (RTC8) (12)

^{13}C NMR peaks: 171.2, 151.7, 144.4, 128.8, 128.0, 128.0, 128.0, 127.9, 126.8, 126.8, 126.4, 126.1, 125.9, 125.6, 124.9, 124.9, 124.8, 124.8, 124.6, 124.6, 123.3, 122.5, 120.4, 120.3, 51.2, 50.7, 45.6, 41.6, 32.1, 29.3, 27.0
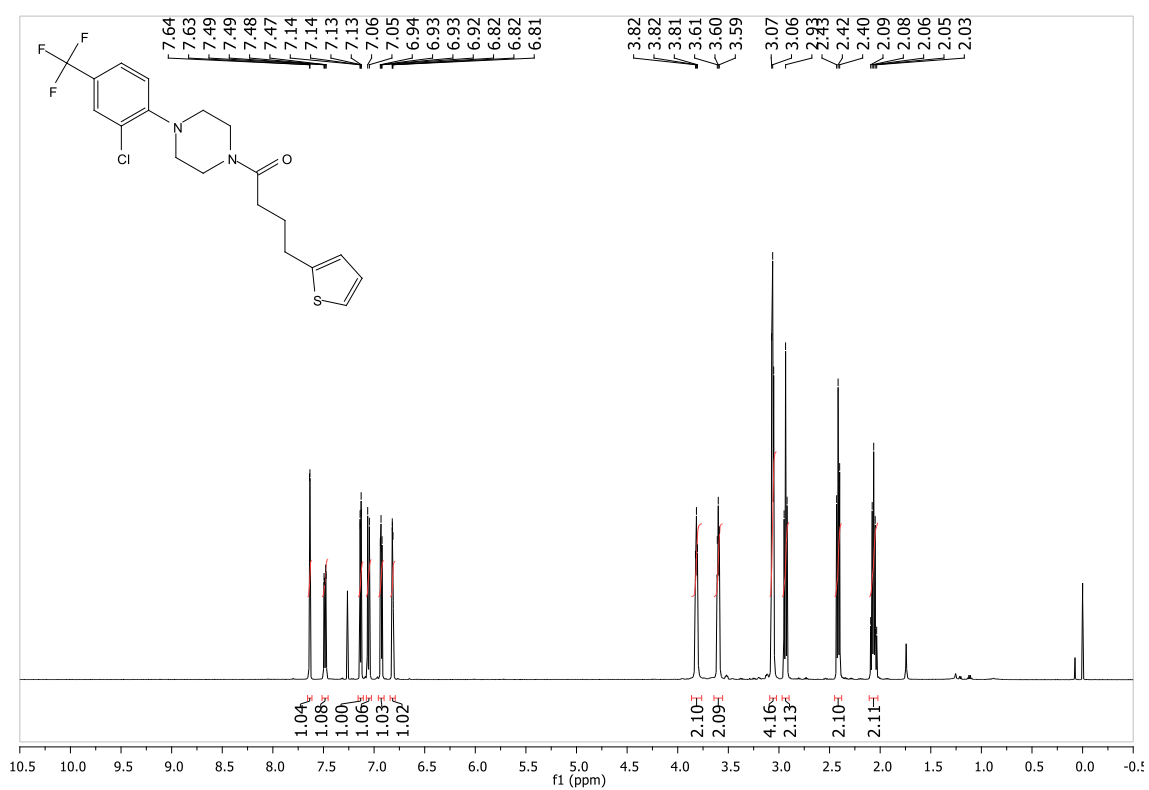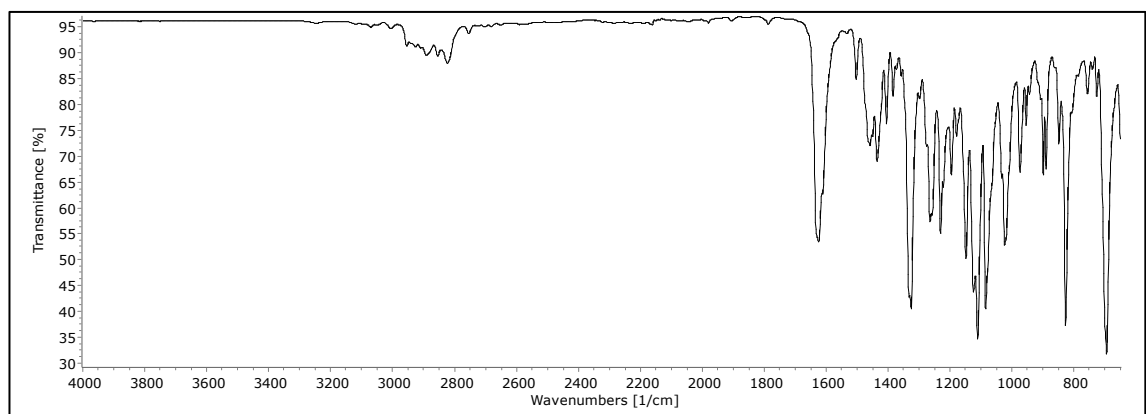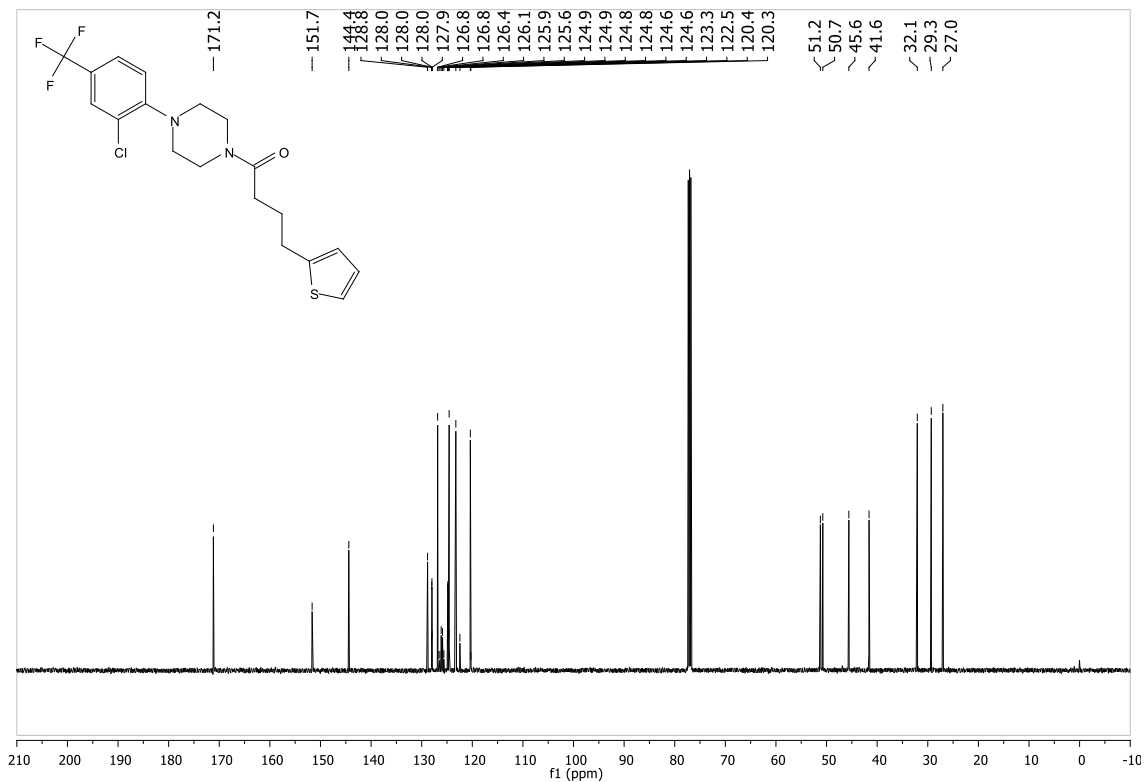
6.13 Spectra for 4-(thiophen-3-yl)-1-(4-(5-(trifluoromethyl)pyridin-2-yl)piperazin-1-yl)butan-1-one (MK42) (RTC5) (13)
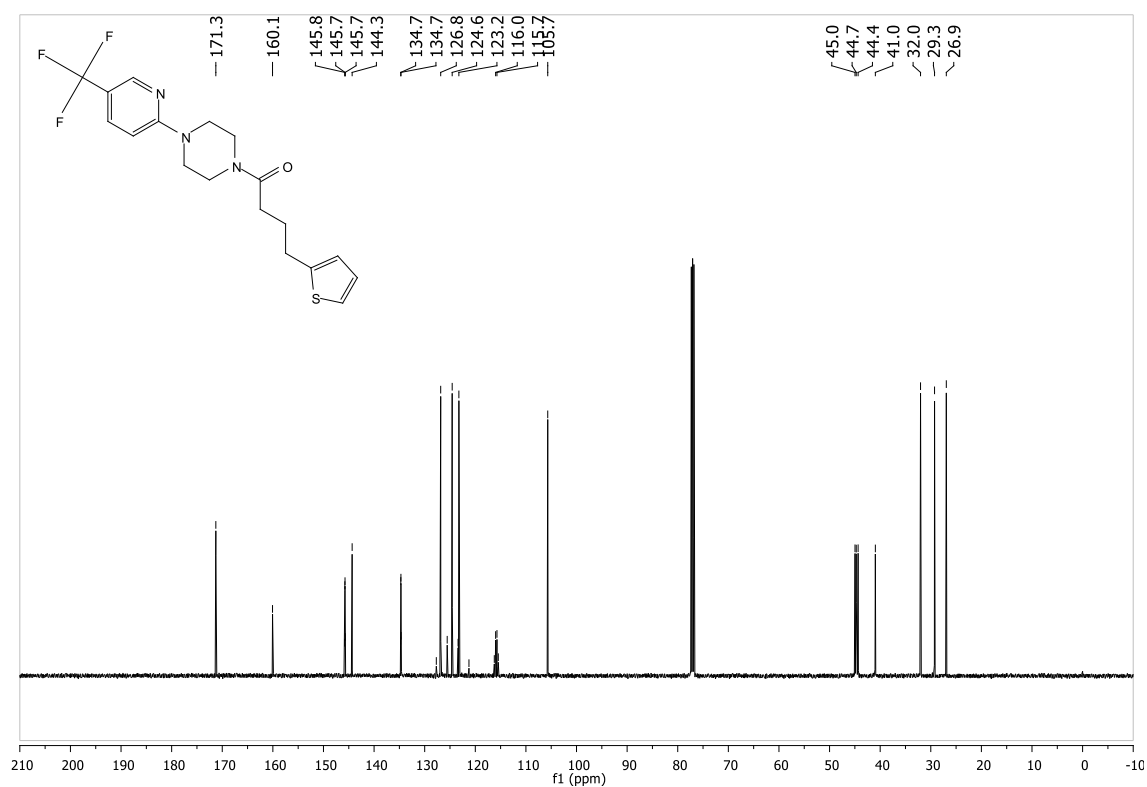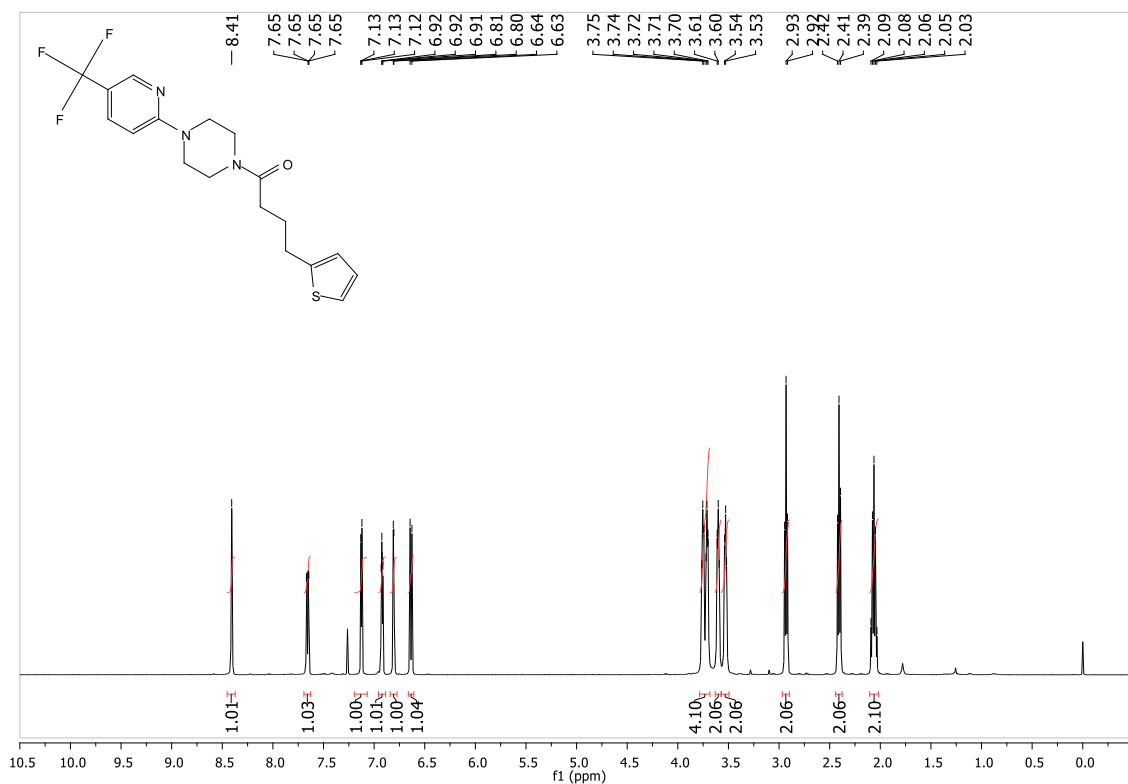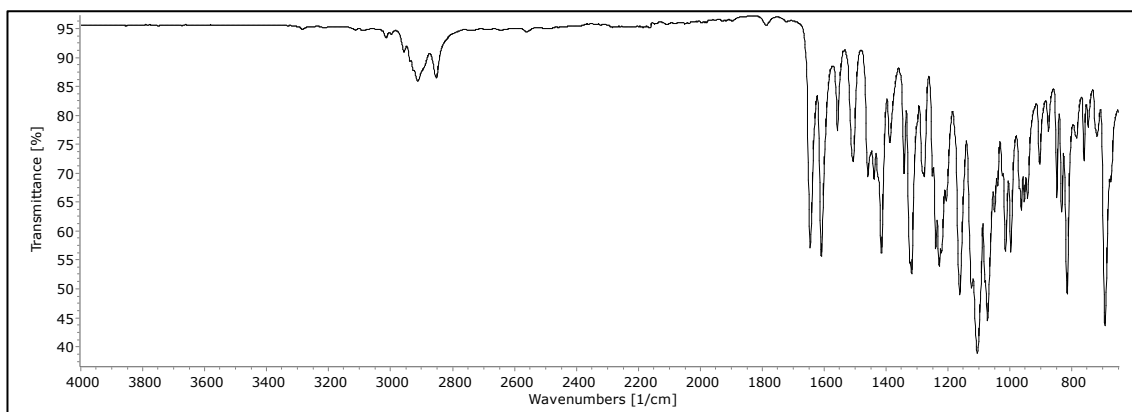
6.14   Spectra for 1-(4-(3-chloro-5-(trifluoromethyl)pyridin-2-yl)piperazin-1-yl)-4-(thiophen-2-yl)butan-1-one (MK45) (RTC6) (14)
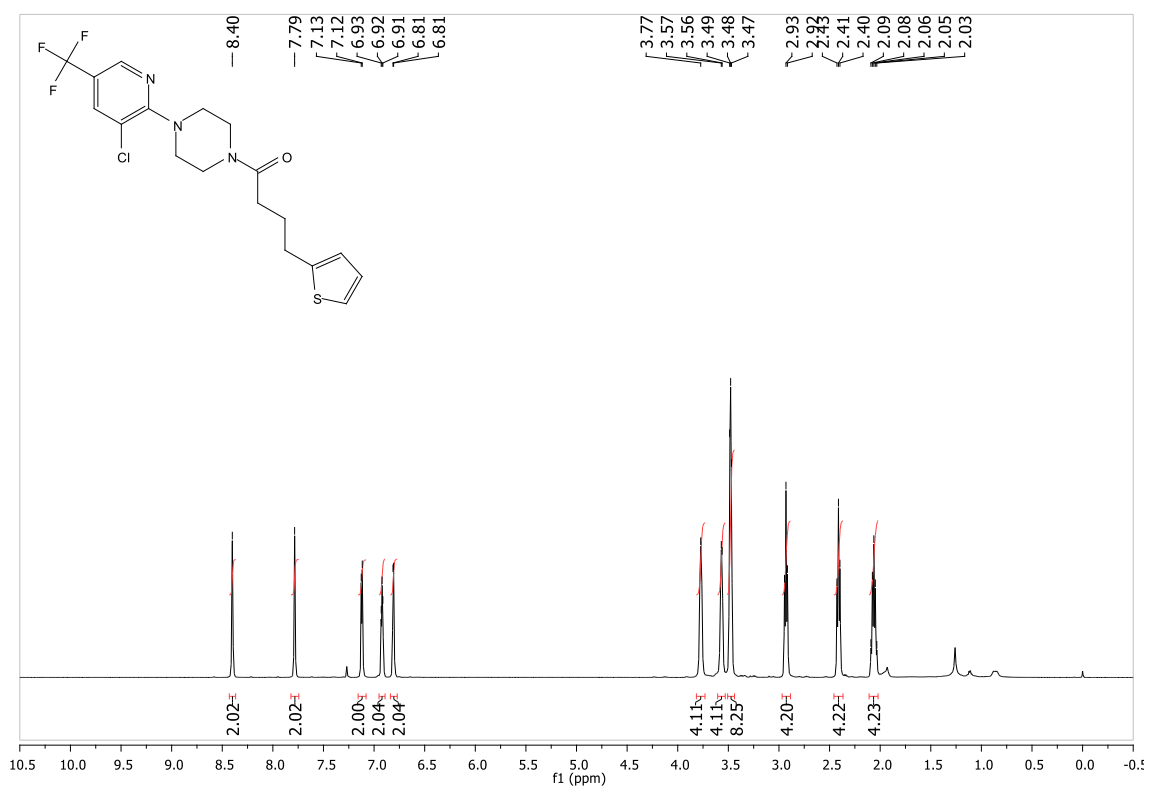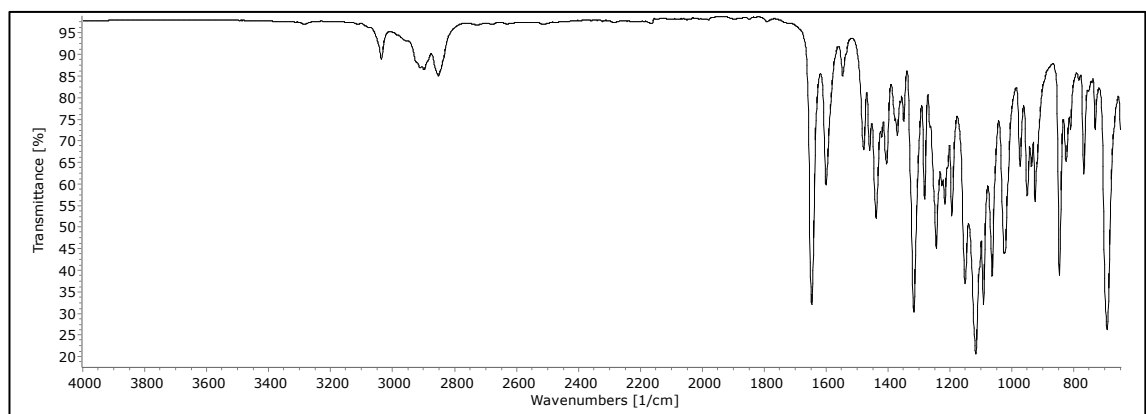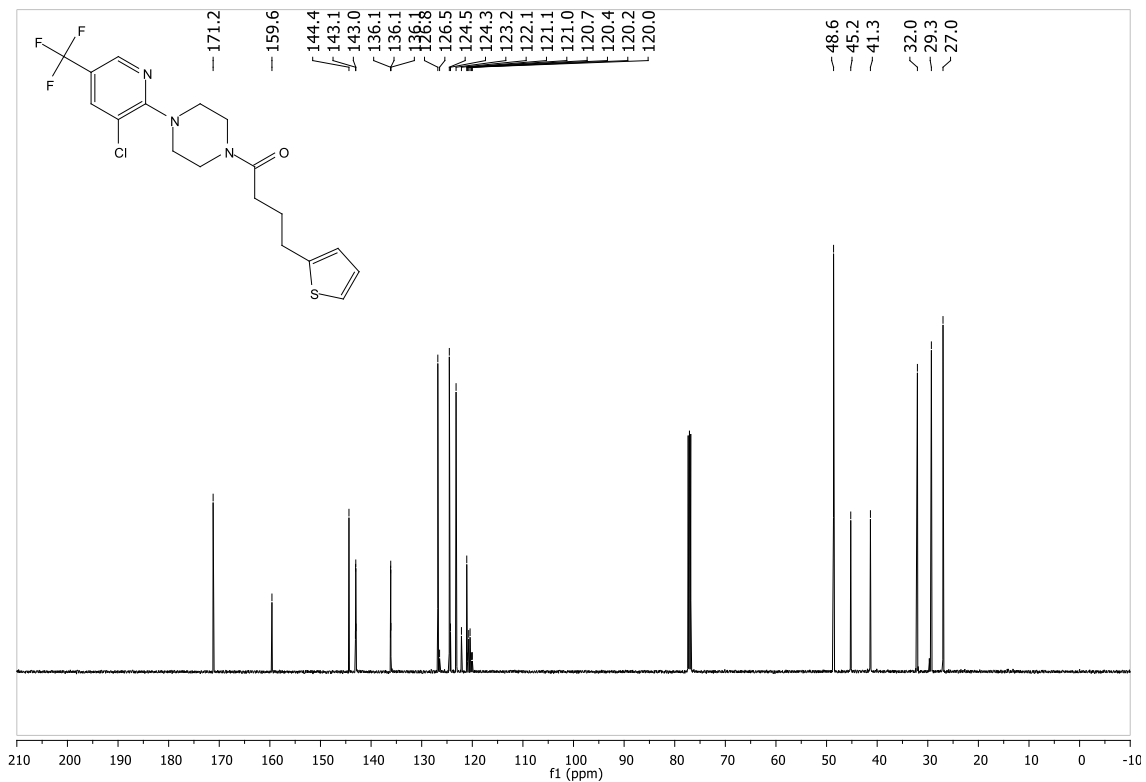
6.15 Spectra for 1-(4-methylpiperazin-1-yl)-4-(thiophen-2-yl)butan-1-one (MK36) (RTC32) (15)
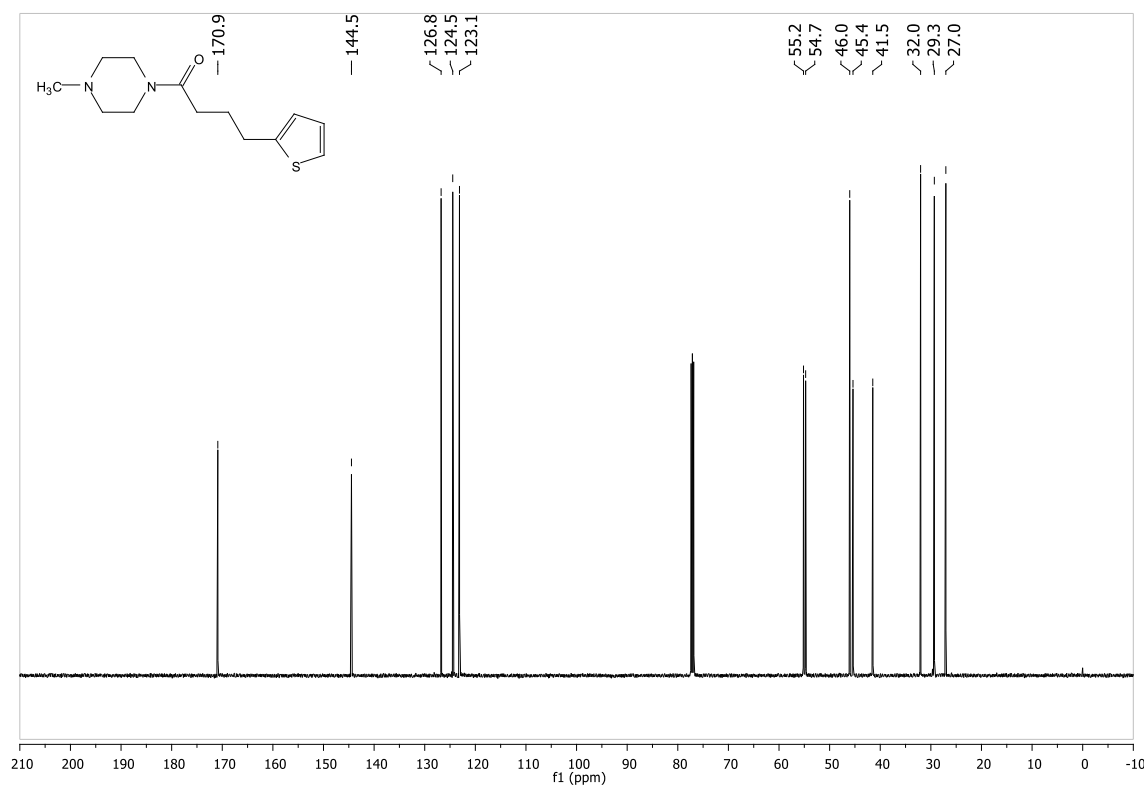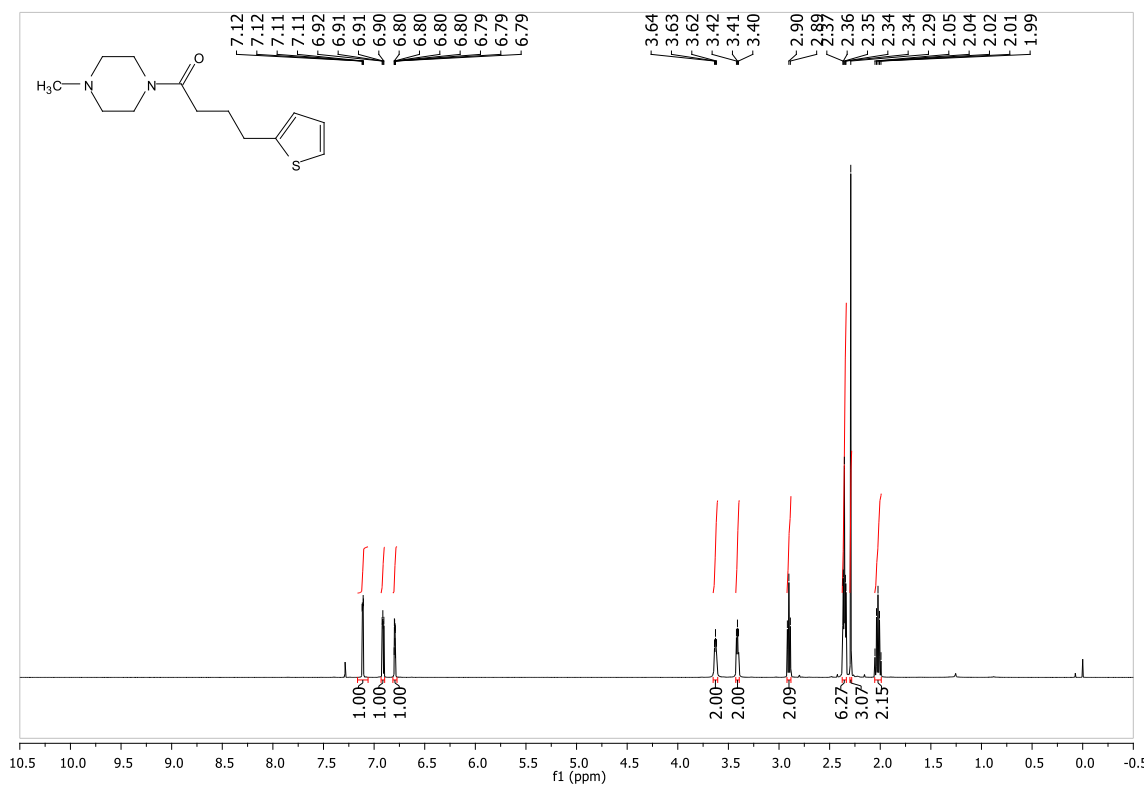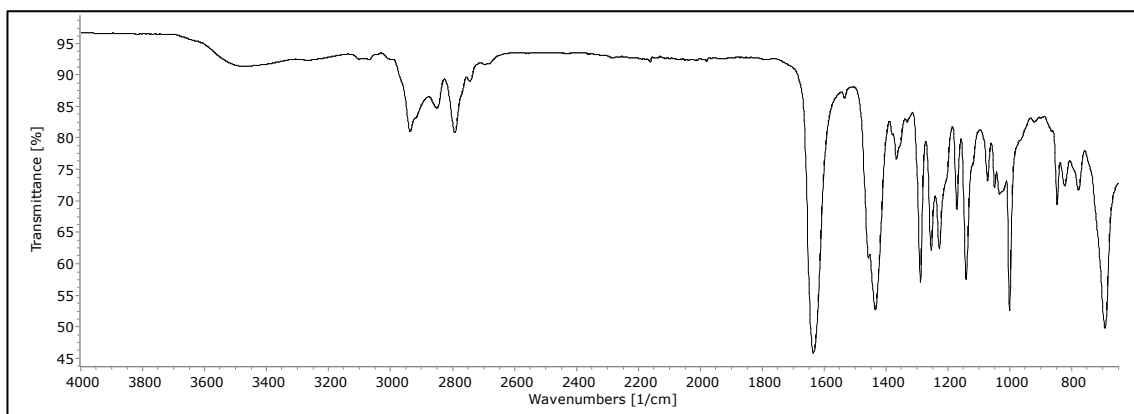
6.16   Spectra for 4-(thiophen-2-yl)-1-(4-(4-(trifluoromethyl)phenyl)piperidin-1-yl)butan-1-one (MK19) (RTC196) (16)

^{13}C NMR peaks: 170.9, 149.2, 144.5, 129.3, 129.0, 128.8, 128.5, 127.5, 127.1, 126.8, 125.6, 125.6, 125.5, 125.5, 125.3, 124.5, 123.2, 123.1, 121.0, 46.0, 42.7, 42.2, 33.7, 32.6, 32.2, 29.4, 27.1
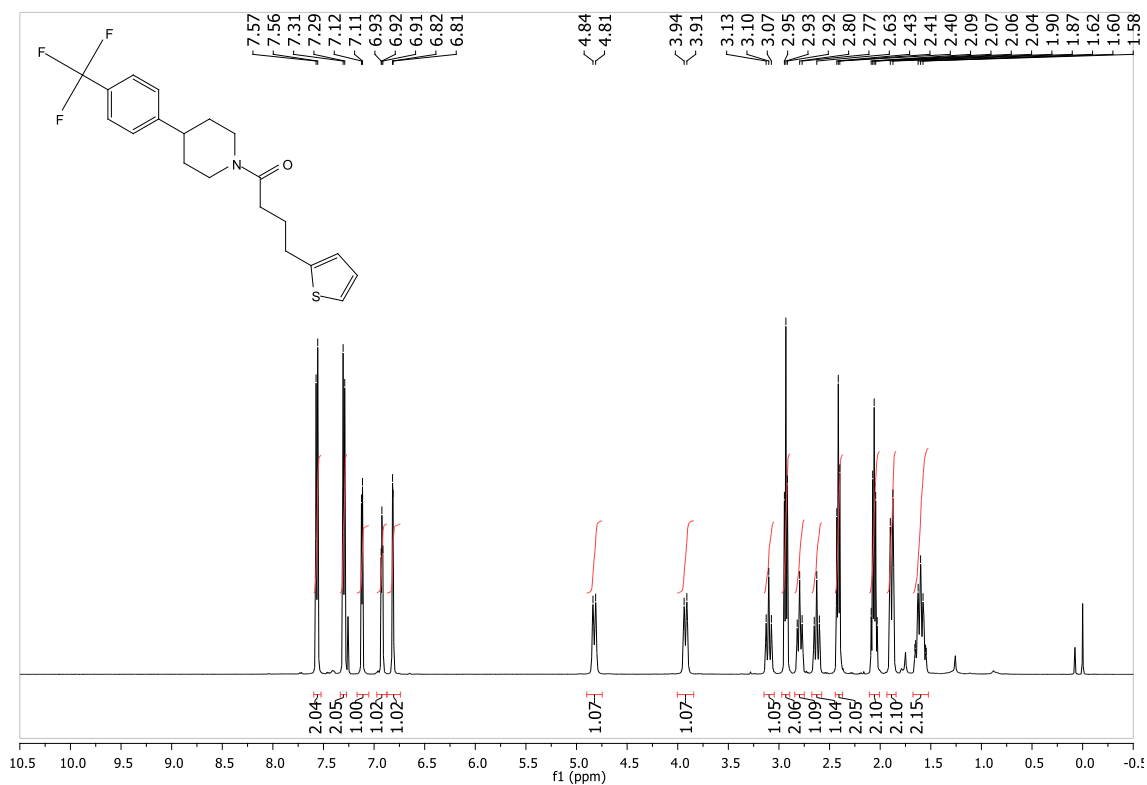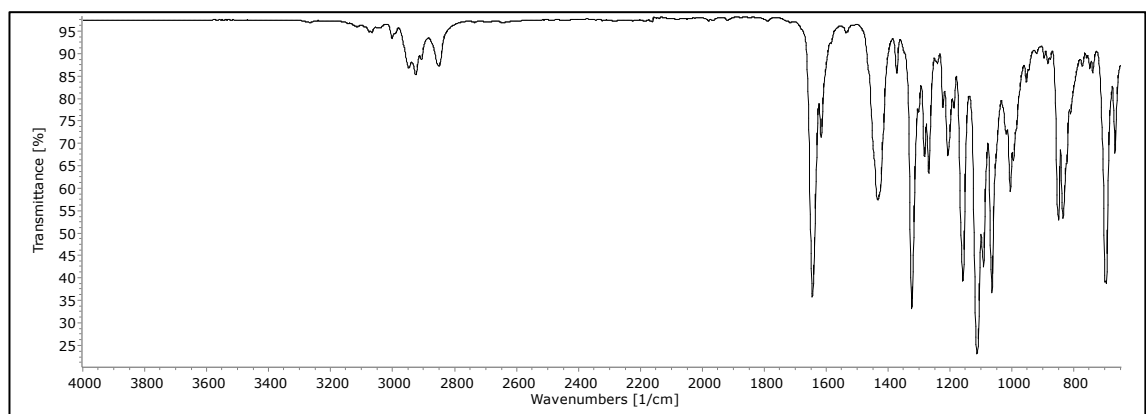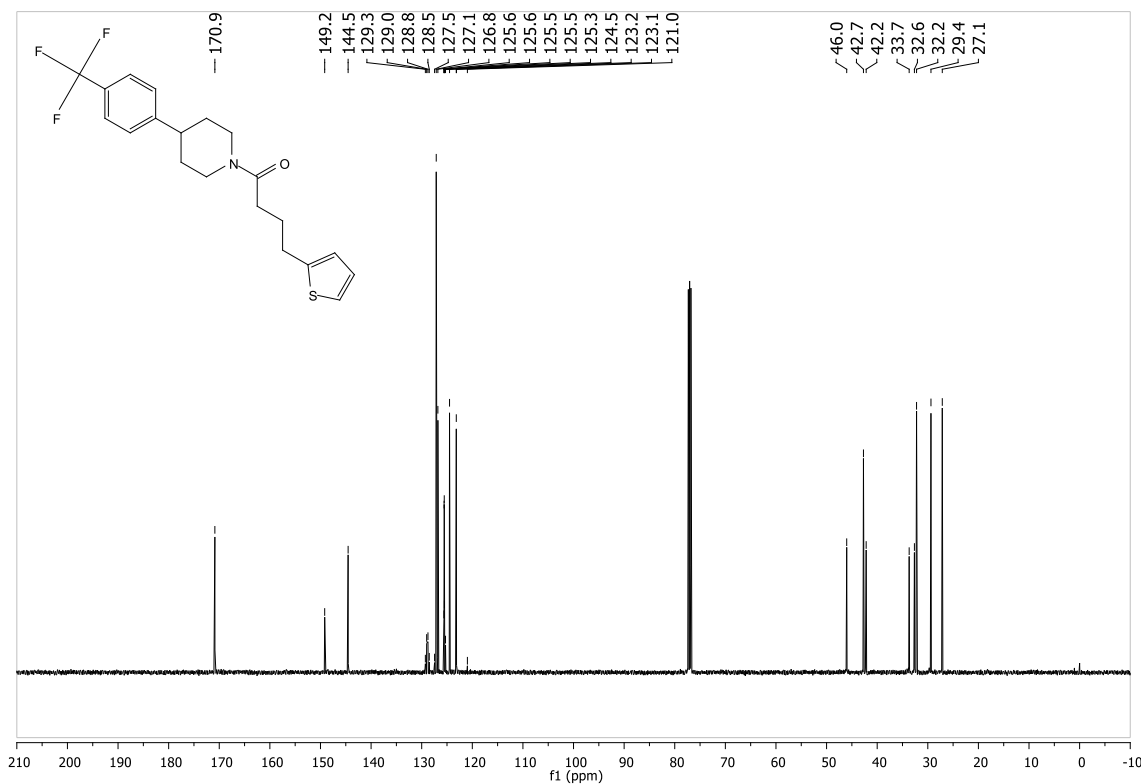
6.17 Spectra for 4-(thiophen-2-yl)-N-(4-(trifluoromethyl)phenyl)butanamide (MK90) (17)
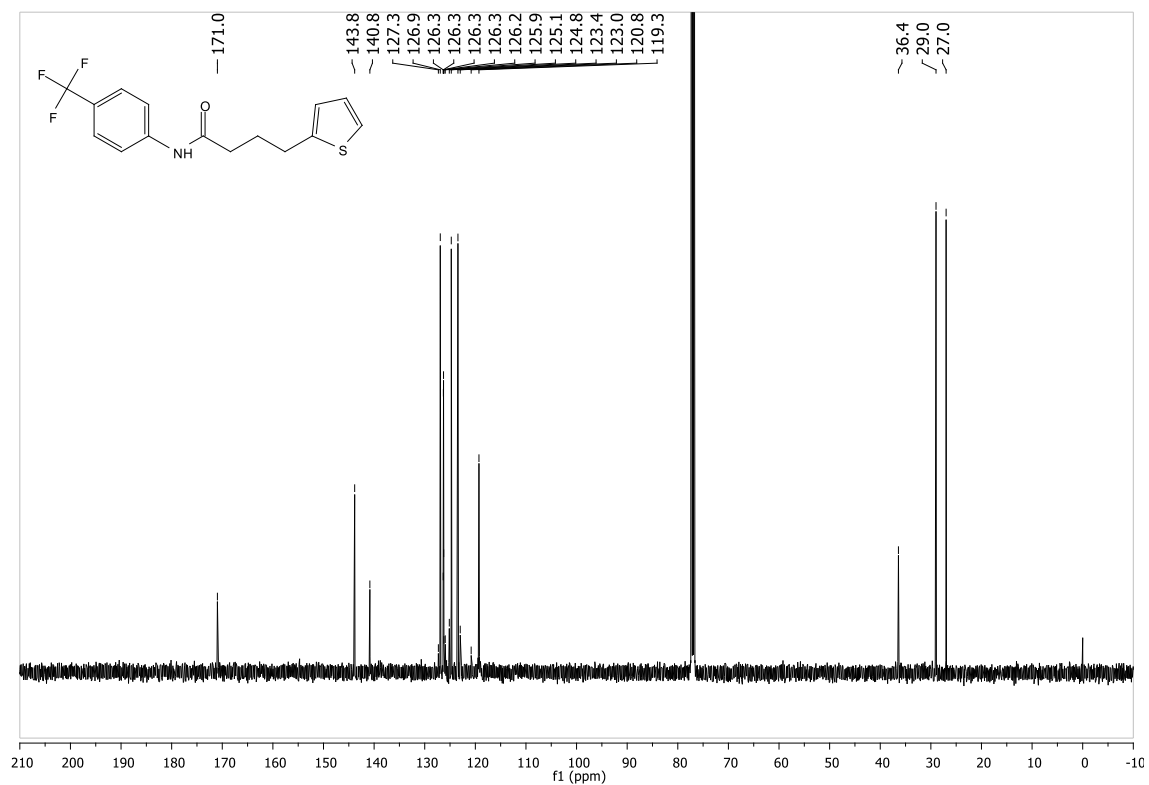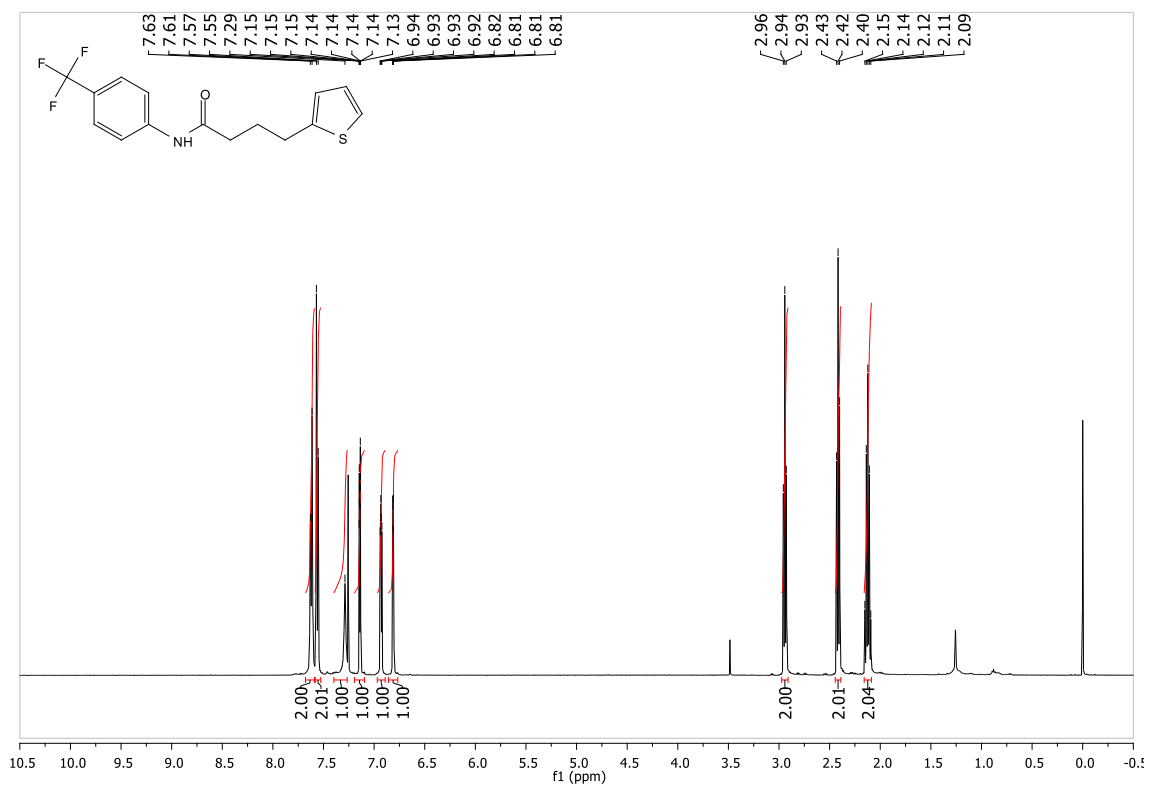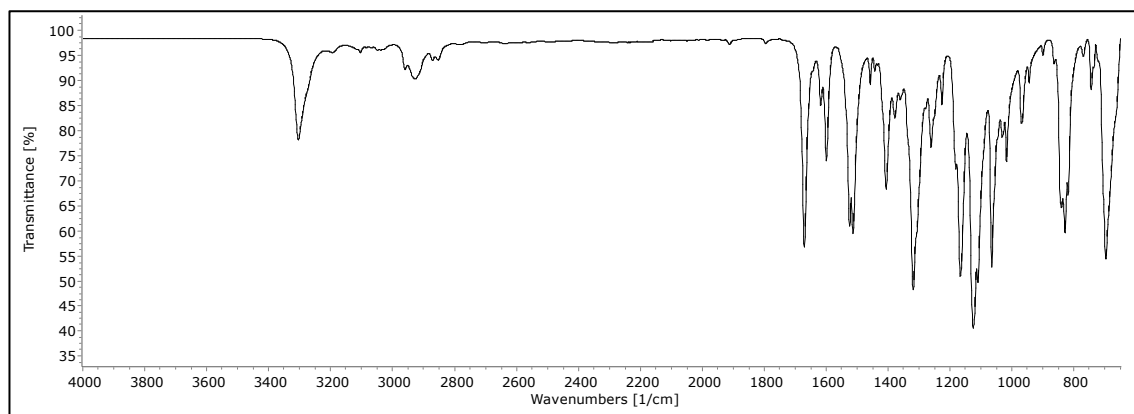
6.18 Spectra for 1-(4-(thiophen-2-yl)butyl)-4-(4-(trifluoromethyl)phenyl)piperazine (MK34) (RTC46) (18)
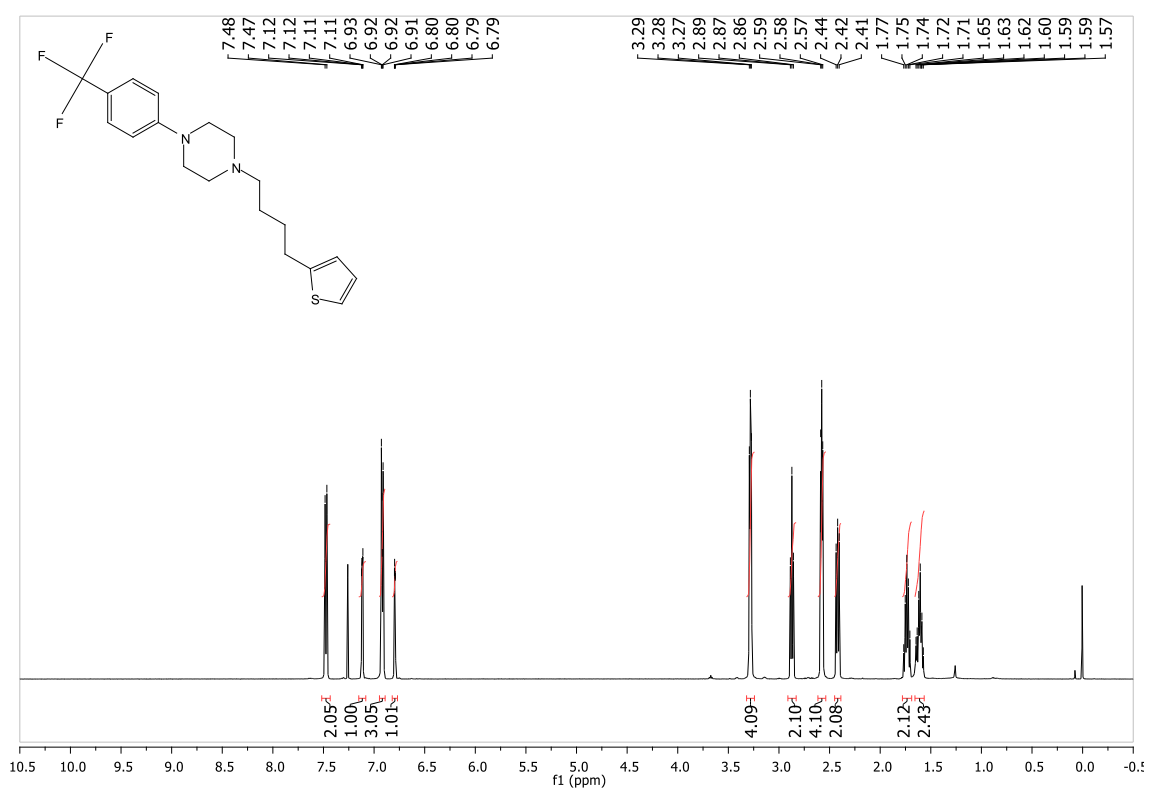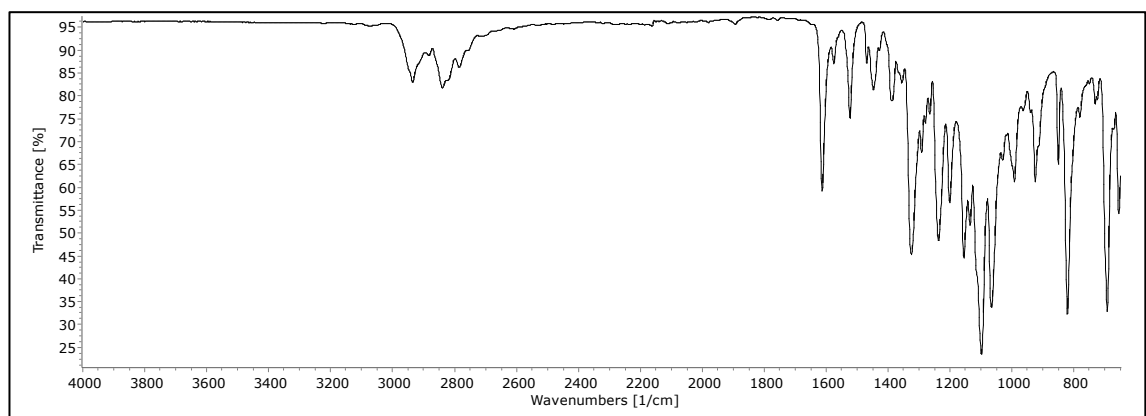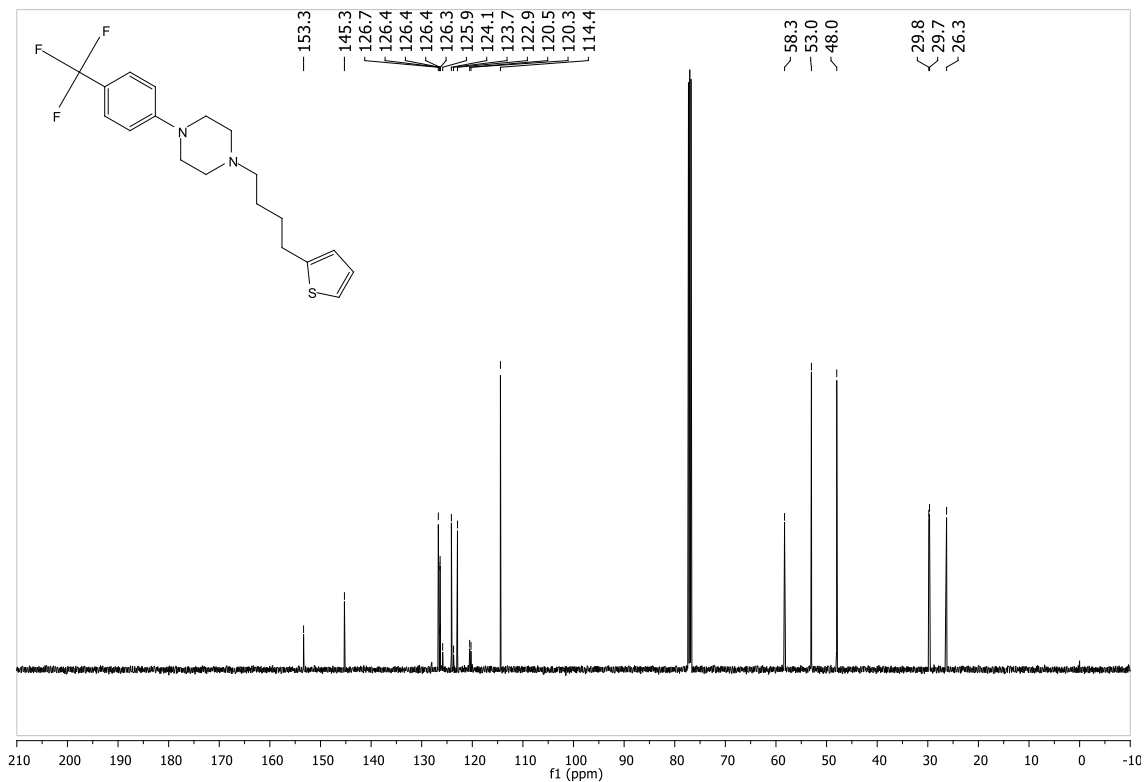
6.19 Spectra for 4-(thiophen-2-yl)butan-1-ol (MK32) (RD28) (19)
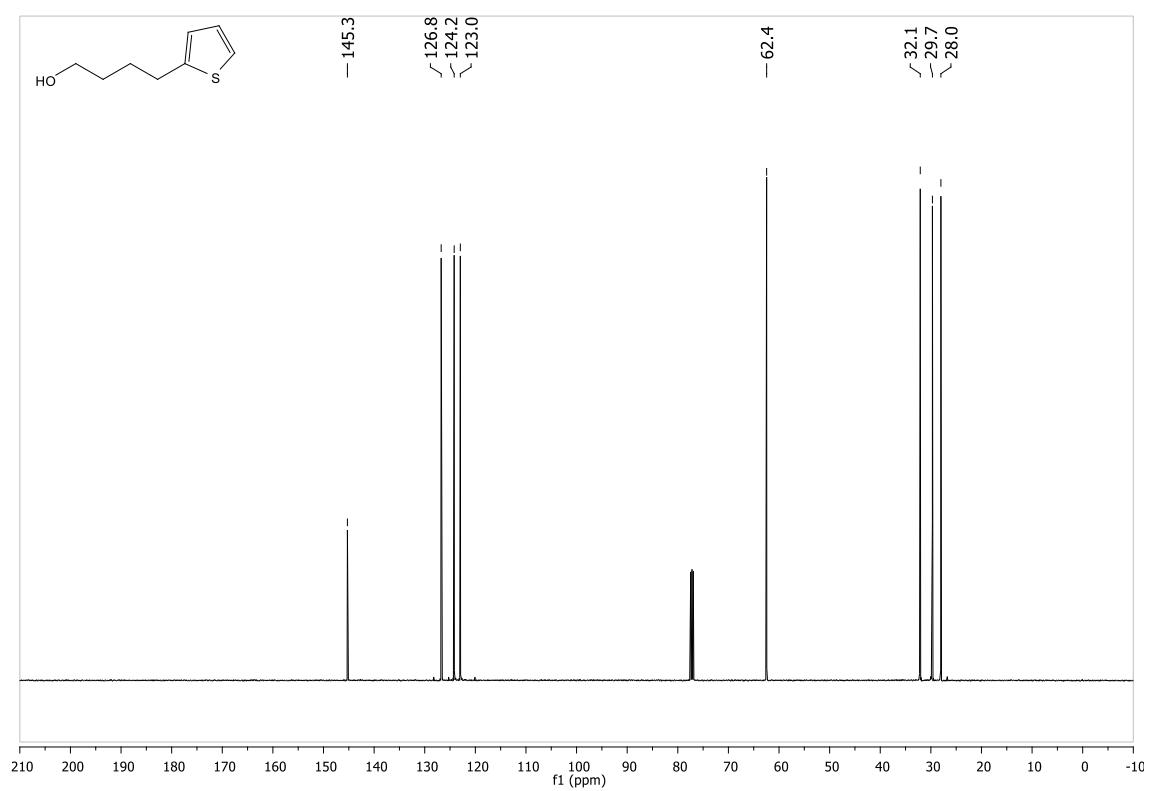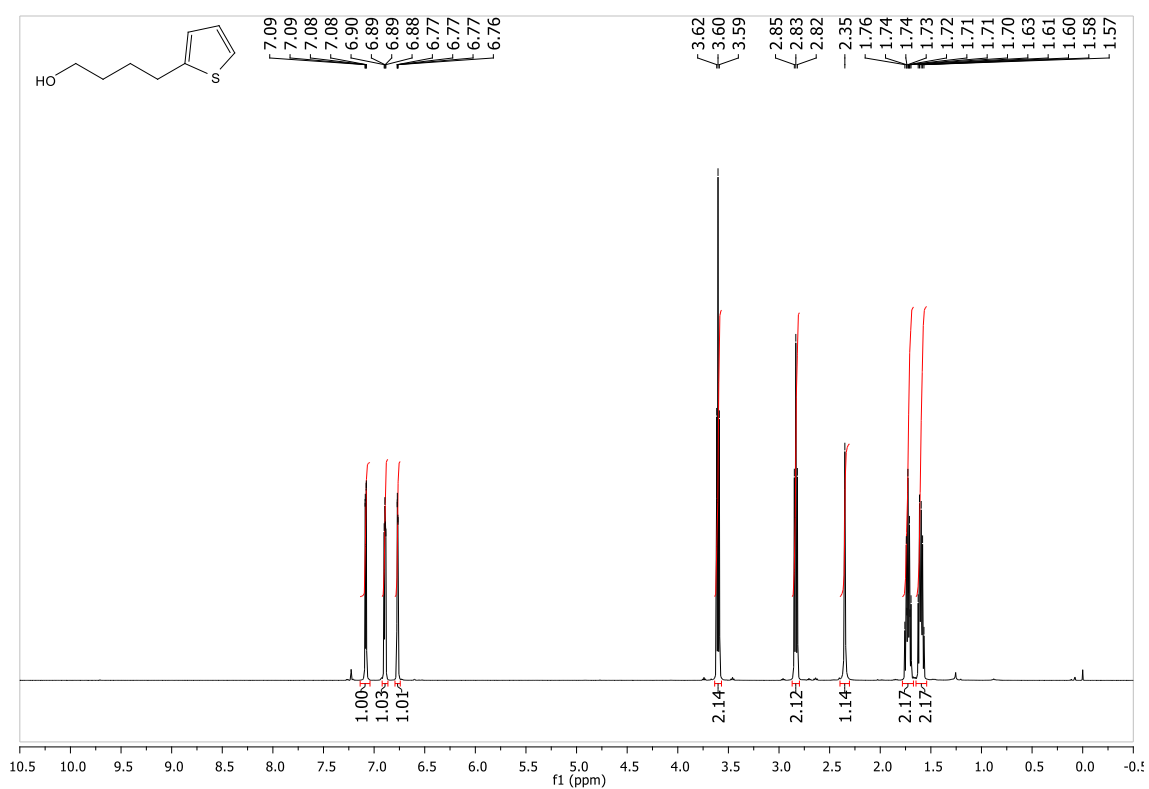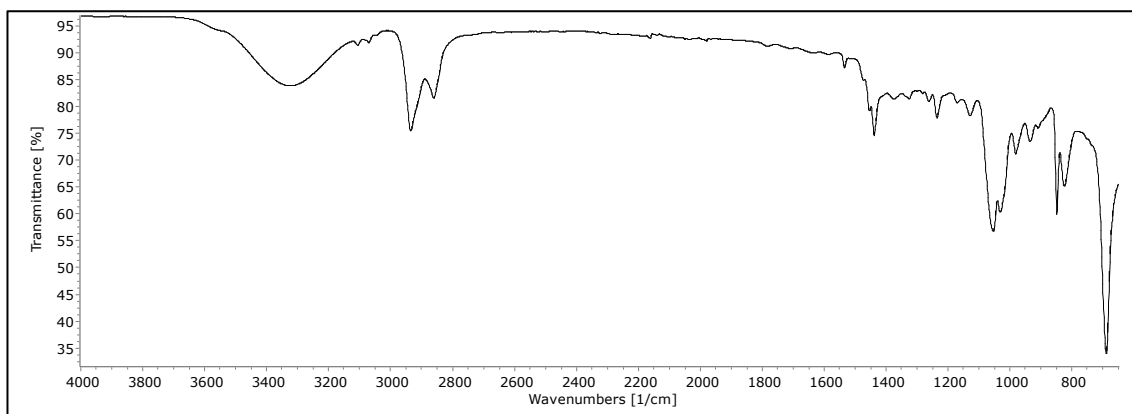
6.20   Spectra for 4-(thiophen-2-yl)butyl methanesulfonate (MK33) (RD31) (20)
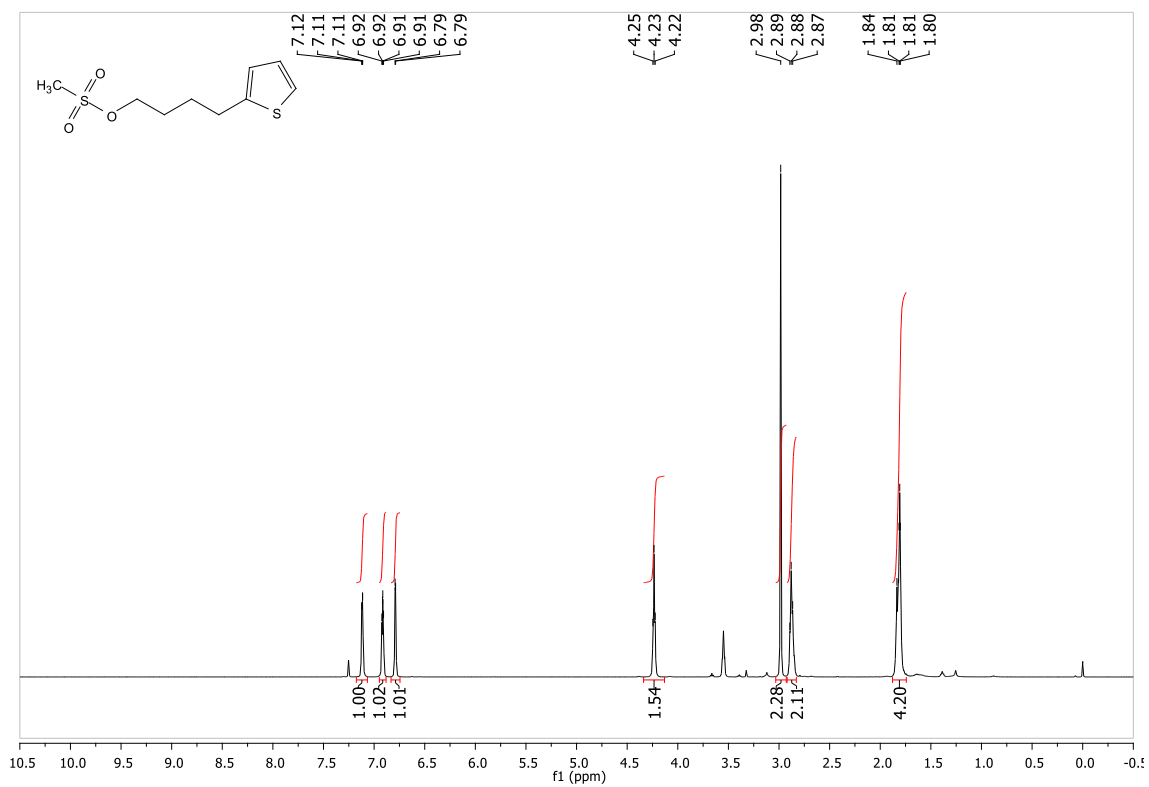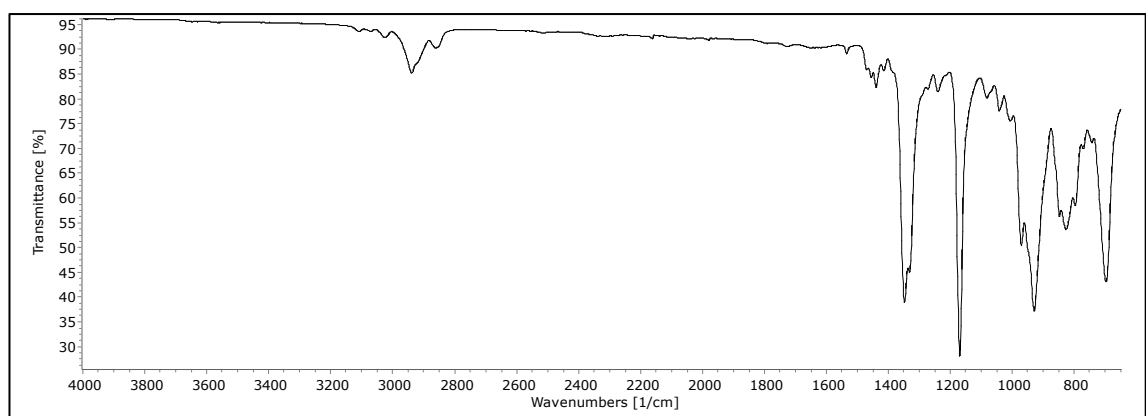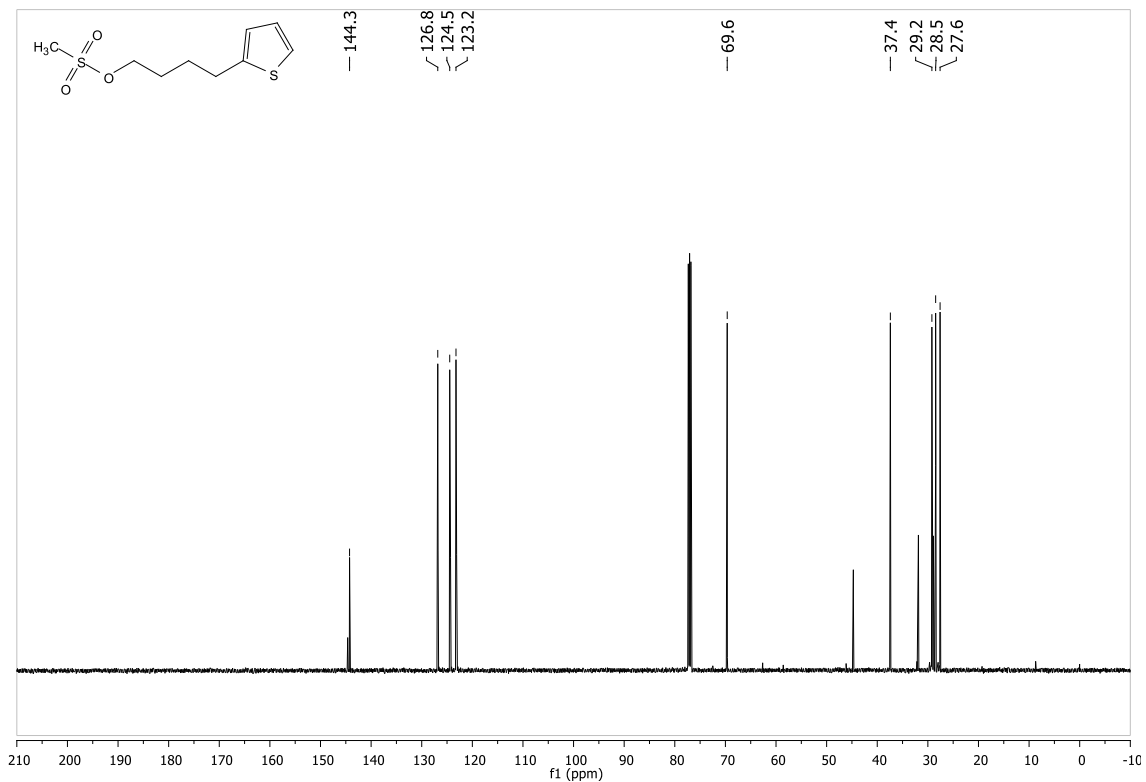
6.21 Spectra for thiophen-2-yl (4-(4-(trifluoromethyl)phenyl)piperazin-1-yl) methanone (MK37) (RTC93) (21)
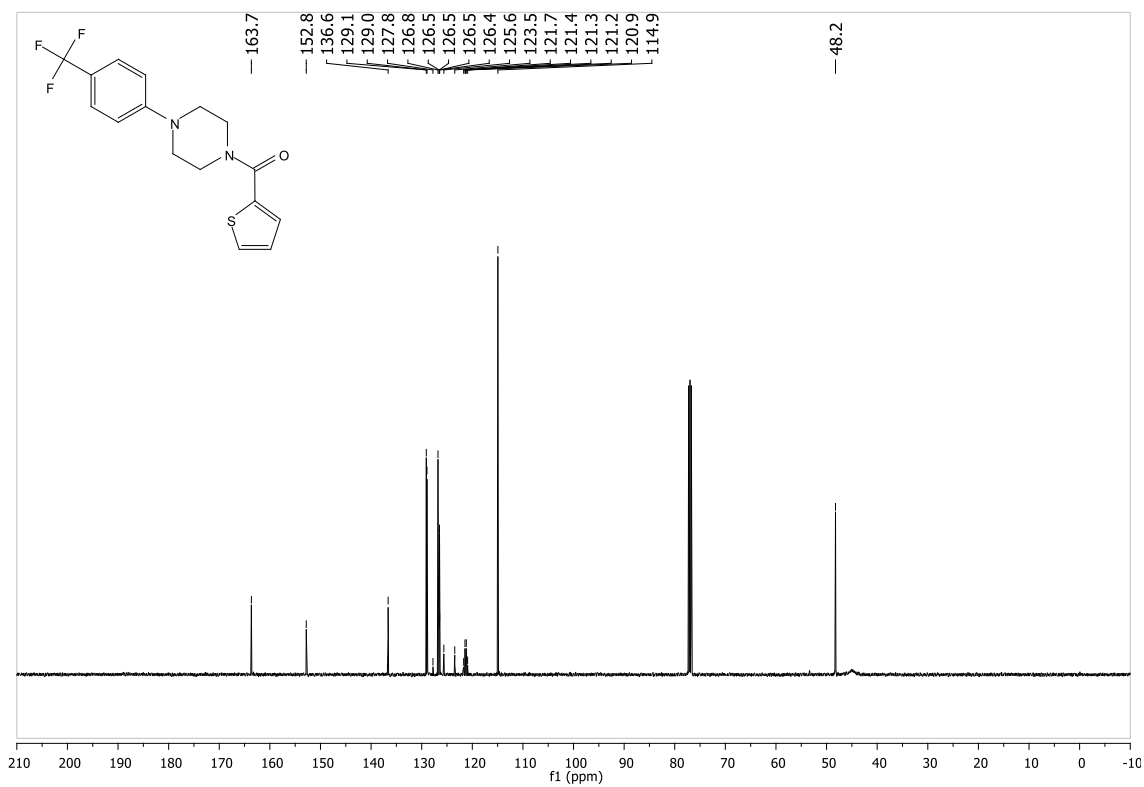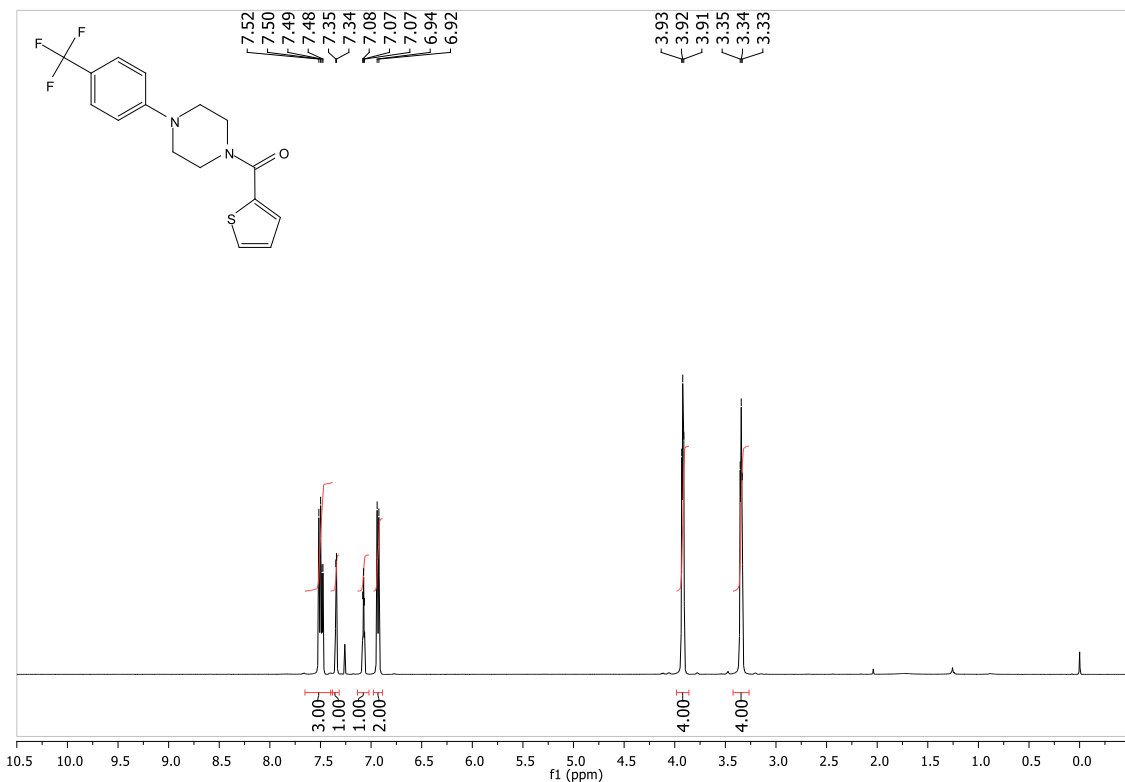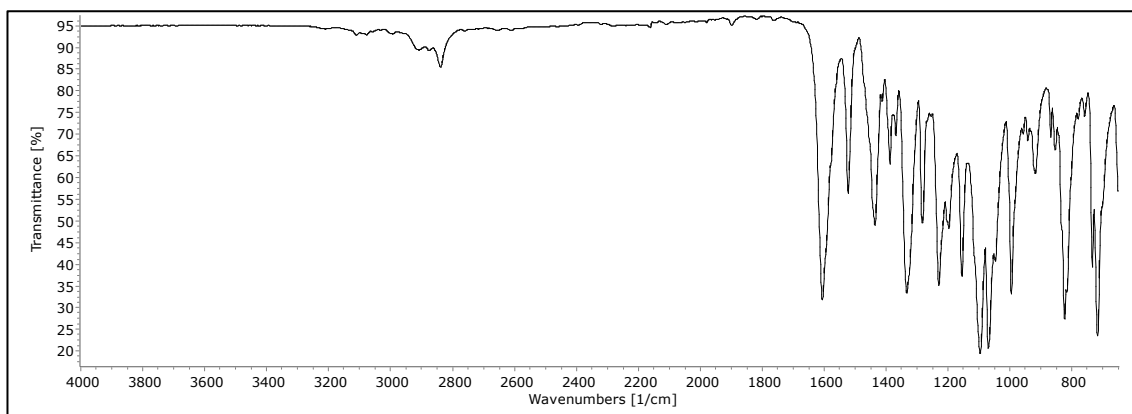
6.22 Spectra for 2-(thiophen-2-yl)-1-(4-(4-(trifluoromethyl)phenyl)piperazin-1-yl)ethanone (MK47) (RTC536) (22)
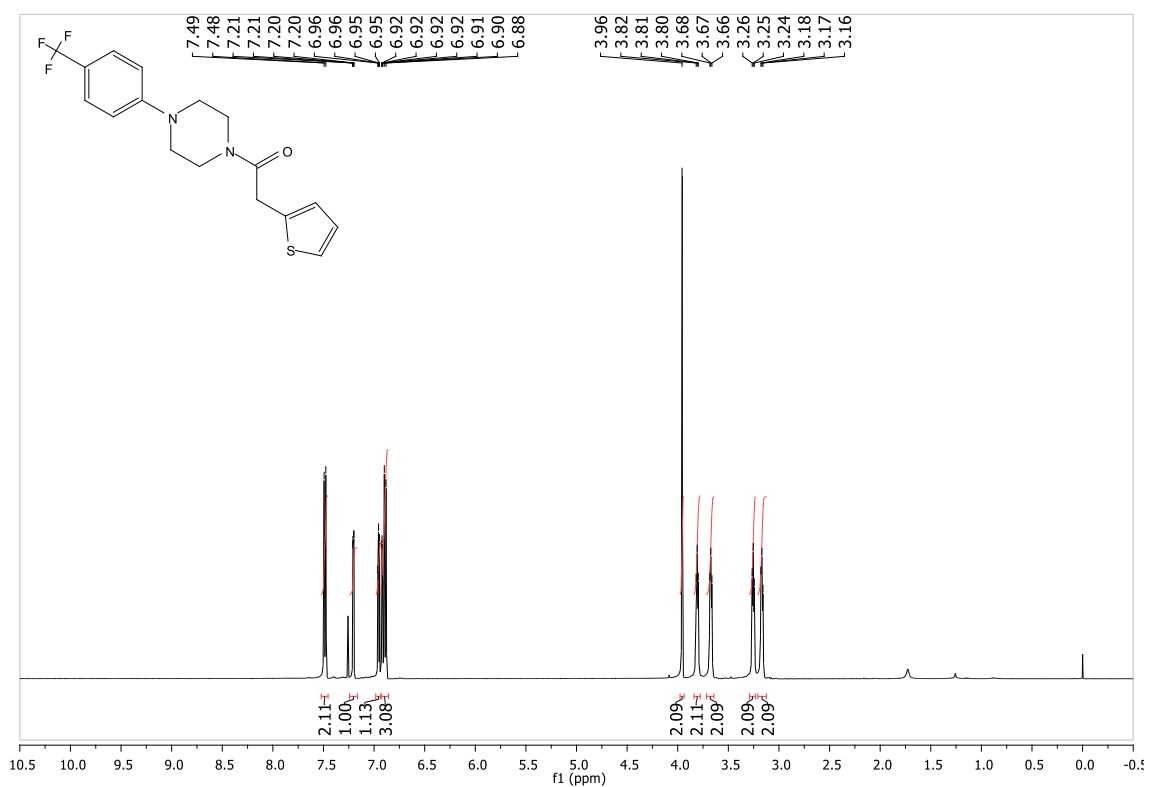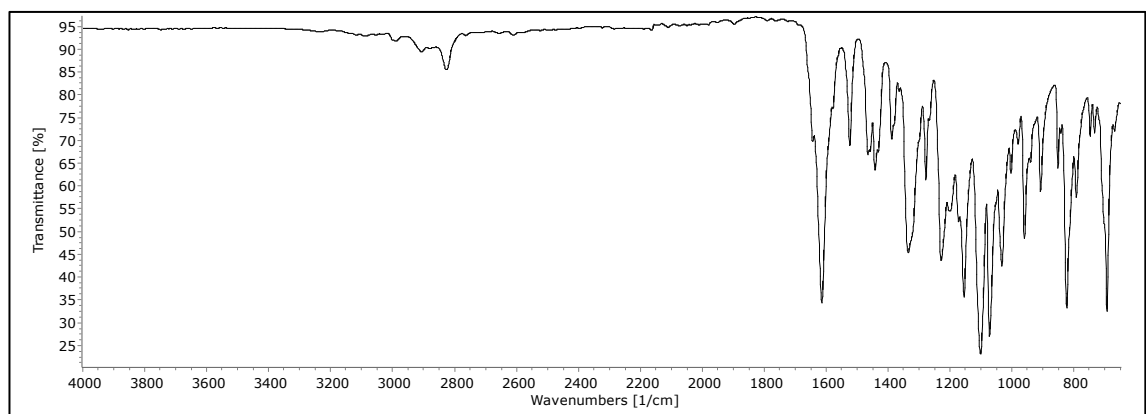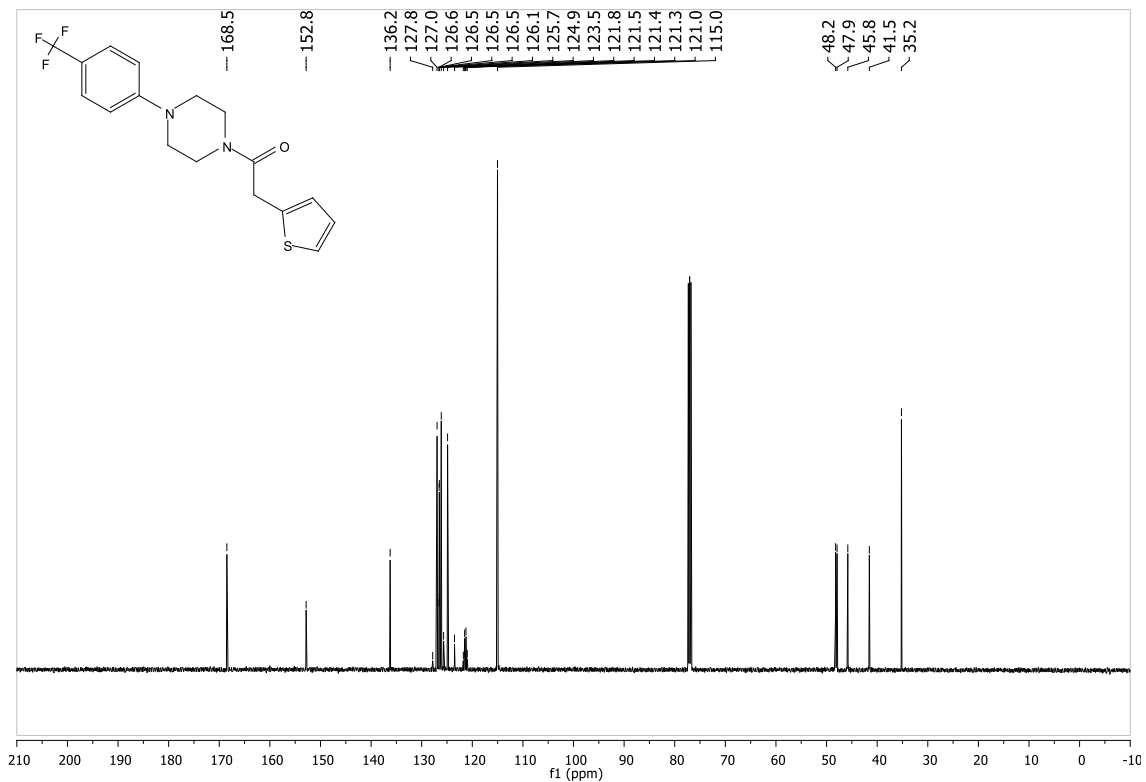
6.23 Spectra for 5-(thiophen-2-yl)-1-(4-(4-(trifluoromethyl)phenyl)piperazin-1-yl)pentan-1-one (MK18) (RTC195) (23)
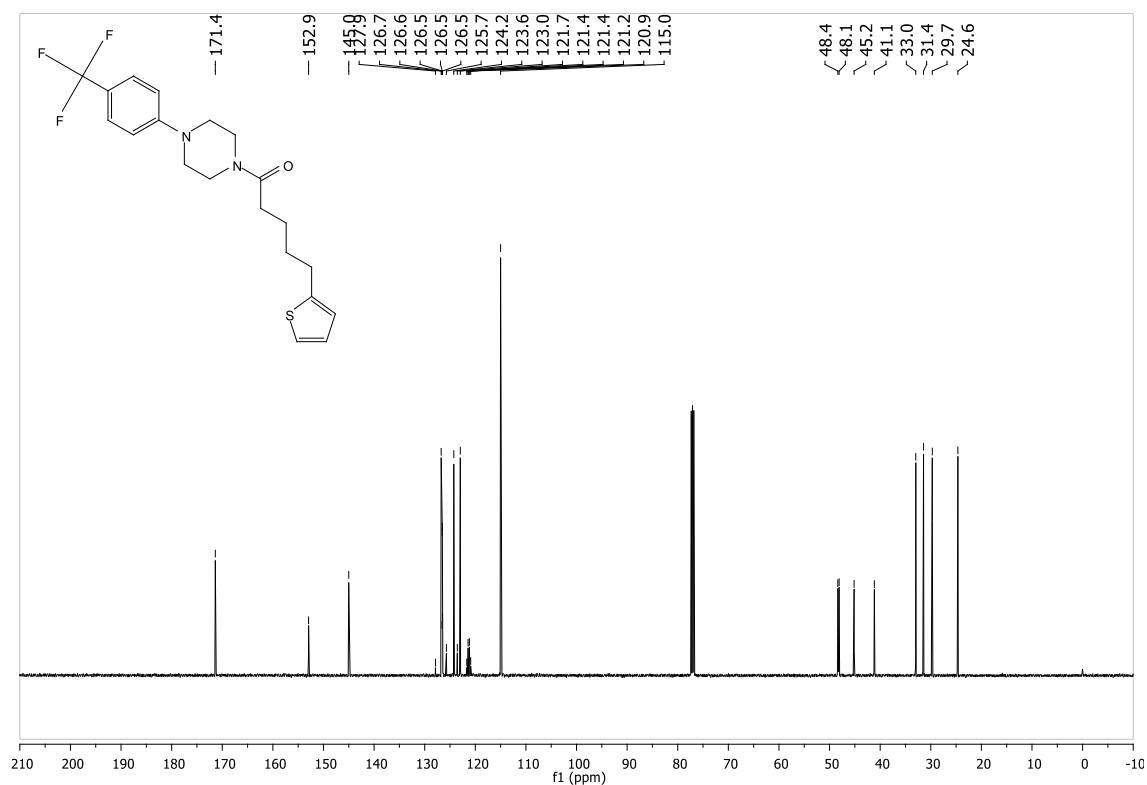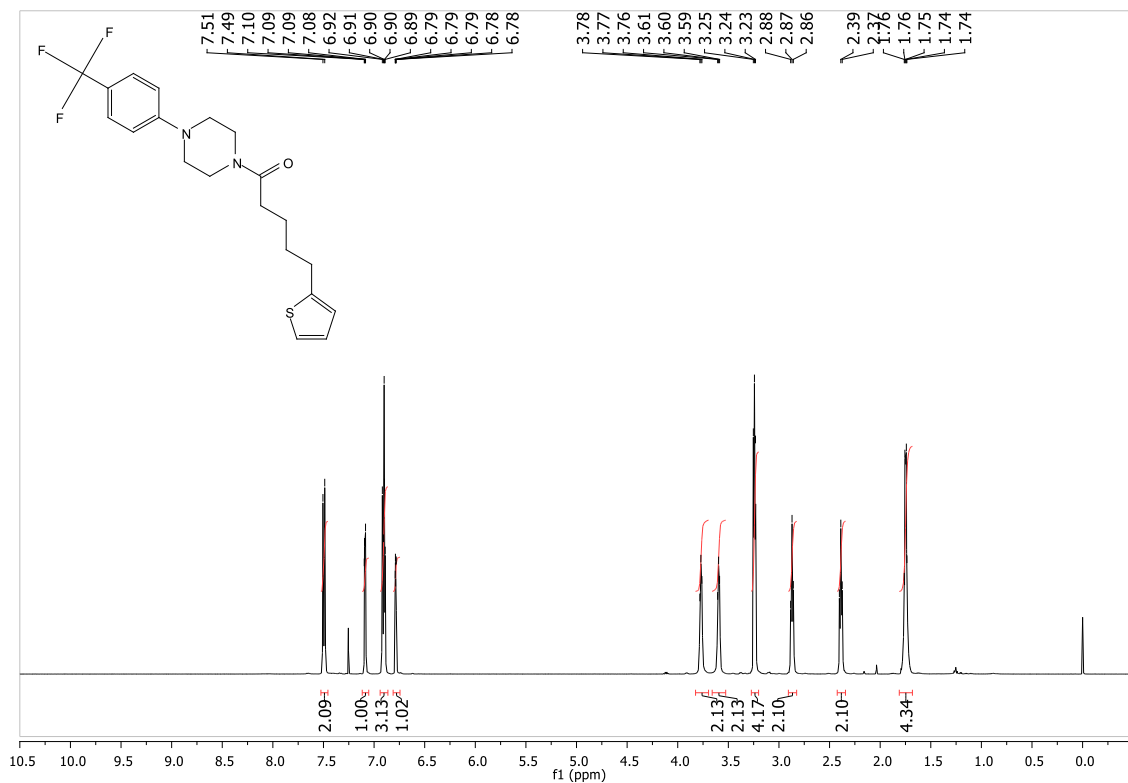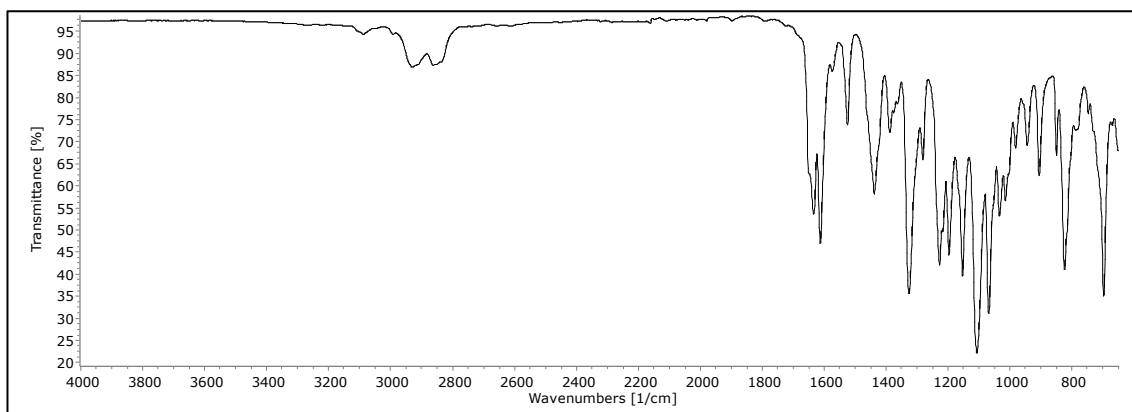
6.24 Spectra for 1-(thiophen-2-yl)-4-(4-(4-(trifluoromethyl)phenyl)piperazin-1-yl)butane-1,4-dione (MK40) (RTC2) (24)
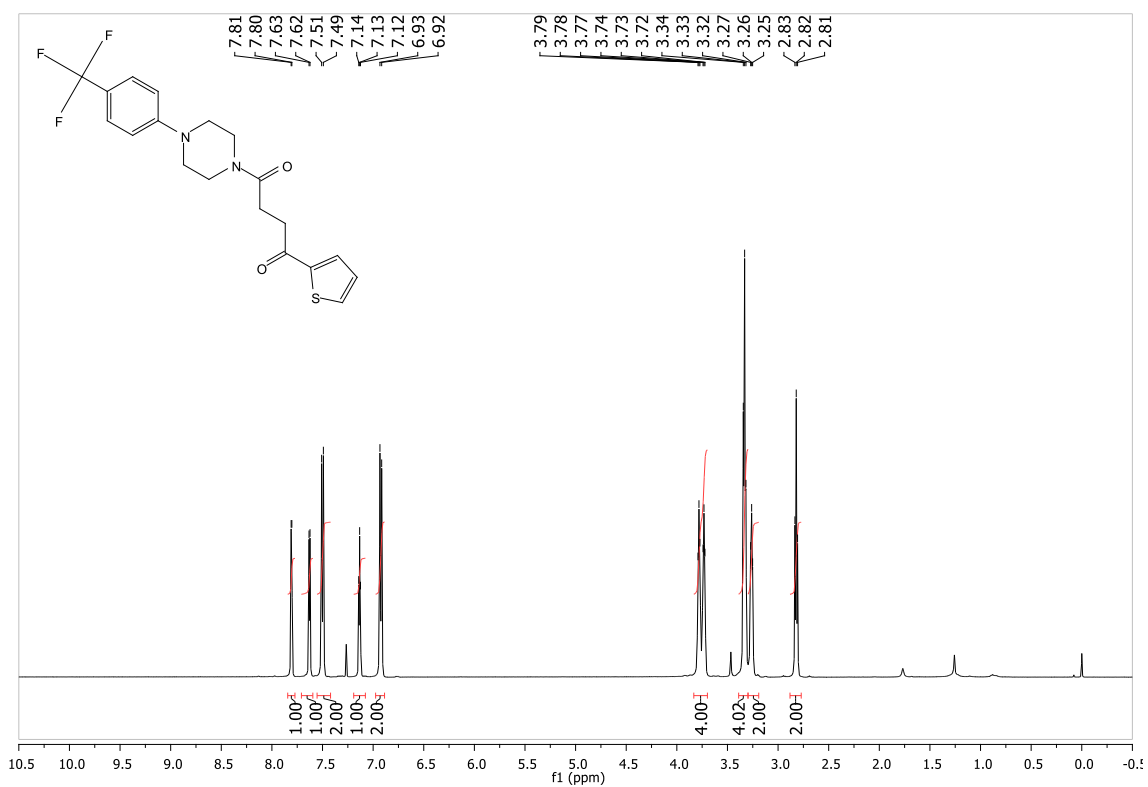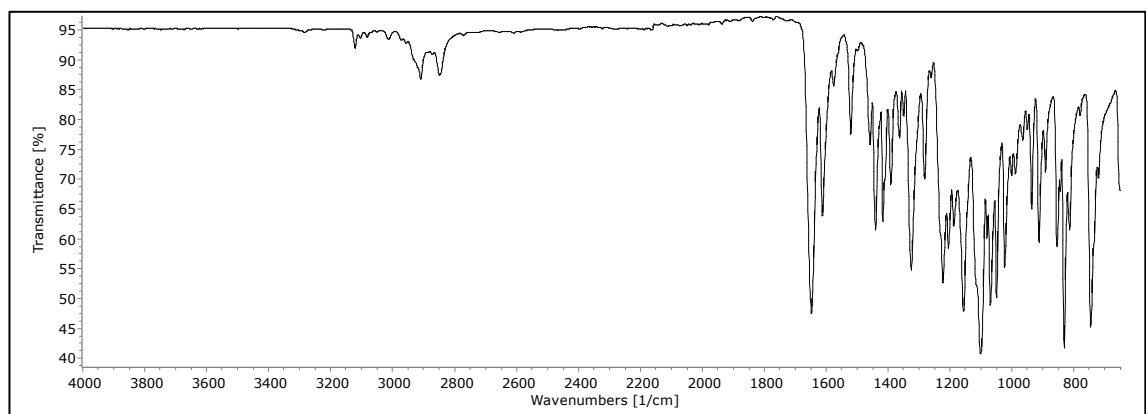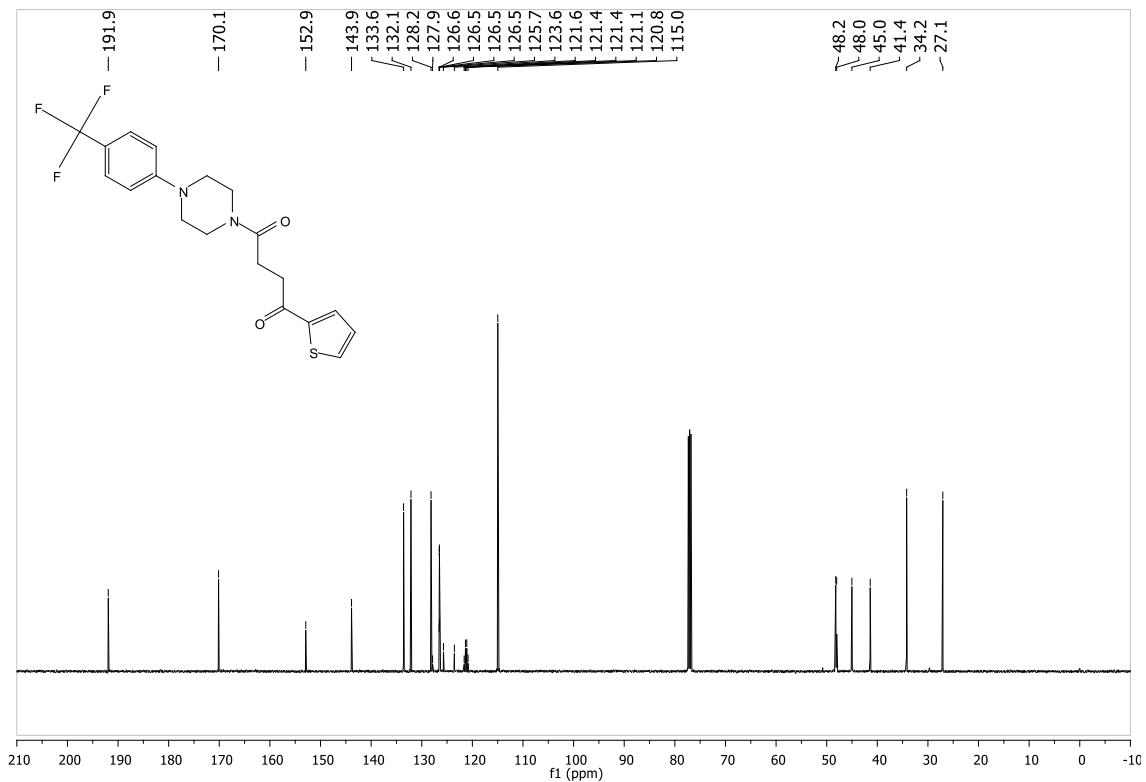
6.25   Spectra for 3-(thiophen-2-ylthio)-1-(4-(4-(trifluoromethyl)phenyl)piperazin-1-yl)propan-1-one (MK22) (RTC7) (25)
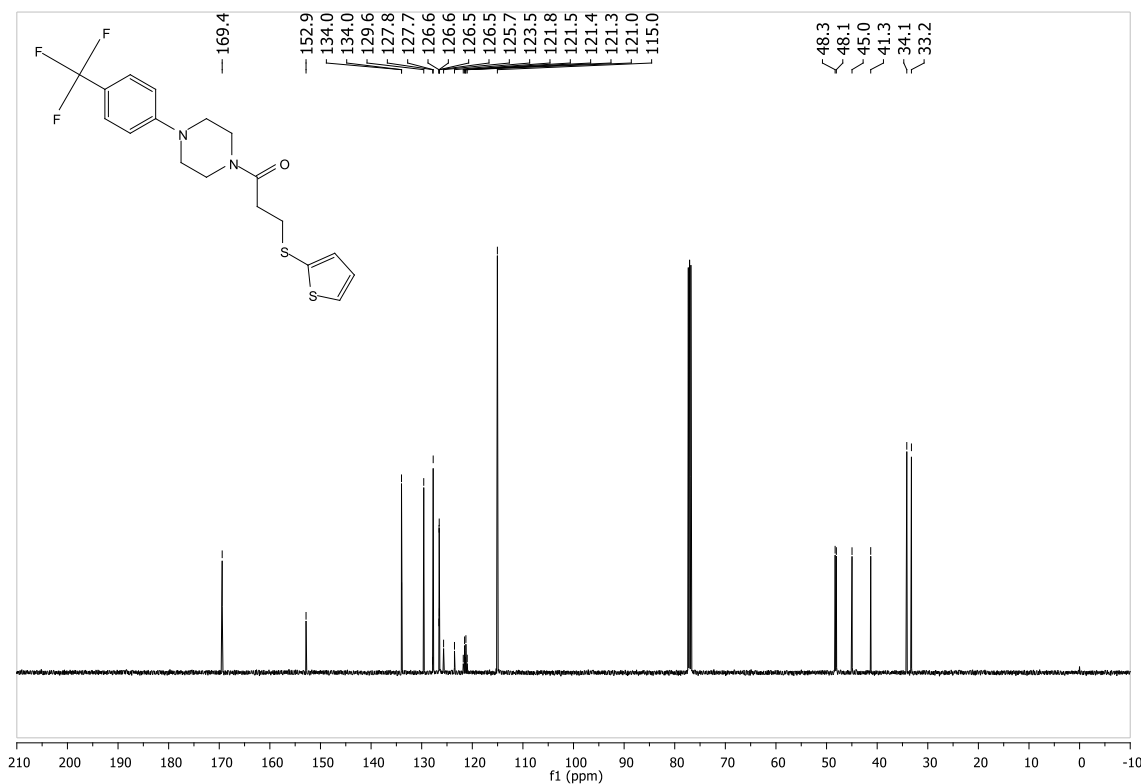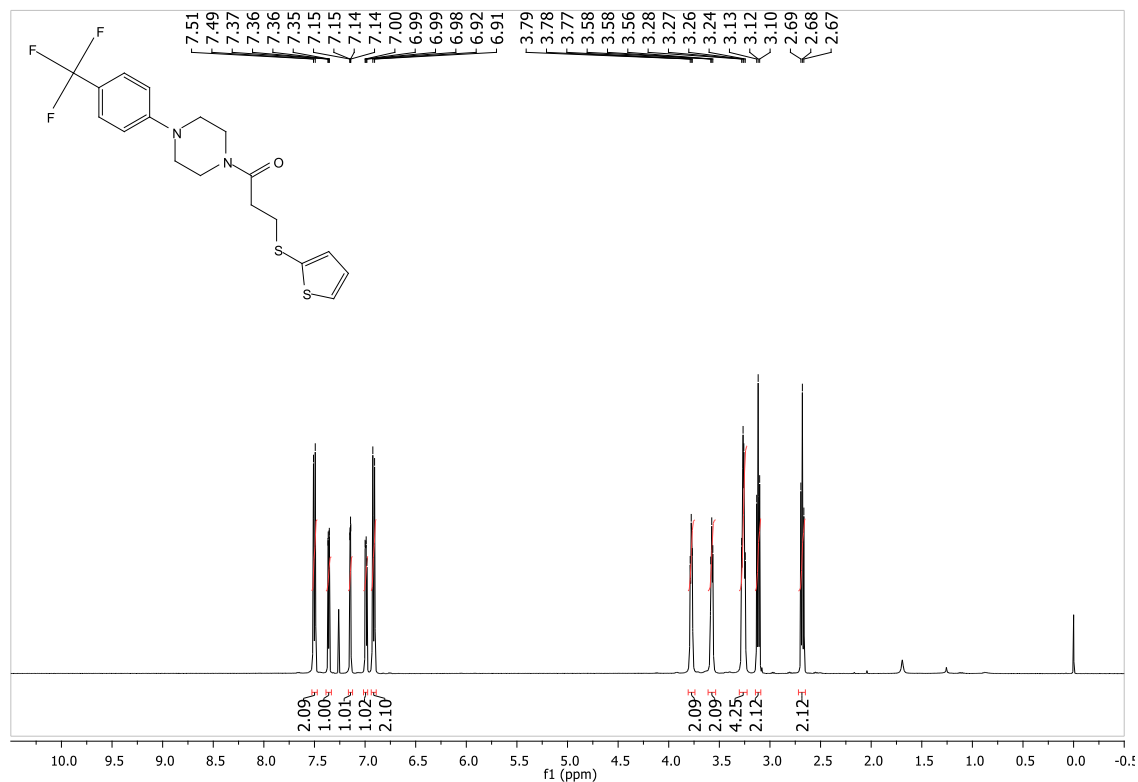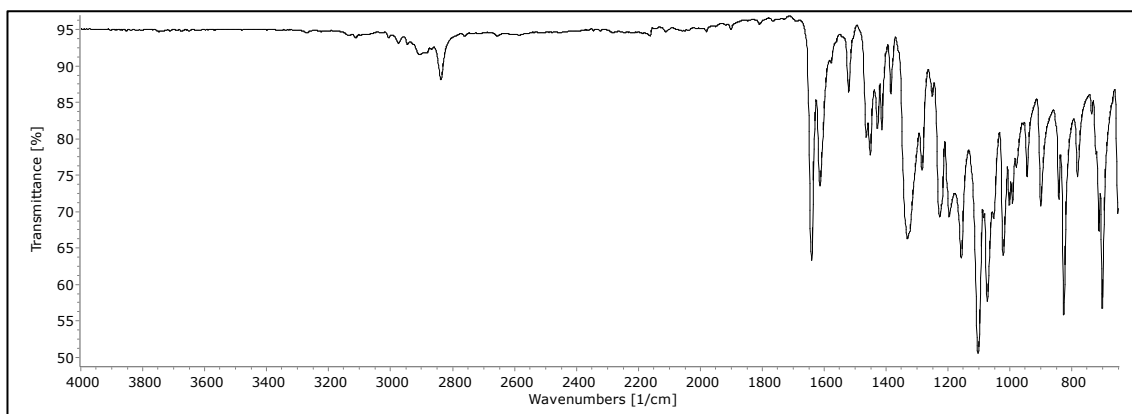
6.26   Spectra for *N,N*-dimethyl-4-(thiophen-2-yl)butanamide (MK46) (26)

178.8
172.9

144.6
143.9

126.8
126.8
124.6
124.5
123.3
123.1

37.3
35.5
33.0
32.2
29.3
29.0
26.9
26.6

H₃C
N
H₃C
O
S

210 200 190 180 170 160 150 140 130 120 110 100 90 80 70 60 50 40 30 20 10 0 -10
f1 (ppm)

6.27 Spectra for 1-(4-phenylpiperidin-1-yl)-4-(thiophen-2-yl)butan-1-one (MK89) (27)

7.34
7.32
7.31
7.24
7.23
7.21
7.19
7.13
7.12
7.12
6.94
6.93
6.93
6.92
6.83
6.83
4.83
4.81
3.92
3.90
3.09
2.96
2.94
2.93
2.76
2.74
2.73
2.71
2.63
2.63
2.44
2.44
2.42
2.42
2.41
2.10
2.09
2.07
2.06
2.04
1.90
1.88
1.64
1.64
1.62
1.61
1.60
1.58
1.58

2.00
3.00
1.00
1.00
1.00

1.00

1.00

1.01
2.00
1.03
1.01
2.00
2.02
2.01
2.05

10.5 10.0 9.5 9.0 8.5 8.0 7.5 7.0 6.5 6.0 5.5 5.0 4.5 4.0 3.5 3.0 2.5 2.0 1.5 1.0 0.5 0.0
f1 (ppm)

6.28 Spectra for 1-(thiophen-2-yl)-4-(4-(4-(trifluoromethyl)phenyl)piperidin-1-yl)butane-1,4-dione (MK88) (28)

6.29 Spectra for 5-phenyl-1-(4-(4-(trifluoromethyl)phenyl)piperazin-1-yl)pentan-1-one (MK30) (RTC16) (29)

13C NMR peaks: 171.5, 153.0, 142.2, 128.5, 128.4, 127.9, 126.6, 126.5, 126.5, 125.8, 125.8, 123.6, 121.6, 121.5, 121.3, 121.0, 120.8, 115.0, 48.3, 48.1, 45.1, 41.1, 35.7, 33.1, 31.1, 24.9
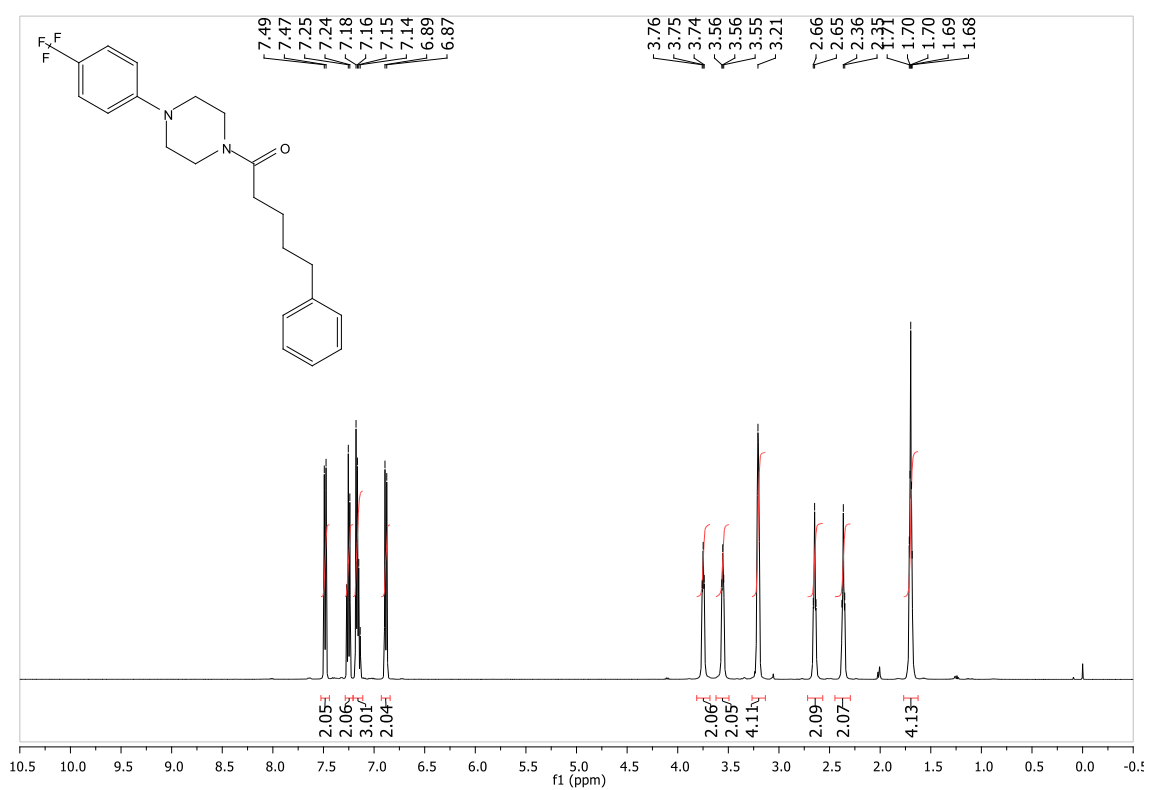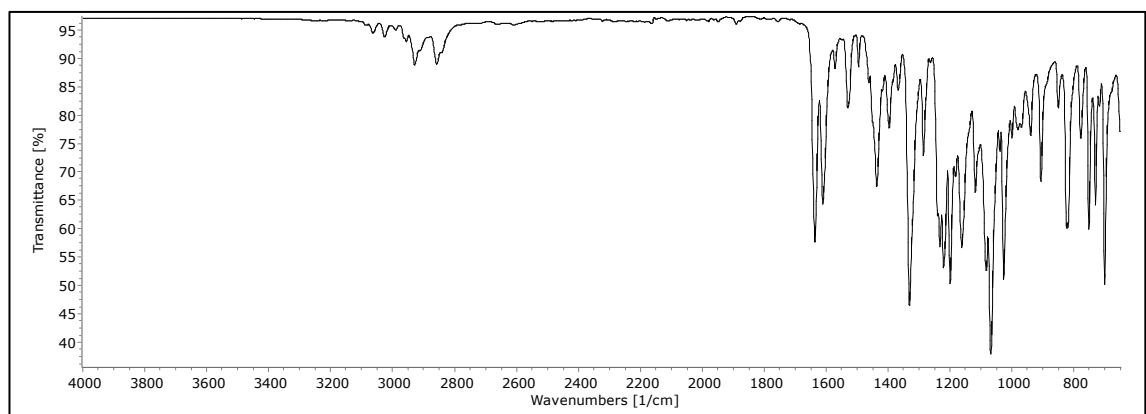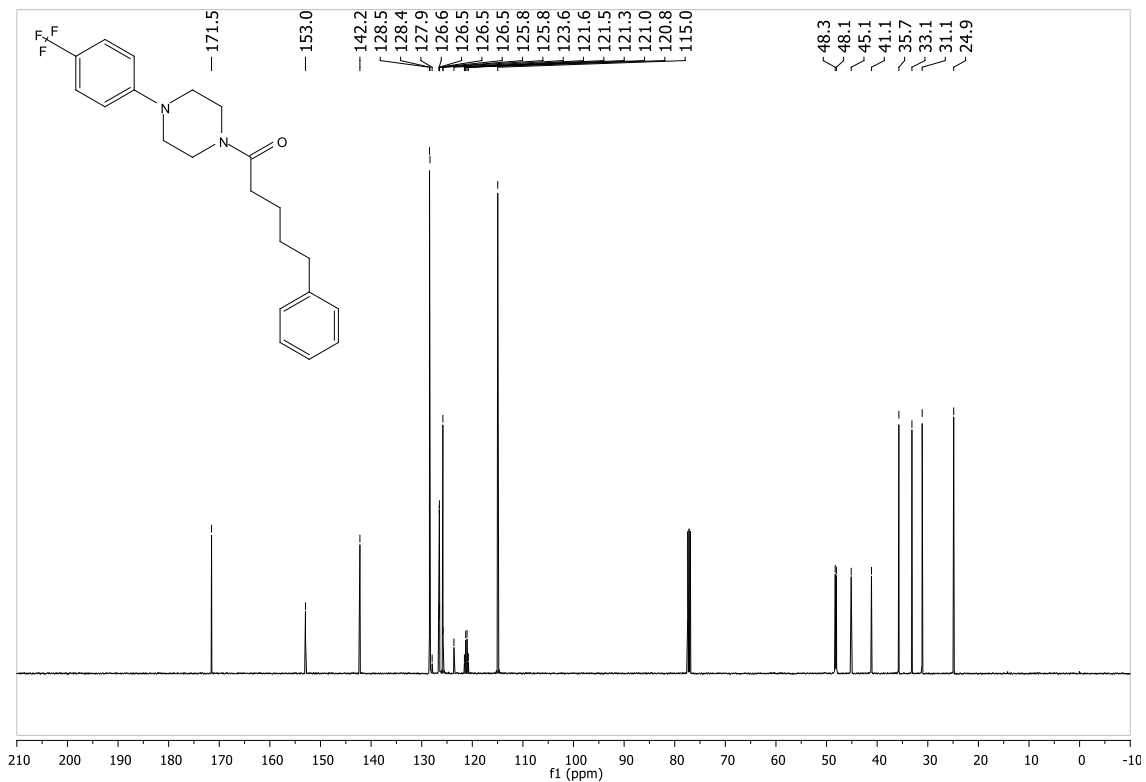
6.30 Spectra for 1-(4-(4-(trifluoromethyl)phenyl)piperazin-1-yl)ethanone (MK29) (RTC12) (30)
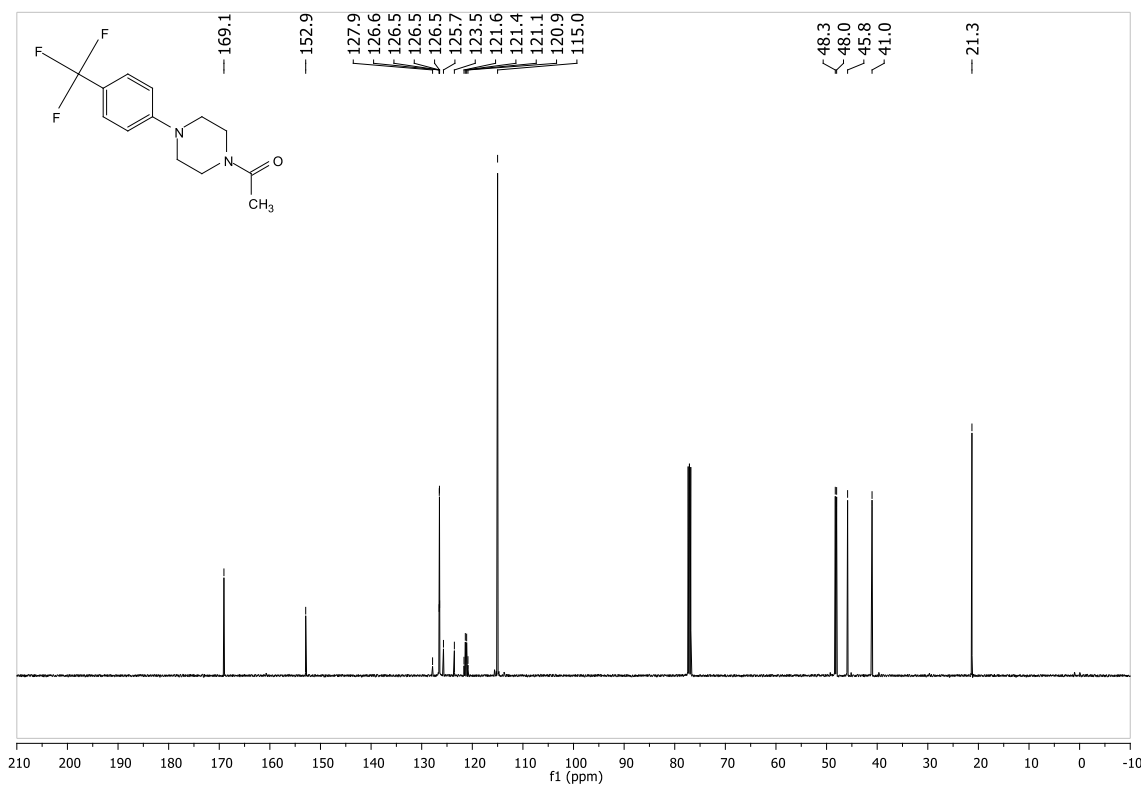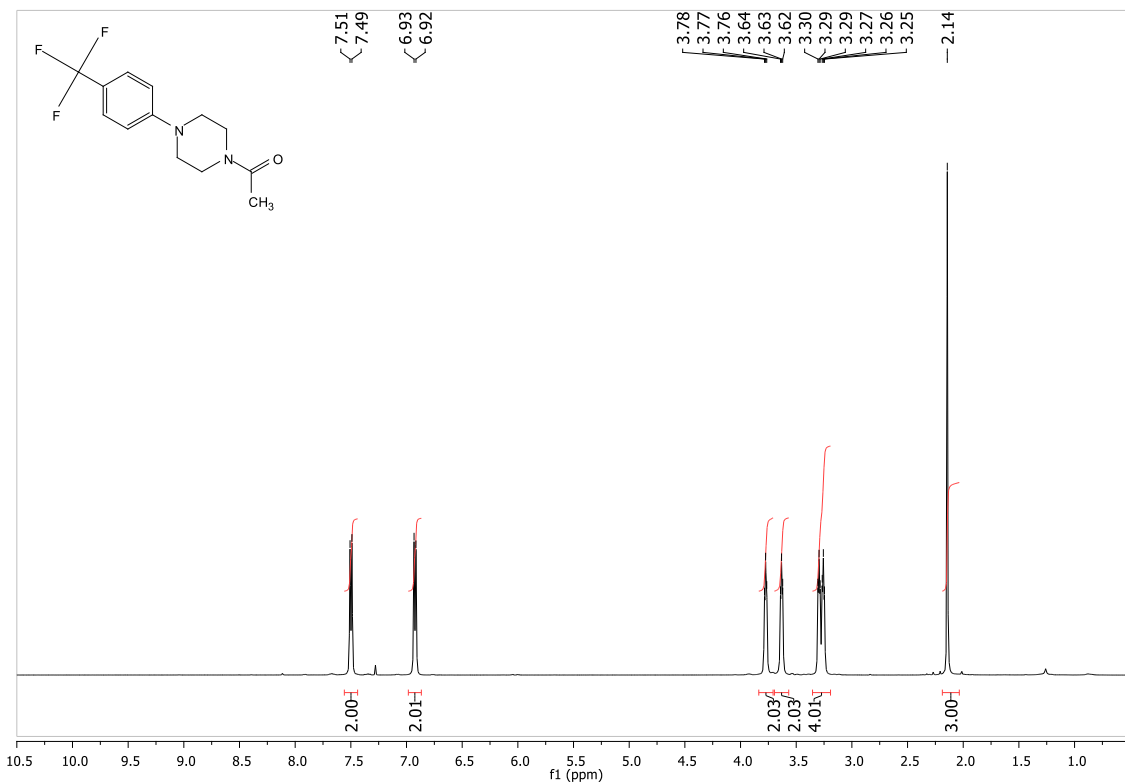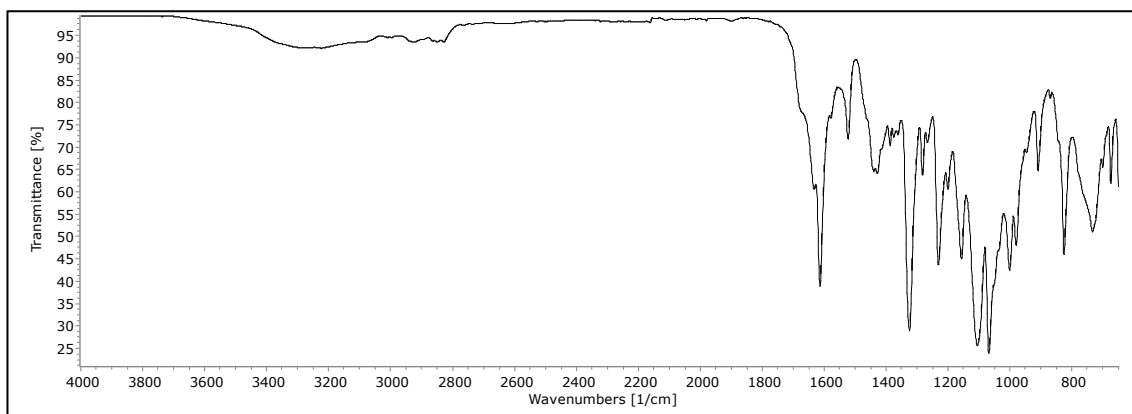
6.31 Spectra for 1-methyl-4-(4-(trifluoromethyl)phenyl)piperazine (MK35) (RTC31) (31)

153.3

128.0
126.4
126.4
126.4
126.3
125.8
123.7
121.5
120.9
120.6
120.3
120.1
114.5

54.8
48.0
46.1

f1 (ppm)

Transmittance [%]

Wavenumbers [1/cm]
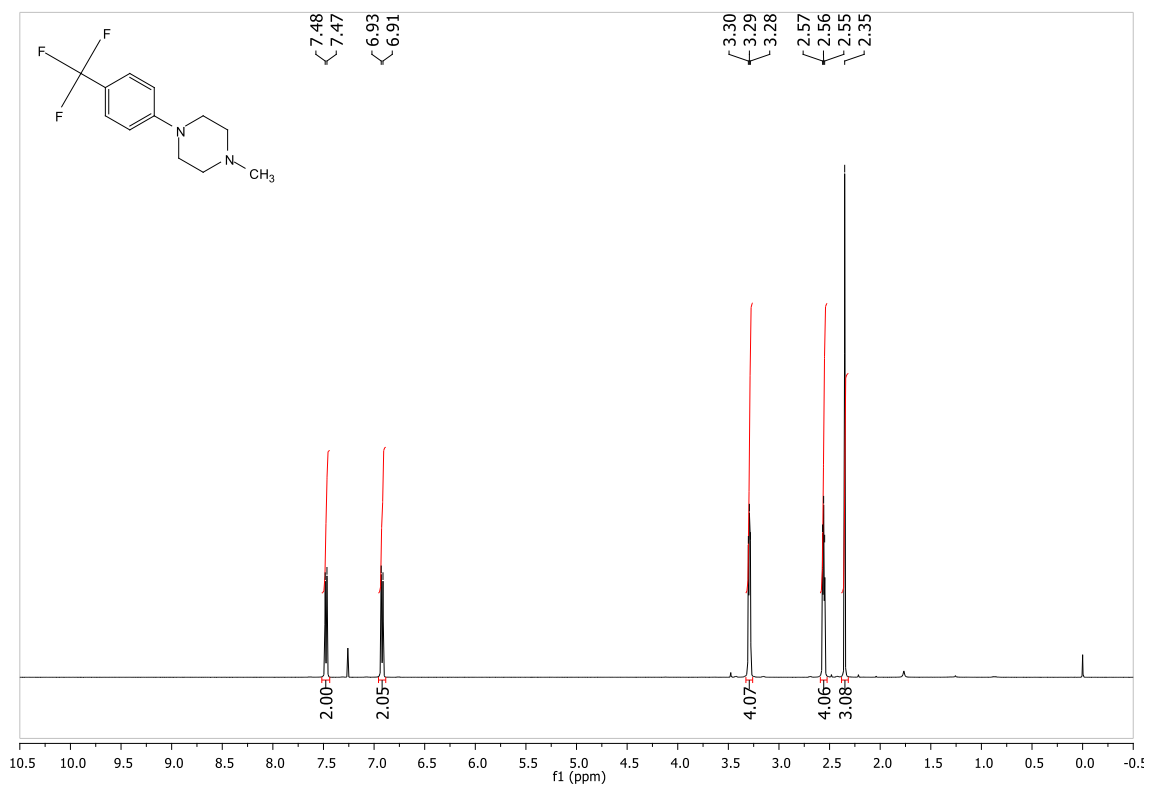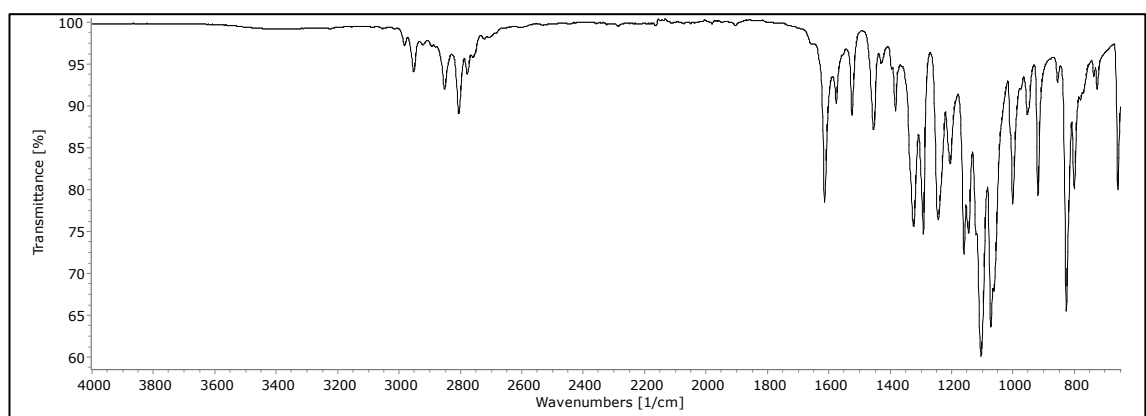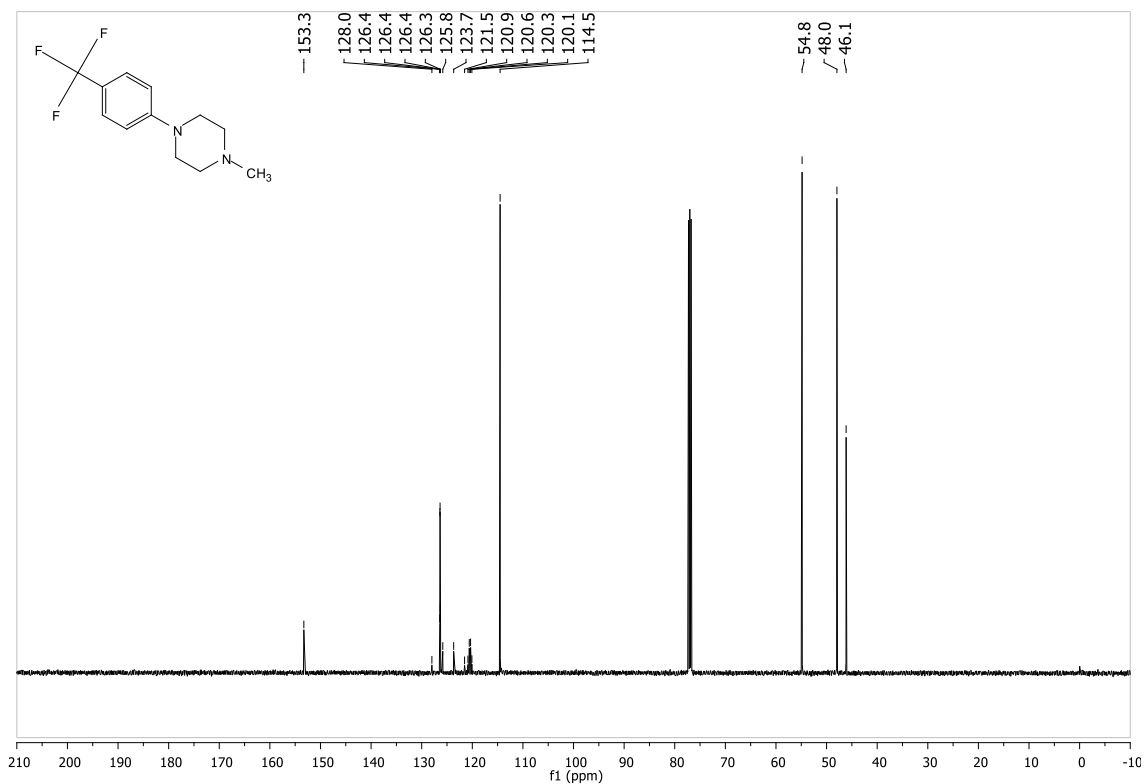
6.32 Spectra for 3-phenyl-1*H*-pyrazol-5-amine (MK12, MK60, MK64, MK67) (32)
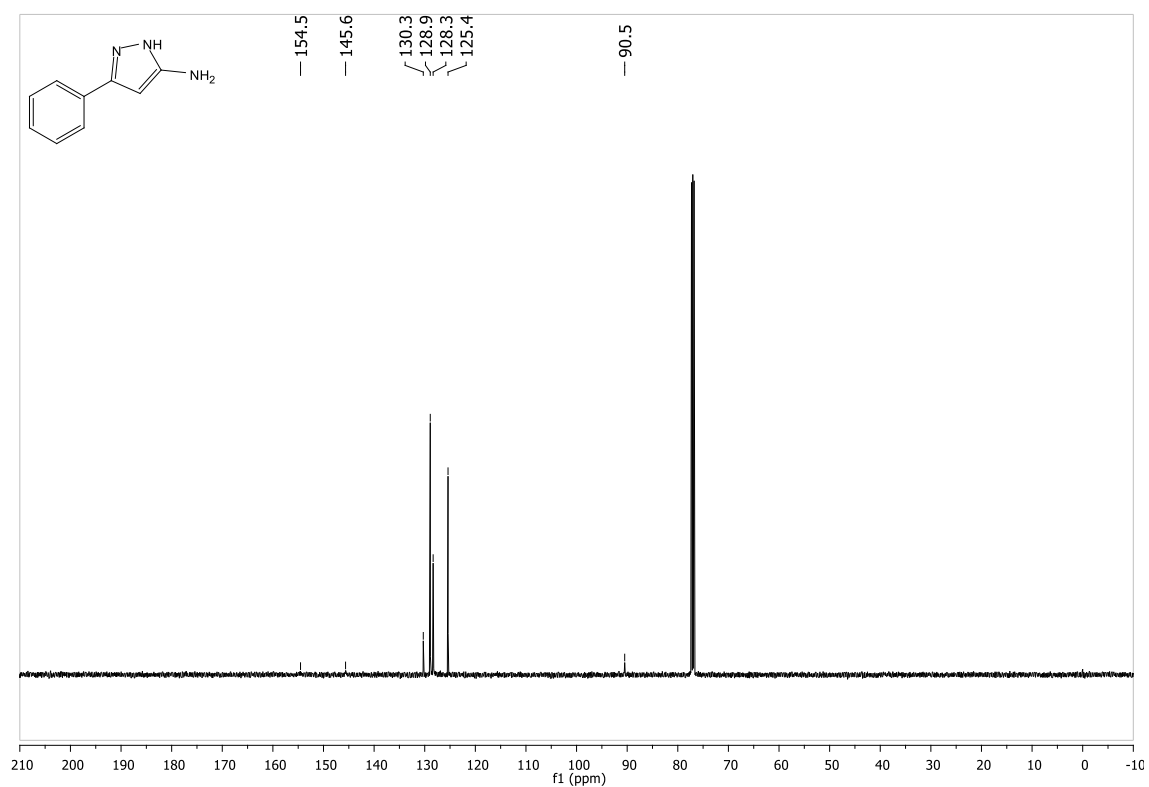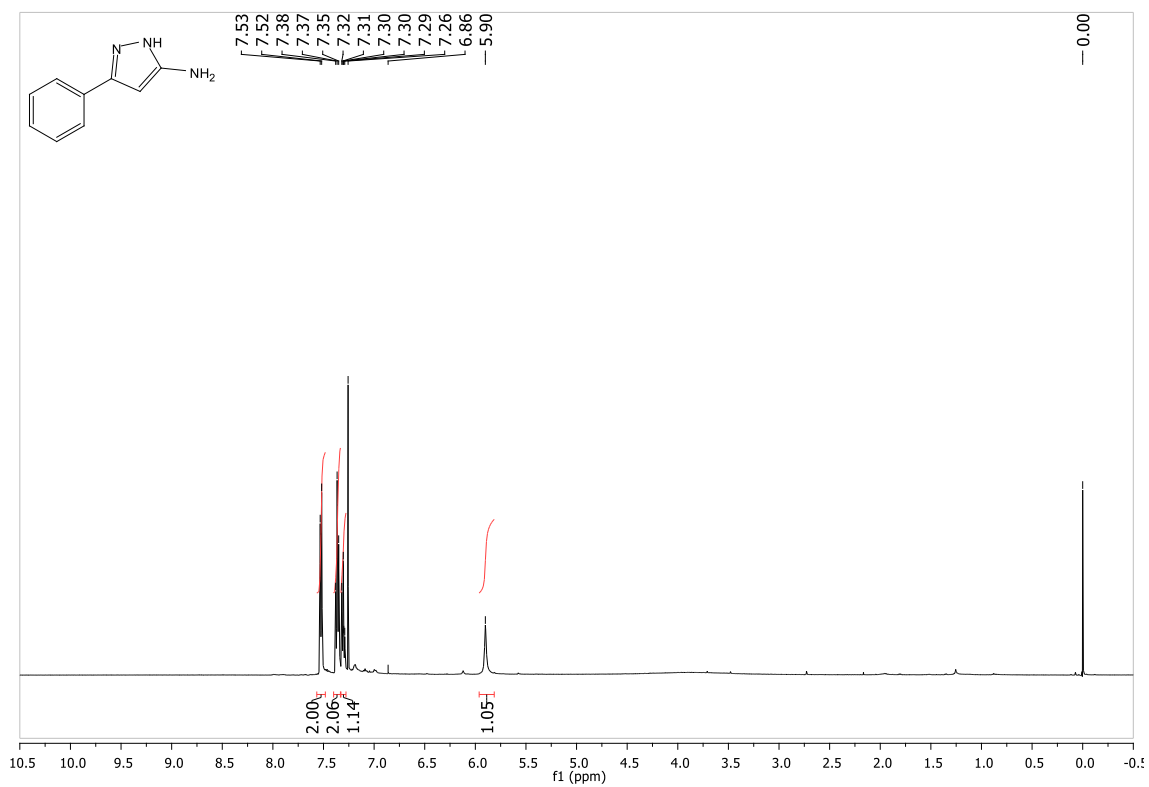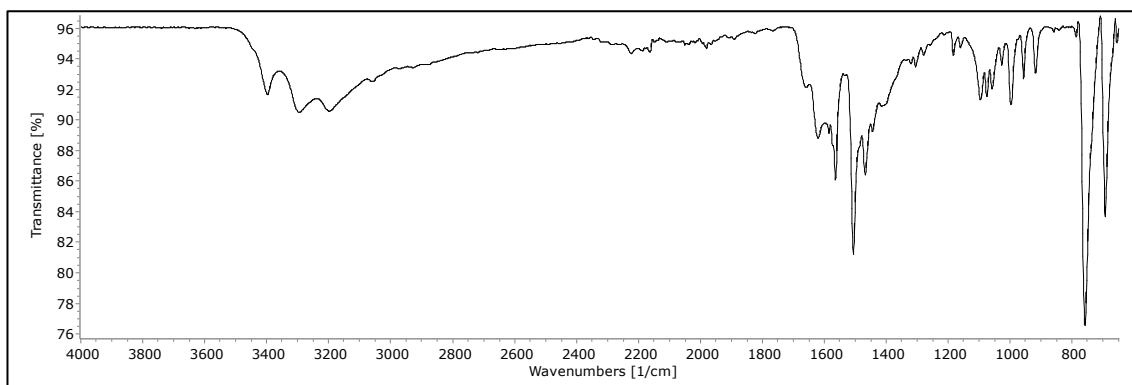
6.33   Spectra for 3-(3-chlorophenyl)-1H-pyrazol-5-amine (MK14) (33)
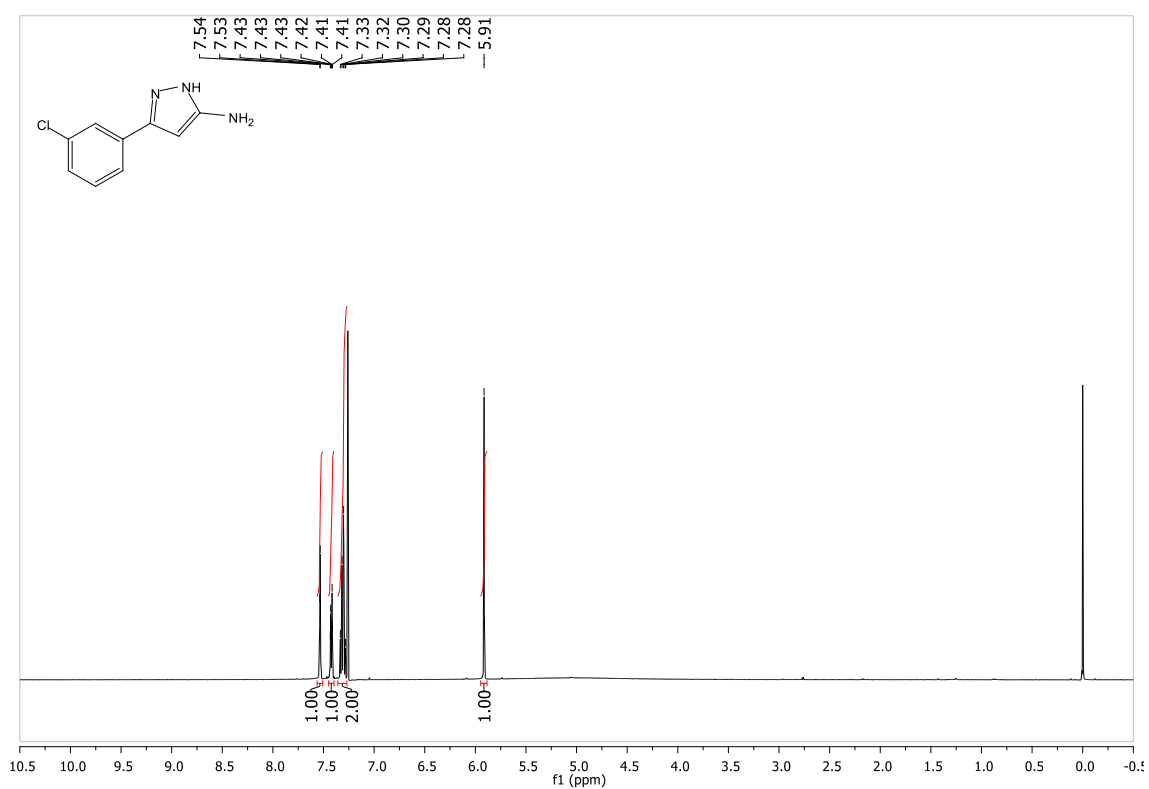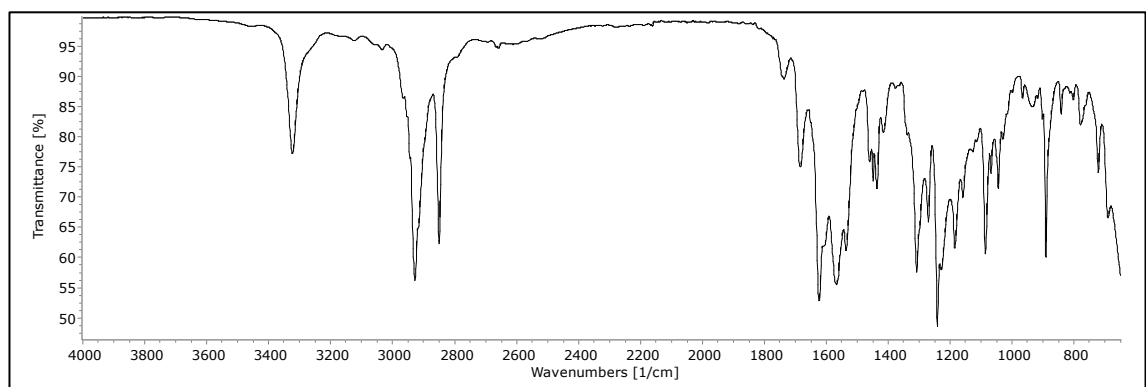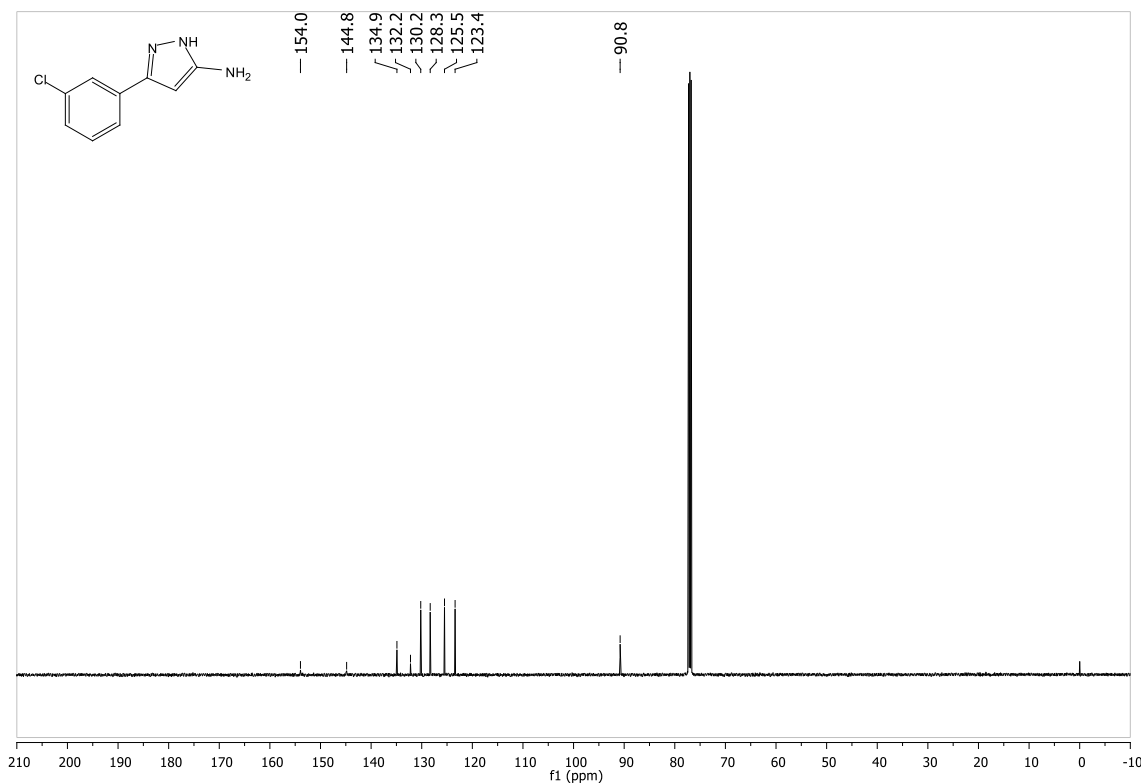
6.34   Spectra for 3-(3-methoxyphenyl)-1*H*-pyrazol-5-amine (MK50) (34)
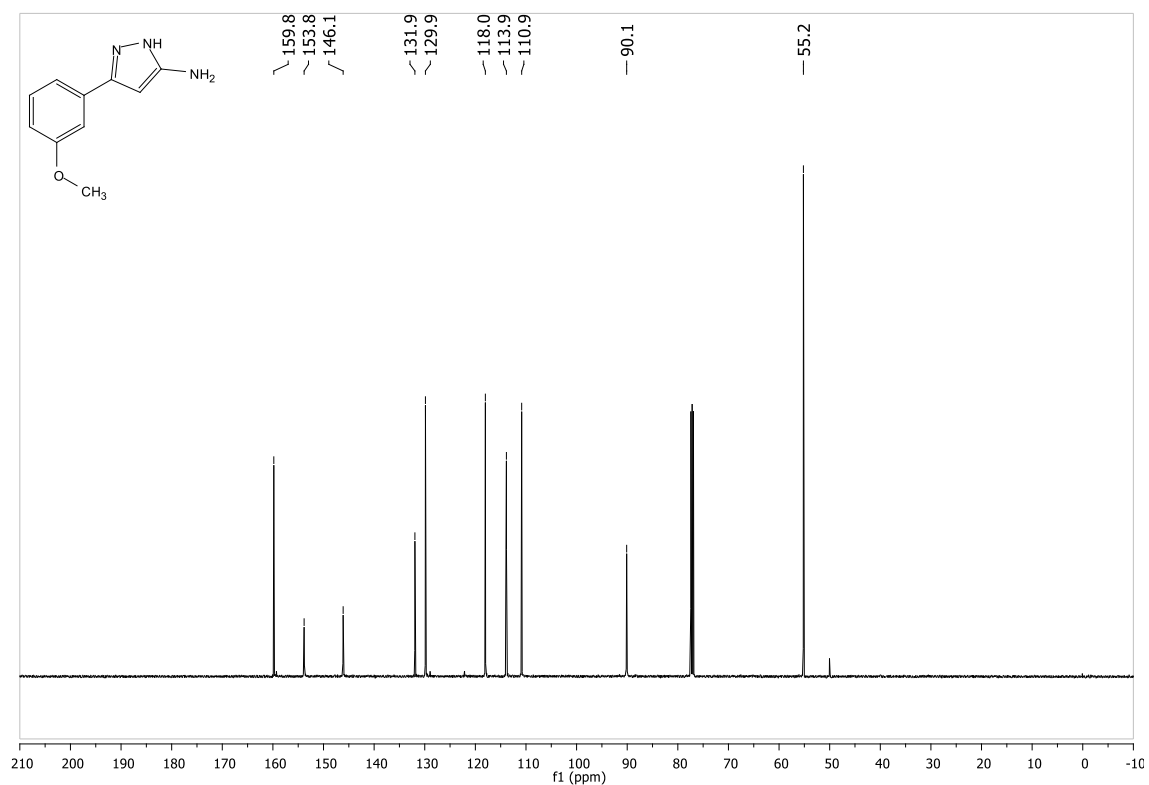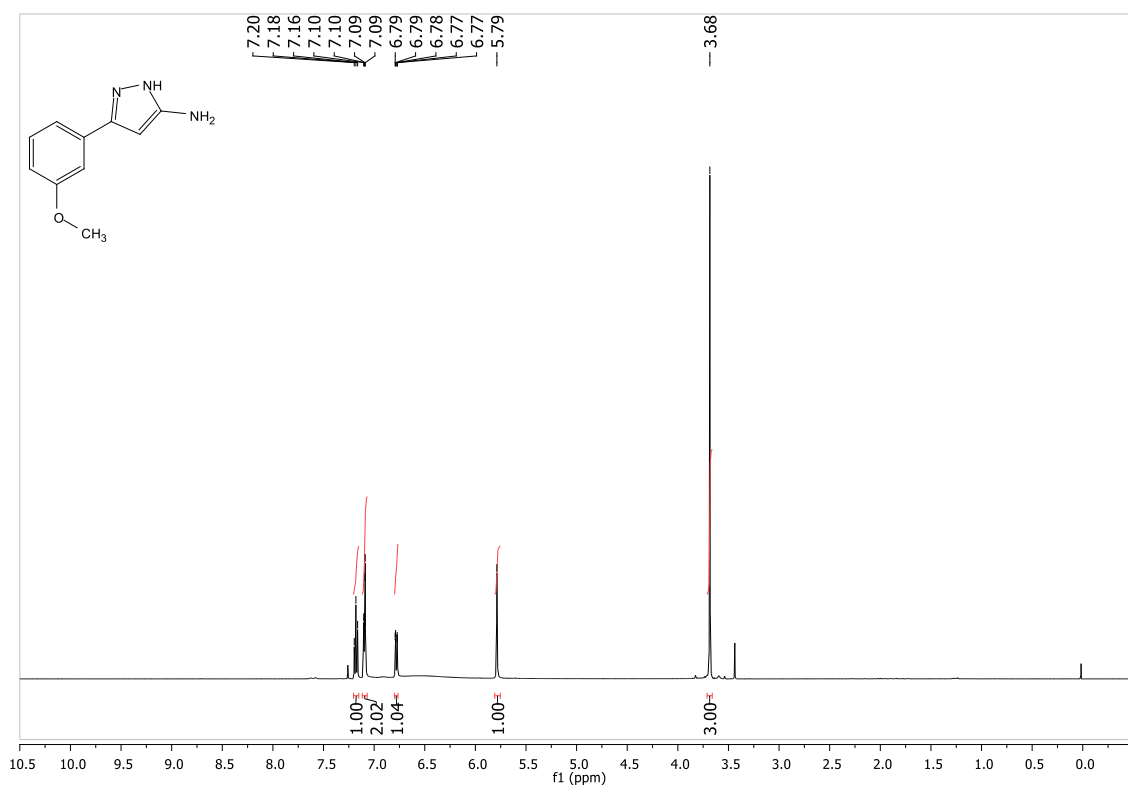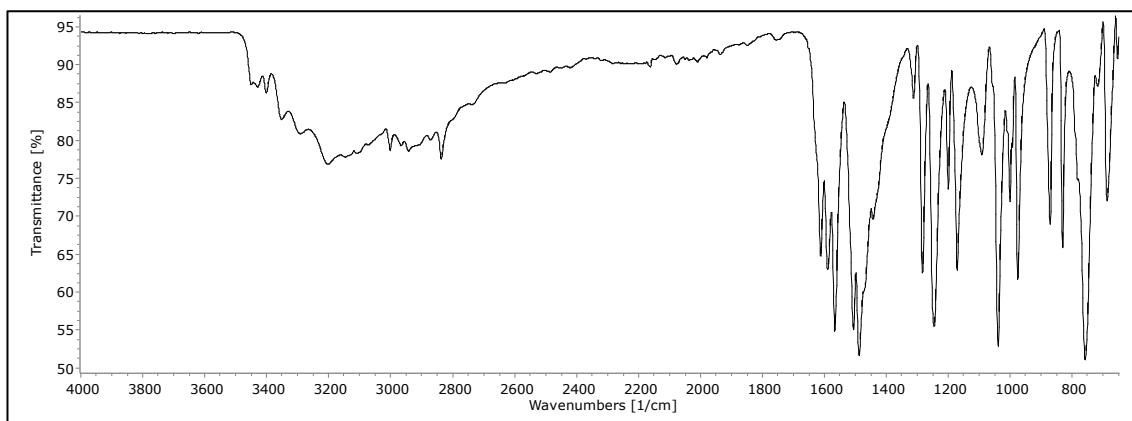
6.35 Spectra for 3-(3-nitrophenyl)-1*H*-pyrazol-5-amine (MK57) (35)

13C NMR peaks: 152.3, 148.6, 146.3, 133.8, 130.8, 129.6, 121.8, 119.4, 88.3
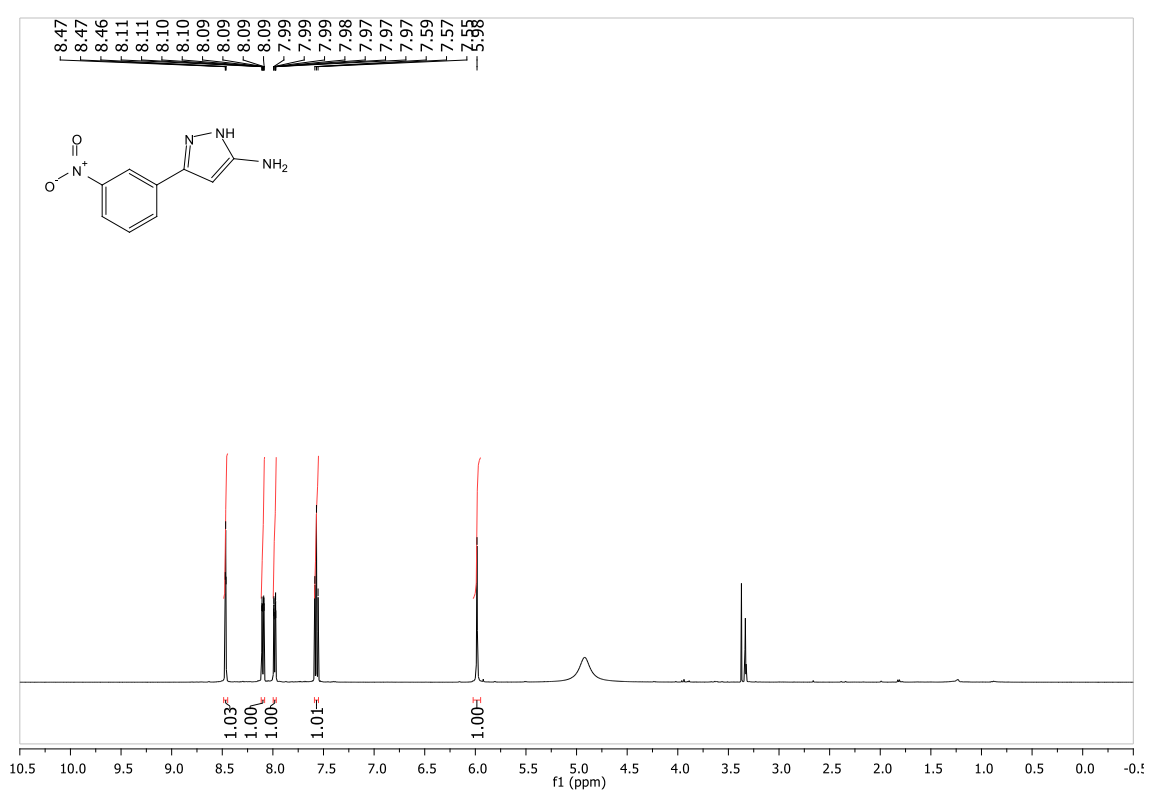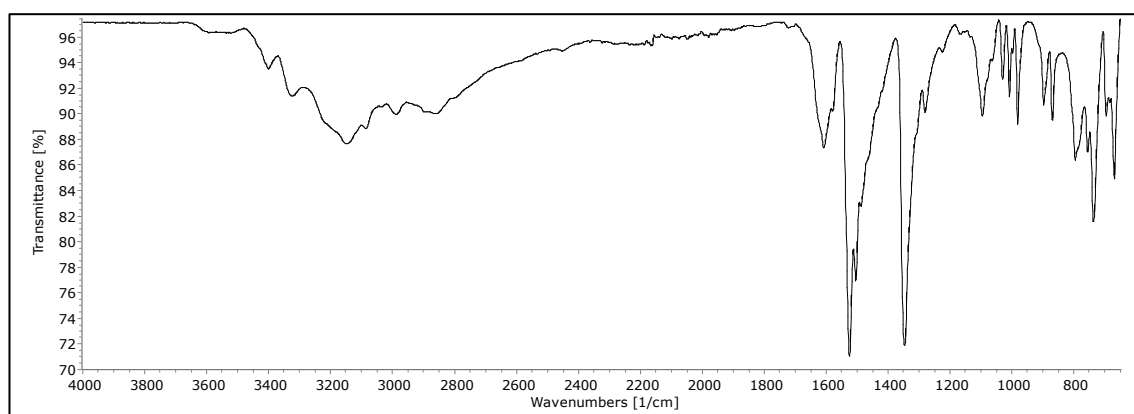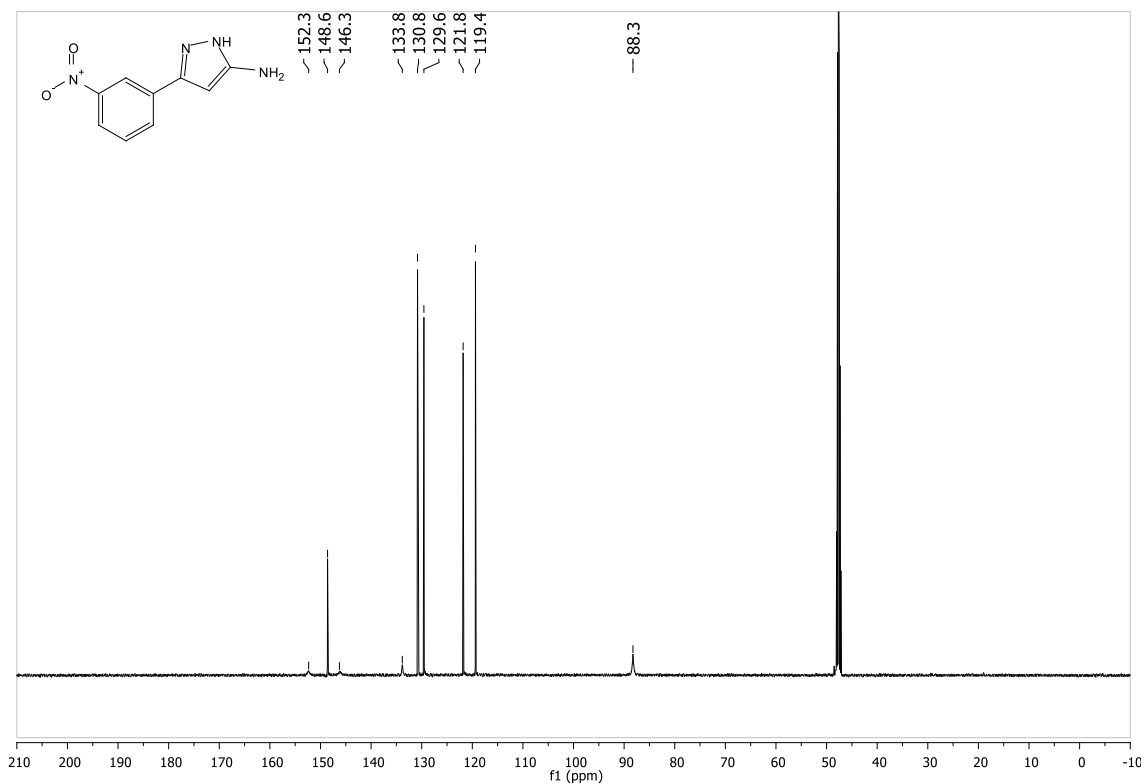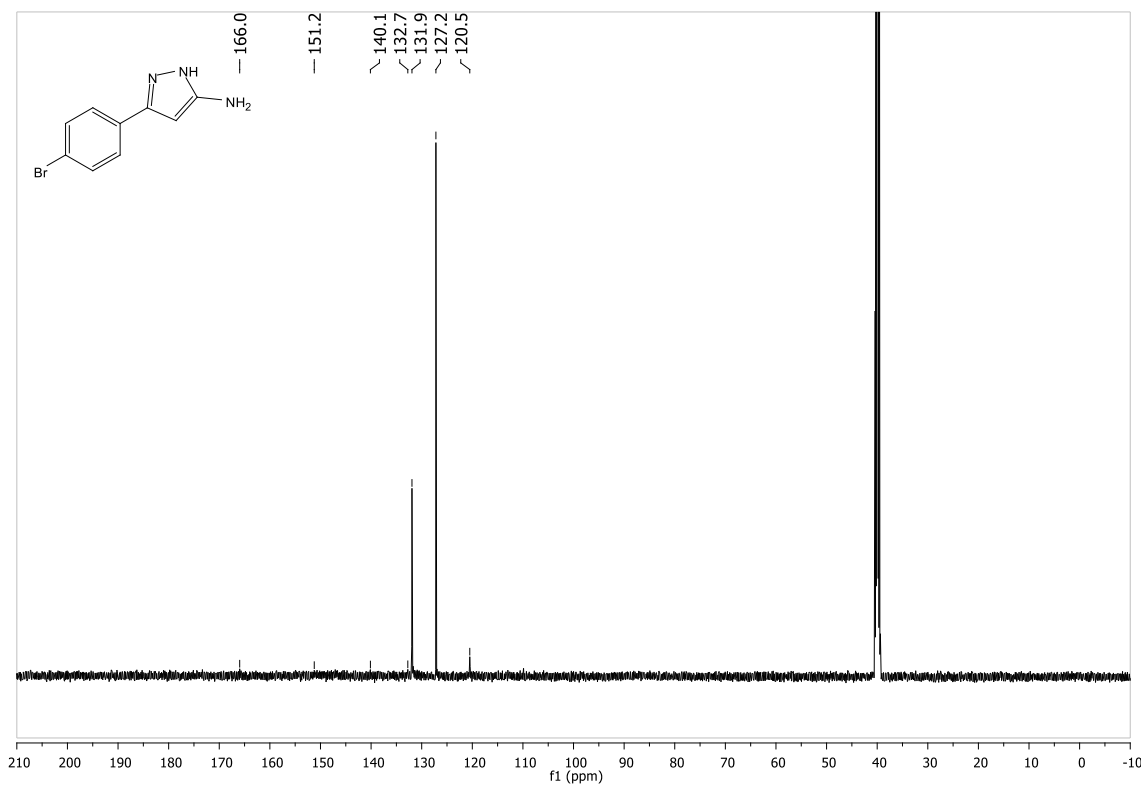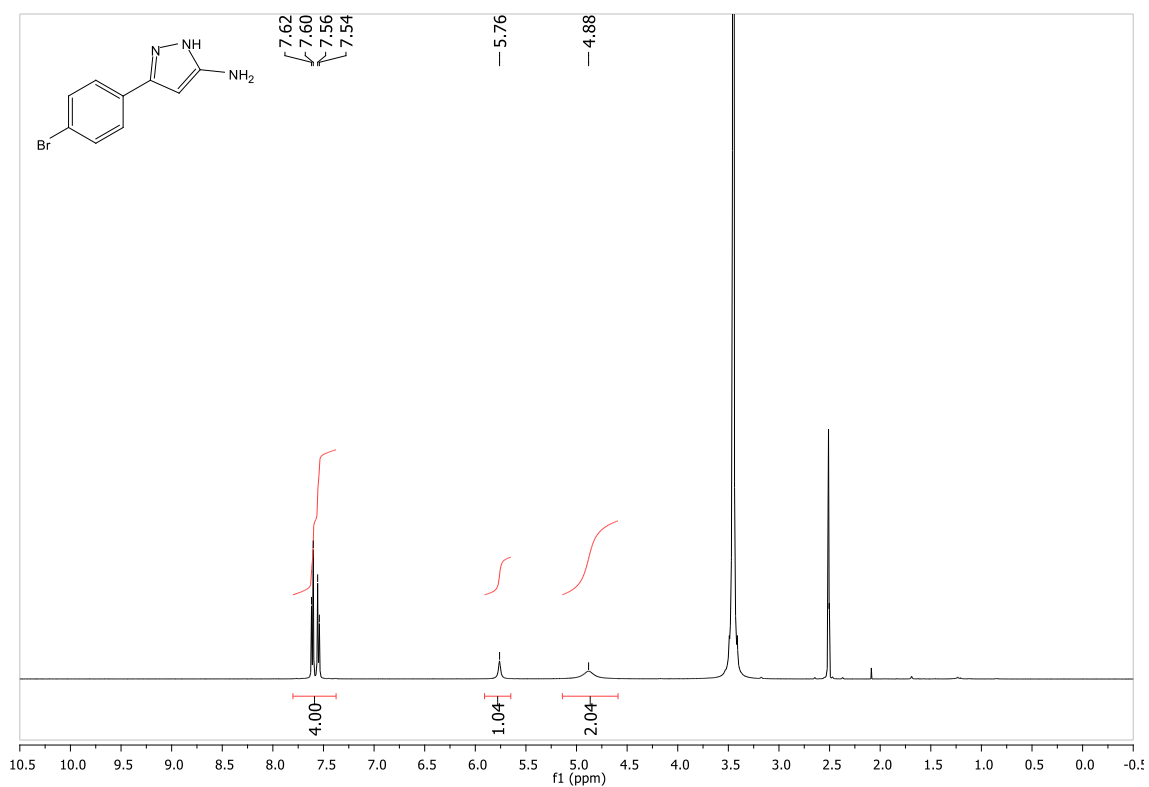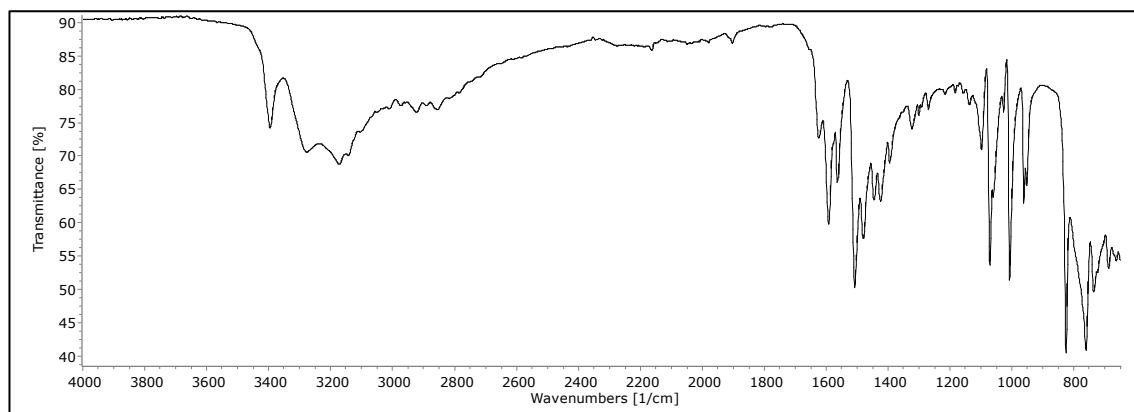
6.37 Spectra for 3-(thiophenyl-2-yl)-1*H*-pyrazol-5-amine (MK51) (37)
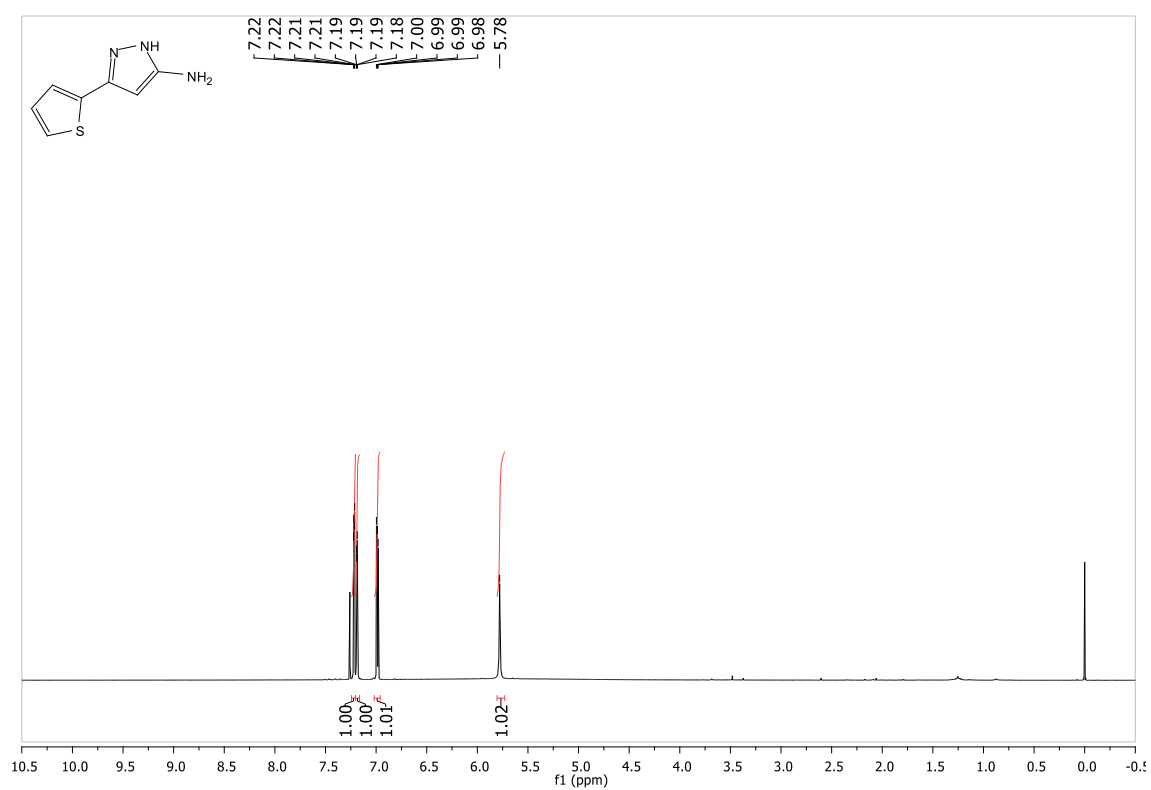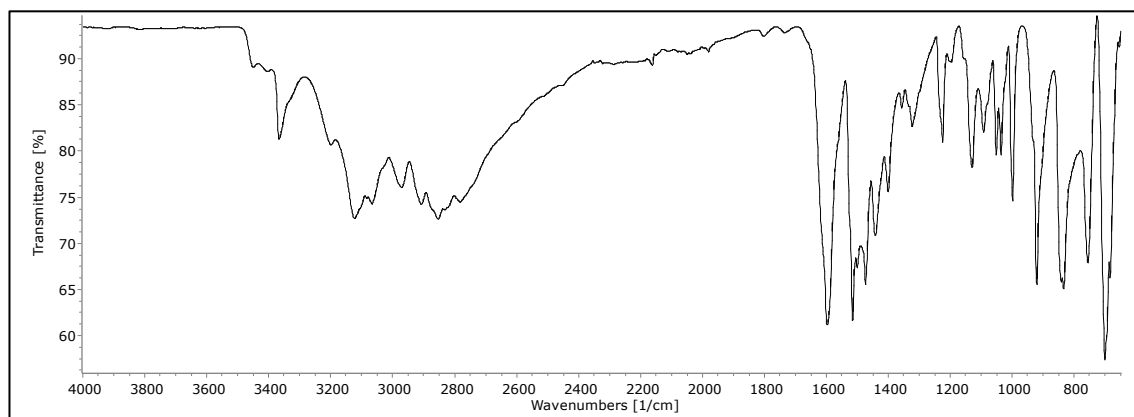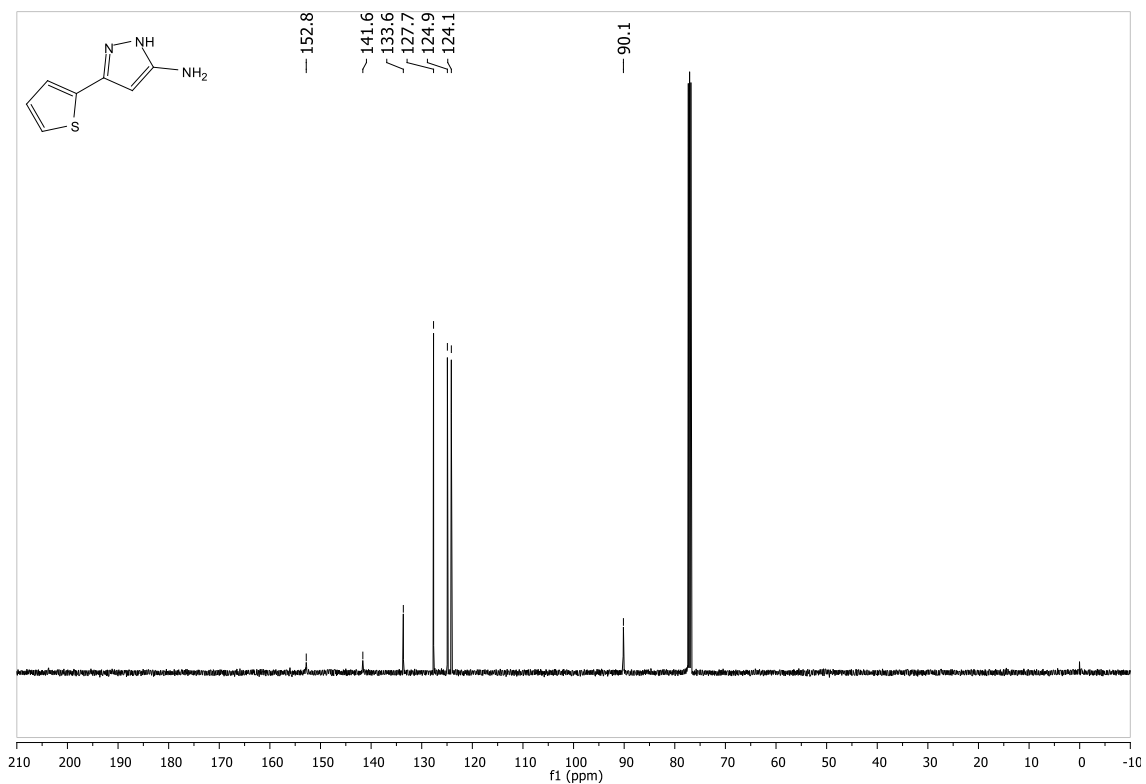
6.38 Spectra for 3-ethyl-1*H*-pyrazol-5-amine (MK54) (38)
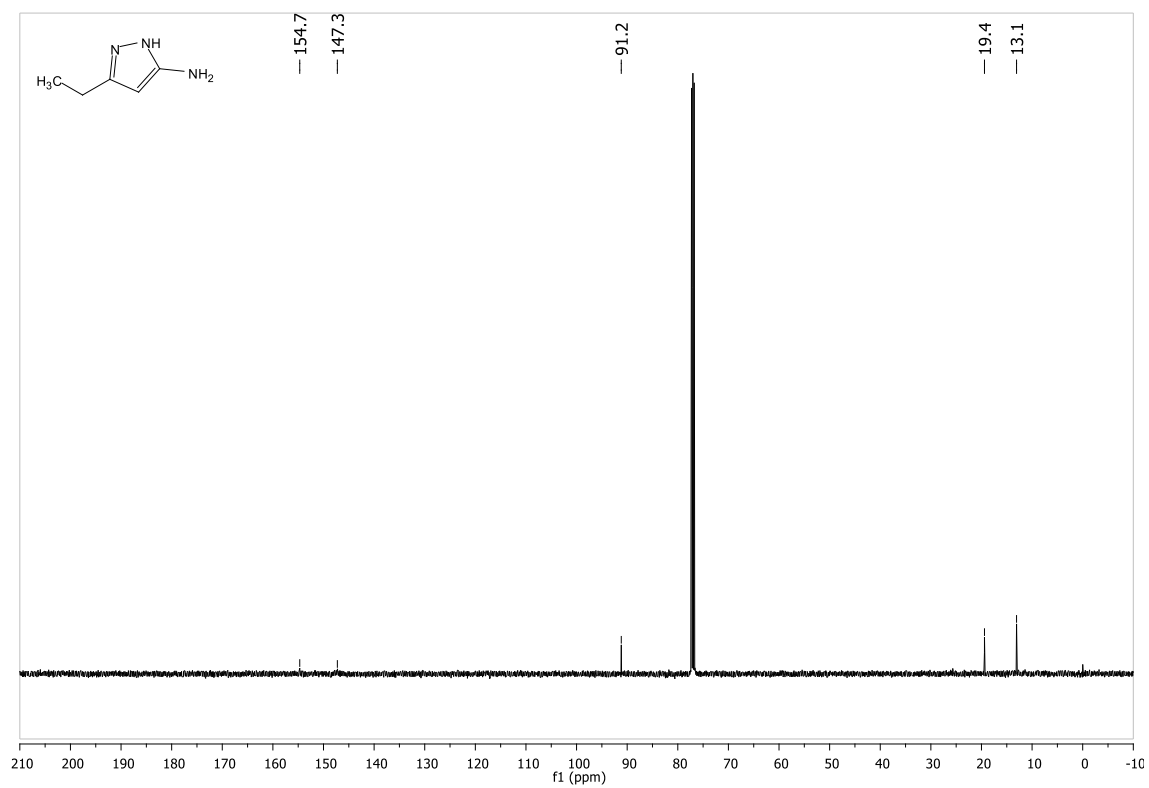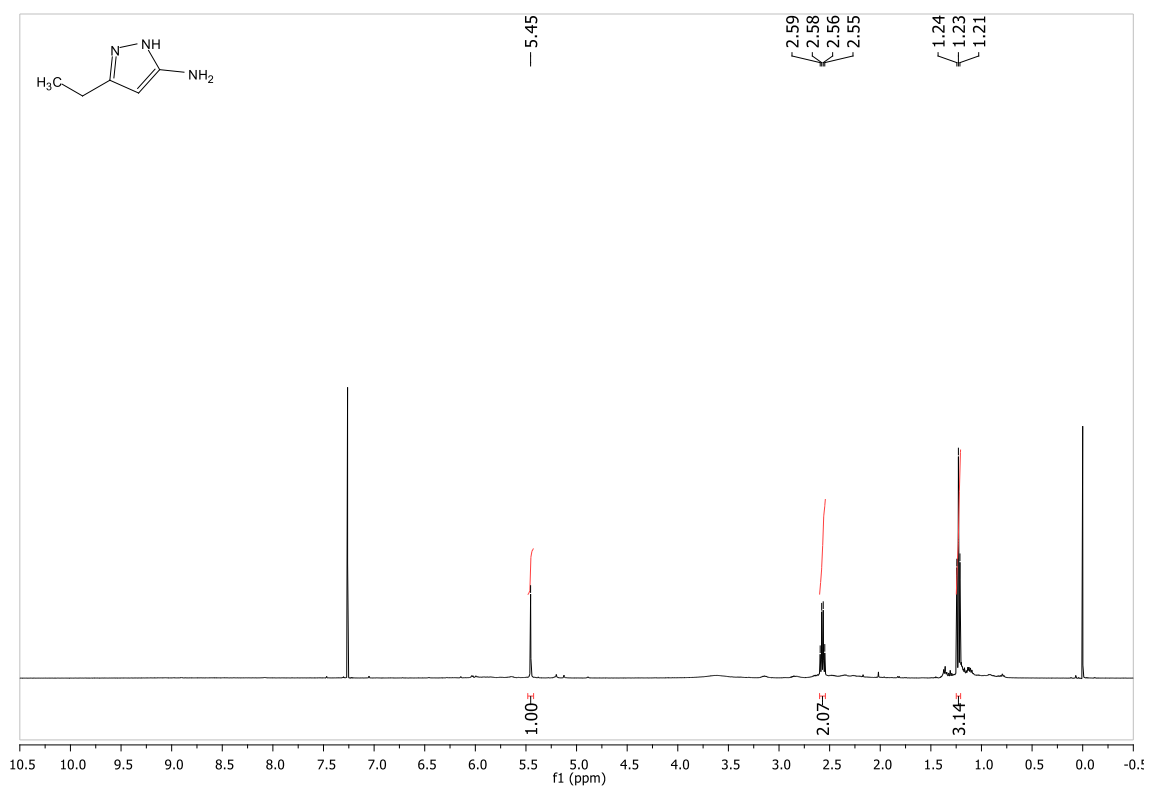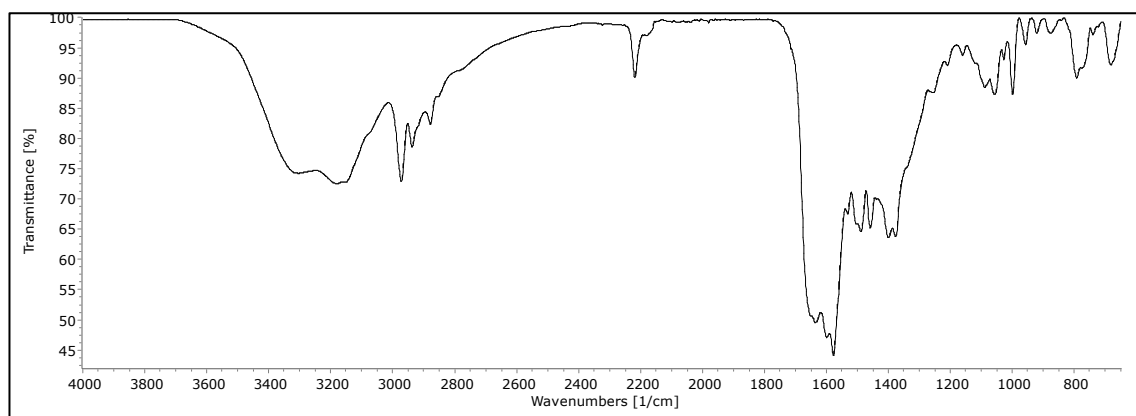
6.39   Spectra for 3-(*tert*-butyl)-1*H*-pyrazol-5-amine (MK53) (39)
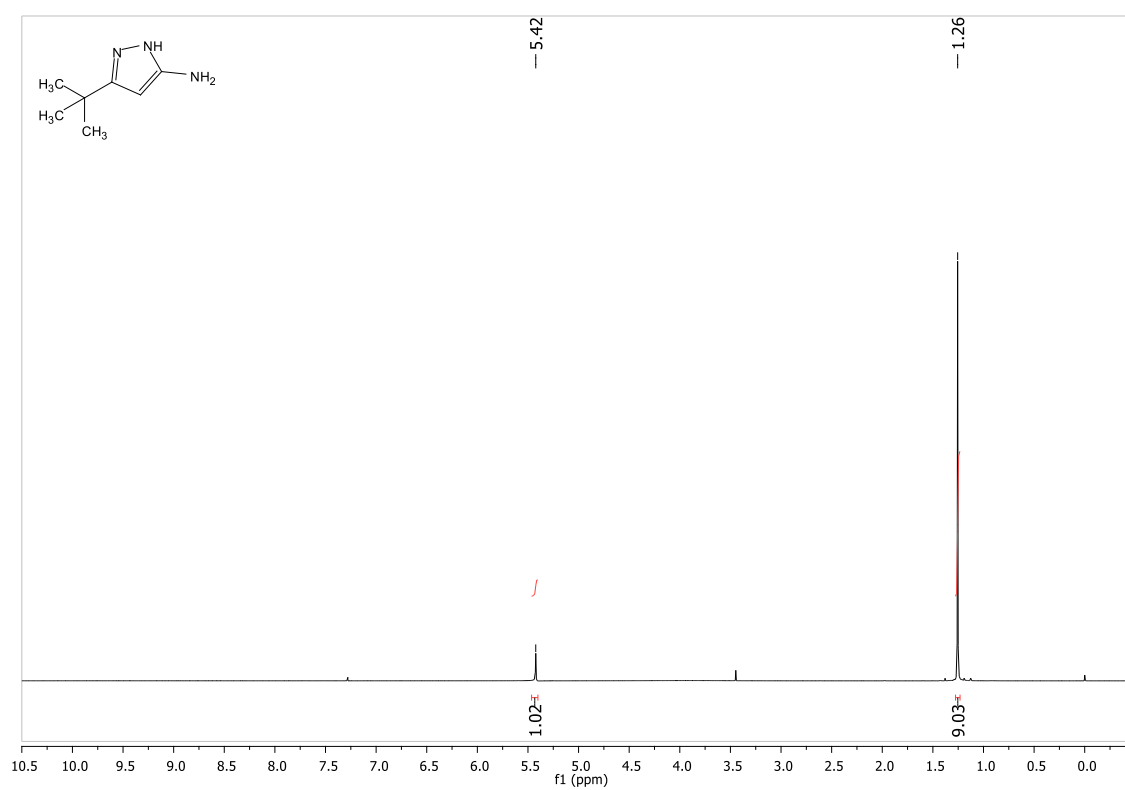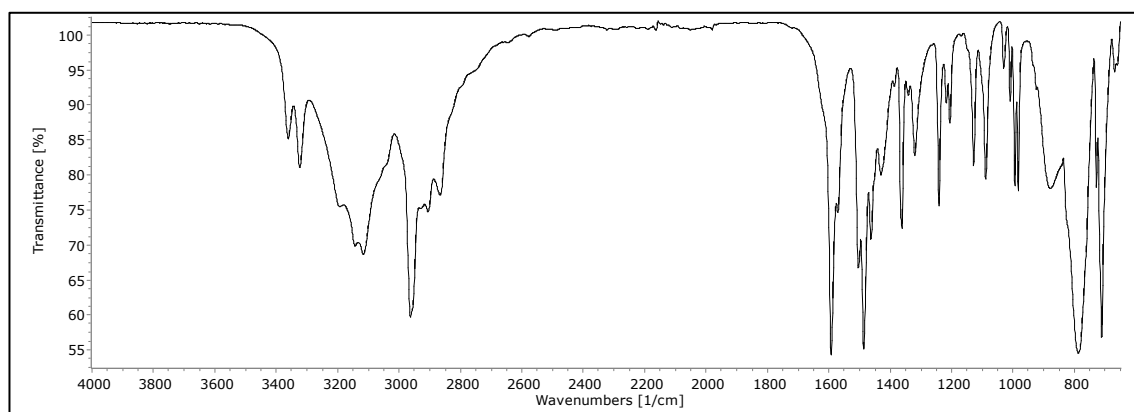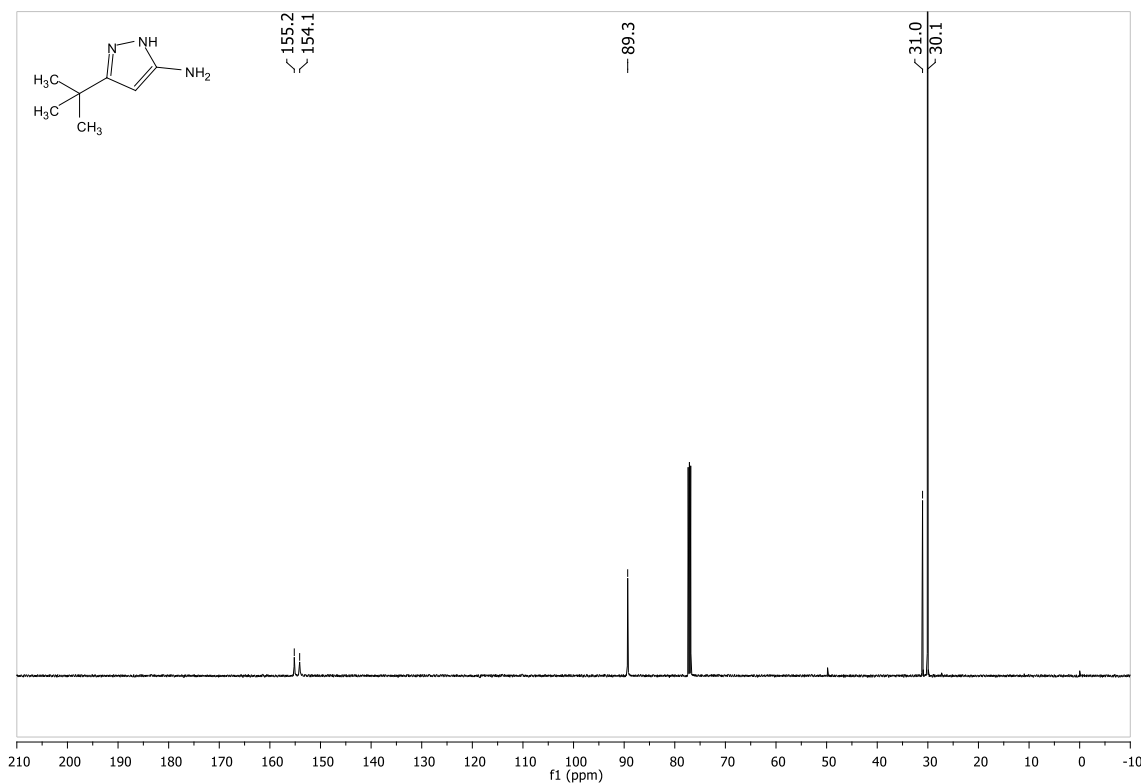
6.40   Spectra for 2,5-diphenylpyrazolo[1,5-*a*]pyrimidin-7(4*H*)-one (MK15, MK65, MK68) (40)
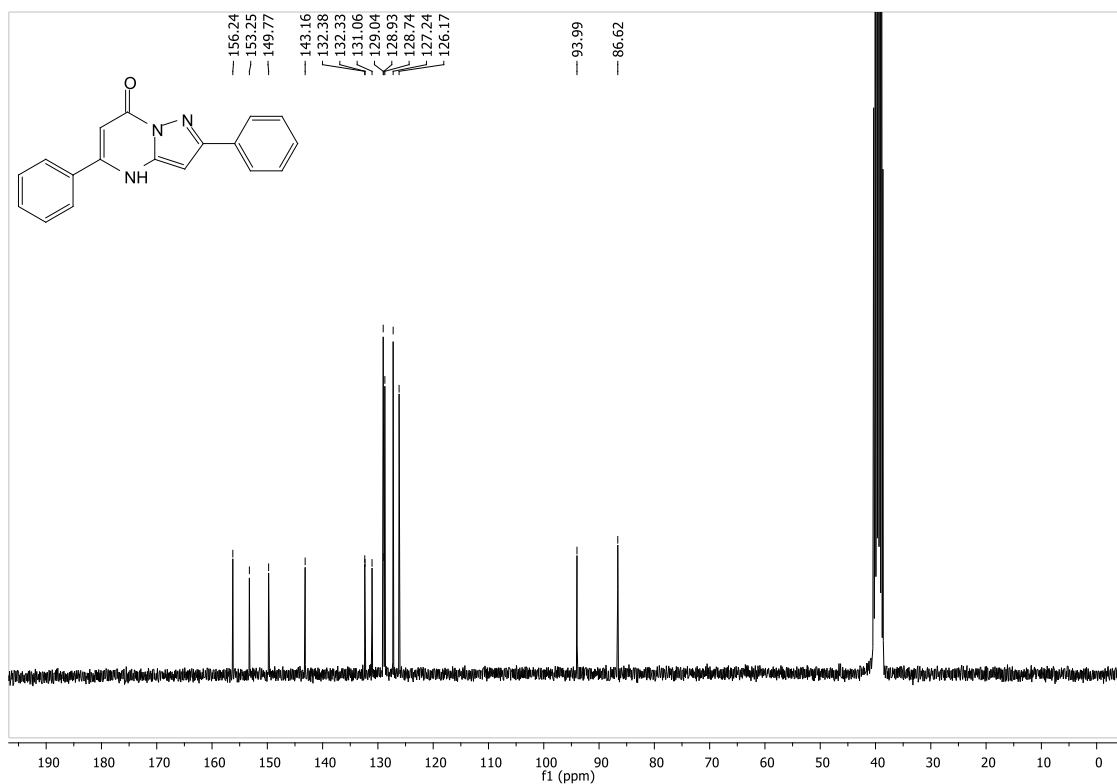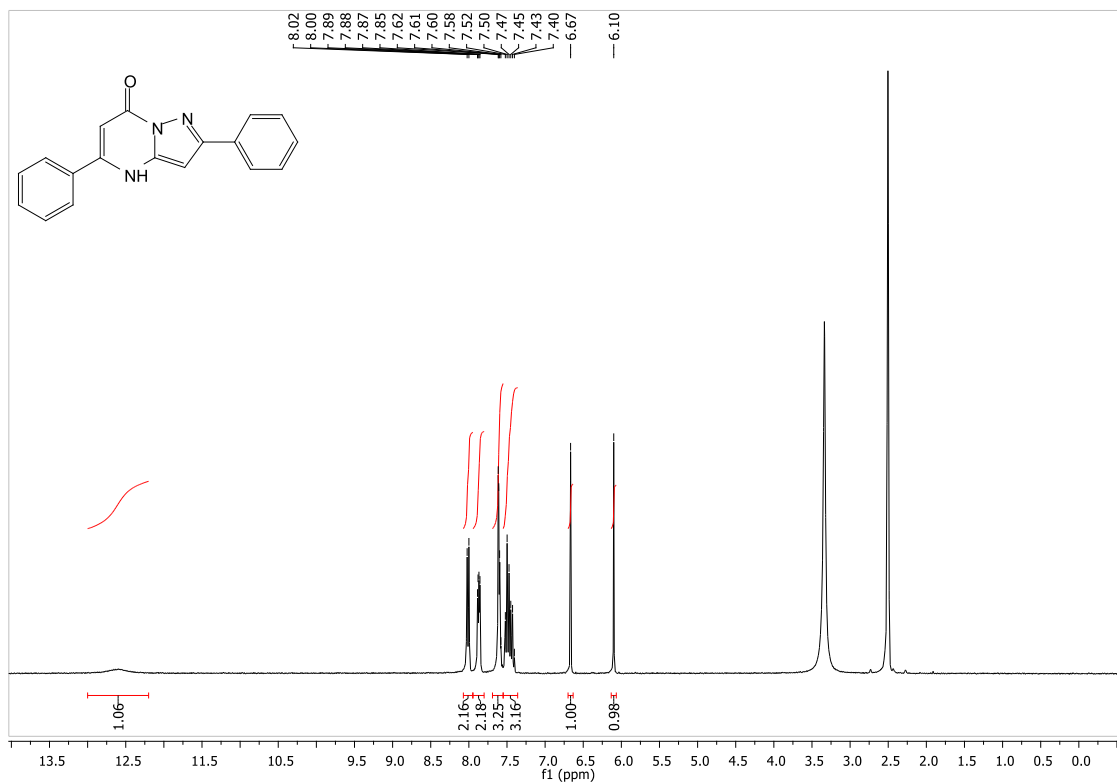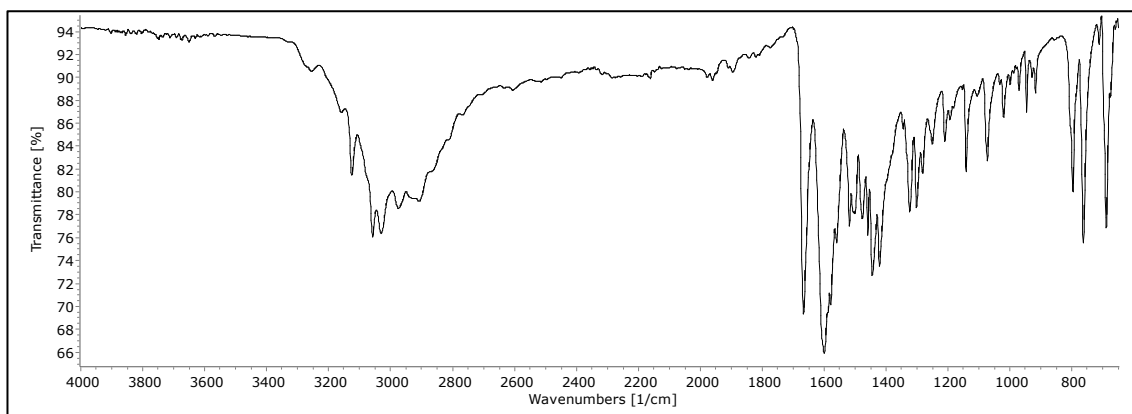
6.41 Spectra for 2-(furan-2-yl)-5-phenylpyrazolo[1,5-*a*]pyrimidin-7(4*H*)-one (MK56) (41)

156.7
150.5
148.3
146.2
144.2
143.6
133.0
131.5
129.5
127.7
112.4
109.0
94.5
86.8

f1 (ppm)
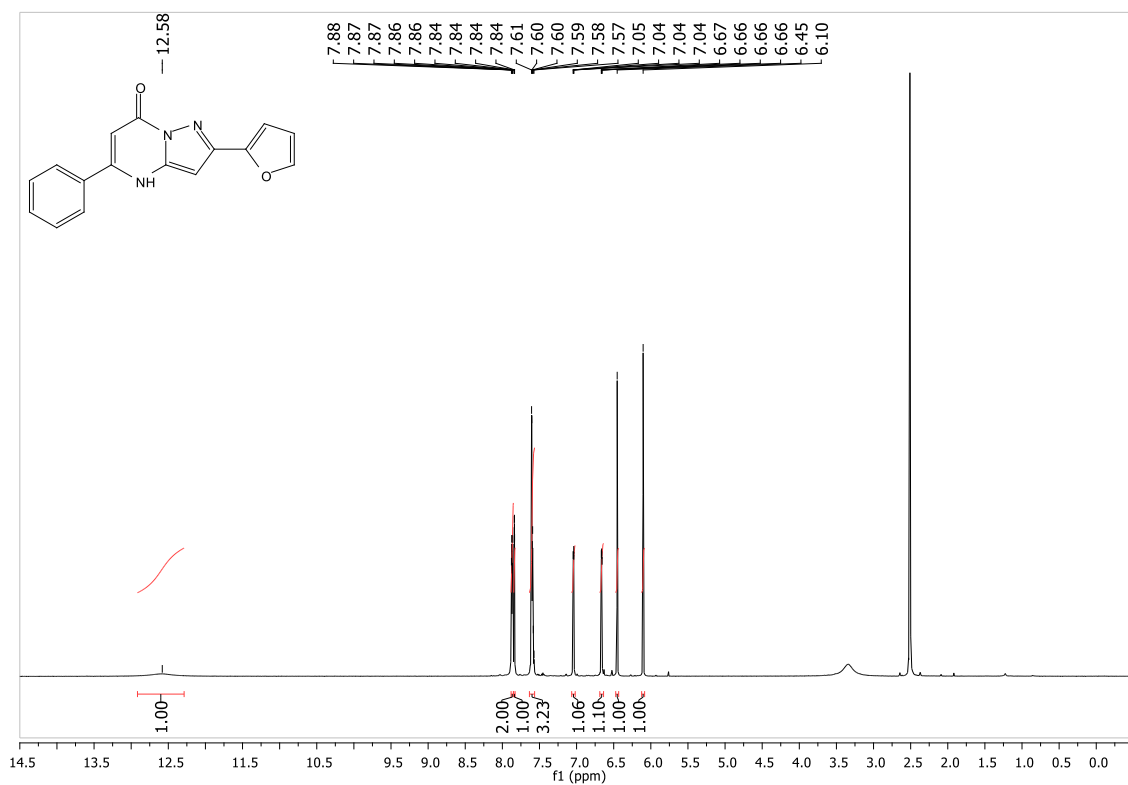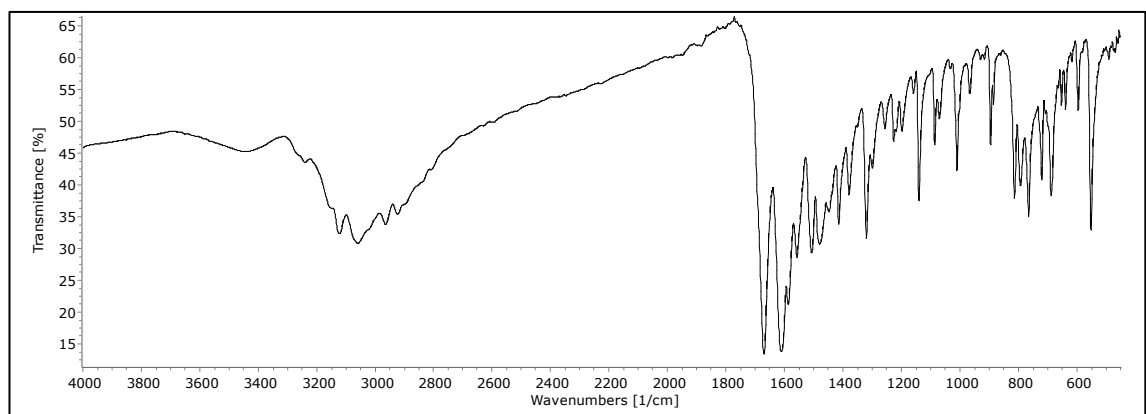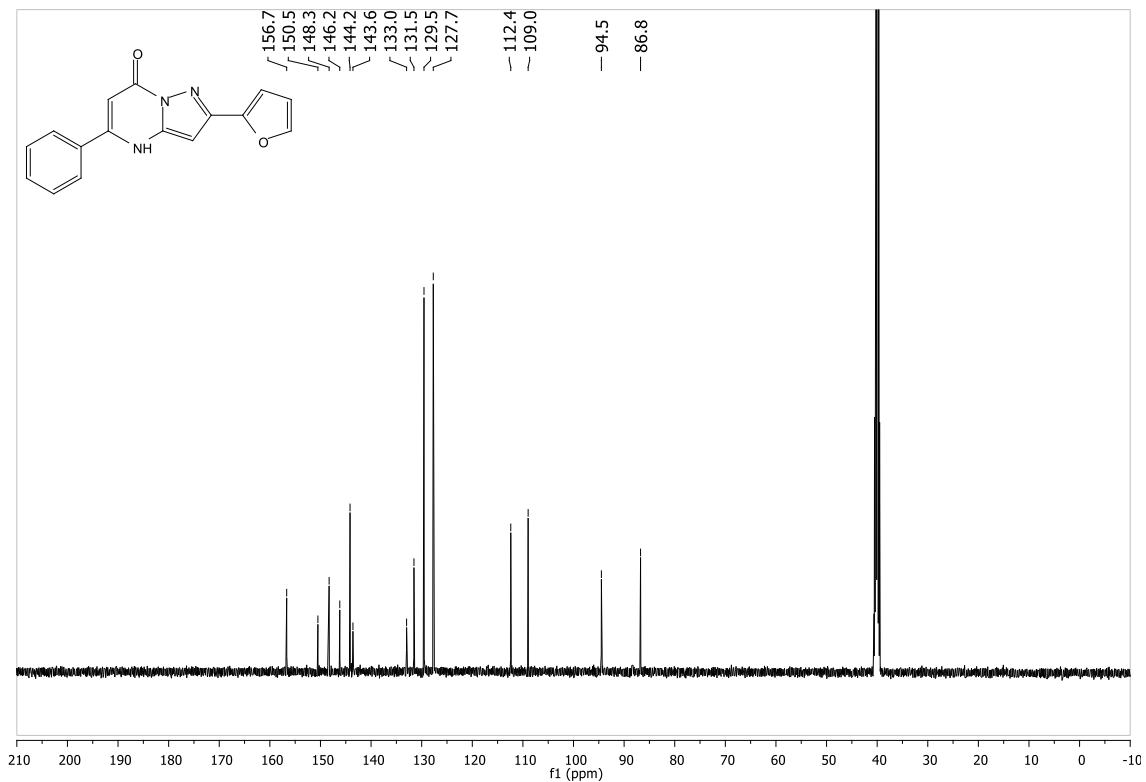
6.42 Spectra for 5-phenyl-2-(thiophen-2-yl)pyrazolo[1,5-*a*]pyrimidin-7(4*H*)-one (MK55) (42)
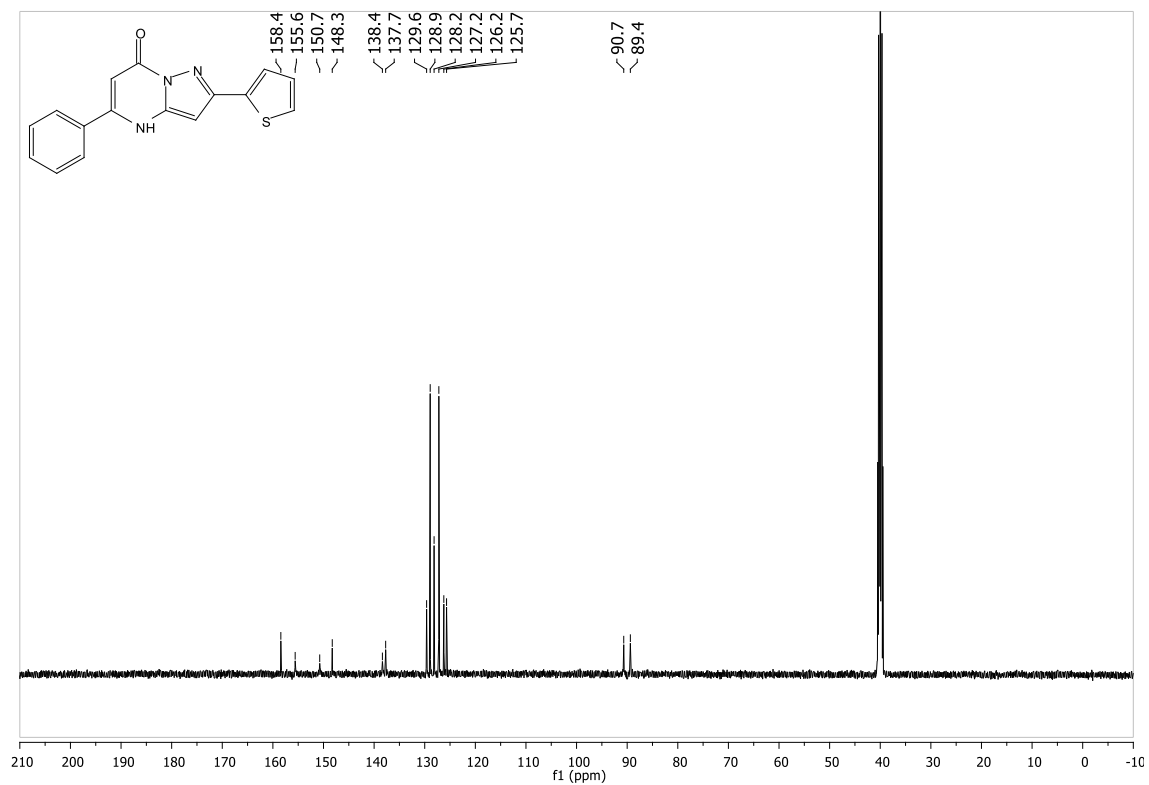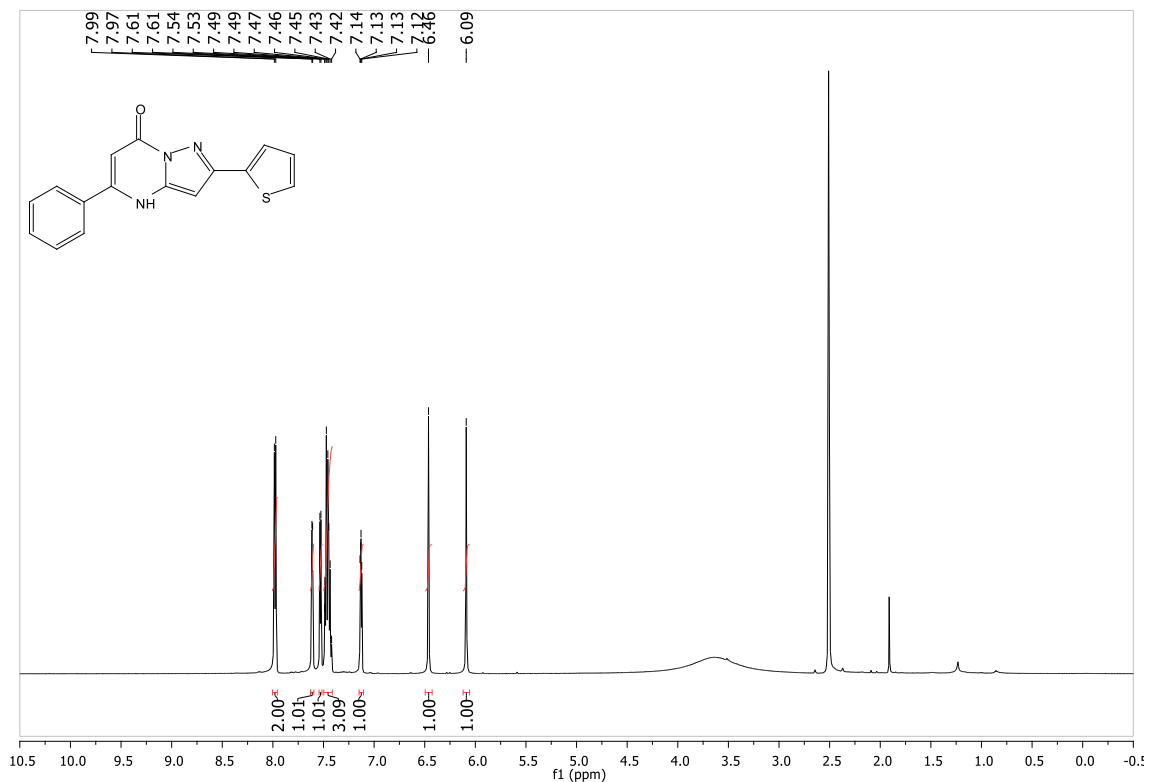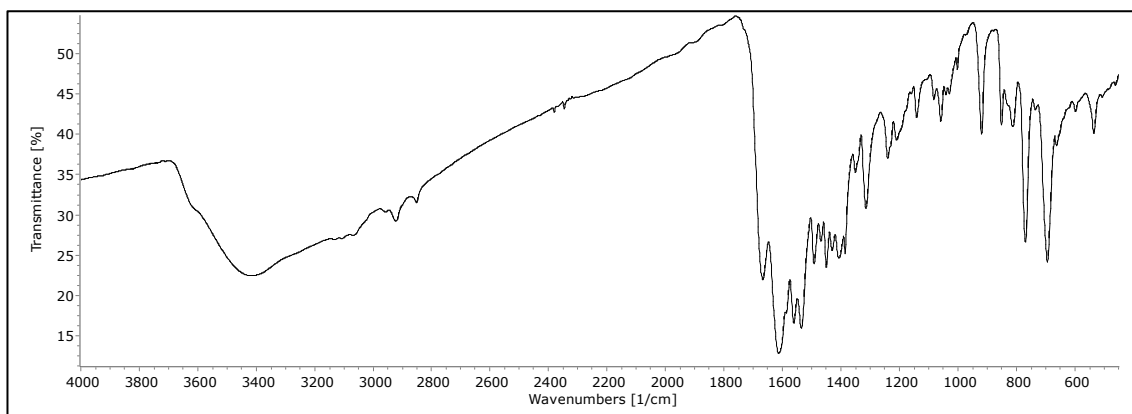
6.43 Spectra for 2-methyl-5-phenylpyrazolo[1,5-*a*]pyrimidin-7(4*H*)-one (MK62) (43)

13C NMR peaks: 156.6, 152.6, 149.7, 142.9, 132.9, 131.5, 129.5, 127.6, 94.1, 89.7, 14.6

f1 (ppm)

Transmittance [%]

Wavenumbers [1/cm]
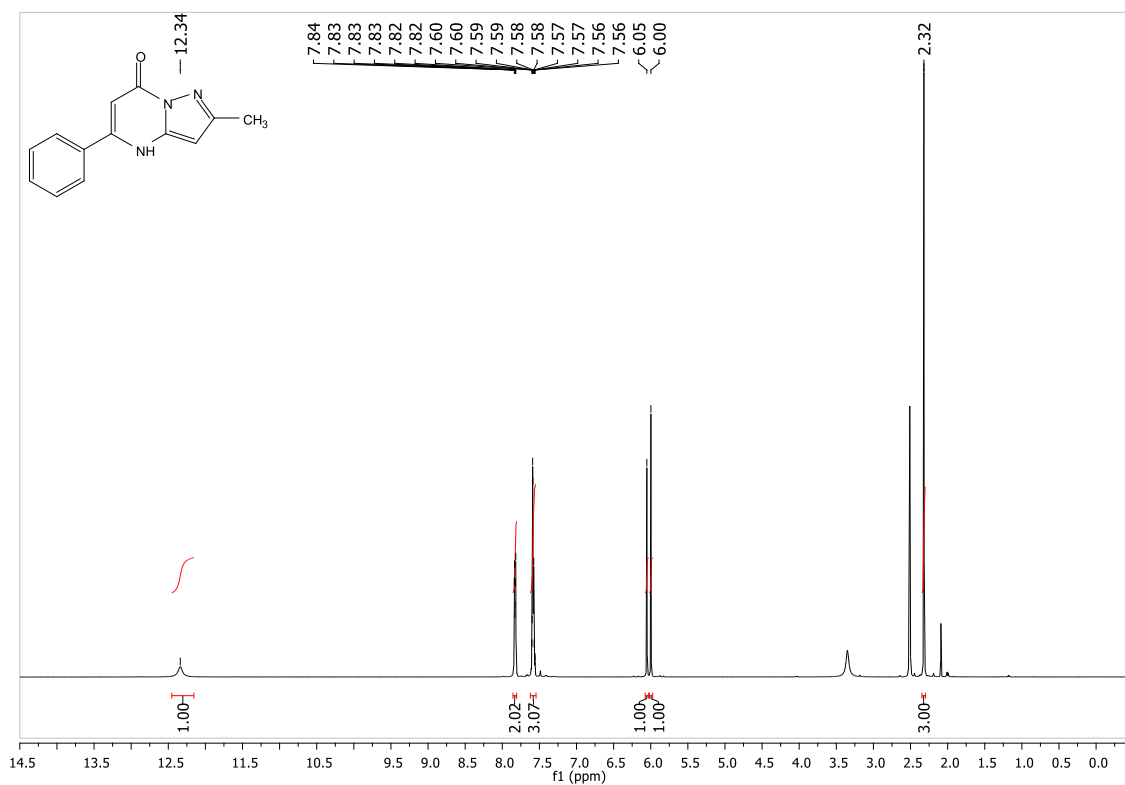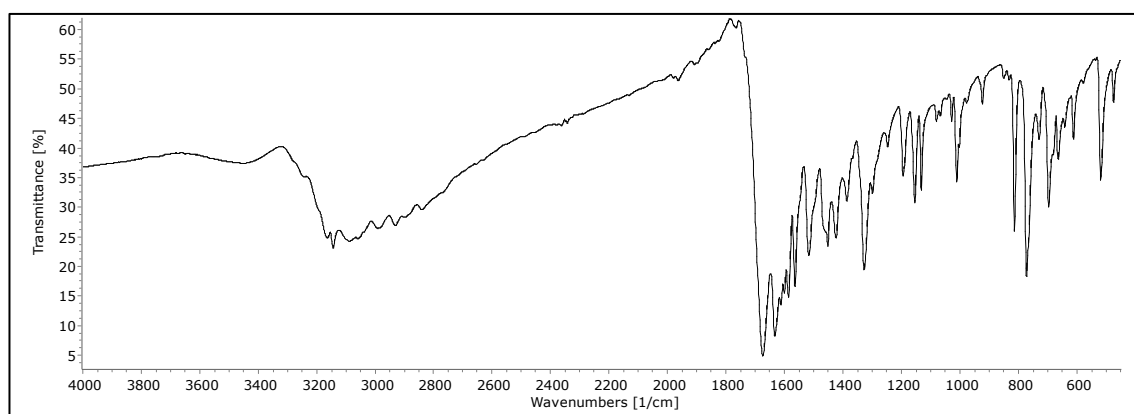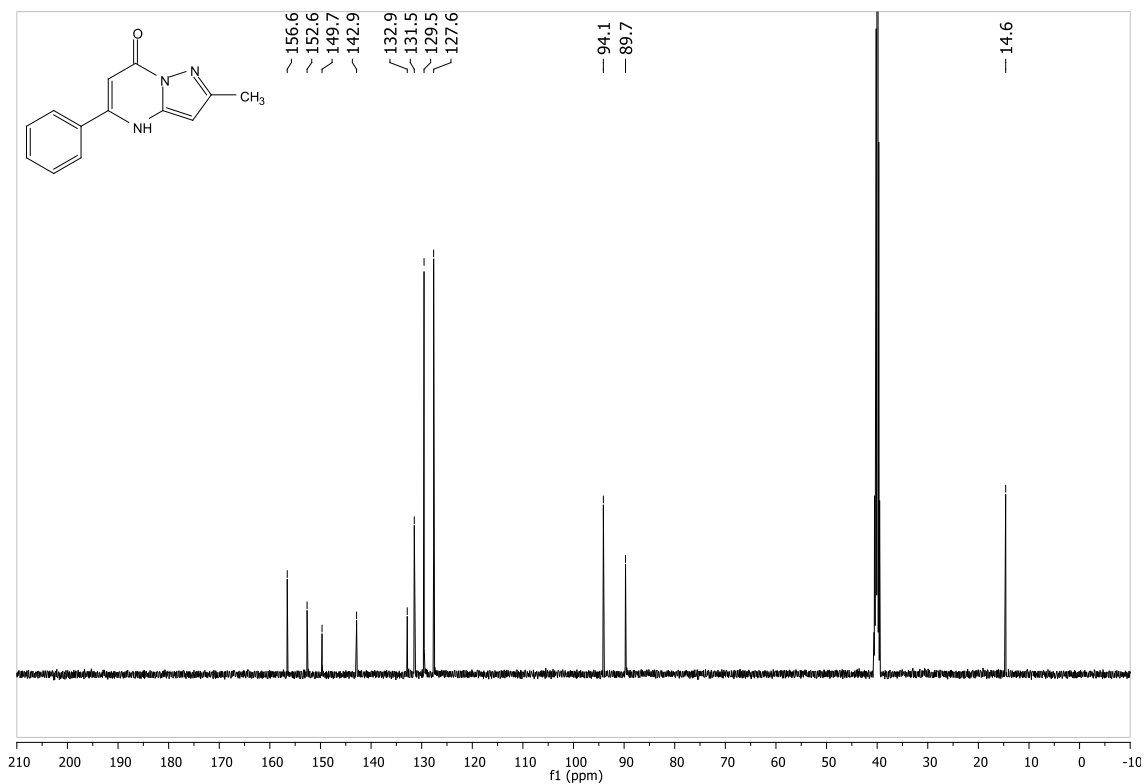
6.44 Spectra for 2-(*tert*-butyl)-5-phenylpyrazolo[1,5-*a*]pyrimidin-7(4*H*)-one (MK59) (RTC81) (44)
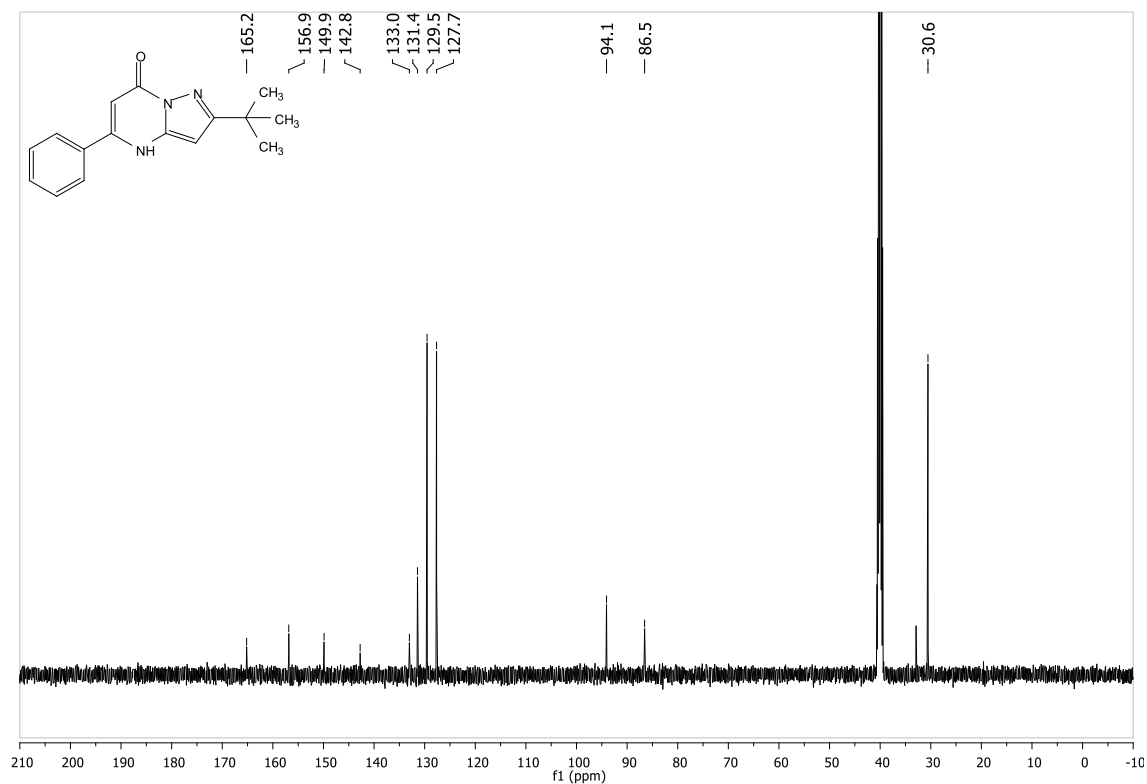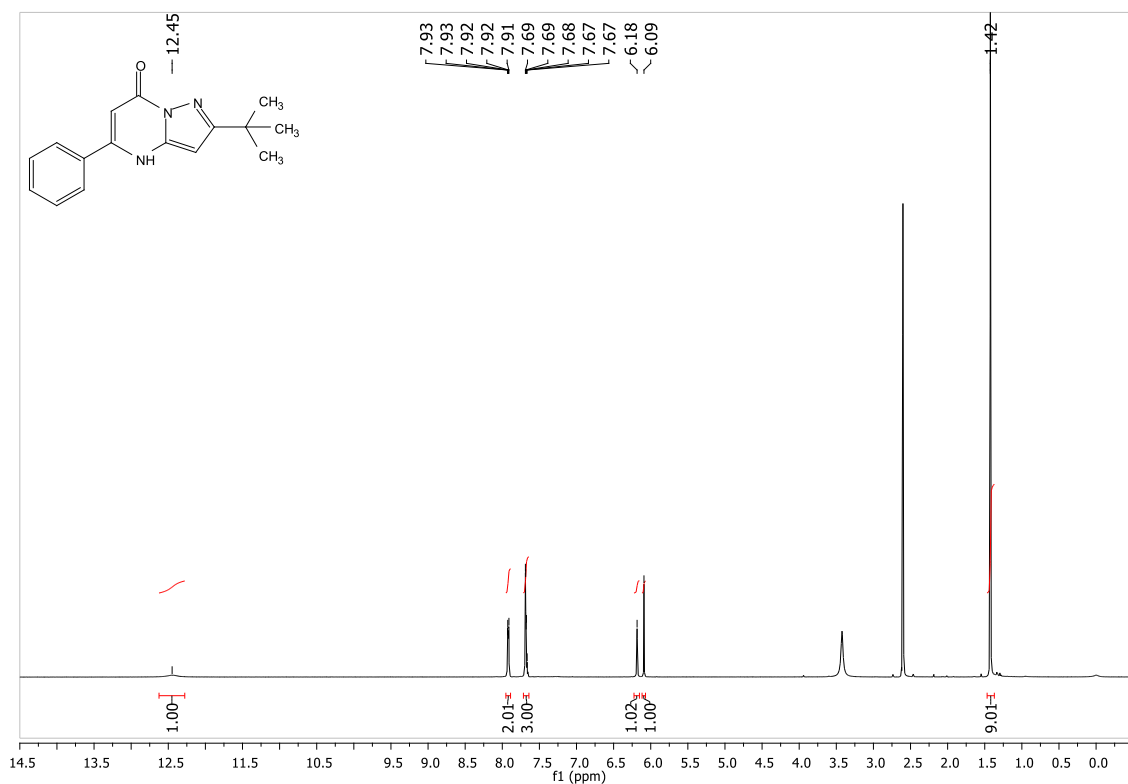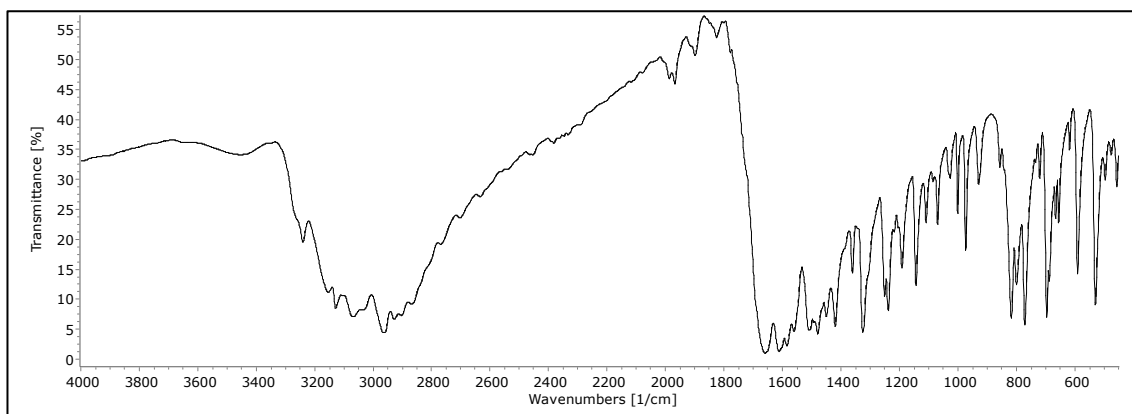
6.45 Spectra for 2-(2-methoxyphenyl)-5-phenylpyrazolo[1,5-*a*]pyrimidin-7(4*H*)-one (MK58) (45)
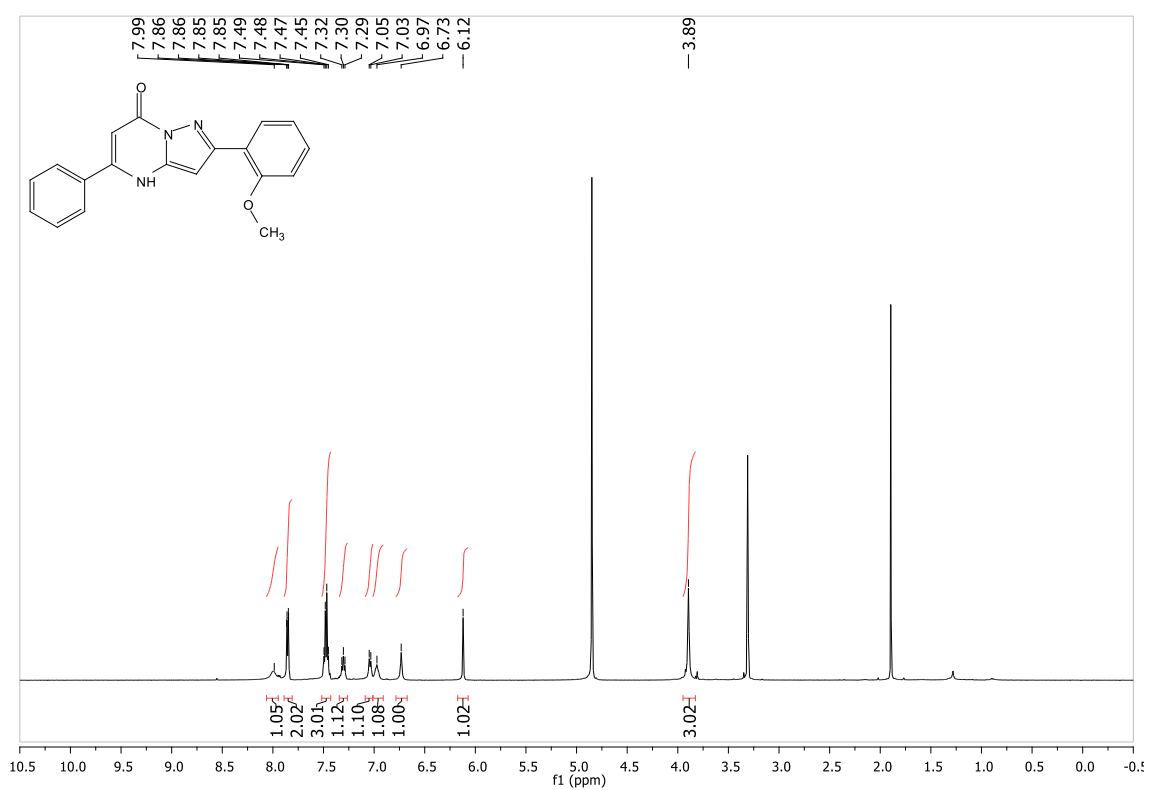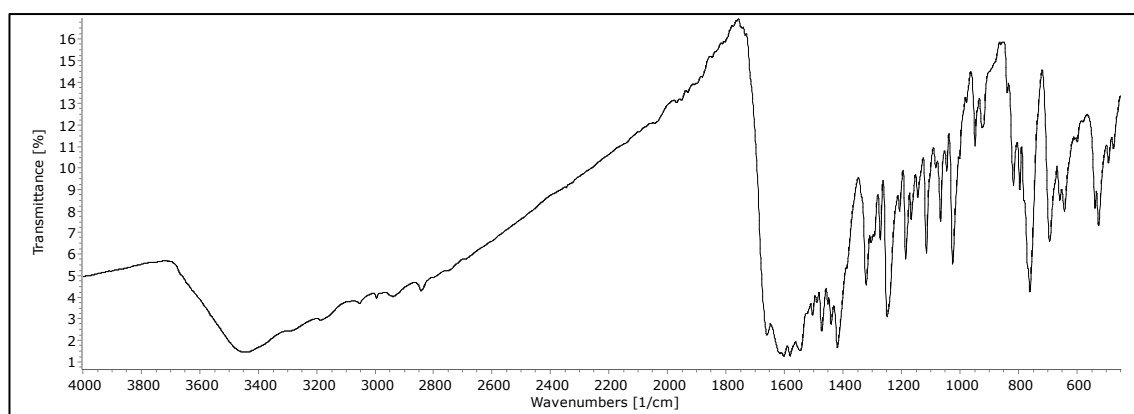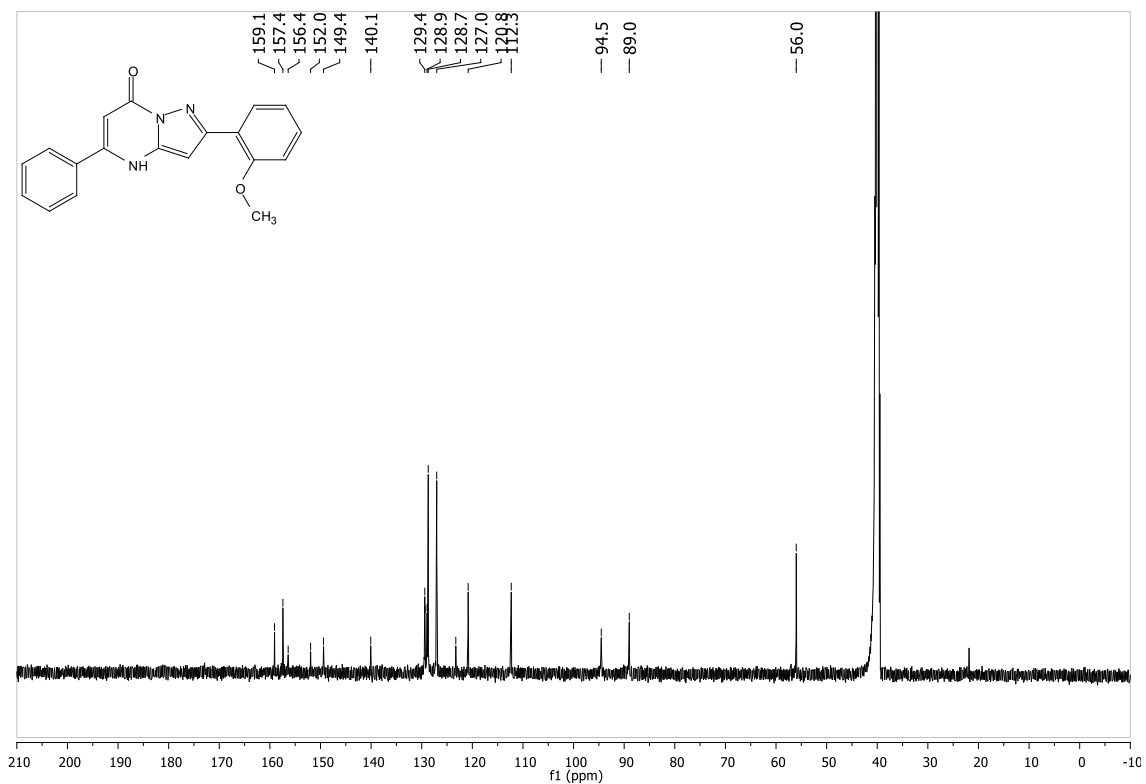
6.46 Spectra for 2-(3-chlorophenyl)-5-phenylpyrazolo[1,5-*a*]pyrimidin-7(4*H*)-one (MK7) (46)
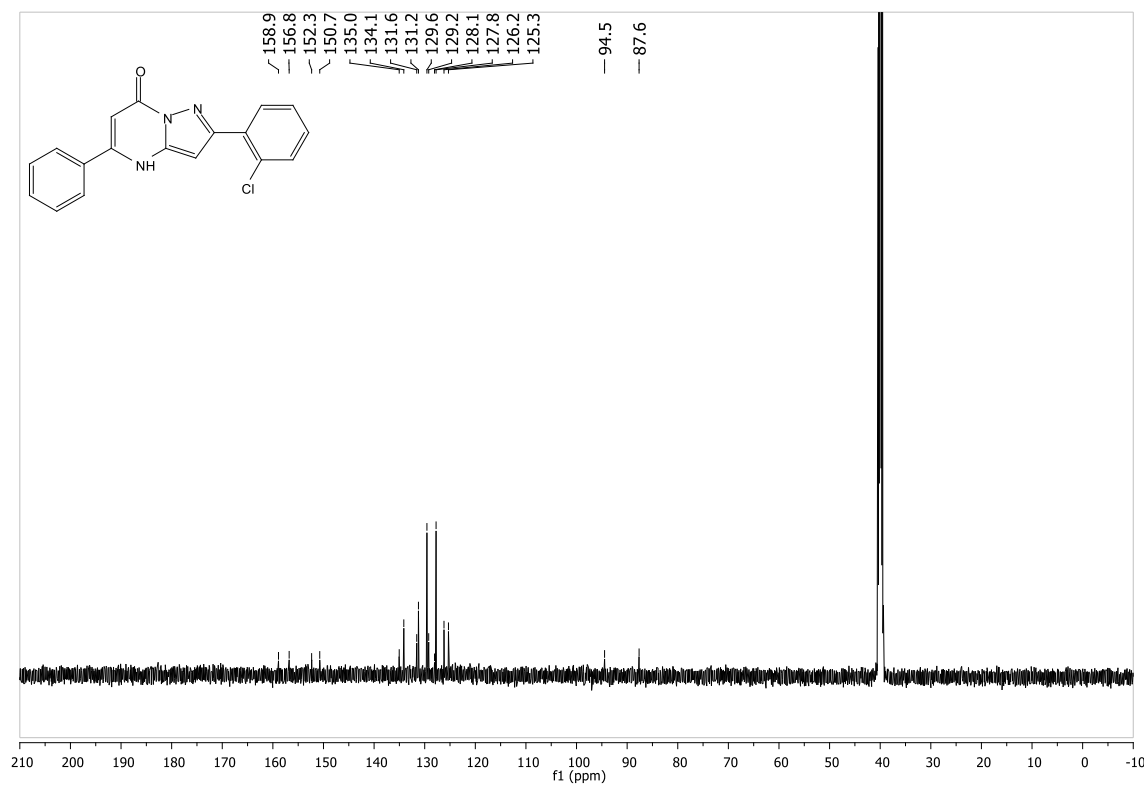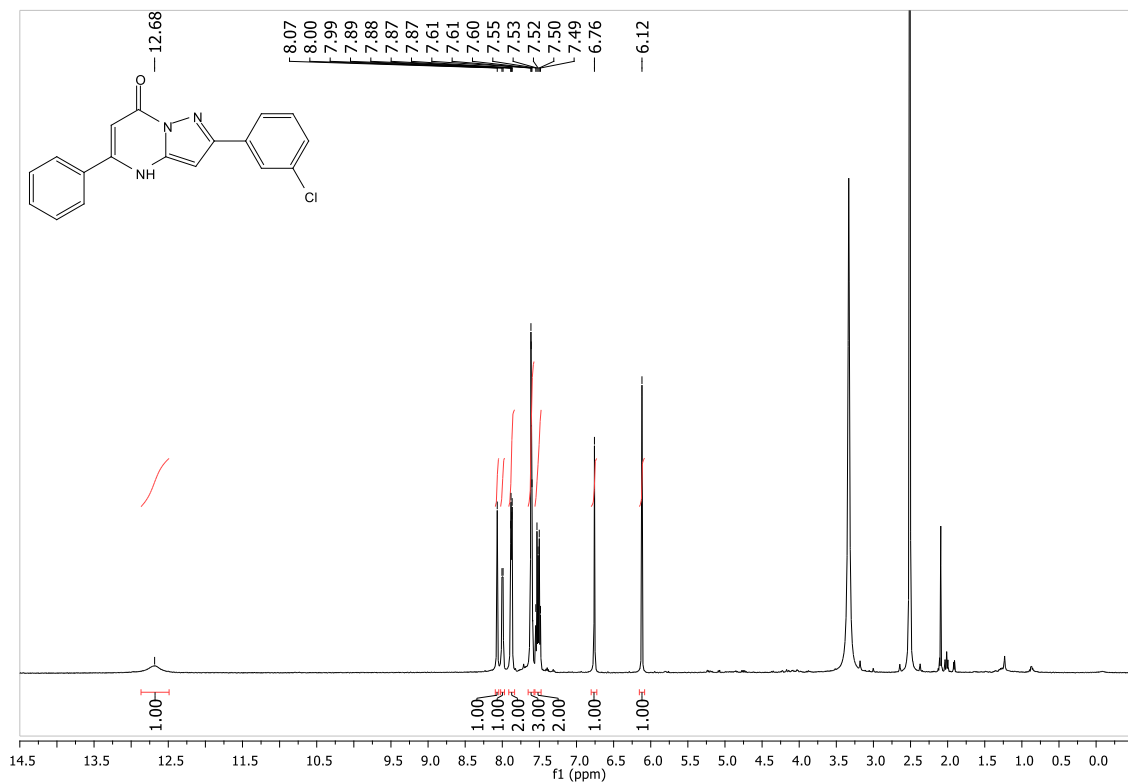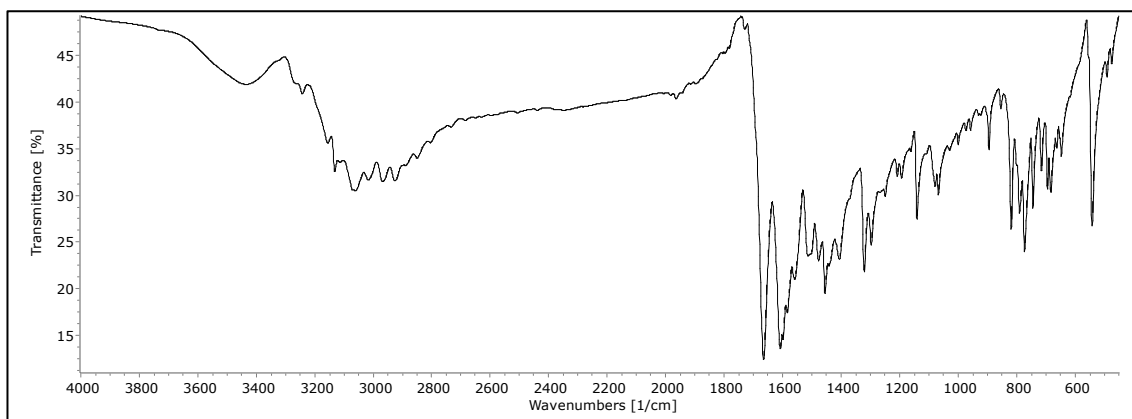
6.47 Spectra for 2-(4-fluorophenyl)-5-phenylpyrazolo[1,5-*a*]pyrimidin-
7(4*H*)- one (MK8) (47)
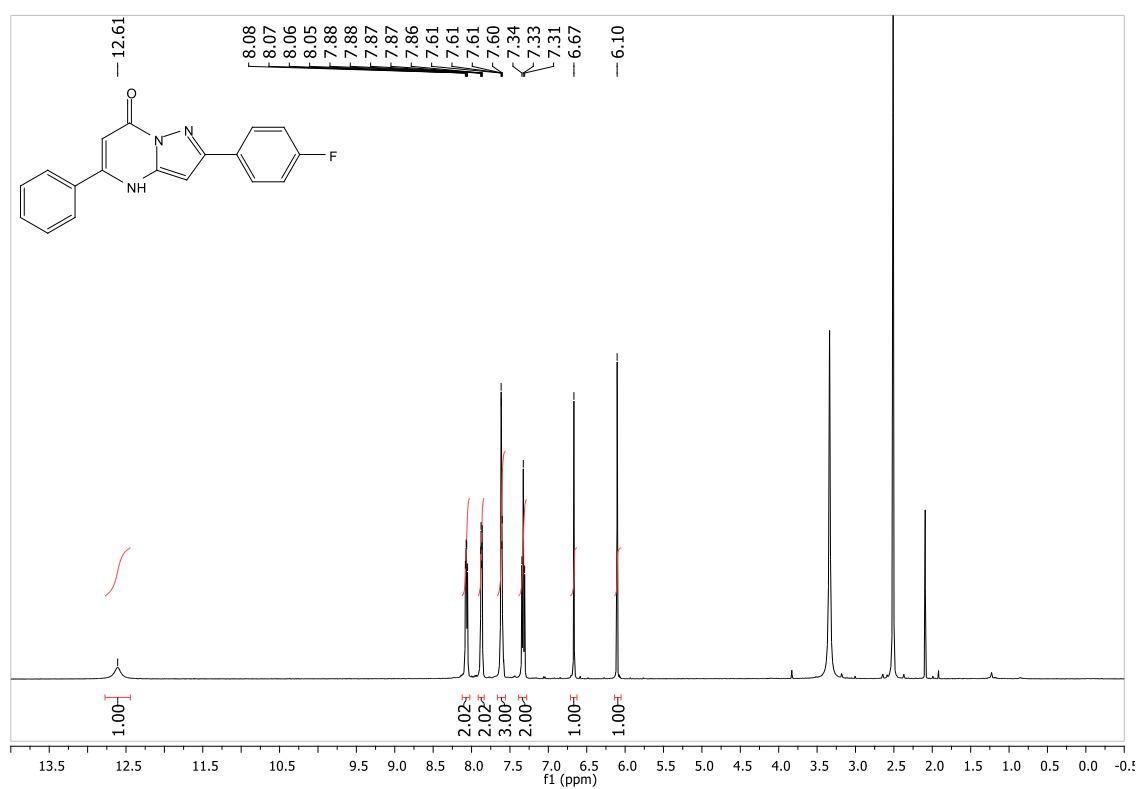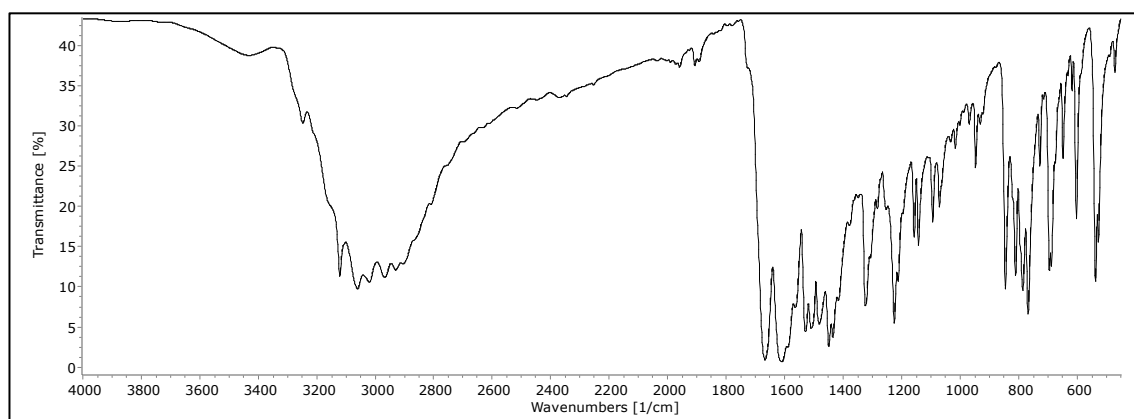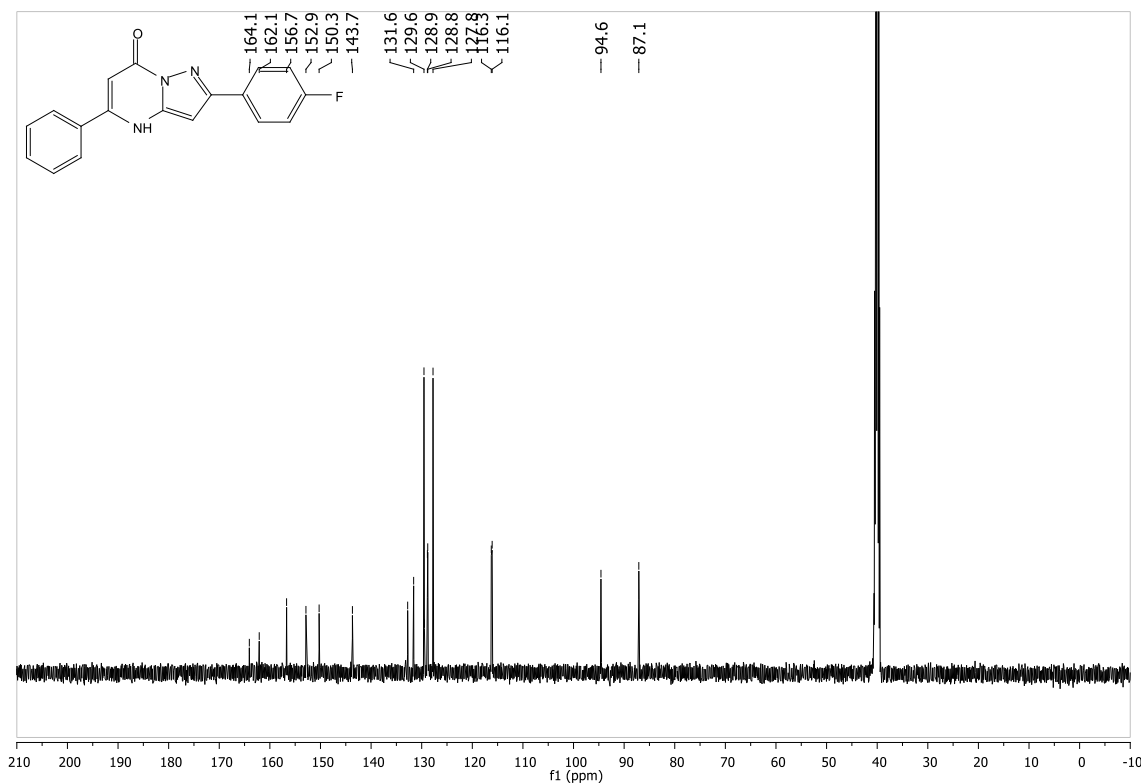
6.48 Spectra for 5-phenyl-2-(*p*-tolyl)pyrazolo[1,5-*a*]pyrimidin-7(4*H*)-one (MK9) (48)
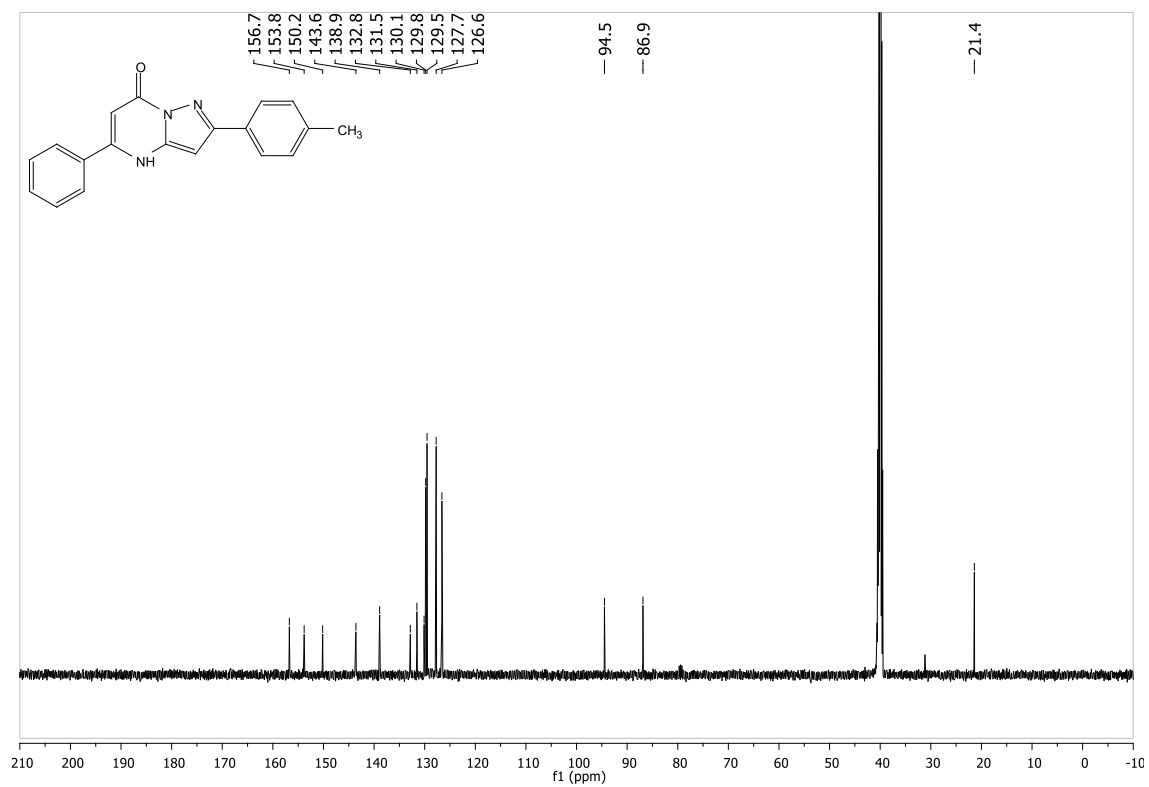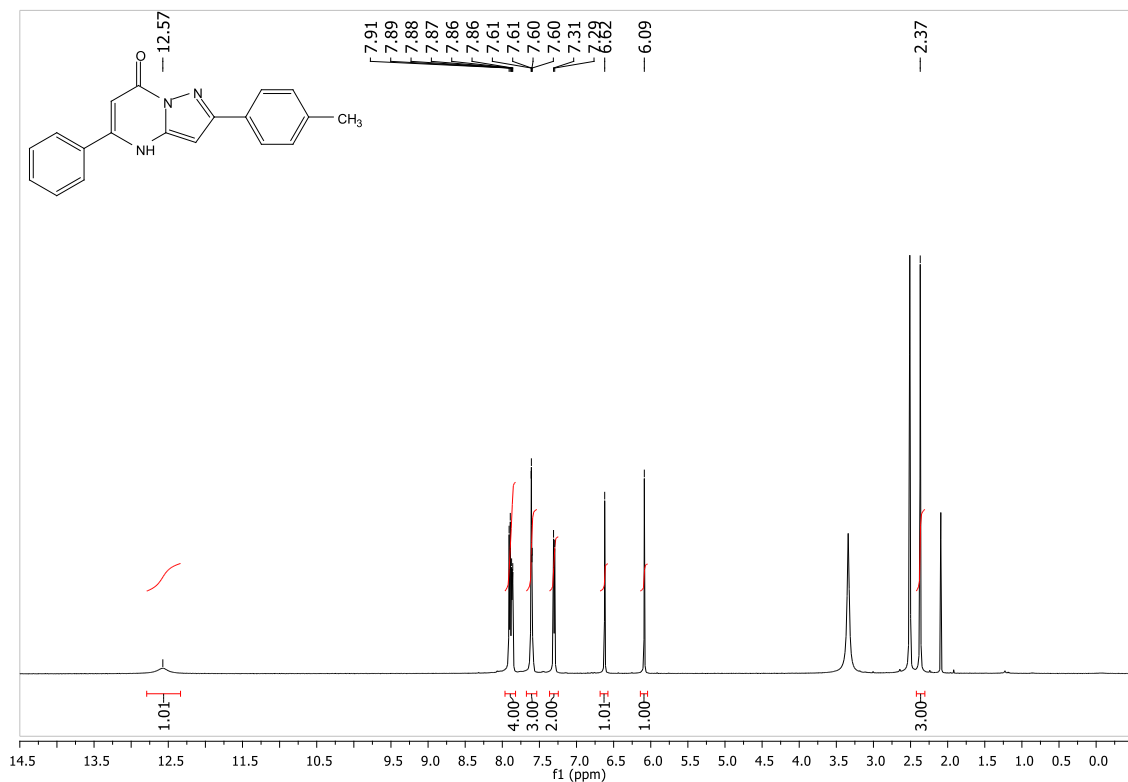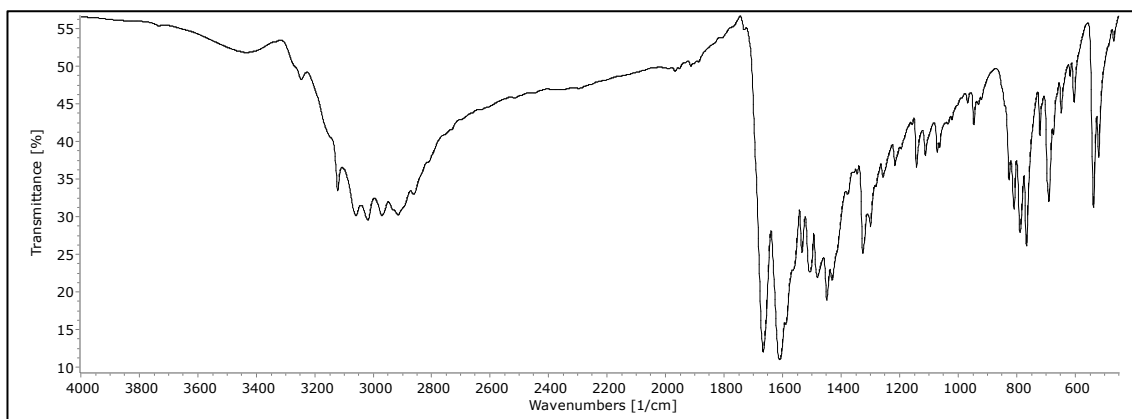
6.49 Spectra for 5-(4-nitrophenyl)-2-phenylpyrazolo[1,5-*a*]pyrimidin-7(4*H*)-one (MK61) (49)

155.9
153.6
148.9
147.7
143.3
138.6
132.4
128.9
128.8
128.7
126.3
123.9

95.6
86.9

210 200 190 180 170 160 150 140 130 120 110 100 90 80 70 60 50 40 30 20 10 0 -10
f1 (ppm)
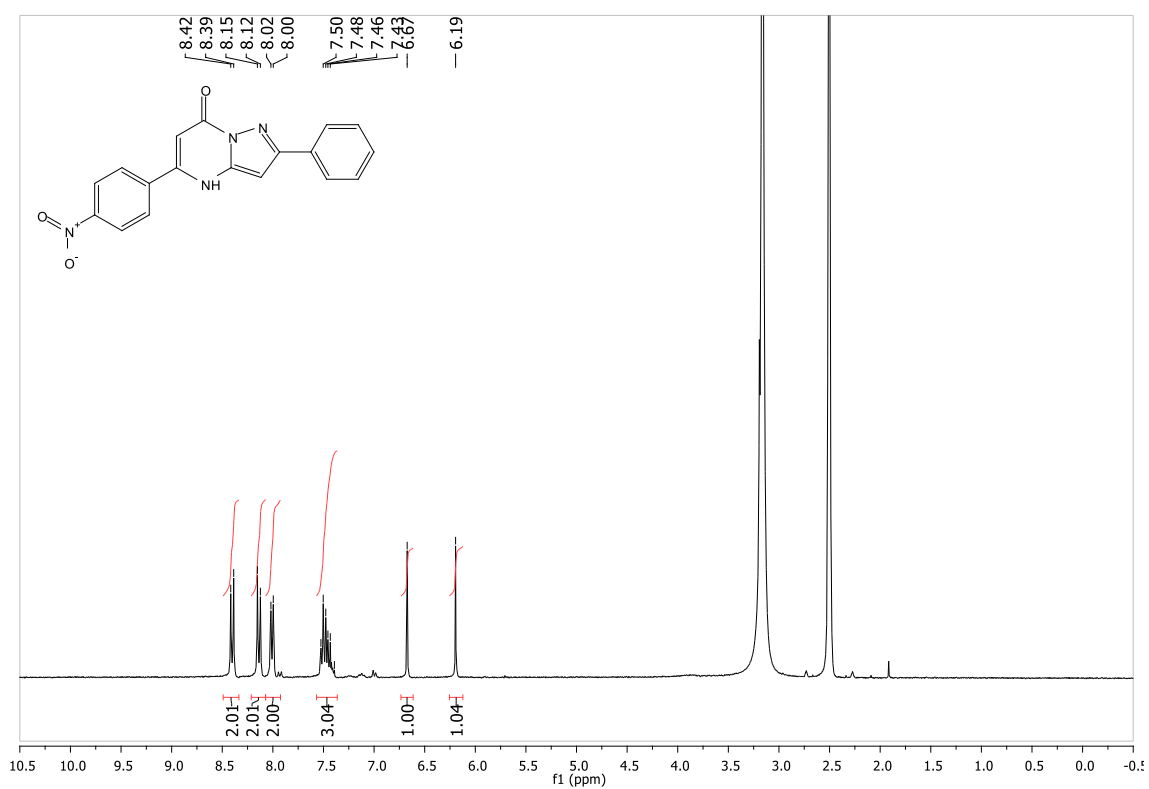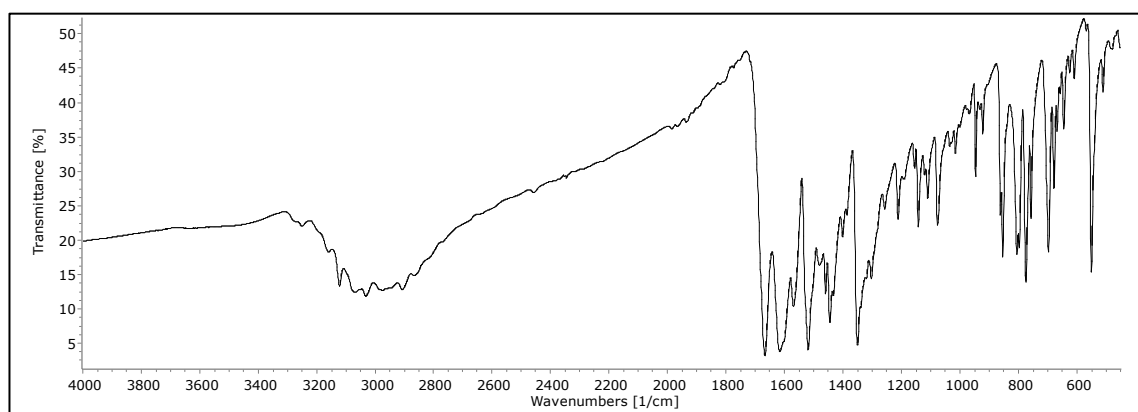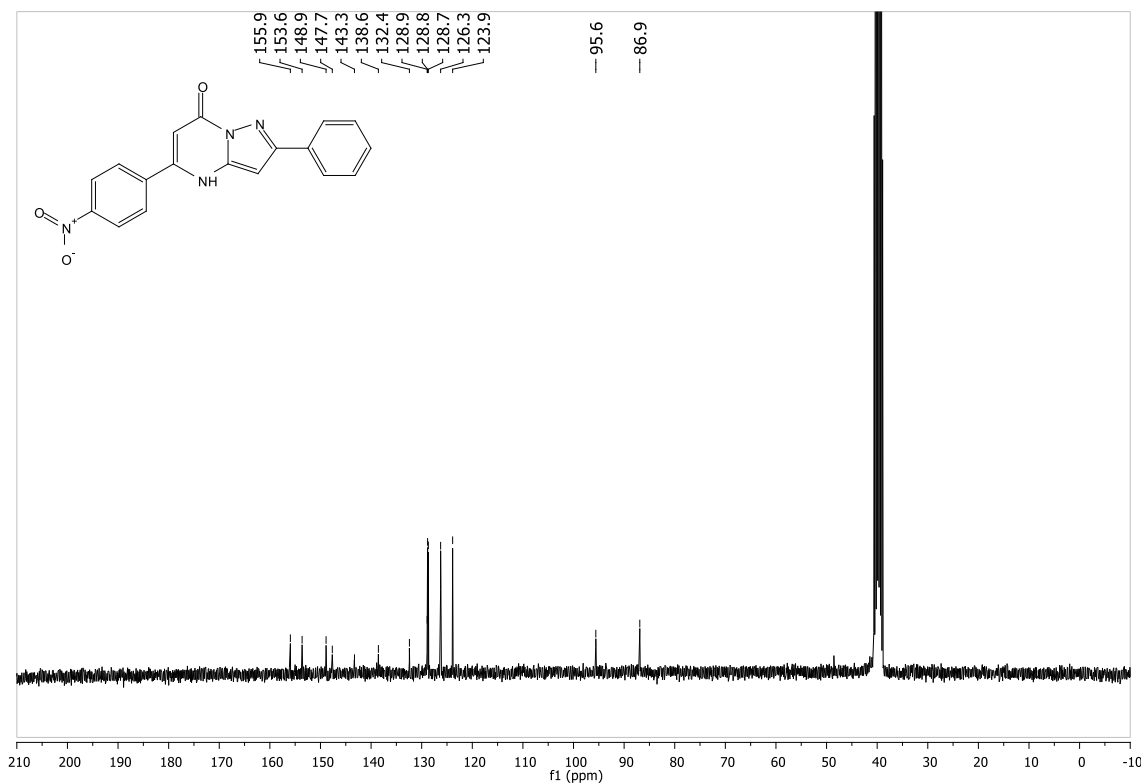
6.50 Spectra for 5-(4-methoxyphenyl)-2-phenylpyrazolo[1,5-*a*]pyrimidin-7(4*H*)-one (MK66) (50)
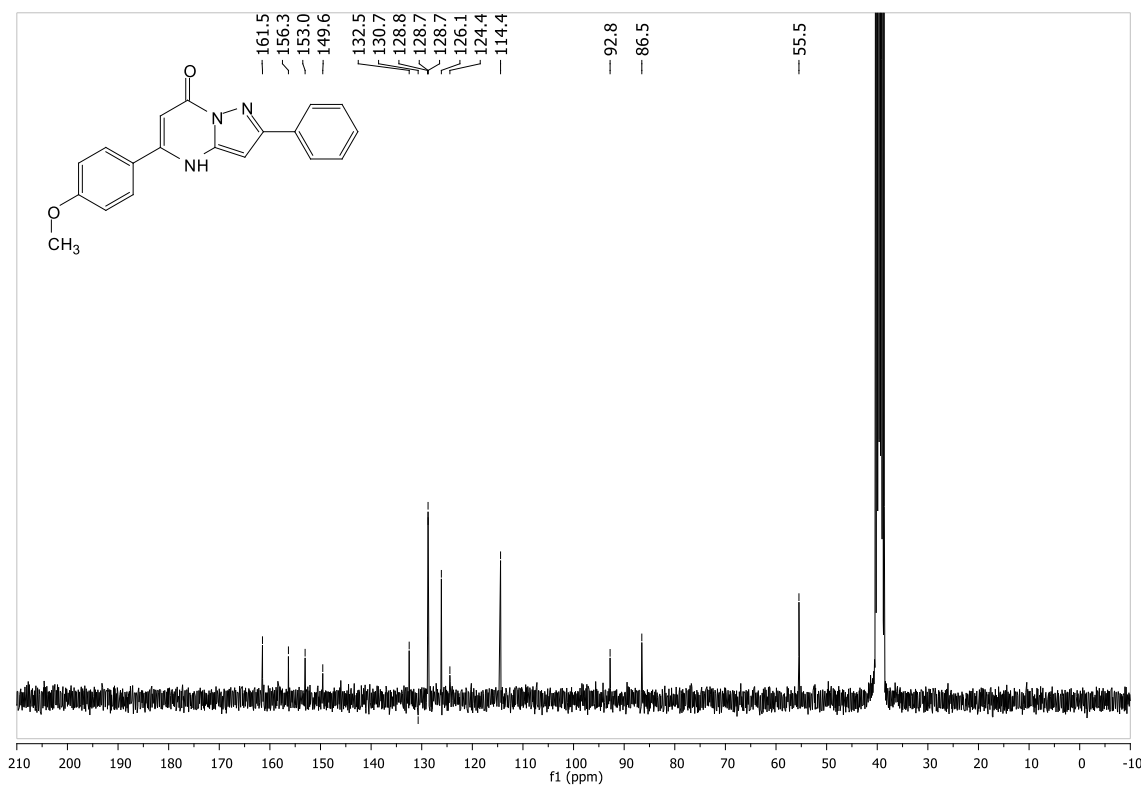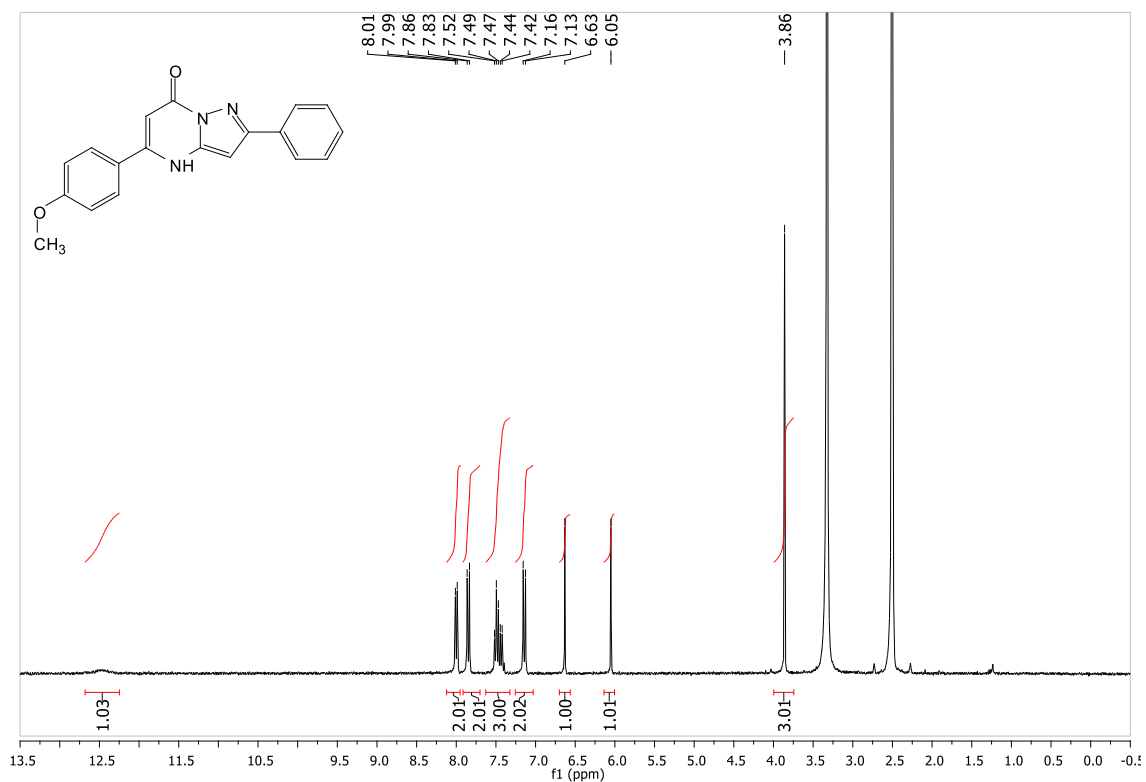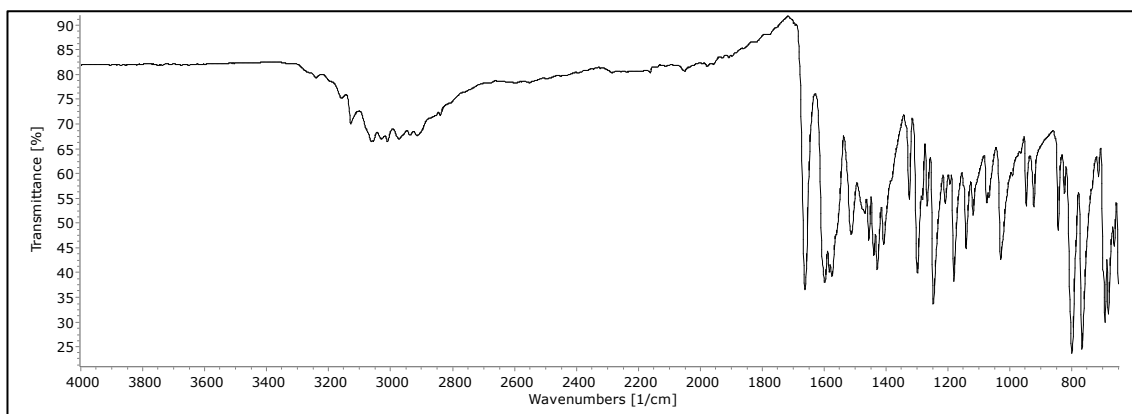
6.51   Spectra for 2-phenyl-5-(2,3,4,5-tetrafluorophenyl)pyrazolo[1,5-a]pyrimidin-7(4H)-one (MK63) (51)
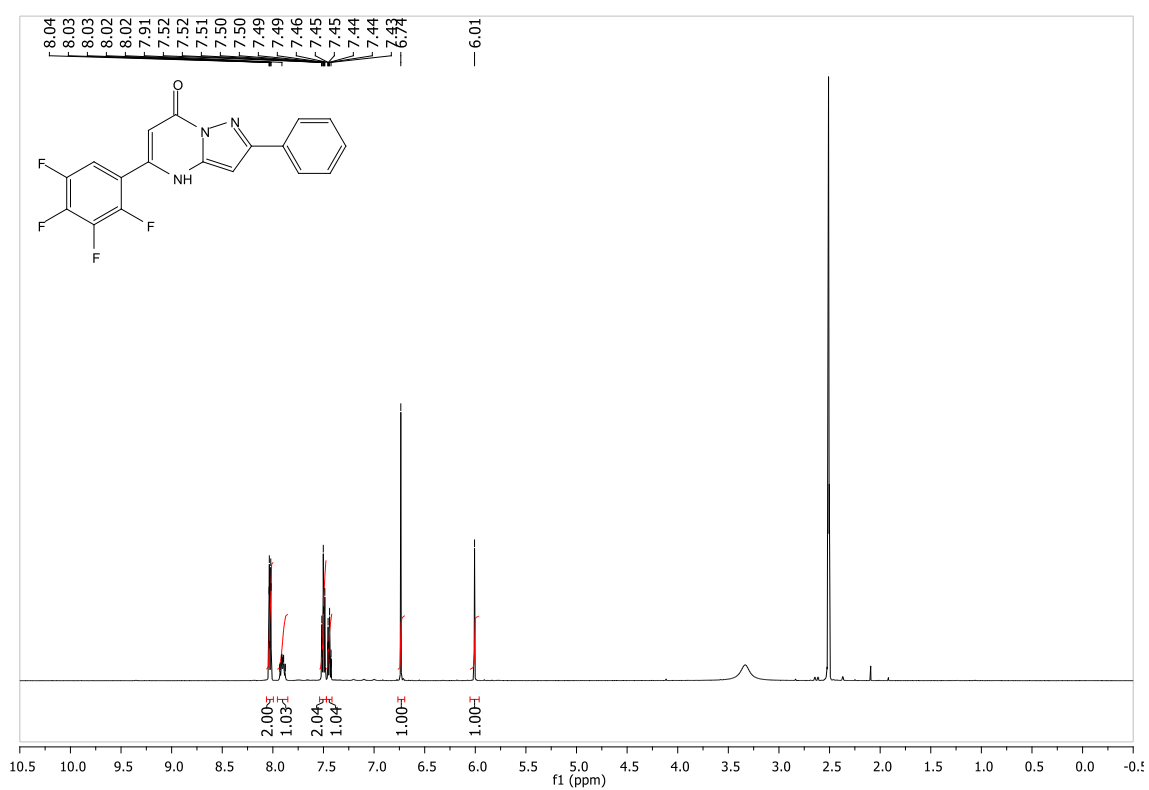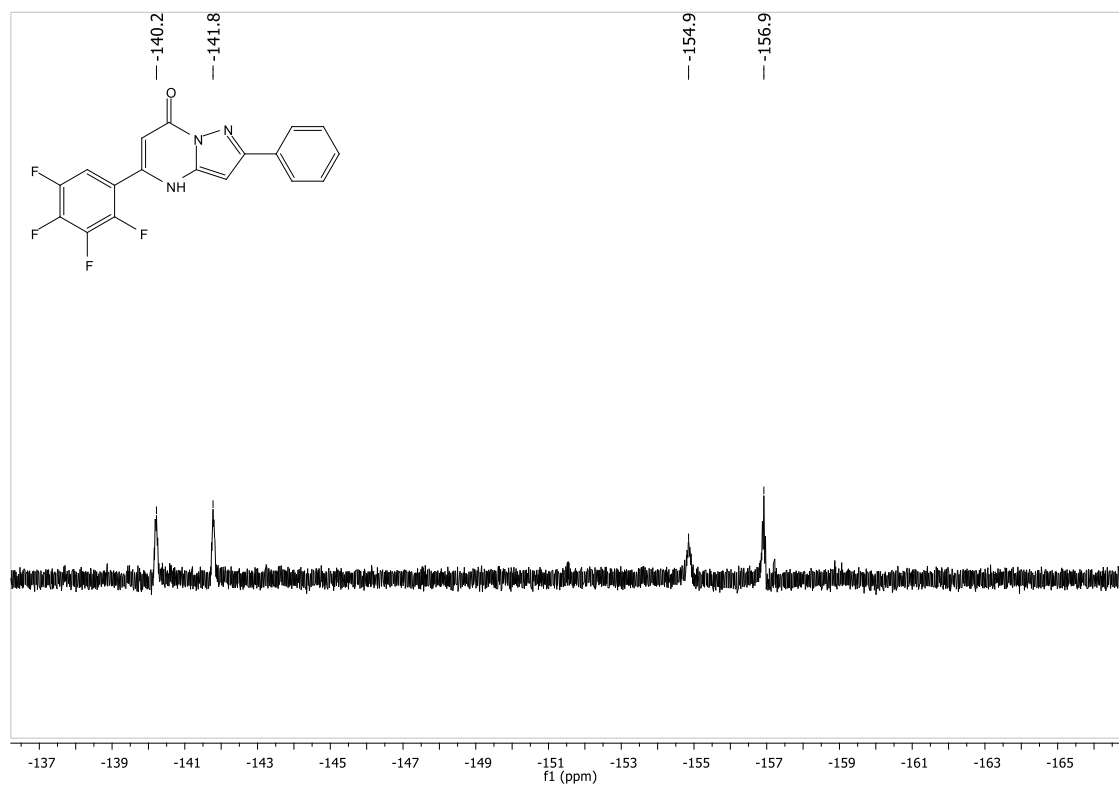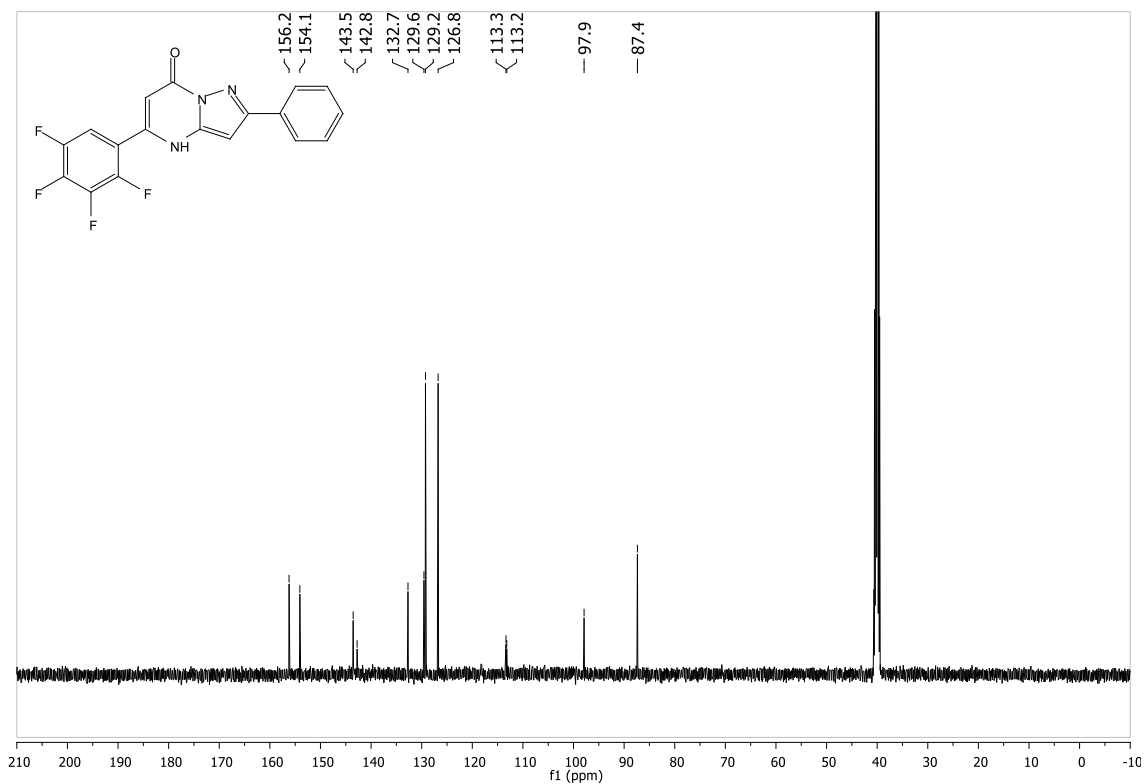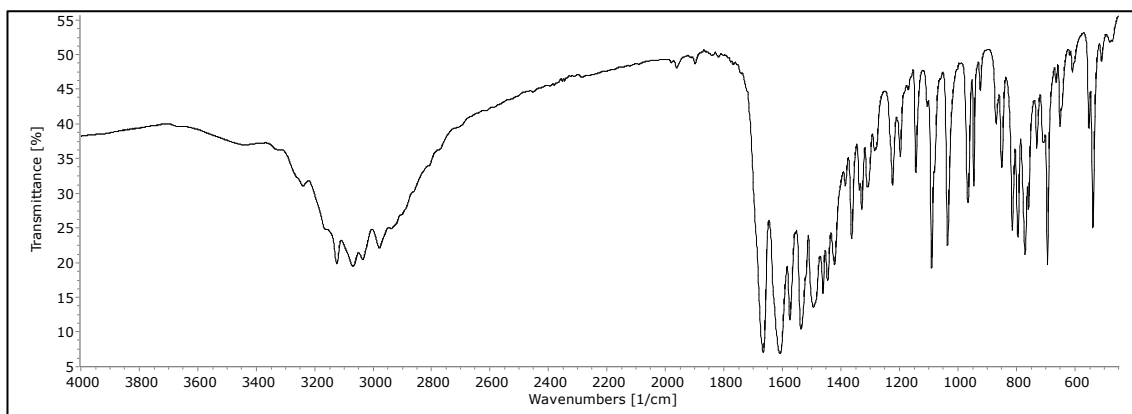
388

6.52 Spectra for 5-(3,5-dimethylphenyl)-2-methylpyrazolo[1,5-*a*]pyrimidin-7(4*H*)-one (MK2) (52)

138.9
132.3
124.5
19.9

f1 (ppm)

Transmittance [%]

Wavenumbers [1/cm]
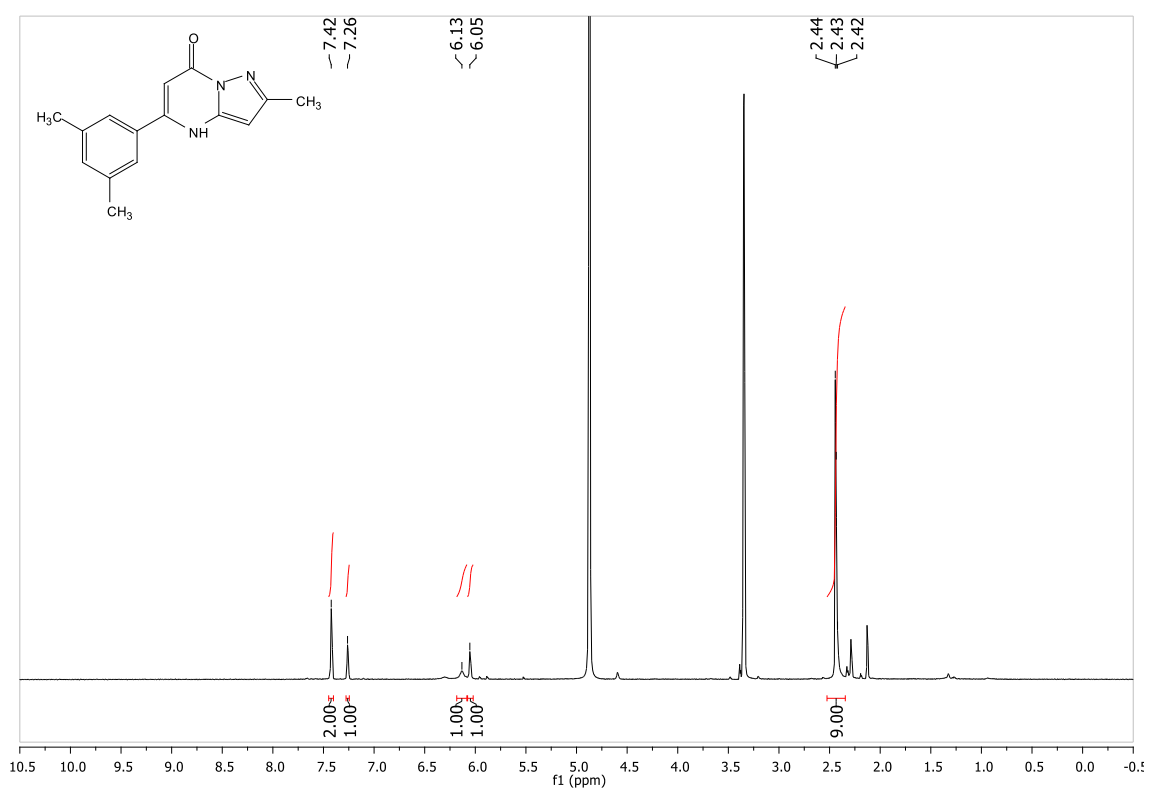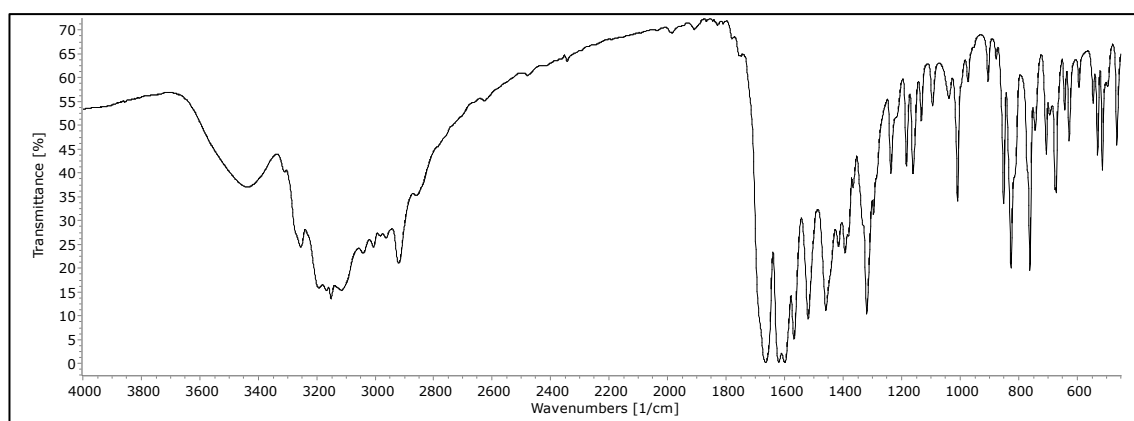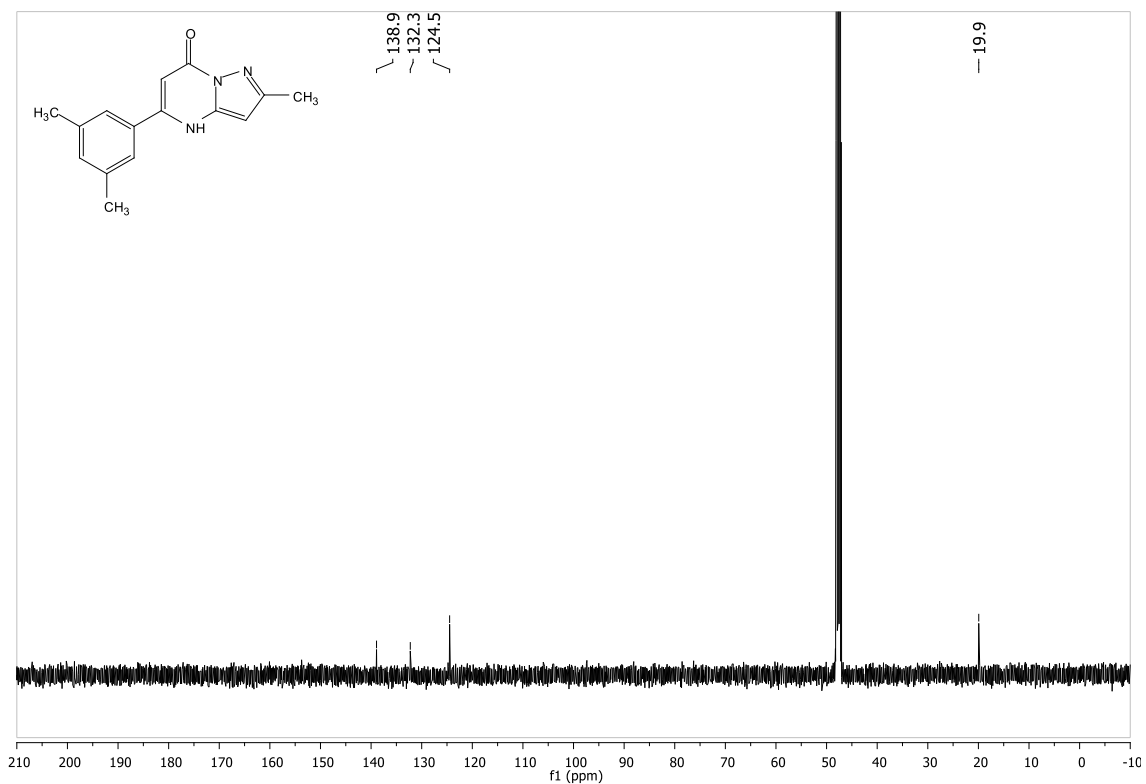
6.53 Spectra for ethyl 3-(3,5-dimethylphenyl)-3-oxopropanoate (MK1) (53)
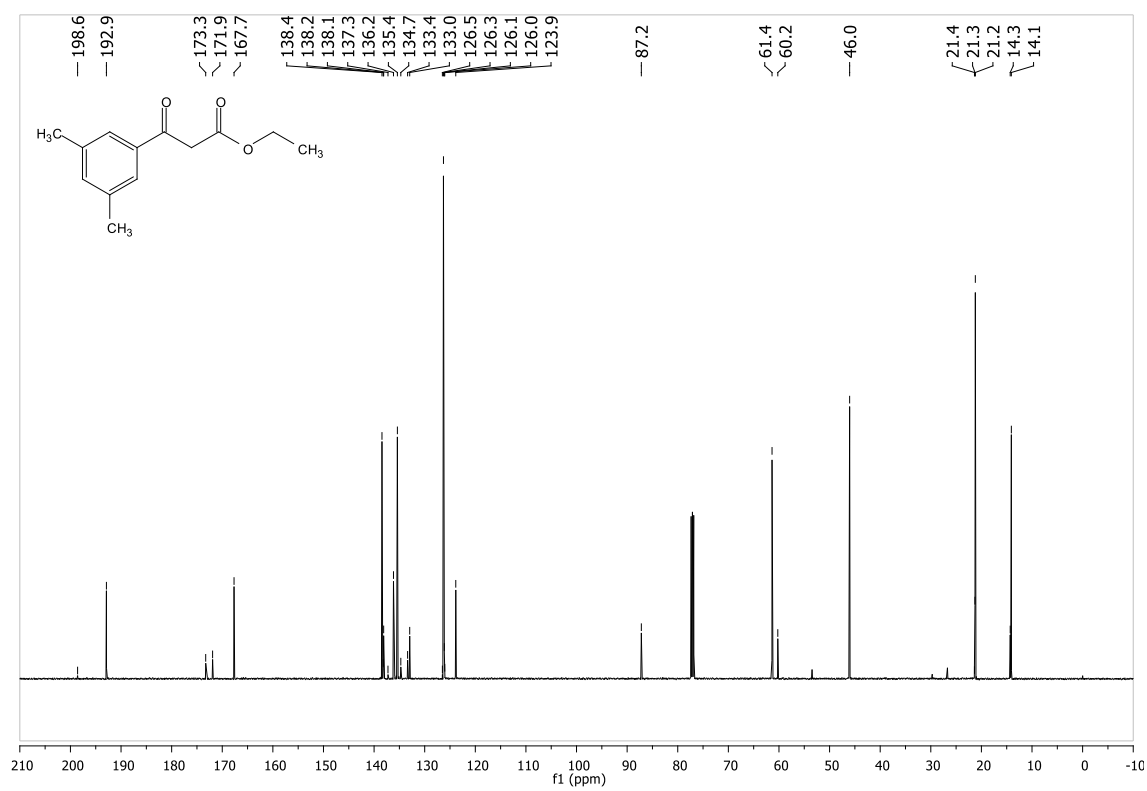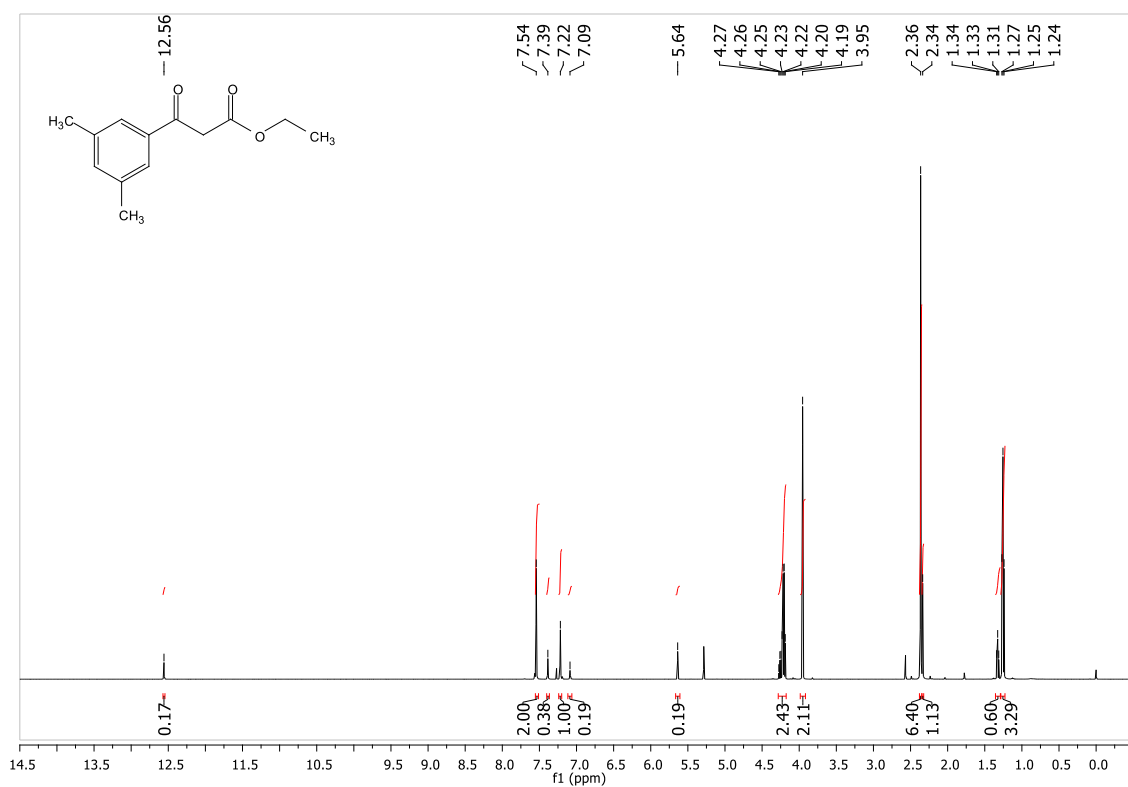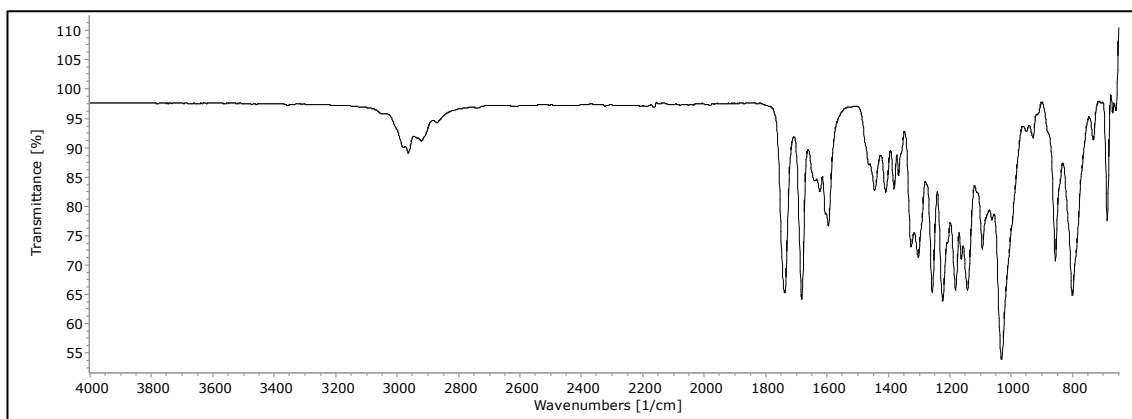
6.54 Spectra for ethyl 3-(3,5-diethylphenyl)-3-oxopropanoate (MK4) (54)
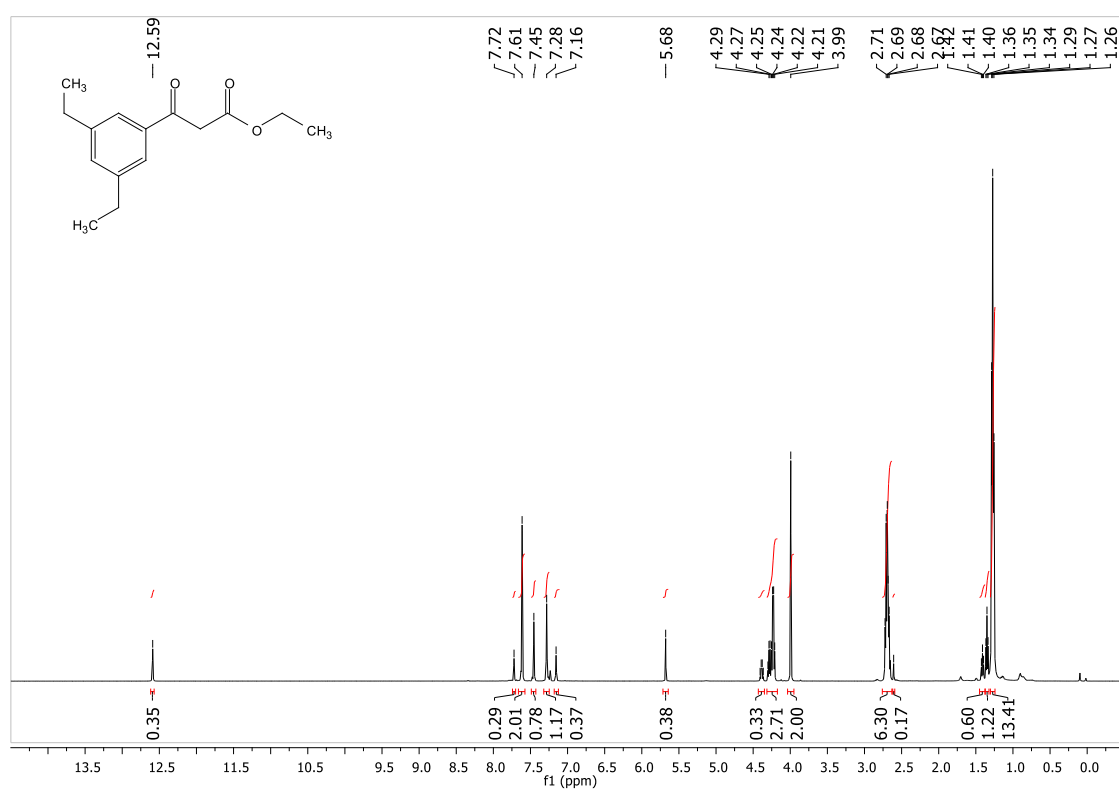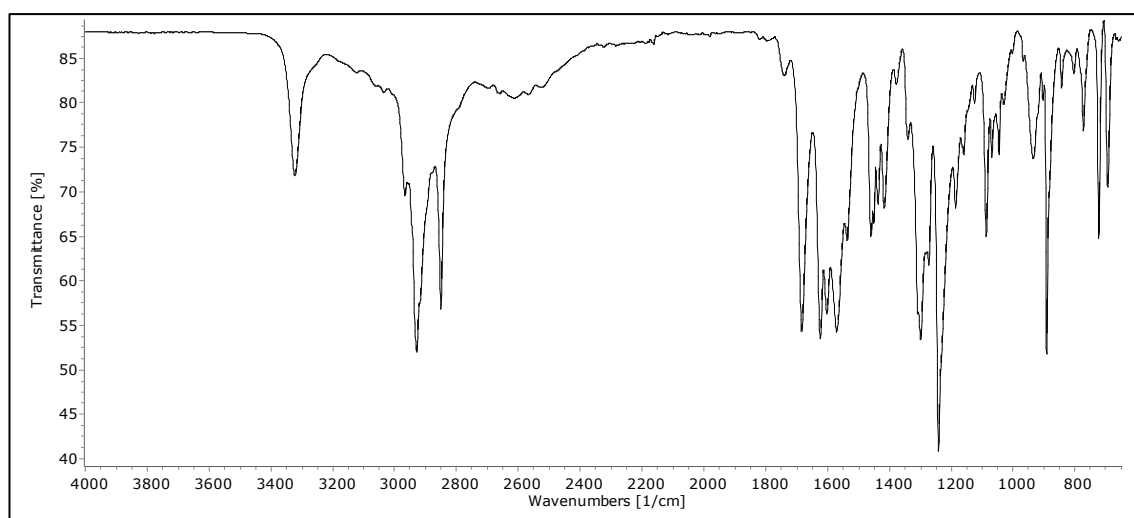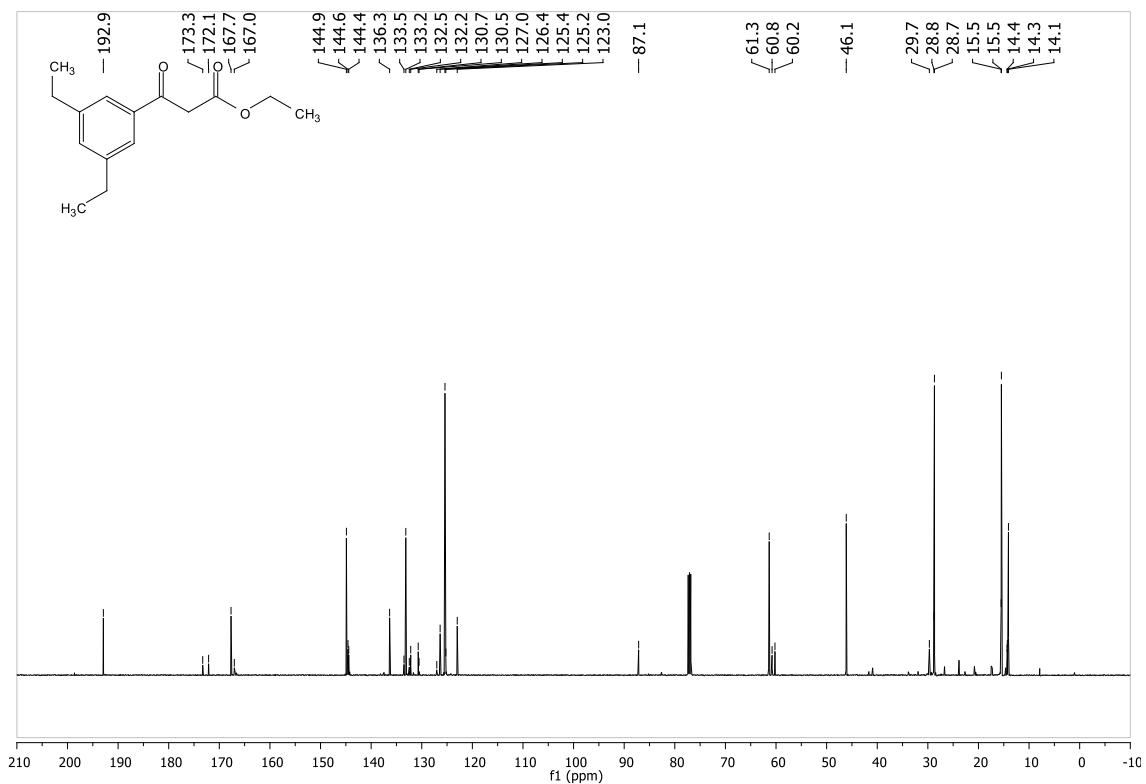
6.55   Spectra for ethyl 3-(3,5-dimethoxyphenyl)-3-oxopropanoate (MK10) (55)
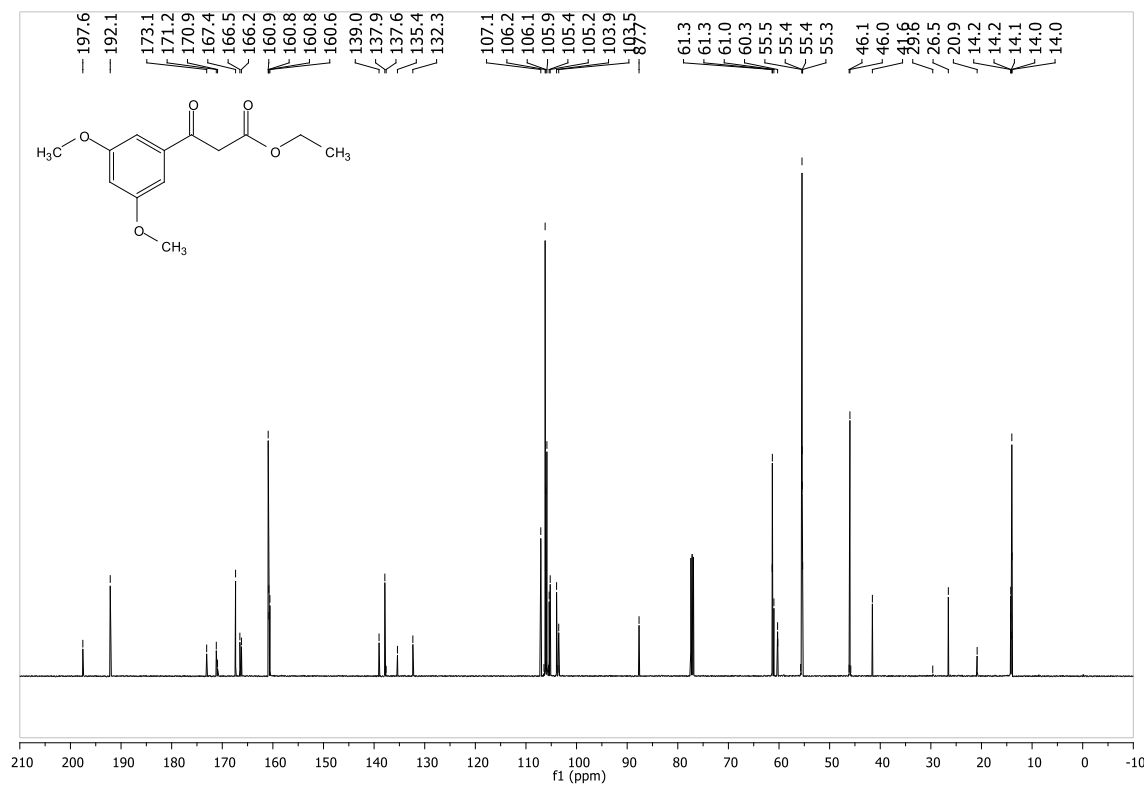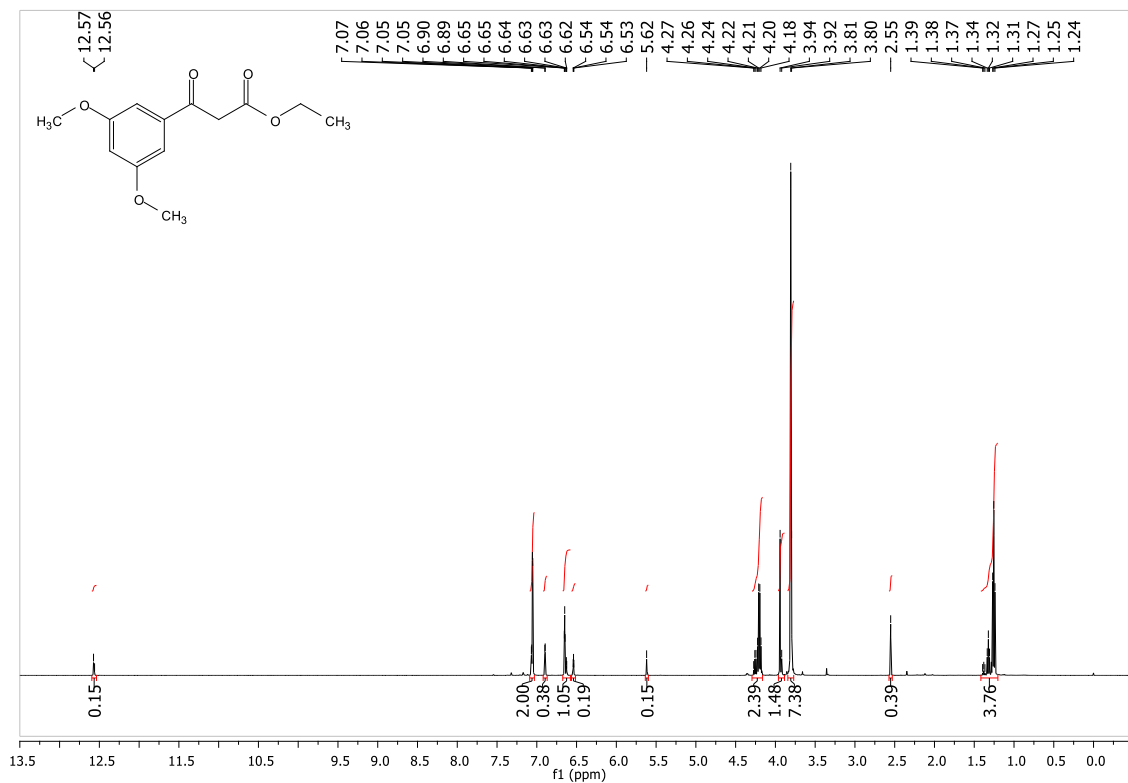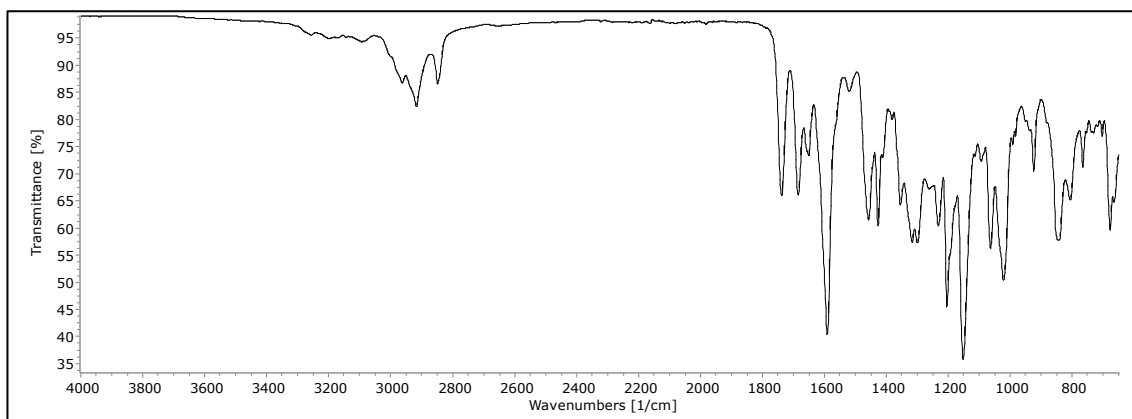
6.56   Spectra for ethyl 3-(3,5-dinitrophenyl)-3-oxopropanoate (MK11) (56)

396
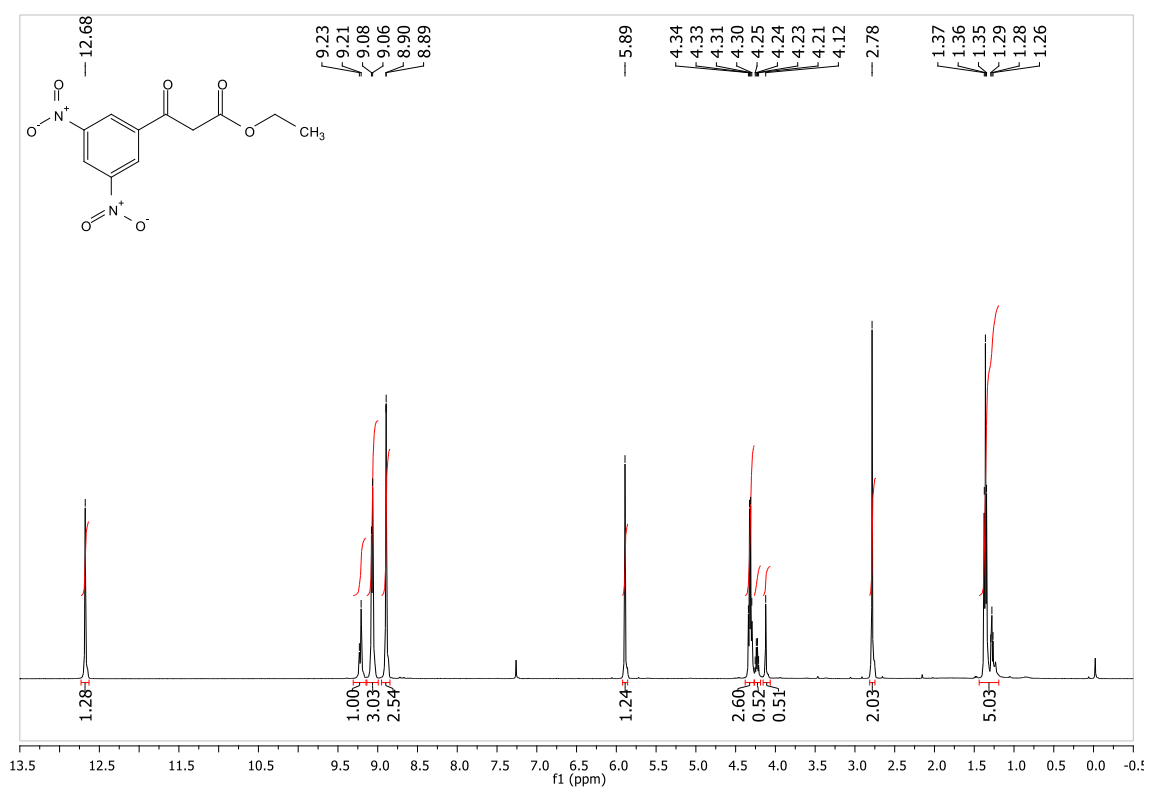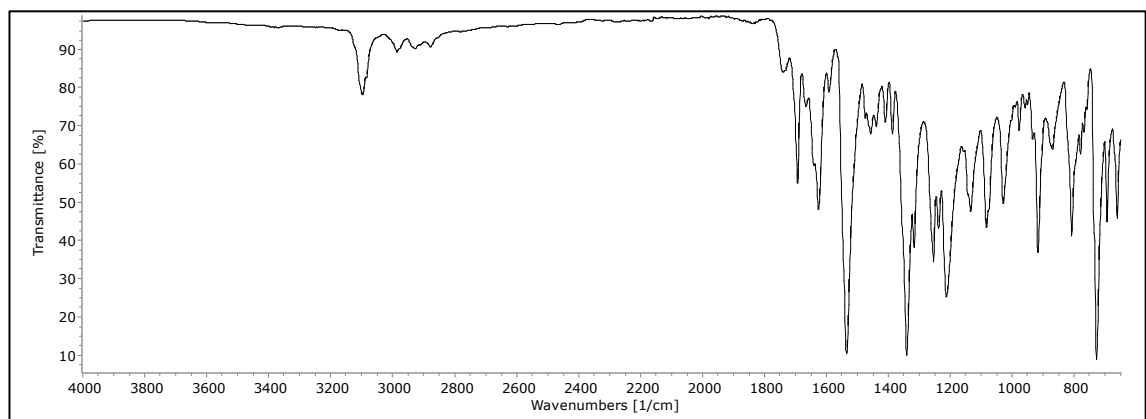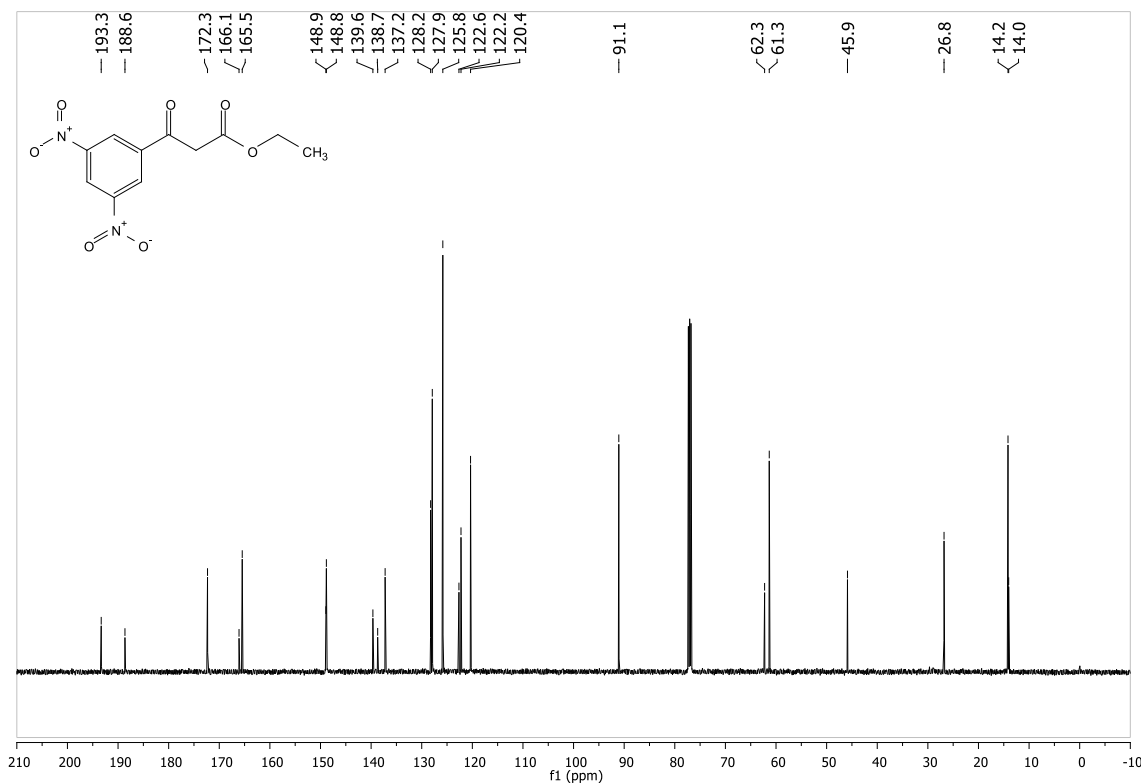
6.57   Spectra for 3,5-diethylbenzoic acid (MK3) (57)
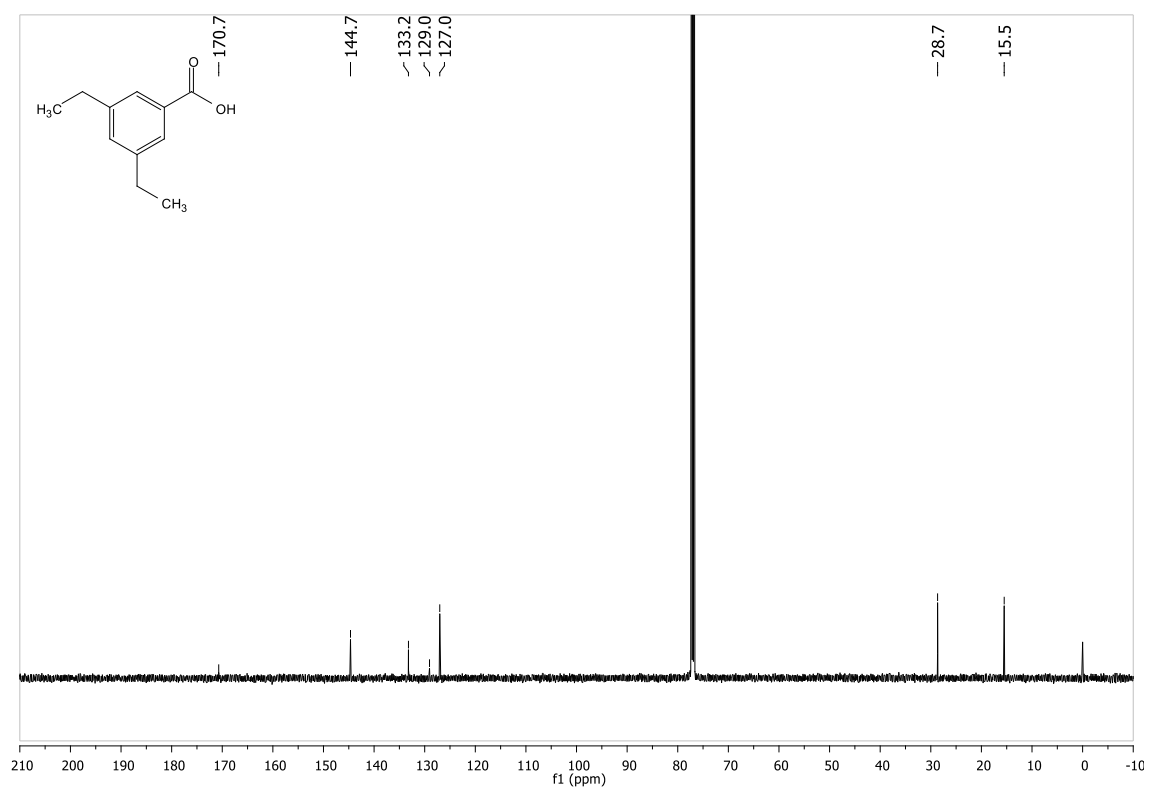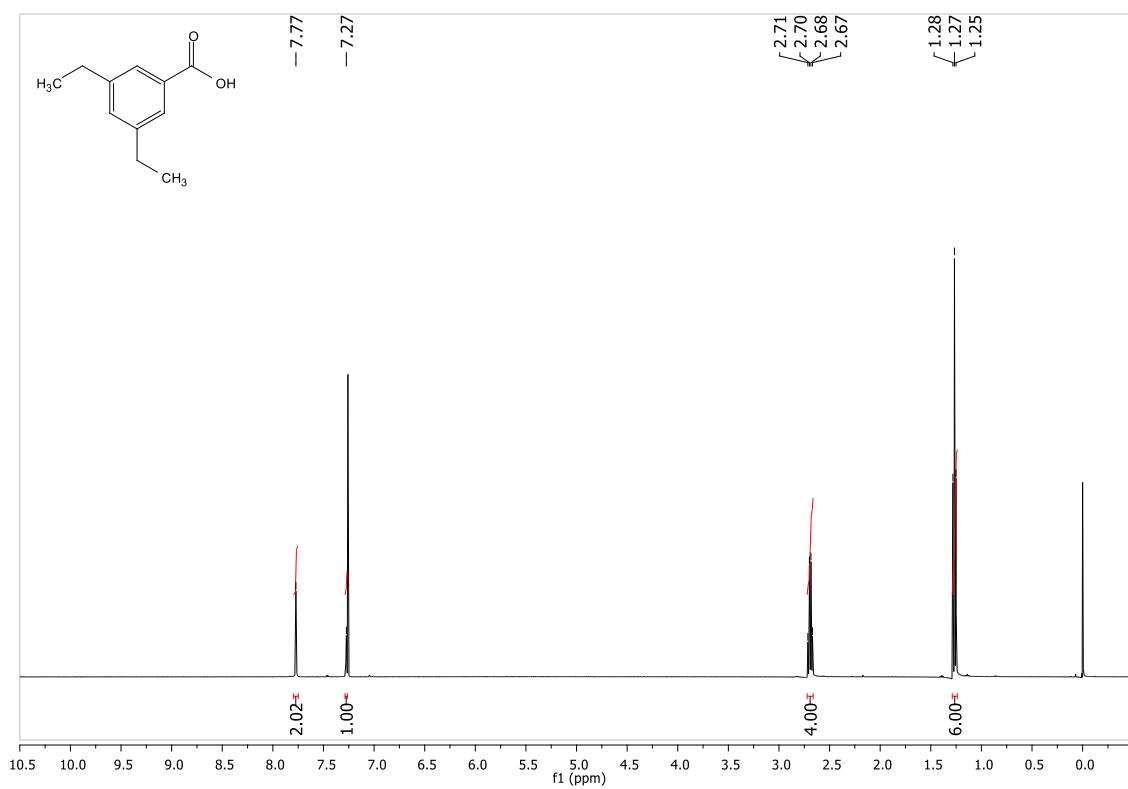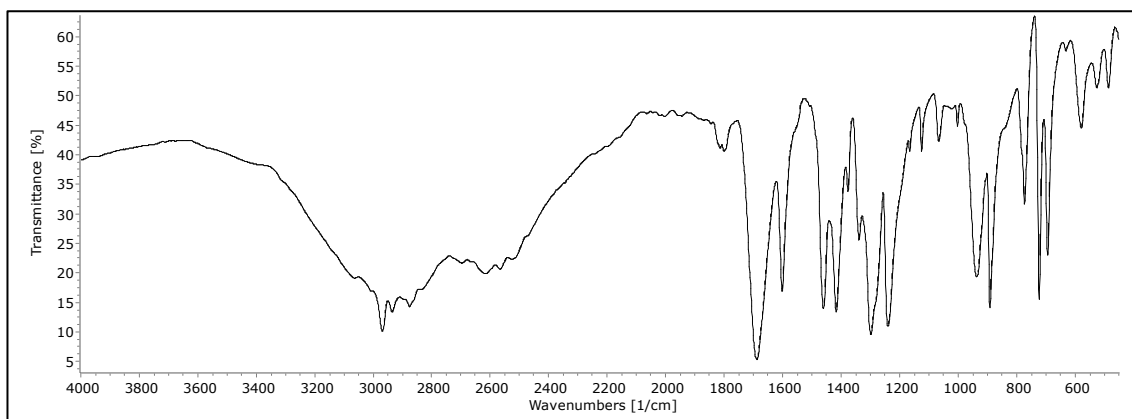
6.58 Spectra for 5-(3,5-dimethylphenyl)-2-isopropylpyrazolo[1,5-*a*]pyrimidin-7(4*H*)-one (MK6) (58)
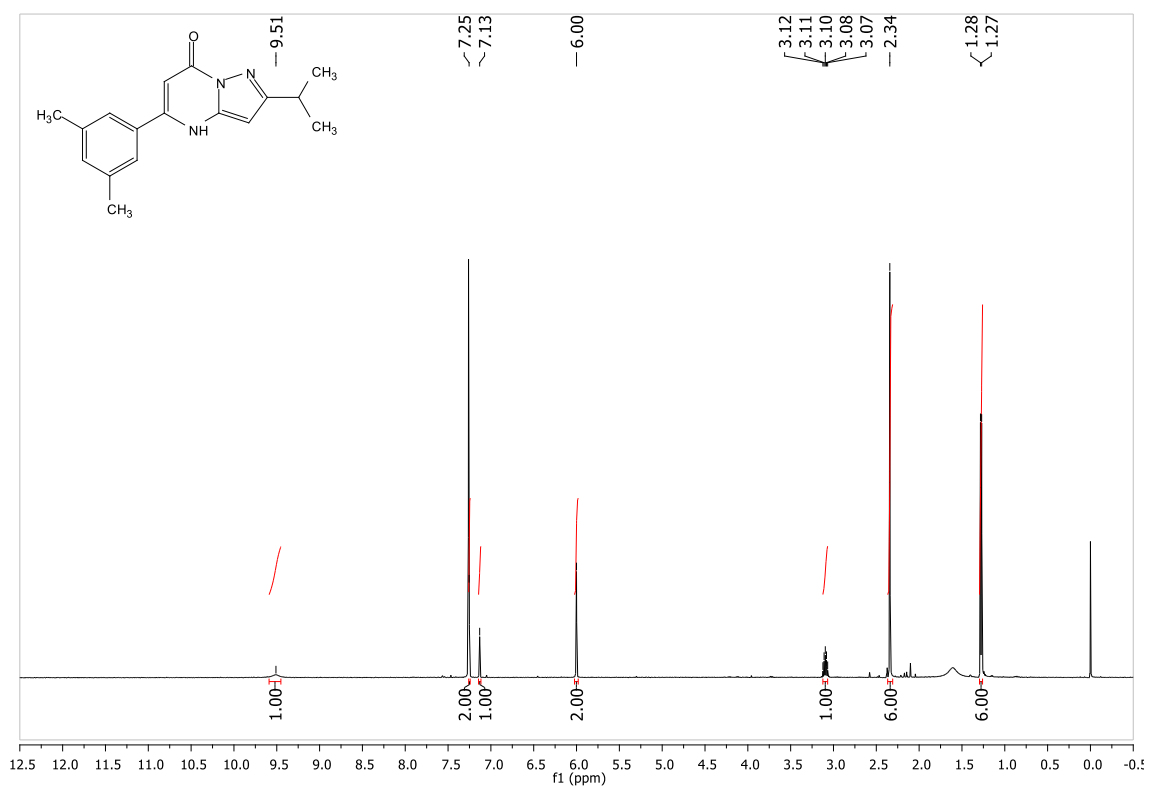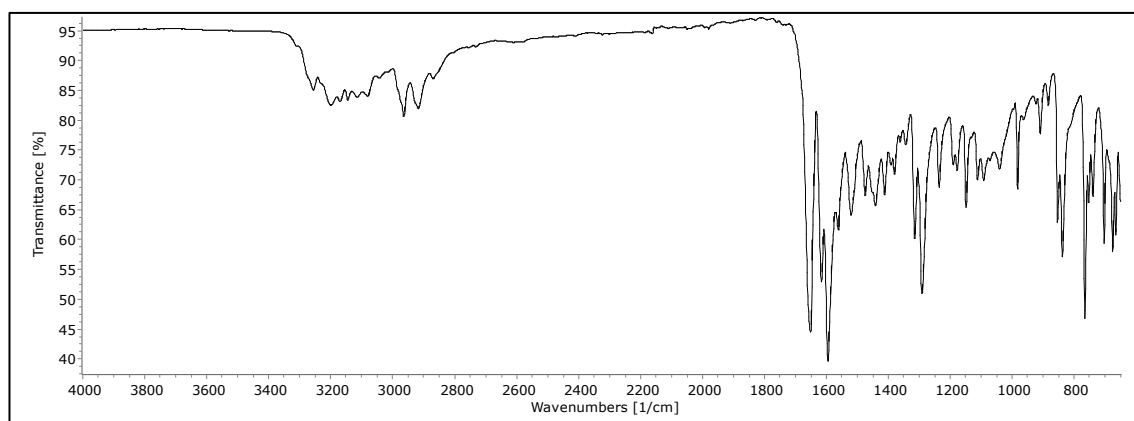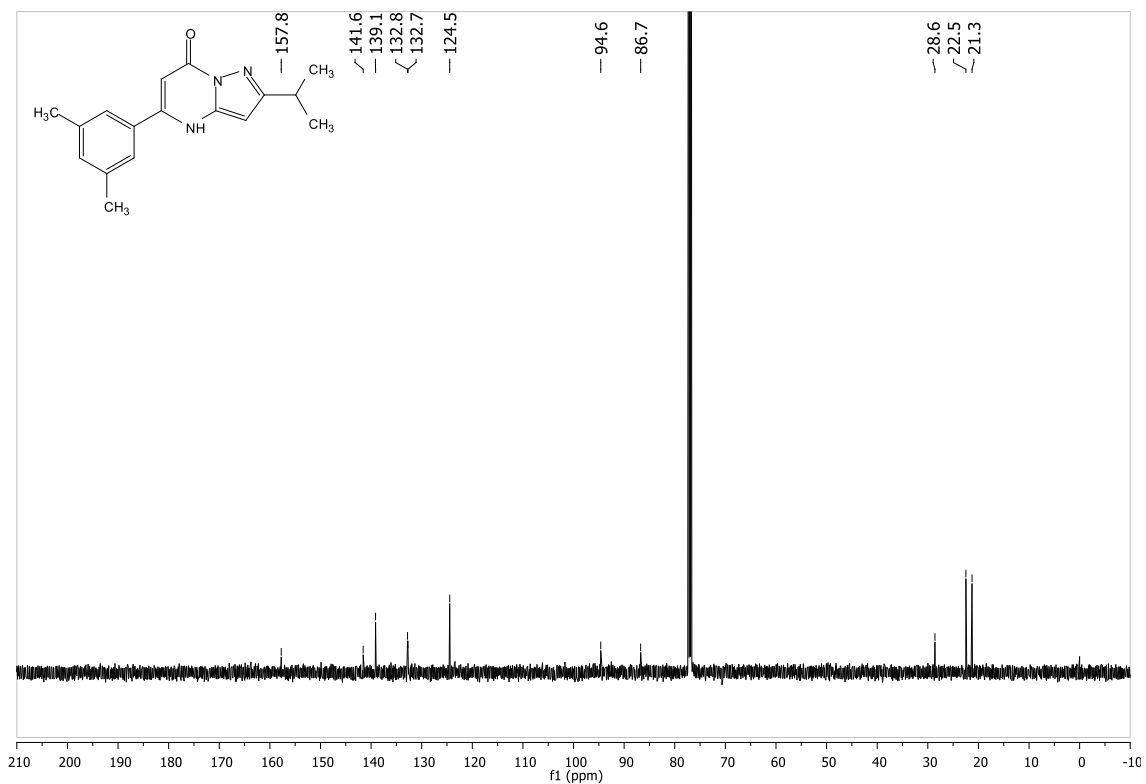
6.59 Spectra for 5-(3,5-diethylphenyl)-2-isopropylpyrazolo[1,5-*a*]pyrimidin-7(4*H*)-one (MK5) (59)
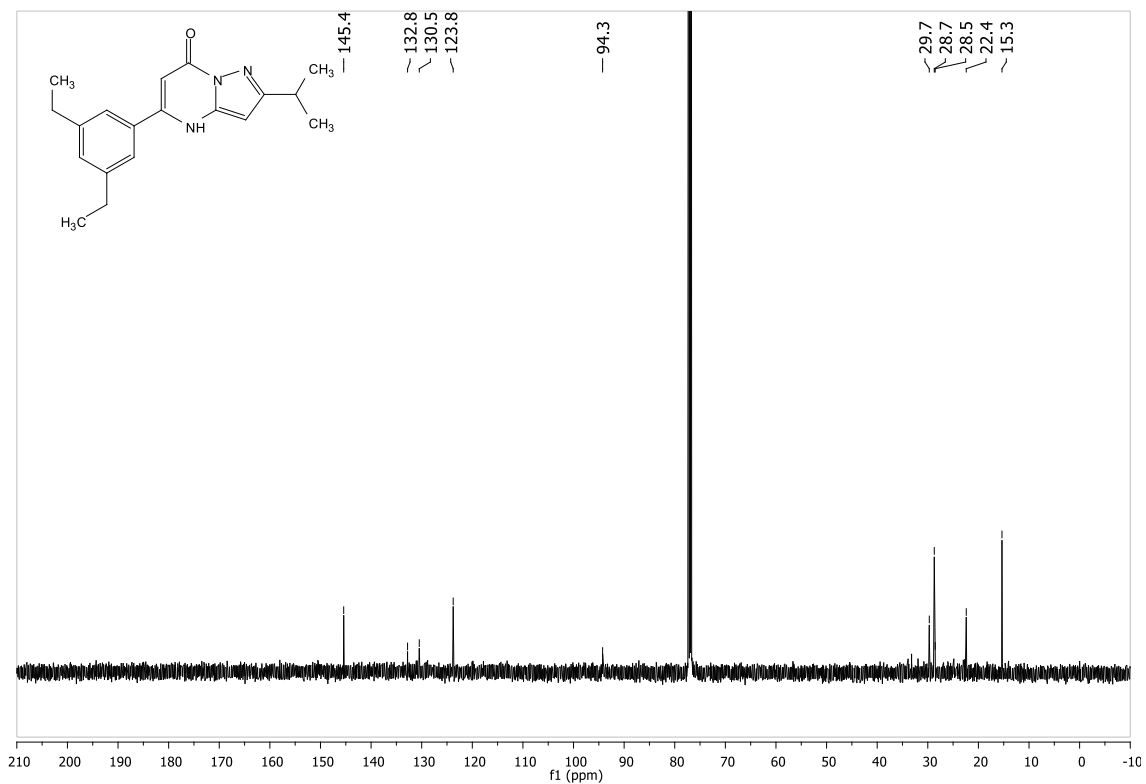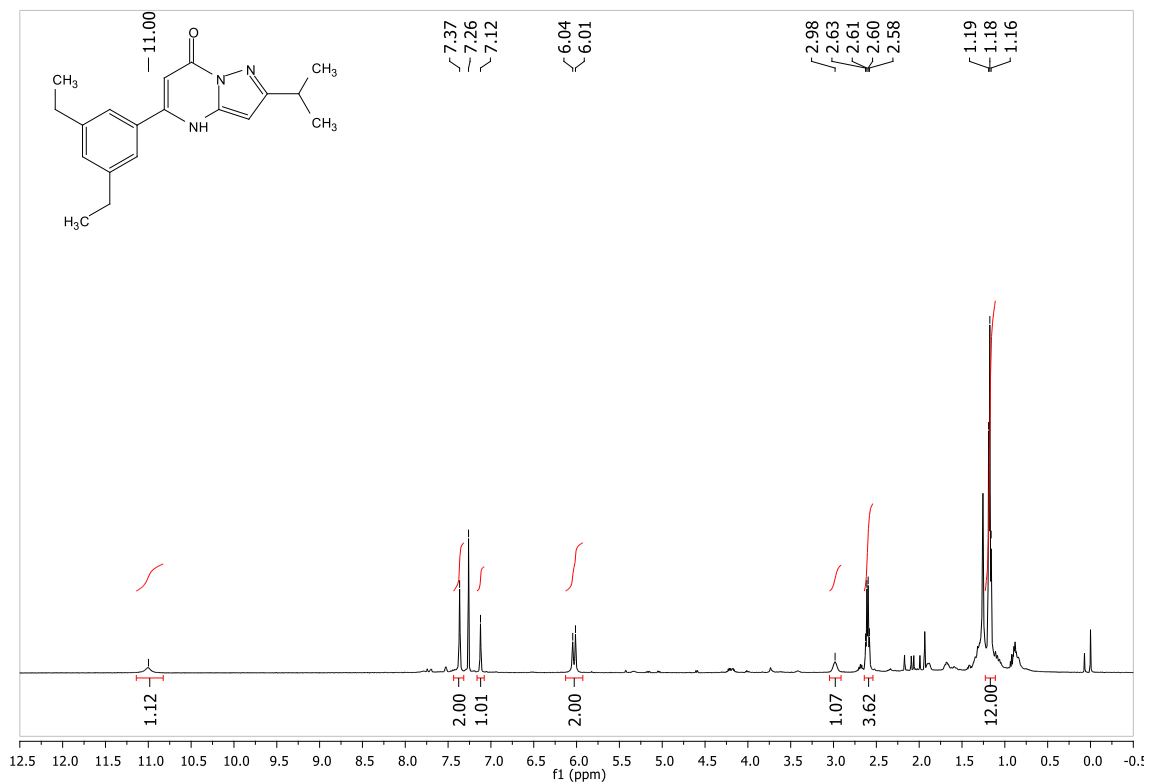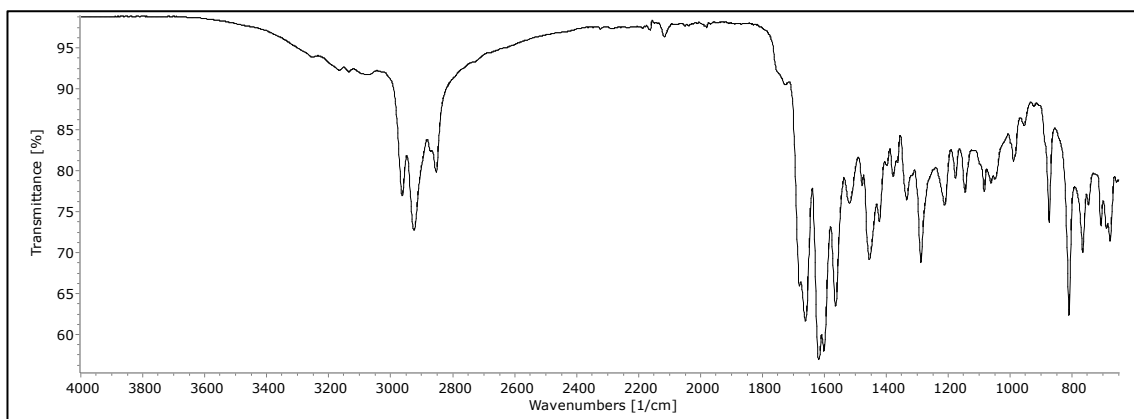
6.60 Spectra for 5-(3,5-dimethoxyphenyl)-2-isopropylpyrazolo[1,5-a]pyrimidin-7(4H)-one (MK13) (60)

13C NMR peaks: 162.4, 161.0, 153.7, 147.5, 138.8, 105.4, 102.1, 91.0, 88.5, 55.9, 28.2, 23.2

f1 (ppm)

Transmittance [%]

Wavenumbers [1/cm]

402
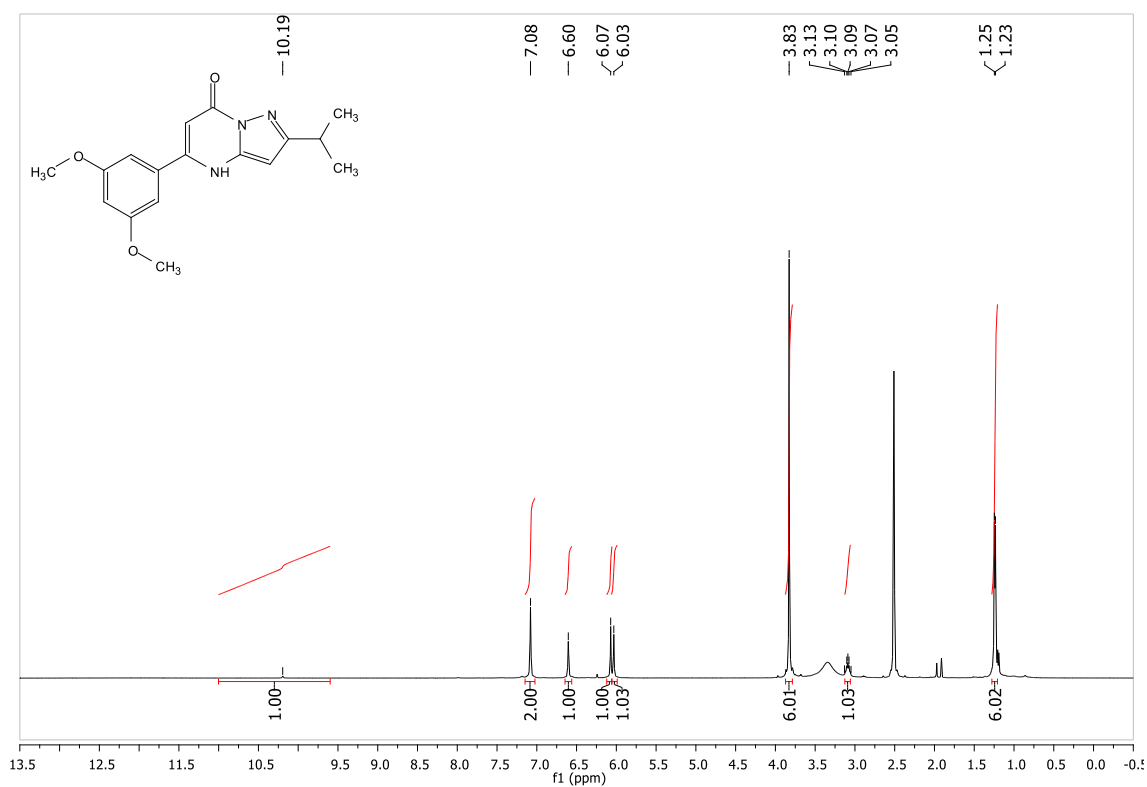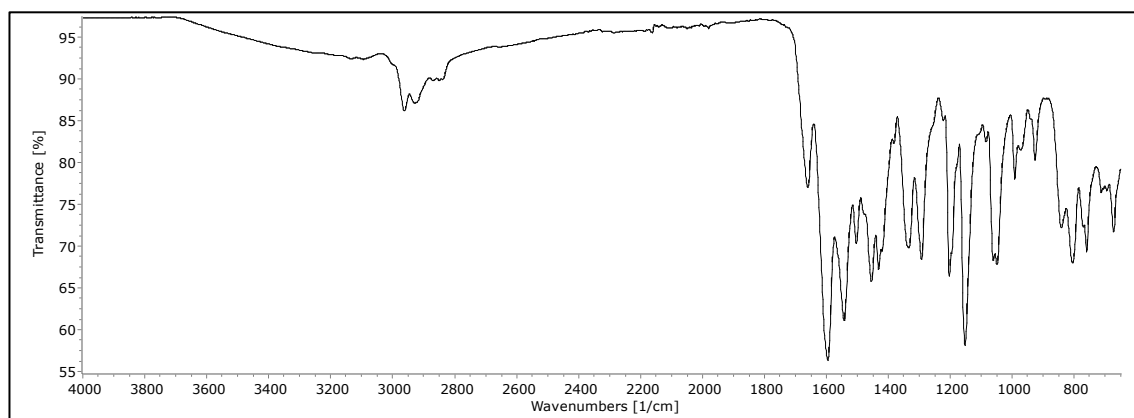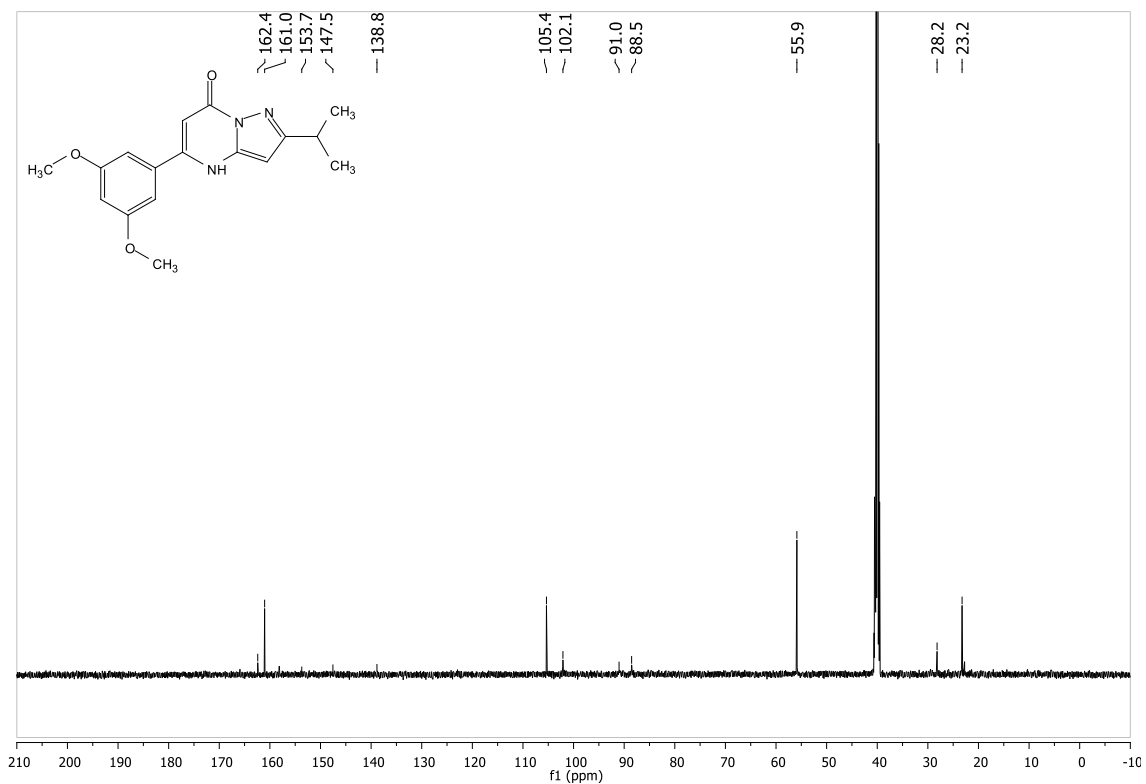
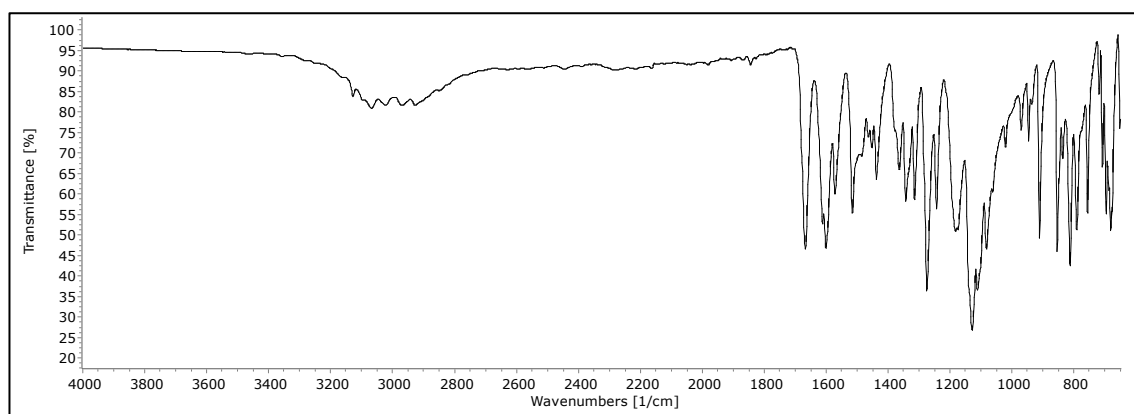## 6.61 Spectra for 5-(3,5-dinitrophenyl)-2-isopropylpyrazolo[1,5-*a*]pyrimidin-7(4*H*)-one (MK49) (61)
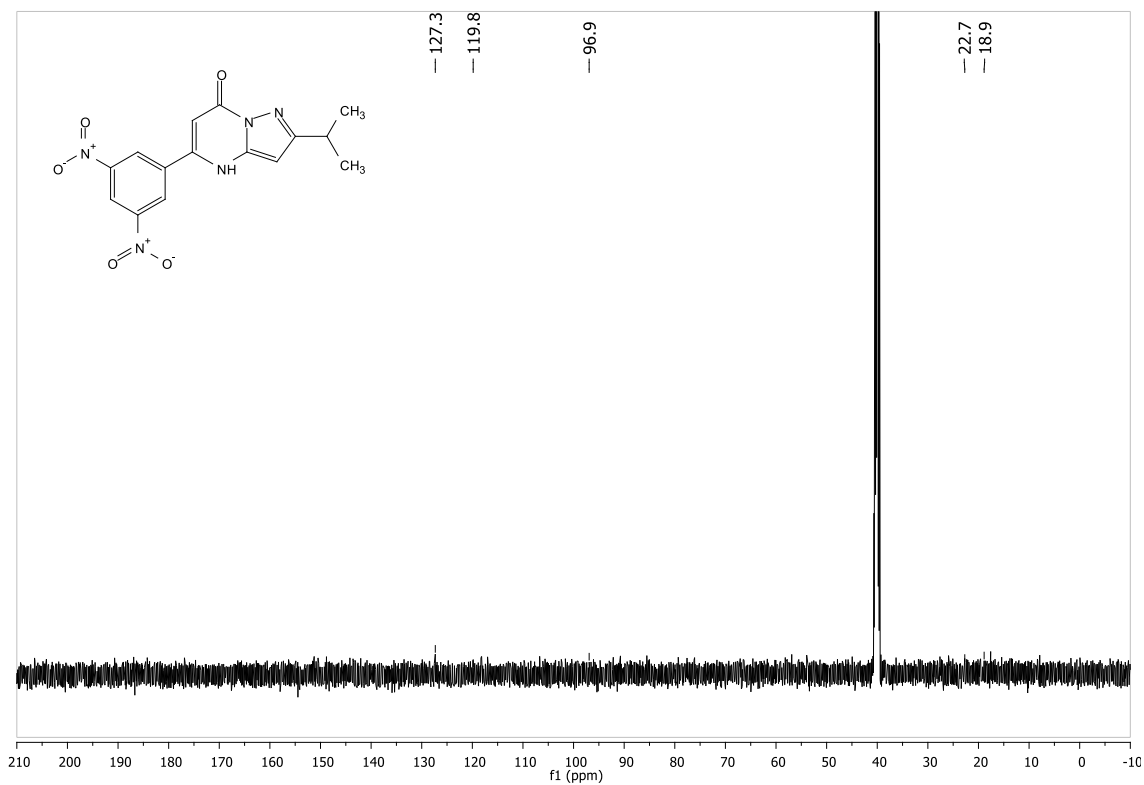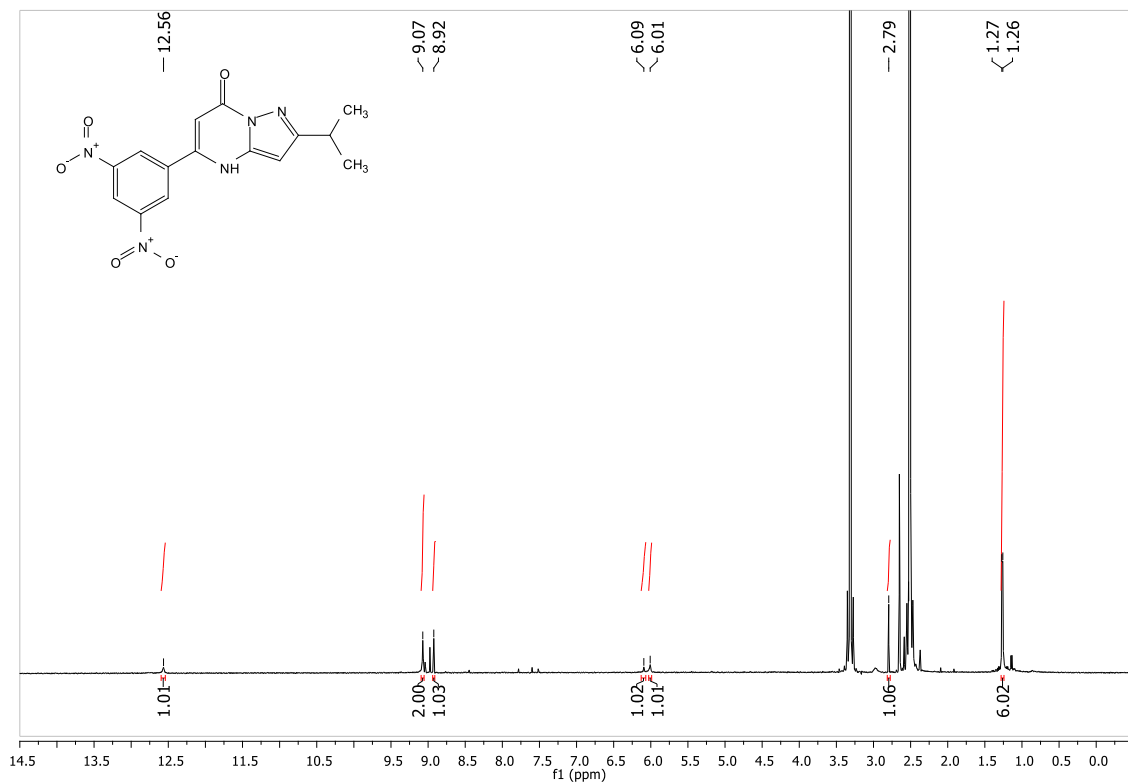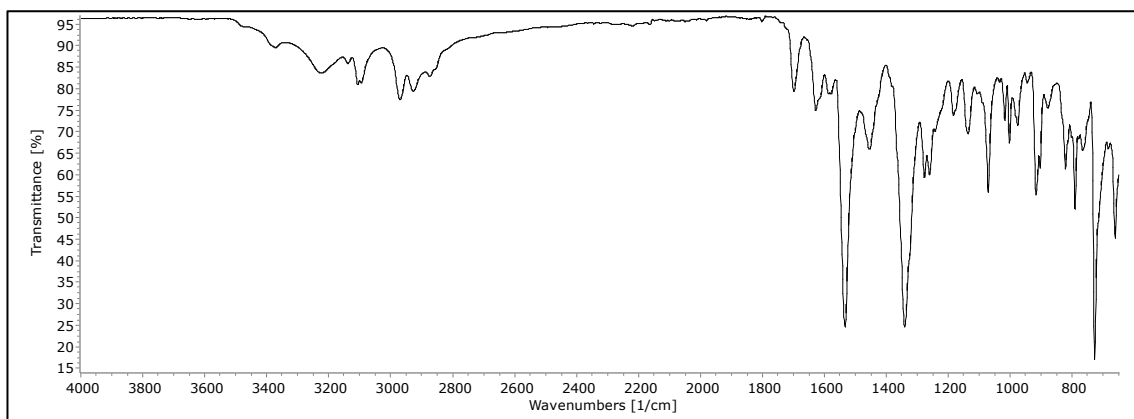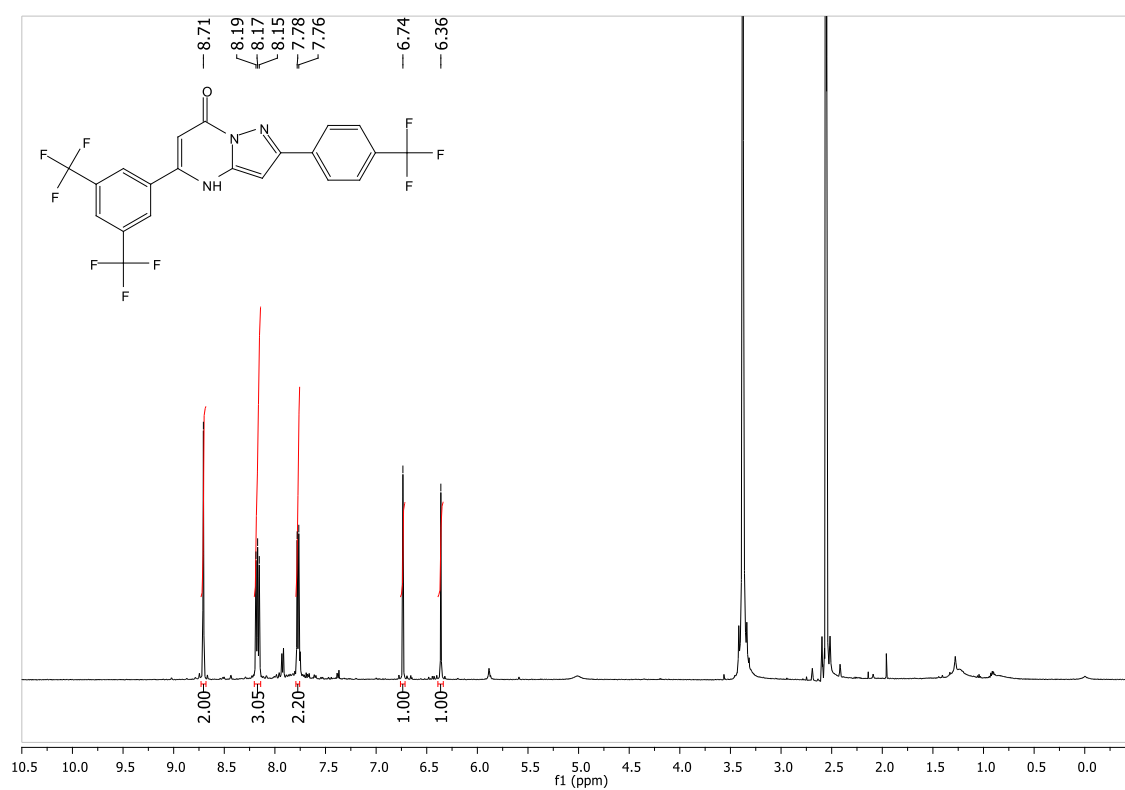
6.62   Spectra for 5-(3,5-bis(trifluoromethyl)phenyl)-2-(2-chlorophenyl)pyrazolo[1,5-*a*]pyrimidin-7(4*H*)-one (MK80) (62)
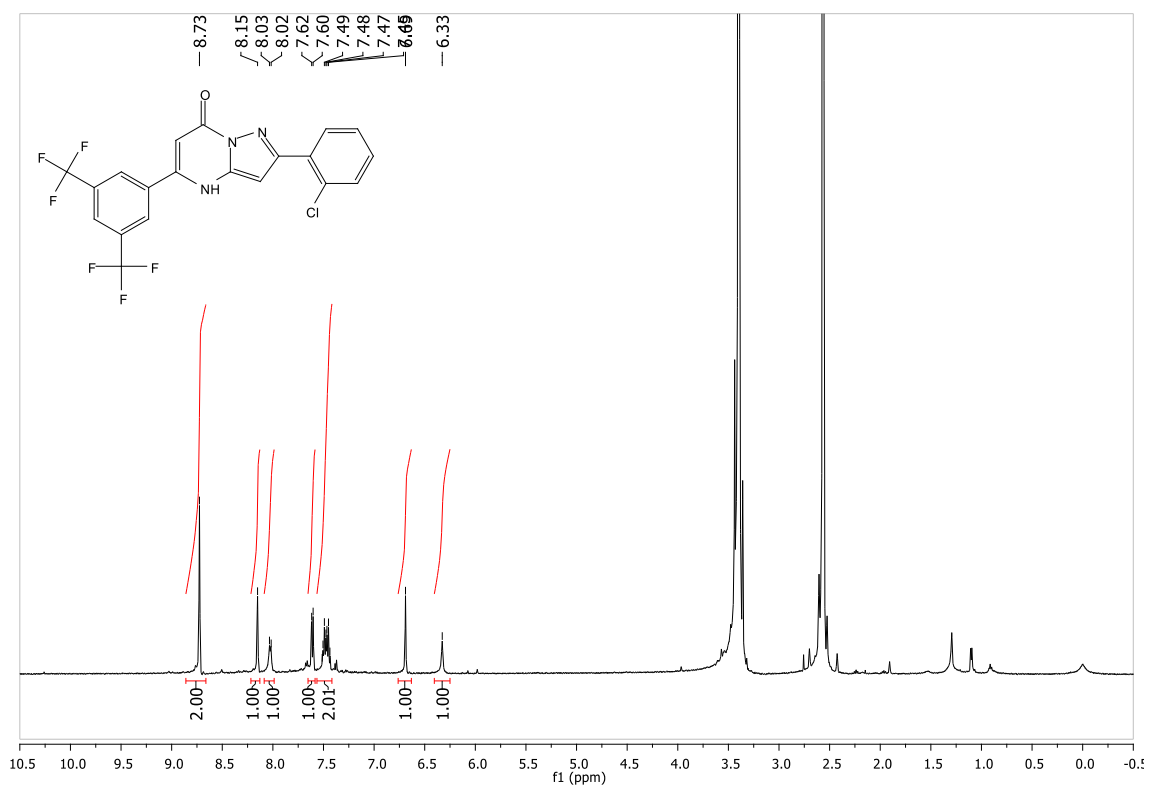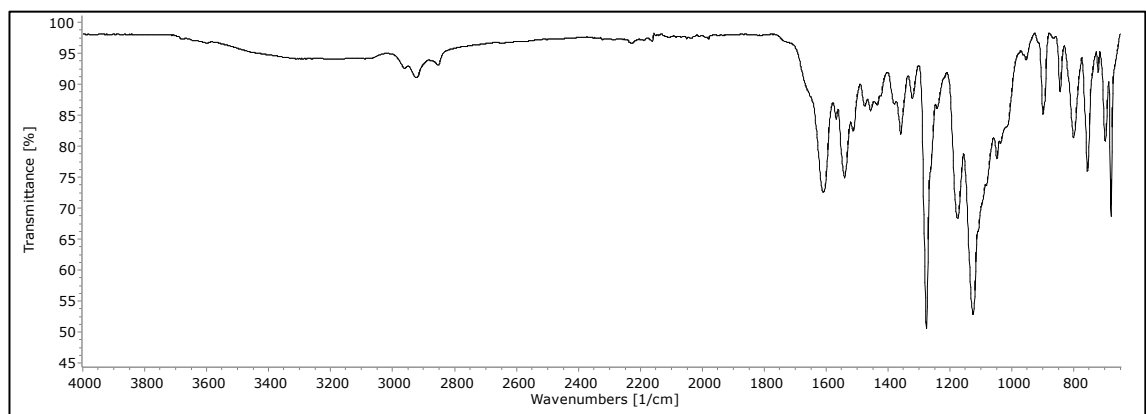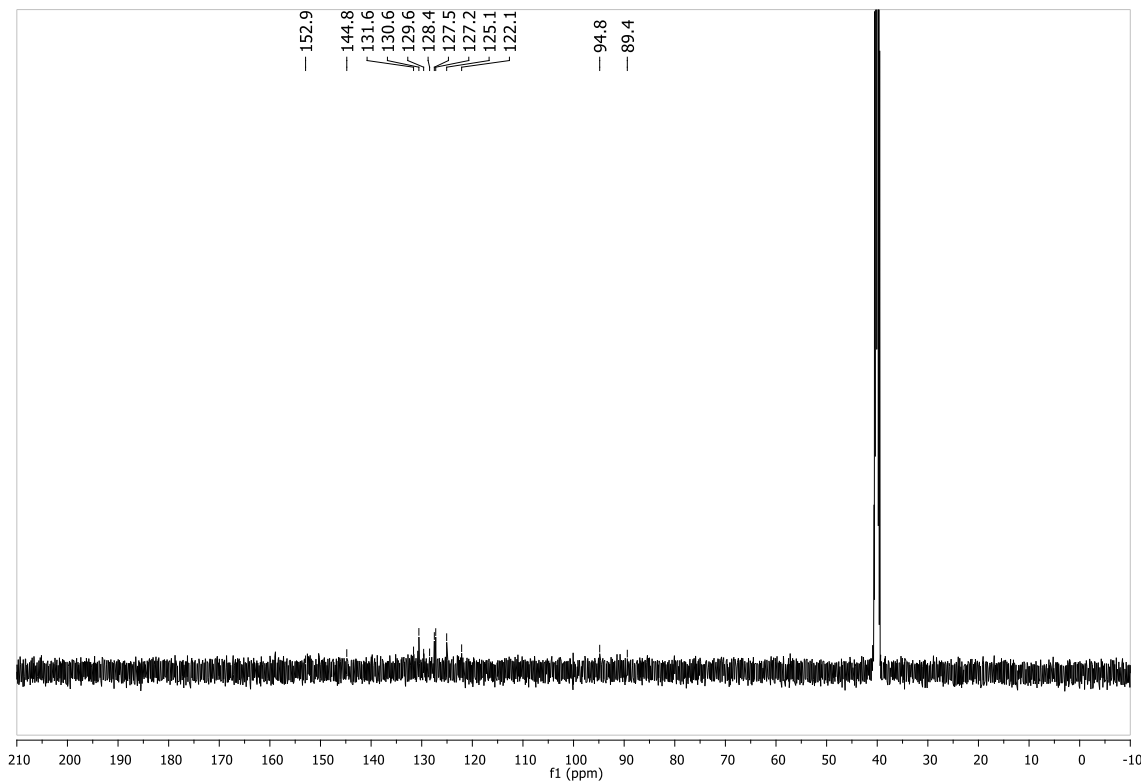
6.63   Spectra for 5-(3,5-bis(trifluoromethyl)phenyl)-2-(2-methoxyphenyl)pyrazolo[1,5-*a*]pyrimidin-7(4*H*)-one (MK79) (63)
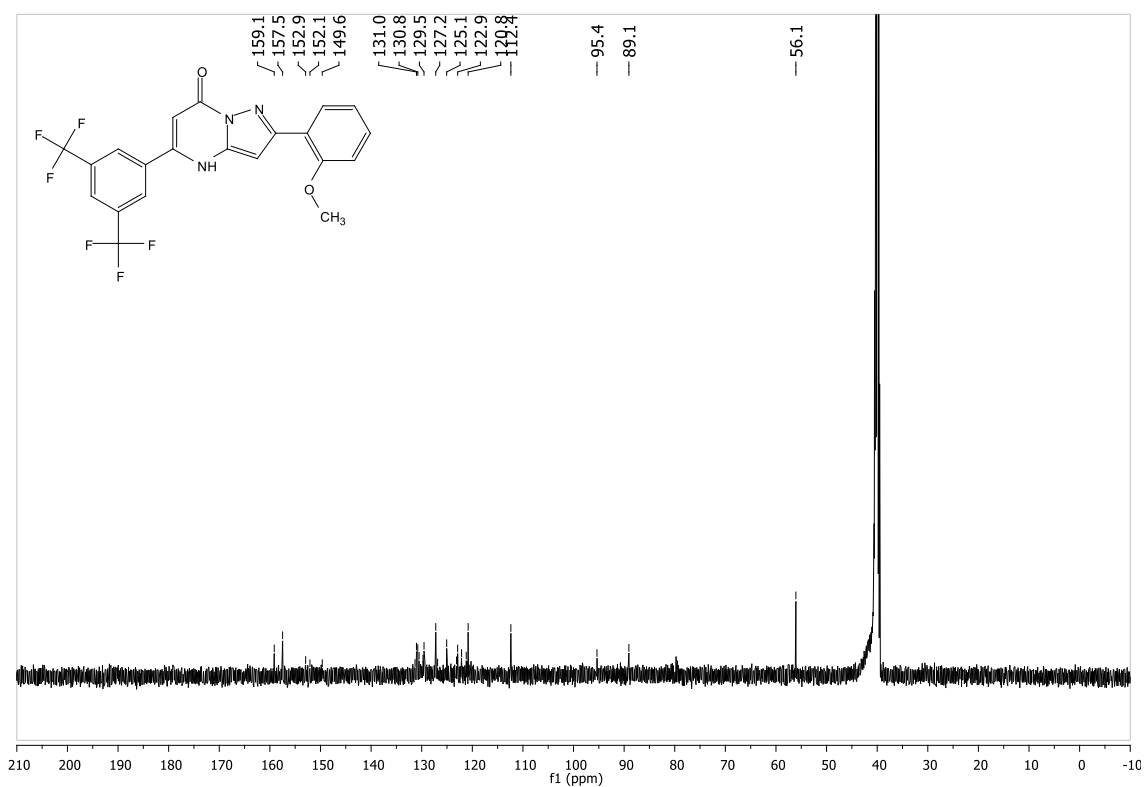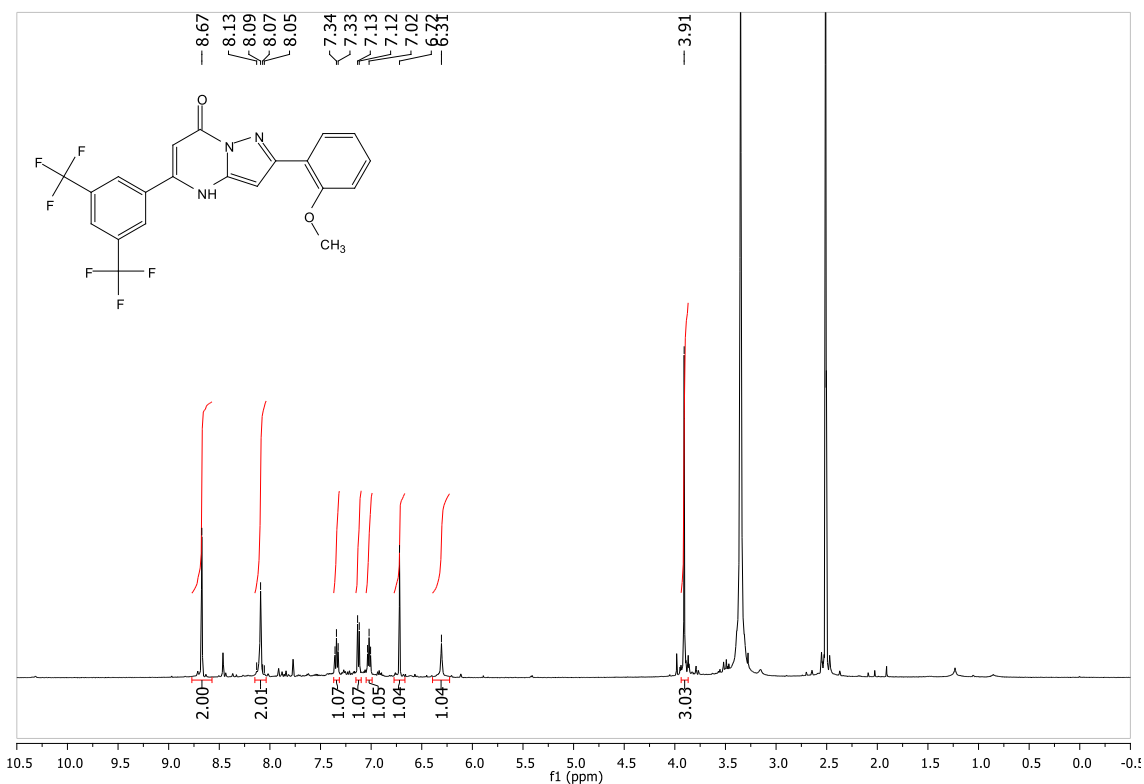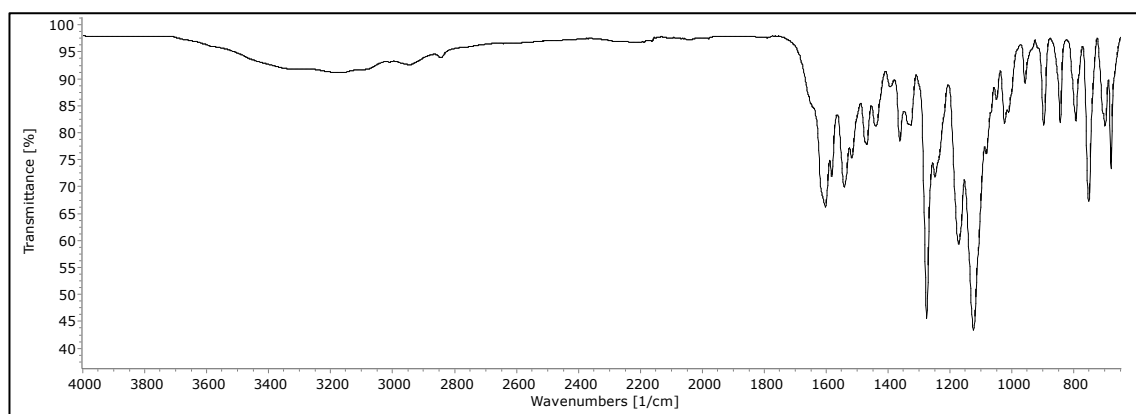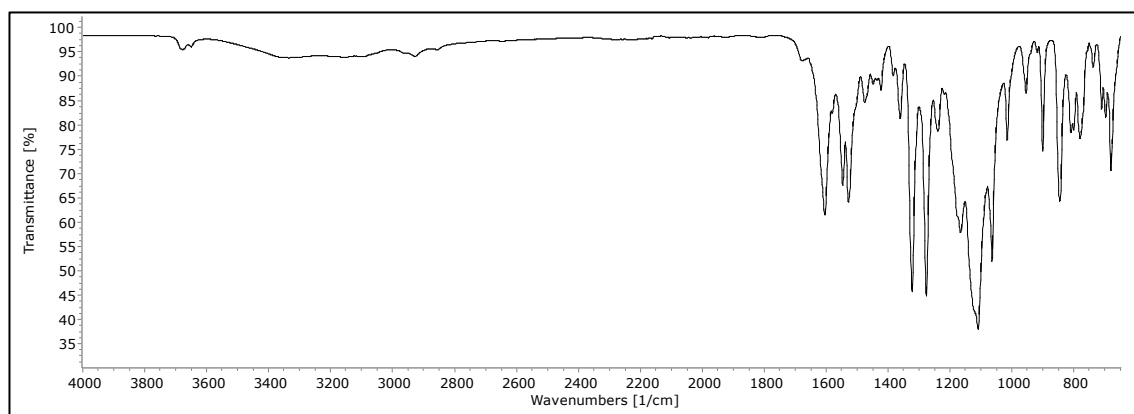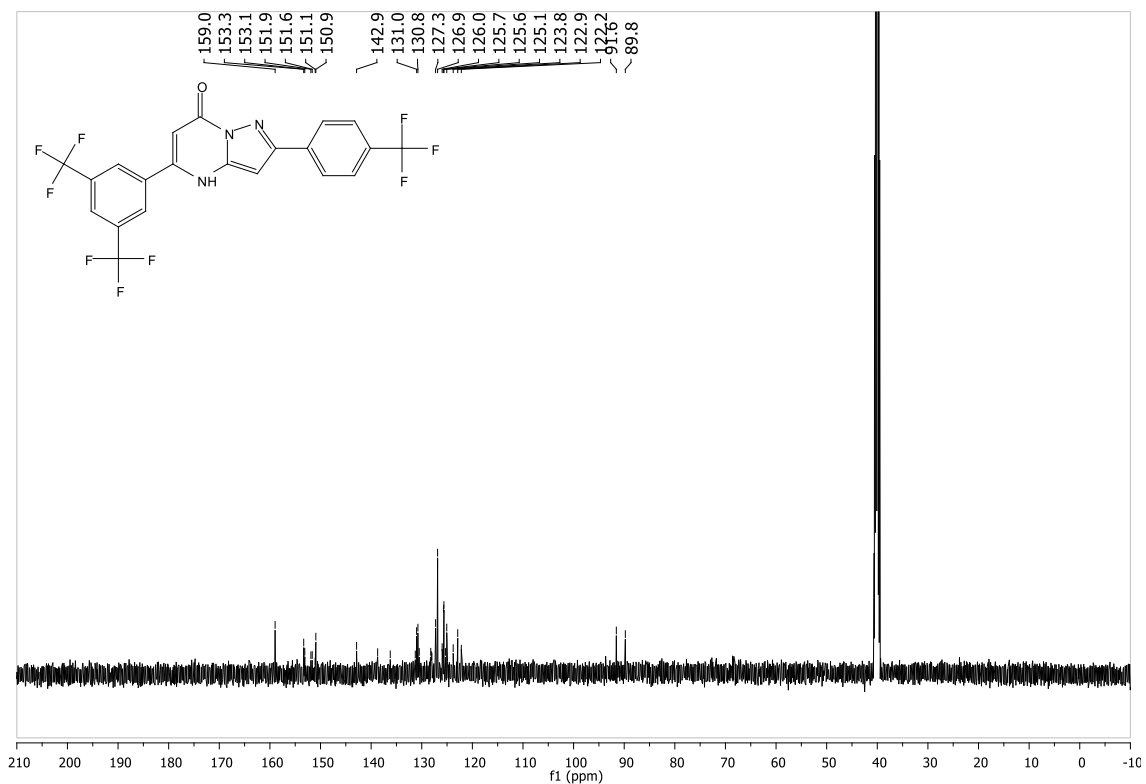
6.64 Spectra for 5-(3,5-bis(trifluoromethyl)phenyl)-2-(3-chlorophenyl)pyrazolo[1,5-*a*]pyrimidin-7(4*H*)-one (MK82) (64)
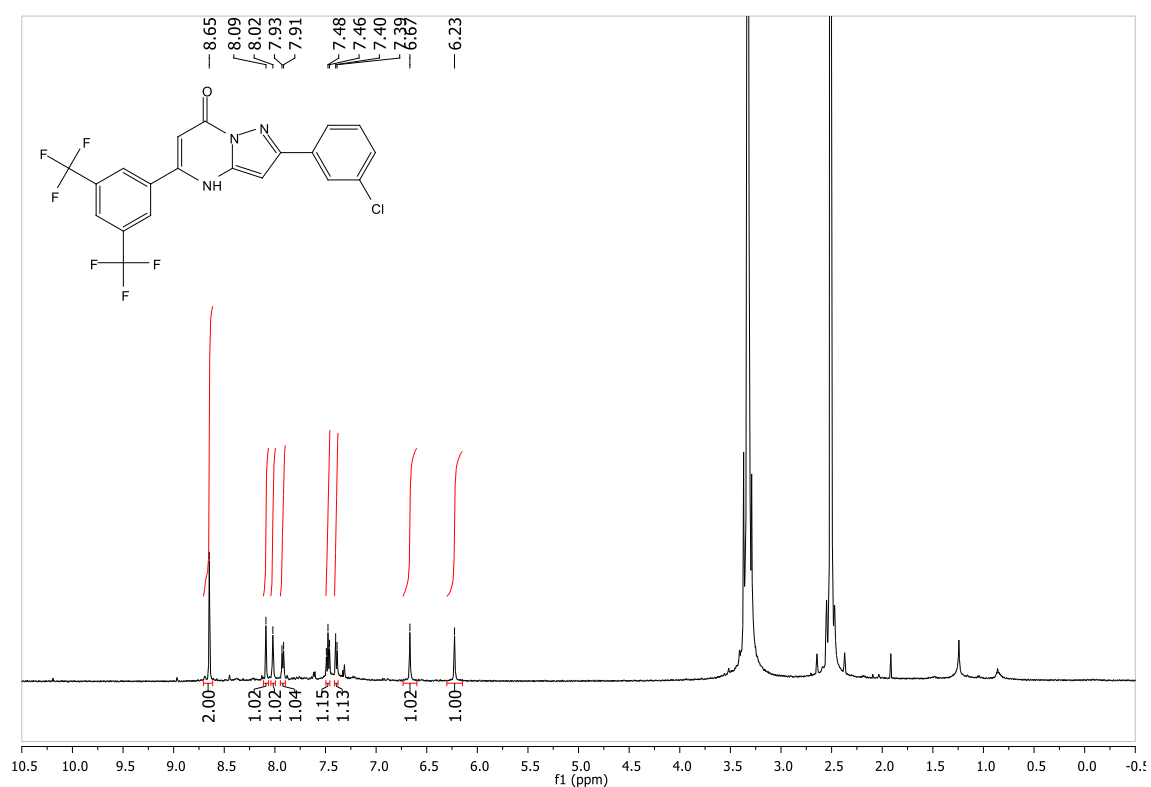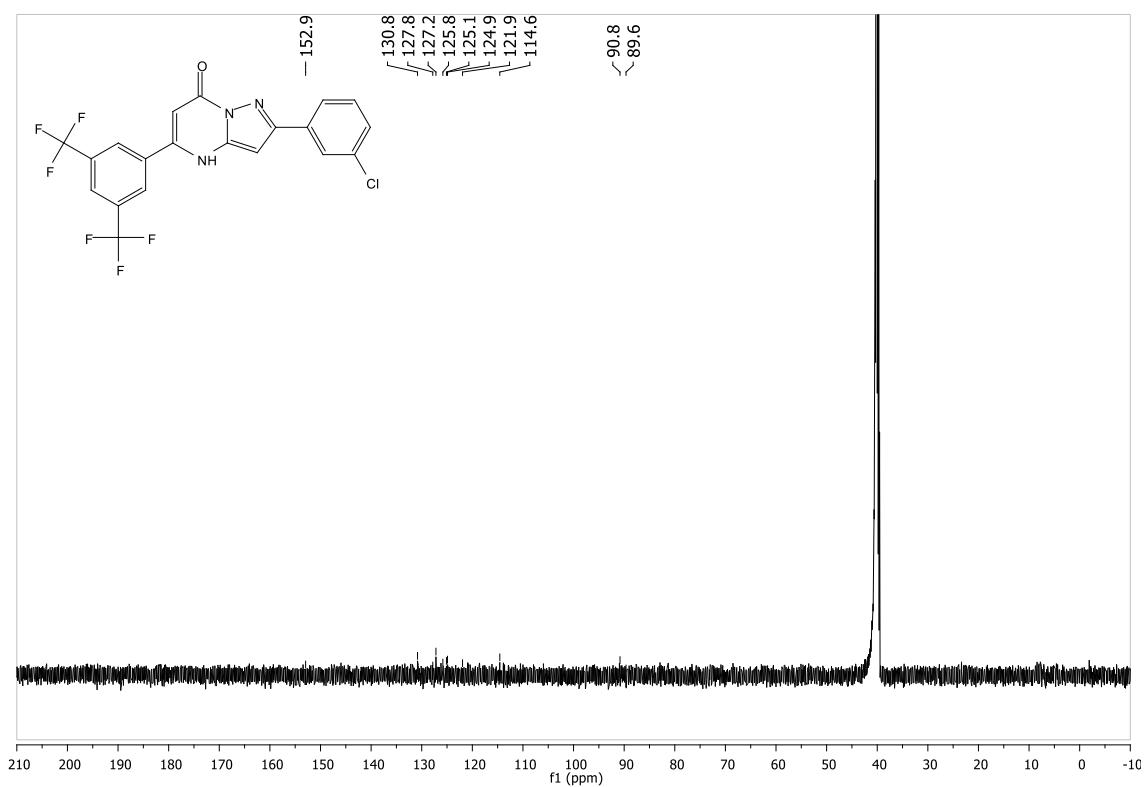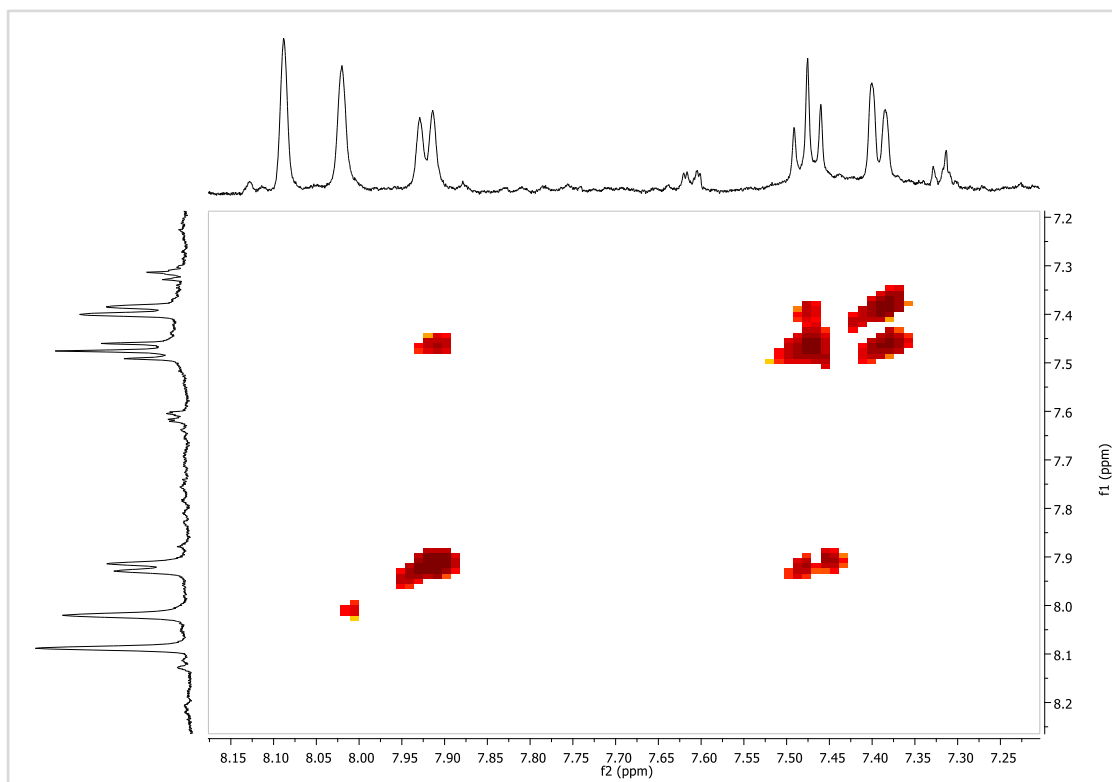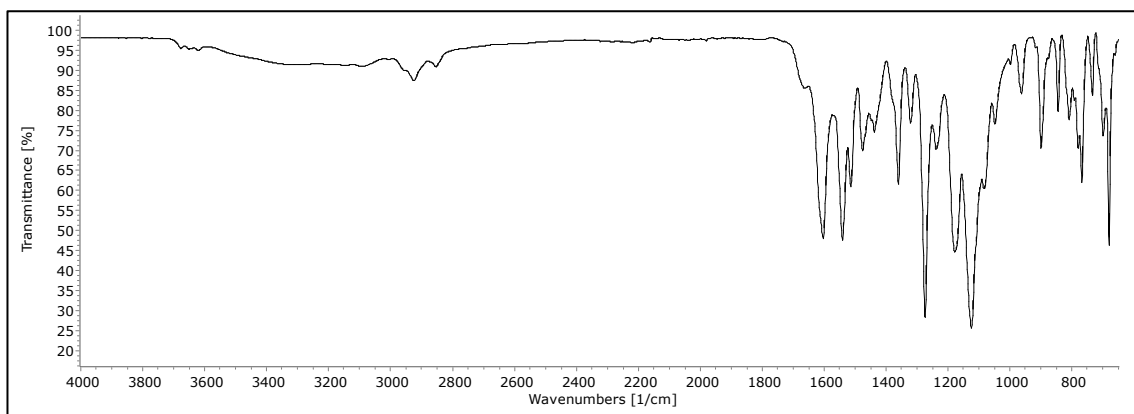
6.65 Spectra for 5-(3,5-bis(trifluoromethyl)phenyl)-2-(3-methoxyphenyl)pyrazolo[1,5-*a*]pyrimidin-7(4*H*)-one (MK81) (65)
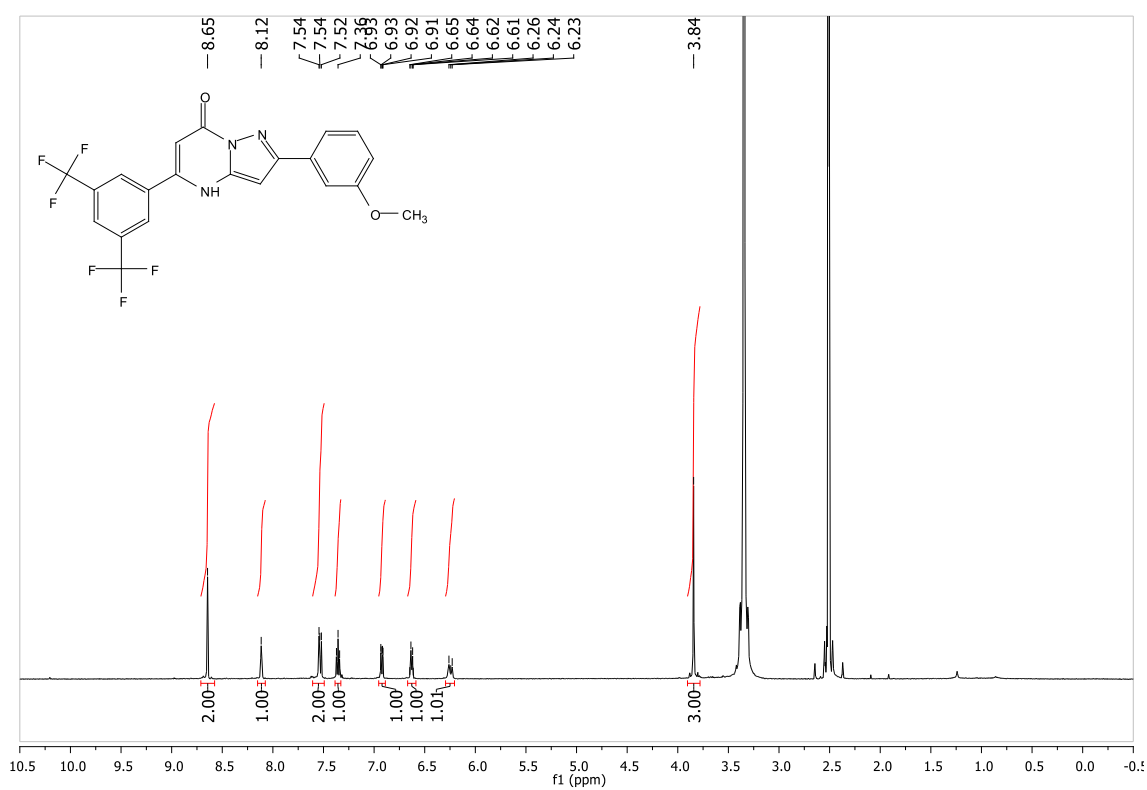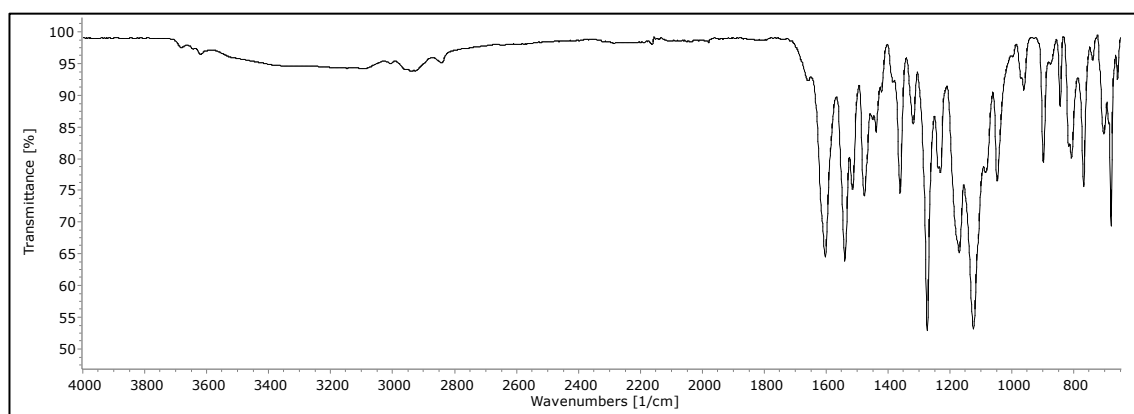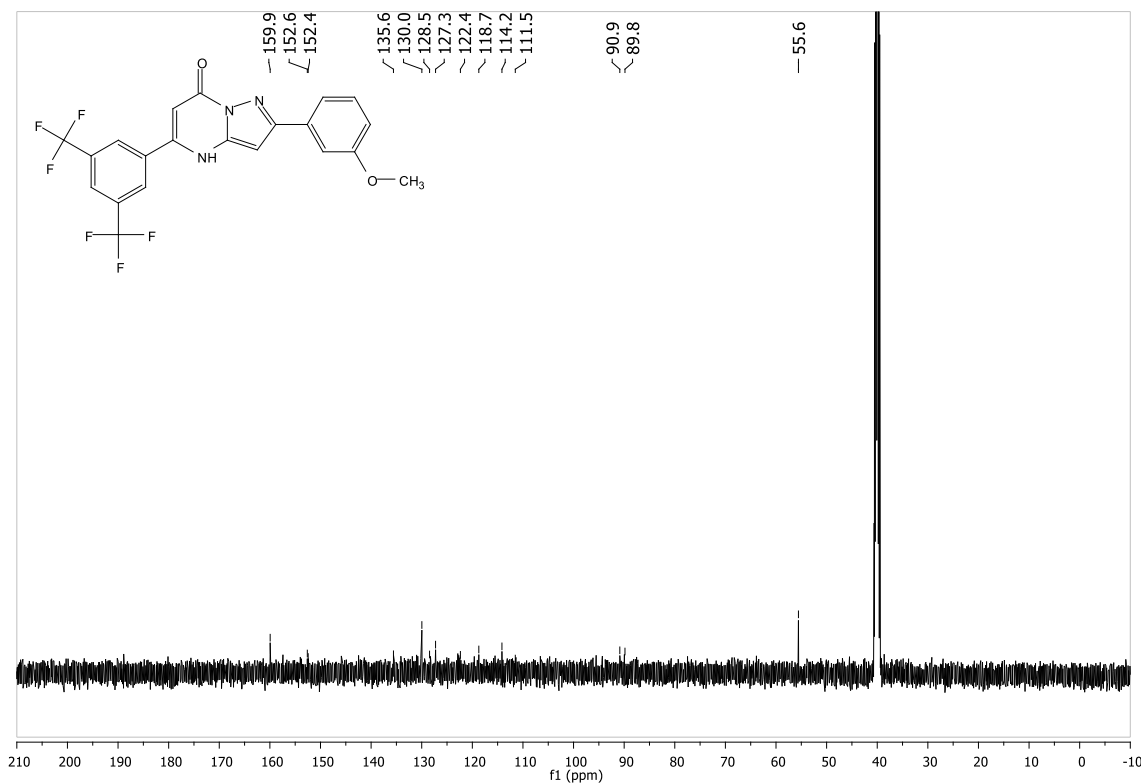
6.66   Spectra for 5-(3,5-bis(trifluoromethyl)phenyl)-2-(3-nitrophenyl)pyrazolo[1,5-*a*]pyrimidin-7(4*H*)-one (MK83) (66)

6.67 Spectra for 5-(3,5-bis(trifluoromethyl)phenyl)-2-(p-tolyl)pyrazolo[1,5-a]pyrimidin-7(4*H*)-one (MK71) (67)

153.9
147.4
143.8
138.9
135.7
131.2
129.8
128.9
126.7
124.6
122.4

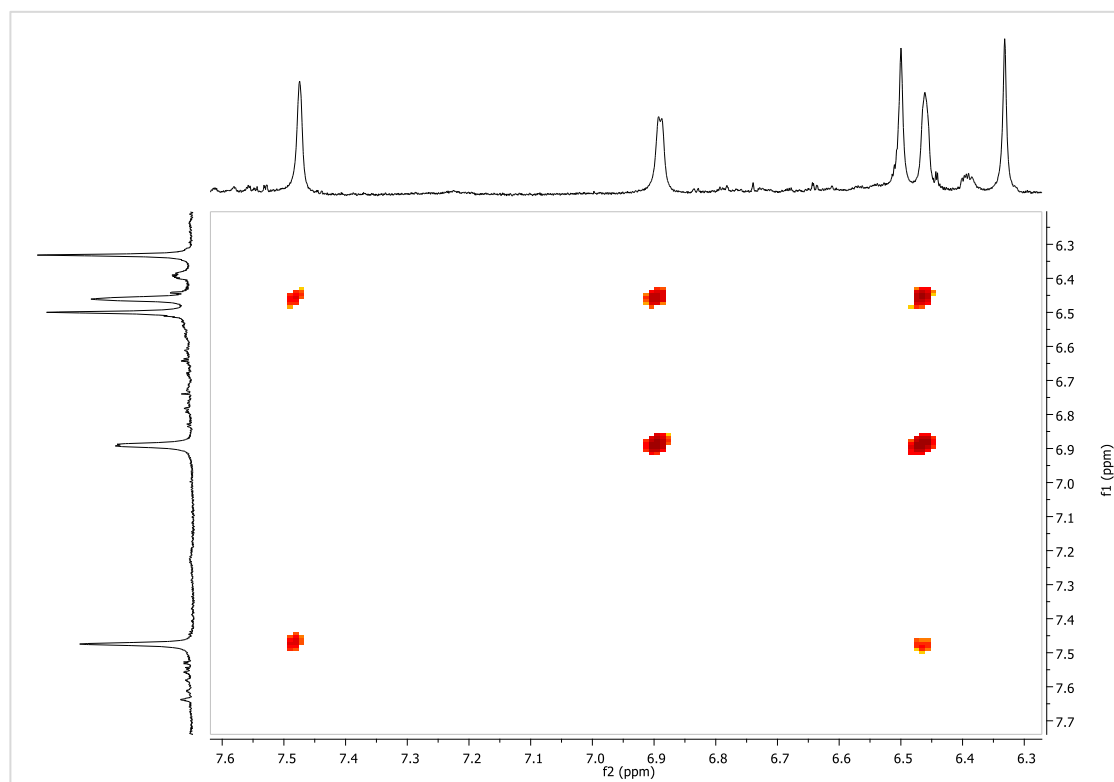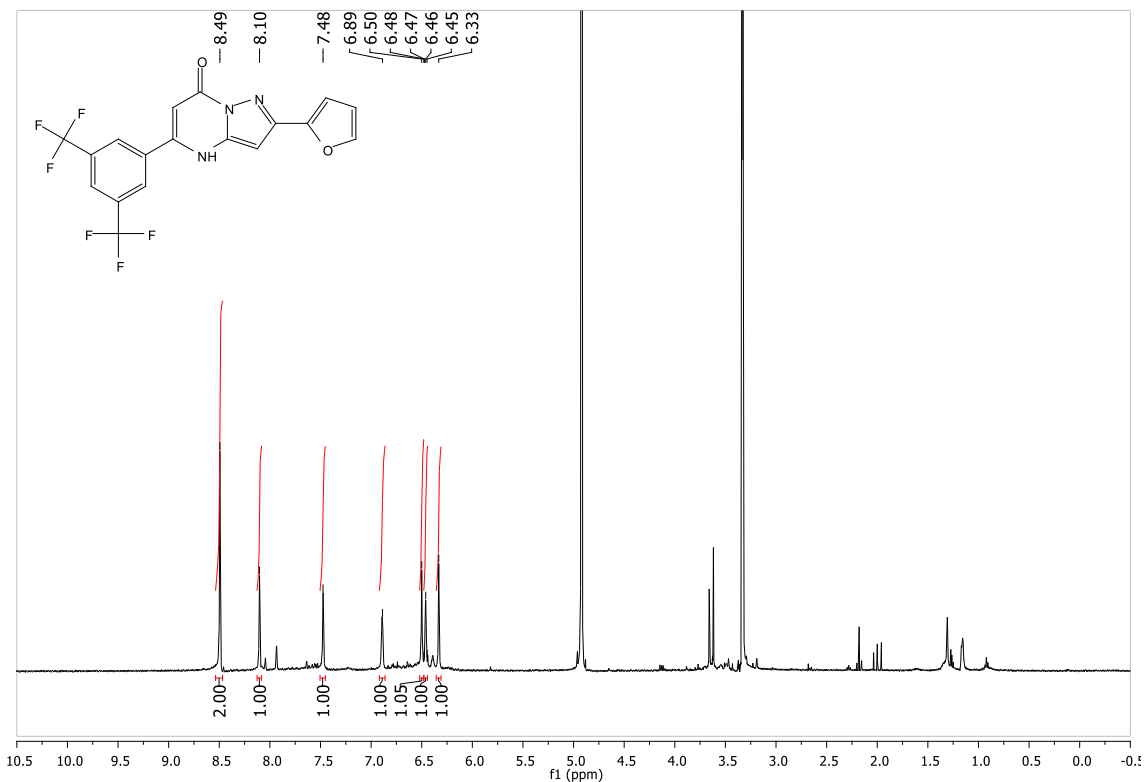95.8
87.2

21.4

f1 (ppm)

Transmittance [%]

Wavenumbers [1/cm]

413
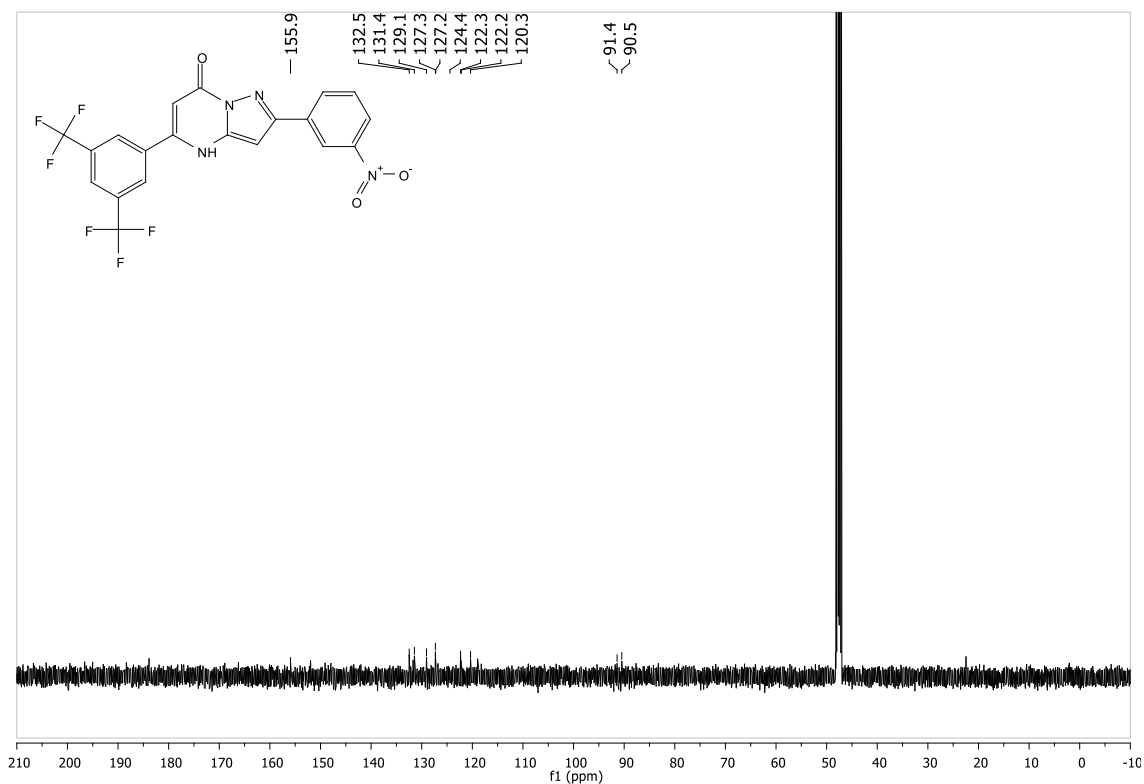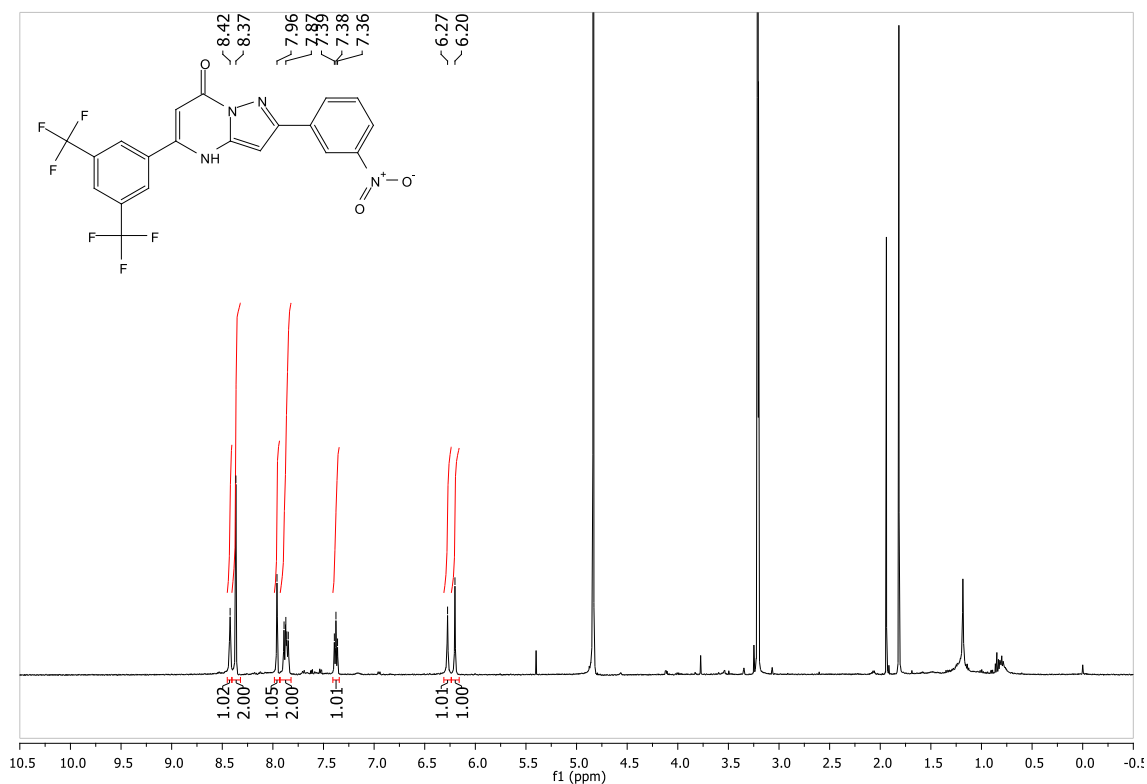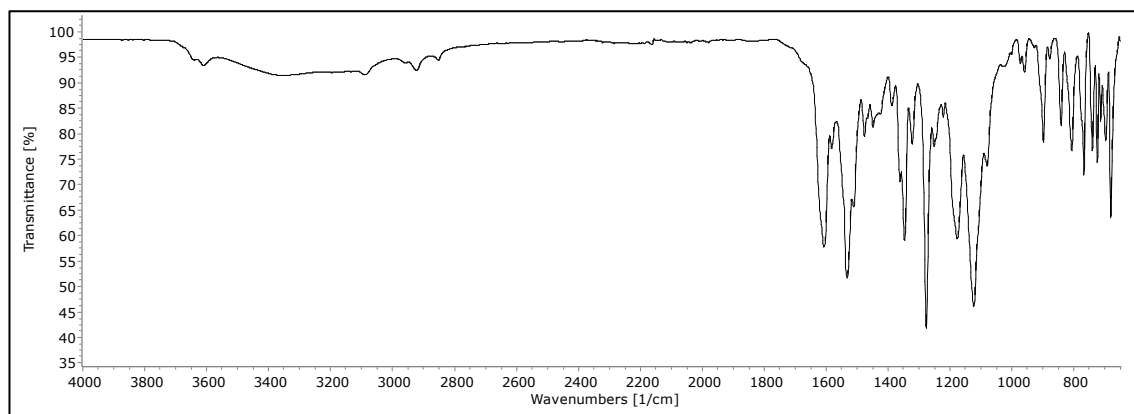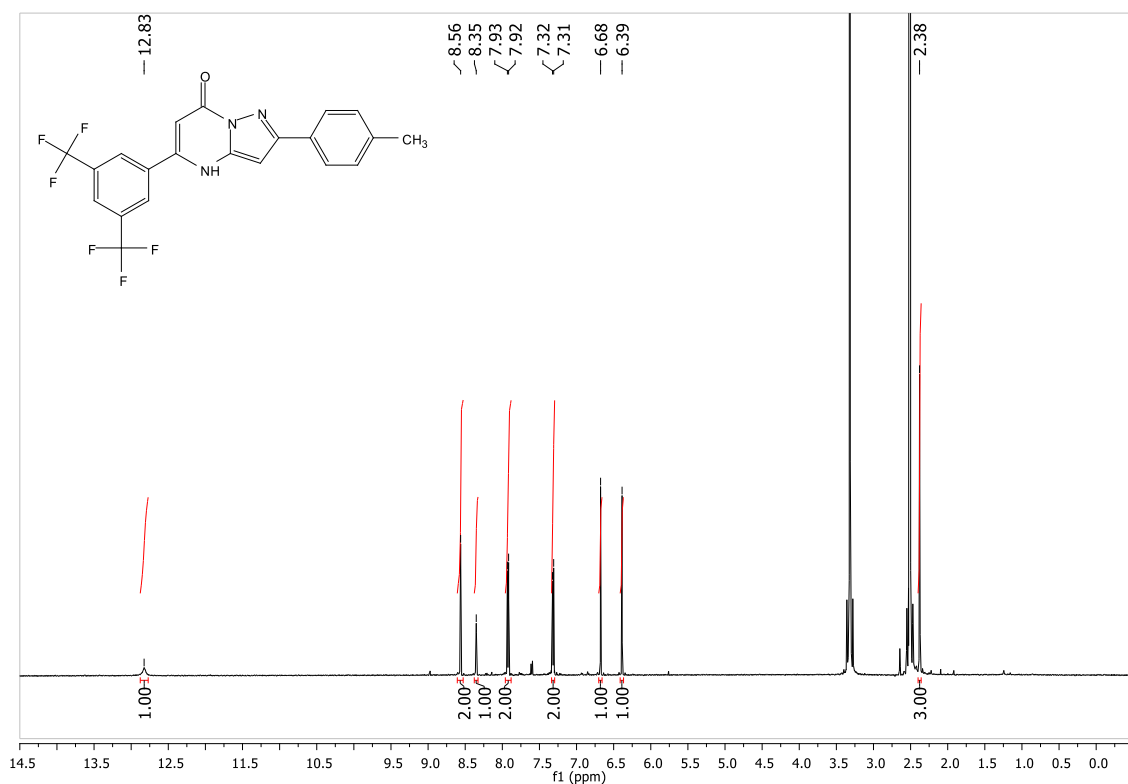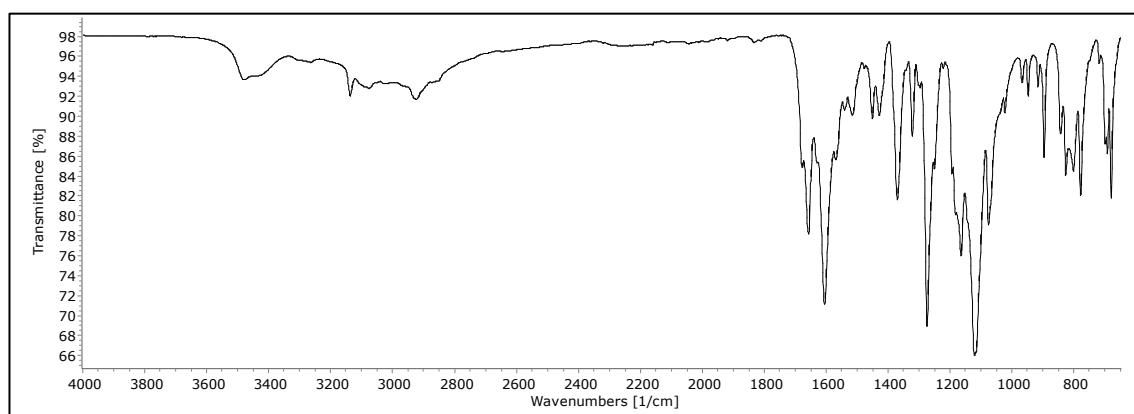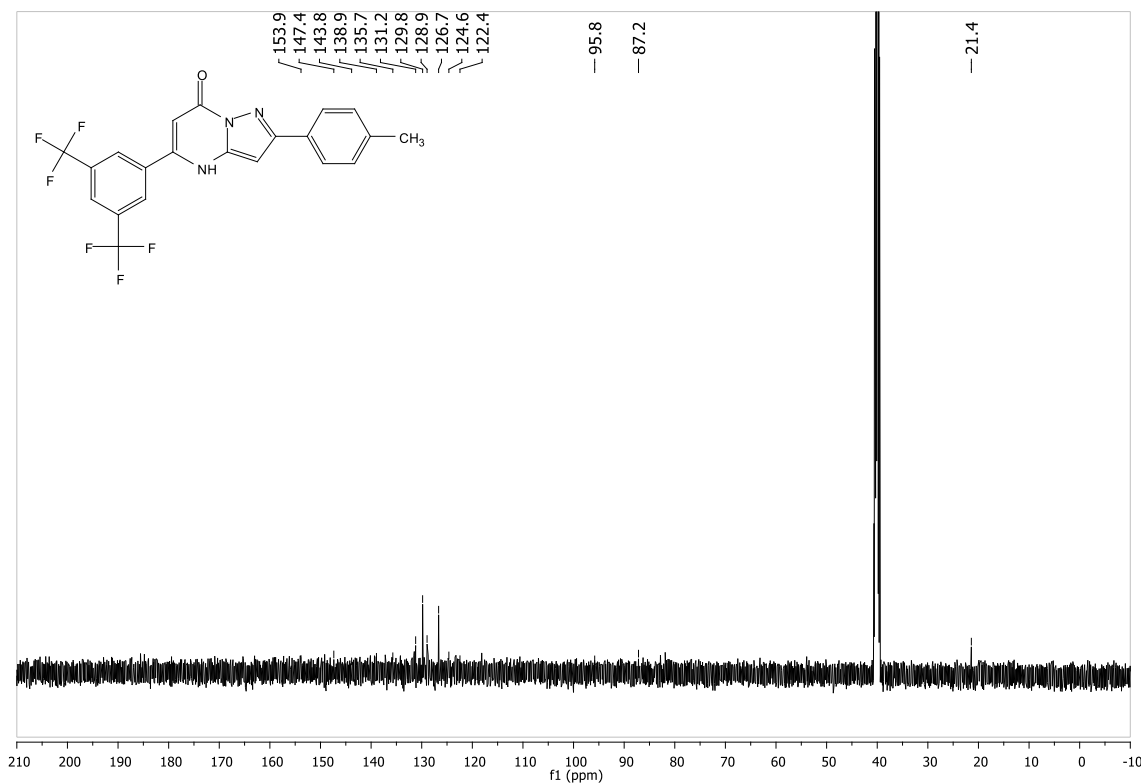
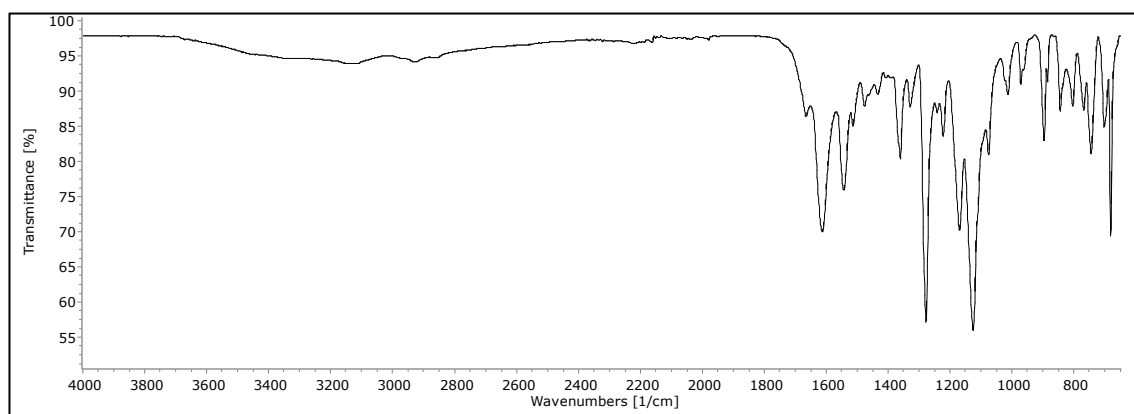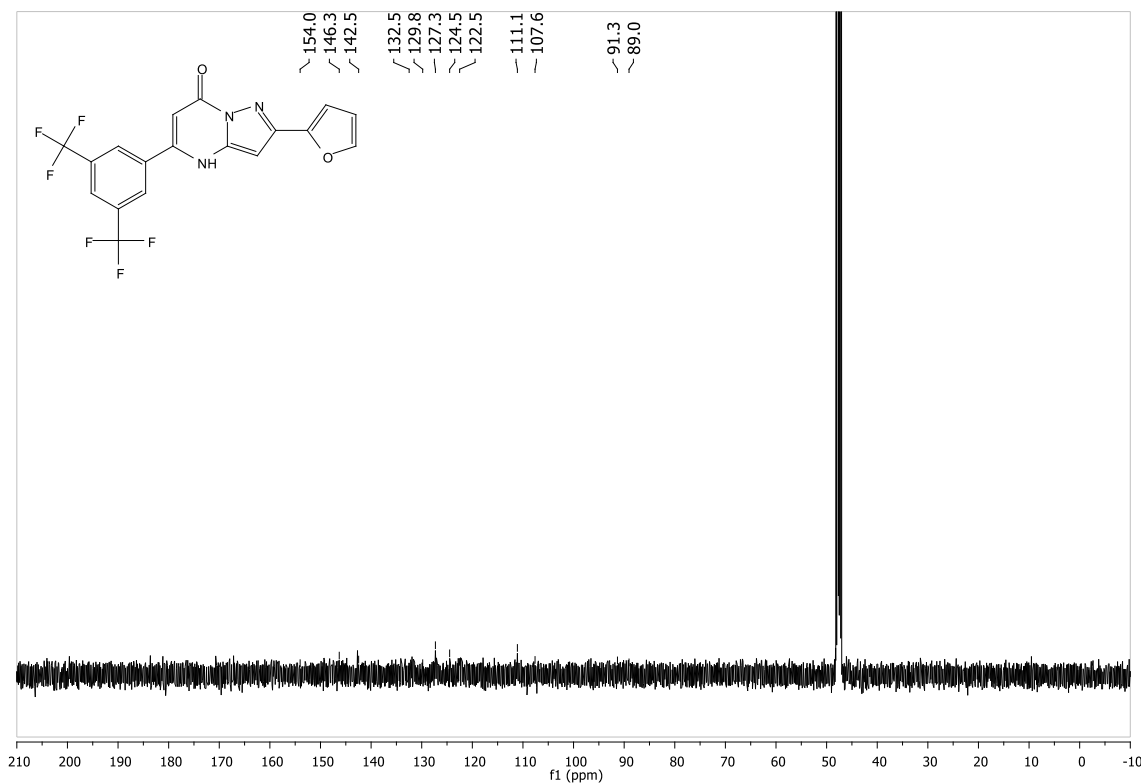## 6.68   Spectra for 5-(3,5-bis(trifluoromethyl)phenyl)-2-(4-fluorophenyl)pyrazolo[1,5-*a*]pyrimidin-7(4*H*)-one (MK72) (68)

6.69   Spectra for 5-(3,5-bis(trifluoromethyl)phenyl)-2-(4-chlorophenyl)pyrazolo[1,5-*a*]pyrimidin-7(4*H*)-one (MK75) (69)

128.9
128.1
127.4
122.9

90.4
90.1

210 200 190 180 170 160 150 140 130 120 110 100 90 80 70 60 50 40 30 20 10 0 -10
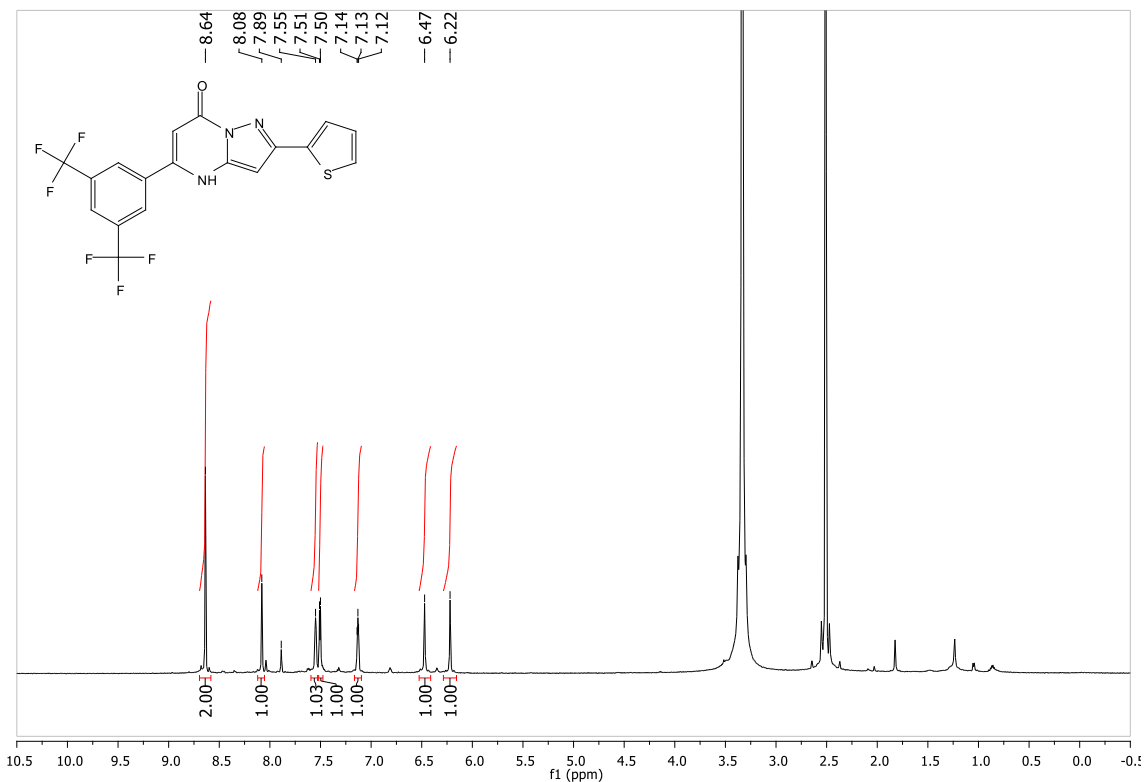f1 (ppm)
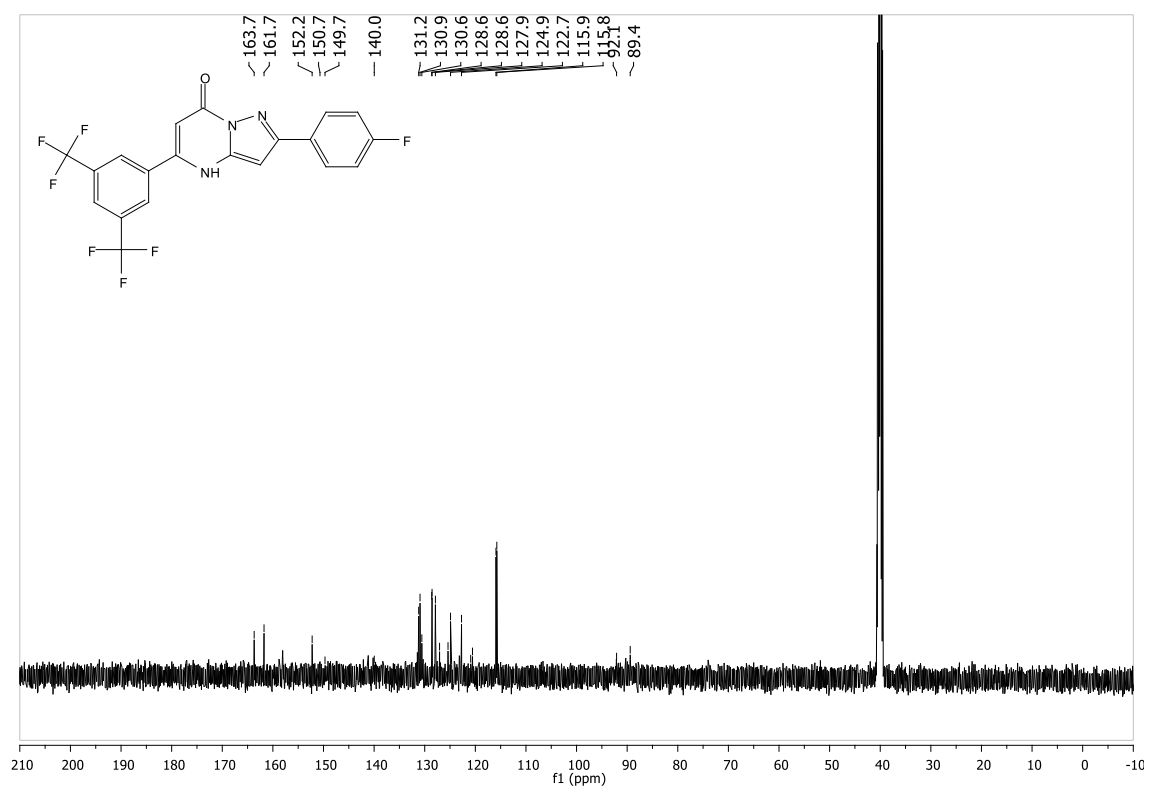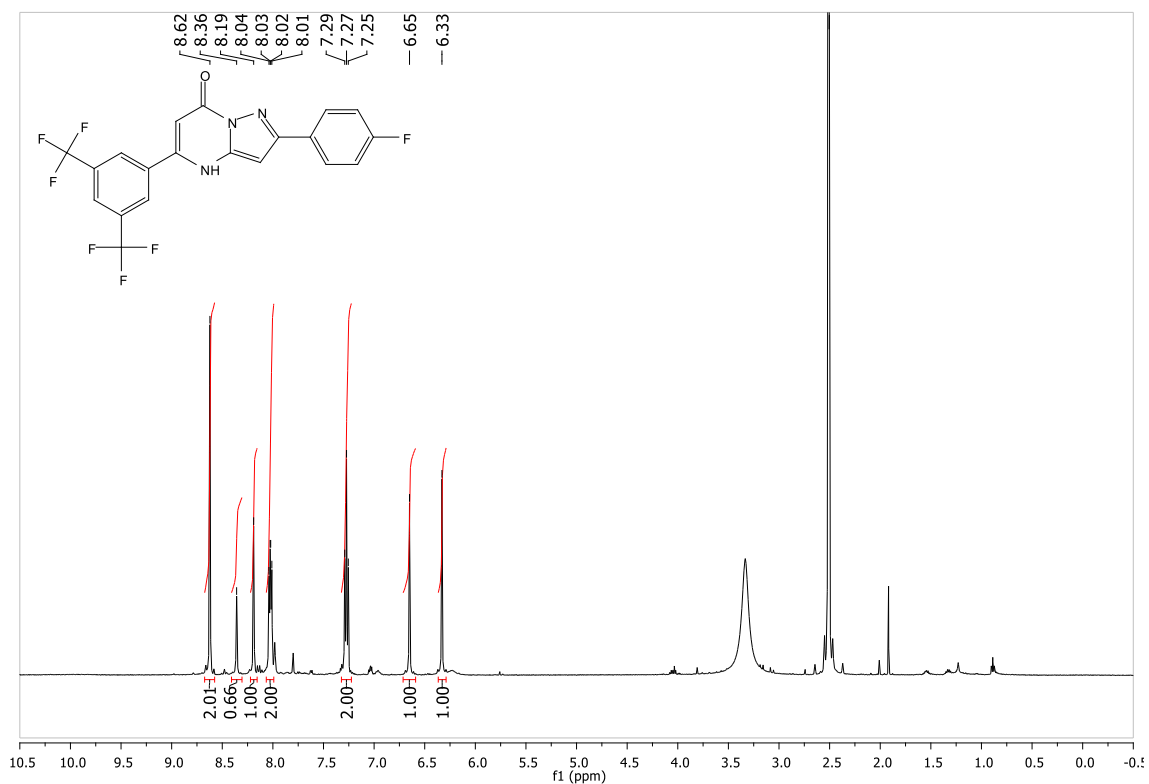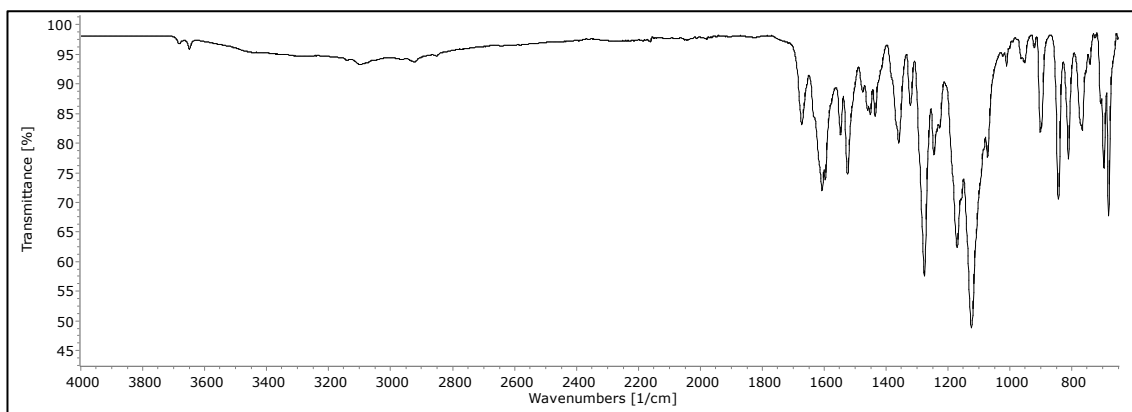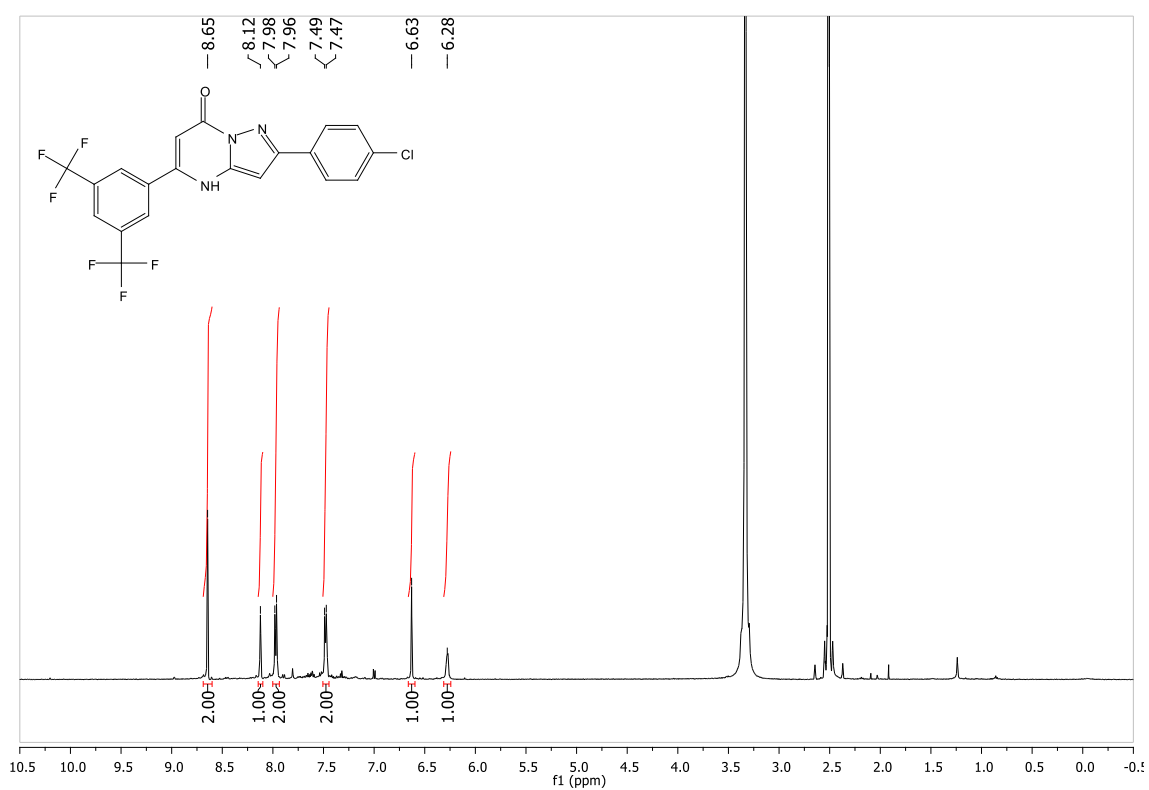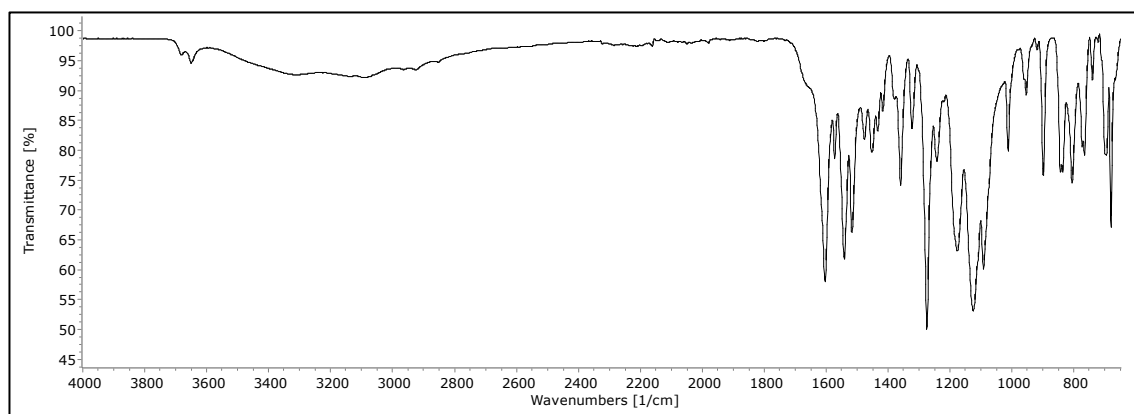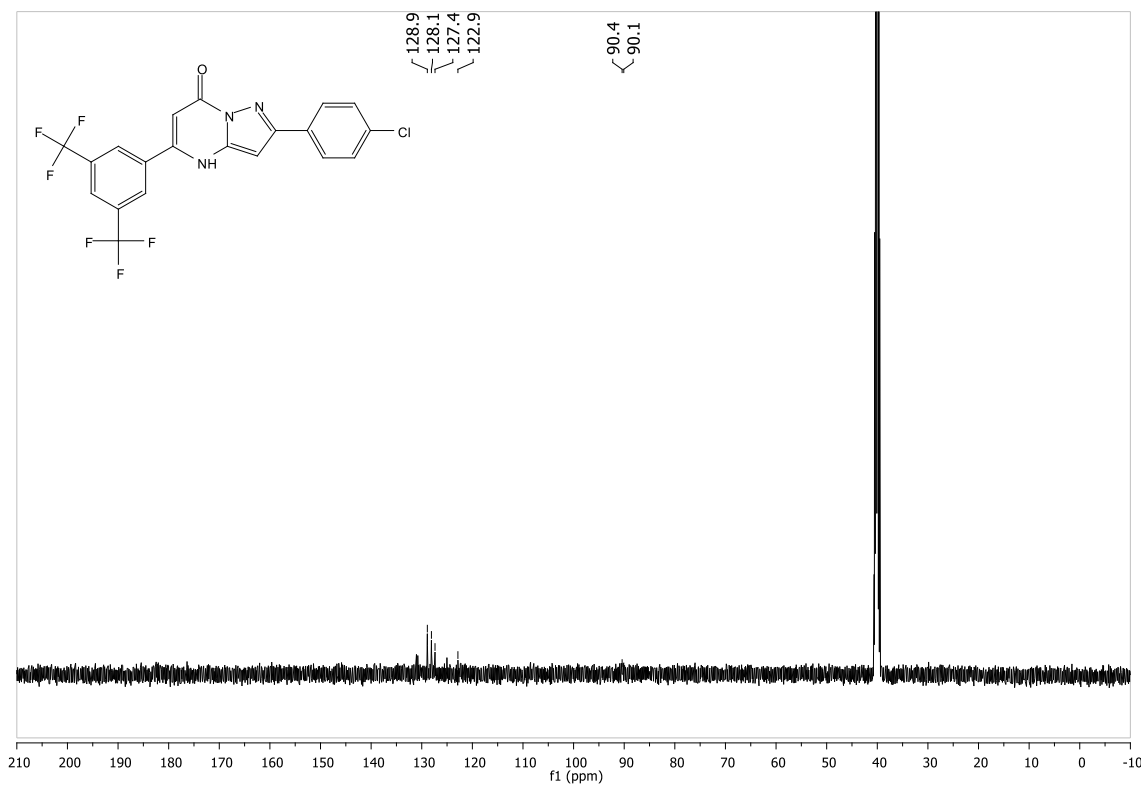
6.70 Spectra for 5-(3,5-bis(trifluoromethyl)phenyl)-2-(4-bromophenyl)pyrazolo[1,5-*a*]pyrimidin-7(4*H*)-one (MK73) (70)
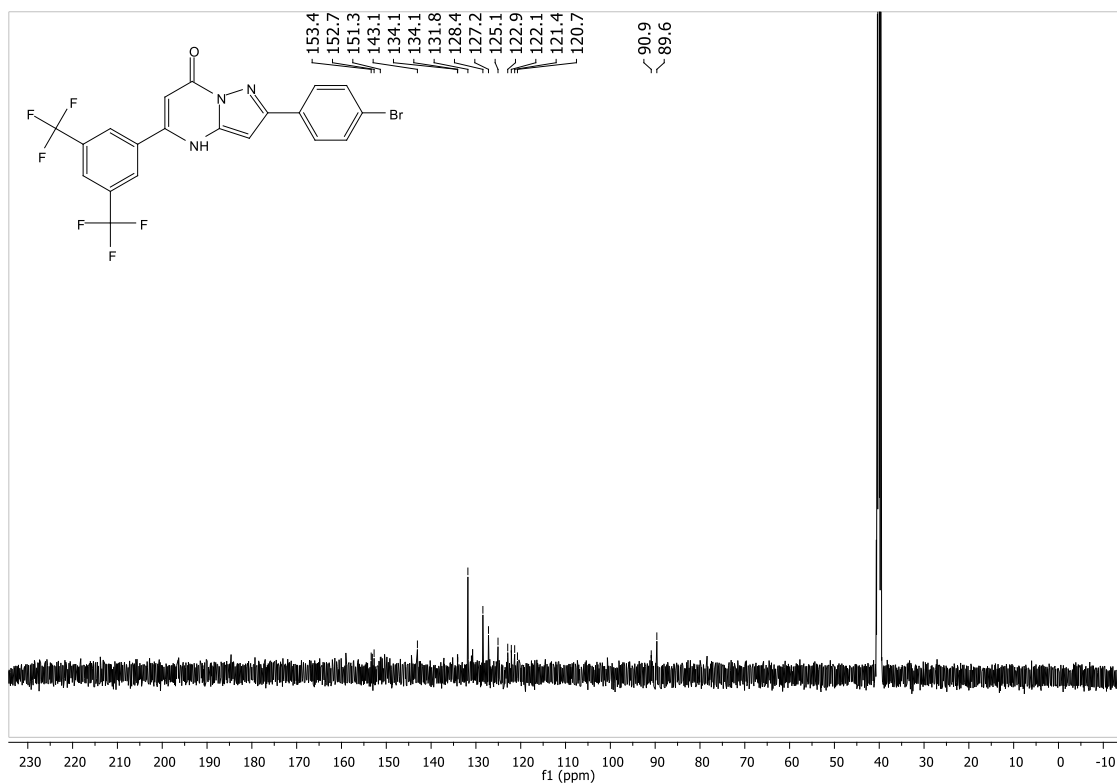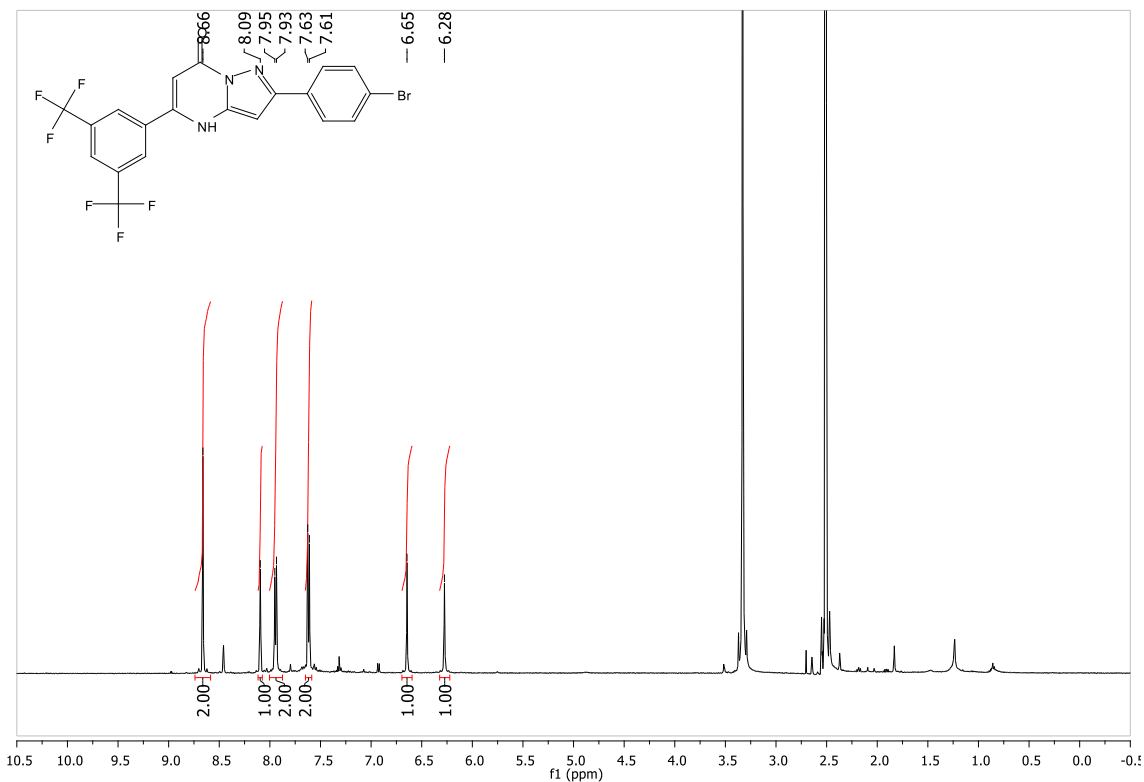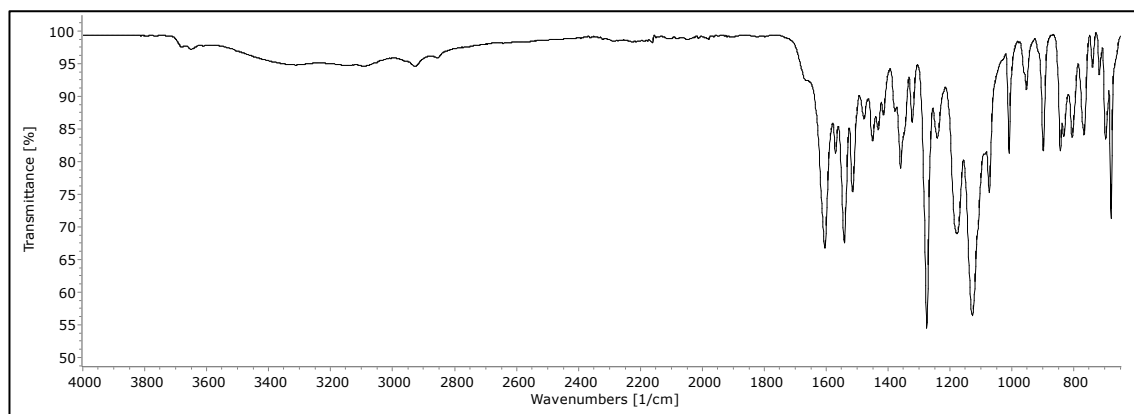
6.71 Spectra for 5-(3,5-bis(trifluoromethyl)phenyl)-2-(4-methoxyphenyl)pyrazolo[1,5-*a*]pyrimidin-7(4*H*)-one (MK74) (71)
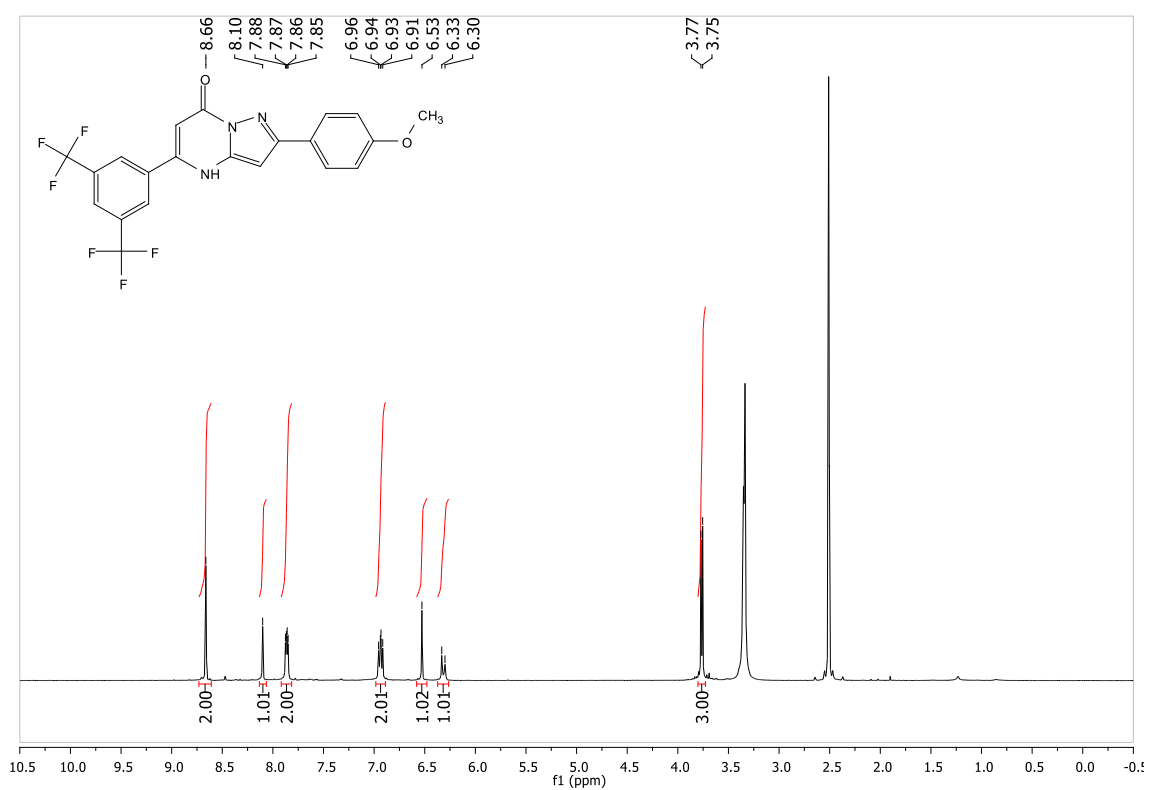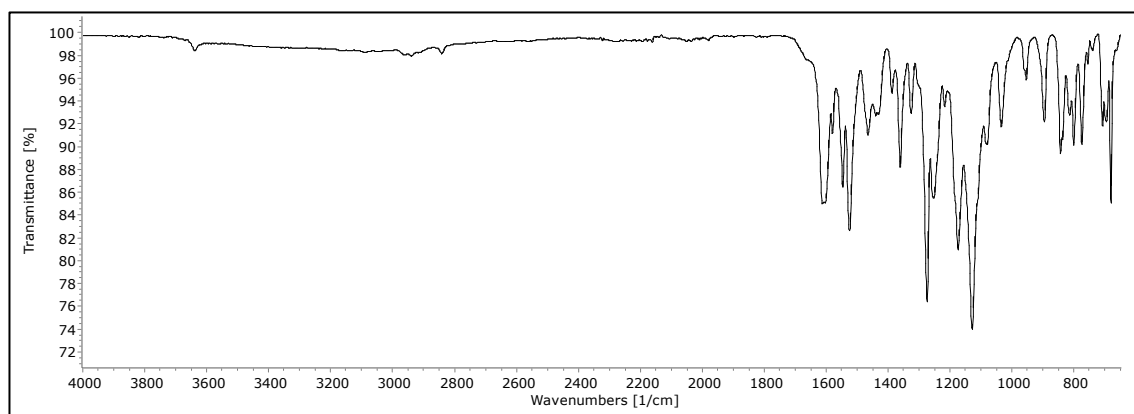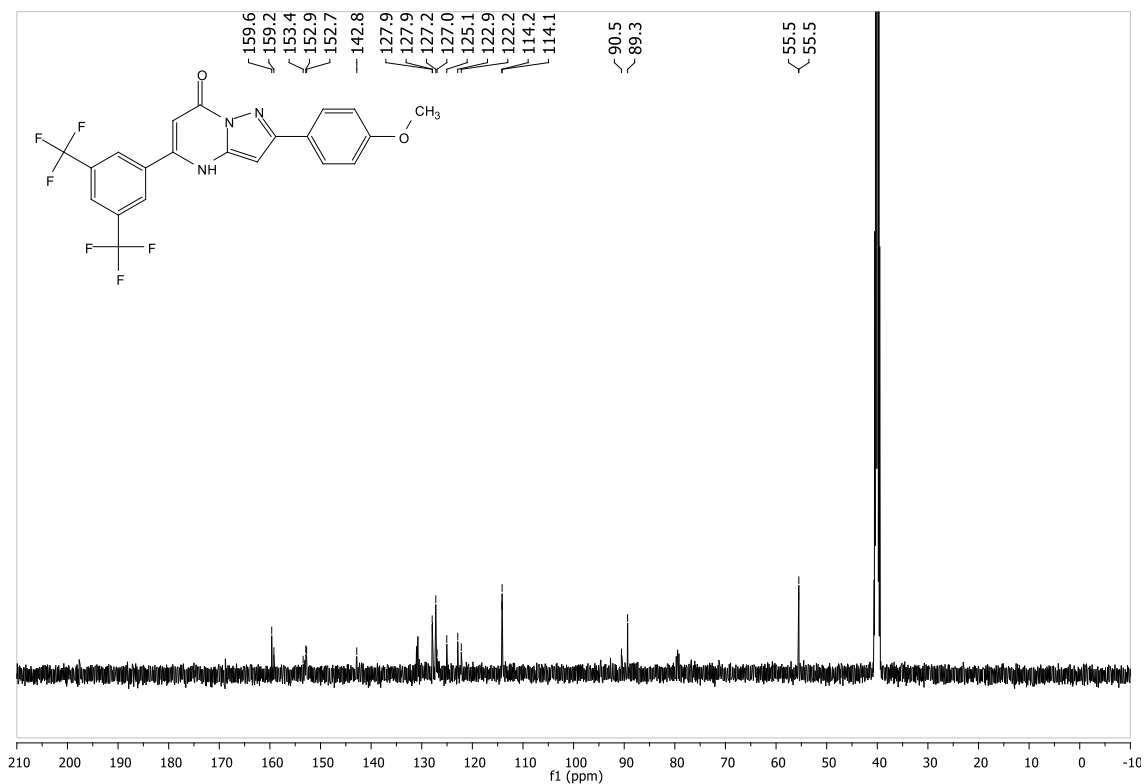
6.72 Spectra for 5-(3,5-bis(trifluoromethyl)phenyl)-2-(4-nitrophenyl)pyrazolo[1,5-*a*]pyrimidin-7(4*H*)-one (MK76) (72)
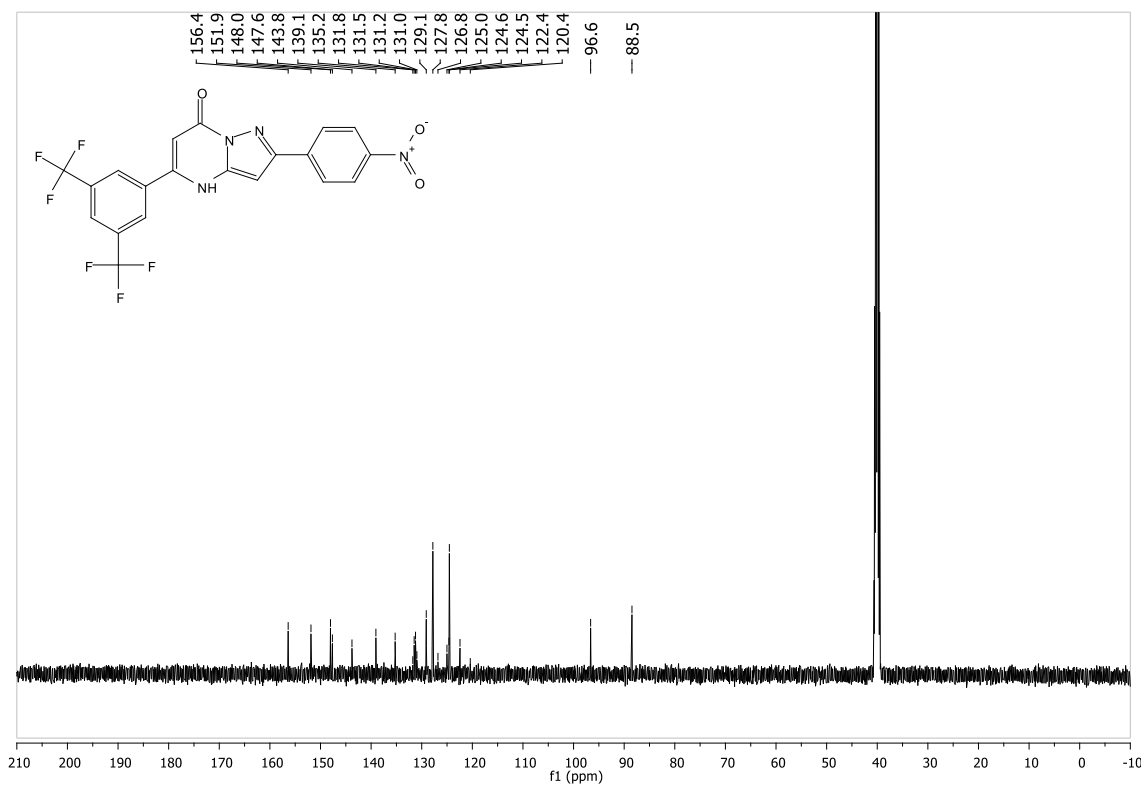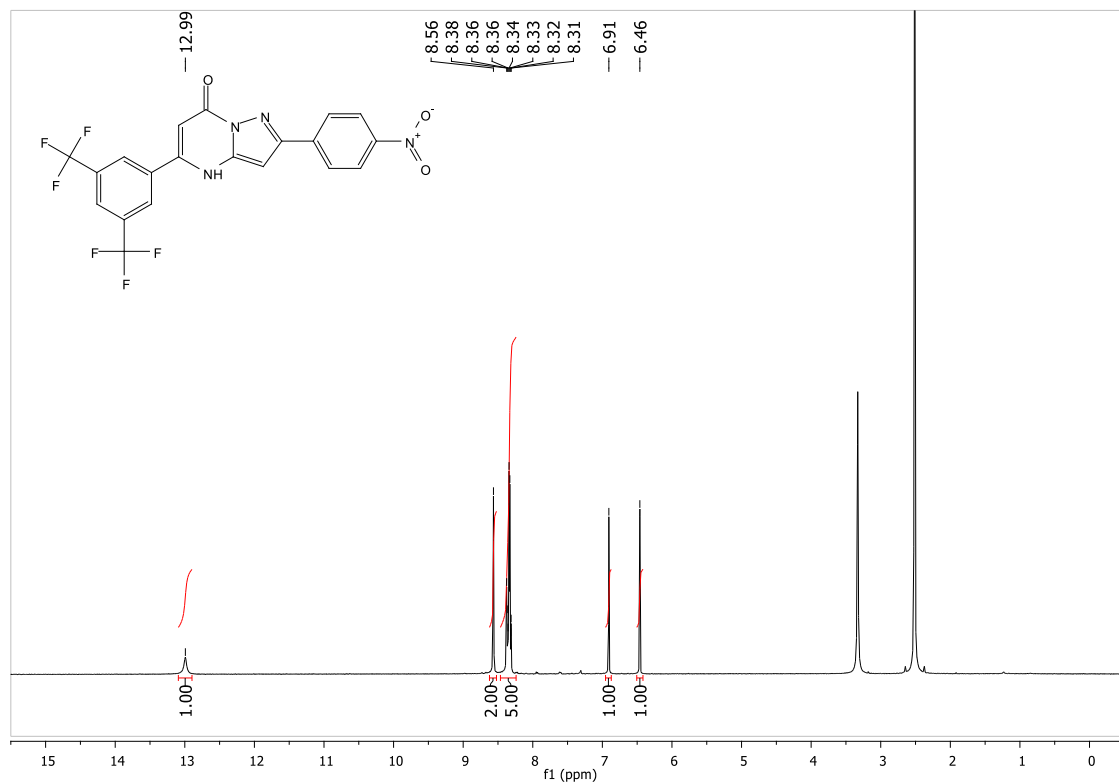
6.73　Spectra for 5-(3,5-bis(trifluoromethyl)phenyl)-2-(4-(trifluoromethyl)phenyl)pyrazolo[1,5-*a*]pyrimidin-7(4*H*)-one (MK78) (73)
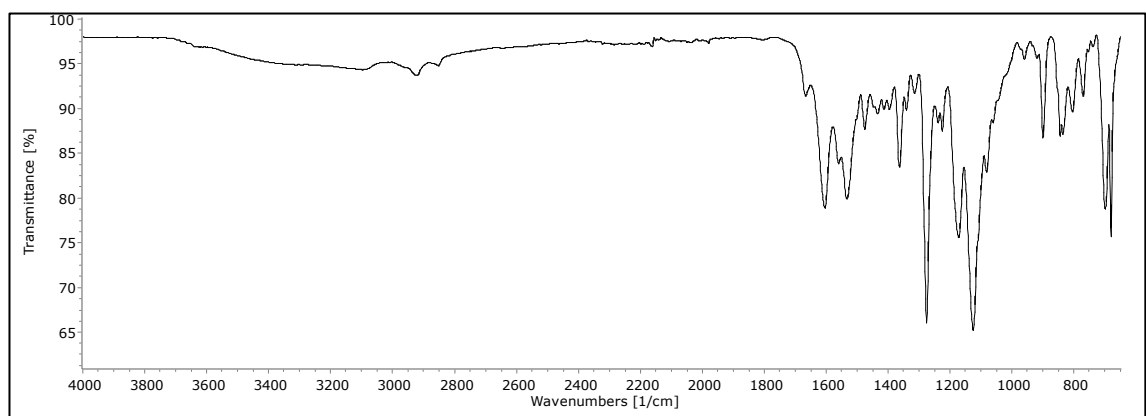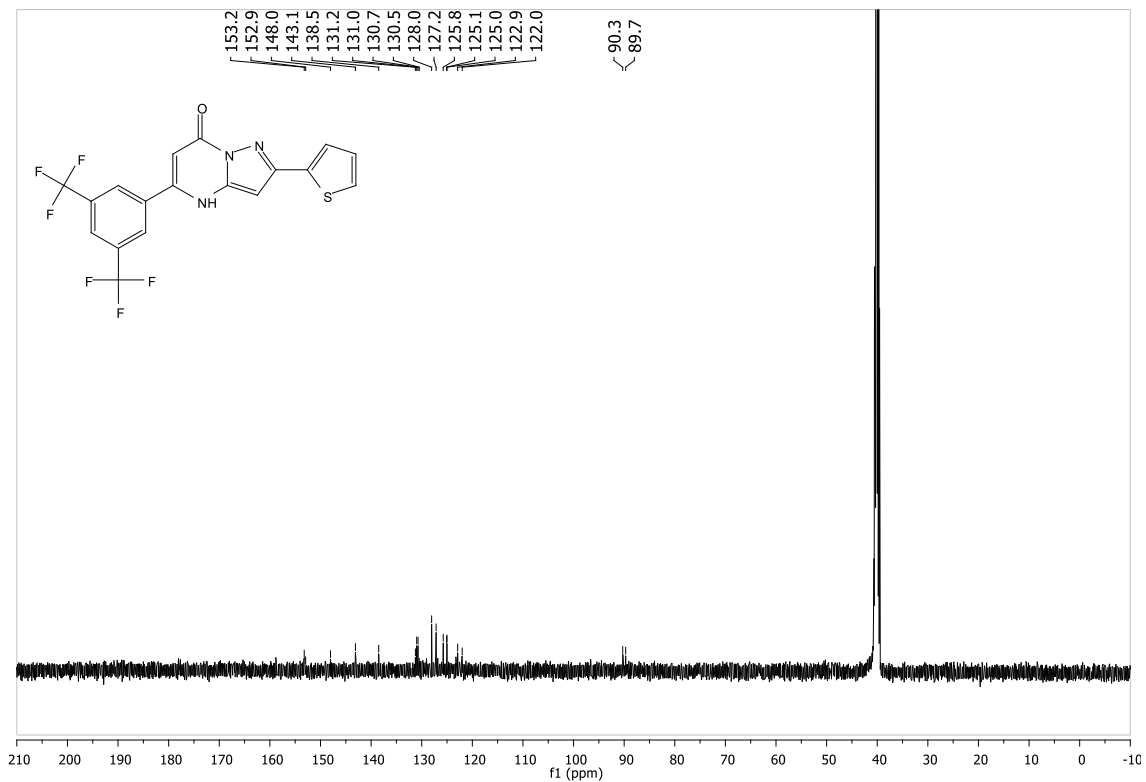
159.0
153.3
153.1
151.9
151.6
151.1
150.9
142.9
131.0
130.8
127.3
126.9
126.0
125.7
125.6
125.1
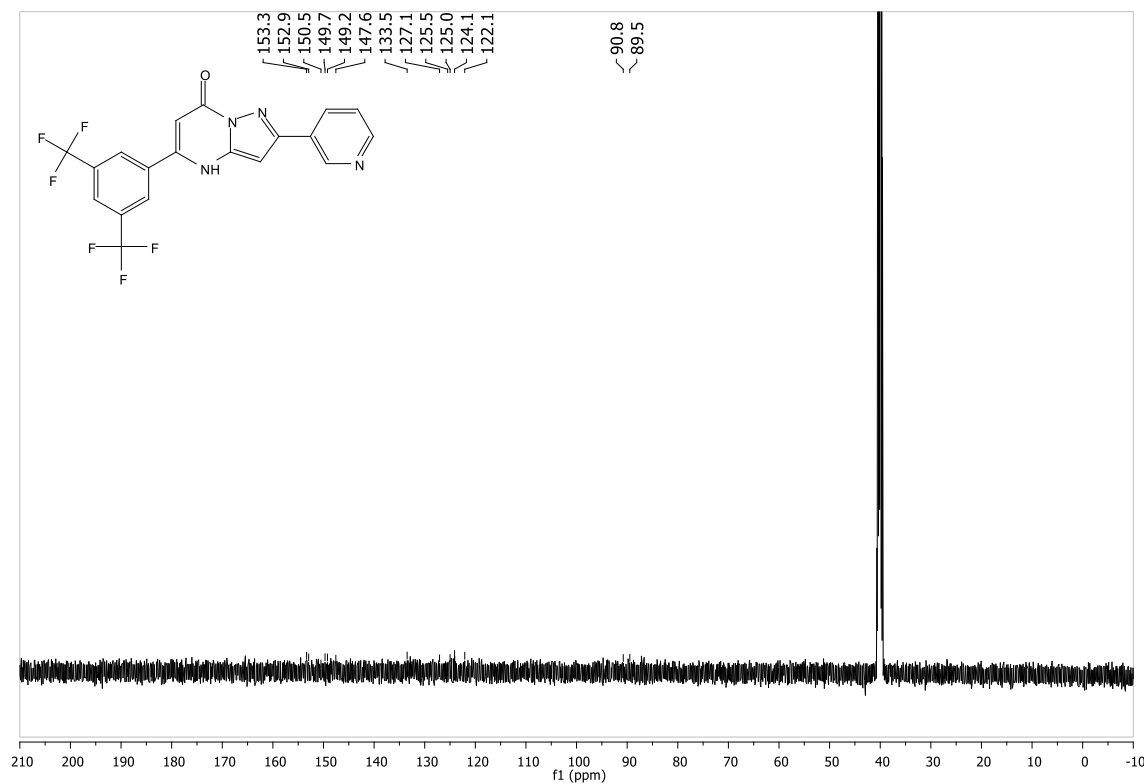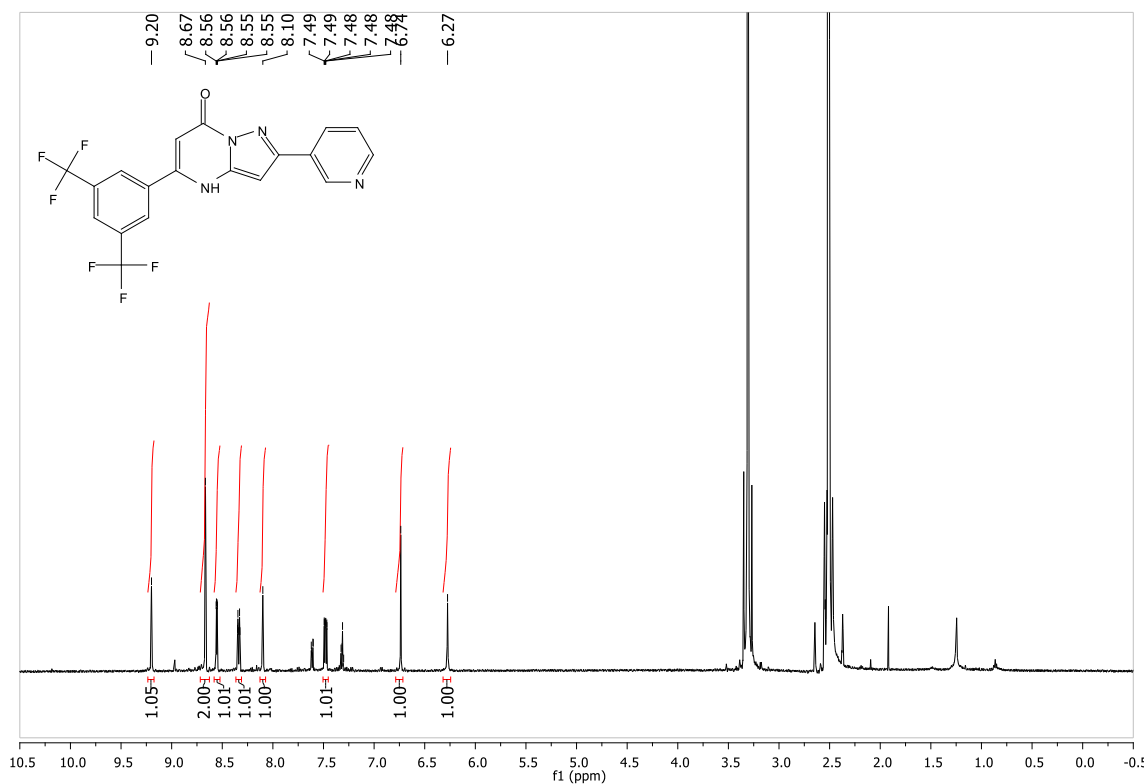123.8
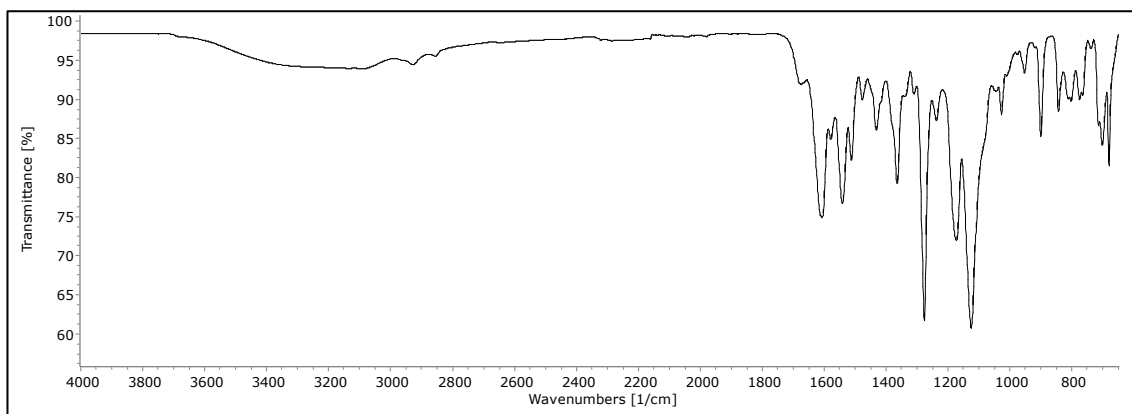122.9
122.2
91.5
89.8

f1 (ppm)

6.75 Spectra for 5-(3,5-bis(trifluoromethyl)phenyl)-2-(thiophen-2-yl)pyrazolo[1,5-*a*]pyrimidin-7(4*H*)-one (MK85) (75)
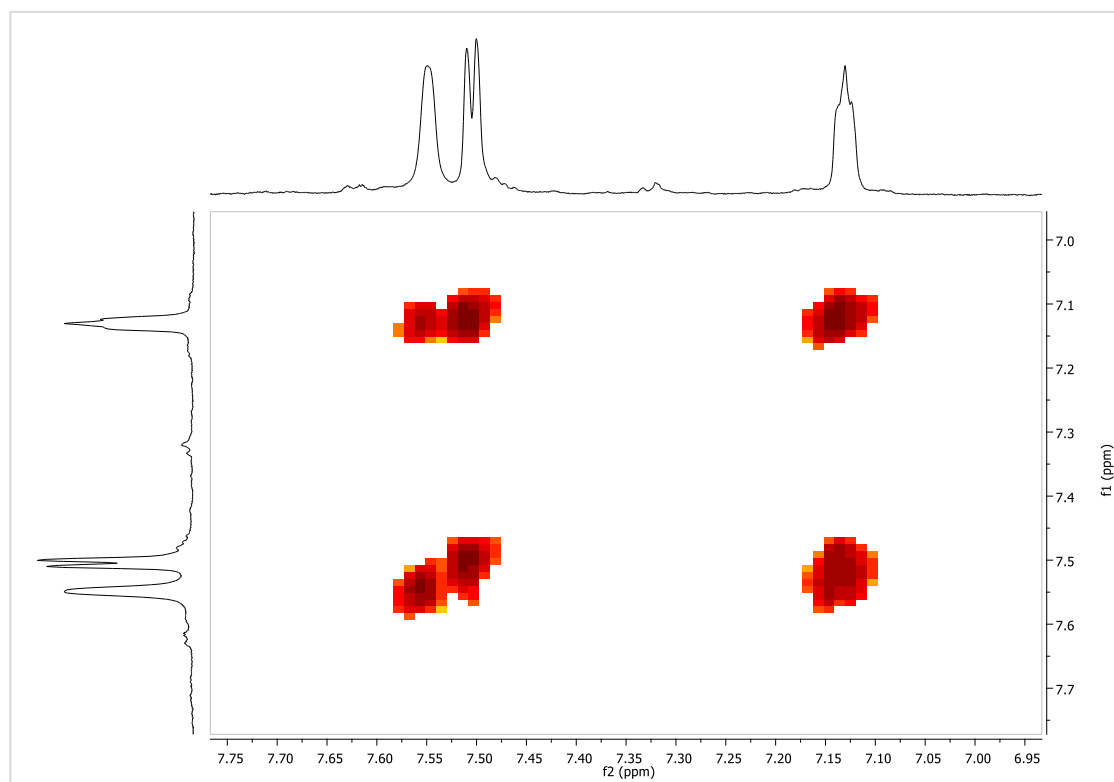
6.76 Spectra for 5-(3,5-bis(trifluoromethyl)phenyl)-2-(pyridin-3-yl)pyrazolo[1,5-*a*]pyrimidin-7(4*H*)-one (MK86) (76)

X-Ray Crystallographic Data

An Oxford Diffraction Xcalibur system was used to collect X-ray diffraction data at room temperature. The crystal structures were solved using ShelxT and refined using ShelxL within the Oscail package.[120,121]

Crystallographic data (excluding structure factors) for MK56b (compound **41**) have been deposited with the Cambridge Crystallographic Data Centre as supplementary publication CCDC 1588686. Copies of the data can be obtained, free of charge, on application to CCDC, 12 Union Road, Cambridge CB2 1EZ, UK, (fax: +44-(0)1223-336033 or e-mail: deposit@ccdc.cam.ac.uk).

Table 1. Crystal data and structure refinement for mk56b.

Identification code	mk56b	
Empirical formula	C16 H11 N3 O2	
Formula weight	277.28	
Temperature	298.5(9) K	
Wavelength	0.71073 Å	
Crystal system	Triclinic	
Space group	P-1	
Unit cell dimensions	a = 6.6464(6) Å	$\alpha = 82.880(10)°$.
	b = 7.0114(9) Å	$\beta = 86.962(8)°$.
	c = 15.0626(16) Å	$\gamma = 72.352(10)°$.
Volume	663.64(13) Å^3	
Z	2	
Density (calculated)	1.388 Mg/m^3	
Absorption coefficient	0.095 mm^{-1}	
F(000)	288	
Crystal size	0.50 x 0.40 x 0.02 mm^3	
Theta range for data collection	3.723 to 29.168°.	

Index ranges	-8<=h<=7, -9<=k<=9, -16<=l<=20
Reflections collected	4838
Independent reflections	3011 [R(int) = 0.0233]
Completeness to theta = 25.242°	99.7%
Absorption correction	Semi-empirical from equivalents
Max. and min. transmission	1.00000 and 0.69643
Refinement method	Full-matrix least-squares on F^2
Data / restraints / parameters	3011 / 1 / 195
Goodness-of-fit on F^2	1.048
Final R indices [I>2sigma(I)]	R1 = 0.0593, wR2 = 0.1313
R indices (all data)	R1 = 0.1145, wR2 = 0.1614
Extinction coefficient	0.010(4)
Largest diff. peak and hole	0.203 and -0.167 e.Å^{-3}

Table 2. Atomic coordinates (x 10^4) and equivalent isotropic displacement parameters (Å^2x 10^3)

for mk56b. U(eq) is defined as one third of the trace of the orthogonalized U^{ij} tensor.

_____

	x	y	z	U(eq)
O(1)	1978(2)	2474(3)	5142(1)	69(1)
N(2)	5084(2)	2450(3)	5702(1)	43(1)
N(1)	8044(2)	2440(3)	4783(1)	42(1)
N(3)	4405(3)	2463(3)	6565(1)	55(1)
O(2)	7624(5)	2616(4)	8381(2)	112(1)
C(1)	6930(3)	2451(3)	4051(2)	42(1)
C(2)	4879(3)	2453(3)	4156(2)	46(1)
C(3)	3826(3)	2448(3)	4985(2)	47(1)
C(4)	6113(4)	2433(4)	7007(2)	56(1)
C(5)	7855(4)	2418(4)	6447(2)	50(1)
C(6)	7159(3)	2425(3)	5612(2)	40(1)
C(7)	8036(4)	2469(4)	3182(2)	50(1)
C(8)	9609(4)	3399(4)	3023(2)	62(1)
C(9)	10656(5)	3352(5)	2210(2)	89(1)
C(10)	10129(7)	2453(6)	1545(2)	110(1)
C(11)	8543(7)	1565(6)	1691(2)	107(1)
C(12)	7509(5)	1561(5)	2504(2)	75(1)
C(13)	5920(5)	2488(4)	7964(2)	74(1)
C(14)	4379(7)	2428(6)	8561(3)	112(1)

C(15)	5162(11)	2539(8)	9408(3)	148(2)
C(16)	7086(11)	2670(8)	9265(3)	153(2)

_____

Table 3. Bond lengths [Å] and angles [°] for mk56b.

_____

O(1)-C(3)	1.233(2)
N(2)-N(3)	1.354(2)
N(2)-C(6)	1.374(2)
N(2)-C(3)	1.400(3)
N(1)-C(6)	1.352(3)
N(1)-C(1)	1.358(3)
N(1)-H(1N1)	0.898(16)
N(3)-C(4)	1.340(3)
O(2)-C(13)	1.356(4)
O(2)-C(16)	1.363(4)
C(1)-C(2)	1.363(3)
C(1)-C(7)	1.468(3)
C(2)-C(3)	1.399(3)
C(2)-H(2)	0.9300
C(4)-C(5)	1.395(3)
C(4)-C(13)	1.444(4)
C(5)-C(6)	1.361(3)
C(5)-H(5)	0.9300
C(7)-C(12)	1.380(3)
C(7)-C(8)	1.387(3)
C(8)-C(9)	1.374(4)
C(8)-H(8)	0.9300

C(9)-C(10)	1.360(4)
C(9)-H(9)	0.9300
C(10)-C(11)	1.373(4)
C(10)-H(10)	0.9300
C(11)-C(12)	1.373(4)
C(11)-H(11)	0.9300
C(12)-H(12)	0.9300
C(13)-C(14)	1.334(4)
C(14)-C(15)	1.422(6)
C(14)-H(14)	0.9300
C(15)-C(16)	1.314(6)
C(15)-H(15)	0.9300
C(16)-H(16)	0.9300
N(3)-N(2)-C(6)	111.99(17)
N(3)-N(2)-C(3)	124.04(16)
C(6)-N(2)-C(3)	123.97(18)
C(6)-N(1)-C(1)	121.26(16)
C(6)-N(1)-H(1N1)	120.1(16)
C(1)-N(1)-H(1N1)	118.6(16)
C(4)-N(3)-N(2)	103.34(17)
C(13)-O(2)-C(16)	106.5(3)
N(1)-C(1)-C(2)	119.2(2)
N(1)-C(1)-C(7)	116.95(18)

434

C(2)-C(1)-C(7)	123.8(2)
C(1)-C(2)-C(3)	123.7(2)
C(1)-C(2)-H(2)	118.2
C(3)-C(2)-H(2)	118.2
O(1)-C(3)-C(2)	128.1(2)
O(1)-C(3)-N(2)	118.6(2)
C(2)-C(3)-N(2)	113.33(17)
N(3)-C(4)-C(5)	113.1(2)
N(3)-C(4)-C(13)	118.0(2)
C(5)-C(4)-C(13)	128.9(2)
C(6)-C(5)-C(4)	104.43(19)
C(6)-C(5)-H(5)	127.8
C(4)-C(5)-H(5)	127.8
N(1)-C(6)-C(5)	134.34(18)
N(1)-C(6)-N(2)	118.54(18)
C(5)-C(6)-N(2)	107.12(19)
C(12)-C(7)-C(8)	118.9(2)
C(12)-C(7)-C(1)	120.0(2)
C(8)-C(7)-C(1)	121.1(2)
C(9)-C(8)-C(7)	119.9(3)
C(9)-C(8)-H(8)	120.0
C(7)-C(8)-H(8)	120.0
C(10)-C(9)-C(8)	120.9(3)
C(10)-C(9)-H(9)	119.6

C(8)-C(9)-H(9)	119.6
C(9)-C(10)-C(11)	119.6(3)
C(9)-C(10)-H(10)	120.2
C(11)-C(10)-H(10)	120.2
C(12)-C(11)-C(10)	120.4(3)
C(12)-C(11)-H(11)	119.8
C(10)-C(11)-H(11)	119.8
C(11)-C(12)-C(7)	120.3(3)
C(11)-C(12)-H(12)	119.8
C(7)-C(12)-H(12)	119.8
C(14)-C(13)-O(2)	109.8(3)
C(14)-C(13)-C(4)	133.6(3)
O(2)-C(13)-C(4)	116.5(3)
C(13)-C(14)-C(15)	106.5(4)
C(13)-C(14)-H(14)	126.7
C(15)-C(14)-H(14)	126.7
C(16)-C(15)-C(14)	106.6(4)
C(16)-C(15)-H(15)	126.7
C(14)-C(15)-H(15)	126.7
C(15)-C(16)-O(2)	110.5(4)
C(15)-C(16)-H(16)	124.7
O(2)-C(16)-H(16)	124.7

_____

Symmetry transformations used to generate equivalent atoms:

Table 4. Anisotropic displacement parameters ($\text{Å}^2 \times 10^3$) for mk56b. The anisotropic displacement factor exponent takes the form: $-2\pi^2[\,h^2\,a^{*2}U^{11} + ... \, + 2\,h\,k\,a^*\,b^*\,U^{12}\,]$

	U^{11}	U^{22}	U^{33}	U^{23}	U^{13}	U^{12}
O(1)	26(1)	87(1)	100(2)	-6(1)	-5(1)	-26(1)
N(2)	29(1)	46(1)	58(1)	-7(1)	2(1)	-15(1)
N(1)	23(1)	48(1)	56(1)	-1(1)	-7(1)	-14(1)
N(3)	52(1)	52(1)	65(2)	-10(1)	11(1)	-21(1)
O(2)	174(3)	130(2)	63(2)	-3(1)	-20(2)	-94(2)
C(1)	34(1)	40(1)	54(1)	-1(1)	-7(1)	-14(1)
C(2)	33(1)	49(1)	59(2)	-3(1)	-12(1)	-14(1)
C(3)	26(1)	42(1)	74(2)	-5(1)	-9(1)	-12(1)
C(4)	65(2)	45(2)	62(2)	-6(1)	0(1)	-23(1)
C(5)	46(1)	49(2)	59(2)	-1(1)	-14(1)	-20(1)
C(6)	27(1)	37(1)	57(2)	-2(1)	-5(1)	-12(1)
C(7)	46(1)	49(2)	54(2)	3(1)	-6(1)	-16(1)
C(8)	54(2)	68(2)	66(2)	6(1)	1(1)	-26(1)
C(9)	88(2)	102(3)	82(2)	11(2)	13(2)	-49(2)
C(10)	143(3)	134(4)	68(2)	-8(2)	34(2)	-72(3)
C(11)	156(4)	128(3)	60(2)	-13(2)	11(2)	-80(3)
C(12)	93(2)	86(2)	59(2)	-3(2)	2(2)	-50(2)
C(13)	111(2)	60(2)	59(2)	-10(1)	6(2)	-36(2)
C(14)	148(4)	120(3)	72(3)	-26(2)	33(3)	-45(3)

437

C(15)	255(7)	127(4)	71(3)	-25(3)	41(4)	-73(5)
C(16)	295(8)	154(5)	50(3)	-8(2)	-10(3)	-127(5)

_____

Table 5. Hydrogen coordinates (x 10^4) and isotropic displacement parameters (Å^2x 10^3)

for mk56b.

_____

	x	y	z	U(eq)
H(2)	4140	2458	3649	60
H(5)	9191	2407	6607	65
H(8)	9954	4055	3465	81
H(9)	11739	3942	2114	115
H(10)	10838	2439	996	143
H(11)	8168	963	1235	139
H(12)	6448	943	2599	97
H(14)	3054	2332	8447	146
H(15)	4450	2523	9956	192
H(16)	7958	2783	9706	199
H(1N1)	9390(30)	2460(40)	4707(16)	71(8)

_____

Table 6. Hydrogen bonds for mk56b [Å and °].

_____

D-H...A	d(D-H)	d(H...A)	d(D...A)	<(DHA)
N(1)-H(1N1)...O(1)#1	0.898(16)	1.879(19)	2.7064(19)	152(2)

_____

Symmetry transformations used to generate equivalent atoms:

#1 x+1,y,z

Table of Figures

Table of Schemes

Publication and Presentations

Publication

Kelada, M., Walsh, J. M. D., Devine, R. W., Mcardle, P. & Stephens, J. C. Synthesis of pyrazolopyrimidinones using a ' one-pot ' approach under microwave irradiation. *Beilstein J. Org. Chem.* 1222–1228 (2018). doi:10.3762/bjoc.14.104

Presentations

Poster presentation: "The design and synthesis of novel small molecules as possible anti-diabetic agents" – "Recent Advances in Synthesis and Chemical Biology XIIII", Royal College of Surgeons Ireland, December 2015.

Poster presentation: "Developing new anti-diabetic agents" – Publications Festival, Maynooth University, January 2016.

Poster presentation: "Anti-diabetic agents: design, synthesis and evaluation" – Royal Society of Chemistry conference, Trinity College Dublin, May 2016.

Poster presentation: "Heterocyclic anti-diabetic agents: design, synthesis and evaluation" – 1st Medicinal Chemistry Conference in Ireland, Trinity College Dublin, July 2016.

Oral international presentation: "The design, synthesis and evaluation of novel small molecules with potential as anti-diabetic agents" – 19th Chemistry Postgraduate Conference, University of Crete, May 2017.

Flash presentation: "The Design, Synthesis and Evaluation of Novel Small Molecules with Potential as Anti-Diabetic Agents" – 69th Irish Universities Chemistry Research Colloquium, Dublin City University, June 2017 (awarded best presentation).

Poster presentation: "The Design, Synthesis and Evaluation of Novel Small Molecules with Potential as Anti-Diabetic Agents" – Research Week, Maynooth University, October 2017.

Oral international presentation: "The design, synthesis and evaluation of novel small molecules with potential as anti-diabetic agents" – European Young Chemists' Network symposium, Turin, Italy, May 2018.

Oral presentation: "The design, synthesis and evaluation of novel small molecules with potential as anti-diabetic agents" – 70th Irish Universities Chemistry Research Colloquium, Queen's University Belfast, June 2018.

Poster presentation: "The Design, Synthesis and Evaluation of Novel Small Molecules with Potential as Anti-Diabetic Agents" – 2nd Medicinal Chemistry Conference, Dublin City University, July 2018.

Modules

Chemistry modules

CH801: Core Skills and Research Techniques in Chemistry.

CH803: Teaching Skills in Chemistry.

CH804: Thesis Plan.

CH806: Research Training Workshops in Chemistry.

CH807: Review of Research Papers.

CH808: Research Supervision Training.

CH863: Presentation of Research Work at Conferences.

Transferable modules

GST1: Personal Development and Employability.

GST5: Creative Thinking and Problem Solving.

GSS3: Professional Skills – Thesis Completion and Career Development.

Other

Masterclass with Dr David Birkett – Royal Irish Academy, April 2018

Abbreviations

°C = Degrees Celsius

AcOH = Acetic acid

ADA = American Diabetes Association

ADP = Adenosine diphosphate

AMPK = Adenosine monophosphate-activated protein kinase

ANOVA = One-way analysis of variance

Ar = Aryl

ATP = Adenosine triphosphate

ATR = Attenuated total reflection

BOP = Benzotriazol-1-yloxy)tris(dimethylamino)phosphonium hexafluorophosphate

bs = Broad singlet

BSA = Bovine serum albumin

CA = Commercially available

CD_3OD = Deuterated methanol

$CDCl_3$ = Deuterated chloroform

CF_3 = Trifluoromethyl

CFRD = Cystic fibrosis-related diabetes

cm^{-1} = Wavenumbers

COSY = Homonuclear Correlation Spectroscopy

d = Doublet

DCC = *N, N'*-Dicyclohexylcarbodiimide

DCM = Dichloromethane

DCU = N,N'-dicyclohexylurea

DEPT = Distortionless Enhancement of Polarization Transfer

DMAP = 4-(Dimethylamino)pyridine

DMEM = Dulbecco's Modified Eagle's Medium

DMF = Dimethylformamide

DMSO = Dimethyl sulfoxide

DPP-IV = Dipeptidyl peptidase IV

EASD = European Association for the Study of Diabetes

eHiTS = Electronic High Throughput Screening

ETC = Electron transport chain

ETF = Electron-transferring flavoproteins

EtOAc = Ethyl acetate

EtOH = Ethanol

$FAD/FADH_2$ = Flavin adenine dinucleotide

FeS = Iron-sulphur

FMN = Flavin mononucleotide

FTIR = Fourier-transform infrared

GIP = Glucose Dependent Insulinotropic Polypeptide

GLP-1 = Glucagon Like Peptide-1

GTT = Glucose tolerance test

GU = Glucose uptake

H_2O = Water (deionised)

HCl = Hydrochloric acid

HFD = High-fat diet

HMBC = Heteronuclear Multiple Bond Correlation

HOBt = Hydroxybenzotriazole

Hr(s) = Hour(s)

HR-MS = High-resolution mass spectrometry

HSE = Health Service Executive

HSQC = Heteronuclear Single Quantum Correlation

Hz = Hertz

IDF = International Diabetes Federation

iNKT = Invariant natural killer T

IR = Infrared

ITT = Insulin tolerance test

J = Coupling constant

KBR = Potassium bromide

KRB = Krebs' Ringer Buffer

$LiAlH_4$ = Lithium aluminium hydride

m = Meta

M = Molar

m = Multiplet

m.p. = Melting point

Me = Methyl

MeOH = Methanol

$MgSO_4$ = Magnesium sulfate

mins = Minutes

mmol = Millimole

MODY = Maturity-onset diabetes of the young

MS = Mass spectrometry

MW = Microwave

N_2 = Nitrogen

Na_2CO_3 = Sodium carbonate

NAD/NADH = Nicotinamide adenine dinucleotide

$NaHCO_3$ = Sodium hydrogen carbonate

NCD = Non-communicable diseases

NEt_3 = Triethylamine

NMP = *N*-methyl-2-pyrrolidone

NMR = Nuclear magnetic resonance

o = Ortho

O.N. = Overnight

p = Para

Pet. Ether = Petroleum ether

Ph = Phenyl

PPAR = Peroxisome proliferator-activated receptor

ppm = Parts per million

PtO_2 = Platinum oxide (Adam's catalyst)

p-TSA.H_2O = *Para* Toluene sulfonic acid monohydrate

q = Quartet

RBP4 = Retinol binding protein 4

rt = Room temperature

s = Singlet

SAR = Structure activity relationship

SEM = Standard Error of the Means

SPR = Surface plasmon resonance

t = Triplet

TBTU = N,N,N',N'-Tetramethyl-O-(benzotriazol-1-yl)uronium tetrafluoroborate

THF = Tetrahydrofuran

TLC = Thin layer chromatography

TTR = Transthyretin

W = Watts

Bibliography

1. IDF Diabetes Atlas (8th Edition), *International Diabetes Federation* (2017). doi:10.1016/j.diabres.2009.10.007

2. Skyler, J. S. Diabetes mellitus: Pathogenesis and treatment strategies. *J. Med. Chem.* **47,** 4113–4117 (2004).

3. Medeiros, D. M., Wildman, R. E. C. & Wildman, R. E. C. *Advanced human nutrition - Chapter 7: Metabolism*. (Jones & Bartlett Learning, 2012).

4. Gandica, R. G., Chung, W. K., Deng, L., Goland, R. & Gallagher, M. P. Identifying monogenic diabetes in a pediatric cohort with presumed type 1 diabetes. **16,** 227–233 (2015).

5. O'Shea, D. & O'Connell, J. Cystic fibrosis related diabetes. *Curr. Diab. Rep.* **14,** (2014).

6. Ripsin, C. M., Kang, H. & Urban, R. J. Management of blood glucose in type 2 diabetes mellitus. *Am. Fam. Physician* **79,** 29–36 (2009).

7. Spencer, E., Pirie, K. L., Stevens, R. J., Beral, V., Liu, B., Green, J., Reeves, G. K., Diabetes and Modifiable Risk Factors for Cardiovascular Disease : The Prospective Million Women Study. *Eur. J. Epidemiol.* **23,** 793–799 (2016).

8. Negoro, N., Sasaki, S., Mikami, S., Ito, M., Tsujihata, Y., Ito, R., Suzuki, M., Takeuchi, K., Suzuki, N., Miyazaki, J., Santou, T., Odani, T., Kanzaki, N., Funami, M., Morohashi, A., Nonaka, M., Matsunaga, S., Yasuma, T., Momose, Y.*,* Optimization of (2,3-dihydro-1-benzofuran-3-yl)acetic acids: Discovery of a non-free fatty acid-like, highly bioavailable G protein-coupled receptor 40/free fatty acid receptor 1 agonist as a glucose-dependent insulinotropic agent. *J. Med. Chem.* **55,** 3960–3974 (2012).

9. Kitabchi, A. E., Umpierrez, G. E., Miles, J. M. & Fisher, J. N. Hyperglycemic crises in adult patients with diabetes. *Diabetes Care* **32,** 1335–1343 (2009).

10. Carolan, E., Hogan, A., Connell, J O., Fallon, M., Byrne, D., Shea, D O., Cody, D.*,* The Prevalence of Cardiovascular Risk Factors in Obese Children. *Ir. Med. J.* 1–4 (2015).

11. Maori, L., Ezekiel, D. & Bilal, J. Prevalence of Diabetes in Zambuk General Hospital. *Rep. Opin. Rep Opin.* **44,** 54–57 (2012).

12. You, W. P. & Henneberg, M. Type 1 diabetes prevalence increasing globally and regionally: the role of natural selection and life expectancy at birth. *BMJ Open Diabetes Res. Care* **4,** e000161 (2016).

13. Interact, T. Consumption of sweet beverages and type 2 diabetes incidence in European adults: Results from EPIC-InterAct. *Diabetologia* **56,** 1520–1530 (2013).

14. World Health Organization. Diagnostic Criteria and Classification of Hyperglycaemia First Detected in Pregnancy. *World Heal. Organ.* 1–63 (2013). doi:10.1016/j.diabres.2013.10.012

15. Fendler, W., Borowiec, M., Baranowska-Jazwiecka, A., Szadkowska, A., Skala-Zamorowska, E., Deja, G., Jarosz-Chobot, P., Techmanska, I., Bautembach-

Minkowska, J., Mysliwiec, M., Zmyslowska, A., Pietrzak, I., Malecki, M. T., Mlynarski, W., Prevalence of monogenic diabetes amongst Polish children after a nationwide genetic screening campaign. *Diabetologia* **55,** 2631–2635 (2012).

16. Kropff, J., Selwood, M. P., McCarthy, M. I., Farmer, a. J. & Owen, K. R. Prevalence of monogenic diabetes in young adults: A community-based, cross-sectional study in Oxfordshire, UK. *Diabetologia* **54,** 1261–1263 (2011).

17. Basu, S., Yoffe, P., Hills, N. & Lustig, R. H. The Relationship of Sugar to Population-Level Diabetes Prevalence: An Econometric Analysis of Repeated Cross-Sectional Data. *PLoS One* **8,** (2013).

18. Nolan, J. J., O'Halloran, D., McKenna, T. J., Firth, R. & Redmond, S. The cost of treating type 2 diabetes (CODEIRE). *Ir. Med. J.* **99,** 307–10 (2006).

19. Lorenzati, B., Zucco, C., Miglietta, S., Lamberti, F. & Bruno, G. Oral hypoglycemic drugs: Pathophysiological basis of their mechanism of action. *Pharmaceuticals* **3,** 3005–3020 (2010).

20. Harrigan, R., Nathan, M. S. & Beattie, P. Oral agents for the treatment of type 2 diabetes mellitus: Pharmacology, toxicity, and treatment. *Ann. Emerg. Med.* **38,** 68–78 (2001).

21. Upadhyay, J., Polyzos, S., Perakakis, N., Thakkar, B., Paschou, S., Katsiki, N., Underwood, P., Park, K., Seufert, J., Kang, E., Sternthal, E., Karagiannis, A., Mantzoros, C. S., Pharmacotherapy of type 2 diabetes: An update. *Metabolism.* **78,** 13–42 (2018).

22. Biederman, J. I., Vera, E., Rankhaniya, R., Hassett, C., Giannico, G., Yee, J., Cortes, P., Effects of sulfonylureas, α-endosulfine counterparts, on glomerulosclerosis in type 1 and type 2 models of diabetes. *Kidney Int.* **67,** 554–565 (2005).

23. Abrahamsson, H., Berggren, P. O. & Rorsman, P. Direct measurements of increased free cytoplasmic Ca2+ in mouse pancreatic beta-cells following stimulation by hypoglycemic sulfonylureas. *FEBS Lett.* **190,** 21–24 (1985).

24. Gómez-Huelgas, R., Gómez Peralta, F., Rodríguez Mañas, L., Formiga, F., Puig Domingo, M., Mediavilla Bravo, J.J., Miranda, C., Ena, J., Treatment of type 2 diabetes mellitus in elderly patients. *Rev. Clínica Española,* **218,** 74–88 (2018).

25. Madiraju, A. K., Qiu, Y., Perry, R. J., Rahimi, Y., Metformin inhibits gluconeogenesis via a redox-dependent mechanism in vivo. *Nat. Med.* 1 (2018). doi:10.1038/s41591-018-0125-4

26. Oh, S., Kim, S., Hwang, J., Lee, H., Antidiabetic and antiobesity effects of ampkinone (6f), a novel small molecule activator of AMP-activated protein kinase. *J. Med. Chem.* **53,** 7405–7413 (2010).

27. Zhou, T., Xu, X., Du, M., Zhao, T. & Wang, J. A preclinical overview of metformin for the treatment of type 2 diabetes. *Biomed. Pharmacother.* **106,** 1227–1235 (2018).

28. Wu, J., Luo, X., Thangthaeng, N., Sumien, N., Pancreatic mitochondrial complex I exhibits aberrant hyperactivity in diabetes. *Biochem. Biophys. Reports* **11,** 119–129 (2017).

29. Cameron, A. R., Logie, L., Patel, K., Erhardt, S., Metformin selectively targets redox control of complex I energy transduction. *Redox Biol.* **14,** 187–197 (2018).

30. Tan, M. H., Alquraini, H., Mizokami-Stout, K. & MacEachern, M. Metformin: From Research to Clinical Practice. *Endocrinol. Metab. Clin. North Am.* **45,** 819–843 (2016).

31. Gante, I., Melo, L., Dores, J., And, L. R. & Almeida, M. do C. Metformin in Gestational Diabetes Mellitus: predictors of poor response. *Eur. J. Endocrinol.* **178,** 129–135 (2018).

32. Insuela, D. B. R. & Carvalho, V. F. Glucagon and glucagon-like peptide-1 as novel anti-inflammatory and immunomodulatory compounds. *Eur. J. Pharmacol.* **812,** 64–72 (2017).

33. Hogan, A. E., Gaoatswe, G., Lynch, L., Corrigan, M. A., Glucagon-like peptide 1 analogue therapy directly modulates innate immune-mediated inflammation in individuals with type 2 diabetes mellitus. *Diabetologia* **57,** 781–784 (2014).

34. Hogan, A. E., Tobin, A. M., Ahern, T., Corrigan, M. A., Gaoatswe, G., Jackson, R., OReilly, V., Lynch, L., Doherty, D. G., Moynagh, P. N., Kirby, B., O'connell, J., OShea, D., Glucagon-like peptide-1 (GLP-1) and the regulation of human invariant natural killer T cells: Lessons from obesity, diabetes and psoriasis. *Diabetologia* **54,** 2745–2754 (2011).

35. Campbell, N. A. Reece, J., Urry, L., Cain, M., Wasserman, S.*, Biology (11th Edition)* (Pearson Education, 2016).

36. Garrett, R. H. & Grisham, C. M. *Biochemistry (5th Edition).* (Twayne Publishers, 2008).

37. Raven, P. H. *Biology (9th Edition)* (Twayne Publishers, 2010).

38. Mitochondria function: the electron transport system. Available at: http://www.ruf.rice.edu/bioslabs/studies/mitochondria/mitets.html.

39. Sazanov, L. A. & Hinchliffe, P. Structure of the hydrophilic domain of respiratory complex I from Thermus thermophilus. *Science* **311,** 1430–6 (2006).

40. Sazanov, L. A., Baradaran, R., Berrisford, J. M. & Minhas, G. S. Crystal structure of the entire respiratory complex I. *Nature* **494,** 443–8 (2013).

41. Miyazaki, R., Yamazaki, T., Yoshimatsu, K., Kojima, K., Bioelectrochemistry Elucidation of the intra- and inter-molecular electron transfer pathways of glucoside 3-dehydrogenase. *Bioelectrochemistry* **122,** 115–122 (2018).

42. Watabe, M. & Nakaki, T. Mitochondrial complex I inhibitor rotenone inhibits and redistributes vesicular monoamine transporter 2 via nitration in human dopaminergic SH-SY5Y cells. *Mol. Pharmacol.* **74,** 933–940 (2008).

43. Li, N. *et al.* Mitochondrial complex I inhibitor rotenone induces apoptosis through enhancing mitochondrial reactive oxygen species production. *J. Biol. Chem.* **278,** 8516–8525 (2003).

44. Martin, D. S. D., Leonard, S., Devine, R., Redondo, C., Kinsella, G. K., Breen, C. J., McEneaney, V., Rooney, M. F., Munsey, T. S., Porter, R. K., Sivaprasadarao, A., Stephens, J. C., Findlay, J. B. C., Novel mitochondrial complex I inhibitors restore glucose-handling abilities of high-fat fed mice. *J. Mol. Endocrinol.* **56,** 261–271 (2016).

45. Devine, R. Design, synthesis and biological evaluation of anti-diabetic agents. Thesis, Maynooth University (2013).

46. Preitner, F., Mody, N., Graham, T. E., Peroni, O. D. & Kahn, B. B. Long-term Fenretinide treatment prevents high-fat diet-induced obesity, insulin resistance, and hepatic steatosis. *AJP Endocrinol. Metab.* **297,** E1420–E1429 (2009).

47. Campos-sandoval, A., Redondo, C., Kinsella, G., Pal, A., Jones, G., Fenretinide Derivatives Act as Disrupters of Interactions of Serum Retinol Binding Protein (sRBP) with Transthyretin and the sRBP Receptor. 4378–4387 (2011). doi:10.1021/jm200256g

48. Stephens, J.; Kinsella, G.; Martin, D.; Devine, R.; Velasco-Torrijos, T.; Findlay, J. B. C. WO2013060860A1. (2013).

49. STEPHENS, J. *et al.* N-acyl-n'-phenylpiperazine derivatives as SRBP modulators for use in the treatment of diabetes and obesity (Patent WO2013060860). (2013).

50. Yun, J. *et al.* Glucose deprivation contributes to the development of KRAS pathway mutations in tumor cells. *Science* **325,** 1555–9 (2009).

51. Leonard, S., Tobin, L. M. & Findlay, J. B. C. The signalling mechanisms of a novel mitochondrial complex I inhibitor prevent lipid accumulation and attenuate TNF-α-induced insulin resistance in vitro. *Eur. J. Pharmacol.* **800,** 1–8 (2017).

52. Nilsson, B. M. 5-Hydroxytryptamine 2C (5-HT2C) receptor agonists as potential antiobesity agents. *J. Med. Chem.* **49,** 4023–4034 (2006).

53. Yokoshima, S., Watanabe, K., Uehara, F., Usui, Y. & Tanaka, H. Asymmetric synthesis of 2-arylpiperazines. *Bioorganic Med. Chem. Lett.* **24,** 5749–5751 (2014).

54. Chen, H., Wang, C., Sun, T., Zhou, Z., Synthesis, biological evaluation and SAR of naftopidil-based arylpiperazine derivatives. *Bioorganic Med. Chem. Lett.* **28,** 1534–1539 (2018).

55. Chen, H., Xu, F., Xu, B., Xu, J., Shao, B., Design, synthesis and biological evaluation of novel arylpiperazine derivatives on human prostate cancer cell lines. *Chinese Chem. Lett.* **27,** 277–282 (2016).

56. Montalbetti, C. A. G. N. & Falque, V. Amide bond formation and peptide coupling. *Tetrahedron* **61,** 10827–10852 (2005).

57. Ghose, A. K., Viswanadhan, V. N. & Wendoloski, J. J. A knowledge-based approach in designing combinatorial or medicinal chemistry libraries for drug discovery. 1. A qualitative and quantitative characterization of known drug databases. *J. Comb. Chem.* **1,** 55–68 (1999).

58. Manetti, D., Ghelardini, C., Bartolini, A., Dei, S., Galeotti, N., Gualtieri, F., Romanelli, M. N., Teodori, E., Molecular simplification of 1,4-diazabicyclo[4.3.0]nonan-9-ones gives piperazine derivatives that maintain high nootropic activity. *J. Med. Chem.* **43,** 4499–4507 (2000).

59. Gierczyk, B., Kaźmierczak, M., Popenda, Ł., Sporzyński, A., Influence of fluorine substituents on the NMR properties of phenylboronic acids. *Magn. Reson. Chem.* **52,** 202–213 (2014).

60. Cobb, S. L. & Murphy, C. D. 19F NMR applications in chemical biology. *J. Fluor. Chem.* **130,** 132–143 (2009).

61. Takamura, A., Watanabe, K., Akutsu, T. & Ozawa, T. Soft and Robust Identification of Body Fluid Using Fourier Transform Infrared Spectroscopy and Chemometric

Strategies for Forensic Analysis. *Sci. Rep.* **8,** 1–10 (2018).

62. Wessel, E. *et al.* Observation of a penetration depth gradient in attenuated total reflection fourier transform infrared spectroscopic imaging applications. *Appl. Spectrosc.* **60,** 1488–92 (2006).

63. Greener, J., Abbasi, B. & Kumacheva, E. Attenuated total reflection Fourier transform infrared spectroscopy for on-chip monitoring of solute concentrations. *Lab Chip* **10,** 1561–1566 (2010).

64. Dhara, M. G. & Banerjee, S. Fluorinated high-performance polymers: Poly(arylene ether)s and aromatic polyimides containing trifluoromethyl groups. *Prog. Polym. Sci.* **35,** 1022–1077 (2010).

65. Sandford, G. Elemental fluorine in organic chemistry (1997-2006). *J. Fluor. Chem.* **128,** 90–104 (2007).

66. True, J. E., Thomas, T. D., Winter, R. W. & Gard, G. L. Electronegativities from core-ionization energies: Electronegativities of SF5 and CF3. *Inorg. Chem.* **42,** 4437–4441 (2003).

67. Nenajdenko, V. G., Sanin, A. V. & Balenkova, E. S. Preparation of α,β-unsaturated ketones bearing a trifluoromethyl group and their application in organic synthesis. *Molecules* **2,** 186–232 (1997).

68. Yale, H. L. The Trifluoromethyl Group in Medicinal Chemistry. *J. Med. Chem.* **1,** 121–133 (1959).

69. Rikimaru, K., Wakabayashi, T., Abe, H., Tawaraishi, T., Structure-activity relationships and key structural feature of pyridyloxybenzene-acylsulfonamides as new, potent, and selective peroxisome proliferator-activated receptor (PPAR) γ Agonists. *Bioorganic Med. Chem.* **20,** 3332–3358 (2012).

70. Bassetto, M., Leyssen, P., Neyts, J., Yerukhimovich, M., In silico identification, design and synthesis of novel piperazine-based antiviral agents targeting the hepatitis C virus helicase. *Eur. J. Med. Chem.* **125,** 1115–1131 (2017).

71. Kumar, J., Chawla, G., Akhtar, M., Sahu, K., Design, synthesis and pharmacological evaluation of some novel derivatives of 1-{[3-(furan-2-yl)-5-phenyl-4,5-dihydro-1,2-oxazol-4-yl]methyl}-4-methyl piperazine. *Arab. J. Chem.* **10,** 141–149 (2017).

72. Sata, F., Nishino, C., Uetake, T. & Fukunishi, H. N-acylpiperazine derivative, antibacterial drug and anti-ulcer drug. (1998).

73. Harder, A. The Biochemistry of Haemonchus contortus and Other Parasitic Nematodes. in *Advances in Parasitology* **93,** 69–94 (Academic Press, 2016).

74. Page, S. W. *Antiparasitic drugs*. *Small Animal Clinical Pharmacology* (W.B. Saunders, 2008). doi:10.1016/B978-070202858-8.50012-9

75. Safko, J. P., Kuperstock, J., McCullough, S., Noviello, A., Network formation and photoluminescence in copper(i) halide complexes with substituted piperazine ligands. *Dalt. Trans.* **41,** 11663 (2012).

76. Yamamoto, J., Hitomi, K., Hayashi, R., Getzoff, E. D. & Iwai, S. Role of the carbonyl group of the (6-4) photoproduct in the (6-4) photolyase reaction. *Biochemistry* **48,** 9306–9312 (2009).

77. Liao, H. Y. & Chu, S. Y. Hydrogen bond acceptor capability of carbonyl π-

electrons—case study of the hydrogen-bonded urea dimer. *New J. Chem.* **27,** 421–424 (2003).

78. Swanston, J. Thiophene. in *Ullmann's Encyclopedia of Industrial Chemistry* (Wiley-VCH Verlag GmbH & Co. KGaA, 2006). doi:10.1002/14356007.a26_793.pub2

79. Mancuso, R. & Gabriele, B. *Recent advances in the synthesis of thiophene derivatives by cyclization of functionalized alkynes*. *Molecules* **19,** (2014).

80. Landman, M., Görls, H. & Lotz, S. Synthesis of molybdenum carbene complexes of thiophene derivatives. *Zeitschrift fur Anorg. und Allg. Chemie* **628,** 2037–2043 (2002).

81. Chapter 14: Thiophenes: reactions and synthesis, *Heterocyclic Chemistry 4th Edition* (1882).

82. Pine, S. H. The Eschweiler-Clark methylation of amines: An organic chemistry experiment. *J. Chem. Educ.* **45,** 118 (1968).

83. Lin, H.; Moore, M. L.; Qu, J.; Rivero, R. A.; Tedesco, R.; Yu, H.;Luengo, J. I. Pyrazolopyrimidine derivatives as PI3 kinase inhibitors. (2013).

84. Griffith, D. A. Pyrazolo [1,5-a] pyrimidin-7-one compounds and uses thereof. (2005).

85. Binch, H., Grootenhuis, Peter, D. J., Pierce, A. & Fanning, Lev, T. D. Modulators of cystic fibrosis transmembrane conductance regulator. (2009).

86. Qi, J., F., Mi, Y., Fu, Y., Design, synthesis and biological activity of pyrazolo[1,5-a]pyrimidin-7(4H) -ones as novel Kv7/KCNQ potassium channel activators. *Eur. J. Med. Chem.* **46,** 934–943 (2011).

87. Portilla, J., Quiroga, J., Nogueras, M. & Cobo, J. Regioselective synthesis of fused pyrazolo[1,5-a]pyrimidines by reaction of 5-amino-1H-pyrazoles and b-dicarbonyl compounds containing five-membered rings. *Tetrahedron* **68,** 988–994 (2012).

88. Felipe, L., Azeredo, S., Coutinho, J., Jabor, V., Evaluation of 7-arylaminopyrazolo[1,5-a]pyrimidines as anti- Plasmodium falciparum, antimalarial, and Pf-dihydroorotate dehydrogenase inhibitors. *Eur. J. Med. Chem.* **126,** 72–83 (2017).

89. Kelada, M., Walsh, J. M. D., Devine, R. W., Mcardle, P. & Stephens, J. C. Synthesis of pyrazolopyrimidinones using a 'one-pot' approach under microwave irradiation. *Beilstein J. Org. Chem.* 1222–1228 (2018). doi:10.3762/bjoc.14.104

90. Velcicky, J., Feifel, R., Hawtin, S., Heng, R., Novel 3-aminopyrazole inhibitors of MK-2 discovered by scaffold hopping strategy. *Bioorganic Med. Chem. Lett.* **20,** 1293–1297 (2010).

91. Rodríguez, A. M., Prieto, P., De La Hoz, A., Díaz-Ortiz, Á., Influence of Polarity and Activation Energy in Microwave-Assisted Organic Synthesis (MAOS). *ChemistryOpen* **4,** 308–317 (2015).

92. Hoz, A. de la & Loupy, A. *Microwaves in organic synthesis*. (Wiley-VCH, Weinheim, 2012).

93. Nayak, J., Devi, C. & Vidyapeeth, L. Microwave assisted synthesis : a green chemistry approach. *Int. Res. J. Pharm. Appl. Sci.* **3,** 278–285 (2016).

94. Bagley, M. C., Davis, T., Dix, M. C., Widdowson, C. S. & Kipling, D. Microwave-

assisted synthesis of N-pyrazole ureas and the p38a inhibitor BIRB 796 for study into accelerated cell ageing. *Org. Biomol. Chem.* **4,** 4158 (2006).

95. Chen, W., Gutmann, B. & Kappe, C. O. Characterization of Microwave-Induced Electric Discharge Phenomena in Metal-Solvent Mixtures. *ChemistryOpen* **1,** 39–48 (2012).

96. Greis, K. D., Zhou, S., Siehnel, R., Klanke, C., Development and validation of a whole-cell inhibition assay for bacterial methionine aminopeptidase by surface-enhanced laser desorption ionization-time of flight mass spectrometry. *Antimicrob. Agents Chemother.* **49,** 3428–3434 (2005).

97. McMahon, D. K., Anderson, P. A., Nassar, R., Bunting, J. B., Saba, Z., Oakeley, A. E., Malouf, N. N., C2C12 cells: biophysical, biochemical, and immunocytochemical properties. *Am. J. Physiol. Physiol.* **266,** C1795–C1802 (1994).

98. Struhl, K. Subcloning of DNA Fragments. *Curr. Protoc. Mol. Biol.* **13,** 3.16.1-3.16.2 (1991).

99. Sato, T., Ito, Y., Nedachi, T. & Nagasawa, T. Lysine suppresses protein degradation through autophagic-lysosomal system in C2C12 myotubes. *Mol. Cell. Biochem.* **391,** 37–46 (2014).

100. Mohammadtaghvaei, N., Meshkani, R., Taghikhani, M., Larijani, B. & Adeli, K. Palmitate enhances protein tyrosine phosphatase 1B (PTP1B) gene expression at transcriptional level in C2C12 skeletal muscle cells. *Inflammation* **34,** 43–48 (2011).

101. Zeng, X. Q. *et al.* Knockdown of NYGGF4 increases glucose transport in C2C12 mice skeletal myocytes by activation IRS-1/PI3K/AKT insulin pathway. *J. Bioenerg. Biomembr.* **44,** 351–355 (2012).

102. Pegg, D. E. Principles of Cryopreservation. in *Methods in molecular biology (Clifton, N.J.)* **368,** 39–57 (2007).

103. Smith, P. K., Krohn, R.I., Hermanson, G.T., Mallia, A.K., Gartner, F.H., Provenzano, M.D., Fujimoto, E.K., Goeke, N.M., Olson, B.J., Klenk, D.C., Measurement of protein using bicinchoninic acid. *Anal. Biochem.* **150,** 76–85 (1985).

104. Sadakiyo, M., Yamada, T. & Kitagawa, H. Hydroxyl Group Recognition by Hydrogen-Bonding Donor and Acceptor Sites Embedded in a Layered Metal–Organic Framework. *J. Am. Chem. Soc.* **133,** 11050–11053 (2011).

105. Platts, J. A., Howard, S. T. & Bracke, B. R. F. Directionality of Hydrogen Bonds to Sulfur and Oxygen. *J. Am. Chem. Soc.* **118,** 2726–2733 (1996).

106. Chappell, J. B. & Hansford, R. G. Preparation of mitochondria from animal tissues and yeasts. *Subcell. Components* 77–91 (1972). doi:10.1016/B978-0-408-70360-4.50009-2

107. Choi, W.-S., Kruse, S. E., Palmiter, R. D. & Xia, Z. Mitochondrial complex I inhibition is not required for dopaminergic neuron death induced by rotenone, MPP+, or paraquat. *Proc. Natl. Acad. Sci.* **105,** 15136–15141 (2008).

108. Heinz, S., Freyberger, A., Lawrenz, B., Schladt, L., Mechanistic Investigations of the Mitochondrial Complex i Inhibitor Rotenone in the Context of Pharmacological and Safety Evaluation. *Sci. Rep.* **7,** 1–13 (2017).

109. Hollenback, D., Bonham, L., Law, L., Rossnagle, E., Substrate specificity of

lysophosphatidic acid acyltransferase β—evidence from membrane and whole cell assays. *J. Lipid Res.* **47,** 593–604 (2006).

110. Hernandez, L., Kodali, S., Cully, D., Singh, S. & Wang, J. A target-specific whole cell assay for antibacterial drug discovery. *Protoc. Exch.* (2006). doi:10.1038/nprot.2006.130

111. Rutkowska, E., Pajǎk, K. & Jóźwiak, K. Lipophilicity - Methods of determination and its role in medicinal chemistry. *Acta Pol. Pharm. - Drug Res.* **70,** 3–18 (2013).

112. Brenner, E., Schneider, R. & Fort, Y. Nickel-catalysed selective N -arylation or N,N′-diarylation of secondary diamines. *Tetrahedron* **58,** 6913–6924 (2002).

113. Pinard, E., Alanine, A., Alberati, D., Bender, M., Selective GlyT1 inhibitors: Discovery of [4-(3-fluoro-5- trifluoromethylpyridin-2-yl)piperazin-1-yl][5-methanesulfonyl-2-((S)-2,2, 2-trifluoro-1-methylethoxy)phenyl]methanone (RG1678), a promising novel medicine to treat schizophrenia. *J. Med. Chem.* **53,** 4603–4614 (2010).

114. Krasavin, M. & Konstantinov, I. O. Minimizing side reactions in classical pyrazole synthesis from B-oxonitriles: The use of acetylhydrazine. *Lett. Org. Chem.* **5,** 594–598 (2008).

115. Nam, N. L., Grandberg, I. I. & Sorokin, V. I. Condensation of 5-aminopyrazoles unsubstituted in position 1 with β-keto esters. *Chem. Heterocycl. Compd.* **39,** 1210–1212 (2003).

116. Tantry, S. J., Shinde, V., Balakrishnan, G., Markad, S., Amit, K., Scaffold morphing leading to evolution of 2,4-diaminoquinolines and aminopyrazolopyrimidines as inhibitors of the ATP synthesis pathway. *Med. Chem. Commun.* **7,** 1022–1032 (2016).

117. Baburajan, P. & Elango, K. P. One pot direct synthesis of β-ketoesters via carbonylation of aryl halides using cobalt carbonyl. *Tetrahedron Lett.* **55,** 3525–3528 (2014).

118. Marcus, A. P., Lee, A. S., Davis, R. L., Tantillo, D. J. & Sarpong, R. Pronounced steric effects of substituents in the Nazarov cyclization of aryl dienyl ketones. *Angew. Chemie - Int. Ed.* **47,** 6379–6383 (2008).

119. Ajioka, N., Suzuki, Y., Yokoyama, A. & Yokozawa, T. Synthesis of Well-Defined Polystyrene- b -Aromatic Polyether Using an Orthogonal Initiator for Atom Transfer Radical Polymerization and Chain-Growth Condensation Polymerization. *Macromolecules* **40,** 5294–5300 (2007).

120. Sheldrick, G. M. SHELXT - Integrated space-group and crystal-structure determination. *Acta Crystallogr. Sect. A Found. Crystallogr.* **71,** 3–8 (2015).

121. Sheldrick, G. M. Crystal structure refinement with SHELXL. *Acta Crystallogr. Sect. C Struct. Chem.* **71,** 3–8 (2015).

END OF THESIS